UNIVERSITÀ DEGLI STUDI DI TRIESTE

UNIVERSITÀ DEGLI STUDI DI UDINE

Dottorato di Ricerca Interateneo in Ingegneria Civile–Ambientale e Architettura

Curriculum: Ingegneria Civile
Settore Scientifico Disciplinare: ICAR/09,
Tecnica delle costruzioni
XXXIII Ciclo

SEISMIC VULNERABILITY EVALUATION OF R.C. AND MASONRY BUILDINGS IN THE CENTRE OF GORIZIA

DOTTORANDA

LJUBA SANCIN

COORDINATORE

PROF. ALBERTO SDEGNO

SUPERVISORE DI TESI

PROF. CLAUDIO AMADIO

ANNO ACCADEMICO 2019/2020

_____

"One thing I have learned in a long life: that all our science, measured against reality, is primitive and childlike --- and yet it is the most precious thing we have."

Albert Einstein

_____

ABSTRACT

The aim of this research study is to investigate the vulnerability of the building heritage in Gorizia, a town in north-eastern Italy, on the border with Slovenia. This town has not been considered seismic until the year 2003 and then in 2010 it has been classified in a higher seismicity class. For this reason, most of the buildings are not designed to resist seismic action at all and an even lower percentage fulfils the requirements of the current technical standard.

Four real existing buildings are analysed as case study buildings, representative of the main structural types that can be found in the town. Two of them are high - rise (11 and 12 storeys) reinforced concrete (RC) framed buildings with a brittle concrete stairwell, designed for gravitational load only and built in the 60's-70's. In the last years, a growing attention has been payed to the seismic vulnerability of existing RC framed structures, but this type of buildings, with a core of concrete walls, has been investigated much less, although it is a structural type that is very spread. The other two case studies are masonry buildings built in 1740 and in 1903, respectively. One of the masonry buildings is the city hall of Gorizia, on which many in-situ tests have been performed within a project of the Department of Engineering and Architecture with the Municipality of Gorizia. For both RC buildings, some considerations are made about the influence of the masonry infills on the seismic behaviour of the building and of the numerical model. The vibration periods found with numerical modelling are also compared to the periods evaluated with vibrational measurements. The two numerical models without infills are then analysed with non-linear static and dynamic analyses. The results are processed with a cloud analysis in order to calculate fragility curves of the buildings, that show a very brittle behaviour. The two masonry buildings are analysed also with pushover analysis.

For the evaluation of the seismic vulnerability of the analysed buildings, two types of seismic hazard assessments have been considered for the extraction of the seismic inputs: Probabilistic Seismic Hazard Assessment (PSHA) method, by the Italian code response spectra and the Scenario Physics-Based Seismic Hazard Assessment (SPBSHA), as an evolution of the Neo Deterministic Seismic Hazard Assessment (NDSHA) method. The response spectra of two specific possible scenarios for the town of Gorizia have been used. The physics-based scenarios are calculated for the two faults that are the closest to Gorizia: Idrija and Medea. A comparison is made between the demand given by the seismic inputs defined with the two methods. The importance of using both methods for the design of low-damage retrofitting solutions is highlighted.

At last, a theoretical study has been carried out within the present research study in order to find an innovative and effective solution for the retrofit of the RC high-rise brittle buildings. It consists in the application of an exo - or endo - skeleton, with the additional introduction of a sliding system at the base of the RC building, in order to decouple its motion from the ground motion. In this way, the exo- or endo-skeleton can be designed independently from the features of the existing building, that remains undamaged. The characteristics of the exo- or endo-skeleton can be calibrated on the seismic input of the site of interest, with the possibility to adapt it to new seismic classifications of the territory.

_____

ACKNOWLEDGEMENTS

_____

_____

INDEX

_____

1. INTRODUCTION

1.1. Vulnerability of Italian building heritage

Italian building heritage is very vulnerable and this endangers the value of the heritage itself that could be lost and the lives of people. The vulnerable buildings are not just residential buildings or touristic ancient structures, but also offices, schools and all kind of built environments. In the last 70 years more than 10 000 casualties have been registered for hydrogeological and seismic phenomena. Economic damage in the same period has been evaluated in around 290 billions of Euros, with a yearly average of 4 billions of Euros and values that are increasing in time [1]. Just for the recent events in Central Italy (summer 2016 to January 2017) the Italian Civil Protection Service has evaluated the cost of the emergency and damage caused by the earthquakes in 23.5 billions of Euros [2].

Italian territory is subjected to various natural hazards. The main ones concerning the building heritage are seismic events, landslides, alluvial phenomena and volcanoes. In order to have a safe built environment in a territory where hazard cannot be avoided, smart solutions should be used. The first rule should be: don't build anything in the most exposed zones (especially for landslides and volcanoes). The second rule should be: build in such a way that at least the expected events can be managed without casualties and with minimal economic loss. A third rule should be: build strategic buildings in even safer places and with even more effective protection against natural events, so that help can be coordinated from there in case of need.

On the other hand, many obstacles can be found, for which these simple rules are not always applicable. It has been evaluated, for instance, that in Italy 20 buildings out of 100 are unauthorized, so that no permission has been given for the location or the building system and its quality [3]. Another challenge, especially regarding seismic risk, is given by the historic buildings and monuments, that are very difficult to adequate without compromising their aesthetic and they were not built to undergo earthquakes. Moreover, there is usually very few information about the structure and its changes over the years.
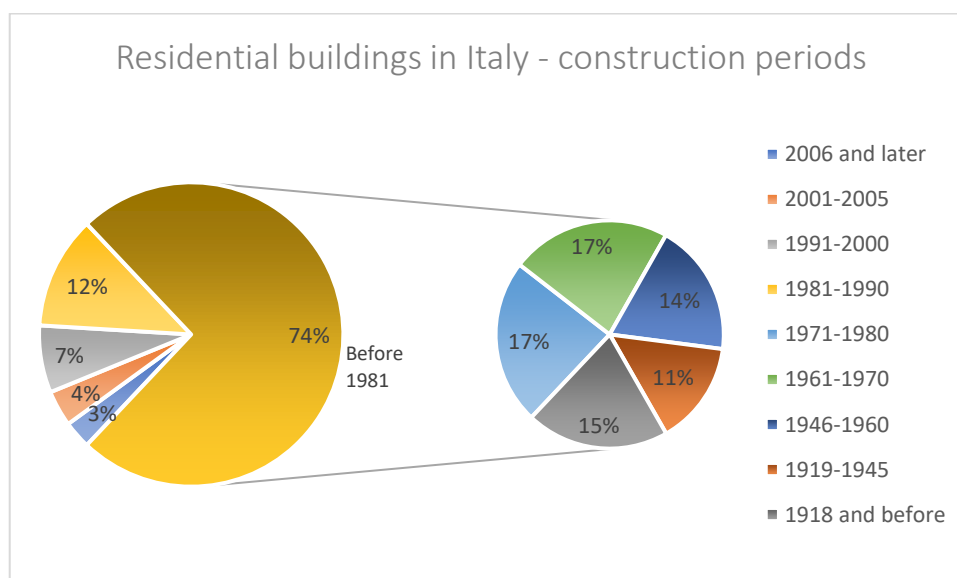
Figure 1-1: Construction periods of the residential building heritage in Italy; on the left side all the buildings constructed before 1981 are positioned in the same piece of the cake graph, on the right side these buildings are subdivided in shorter construction periods. [4]

Also if we exclude the monuments and just take into account residential buildings, that are probably the most important regarding human lives, it can be noticed that they are on average very old and vulnerable. Figure 1-1 shows the percentage of residential buildings in Italy built in different

periods. It can be noticed that 74% of residential buildings in Italy have been constructed before the year 1981. Figure 1-2 shows the main construction systems used in different periods: masonry, reinforced concrete and other materials. We can notice that other materials are used just in few cases, masonry is the main construction system until the 60's or 70's and then reinforced concrete takes its place.
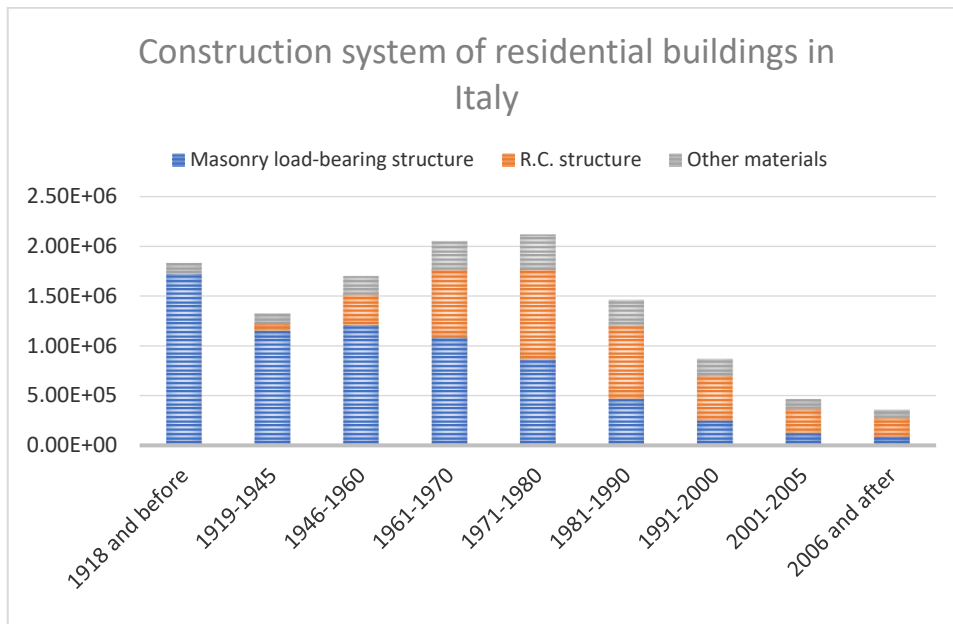
Figure 1-2: Construction systems of residential buildings in Italy, subdivided by construction period. [4]

1.2. Seismic hazard and building code

If we consider just the seismic hazard, the year 1981 is meaningful because it is the year in which the proposal for the reclassification of the national territory in 3 seismic categories has been adopted. The proposal was made by CNR (Consiglio Nazionale delle Ricerche), as part of the finalized project "Geodinamica" and it was aiming at substituting the first categorization of Italian territory that had just 2 seismic categories based on occurred earthquakes (Figure 1-3). Thanks to specific ministerial decrees between years 1981 and 1984, 45% of national territory was classified as seismic and the use of specific construction codes became mandatory (Figure 1-4). The other half of Italian territory has continued to be free to construct without taking earthquakes into account, also because in 1974 for the first time was made the decision that seismic classification needs proven technical-scientific knowledge and not just experience of occurred earthquakes.

Just after the earthquake in Puglia and Molise, in 2002, the Ordinance of the President of the Council of Ministers n. 3274 of 2003 (Ordinanza del Presidente del Consiglio dei Ministri - OPCM n.3274 del 2003 [5]), based on the classification proposal of 1998 (Figure 1-5) classifies the entire Italian territory as seismic, dividing it in 4 zones with different hazard, leaving no zone free of seismic risk (Figure 1-6).

The last important step is the entry into force of "Norme tecniche per le costruzioni 2008 (NTC 2008), that became mandatory on 1 July 2009. Lately a new version of this code has entered into force, NTC 2018 [6], with minor differences compared to the previous one.

Based on the evolution of seismic classification and construction codes, it can be stated that there are plenty of buildings, constructed until years 2000, that have not been properly designed to withstand the earthquakes that nowadays we know could occur in certain territories. Moreover, the knowledge about seismic hazard is continuously changing and improving, so that it cannot be taken for granted that also the structures designed based on the latest codes would resist the strongest earthquakes. This is also due to the choice of basing the seismic input for design on a probability calculation and not on the maximum expected shakes. This topic will be discussed in § 2. In fact, in

the latest strong earthquakes in Italy it has been seen that also new structures, designed based on the latest codes, have collapsed. Connected to this topic there is also the topic about the design philosophy. Until the building codes allow to build structures that are able to protect human lives, but get so damaged that they need to be demolished and rebuilt, we'll always have a lot of economic loss after each strong earthquake. The aim of the new design criteria should be to have structures that remain undamaged after strong events or just need to substitute small parts that are meant to protect the building and are easy and low-cost to substitute.

Figure 1-3: R.D. 640 of 25/03/1935 – 2 categories, based on experienced earthquakes.
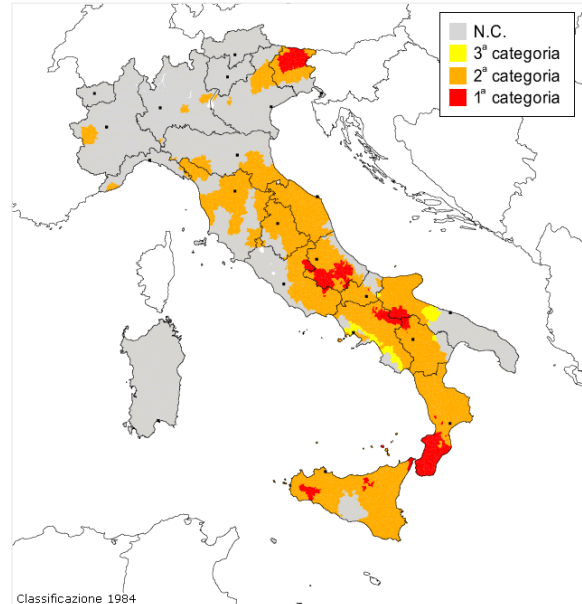
Figure 1-4: D.M 29/02/1984 – 3 categories, based on technical-scientific knowledge.
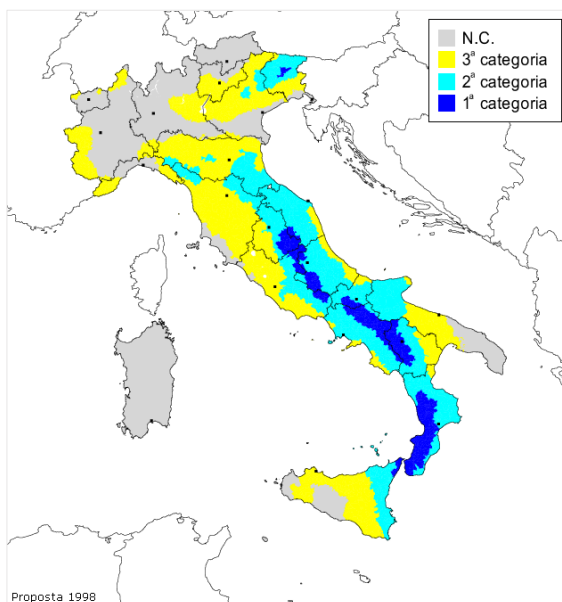
Figure 1-5: 1998 – new proposal of seismic classification.
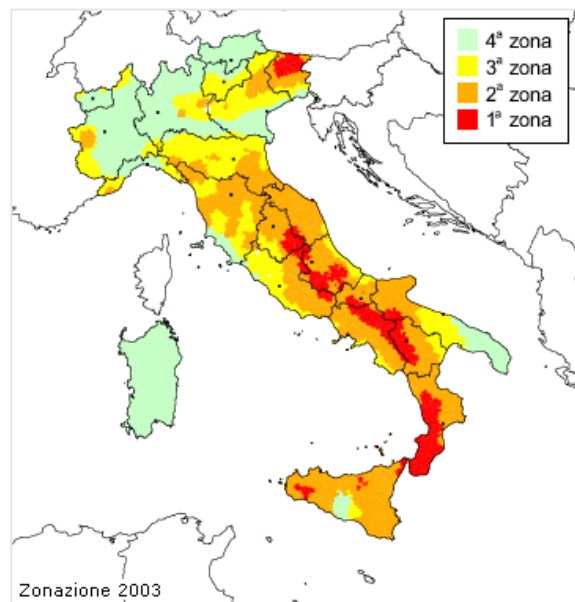
Figure 1-6: OPCM 3274 of 20/03/2003 – 4 zones.

1.3. Seismic hazard in Gorizia

Gorizia is a small town in Friuli Venezia Giulia, a region in North-Eastern Italy, and it is located at the foot of the Julian Alps, bordering Slovenia. It has about 34 000 inhabitants and a long

history, so that here can be found very old buildings, usually built of stone masonry and newer buildings, usually with reinforced concrete structure. This research is focused on seismic vulnerability of the building heritage of this town.

Gorizia was first officially classified as seismic in 2003, by the already mentioned OPCM 3274 and put in zone 3, as it was proposed already in 1998. With a regional update (Delibera della Giunta Regionale 845 del 06/05/2010) in 2010 it was moved to zone 2 (Figure 1-7). The late classification of this town as seismic leads to a very big part of the existing building heritage that is not designed for resisting earthquakes at all (until 2003) or designed to resist seismic events of lower intensity (until 2010). This means that just the very new, not older than 10 years, buildings are designed to withstand the seismic level that could occur in this area, according to the latest studies.
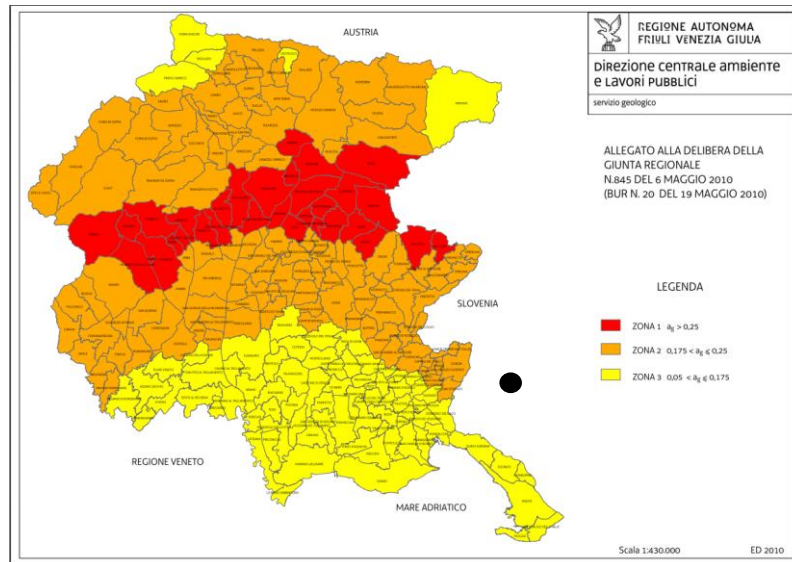
Figure 1-7: Regional update of seismic classification for the region Friuli Venezia Giulia (Delibera della Giunta Regionale 845 del 06/05/2010). Gorizia is in zone 2.

Although Gorizia has not really experienced strong earthquakes in its known history, it is classified as very seismic because it is located at the end of an arch of faults that cut the region almost in half and that have produced strong earthquakes as the one in Friuli in 1976. The town is also positioned between two faults with potentially high magnitudes: Idrija and Medea (Figure 1-8). Research studies show that Idrija fault can potentially produce earthquakes of magnitude 6.8 and Medea fault of 6.4. There are also more recently discovered faults that could affect seismicity of Gorizia. The seismic area of the region can be noticed also on the map of the recorded occurred earthquakes (Figure 1-9). Although the majority of earthquakes on the map have very low magnitude, the epicentres clearly show the shape of the arch of faults and Gorizia is in this arch. One more factor that contributes to form a potentially dangerous territory is the geology of Gorizia and thus its site effects. The bedrock is emerging in some spots, as for example where it forms the hill under the castle of Gorizia, dating back to the 11th century, but the main ground type elsewhere in the town is fluvioglacial and alluvial sediments from Isonzo river. Soft ground, as sediments, could amplificate seismic waves and thus create stronger site effects compared to the effects of an earthquake where just rock is present.

In order to fully introduce the seismicity of Gorizia, Table 1-1 displays the strongest earthquakes that have been felt in the known history of the town. They are located quite far from Gorizia (about 50 km to 100 km) and have not caused big damage to the buildings. The highest intensity felt in Gorizia has been VI or VII, measured on Modified Mercalli Intensity Scale. Degree VI means "Strong earthquake - felt by all and many are frightened. Some heavy furniture is moved; a few instances of fallen plaster occur. Damage is slight." Degree VII means "Very strong earthquake - damage is negligible in buildings of good design and construction; but slight to moderate in well-

built ordinary structures; damage is considerable in poorly built or badly designed structures; some chimneys are broken."
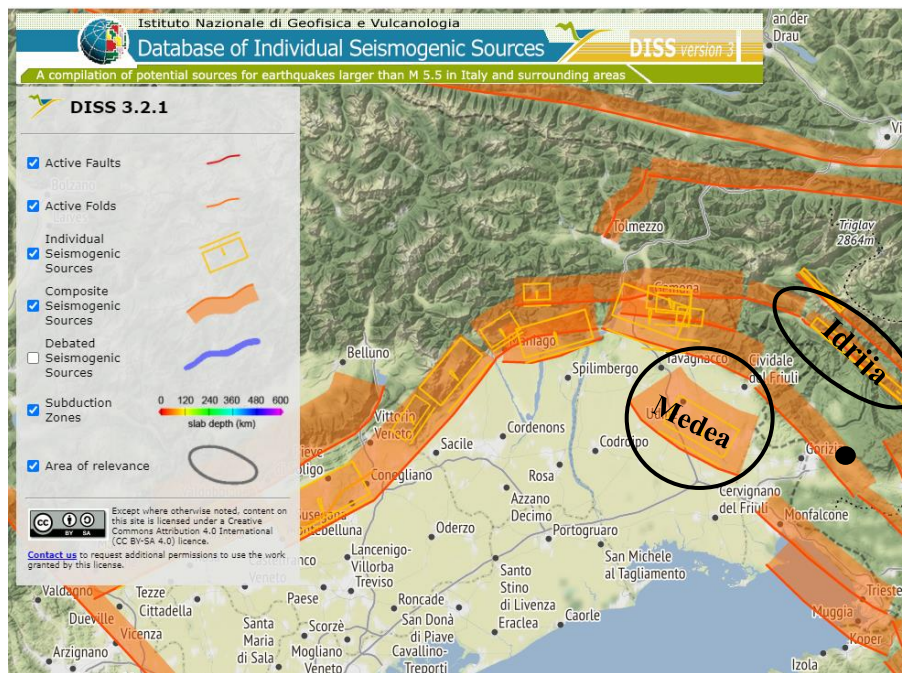
Figure 1-8: Screenshot of the web map created by INGV, where all active faults, individual and composite seismogenic sources are reported. Gorizia town, Medea and Idrija faults are highlighted. [8]
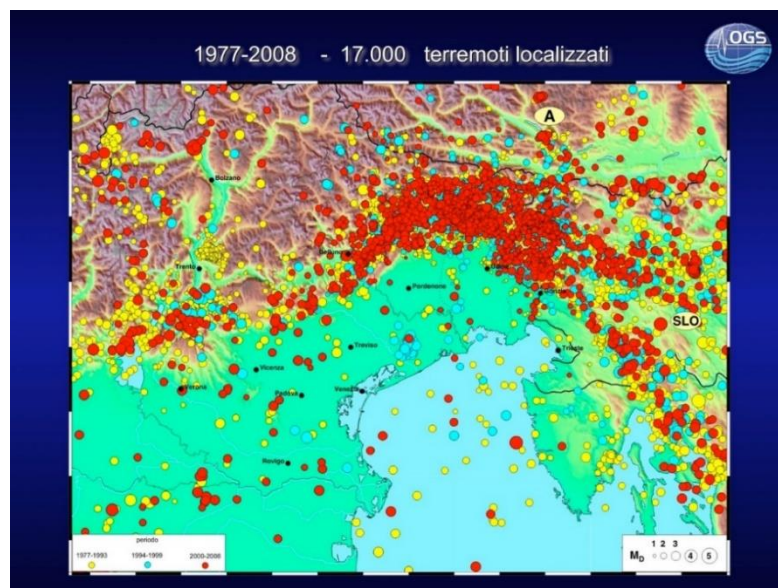
Figure 1-9: Map of occurred earthquakes between years 1977 and 2008 (catalogue of OGS = Istituto Nazionale di Oceanografia e Geofisica Sperimentale) – different colours indicate the range of years of occurrence, the size of the dots indicate the magnitude.

In order to evaluate the greatest peak ground accelerations (PGAs) felt in Gorizia with these seismic events, in Figure 1-10 is reported an image realized by OGS (Istituto Nazionale di Oceanografia e Geofisica Sperimentale), where the data for four significant events are calculated. The attenuation law used for the calculation is Sabetta and Pugliese, 1996 [7]. It can be seen that the values remain quite low, the highest PGA felt in Gorizia is 0.08 g, although the studies and the seismic classification show that the values could be potentially higher. For seismic zone 2, in which

Gorizia is classified, is typical a range of PGA between 0.15 g and 0.25 g with 10% of probability of exceedance in 50 years.

Table 1-1: Table of the strongest earthquakes felt in the town of Gorizia and their intensity there (Modified Mercalli). [9]

Date	Magnitude	Location	Intensity felt in Gorizia
1511/03/26	6.32	Friuli - Slovenia	VI-VII
1873/06/29	6.29	Alpago Cansiglio	VI
1895/04/14	5.98	Ljubljana	V-VI
1926/01/01	5.72	Carniola Interna	VI
1976/05/06	6.45	Friuli	VI-VII
1976/09/15	5.95	Friuli	V-VI
1998/04/12	5.60	Kobarid	
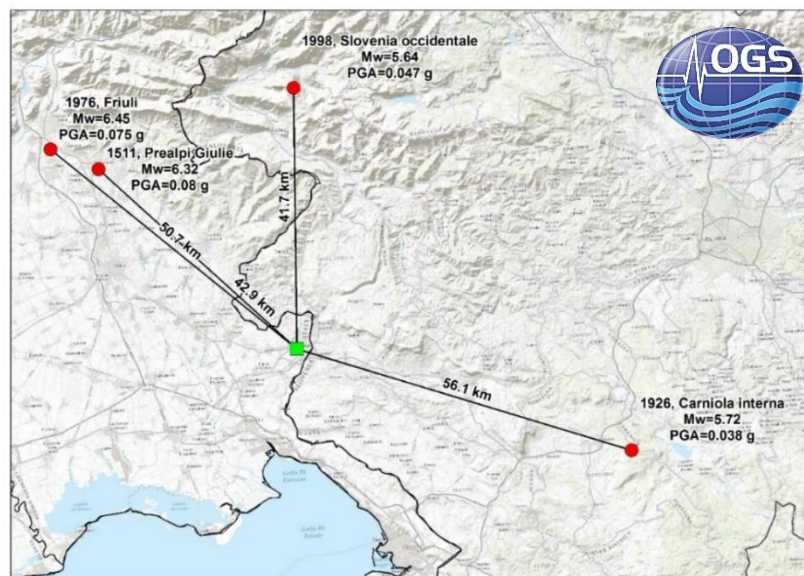
Figure 1-10: Peak ground accelerations calculated at the hospital of Gorizia (green square) for four significant earthquakes in the history of Gorizia, placed within a radius of 60 km from the town. PGA= 0.075 g for the Friuli earthquake in 1976, PGA = 0.08 g for the earthquake in 1511 without certain epicentre, PGA =0.047 g for the earthquake in Western Slovenia in 1998 and PGA = 0.038 g for the Carniola interna earthquake in 1926. The attenuation law used is Sabetta e Pugliese, 1996. (OGS)

1.4. Building heritage in Gorizia

As the aim of this research study is to evaluate the vulnerability of the building heritage in Gorizia, first a survey about its composition has been made. The Italian Institute for Statistics (Istituto Nazionale di Statistica – ISTAT) has some data about the existing buildings in Italy, collected with the census that used to occur every 10 years. The data can be sorted by Province and Municipality and it can be seen the: age, state of preservation, materials, number of storeys and the usage of the buildings. For the Province of Gorizia it is shown that in 2001 (the second-last census) there were 30 038 buildings, of which 26 892 residential and that in 2011 (last census) they increased to 35 507 total and 30 760 residential. Of all the buildings, just 14 674 (47.7%) were in perfect state of preservation. Moreover, it has to be pointed out that the state of preservation is evaluated by the generic citizen that has filled out the census form and it is not a technical evaluation made by an expert. It is also not specific for seismic resistance. It means that just a smaller part of the buildings categorized as "in perfect state of preservation" are probably also earthquake resistant. Table 1-2 shows however that the worse preservation state of RC buildings is mostly present in the buildings constructed between the years 1946 and 1971(highlighted in red in Table 1-2) and that the 70's have been the years when the greatest number of RC buildings have been built (highlighted in green in the

same table). On the other hand, for masonry buildings it can be seen that the ones built before 1919 are in the worst state of preservation (highlighted in brown in the same table).

Table 1-2: Information about residential buildings in the province of Gorizia, aggregated by state of preservation, building system, census year and construction period.

Province of Gorizia (residential)			Construction period							
			Before 1919		From 1919 to 1945		From 1946 to 1961		From 1962 to 1971	
			abs.nr	% on total of the same material	abs.nr	% on total of the same material	abs.nr	% on total of the same material	abs.nr	% on total of the same material
Perfect	Masonry	2001	1172	8%	931	6%	801	5%	580	4%
		2011	1316	8%	872	5%	938	6%	751	5%
	R.C.	2001	0	0%	34	1%	175	5%	318	9%
		2011	0	0%	41	1%	247	4%	599	10%
	Other	2001	235	3%	178	2%	365	5%	496	6%
		2011	280	3%	257	3%	542	7%	626	8%
Total Perfect state 2001			1407	5%	1143	4%	1341	5%	1394	5%
Total Perfect state 2011			1596	6%	1170	4%	1727	6%	1976	7%
Good	Masonry	2001	1825	12%	1621	11%	1650	11%	1176	8%
		2011	1462	9%	1525	9%	1733	10%	1475	9%
	R.C.	2001	0	0%	50	1%	282	8%	470	13%
		2011	0	0%	48	1%	319	5%	563	9%
	Other	2001	460	6%	346	4%	719	9%	879	11%
		2011	201	3%	431	5%	681	8%	670	8%
Total Perfect state 2001			2285	8%	2017	8%	2651	10%	2525	9%
Total Perfect state 2011			1663	6%	2004	7%	2733	10%	2708	10%
Mediocre	Masonry	2001	961	6%	840	5%	609	4%	321	2%
		2011	640	4%	537	3%	556	3%	259	2%
	R.C.	2001	0	0%	24	1%	76	2%	92	3%
		2011	0	0%	24	0%	91	1%	157	3%
	Other	2001	149	2%	109	1%	191	2%	166	2%
		2011	66	1%	162	2%	138	2%	90	1%
Total Perfect state 2001			1110	4%	973	4%	876	3%	579	2%
Total Perfect state 2011			706	3%	723	3%	785	3%	506	2%
Very bad	Masonry	2001	161	1%	101	1%	53	0%	14	0%
		2011	99	1%	62	0%	52	0%	11	0%
	R.C.	2001	0	0%	1	0%	7	0%	1	0%
		2011	0	0%	2	0%	10	0%	8	0%
	Other	2001	29	0%	15	0%	11	0%	5	0%
		2011	10	0%	22	0%	11	0%	10	0%
Total Perfect state 2001			190	1%	117	0%	71	0%	20	0%
Total Perfect state 2011			109	0%	86	0%	73	0%	29	0%
Total Masonry		2001	4119	27%	3493	23%	3113	20%	2091	14%
Total R.C.		2001	0	0%	109	3%	540	15%	881	24%
Total Other		2001	873	11%	648	8%	1286	16%	1546	20%
Total Masonry		2011	3517	21%	2996	18%	3279	20%	2496	15%
Total R.C.		2011	0	0%	115	2%	667	11%	1327	22%
Total Other		2011	557	7%	872	11%	1372	17%	1396	17%
Total buildings		2001	4992	19%	4250	16%	4939	18%	4518	17%
Total buildings		2011	4074	13%	3983	13%	5318	17%	5219	17%

Province of Gorizia (residential)			Construction period							
			From 1972 to 1981		From 1982 to 1991		From 1991 to 2001		From 2001 to 2005	
			abs.nr	% on total of the same material	abs.nr	% on total of the same material	abs.nr	% on total of the same material	abs.nr	% on total of the same material
Perfect	Masonry	2001	458	3%	415	3%	546	4%	-	-
		2011	637	4%	494	3%	537	3%	371	2%
	R.C.	2001	375	10%	410	11%	542	15%	-	-
		2011	726	12%	654	11%	532	9%	518	8%
	Other	2001	724	9%	626	8%	1009	13%	-	-
		2011	596	7%	587	7%	798	10%	515	6%
Total Perfect state 2001			1557	6%	1451	5%	2097	8%	-	-
Total Perfect state 2011			1959	7%	1735	6%	1867	7%	1404	5%
Good	Masonry	2001	650	4%	268	2%	104	1%	-	-
		2011	958	6%	441	3%	245	1%	79	0%
	R.C.	2001	453	12%	172	5%	57	2%	-	-
		2011	518	8%	309	5%	177	3%	34	1%
	Other	2001	676	9%	302	4%	121	2%	-	-
		2011	449	6%	247	3%	131	2%	30	0%
Total Perfect state 2001			1779	7%	742	3%	282	1%	-	-
Total Perfect state 2011			1925	7%	997	4%	553	2%	143	1%
Mediocre	Masonry	2001	74	0%	17	0%	7	0%	-	-
		2011	74	0%	22	0%	6	0%	2	0%
	R.C.	2001	87	2%	4	0%	2	0%	-	-
		2011	78	1%	24	0%	3	0%	2	0%
	Other	2001	73	1%	11	0%	1	0%	-	-
		2011	24	0%	14	0%	1	0%	1	0%
Total Perfect state 2001			234	1%	32	0%	10	0%	-	-
Total Perfect state 2011			176	1%	60	0%	10	0%	5	0%
Very bad	Masonry	2001	2	0%	0	0%	0	0%	-	-
		2011	2	0%	1	0%	0	0%	0	0%
	R.C.	2001	2	0%	0	0%	0	0%	-	-
		2011	0	0%	1	0%	0	0%	0	0%
	Other	2001	5	0%	0	0%	0	0%	-	-
		2011	2	0%	1	0%	0	0%	0	0%
Total Perfect state 2001			9	0%	0	0%	0	0%	-	-
Total Perfect state 2011			4	0%	3	0%	0	0%	0	0%
Total Masonry		2001	1184	8%	700	5%	657	4%	-	-
Total R.C.		2001	917	25%	586	16%	601	17%	-	-
Total Other		2001	1478	19%	939	12%	1131	14%	-	-
Total Masonry		2011	1671	10%	958	6%	788	5%	452	3%
Total R.C.		2011	1322	21%	988	16%	712	12%	554	9%
Total Other		2011	1071	13%	849	11%	930	12%	546	7%
Total buildings		2001	3579	13%	2225	8%	2389	9%	0	0%
Total buildings		2011	4064	13%	2795	9%	2430	8%	1552	5%

Province of Gorizia (residential)			From 2006 to 2011		Total		
			abs.nr	% on total of the same material	abs.nr	% among the same category	% on the total of buildings
Preservation state	Perfect	Masonry	2001	-	-	4903	32%	18.2%

Province of Gorizia (residential)			abs.nr (2006-2011)	% on total of the same material	abs.nr (Total)	% among the same category	% on the total of buildings
Perfect	Masonry	2001	-	-	4903	32%	18.2%
		2011	375	2%	6291	38%	20.5%
	R.C.	2001	-	-	1854	51%	6.9%
		2011	447	7%	3764	61%	12.2%
	Other	2001	-	-	3633	46%	13.5%
		2011	418	5%	4619	57%	15.0%
Total Perfect state 2001			-	-	**10390**	39%	38.6%
Total Perfect state 2011			1240	5%	**14674**	55%	**47.7%**
Good	Masonry	2001	-	-	7294	47%	27.1%
		2011	28	0%	7946	48%	25.8%
	R.C.	2001	-	-	1484	41%	5.5%
		2011	31	1%	1999	32%	6.5%
	Other	2001	-	-	3503	44%	13.0%
		2011	21	0%	2861	36%	9.3%
Total Perfect state 2001			-	-	**12281**	46%	45.7%
Total Perfect state 2011			80	0%	**12806**	48%	41.6%
Mediocre	Masonry	2001	-	-	2829	18%	10.5%
		2011	1	0%	2097	13%	6.8%
	R.C.	2001	-	-	285	8%	1.1%
		2011	2	0%	381	6%	1.2%
	Other	2001	-	-	700	9%	2.6%
		2011	2	0%	498	6%	1.6%
Total Perfect state 2001			-	-	**3814**	14%	14.2%
Total Perfect state 2011			5	0%	**2976**	11%	9.7%
Very bad	Masonry	2001	-	-	331	2%	1.2%
		2011	0	0%	227	1%	0.7%
	R.C.	2001	-	-	11	0%	0.0%
		2011	0	0%	21	0%	0.1%
	Other	2001	-	-	65	1%	0.2%
		2011	0	0%	56	1%	0.2%
Total Perfect state 2001			-	-	**407**	2%	1.5%
Total Perfect state 2011			0	0%	**304**	1%	1.0%
Total Masonry		2001	-	-	**15357**		**57.1%**
Total R.C.		2001	-	-	**3634**		**13.5%**
Total Other		2001	-	-	**7901**		29.4%
Total Masonry		2011	404	2%	**16561**		**53.8%**
Total R.C.		2011	480	8%	**6165**		**20.0%**
Total Other		2011	441	5%	**8034**		26.1%
Total buildings		2001	0	0%	**26892**		
Total buildings		2011	1325	4%	**30760**		

From Table 1-2 it can be also learned that, until 2001, 57.1% of the buildings had masonry structure and just 13.5% reinforced concrete structure. In 2011, instead, the number of R.C. buildings increased to 20%, when the masonry remained similar, at 53.8%. The remaining 26.1% of buildings are built with other materials, that can be steel, wood or other, it is not specified in the census data.

These data are reported more concisely in Table 1-3, together with the data for the Municipality of Gorizia (smaller area than the Province). In the Municipality of Gorizia in 2011 the masonry buildings were 49.9% and the R.C. buildings were 37.5%. In the table the buildings are also subdivided by their construction period.

Table 1-3: Percentages of residential buildings with specific parameters – construction system, construction period. Data for the province and for the Municipality of Gorizia. (data ISTAT, census 2001 and 2011)

	Province 2001	Province 2011	Municipality 2001	Municipality 2011
Percentage of masonry on total	57.1%	53.8%	62.2%	49.9%
Percentage of R.C. on total	13.5%	20.0%	14.5%	37.5%
Percentage of "other" on total	29.4%	26.1%	23.3%	12.6%
Total	100.0%	100.0%	100.0%	100.0%
Before 1919	18.6%	13.2%	21.8%	16.9%
1919-1945	15.8%	12.9%	21.5%	16.6%
1946 - 1960 (1961)	18.4%	17.3%	18.0%	16.2%
1961(1962)-1970(1971)	16.8%	17.0%	16.2%	17.2%
1971(1972)-1980(1981)	13.3%	13.2%	10.8%	11.8%
1981(1982)-1990(1991)	8.3%	9.1%	6.4%	7.8%
1991(1992)-2000(2001)	8.9%	7.9%	5.3%	5.0%
2001-2005	0.0%	5.0%		4.5%
2006-2011	0.0%	4.3%		4.0%
Total	100.0%	100.0%	100.0%	100.0%

The graph in Figure 1-11 shows that also if just the data of residential buildings are considered, the percentages on the total are not very different, as the residential buildings are 87% of all the buildings in the province of Gorizia and even 3% of the buildings are not used at all.
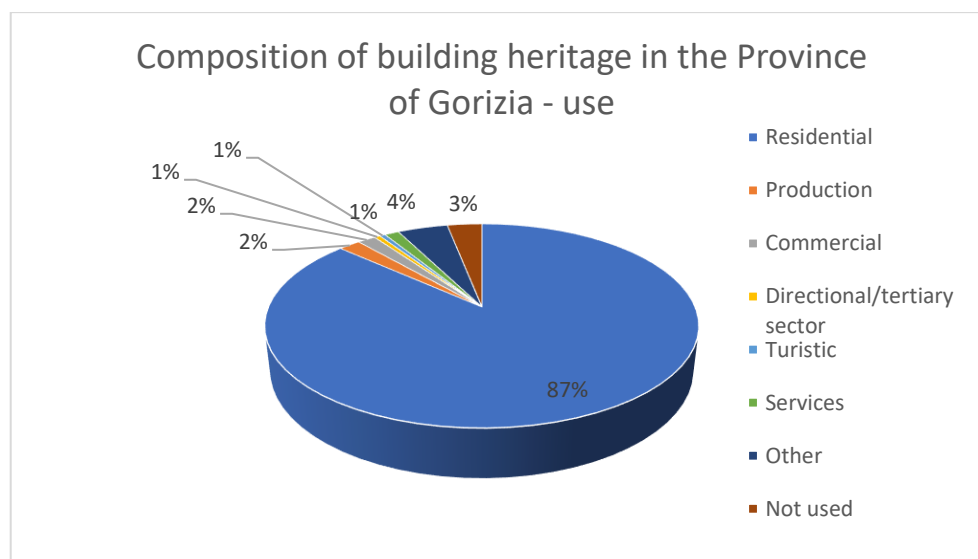
Figure 1-11: Use of the buildings in the province of Gorizia. (ISTAT, census 2011)

The data of how many buildings are used or not used in the Municipality of Gorizia are displayed in Table 1-4. It can be noticed that the percentage of non-used buildings is higher than the one of the Province. The number of masonry buildings and R.C. buildings are displayed in Figure 1-12 and their number of storeys in Figure 1-13, where also the number of residential buildings in the Municipality of Gorizia can be seen, 7636. This number represents the 80.5% of all the buildings in Gorizia and the 83.9% of the used buildings, a slightly lower value than in the Province.

_____

Table 1-4: Data about the use of buildings in the Municipality of Gorizia.

Municipality of Gorizia	Used buildings		Not used buildings		Total
Census 2001	6286	95.4%	300	4.6%	6586
Census 2011	9102	95.9%	386	4.1%	9488
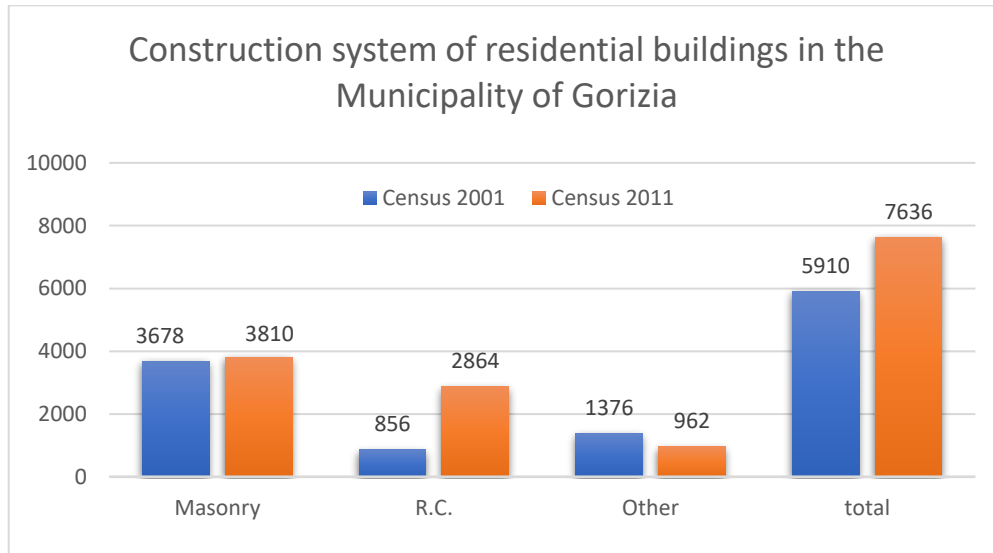
Figure 1-12: Graph of the number of residential masonry and RC buildings in the Municipality of Gorizia.
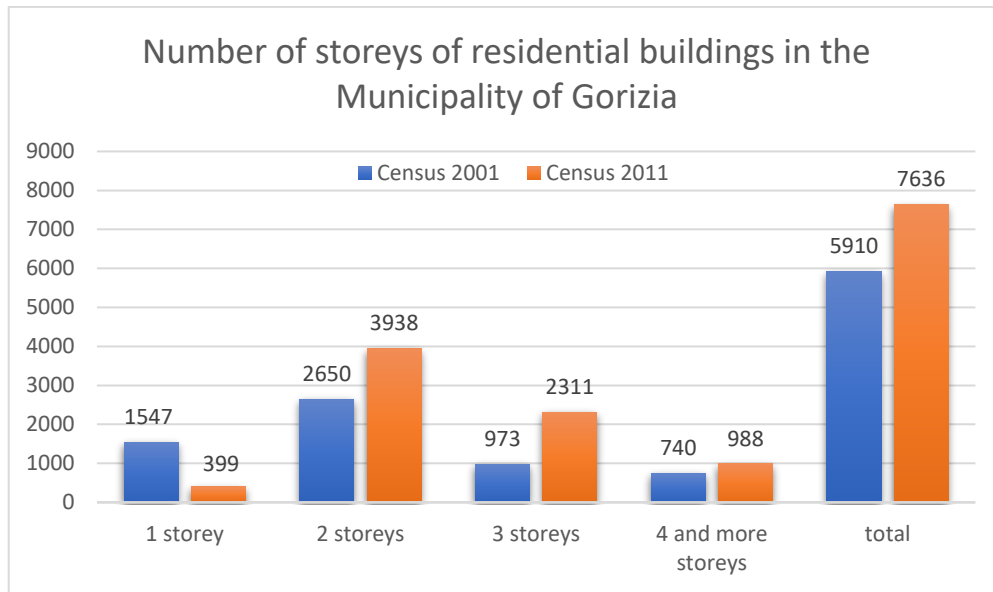
Figure 1-13: Graph of the number of storeys of residential buildings in the Municipality of Gorizia.

All the presented data show that the majority of buildings are residential and that the main construction systems, that covers almost 90% of the total, are masonry and reinforced concrete buildings. The research of this PhD thesis will focus, for this reason, on existing buildings made with these two construction systems.

Another important piece of information that can be read from the data is the age of buildings. It can be seen that just 4% of residential buildings in the Municipality of Gorizia are built between 2006 and 2011 and therefore just very very few are designed considering seismic action and even less with the latest credible seismic action. Moreover, 91.5% of the buildings in the Municipality of Gorizia have been constructed before 2001, when Gorizia was not considered seismic at all. Half of

_____

the existing residential buildings have been constructed before 1960, so they are quite aged. An interesting information is also that more buildings have been built in the period 1961-1970 than in the whole history until 1918. **For this research, old masonry buildings (1900 or before) and R.C. buildings from years 1960/70, the years in which the R.C. was at its first expansion, will be considered.**
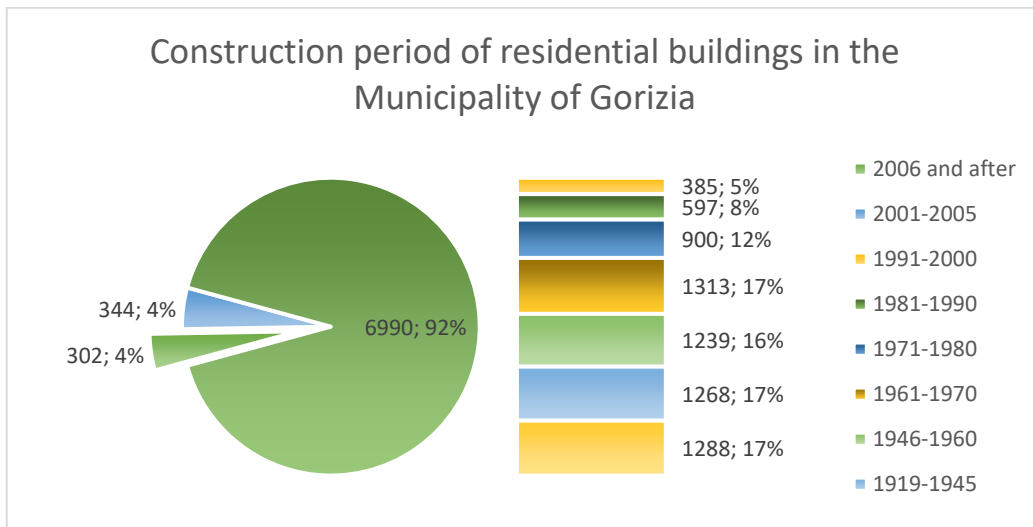
Figure 1-14: Construction period of residential buildings in the Municipality of Gorizia. Just 4% of the buildings are built after 2006, even less after 2010, when Gorizia passed to seismic zone 2.

1.5. Geology of Gorizia

As a preliminary study, the geology of Gorizia has been investigated. Information has been found in some papers and in geological maps. The geological-technical map of the municipality describes the geology of just the first 10 m, but shows also tectonic structures. It is clear that Gorizia lays on sediments, mainly gravel or sandy-gravel. To the East there is arenaceous flysh or marly-arenaceous flysh, as it is under Gorizia castle.
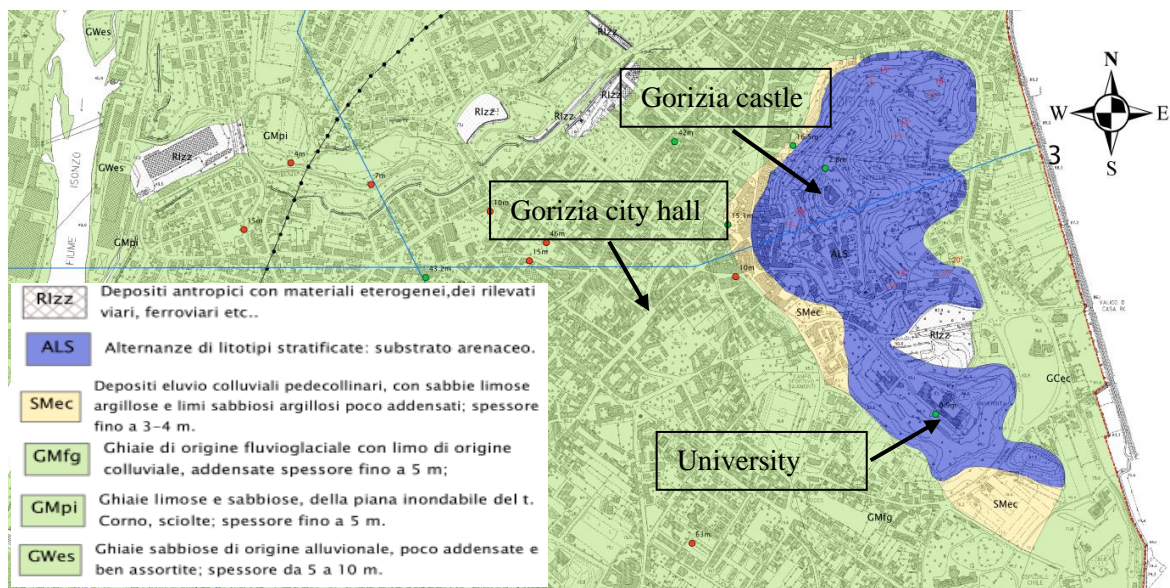
Figure 1-15: Piece of geological map from the seismic microzonation of the municipality of Gorizia (dr. Fulvio Iadarola, March 2017). The gretest part of Gorizia is on soil of type GMfg, that is fluvio-glacial gravel. The zone of the castle lays on sandstone.

Some data have been found in the microzonation of Gorizia, made by the geologist dr. Fulvio Iadarola in March 2017 (Figure 1-15).

_____

In order to better understand the characteristics of the soil under the case - study buildings, also some measurements have been performed. Natural vibrations and vibrations created with a big hammer have been recoded with Tromini and with other geophons in order to catch vibration properties of the ground (seismic prospecting method).

Figure 1-16: Photos from the test-site. On the left: a Tromino is visible, the meter for determining the distances between the vibration source and the instrument and a geophone that measures the same vibration. On the right: vibration source (a piece of wood and a hammer) and measuring instruments.

Some photos from the testing are visible in Figure 1-16 and some results are visible in Figure 1-17. The measurements have been made next to the case study "RC building 1" (see §3.1). The measurements confirmed the presence of gravel and found a possible amplification (site effect) at around 3 Hz and 8 Hz.
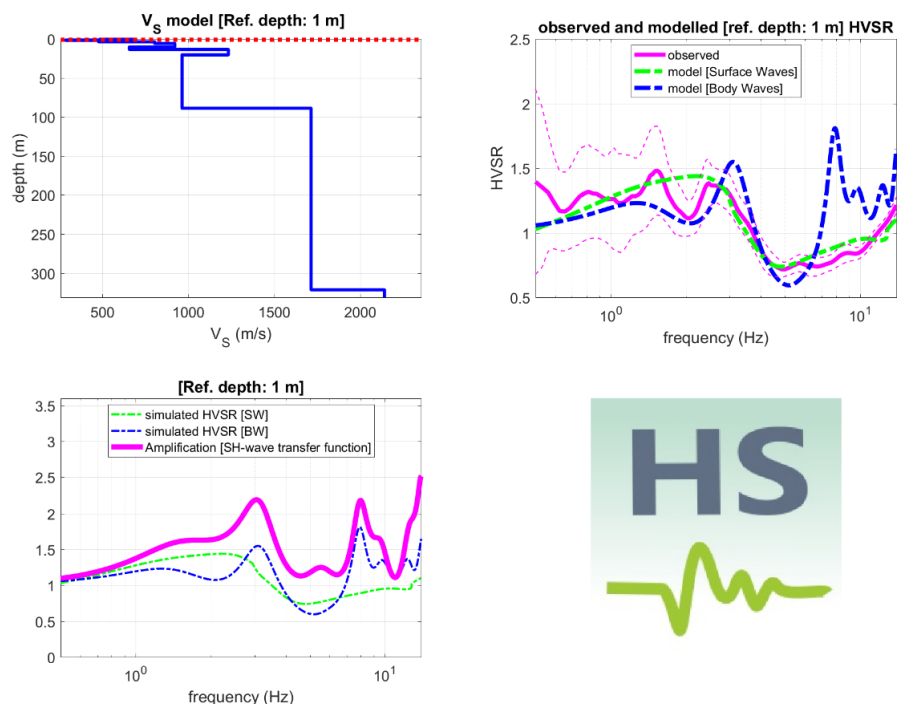
Figure 1-17: Results of the seismic prospection of the ground in the centre of Gorizia. The tests are made next to the case study RC building 1 (see §3.1). Some amplification could be around 3 Hz and 8 Hz. Elaboration made by dr. Giancarlo dal Moro.

_____

_____

2. COMPARISON BETWEEN PSHA AND NDSHA APPROACHES

2.1. Probabilistic Seismic Hazard Analysis (PSHA) method

The current building code in Italy (NTC 2018 [10]), as also the previous version (NTC 2008 [11]) and Eurocodes in Europe [12][13], uses a probabilistic approach for the determination of seismic hazard and also for the seismic input used for the design and dimensioning of structures.

The probabilistic method (PSHA) aims to determine the probability of exceedance of a certain level of shaking of the ground in a certain location and in a certain time window. To do so, it can just rely on the available data and process them to obtain the result. The available data, at the moment, are not so many and, above all, they cover just a short period compared to the tectonic evolution. The first instrumental recordings of earthquakes in Italy are from the 50's, while the concept of an organized and centralized net was born just in 1979. The data that we have for older earthquakes are based just on written testimonials of observed damage after the most catastrophic events in inhabited areas.

The method can be summarized with four steps [14][15]:

- **Create a seismic hazard source model**: take all the available information on the occurred events (historical and "registered" catalogue, map of seismogenic zones – see Figure 2-1 and Figure 2-2) and associate a magnitude and a location to each event to calculate a seismicity rate.
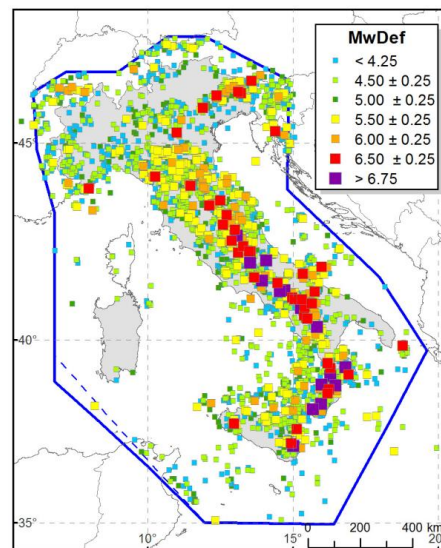
Figure 2-1: Map of epicentres of the earthquakes listed in CPTI15, divided by Mw classes. The border of the new areal coverage is shown together with the old border – dashed line (CPTI11). For the map of seismic hazard of 2004 a previous version of the catalogue has been used – CPTI2 [16].

Figure 2-2: Seismogenetic zonation ZS9. The blue borders separate zones with the same kinematic significate, that differ mainly for seismicity characteristics. The seismic zones (ZS) with dashed border, identified by a letter, have not been used in the hazard evaluation [17].

Note that especially for the older earthquakes, not registered, the catalogue presents many uncertainties, that's why at each new version the locations and magnitudes of the events are calculated again and again.
In order to calculate the seismicity rate the available data are processed in various steps, from the evaluation of the completeness of the catalogue of earthquakes, with historical and statistical approaches, to the use of curves that link the magnitude to the frequency of occurrence. For the seismic hazard map used by the building code,

_____

realized by the National Institute for Geophysics and Volcanology (Istituto Nazionale di Geofisica e Vulcanologia INGV) in 2004, individual rates (AR= Activity rates) calculated for each magnitude class and for each seismogenic zone (ZS) and also truncated Gutemberg-Richter relations have been used – see Figure 2-3. Gutemberg-Richter relations sets that:

$$log_{10}N = a - bM \qquad (2.1)$$

where

N = number of events that exceeds a given interval of magnitude M

a = constant that quantifies the number of earthquakes with magnitude ≥ 0 (represents the level of seismicity of the considered zone)

b = ratio between earthquakes with low and high magnitude (gives the slope of the line)

The values of a and b are obtained with regressions on the seismic database of the zone of interest (in case of the Italian seismic hazard map, they are calculated for every seismogenic zone). In Figure 2-3 some examples of used curves can be seen.
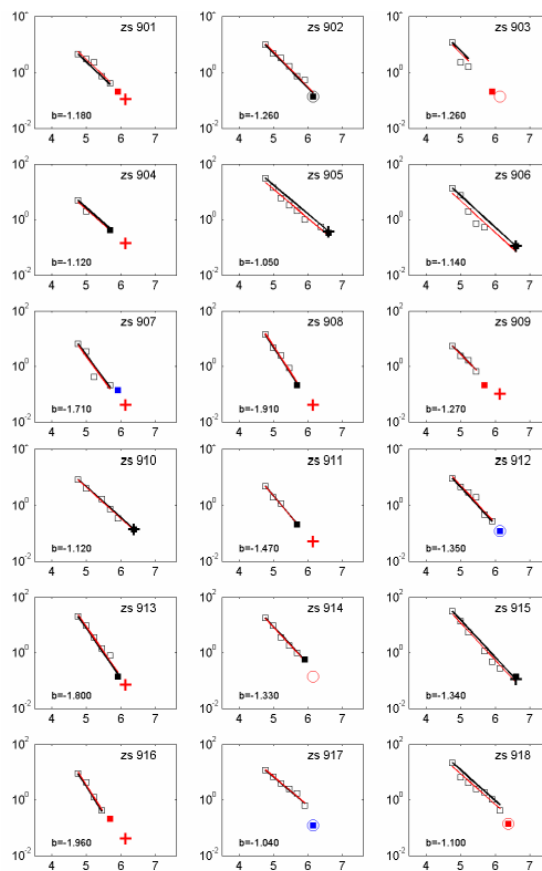
Figure 2-3: Example of Gutemberg-Richter (G-R) curves, used for the construction of the seismic hazard map in 2004. Comparison between activity rates AR (empty squares), b values, G-R interpolated on the rates (red lines) and their balanced version (black lines), Mmax values and their rates, for the ZS from 901 to 918 and for "historical" completeness intervals CO-04.2 [17].

- **Create a ground motion model** by using attenuation laws (Ground Motion Prediction Equations – GMPE). There are plenty of different GMPE's that try to adapt to different seismic zones of the world (some of them can be seen in the list published by John Douglas at the link http://www.gmpe.org.uk/gmpereport2014.html). They are frequently modified after new seismic events. Some of them distinguish more parameters, some of them less, as for instance the ground type or the rupture mode of the fault. In every case the

GMPE's of the peak accelerations (also some other parameters could be evaluated) are curves that fit observations, they are graphs of PGA (Peak Ground Acceleration), or of spectral accelerations at given periods, versus the distance from the epicentre, given the magnitude. They are thus statistically processed empiric relations. Since the observations are rare and scattered on the graph, it is necessary to make assumptions about their distribution. Usually a log-normal distribution of the PGA is assumed for a certain distance from the epicentre and based on this assumption the median curve and the percentiles are found. The main problem is that usually there is a lack of data for earthquakes at short distance, especially for stronger earthquakes, so that the fitting of the low part of the curve is usually based on very few or zero data. The evaluation error could then be potentially high and the PSHA method in very seismic areas is even more sensitive to the lack of data, so that the predictions in these zones could have even larger errors than in less seismic areas. Moreover, different attenuation laws use different definitions of distance from the plane of the fault and they are not always used with the right distances. Figure 2-4 shows the comparison between two GMPE curves (ASB96 and SP96) with data of really occurred earthquakes. In Figure 2-5 also the hypothesis of the log-normal distribution of the observations is represented, for each distance from the epicentre.
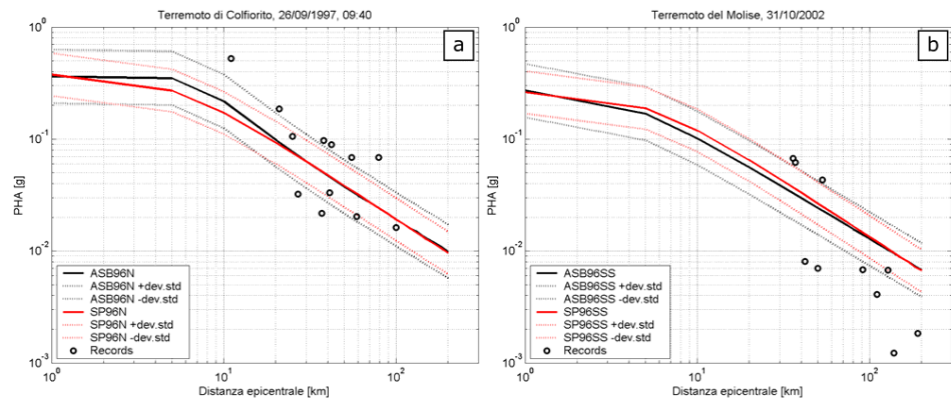
Figure 2-4: a) Comparison between the curves ASB96 for normal faults (ASB96N, in black) and SP96 for normal faults (SP96N, in red) for Ms 6.0 with the data of the earthquake of Colfiorito (Ms 6.0). b) Comparison of the same relations modulated for transcurrent faults (ASB96SS, in black, and SP96SS in red) for Ms 5.5 with the data of the earthquake of Molise (Ms 5.6) [17]. PHA= peak horizontal acceleration.
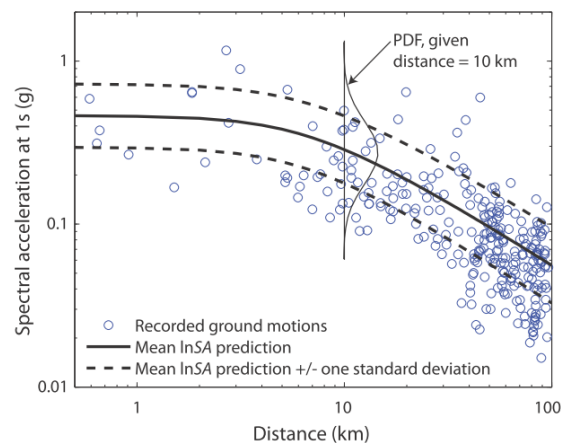
Figure 2-5: Spectral acceleration values for 1 s observed during the earthquake of Chi-Chi, Taiwan, in 1999. The variability of the acceleration at distances between 1 km and 3 km vary from 0.15 g to more than 1 g. A log-normal distribution is considered for every distance.[14]

In general, the functional form for evaluating the attenuation is of the kind:

$$f(y) = a + f_1(M) + f_2(R) + f_3(S) \pm \varepsilon \qquad (2.2)$$

Where y is the parameter to evaluate (for example the PGA), M is the magnitude, R the distance and S a variable that represents the geological characteristics of the site. ε is the uncertainty of the estimate. The mathematical model used for the GMPE of Sabetta and Pugliese, 1996 (SP96), utilized also for the redaction of the Italian seismic hazard map, is the following:

$$log(y) = a + b(M) - log\sqrt{(R^2 + h^2)} + e_1(S_1) + e_2(S_2) \pm \sigma \qquad (2.3)$$

where the coefficients $a, b, h, e_1, e_2, \sigma$ are estimated with a linear regression.

- **Probabilistic calculation**: let's suppose that among the parameters of shaking, we are interested to the maximum acceleration on rigid soil (PGA) (spectral acceleration could be another option). If we take the available seismic events, with their magnitude, localization and seismicity rates, we can calculate the distance of each from the site of interest and then with the GMPE find for each event the distribution of the possible levels of PGA (or spectral acceleration) in the site (the already mentioned log-normal distribution). By integration on the distribution the probability of exceedance of the various levels of shaking for the single event can be calculated (cumulative density function):

$$P(PGA > x|m,r) = \int_x^\infty \frac{1}{\sigma_{ln\,PGA}\sqrt{2\pi}} \, e^{\left(-\frac{1}{2}\left(\frac{\ln u - \overline{\ln PGA}}{\sigma_{ln\,PGA}}\right)^2\right)} du \qquad (2.4)$$

where m, r are the magnitude and the distance.

If we multiply this probability for the seismicity rate (λ), we find the annual rate of exceedance of the PGA for each event. If we sum all the seismic events, we find the total annual rate of exceedance of each PGA or of another intensity measure (IM) of shaking:

$$\lambda_{IM}(IM > x) = \sum_{i=1}^{n_{sources}} \lambda(M_i \qquad (2.5)$$
$$> m_{min}) \sum_{j=1}^{n_M} \sum_{k=1}^{n_R} P(IM > x|m_j, r_k) P(M_i = m_j) P(R_i = r_k)$$

where:

$n_{sources}$ = number of seismic sources that affect the site of interest

$\lambda(M_i > m_{min})$ = seismicity rate of earthquakes with magnitude higher than the minimum one, for the source i

$n_M\ e\ n_R$ = total number j and k of intervals used to discretize the range of magnitudes M_i (from m_{min} to m_{max}) and distances R_i (from r_{min} to r_{max})

$P(IM > x|m_j, r_k)$ = conditional probability of exceedance of an IM (eg. PGA) for a given event of magnitude m_j and for a given distance of the source from the site of interest r_k.

$P(M_i = m_j) P(R_i = r_k)$ = probabilities that a given event has a given magnitude and a given distance from the site of interest.

Through this formula, considered the representative formula of the PSHA method, the hazard curve can be calculated for the site of interest. This gives the estimate of how many times per year a given level of shaking (eg. In terms of PGA) is exceeded in the site of interest. Figure 2-6 shows an example of a hazard curve of a site with just 2 seismic sources.

For the sake of completeness, every hazard curve should be reported with its range of variation, as there are always epistemic uncertainties (uncertainties on the

calculation methods, as eg. the evaluation of completeness of the catalogue or the use of GMPE). The result should be a distribution of hazard curves and not just one curve, that means that the hazard curve itself is uncertain. In order to have just one hazard curve it is necessary to choose weather take simply the average or a percentile of some kind. Usually the epistemic uncertainties (of the method) are taken into account through logic trees, whereas the aleatory uncertainties (natural variability of the phenomenon) are treated with probability distributions.
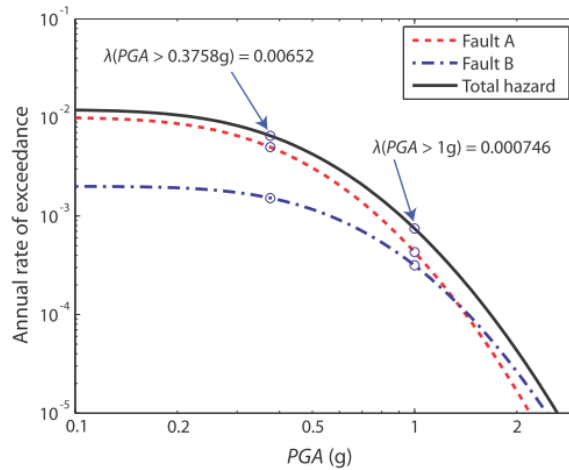
Figure 2-6: Example of hazard curve in terms of PGA for a site with 2 seismic sources [14].

Eventually, in order to calculate the probability of exceedance from the rate of exceedance in a given time range, it is necessary to know the probability distribution of the time between seismic events. A Poisson distribution is usually considered, as it has simple mathematic equations, it seems to well approximate the observations and more complex models don't seem to lead to better final results. With this choice the hazard curve that gives the probability of Poisson that a given PGA is exceeded in a given time period (e.g. 50 years) and in a given site can be calculated. The probability is independent from the occurrence of recent earthquakes.

Poisson distribution is a discrete probability distribution that tells the probability of a number of events n to occur independently in a given time period, knowing that on average a number γ of events occur. In our case we know from the previous elaborations that the expected number of events that exceed a given value of IM in a given time period T is $\gamma = \lambda_{IM}T$. The probability of observing n of these events in the time period T is given by the Poisson distribution:

$$P(n.\,of\,events\,in\,time\,period\,T) = \frac{(\lambda_{IM}T)^n e^{-(\lambda_{IM}T)}}{n!} \tag{2.6}$$

We want to know the probability that a given value of IM is exceeded <u>at least ones</u> in the time period T. In other words, this is the probability that the time t between two events that exceed the given IM value in a given site is minor or equal to T:

$$P(t \leq T) = 1 - P(t > T) = 1 - P(n = 0\,in\,T) \tag{2.7}$$

If we use equation (6), the probability of exceedance of a given value of IM in a given time period T can be written as:

$$P_{EY} = 1 - e^{-(\lambda_{IM}T)} \tag{2.8}$$

Usually the reciprocal value of the annual seismicity rate is called "average return period" of exceedance of IM:

$$T_R = \frac{1}{\lambda_{IM}} \tag{2.9}$$

Using equation (8) for calculating λ_{IM} and substituting in (9), T_R can be expressed as:

$$T_R = \frac{-T}{\ln\left(1 - P_{EY}\right)}$$ (2.10)

Equation (10) is the one that can be found in the instructions for the application of the building code NTC08 (Circolare 02.02.2009, n. 617 [18]), at the chapter C.3.2.1 with slightly different naming. Here T is the reference average life (period) of the examined structure (V_R in the code) and P_{EY} the probability of exceedance in that reference period (P_{V_R} in the code).

This is the end of the part exclusively connected to the PSHA method, then the choices made by the code writers to draw up the national seismic hazard map and the inputs for structural design intervene.

- **Code choices for use in design of structures**: as it has been explained, every hazard curve is then processed, through the Poissonian distribution, in order to connect it to a specific time period, so that every time period (eg. 50 years or 70 years) has its hazard curve. After choosing the probability of exceedance that is considered acceptable in a given time period (eg. 10% in 50 years), the PGA (or other IM) can be taken in the hazard curve of the chosen time period, obtaining one value. If we repeat this for every site in a predefined net, for the same time period and for the same probability of exceedance, **a map can be drawn with the values of PGA (or other IM) with a given probability of exceedance in T years** (eg. 10% in 50 years). If the analysis is done for different natural periods and not just for the PGA, a response spectrum with uniform probability can be created (Uniform Hazard Spectrum = UHS) for each site of interest.

  A UHS is built with the following procedure: an exceedance rate is chosen and its spectral acceleration is identified for each period. By plotting the accelerations versus the periods, the spectrum is found, where every spectral acceleration has the same probability of exceedance in the chosen time period. The user must be aware that this kind of response spectrum is an envelope of accelerations for different natural periods and every acceleration could come from a different earthquake. If we want to go back to the single events (earthquakes), the disaggregation can be used to find the earthquake that has given that acceleration. This process can be very useful when we want to find spectro-compatible accelerograms to run nonlinear dynamic analyses on structures.

In order to use this method for the building code purposes, some choices have been done. In the following paragraph the choices made for the seismic hazard curve created for the OPCM 2003 n. 3274 [5] and now used (with updates) by the current code (NTC2018 [10]). The map has been prepared by INGV. **It was chosen to**:

1) Consider **PGA as the main parameter of earthquakes (a$_{max}$)**: All. 1 of OPCM 2003 n.3274 requires that the map should be produced in terms of maximum acceleration at the ground.
2) Consider a **nominal life for ordinary structures** of 50 years and associate an **"acceptable" probability of exceedance** of 10% in this time period (also this standard is required by the All. 1 of the OPCM 2003). The average return period of seismic events becomes then 475 years. For strategic buildings longer periods are considered.
3) Produce the national map based on a **ground with Vs>800 m/s** (the OPCM categorizes it as ground type A). The Regions are in charge of identifying the local site effects.

4) Consider the epistemic uncertainties by using a **logic tree** with different weights in different branches. The branches take into account the uncertainties in: a) methods for the evaluation of the completeness of the catalogue, b) methods for determining the seismicity rates, c) the choice of the GMPEs, d) the determination of the maximum magnitude. There are thus 16 different maps, corresponding to the 16 branches of the logic tree and the final hazard map is calculated as the weighted median. The map is always presented with an uncertainty measure, in terms of distribution of values of the 84th percentile of the sample of the 16 maps.

5) The method used for the calculation of the hazard map in 2004 is the same already used in 1998 (established methods), but the knowledge was updated (seismicity, seismogenic potential, mode of energy propagation). The methodology is also commonly used around the world for the evaluations of seismic hazard and for seismic codes. In particular, the **Cornell's approach** from 1968 with updates has been used.

6) Among the **GMPEs used** (4 different have been used), also the one from Ambraseys et al. (1996) – ASB96, that does not use an unambiguous definition of distance, has been used; it assumes the distance from the surface projection of the fault for events with Ms>=6.0 and the epicentral distance for weaker earthquakes. In the common use of probabilistic hazard analyses, the distance is calculated by subdividing the source areas into cells and by considering the geometric distance between the baricenter of each cell, considered an earthquake site, and the nodes of a net of points/sites. This measure does not correspond to any of the two definitions of distance. It has not been found a research about the influence that the choice of distance could have on the final result. However, for this map, a correction of the distances for earthquakes with Ms>= 6.0 has been made. Figure 2-7 shows the ASB96 attenuation law used, modulated for different rupture mechanisms of the fault.
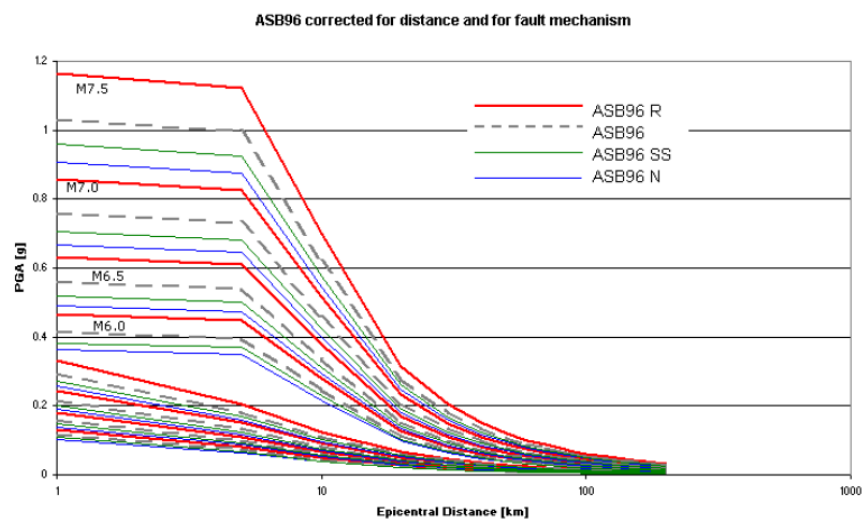
Figure 2-7: GMPE ASB96 modulated on the fault rupture mechanism. The dashed line is the average, the red one is the correction for reverse faults, in green the one for transcurrent faults, in blue for normal faults [17].

7) As the earthquake catalogue is certainly not complete, especially for lower magnitudes, the completeness estimates of site historical data have been used (that are based on statistical elaborations, but also on an "**expert opinion**", that is for sure subjective).

8) In the method the choice of the **maximum magnitude Mmax** is usually made in order to guarantee the possibility of the occurrence of earthquakes with higher magnitude than the ones in the catalogue. This choice shows the lack of knowledge about the seimogenic potential of the analysed region. The value of Mmax is

calculated with different approaches, mainly statistic. Often the difference between the assumed Mmax and the maximum magnitude reported in the catalogue is very high in medium-low seismic regions.

2.1.1. Limitations of the method

The PSHA method is based on two assumptions: a) that earthquakes occur randomly and by following a parametric model; b) that the parameters of such a model can be well estimated, based on available data. None of the two assumptions seems realistic.

PSHA method is also based on the theory of the "characteristic earthquake" and of the "elastic-rebound paradigm", that are also not scientifically demonstrated or demonstrable.

The hypothesis of the earthquakes occurring independently from the time and the hypothesis of the existence of a return period are also not scientifically proved, conversely, it seems that earthquakes are not independent from time. The hypothesis is thus in conflict with the physics of earthquakes.

When evaluating the seismicity rates of earthquakes, it should be noted that statistical laws for earthquakes, such as the Gutemberg-Richter (magnitude vs. frequency of occurrence) give the frequency of occurrence and not probability distributions.

Already the fact that the frequencies of the historical catalogue are used as future probabilities of occurrence, it means that we suppose that earthquakes occur randomly, without memory and connection to past events.

PSHA has also been frequently criticized for the mathematical methods used, in addition to the critics about the assumptions in contrast with physics.

Even if it were a mathematically correct method, the available data on which is based are too few to give reliable estimates.

The use of the "expert opinion" in the process of PSHA shows that the approach is "not scientific".

It is not a scientific method also because it cannot be tested or objectively comparable with the observations and in case rejectable, if it does not agree with them.

Regarding the completeness of available data in the historical catalogue, it is clear that it does not depend just on the magnitude (information is available just for the strong earthquakes or the ones that have caused greater damage), but also on the location. In the past the territories were not so densely populated and built as now and for sure nobody was caring about what was happening in non-populated areas or in zones with populations that were not writing. Maybe Italy has been quite populated also centuries ago, but in the world there are for sure enormous areas that are not or were not very populated and for sure this causes huge lack of data in the catalogues. If there is now a city in those areas, the seismicity there could be highly underestimated.

In order to avoid the uncertainty of the GMPEs (they are many and have very variable data in some cases, while in other cases they totally miss data) the attenuation of the seismic waves could be evaluated with physics-based simulation, always associated with a probabilistic method. In this way, also *simulated accelerograms* would be obtained, that are specific for the site of interest. The lack of accelerograms with properties that are specific for the site of interest is in fact another problem of current codes. On the other hand, using physical simulation would not be a brand new idea as it is already used for calculating the amplification factors for site effects.

Poisson probability distribution is usually used for calculating the hazard curve. This distribution assumes that the occurrence of earthquakes is independent from time, and thus also from previously occurred earthquakes, but just depends on the considered time window. With such assumptions earthquakes are characterized by a stationary stochastic process without memory. This

is not what happens in real world and it excludes some natural phenomena as seismic swarms, aftershocks and foreshocks and it excludes in general the probability (as it is very low) of the occurrence of more than one earthquake in a short time period.

It should be noted that also the lower cut of the magnitude influences the final calculation of the hazard curve. If, eg. a minimum magnitude of 5 is assumed, the exceedance rates of low PGAs will be lower than in the case of assuming the minimum magnitude 4.5.

Errors in the estimates of the hazard made with PSHA method could be greater than the estimates themselves.

Decisions (political, social) that are based on information that is assumed as more or less correct, but is not correct at all or too uncertain, can lead to even worse results as in case of decisions made based on the awareness of the existence of uncertainty.

PSHA method is based on Cornell's approach (1968) [19], very used all around the world since 90's, but that has underestimated very seismic zones in many cases. Therefore, it has not been "validated".

It is of great importance that professionals, but also people in general, realize, that assuming that there is a return period of the earthquakes, the presumption of evaluating it more or less precisely and the choice of a drawing the hazard maps with an arbitrary probability of 10% of exceedance in 50 years, means to accept a certain probability that the design seismic events can be largely exceeded by real earthquakes.

Even if the arbitrary choice of the probability of exceedance and of the nominal life could be avoided by setting the probability to zero, the PSHA method gives extremely high and not realistic accelerations, especially for low-seismic zone, so that it cannot be done. [20]

2.2. Neo-Deterministic Seismic Hazard Analysis (NDSHA) method

In order to avoid some of the limitations of the probabilistic method and of other purely deterministic methods, already in the 80's (precisely in 1985) a group of researchers of the University of Trieste started to develop a method that uses numerical simulations based on the knowledge of the process of generation of earthquakes and of the propagation of waves in a visco-elastic medium. They called this method "Neo-Deterministic Seismic Hazard Assessment" (NDSHA), because it is not a classical deterministic method, based on occurred events, but it gives deterministic results, independent from the probability of occurrence of earthquakes and it does not calculate or use a return period of the earthquakes. In the years when the method started to develop, computer performances were much lower than nowadays. With time and with technological development, the method has developed and it is now able to run a number of simulations that were until now impossible. This possibility gives the opportunity to perform parametric analyses that are very useful to deal with the uncertainties in the analysed phenomenon.

This method is a multi-scenario procedure that aims at calculating realistic time histories of the ground shaking (physics-based synthetic seismograms) as the tensor product of the earthquake source functions and the Green's functions of the transmitting medium [21][22][23]. At the moment the program uses the Modal Summation technique for models with parallel and homogeneous layers (suitable for far-field conditions, evaluations at national or regional scale, as it is working just for distances of the site of interest from the epicentre that are larger or equal to the depth of the hypocentre) and another technique, called DWN (Discrete Wave Number) for the local site effects (near field conditions). With this technique it is possible to model a laterally heterogeneous profile. Moreover, in order to improve the model of the seismic source, a program has been developed for modelling an Extended-Source [24]. This kind of seismic source can be used with both techniques (Modal Summation and DWN). The method can then calculate time histories of different possible situations and tries to define maximum values of ground displacement, velocity and acceleration for

different scenarios. Also response spectra can then be calculated as envelopes of the different simulated events, without using GMPE.

The main steps of NDSHA method are:

- **Identification and characterization of seismic sources**: the input data of the method is the available information about seismic sources. This is taken from the catalogue of earthquakes (Figure 2-8), from the map of seismogenic zones with their focal mechanisms (Figure 2-9) and from the map of seismogenic nodes (Figure 2-10) [25][26][27]. These maps are compared and integrated among them (eg. for the determination of the maximum magnitude). The aim of NDSHA is to consider all the seismogenic sources, without caring about return periods or occurrence probability. Seismogenic zones are homogeneous seismotectonic areas that are able to produce earthquakes. Seismogenic nodes are zones that have the tendency to generate strong earthquakes ($M \geq 6$) and are identified based on a morfostructural analysis.
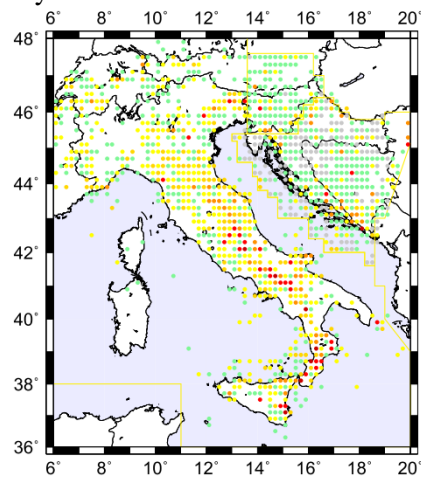
Figure 2-8: Discretized seismicity from the catalogue CPTI04 and from the Slovenian and Croatian catalogue [28][29][30].
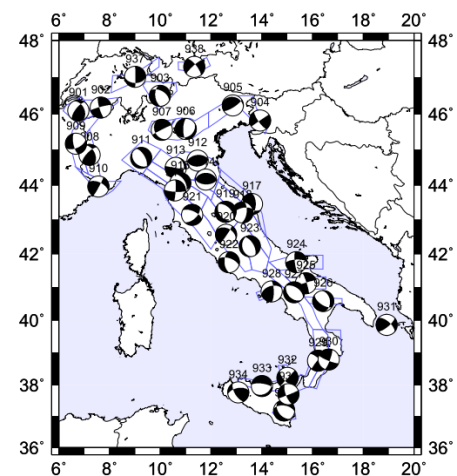
Figure 2-9: Map of seismogenic zones ZS9 and their focal mechanisms [31].
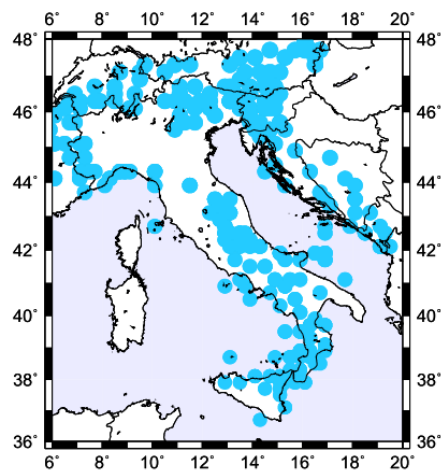
Figure 2-10: Map of seismogenic nodes [25][26][27].

National territory is divided in cells of 0.2° x 0.2°, corresponding approximately to 10 km x 10 km. For each cell just the maximum magnitude is considered (maximum among the smoothing procedure described in the following, the magnitude of the seismogenic nodes and a minimum magnitude of 5). In order to consider the uncertainty in the location of earthquakes from the catalogue and the fault dimensions, the creation of the map of magnitudes goes through a smoothing process, where the magnitude of a given point of the map is assigned also to the

neighbour cells all around the point, for a radius of three cells) and truncation (the magnitudes are assigned just within the borders of seismogenic zones). The uncertainty about the source of the earthquake that is simulated will then be considered additionally by executing more simulations and varying the parameters of the source (location, rupture mode and velocity). Rupture mode of the seismic source (focal mechanism) is defined by 3 angles: the strike-receiver angle (angle between the fault direction and the site of interest), the dip angle (slope of the fault plane) and the rake angle (angle between the direction of the rupture and the direction of the fault). The three angles are depicted in Figure 2-11. If these parameters are varied within their possible ranges (given by the focal mechanism), the effects of the source can be simulated together with the uncertainties.
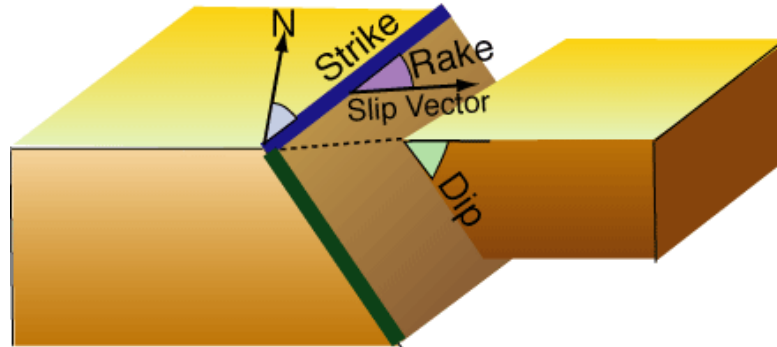
Figure 2-11: Scheme of a generic fault and representation of the three angles that describe the rupture mode.

- **Characterization of the subsoil in which the seismic waves propagate:** for the regional scale analyses (RSA) the national territory is discretized in regional polygons (1° x 1° cells) and the subsoil is modelled with plane and parallel inelastic layers with the average structural properties of the lithosphere in the cell. In order to make simulations at local scale and find topographical and site effects, more detailed profiles of the most superficial layers are introduced (from bedrock to the surface), just the sources that in RSA affect the most the site of interest are considered and seismograms are generated along the input profile.

- **Computation of synthetic seismograms:** along the whole profile of the subsoil, the tensor product of the earthquake source functions and the Green's functions of the transmitting medium is used. [32]

- **Estimation of the earthquake ground motion parameters relevant for seismic hazard assessment:** Figure 2-12 shows the main steps of the just described process.

- **Calculation of the Maximum Credible Seismic Input (MCSI) for engineering use**: NDSHA method has been lately integrated with the work of M. Fasan during his PhD research and it is published as: "*A new design strategy based on deterministic definition of the seismic input to overcome the limits of design procedures based on probabilistic approaches* " [33]. This scientific paper proposes a method for the calculation of the seismic input (design seismic action for structures) for Italian territory, based on NDSHA method, that permits to avoid some of the limits of the currently used PSHA method. This proposed seismic input is called MCSI and can be defined in terms of seismograms, accelerograms or response spectra. The method has two steps: first $MCSI_{BD}$ is defined (the maximum credible seismic input at the bedrock), determined at a regional scale, then it is amplified to account for site effects and obtain $MCSI_{SS}$ (Site Specific). The amplification is calculated by considering local topographic and stratigraphic features through a specific analysis. The proposed method is thus capable of providing a seismic input that is specific for the site of interest and compatible with the earthquakes that can really occur in that site. It is particularly useful for non-linear dynamic analyses of structures, as the MCSI accelerograms are fully compatible with the characteristics of the site and of the seismic source and a great number of them can be calculated.

In this way the dynamic analyses are reliable also in sites where no records of natural earthquakes are available. Available records nowadays are indeed really few, especially for stronger earthquakes.

As already mentioned, the uncertainties about the seismic source are managed by performing a huge number of analyses where the parameters that describe the rupture process are varied. A realistic estimate is then obtained by determining the probability distribution of the realizations with the use of Monte-Carlo method, and not by assigning an "a priori" probability distribution as in PSHA, that considers a log-normal distribution. After that, for each site the medians of the distributions are compared and the distribution with the highest median is considered as representative of the parameter describing the ground shaking. In this way, just the seismic source that gives the worse scenario is considered. This procedure can be used for every ground motion parameter (PGA, PGV, SA…). If a response spectrum is needed, the procedure is repeated for more natural periods. In the obtained spectrum the maximum acceleration for each period could be controlled by a different scenario, as in the Uniform Hazard Spectra (UHS). The MCSI should be the envelope of the response spectra of all the simulated events (100th percentile), but it was chosen to fix the value of $MCSI_{BD}$ at the 95th percentile of 300 simulations of rupture process (for each seismic source), as a sensitivity test has shown that, for each source, this value remains stable for a number of simulations greater or equal to 300. Moreover, the 95th percentile is in tune with the code (NTC2018) where the actions are calculated with the same value of the percentile.
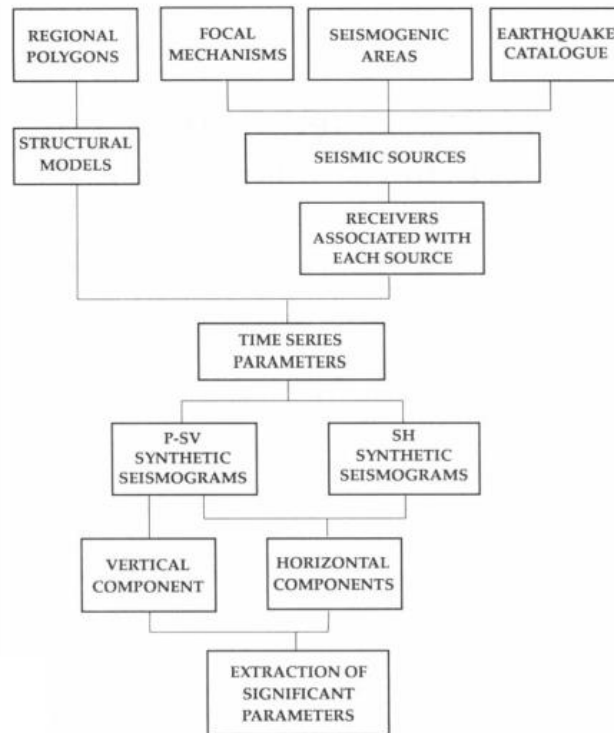
Figure 2-12: Flow chart of the NDSHA method [32].

The method is very flexible, as the input data can be easily updated, based on new findings in the field of seismology, seismotectonic, geology, geotechnique and geophysics of the site of interest. Moreover, in the sites where there is no knowledge about faults, historical and geomorphological data can be used. Although it is not an aim of the method, also the average return periods of earthquakes can be evaluated and hazard maps based on return periods can be drawn [34].

_____

As stated in the book "Difendersi dal terremoto si può" (Keeping safe from earthquakes is possible) by Giuliano Panza and Antonella Peresan [35]. "*An earthquake that is compatible with the seismogenic characteristics of a certain zone, although sporadic and thus declared as "with low probability of occurrence", can occur in every moment*." This assumption is the base of the method.

A flow chart of the procedure to calculate MCSI in terms of response spectrum is shown in Figure 2-13.
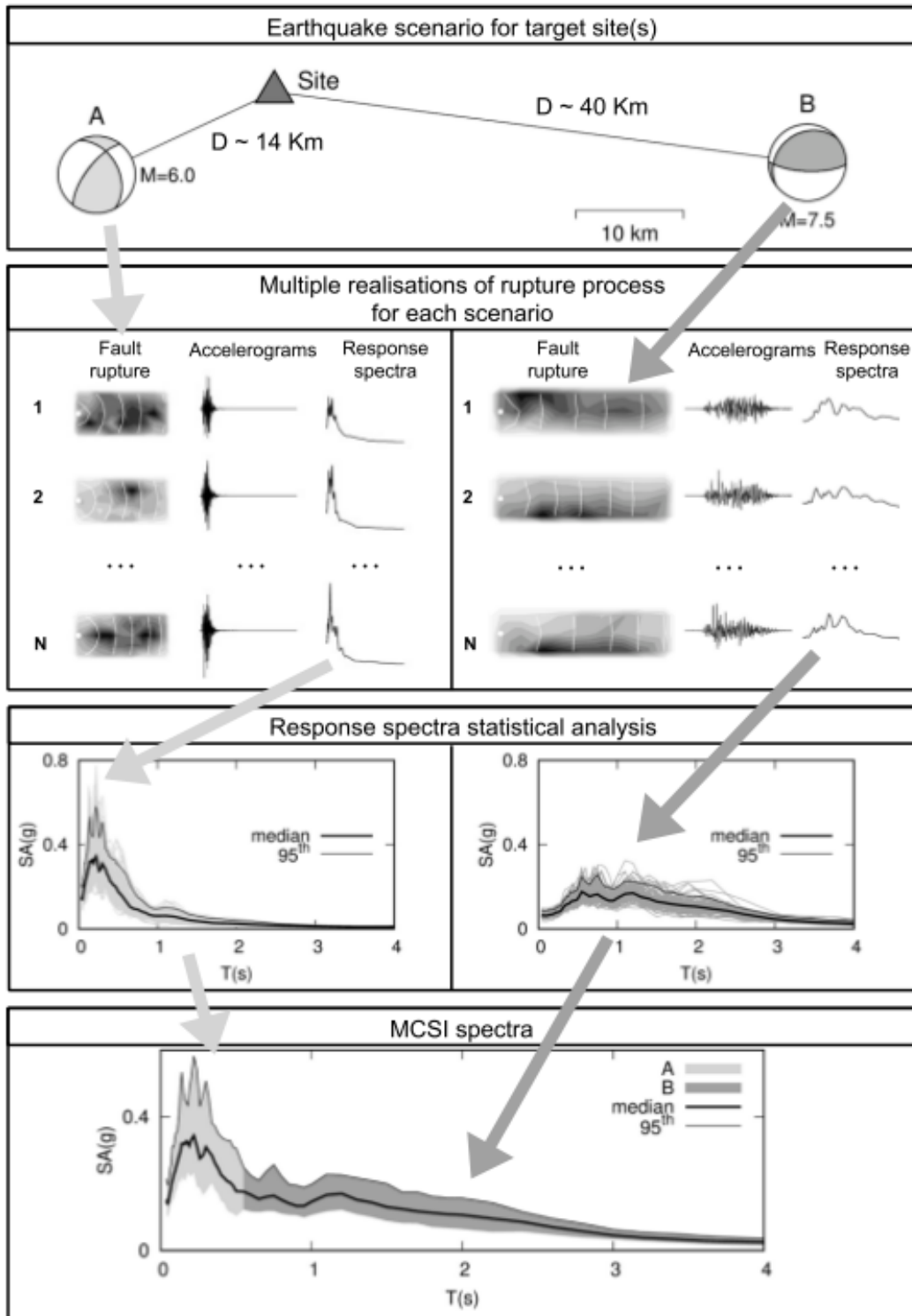
Figure 2-13: Flow chart of the procedure to calculate MCSI [20].

_____

2.2.1. Strength of the method

Every information about the subsoil is considered and can be easily updated.

An "expert opinion" is not needed, the method is then objective.

It uses advanced physics simulation instead of empiric attenuation laws (GMPE). With this method also a useful database for the design of structures can be produced (seismograms and accelerograms).

The intrinsic uncertainty of the probabilistic analyses is avoided by considering an adequate number of scenarios found with parametric analyses, on the contrary of PSHA that often has lack of data.

The Poisson probability distribution (that goes against physic laws) is not used, as the average return periods of earthquakes and the probability of exceedance of a given shaking level are not used.

As the method uses physic-based modelling of the phenomenon, it can create also displacement time histories of the expected earthquakes and this can be useful especially for the design of seismically isolated structures. When using PSHA method, the displacements are obtained as the second integration of acceleration and this can cause quite high errors [36]. In the Italian code NTC2018, at chapter 3.2.3.2.3, the elastic response spectrum for displacements is defined directly from the acceleration spectrum, through a multiplier that depends on the square of the natural period of the structure. The opportunity of using NDSHA method beside traditional PSHA method has been recognized by the Parliament of the Republic with the approval by the VIII Permanent Commission for the Environment, Territory and Public work of the House of Representatives of the final resolution 8-00124/2011 in matter of seismic isolation of civil and industrial constructions, with which has been stated the need to consider a deterministic method beside the probabilistic one, when evaluating seismic hazard and in any case, that the designer of seismically isolated structures should also refer to deterministic data in order to set the maximum design displacement of the isolators. This opportunity has been recalled among the motivations in DDL C. 1184 of the 11 June 2013 - XVII Legislatura ad oggetto "Delega al Governo per l'adozione del Piano antisismico nazionale". Unluckily the legislative proposal has not been followed by a proper law.

2.2.2. Limitations of the method

The calculation of the propagation of the seismic waves is done without considering the non-linearity of the medium and this could lead to an overestimation of the surface shaking.

The method needs site investigation that is deeper than 30 m (the code standard) in order to have a more reliable evaluation.

Also this method is based on the current knowledge of the subsoil and of the seismic sources, so, if a fault is not known, also this method is not useful for the determination of the hazard in the sites near the fault. The lack of data, on the other hand, influences less the result, compared to the PSHA method.

The precision of the result depends on the frequency cut-off of the signal: 1 Hz is used for the national and regional scale analyses; 10 Hz is used for local scale analyses.

2.3.Step by step comparison between PSHA and NDSHA

In order to summarize all the differences and similarities between the two methods, a table is presented (Table 2-1).

Table 2-1: Comparison between PSHA and NDSHA, step by step.

Step of the method	PSHA	NDSHA
Input data	Catalogue of earthquakes, map of seismogenic zones with their focal mechanisms.	Catalogue of earthquakes, map of seismogenic zones with their focal mechanisms + map of seismogenic nodes.
Dealing with uncertaintes about magnitudes and locations in the catalogue	Statistic and precautionary evaluation of maximum magnitude (the error about Mmax is considered also through the logic tree). The error about the location is considered through the probability distribution of distance.	The uncertainty about magnitude is considered by using more information sources (see below), the uncertainty about the location is considered through the smoothing process.
Determination of the maximum magnitude	Maximum observed value in history + 0.2 (precautionary), with statistic elaboration of data from the catalogue, if needed, or from the geometry of the seismic source; it is needed for the calibration of Gutemberg – Richter's law.	Takes the maximum among the values of the catalogue of earthquakes (after the smoothing process), the values of the map of seismogenic nodes and a minimum of 5; it is used just as an input parameter for performing the simulations of earthquakes.
Determination of the minimum magnitude	The minimum magnitude that produces damage; it is needed for the calibration of Gutemberg – Richter's law.	Not needed.
Calculation of seismicity rate	With evaluation of the completeness of the catalogue of earthquakes, with historical and statistical approaches, through "expert opinions", with evaluation of individual activity rates (AR) and assessment with G-R law.	Not calculated.
Characterisation of seismic source (point, linear or volumetric)	The uncertainty is considered through the probability distribution of the distance from the site of interest and it enters directly in the computation of the hazard curve.	The uncertainty is considered through the simulation with the use of point source and extended source models and by performing parametric sensitivity analysis.
Attenuation of seismic waves	Use of GMPE (empiric laws, based on usually few data, especially in some parts of the curve), that assume log-normal distributions of the IM for each distance from the site of interest. Numerous laws exist.	Simulation of wave propagation in visco-elastic medium, with the possibility of improvement of the model (e.g. the detail of stratigraphic profiles of the subsoil and the calculation technique)

Computation of IM in the site of interest	Calculation of hazard curve based on the seismicity rates and on log-normal distribution of the IM of a given event at a given distance. The probability of exceedance of a given IM in a given time range in the site of interest is calculated through the hypothesis of Poisson distribution of the time between two consecutive events of the same energy. The considered IM has to be chosen at the beginning.	From the performed physics-based simulations synthetic seismograms, velocity and acceleration time histories can be extracted and the worse scenario for the site of interest can be chosen. The IM can be chosen after the simulations.
Evaluation of epistemic uncertaintes (of the method)	With logic tree (for the evaluation of the completeness of the catalogue, maximum magnitude, use of GMPE and seismicity rates).	As seismicity rates are not considered, errors can occur just concerning the maximum magnitude and the quality of the physics-based model. For the maximum magnitude parametric analyses can be performed, the model can be just improved with time and development of computational capacity. In order to validate the quality of the model, the synthetic time histories can be compared to the natural recorded ones.
Final product	Response spectra in terms of accelerations, maps of maximum accelerations on rigid soil for each site, **with a certain probability of exceedance in T years**; NO time histories.	Displacement, velocity and acceleration time histories, with specific characteristics of the site of interest, response spectra. From these it is possible to calculate the **maximum credible earthquake** (without return period limitations).
Site effects and necessary data to obtain them	They are considered by amplifying the spectrum at the bedrock with average coefficients. For the calculation of the coefficients, the average velocity of S waves in the last 30 m of subsoil is considered.	They are considered by modelling the stratigraphic profile of the site of interest in more detail. The profile should be at least 100 m deep and 20 km long in the model, in order to obtain good results.

2.4. Conclusions

The two methods both start from the available knowledge about the earthquakes and the underground. We cannot say that we know everything about them, on the opposite, the knowledge in this field is limited, but the use of the available information in the two methods is different. PSHA tries to make some assumptions and some approximation, NDSHA is aware of the lack of knowledge and uses the available knowledge as it is.

For sure none of the two methods can be considered 100% reliable, but the awareness of dealing with uncertain data is important. For sure in the past, when PSHA was first invented, NDSHA was not an option because it needs huge computational ability, that was not available at the time.

PSHA allowed to somehow study the earthquakes and give a more or less credible seismic input for the design of structures. Now we have huge computational ability and so a lot more complex calculation can be performed. NDSHA is a method that can evolve and update together with the advances in knowledge and in technology. Calculation methods can be optimized, for a more and more detailed modelling of the phenomena and input data can be updated, so that the method gives the right direction to follow for the future. In fact, the method is rapidly evolving, putting more and more attention on the importance and possibilities given by the physics-based simulations, more than on the differences in the hazard assessment methods. The great number of simulations (simulation of a great number of seismic sources and a great number of events for each seismic source) allows to treat the realizations with the Monte Carlo method in order to calculate physics-based ground shaking scenarios that take into account the complexity of the kinematic source rupturing process [37]. In such a way, the simulations allow to use a real probabilistic approach (based on a huge number of data), that could better describe the physical events. This extension is used in this research work, as specified in §2.5.

2.5. Scenario Physics-Based Seismic Hazard Assessment (SPBSHA)

In this research PSHA method and a scenario physics-based seismic hazard assessment are used to evaluate seismic vulnerability of four case-study buildings. The SPBSHA method makes use of the same modelling of the ground and wave propagation of the NDSHA method, but it extends the use of the simulations based on a Monte Carlo method. When performing non-linear static (pushover) analyses, both types of response spectra are used to find the seismic demand and the results are compared to each other. The physics-based simulations are used to find the seismic input of two scenarios that are possible for Gorizia town: Medea fault and Idrija fault. For each scenario, 100 realizations are performed and percentile response spectra are found.

2.5.1. SPBSHA response spectra

As already described in §2.2 the accelerograms are calculated as the tensor product of the earthquake source functions and the Green's functions of the transmitting medium. In this research study two scenarios have been considered, calculated based on the characteristics of earthquakes that could derive from the two faults that are the closest to the town of Gorizia: Medea and Idria [38]. The main characteristics of the two faults are shown in Figure 2-14**Errore. L'origine riferimento non è stata trovata.** and Figure 2-15.

The faults have been modelled as an extended source. Such source is modelled as a grid of point sources, where each of those can generate a different realization. For each of the two scenarios (Medea and Idrija), 100 realizations of the rupture process have been calculated. In this way, the stochastic nature of the rupture process is considered. The subsoil is modelled with a semi-infinite space with inelastic plane and parallel layers. The characteristics of the layers have been inferred from geological studies of Panza et. al. [39][40]. For the site effects, the Municipality of Gorizia has been subdivided in 286 census areas, each one with its own superficial stratigraphy, inferred from past geological studies made for Gorizia [41][42].

For this study on the case-study buildings, 100 couples of accelerograms (E-W and N-S – vertical component is also calculated but is not of interest in this case) and their corresponding response spectra have been calculated. The response spectra for each realization are actually three (excluding the vertical component): two of the two main directions and one of the resultant (considering both components of the signal). The resultant response spectrum is calculated as every response spectrum: for each period a SDOF is analysed and the maximum is taken from its response. In this case the SDOF is analysed in both directions, the resultant response is calculated and then the maximum is taken for defining the resultant response spectrum of each realisation.

With the aim of reducing the number of response spectra for the calculation of seismic vulnerability with pushover analyses, without losing information, the response spectra have been statistically processed and the percentiles have been calculated. The 50th, 84th and 95th percentile have

been considered. Such response spectra are shown in Figure 2-16 and Figure 2-17, compared to code response spectra for four different limit states and reference life 50 and 100 years.

PARAMETRIC INFORMATION

PARAMETER	QUALITY		EVIDENCE
Min depth [km]	1.0	LD	Based on various geological data (Nicolich et al., 2004; Ponton et al., 2010).
Max depth [km]	12.0	LD	Based on various geological data (Ponton et al., 2010; Bressan et al., 2016).
Strike [deg] min... max	290...330	LD	Based on geological data from Nicolich et al. (2004).
Dip [deg] min... max	30...50	LD	Based on geological data from Nicolich et al. (2004).
Rake [deg] min... max	110...130	EJ	Inferred from the regional stress orientation.
Slip Rate [mm/y] min... max	0.14...0.21	OD	Based on modeling of subsurface geological data.
Max Magnitude [Mw]	6.5	EJ	Inferred from the geometrical parameters of the source.

LD=LITERATURE DATA; OD=ORIGINAL DATA; ER=EMPIRICAL RELATIONSHIP; AR=ANALYTICAL RELATIONSHIP;EJ=EXPERT JUDGEMENT;

Figure 2-14: Characteristics of the fault of Medea [8]

PARAMETRIC INFORMATION

PARAMETER	QUALITY		EVIDENCE
Min depth [km]	1.0	EJ	Inferred from geologic and regional structural setting.
Max depth [km]	14.0	EJ	Inferred from geologic and regional structural setting.
Strike [deg] min... max	290...330	LD	Based on geologic and geomorphological maps and data.
Dip [deg] min... max	70...85	EJ	Inferred from geological and geomorphological observations.
Rake [deg] min... max	160...180	EJ	Inferred from geological and geodetic data.
Slip Rate [mm/y] min... max	0.1...0.25	EJ	Inferred from geodynamic data and geological considerations.
Max Magnitude [Mw]	6.8	LD	Derived from the largest associated historical earthquake (CPTI04).

LD=LITERATURE DATA; OD=ORIGINAL DATA; ER=EMPIRICAL RELATIONSHIP; AR=ANALYTICAL RELATIONSHIP;EJ=EXPERT JUDGEMENT;

Figure 2-15: Characteristics of the fault of Idrija [8]
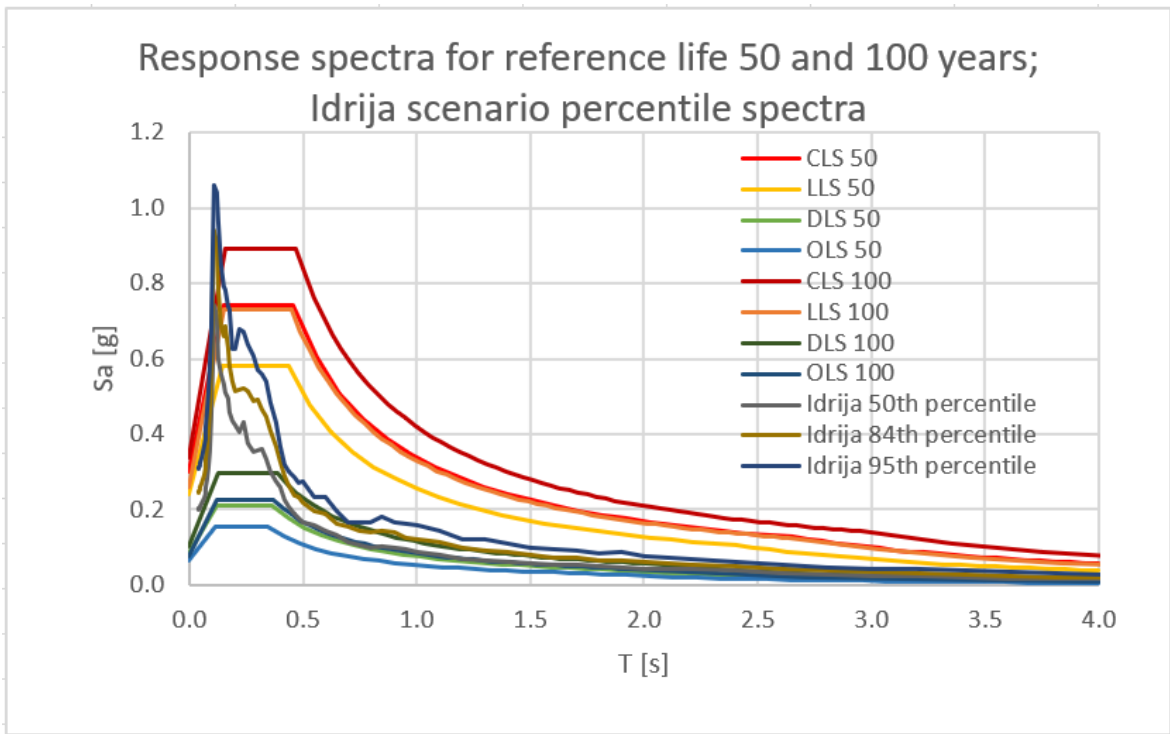
Figure 2-16: Scenario response spectra for Idrija fault – 50th, 84th and 95th percentile and code spectra for comparison (CLS, LLS, DLS, OLS), for reference life 100 years and 50 years.
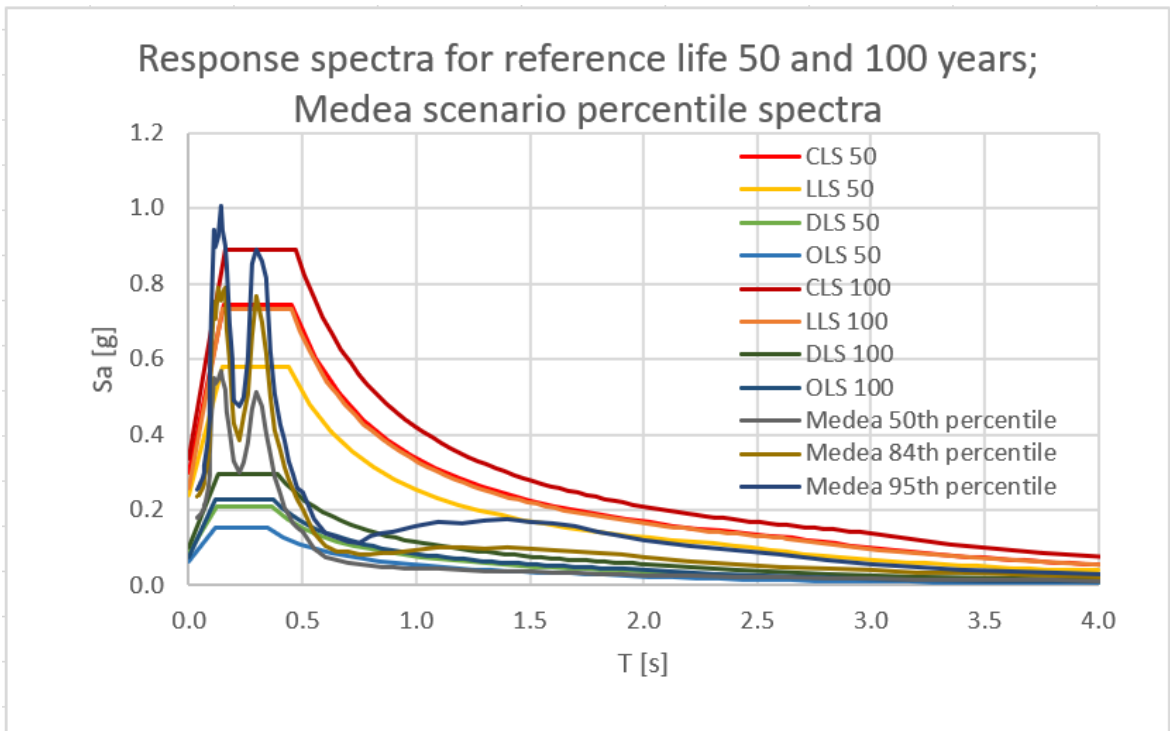
Figure 2-17 Scenario response spectra for Medea fault – 50th, 84th and 95th percentile and code spectra for comparison (CLS, LLS, DLS, OLS), for reference life 100 years and 50 years.

For the sake of completeness, also all the spectra (of all the 100 realisations) are reported in Figure 2-18 and Figure 2-19, together with the percentile spectra.
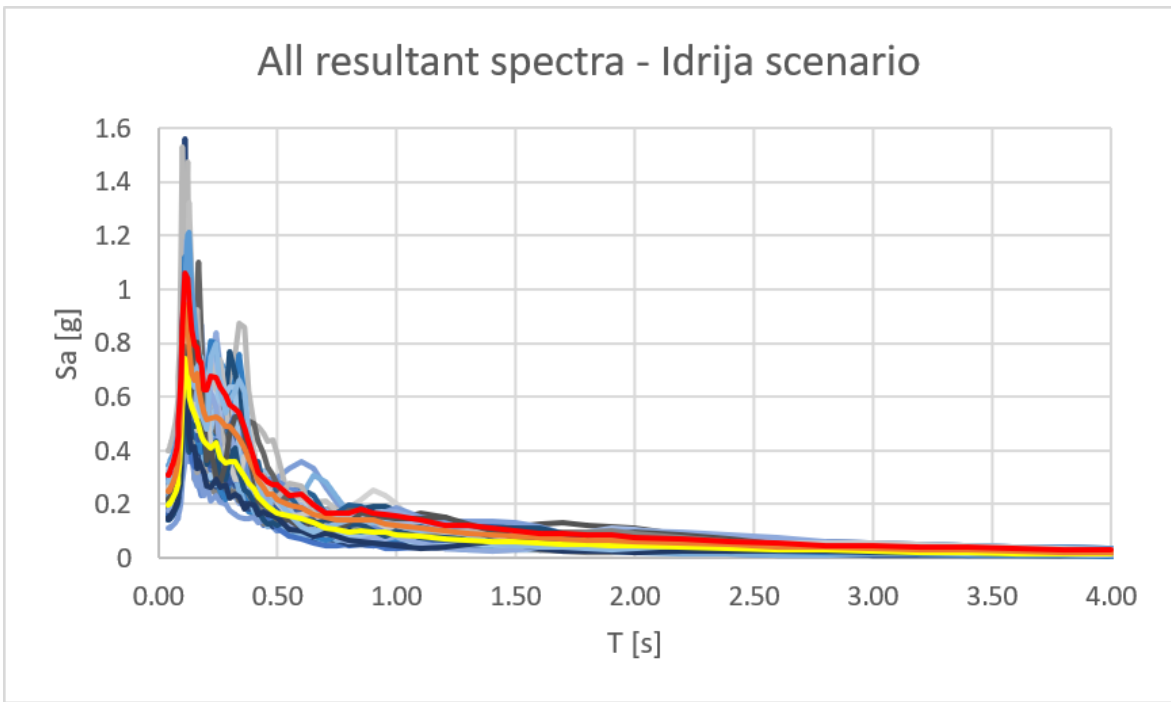
Figure 2-18: Resultant response spectra for all the 100 realisations for Idrija scenario. In the same graph also the percentiles spectra (50th in yellow, 84th in orange and 95th in red) are reported.
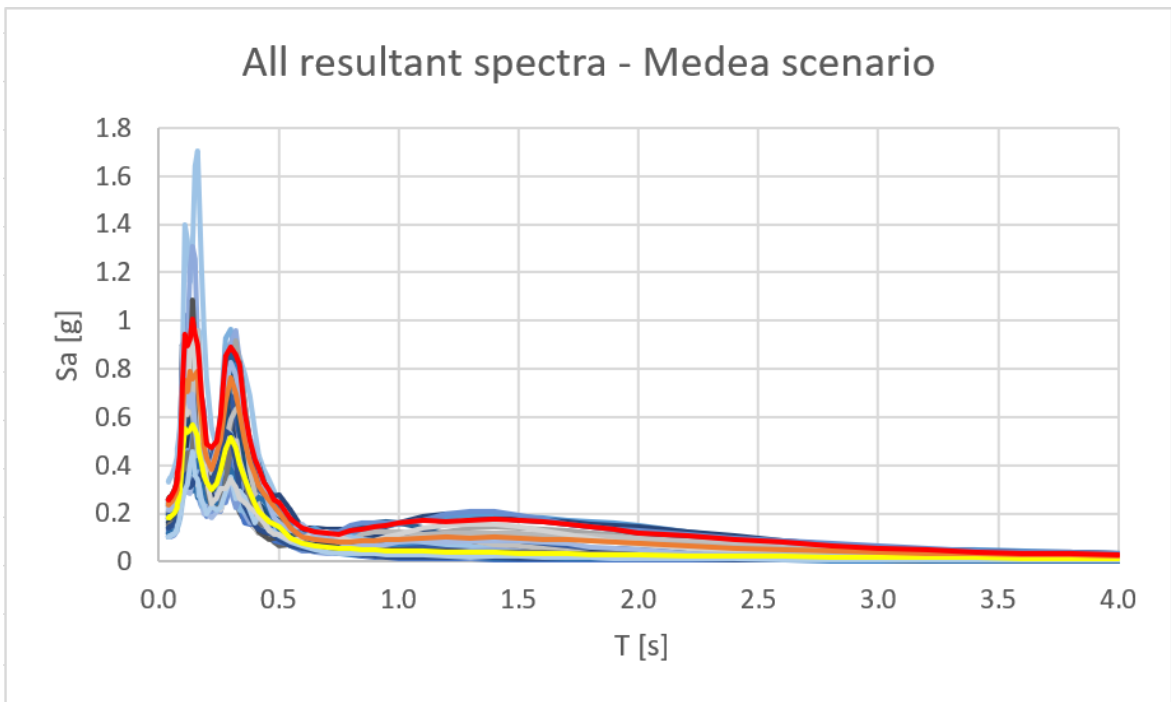
Figure 2-19: Resultant response spectra for all the 100 realisations for Medea scenario. In the same graph also the percentiles spectra (50th in yellow, 84th in orange and 95th in red) are reported.

It can be seen that the scenario response spectra have higher accelerations than code response spectra for very short periods, but both scenarios have very low accelerations for periods around 0.3 s (especially Medea) and for higher periods. The period around 0.3 s could be typical for masonry buildings, while higher RC buildings usually have longer periods. The shape of the response spectra is due to the specific position and soil of Gorizia and it could cause a lower seismic demand for some buildings than the one expected with the code seismic inputs.

3. CASE STUDY BUILDINGS

The aim of this research is to investigate the vulnerability of the building heritage in Gorizia. As shown in § 1, the majority of buildings in the town are old masonry buildings and "newer" reinforced concrete buildings from the 60's-70's. All the buildings built before the year 2003 were not considering earthquake hazard at all and just after 2010 the seismic hazard has been considered at the level that we now consider credible.

Based on the statistical data about the building heritage in Gorizia, some buildings have been chosen and analysed with different methods in order to evaluate their seismic vulnerability and retrofit options. For privacy reasons the residential buildings will be described without revealing their exact location.

For R.C. buildings the software SAP2000 from CSI [43] is used for numerical modelling and analysis. For masonry buildings the software TreMuri from STA DATA is used.

3.1. RC building 1

The building (Figure 3-1) was built between years 1967 and 1968 and it well represents the RC buildings of the 60's-70's in Gorizia. The RC buildings of that times were usually designed to withstand exclusively gravitational loads, so their structure used to have frames just in one direction, while in the other direction, just the slabs were connecting the frames. They are usually also in a bad state of preservation, as seen at §1.4.

The documentation has been difficult to find and the finding has been accidental. In the public offices, as e.g. the state archive (Archivio di Stato) and at the City hall there was no documentation stored about this building. No testing certificate (certificato di collaudo) has been handed to the offices or at least has not been found when needed. The exact information about the year of construction is thus missing, it is just known that in 1971, when other two nearby buildings have been constructed, partially connected to this through an underground garage, the RC building 1 was already built. This information has been extracted from the testing certificate of these neighbour buildings. The projects on which all the modelling and the knowledge about the structure is based, have been kindly provided by a colleague of the structural designer of the building. The provided documentation consists of some architectural drawings, updated at different dates, of 31 drawings of the final project of the structure, with dimensions, rebar, type of slabs and of a handwritten calculation report, with very simple calculation of beams and columns.

The collection of information about old buildings is always very difficult. Before finding the documentation about this building, some other buildings have been considered, but it has been impossible to find the minimum necessary information to understand the structure and model it without invasive in situ investigations and tests. This is a common problem in Italy. As it was not mandatory to deliver the projects or even to have a design project with some calculation in the past, for the major part of buildings no information is available and this makes it even more difficult and uncertain to evaluate their vulnerability or even to retrofit them in a proper way. The structure and the construction details can be just discovered by executing invasive and expensive in situ tests.

As there was no possibility of performing tests on the structure during this research, the building with more information available has been chosen. More information about the building has been collected from an inhabitant, that lives there from the real beginning, when the structure was built. Since the construction, no big changes have been made to the structure, so that the model can follow the information given by the design documentation.

Nevertheless some measurements of dimensions and distances have been performed to check the correspondence of reality with the project and the quantity of rebars has been checked in some elements (columns – see Table 3-1) with a covermeter (Elcometer CoverMaster). As an additional

test, some vibrational measurements have been performed in order to evaluate the natural period of the structure and compare it with the period given by the numerical model.

Figure 3-1: View of the back façade of case study RC building 1.

Table 3-1: Rebar and stirrup check with covermeter.

Column nr. and storey nr.	Project rebars and stirrups	Detected rebars and stirrups
20 – IX storey	$4\phi12$, stirrup $\phi6/15$ cm	$4\ \phi\ 14$, stirrup $\phi\ 8/14$ cm, concrete cover 30 mm
21 – IX storey	$4\phi12$, stirrup $\phi6/15$ cm	$4\phi14$, stirrup $\phi8/14$ cm
22 – IX storey	$4\phi12$, stirrup $\phi6/15$ cm	$4\phi14$, stirrup $\phi6/14$ cm
17 - basement	$6\phi16$, stirrup $\phi6/20$ cm	$6\phi16$, stirrup $\phi6/20$ cm
18 - basement	$6\phi18$, stirrup $\phi6/20$ cm	6ϕ?
Shear walls of stairwell	No info	Vert. $\phi10/20$ cm; horiz. ϕ?/70 cm

The standard used for the design of this building is Regio Decreto 16/11/1939 n. 2229 – Norme per la esecuzione delle opere in conglomerato cementizio semplice od armato. This law was specific for concrete structures. It has been then integrated with:

- Circ. Min. LL. PP. n. 1472/1957 – Armature delle strutture in cemento armato;
- Circ. Min. LL.PP. n.1547/1965 - Caratteristiche e modalità di impiego nel cemento armato degli acciai ad aderenza migliorata;
- Circ. Min. LL.PP. n. 3525/1967 - Caratteristiche e modalità d'impiego nel cemento armato degli acciai ad aderenza migliorata. Carichi di snervamento e rottura;
- Circ. Min. LL.PP. n.6090/1969 - Norme tecniche per la progettazione, il calcolo, l'esecuzione e il collaudo di costruzioni prefabbricate in zone sismiche e asismiche.

3.1.1. Geometry of the building and load-bearing elements

The first case study building has a RC frame structure, with frames in just one direction and not continuous along all the length of the building, but divided essentially in 3 parts (Figure 3-2). The plan of the building is inscribable in a rectangle with dimensions 30.00 m x 12.05 m, when considering the outer border of the structure (load-bearing elements) and considering also the stairwell. The stairwell is made of very little armed concrete, as shown in Table 3-1. The building is standing alone, without connections to other buildings, apart from some connections in the basement/garage under the ground level, through some concrete beams of the ceiling of the garage that is in common with other two buildings that are about 30 m away. The interaction is considered neglectable.

From architectural drawings it can be learned that each floor of the building contains 2 or 3 apartments, although it is not specified which floors have 2 and which 3 apartments, but in both cases the geometry is quite symmetric, so that it does not noticeably influence the centre of mass. During a site inspection it has been ascertained that the only floors with just 2 apartments are the ground floor (because a part of the plan is occupied by the entrance), the fifth floor (where 2 flats have been transformed in 1), the ninth and the eleventh floors. All the other floors have 3 flats.
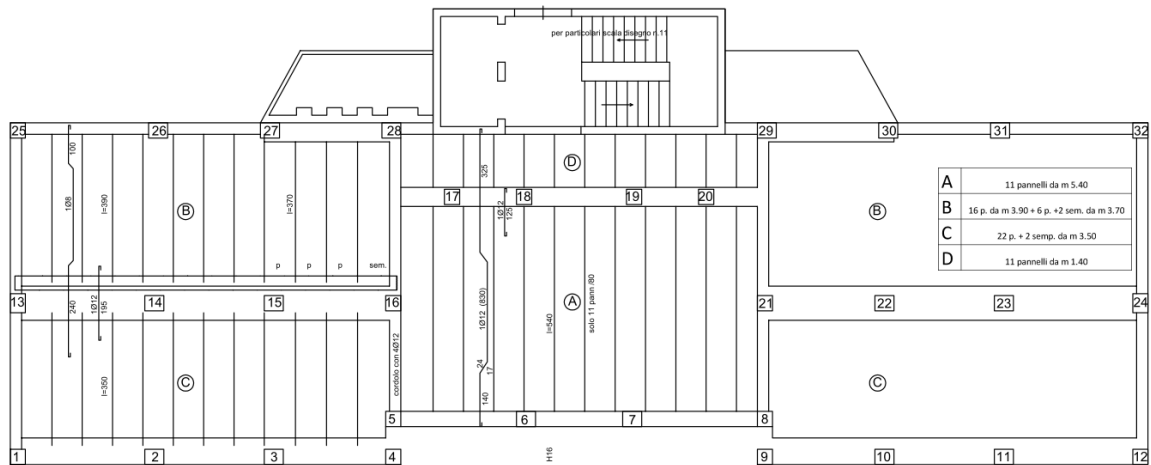
Figure 3-2: First storey plan, where the structure of the building can be seen (Autocad reproduction of the found design documents) – one directional and non-continuous r.c. frames along the length of the building; in the transversal direction just slabs and curbs are present.
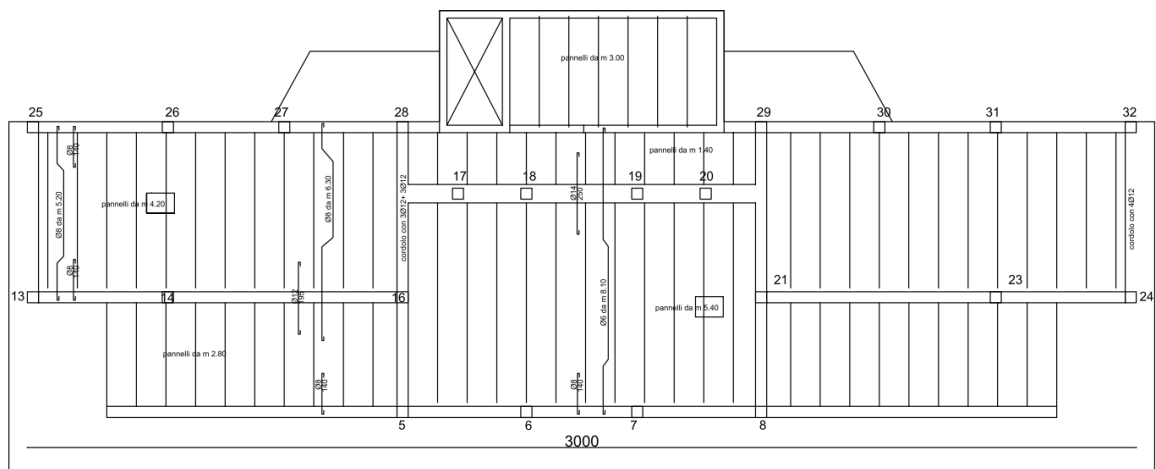
Figure 3-3: Plan of the roof of the attic (Autocad reproduction of the found design documents).

The building has 12 storeys over the ground level and one under the ground, for the basements. The 32 columns, that are continuous from the basement to the 10th floor, vary in

dimensions, from storey to storey, becoming smaller and smaller, until the minimum dimension of 30 cm x 30 cm. In the basement there are two more columns, that do not continue to the upper floors, in the attic the plan is smaller, so that some columns are not needed there and they do not arrive to the roof (Figure 3-3). The stairwell continues one more storey over the end of the twelfth floor (that will be called 11th floor, because the ground floor is counted as floor 0) and the building is covered with a flat roof (slope of 14°), where it is possible to walk.
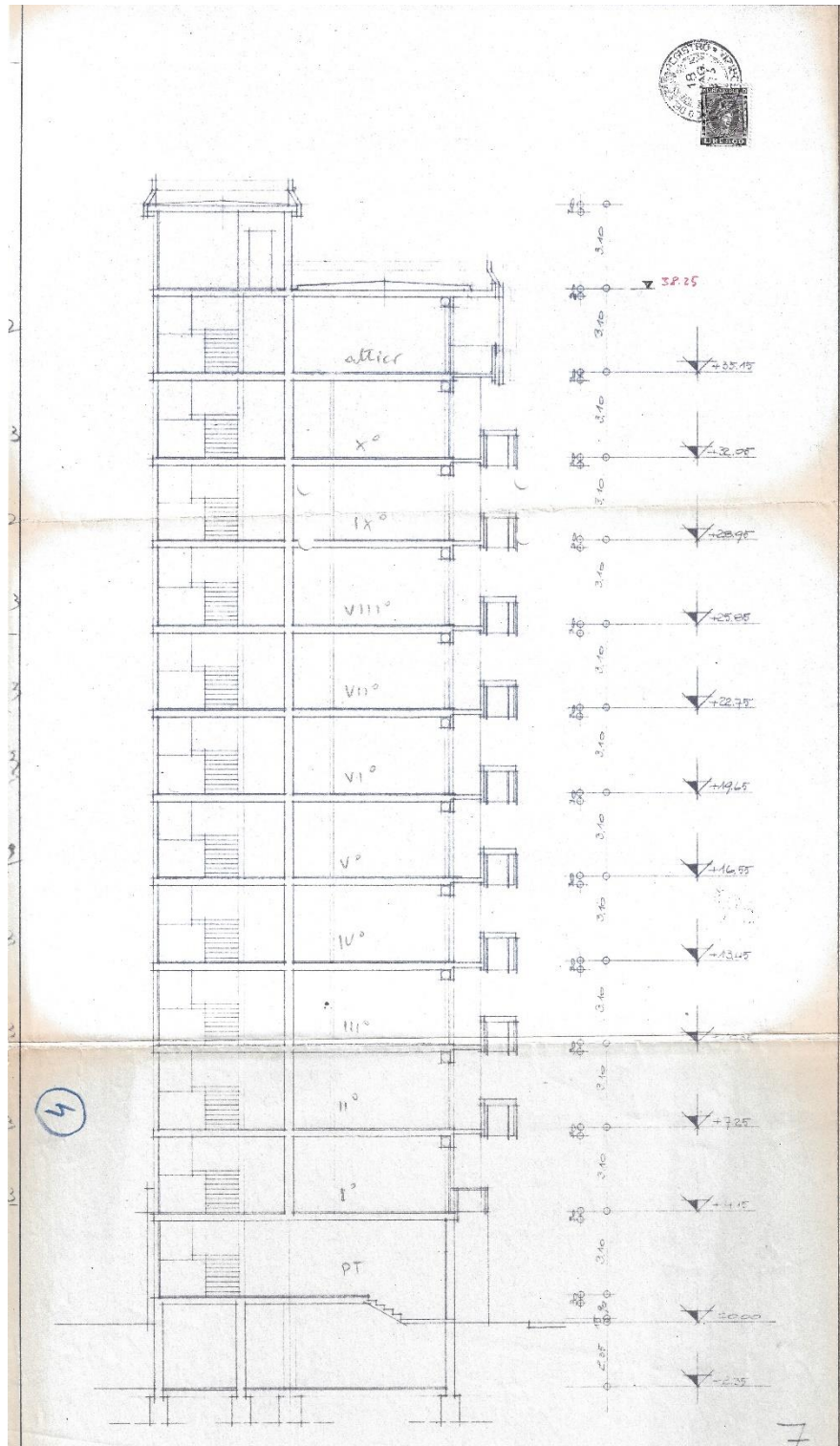
Figure 3-4: Architectural design project of the building (scan of the original document) – section updated at the 3rd of June 1968.

The storeys are all the same from the 2nd to the 10th floor, on the contrary the ground floor, the first and the 11th floor (attic) have some slight differences in the plan and in the structure. The inter-storey height is equal to 3.1 m, just the basement is higher, 3.4 m. The total height of the building over the ground level is 40.3 m (Figure 3-4).

The load-bearing elements are beams and columns also in the basement, so that the foundation is made of plinths that support the "internal" columns and of inverted T beam foundations along the whole perimeter of the building. Plinths are not connected to the beams at all and also not among them, as at the time when the building was designed there was no common practice of using foundation lattices, also because Gorizia was not considered seismic, so there was no reason to use them.

The beams have various dimensions, some of them have the same thickness of the slab, some of them are deeper. In the transversal direction there are just the hollow pot slabs and some curbs that connect the various frames. This type of structure is extremely frequent in the buildings of that time, as they were designed exclusively for vertical loads, often "forgetting" even the wind action. On the other hand, at the time when this building was designed even the Friuli earthquake of 1976 has not occurred yet, so the town was not aware about earthquakes at all.

Columns

In the design documents are specified the dimensions and the rebars of the foundations, beams and columns at each storey. The drawings show the plans of the storeys and the plans of the slabs with the rebars of the columns and some drawings specify the rebars of the beams and foundations. As it can be seen in Figure 3-2 and Figure 3-3, every column is characterized by a number that remains the same over all the storeys. A table with all the dimensions and rebars of the columns, that are considered in the numerical model of the building, is reported in Attachment, in Table 0-1.

Slabs

The building has more than one type of slab. The main direction of the slab is perpendicular to the RC frames, so along the short side of the building, as it can be seen in Figure 3-2, except for the central part of the ground floor slab, that has the other direction. In Table 3-2 are summarized all the types of slabs in the building, specifying the floor at which they are, their weight and accidental loads. The data are taken from the design documentation (drawings and calculation report) and from the manuals of the slabs. In the calculation report is not always clear which is the dead load and which is the accidental load, as at the time of design was not necessary to subdivide the loads in order to assign them different safety factors, as we do nowadays. The professional was considering just one load, comprising all the needed actions.

In Figure 3-5 the properties of the prestressed joists of the hollow slab Celersap, used at the ground floor of the building, can be seen. Also a table with some data for the rapid calculation of the more suitable height of the slab to use is shown in Figure 3-6. Dead loads of the slabs are also specified. The plan of the attic is shown in Figure 3-7, with a zoom on the part where the slab Bisap H16.5 with 3 cm concrete topping is used, instead of Bisap H20, that is used in all the other storeys. It should be noted that none of the slabs, except for the slab of the ground floor, a part of the attic and the ceiling of the attic, have a concrete topping. As at the time when the building was designed there was no need of having rigid diaphragms (as no horizontal action was considered), this kind of slabs were used, where the upper part of the hollow pots was made more resistant in order to use it without concrete topping.

Table 3-2: Slab types in the building, their weight and loads.

	Ground floor	Storeys I to X	Attic (slab)	Attic (ceiling)
Type of slab	**Celersap H20+3**; spacing 50 cm (prestressed joists type 1) and spacing 52 cm (joists type 2) - Figure 3-5	**Bisap H20**; spacing 80 cm (2 hollow pots); balconies have slabs made of **free blocks** of **H16.5** on the front façade and **H20** on the back façade (next to the stairwell)	**Bisap H20**, except for two zones with **H16.5 + 3.5** with rebars $3\phi8$/m (Figure 3-7)	**Bisap H16.5 + 3**
Self weight	240 kg/m^2	160 kg/m^2	160 kg/m^2 for H20; 140 kg/m^2 for H16.5; 88 kg/m^2 for concrete topping	140 kg/m^2 for H16.5; 75 kg/m^2 for concrete topping
Accidental and permanent load	600 kg/m^2	350 kg/m^2	350 kg/m^2	250 kg/m^2
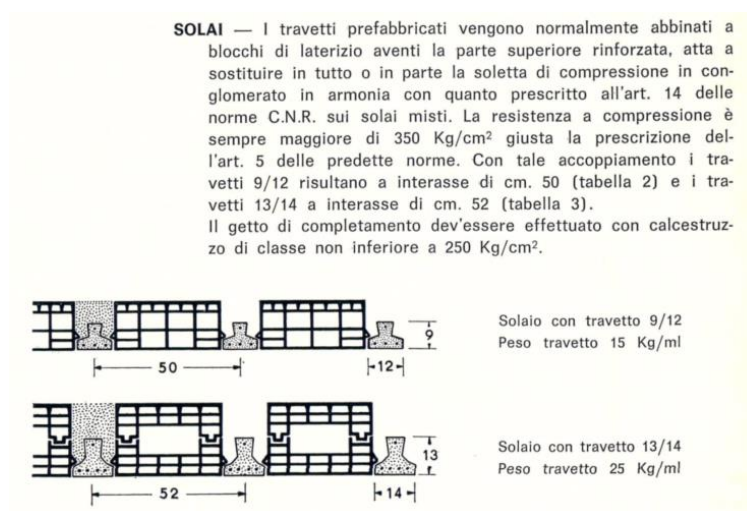
Figure 3-5: Excerpt of the manual of the hollow slab Celersap, where the properties of joists type 1 and type 2 are shown, that are not made explicit in the project documentation.

SOLAIO CELERSAP P. - INTERASSE 50 cm

Altezza solaio H (cm)	Peso blocchi e travetti (Kg/mq)	Conglomerato (l/mq)	Peso del solaio in opera (Kg/mq)	MOMENTI MAX DI SERVIZIO RIFERITI ALLA STRISCIA DI SOLAIO LARGA 1 M — M_{max} (Kgm)							Altezza utile h (cm)	Asse neutro x (cm)	Mom. d'inerz. J (cm⁴)	Mom. resist. di compr. W_s (cm³)	Mom. resist. di traz. W_i (cm³)	Distan. asse baricentrico x_c (cm)	Area sezione A_c (cm²)	Momento d'inerzia baricentrico J_c (cm⁴)	Calore dall'alto al basso r_1	Calore dal basso all'alto r_2
12	80	14	110	438	568	588	732	762	920	1000	10,50	4,98	6875	1375	655	5,79	762	11190	0,22	0,21
12+3		44	175	676	876	910	1132	1176	1424	1548	13,50	5,25	14780	2815	1010	6,73	1062	22850	0,24	0,23
12+5		64	220	810	1026	1120	1394	1450	1752	1904	15,50	5,79	20900	3610	1245	7,50	1262	32980	0,26	0,25
16,5	94	25	150	764	990	1028	1280	1330	1610	1748	15	6,80	16618	2440	1140	8,13	916	26640	0,31	0,29
16,5+3		55	215	958	1212	1400	1686	1798	2166	2374	18	6,70	29885	4460	1555	8,75	1216	47820	0,33	0,31
16,5+5		75	260	1076	1360	1604	1894	2020	2434	2740	20	6,92	39200	5660	1790	9,38	1416	64230	0,35	0,33
20	99	33	175	988	1248	1386	1726	1792	2170	2360	18,50	8,02	27785	3460	1540	9,91	1038	44950	0,36	0,34
20+3		63	240	1166	1470	1738	2050	2188	2634	3044	21,50	7,65	45830	5990	1990	10,35	1338	75470	0,38	0,36
20+5		83	285	1286	1620	1914	2258	2412	2902	3360	23,50	7,82	57815	7400	2245	10,88	1538	99970	0,40	0,38
25	122	44	220	1286	1620	1914	2258	2412	2902	3300	23,50	9,43	50470	5330	2160	12,48	1356	82000	0,49	0,46
25+3		74	285	1466	1840	2184	2572	2746	3304	3828	26,50	8,84	75500	8530	2630	12,95	1656	130240	0,51	0,48
25+5		94	330	1582	1990	2368	2780	2968	3572	4140	28,00	8,94	91475	10220	2900	13,44	1856	165020	0,53	0,50

CARATT. DEI TRAVETTI 9/12 — Peso Kg/ml 15
Area sezione B = 72 cm² — Mom. d'inerzia J_c = 423 cm⁴ — D. baric. bordo s. x_c = 5,65 cm

n°	1	2	3	4	5	6	7		
									Contrassegno che individua il tipo d'armatura
A_p = cm²	0,32	0,40	0,48	0,56	0,60	0,72	0,84		Area armatura metallica contenuta nel travetto
y_a = cm	3,10	2,85	3,10	2,80	2,84	2,66	2,72		Distanza baricentro armat. dal lembo infer. del travetto
σ_{ps} = Kg/cm²	−35,4	−30,7	−51,1	−37,5	−42,8	−35,4	−44,4		Precompressione al lembo superiore del travetto
σ_{pi} = Kg/cm²	−52	−71,9	−75	−97,2	−101,4	−125,9	−138		Precompressione al lembo inferiore del travetto
x_i = cm	5,66	5,67	5,66	5,69	5,68	5,70	5,70		Distanza baricentro sezione ideale dal lembo superiore
J_i = cm⁴	436	437	441	438	443	445	445		Momento d'inerzia baricentrico sez. ideale del travetto

Figure 3-6: Table from the manual of Celersap, used for the slab of the ground floor in the case study building.

Also a figure of the manual of Bisap is reported Figure 3-8. It has been found together with the project documentation.

Figure 3-7: Type of slabs in the attic – entire plan and zoom on a part of it.

Figure 3-8: Manual of the hollow pot slab Bisap, used in most of the storeys of the case study building.

Roof

The roof is made of brick hollow flat blocks (*tavelloni*, in Italian), as it is also specified in the documentation. The construction system is made of small brick walls, built on the last floor slab approximately every 90 cm and that support the flat blocks of the roof. The roof is a hip roof, with 14° slope. As seen during a site inspection, the roof is not covered with tiles, but just with a waterproof sheath. It is not clear if it was designed like this from the very beginning or if it was changed at some point. Figure 3-9 shows the detail of the roof, scanned from the original drawings, Figure 3-10 shows the plan of the roof and Figure 3-11 represents the typical roof made of brick hollow flat blocks.
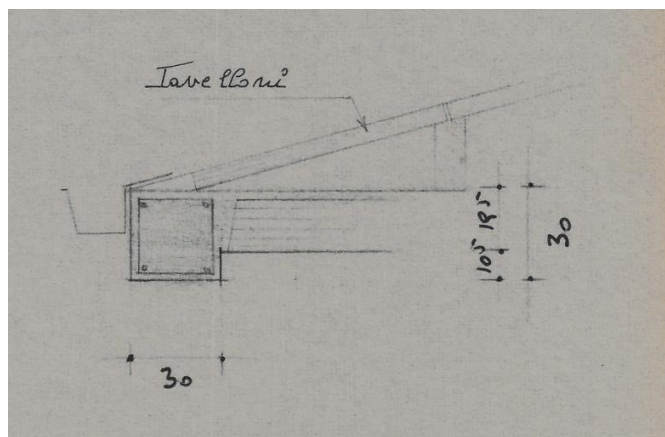
Figure 3-9: Detail of the roof from the original design drawings.
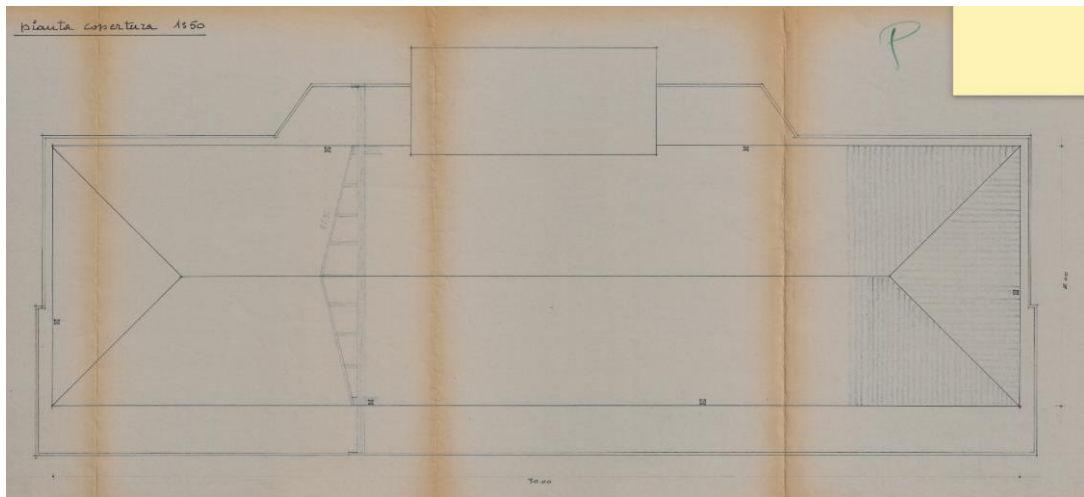
Figure 3-10: Drawing of the roof – scan of the original drawing.

Brick hollow flat blocks (h = 6 cm)

Bastard mortar

Hollow bricks walls (25x12x8)

Hole for ventilation

Eaves overhang

Slab
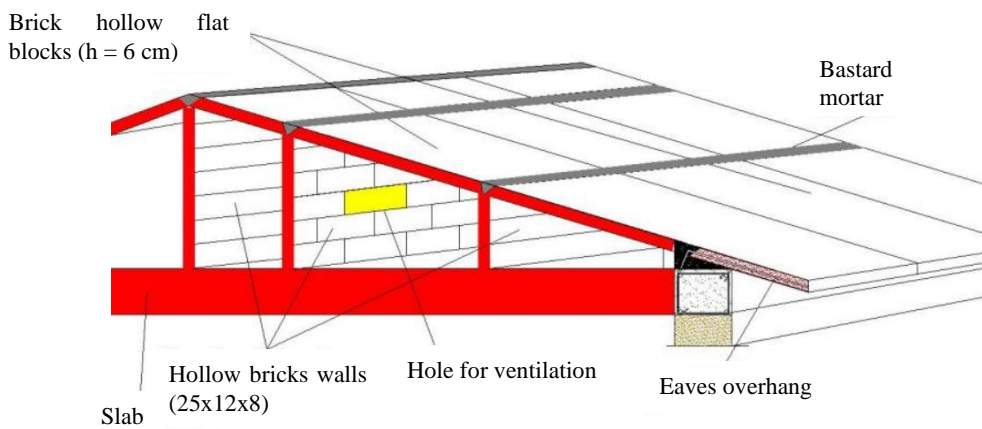
Figure 3-11: Construction system of a roof with brick hollow flat blocks.

Beams

The beams of the same storey have different dimensions, but the scheme is repeated at the other storeys. From the first to the tenth floor, the dimensions and rebars of the beams are exactly the same. The names given to the beams in order to identify them are shown in Figure 3-12. An example of original drawing of the beams, where dimensions and rebars are specified, is shown in Figure 3-13. In Table 3-3 the dimensions and rebars of all the beams of the building are reported.

GROUND FLOOR SLAB AND FOUNDATION
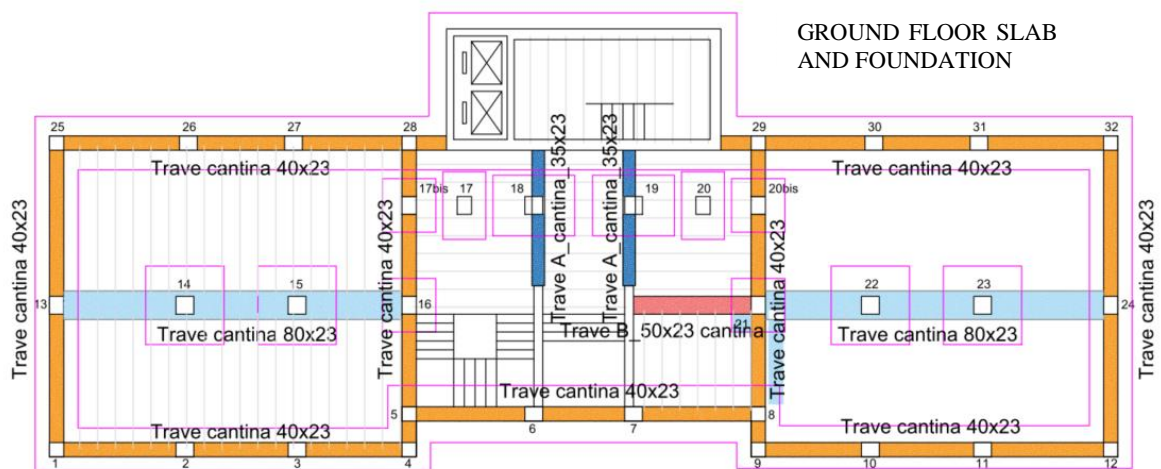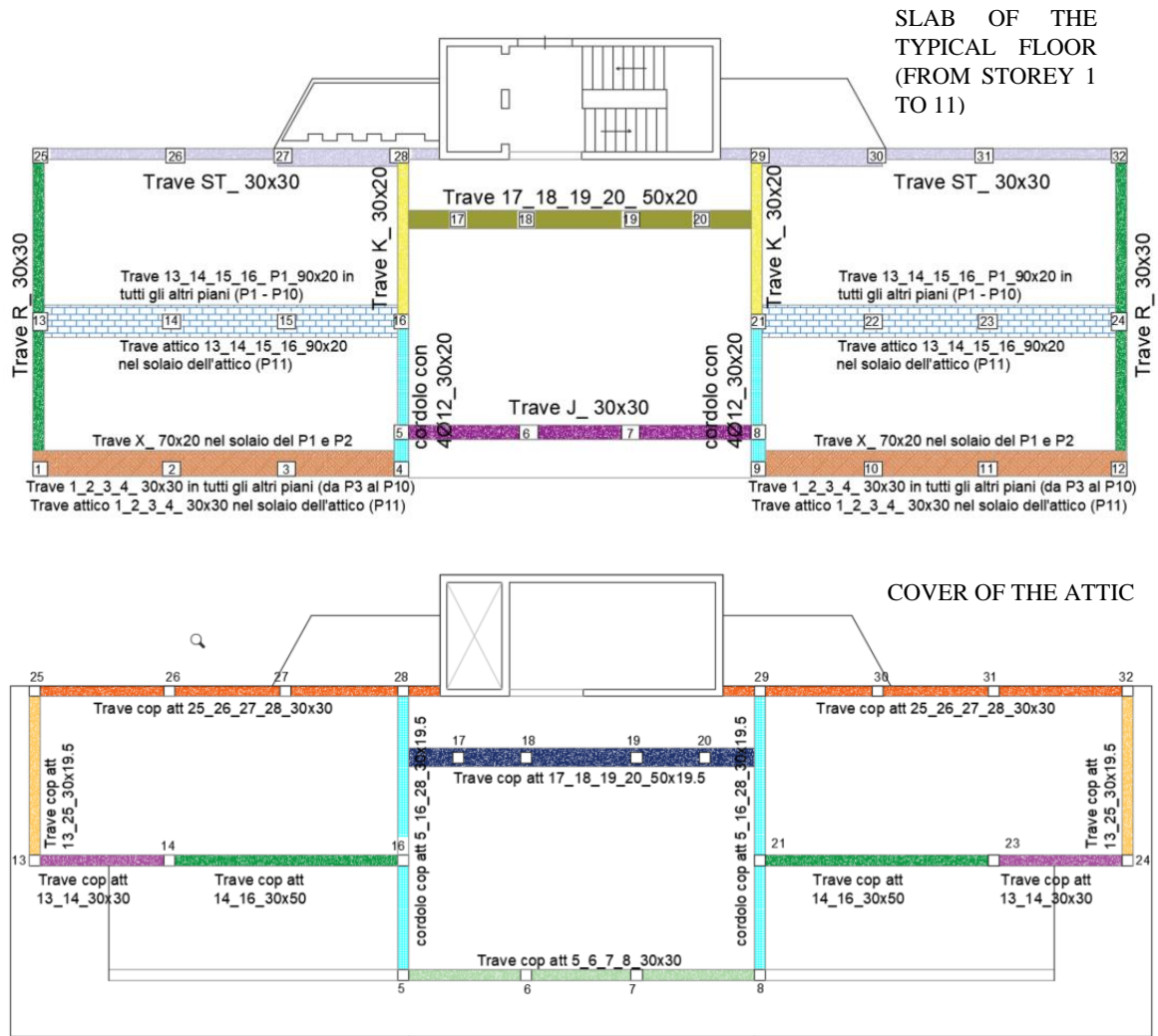
Figure 3-12: Plan of the ground floor, the typical floor and of the cover of the attic, reporting the names given to beams and columns.
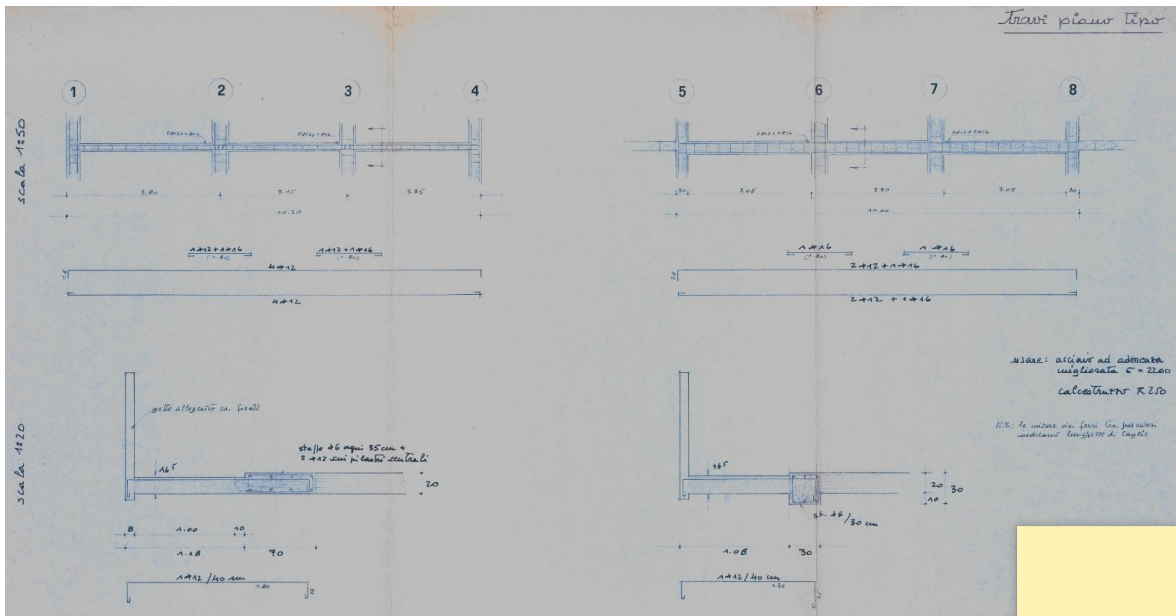
Figure 3-13: Example of an original drawing of the beams with the specification of dimensions and rebars.

Table 3-3: Table of the beams in the case study building (RC building 1) – dimensions and rebars at the endings (N.S. = not specified).

Name of beam	b [cm]	h [cm]	Lmodel [m]	Rebar at the endings				Stirrups
				Top left	Top right	Bottom left	Bottom right	
Cordolo con 4f12_30x20	30	20	3.1	2 ϕ 12	2 ϕ 12	2 ϕ 12	2 ϕ 12	N.S.
Cordolo cop att 5_16_28_30x19.5	30	19.5	3.1	3 ϕ 12	3 ϕ 12	3 ϕ 12	3 ϕ 12	N.S.
Trave 1_2_3_4_30x30	30	30	3.65	3 ϕ 12	2 ϕ 12+ 1 ϕ 16	3 ϕ 12	3 ϕ 12	ϕ 6/35
Trave 13_14_15_16 P1_90x20	90	20	3.65	3 ϕ 12+ 2 ϕ 16	4 ϕ 12+ 1 ϕ 16	3 ϕ 12+ 1 ϕ 16	3 ϕ 12+ 1 ϕ 16	ϕ 6/35
Trave 17_18_19_20_50x20	50	20	1.875	3 ϕ 12	3 ϕ 12+ 1 ϕ 16	3 ϕ 12	3 ϕ 12	ϕ 6/35
Trave A_cantina_35x23	35	23	2	3 ϕ 12	3 ϕ 12	3 ϕ 12	3 ϕ 12	N.S.
Trave attico 1_2_3_4_30x30	30	30	3.65	3 ϕ 12	2 ϕ 12+ 1 ϕ 16	3 ϕ 12	3 ϕ 12	ϕ 6/35
Trave attico 13_14_15_16_90x20	90	20	3.65	3 ϕ 12+ 2 ϕ 16	4 ϕ 12+ 1 ϕ 16	3 ϕ 12+ 1 ϕ 16	3 ϕ 12+ 1 ϕ 16	ϕ 6/35
Trave B_50x23 cantina	50	23	3.35	4 ϕ 12	4 ϕ 12	4 ϕ 12	4 ϕ 12	ϕ 6/30
Trave cantina 40x23	40	23	2.8	2 ϕ 12	2 ϕ 12	2 ϕ 12	2 ϕ 12	N.S.
Trave cantina 80x23	80	23	3.65	2 ϕ 12+ 3 ϕ 16	2 ϕ 12+ 3 ϕ 16	2 ϕ 12+ 2 ϕ 16	2 ϕ 12+ 2 ϕ 16	ϕ 6/30
Trave cop att 13_14_30x30	30	30	3.65	2 ϕ 8	2 ϕ 8+ 3 ϕ 16	2 ϕ 12	2 ϕ 12	ϕ 6/30
Trave cop att 13_25_30x19.5	30	19.5	4.6	2 ϕ 12	2 ϕ 12	2 ϕ 12	2 ϕ 12	N.S.
Trave cop att 14_16_30x50	30	50	6.35	2 ϕ 8+ 3 ϕ 16	2 ϕ 8+ 1 ϕ 16	2 ϕ 16	3 ϕ 16	ϕ 6/30
Trave cop att 17_18_19_20_50x19.5	50	19.5	1.875	3 ϕ 12	3 ϕ 12	3 ϕ 12	3 ϕ 12	ϕ 6/35
Trave cop att 25_26_27_28_30x30	30	30	3.65	2 ϕ 12	3 ϕ 12	2 ϕ 12	2 ϕ 12	N.S.
Trave cop att 5_6_7_8_30x30	30	30	3.175	2 ϕ 12	3 ϕ 12	2 ϕ 12	2 ϕ 12	N.S.
Trave J_30x30	30	30	3.175	2 ϕ 12+ 1 ϕ 16	2 ϕ 12+ 2 ϕ 16	2 ϕ 12+ 1 ϕ 16	2 ϕ 12+ 1 ϕ 16	ϕ 6/30
Trave R_30x30	30	30	4.1	2 ϕ 12	3 ϕ 12	2 ϕ 12	2 ϕ 12	ϕ 6/35
Trave ST_30x30	30	30	3.65	3 ϕ 12	2 ϕ 12+ 1 ϕ 16	3 ϕ 12	3 ϕ 12	ϕ 6/35
Trave X_70x20	70	20	3.65	4 ϕ 12	5 ϕ 12+ 1 ϕ 16	4 ϕ 12	4 ϕ 12	ϕ 6/35
Trave_K_30x20	30	20	4.6	2 ϕ 12+ 1 ϕ 16	2 ϕ 12+ 1 ϕ 16	2 ϕ 12+ 1 ϕ 16	2 ϕ 12+ 1 ϕ 16	ϕ 6/35
Trave collegamento tra setti 30x30	30	30	1.5	0	0	0	0	0

Stairwell and other walls

The plans show that the position of the stairwell is on one side of the building, on the outer side of the "main rectangular shape building", so that is it positioned off-center in Y direction (short side of the building), but it is quite centred in X direction (long side of the building). The stair and elevator well is made of 20 cm thick r.c. walls along the whole height of the building, but the basement, where some of the walls are 30 cm thick. The walls support the loads of the staircase and of the landings. The design project does not give any specification about the reinforcement of the walls. A site inspection with the covermeter has been done in order to check the presence of rebars and very little reinforcement was found: $\Phi 10/20$ cm vertically and $\Phi 10/70$ cm horizontally (see Table 3-1).

Beside the walls of the stairwell, two other walls are present in the basement. These two walls don't continue at upper floors, but support the load of some beams in the ground floor slab, as it can be seen in Figure 3-12.

Infills

All the infills of the outer walls are made of clay bricks, as also the internal partition walls. The material is not specified in the found documentation, but in the calculation report a load of 740 kg/m can be seen, applied to the external beams, that is called "tamponamento" or "muro", meaning infill or wall. This value of load could well correspond to a brick wall made of 13 cm + 8 cm bricks, with an interspace in between, the type of infill that was found in the design project of some other buildings nearby, constructed right after this one.

3.1.2. Knowledge level

When talking about existing buildings, the level of uncertainty is much higher than in new buildings. As already mentioned, often there is no documentation of the building and it is very difficult to know the quality of materials (concrete in the past was not standardised as today and it was made at the construction site, so that the properties were varying also from one day to the other), the construction details cannot be known precisely and also all the rebar cannot be checked. For this reason the building codes as the Eurocode 8-3, but also the Italian NTC 2018, use some safety factors that are connected to the knowledge level of the building.

For the case study RC building 1 a **knowledge level LC2** (NTC 2018) has been assumed, as the final project documentation (drawings and calculation report) has been found and some random elements have been checked (with covermeter and by checking dimensions and distances). The associated confidence factor is then **CF=1.2**. Especially non-linear analyses are going to be performed on the building in order to better understand the behaviour of this not fully regular building.

3.1.3. Materials

The only information about the used materials for the construction of the building are some writings on the project drawings. For the whole structure over the ground level, deformed reinforcing bars (with rib pattern) with σ_f= 2200 are prescribed, without even mentioning the measuring unit (that should be kg/cm^2). The prescribed concrete is R250. Just in the drawings of the foundations, an Aq50 steel is prescribed, probably smooth. This kind of steel was in use in years 1957 to 1972, when the LL.PP.n.1472/1957 was in force.

In order to find the mechanical characteristics of the used materials, data have been taken from literature (indirect sources).

Steel reinforcement

Mechanical characteristics of the steel have been taken from a paper (research of Reluis project): "Le caratteristiche meccaniche degli acciai impiegati nelle strutture in c.a. realizzate dal 1950 al 1980" [44], with the help of the connected software Stil (Figure 3-14). This program gives the minimum and maximum values of the mechanical characteristics of steel, the average and the

median, calculated on the numerous tests that have been performed. The needed input data are just the year(s) of construction (in this case from 1968 to 1970) and the type of rebar (in this case with rib pattern). Table 3-4 is extracted from the same paper and shows the evolution of the rebar classification in Italy.
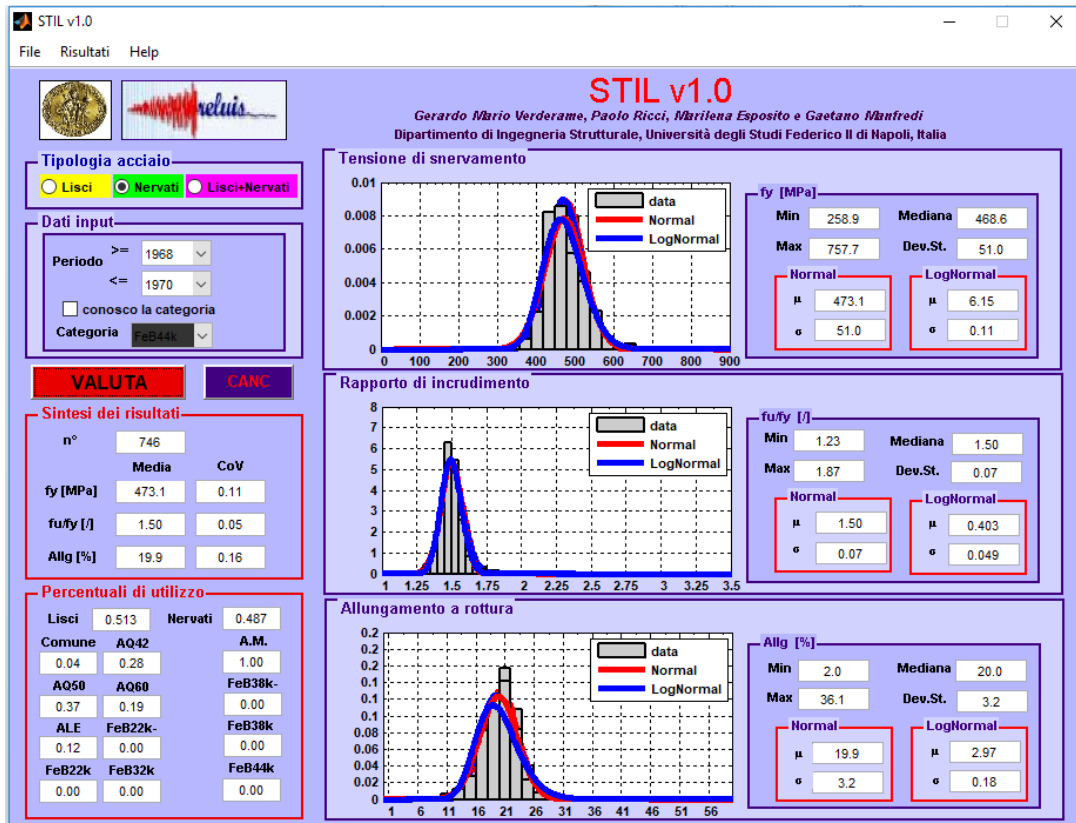
Figure 3-14: Graphical user interface of the software Stil [44] for the determination of the properties of reinforcing bars in existing r.c. structures in Italy.

For the RC building 1 the software gives the value of $f_y = 473.1\ Mpa$ (average yield stress) and, as the rib pattern was prescribed for the structure, that was not common at the time, a steel *Feb44k* is taken as a reference. This type of rebar is actually introduced later, with the D.M. 30/05/1972 [45], but it is the one that has the most similar properties to the values from Stil and to the values prescribed in the project of the building. Assumed that the specified tension $\sigma_f = 2200$ refers to the design value, the steel FeB44k used to have exactly the same design value for the steel not checked in the factory (see Figure 3-15).

Table 3-4: Evolution of reinforcing steel classification in Italian building codes [44].

Normativa	R.D.L n°2229/1939			LL.PP. n°1472/1957				D.M.30/05/1972					D.M. 30/05/1974			
Tipologia	liscio			liscio			a.m.	liscio		aderenza migliorata (a.m)			liscio		a.m.	
Denominazione	Dolce	Semi duro	Duro	Aq42	Aq50	Aq60		FeB22	FeB32	A38	A41	FeB44	FeB22	FeB32	FeB38	FeB44
Snervamento (kgf/mm²)	≥ 23	≥ 27	≥ 31	≥ 23	≥ 27	≥ 31	/	≥22	≥32	≥38	≥41	≥44	≥22	≥32	≥38	≥44
Rottura (kgf/mm²)	42-50	50-60	60-70	42 - 50	50 - 60	60-70	/	≥34	≥50	≥46	≥50	≥55	≥34	≥50	≥46	≥55
Allungamento (%)	≥ 20	≥ 16	≥ 14	≥ 20	≥ 16	≥ 14	≥ 12	≥24	≥23	≥14	≥14	≥12	≥24	≥23	≥14	≥12

The Circolare n. 1547 from 1965 actually defines the properties and the usage rules of reinforcing bars with rib pattern, by classifying them in two categories: normal (A category) and special (B category). Steel of A category should have a rupture elongation not less than 12%, for B category the limit is 10%. Regarding the design stress, it says that it should not be higher than 50%

of the yielding stress or 40% of the rupture stress and in any case it should not exceed the value of 2200 kg/cm² for A category and 2600 kg/cm² for B category. It is also required that this kind of steel is used with a concrete that have a strength of at least R250 for A category and R350 for B category [46]. This information, associated with the prescriptions in the project, show that probably the steel of A category has been used. The properties of this steel are very similar to the ones of FeB44k:

$$f_y = 2200/50\% = 4400 \; kg/cm^2 = 431 \; N/mm^2 \tag{3.1}$$
$$f_u = 2200/40\% = 5500 \; kg/cm^2 = 540 \; N/mm^2 \tag{3.2}$$

For further check, an excerpt of the Circolare n. 1472 del 23 maggio 1957 del Ministero dei Lavori Pubblici – Consiglio Superiore, that was in force at the construction time, is reported in Figure 3-16. Here the design stresses can be seen and it is written that for the reinforcing bars with rib pattern the design stress should not be higher than 50% of the yielding stress or 40% of the rupture stress and in any case it should not exceed the value of 2200 kg/cm². This shows that the steel that was prescribed for the case study building was the best available at the construction time, better than a smooth Aq60 and more similar to a FeB44k.

Figure 3-15: Excerpt from the code D.M. 30/05/1972 [45], where the design stresses of reinforcing bars are specified.

For existing buildings, the current Italian code specifies that the strength values should be determined as the average of the in situ tests, divided by the confidence factor. In this case, as there are no tests available, the characteristic values of the used steel are precautionary taken. The properties of steel FeB44k, according to D.M. 09/01/1996 [47], that regarding this has just different units of measurement compared to [45], are listed in Table 3-5:

Table 3-5: Mechanical properties of reinforcing steel FeB44k.

Characteristic yielding stress	**430 N/mm²**
Characteristic ultimate stress	540 N/mm²
Elongation A_s	12%

The characteristic values are then divided by the confidence factor CF=1.2 to be used as design values in the numerical model (Table 3-6):

Table 3-6: Design properties of reinforcing steel FeB44k.

Design yielding stress (f_y)	**430 N/mm² /1.2** = 358.33 N/mm²
Design ultimate stress (f_u)	540 N/mm² /1.2 = **450.00 N/mm²**
Elastic modulus (E)	**206,000 N/mm²**
Elastic deformation limit (ε_y)	358.33/206000= **0.00174**
Ultimate deformation (ε_u)	0.9*12%= **0.108**

CIRCOLARE n. 1472 in data 23 maggio 1957 del Ministero dei Lavori Pubblici - Consiglio Superiore.

Armatura delle strutture in cemento armato.

Per conoscenza e norma si trascrive il testo dell'articolo delle « Norme sui leganti idraulici », riguardante le armature delle strutture in cemento armato, in corso di elaborazione da parte della apposita Commissione Tecnica del Consiglio Nazionale delle Ricerche:

« Per tutte le armature delle strutture in cemento armato possono essere impiegati soltanto acciai Aq. 42, Aq. 50, Aq. 60 (UNI T. 743) sia in tondo, sia di forma speciale.

« Per gli acciai in tondo, la tensione non deve superare il 50% del carico di snervamento e, in ogni caso, i valori indicati nella tabella III.

Tabella III

Aq. 42	1400	Kg/cm²
Aq. 50	1600	Kg/cm² (¹)
Aq. 60	1800	Kg/cm² (¹)

« Per gli acciai di forma speciale ad aderenza migliorata (ritorti, sagomati, ecc.) la tensione ammissibile non deve superare il 50% del carico di snervamento nè il 40% del carico di rottura con la condizione che l'allungamento di rottura non sia inferiore al 12%.

« La tensione ammissibile per detti acciai non deve inoltre superare il valore di 2200 Kg/cm².

_____

(¹) Per diametri non superiori a 30 mm. Purchè si impieghi conglomerato almeno di classe R. 200 nel caso di sezione rettangolare, conglomerato almeno di classe R. 250 nel caso di sezione a T.

Figure 3-16: Excerpt of the Circolare n. 1472 del 23 maggio 1957 del Ministero dei Lavori Pubblici – Consiglio Superiore, where the design stresses of reinforcing bars used at that time are reported.

Concrete

As already mentioned, in the project documentation a concrete class R250 is prescribed, that corresponds to a R_{ck}= 25 N/mm². The properties of a concrete C20/25 are then considered.

Table 3-7: Mechanical properties of concrete C20/25.

Characteristic cylindric compression strength f_{ck}	**20.00 N/mm²**
Characteristic tensile strength f_{ctm}	2.21 N/mm²
Elastic modulus	29 962 N/mm²

The characteristics of concrete used in the numerical model are:

Table 3-8: Design properties of concrete C20/25.

Design compression strength (f_{ck})	**0.83*25 N/mm² /1.2** = 17.29 N/mm²
Elastic modulus (E_{cm})	**29,962 N/mm²**
Compression deformation (ε_{c1})	**17.29/(29962*0.75)= 0.00075**
Ultimate deformation (ε_{cu})	**0.002**

3.1.4. Loads

Characteristics of the construction site

- Site: Gorizia
- Geographic coordinates: longitude 13.622 °E, latitude 45.937 °N
- Height: 84 m a.s.l. (above sea level)
- Distance from the sea: about 18 km (as the crow flies)
- Ground type (for seismic load): B (deposits of very dense sand, gravel, or very stiff clay, at least several tens of metres in thickness, characterised by a gradual increase of mechanical properties with depth and by average shear wave velocity values $v_{s,30}$ between 360m/s and 800m/s)
- Topographic category: T1 (planar surface, isolated reliefs with average slope i≤15°)
- Roughness of the ground (for wind load): B (suburban zone)
- Zone for wind load: Zone 1 ($v_{b,0}$=25 m/s, a_0= 1000 m, k_r= 0.40)
- Zone for snow load: Zone II (q_{sk}= 1,00 kN/m² for a_s≤200 m)

Permanent and accidental loads

The dead loads of the beams and the columns are automatically considered by the program (SAP2000 is used), by taking into account a specific weight of reinforced concrete of 25 kN/m³. This represents the self-weight of structural members G_1, that for Italian building code is treated separately from the non-structural self-weight, G_2, that is specified in the following.

The non-structural self-weight of slabs and walls (infills of outer walls, partition walls and parapets of balconies), G_2, and imposed loads, Q, are specified in Table 3-9 and Table 3-10. According to the current code, accidental loads are Q_A=2.00 kN/m² in areas for domestic and residential activities and Q_C=4.00 kN/m² in areas where people may congregate (balconies, stairs, entrance at the ground floor).

The area loads from Table 3-10 are then transformed into linear loads applied to beams, based on their influence areas. The load due to the external infills (Table 3-9) is applied to the load-bearing beams by taking into account the presence of windows and balcony doors, so that the full value is taken just where no openings are present. Where there are openings, the percentage of the full infill is considered and uniformly distributed on the beam.

The specified loads are calculated based on the supposed flooring systems (compositions) but are calibrated on the loads that the designer used in the project of the building (in calculation report). In some cases the interpretation of the used loads in the calculation report is difficult, especially the splitting into permanent and imposed loads (e.g. for balconies), so that the total has been considered for comparison with the calculated loads.

For the partition walls, a distributed load of G_2=1.20 kN/m² has been considered all over the slabs, according to the current code, although it is unclear from the original calculation report if any load was considered for partitions and with which value.

Table 3-9: Dimensions and non-structural weight of walls.

Walls	thickness [m]	higth [m]	G_2 [kN/m]	G_2 [kN/m] (NTC 18 § 3.1.3)
External infills	0.3	2.85	7.41	
Partition walls	0.10	2.85	2.74	1.20
Parapet of balconies (lightened concrete)	0.08	1.00	0.8	
Parapet of balconies (hollow bricks)	0.13	1.00	1.04	

Table 3-10: Thickness and non-structural weight of slabs.

_____

Slabs	thickness [m]	G2 [kN/m²]	Q [kN/m²]	load in the project [kg/m²]
Celersap H20+3, basement ceiling	0.33	4.40	4.00	840
Bisap H20	0.30	3.02	2.00	450 - 500
H16.5 + 3.5 attic	0.30	3.70	2.00	
H16.5 balconies	0.25	2.87	4.00	600
H20 terraces	0.30	3.35	4.00	650
H16.5 + 3 attic's ceiling	0.195	2.15	0.50	450
Roof	0.090	1.85	-	

The loads due to the staircase and balconies are applied to the walls of the stairwell in the model. Because of the direction of those elements, some of the walls are loaded with just the self-weight.

Snow load
The snow seems not to be considered in the original project. According to the current code, for the roof shape of the case study building (hip roof with 14° slope), the snow load is:

$$qs = \mu i \cdot qsk \cdot CE \cdot Ct = 0.8 \cdot 1.00 \, kN/m2 \cdot 1 \cdot 1 = 0.8 \, kN/m2 \qquad (3.3)$$

Wind load
Wind load has not been considered in the original project, as just purely gravitational loads has been considered.

Also for this study the wind load is neglected, as seismic forces are considered and they are much higher than wind.

3.1.5. Structural regularity check
Nowadays a structure is considered well designed if it is hyperstatic and regular in plan and in elevation. A detailed check has been executed and here are summarized the main aspects that also help to understand the behaviour of the building subjected to lateral loads. As the basement cannot be considered a rigid box in this case study, it is considered together with all the other floors for the regularity check.

The distribution of masses is symmetric relatively to Y axis (short side), but is slightly asymmetric relatively to X axis (long side). The asymmetry is even higher in terms of stiffness, due to the stiff concrete walls of the stairwell.

Although most of the slabs don't have any concrete topping, as the whole structure is quite flexible (RC frames), the diaphragms are considered rigid in their plans and able to distribute horizontal actions among the vertical load-bearing elements proportionally to their stiffness.

Another positive quality of the case study building is that almost all the vertical load-bearing elements are continuous from the basement to the roof.

For the regularity of the building also the distribution of masses in elevation is important. In a regular building the mass of the individual storeys shall remain constant or reduce gradually (max 25%) from the base to the top of the building. In this case the mass of the 11th and 12th floor are much smaller than the previous floors (more than 25% - see Table 3-11), but at least the mass at the top is smaller and not larger.

Table 3-11: Mass regularity check.

Storey	Heigth	Mass (ton)	Mass variation
Basement	0	338.9	-
GF	3.1	278.9	-18%
1	6.2	282.2	1%
2	9.3	278.4	-1%
3	12.4	277.2	0%
4	15.5	274.1	-1%
5	18.6	272.0	-1%
6	21.7	271.4	0%
7	24.8	270.8	0%
8	27.9	270.8	0%
9	31	270.8	0%
10	34.1	300.6	11%
11	37.2	157.6	-48%
12	40.3	23.0	-85%

The evaluation of the variations of stiffness in elevation is made with the following procedure: the program SAP2000 and the numerical model of the building without infills are used. The concrete walls of the stairwell are modelled with shell elements (model N1 described in §4.2.1). The details of the model are described in §3.1.6. For each direction (X and Y) and for each floor, an arbitrary force F=1000 kN is applied to the centre of stiffness of the slab and the displacement (d) of the same joint is determined. This is repeated for each storey and for each main direction. Every time, all the storeys above the investigated one should freely move (no restrains), while all the storeys below the investigated one should remain fixed (all degrees of freedom are restrained). For each storey and each direction the stiffness can then be calculated as k= F/d. The obtained values are reported in Table 3-12. It can be noticed that the variation of stiffness between the ground floor and the basement in both directions exceeds 30%, that is the limit for the current code in order to be regular in elevation. Also at the last storey (that represents just the upper part of the stair-elevator-well that continues over the roof of the building) there is a noticeable stiffness variation. In X direction the stiffness increases of almost 60%, because there are no openings in the concrete wall, while in the same walls there are openings in the lower storeys. Despite these variations, the building could be considered almost regular in elevation, also because the concrete shear-walls are continuous from the basement to over the roof and, as it will be shown in the results of the analyses, they take a great part of seismic forces.

Table 3-12: Translational stiffness of each storey, computed in X and Y direction and calculation of variations compared to the storey below.

Application point	Direction	Force [kN]	Displacement of application point [m]	Stiffness K= F/d [kN/m]	Variation in X	Variation in Y
P0 (0 m)	x	1000	0.0001267	7892659.826	-	
	y	1000	0.0001781	5614823.133		-
P1 (3.1 m)	x	1000	0.0001887	5299417.064	-33%	
	y	1000	0.0002866	3489183.531		-38%
P2 (6.2 m)	x	1000	0.0001976	5060728.745	-5%	
	y	1000	0.0003081	3245699.448		-7%
P3 (9.3 m)	x	1000	0.0001996	5010020.04	-1%	
	y	1000	0.0003109	3216468.318		-1%

P4 (12.4 m)	x	1000	0.0002003	4992511.233	0%	
	y	1000	0.0003117	3208213.025		0%
P5 (15.5 m)	x	1000	0.0002021	4948045.522	-1%	
	y	1000	0.0003143	3181673.56		-1%
P6 (18.6 m)	x	1000	0.0002062	4849660.524	-2%	
	y	1000	0.0003173	3151591.554		-1%
P7 (21.7 m)	x	1000	0.0002059	4856726.566	0%	
	y	1000	0.0003177	3147623.544		0%
P8 (24.8 m)	x	1000	0.0002063	4847309.743	0%	
	y	1000	0.0003189	3135779.241		0%
P9 (27.9 m)	x	1000	0.0002049	4880429.478	1%	
	y	1000	0.0003192	3132832.08		0%
P10 (31.0 m)	x	1000	0.0002021	4948045.522	1%	
	y	1000	0.0003196	3128911.139		0%
P11 (34.1 m)	x	1000	0.0001964	5091649.695	3%	
	y	1000	0.0003208	3117206.983		0%
P12 (37.2 m)	x	1000	0.0001831	5461496.45	7%	
	y	1000	0.0003278	3050640.635		-2%
P13 (40.3 m)	x	1000	0.0001148	8710801.394	59%	
	y	1000	0.0003963	2523340.903		-17%

3.1.6. Numerical model of the structure

The building is modelled with the software SAP2000, by Computer and Structures inc., Berkeley, distributed in Italy by CSI-Italia s.r.l. [43]. SAP2000 is a software for the three dimensional static and dynamic finite element analysis and design of structures that adapts to every kind of structure.

Geometric model

As already mentioned, the used materials are concrete C20/25 and reinforcing steel FeB44k, modified with confidence factors for knowledge level LC2, as there were no available in-situ tests. The parameters that have not been specified, are taken with default values (specific weight, tangent modulus, Poisson's ratio).

After defining the materials, the sections should be defined. For the linear elements "Frame sections" are defined, for shell elements "Area sections" are defined. Beams and columns are modelled with frame elements, while for concrete walls two different models have been used. First they have been modelled with shell elements, then frame elements have been chosen, combined with rigid links, that are faster and easier to analyse and give very similar results.

In the frame sections of the columns also rebar is defined (material, concrete cover, spacing of stirrups and their diameters, number of bars and diameter – just one diameter can be set, so that equivalent diameters have been used). For the beams just the material, concrete cover and quantity of rebar at the endings of the beam (not number of bars or their diameter and no information about stirrups and about rebar along the beam) can be defined (Figure 3-17).
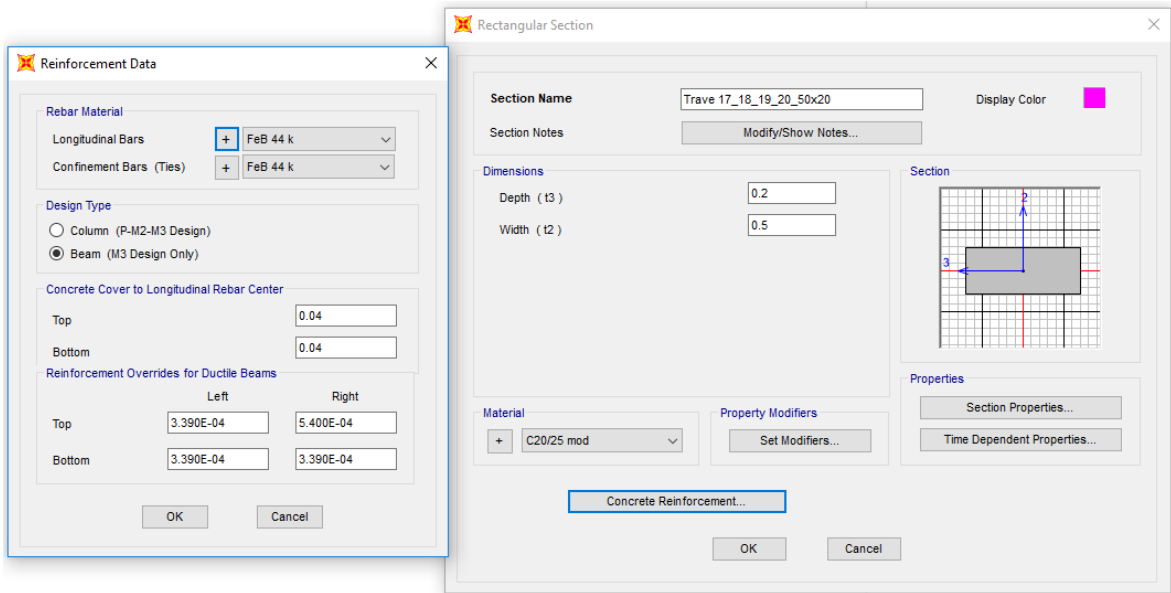
Figure 3-17: Example of definition of the section of a beam.
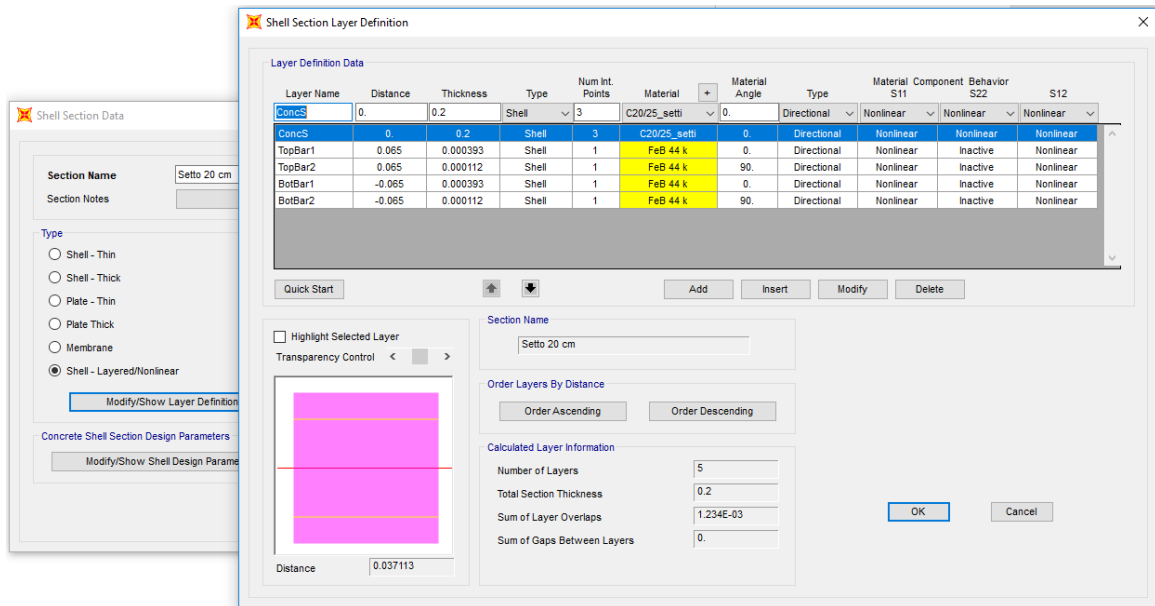
Figure 3-18: Example of definition of the section of non- linear shell elements for the shear-walls.

The Area sections for the shear-walls are defined as Shell-Layered/Nonlinear, as also non-linear analyses are performed. The definition is made for each layer, with the definition of materials and rebar, as shown in Figure 3-18.

In the numerical model the balconies have been considered just as masses (loads) applied to the beams that support them, in the same way as also all the slabs.

The stiffness given by the slabs has been modelled by assigning diaphragm constraints at each storey.

All the columns of the basement are fully restrained and no foundation is modelled.
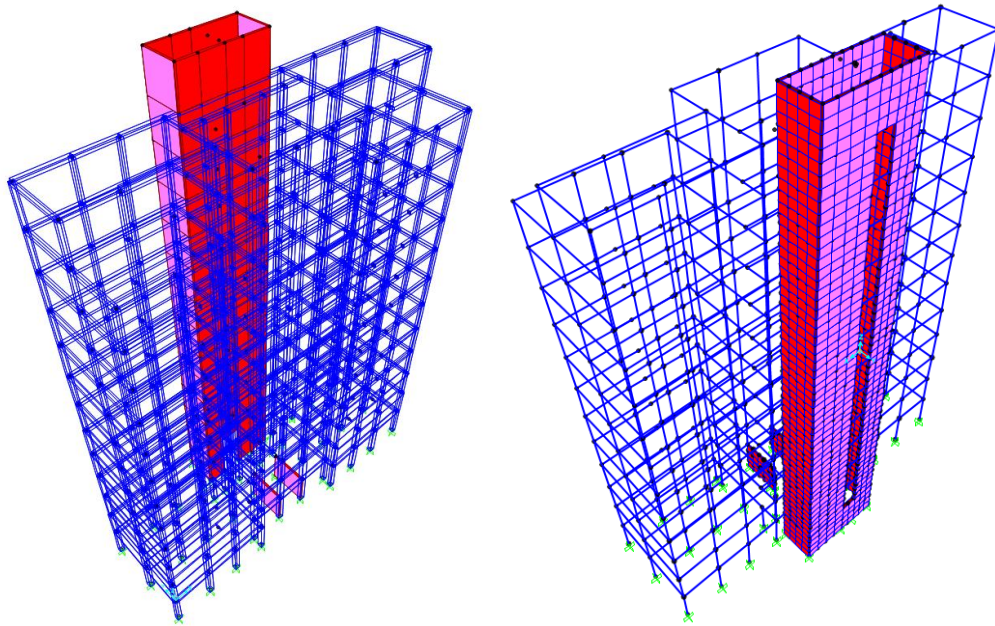
Figure 3-19: 3D view of the numerical model where the stairwell is modelled with shell elements. On the right side the analysis model, with the mesh of the shell elements can be seen.

As non-linear shell elements have no torsional stiffness in their plan, it is necessary to add some beam elements (30 cm x 30 cm) that start at the intersection of the beams with the walls and continue along the whole wall, at each storey, in order to transfer bending forces from beams to walls. The numerical model of the building, where shell elements have been used for the concrete walls, can be seen in Figure 3-19.

The infills of the outer walls have not been modelled for the main analyses. They have been modelled for a comparison that is described in §4.2.1.

Once the structure was modelled, the loads have been added, with the values described in §3.1.4. The mass source has been defined through the Specified Load Patterns.

Modelling of non-linearities

Non-linearities of structures can be dealt with in different ways. In this research study it has been chosen to use concentrated plasticity – all the non-linearities are concentrated in plastic hinges, while all the rest of the elements remain elastic.

When using this method, special attention should be paid to the definition of plastic hinges, that should represent the real non-linear behaviour of the whole element. In this model the length of the hinges is zero and they are positioned at the endings of each element (beam and column). No rigid zones have been applied in the nodes where more structural elements merge.

Basically, three/four types of hinges are applied to the model:

- Deformation controlled moment hinges (M3) to the endings of the beams (relative distance 0.1 and 0.9)
- Deformation controlled Interacting P-M2-M3 hinges to the endings of the columns (relative distance 0.1 and 0.9)
- Force controlled (brittle) shear hinges in the middle of beams and columns (just one direction for beams, two directions for columns).
- Fiber hinges in the shell elements of concrete walls (just in the models with shell elements)

The choice of positioning the shear hinges in the middle of the beams is due to the fact that the seismic action is considered to be prevalent. The shear force given by the vertical load is

considered neglectable, compared to the shear force caused by lateral forces and the positioning of the plastic hinge in the middle of the beam is considered acceptable.

(a) Deformation

(b) Deformation ratio

(c) Component or element deformation acceptance criteria
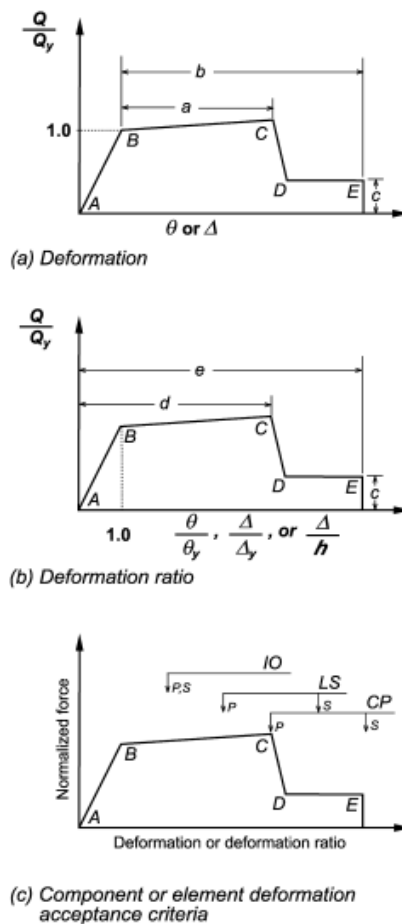
FIG. C7-3. Generalized Component Force-Deformation Relations for Depicting Modeling and Acceptance Criteria

Figure 3-20: Generalized Component Force-Deformation Relations for Depicting Modeling and Acceptance Criteria (ASCE/SEI 41-13).

As the properties of the hinges depend on the dimensions of the elements, on their internal forces (e.g. axial force) and on the quantity of rebar, they are different for almost each beam and column and a manual definition would be too time-consuming (in this model there are 3458 assigned hinges). Automatic hinges, defined by the program based on the American standard ASCE/SEI 41-13 (American Society of Civil Engineers: Seismic Evaluation and Retrofit of Existing Buildings) have been used for the moment (M3) and interacting (P-M2-M3) hinges. This standard defines the generalized force-deformation relations for r.c. elements, through diagrams depending on just three parameters: a, b and c (Figure 3-20). They are usually multilinear moment-rotation diagrams and characterize plastic hinges. For small deformations the hinge remains elastic (A-B), after the yielding (B), stiffness decreases to almost zero, although some hardening can be considered (B-C). Point C corresponds to the ultimate deformation, where the element can be considered damaged, but still has some resistance. After this point/deformation, a local rupture occurs and almost all resistance is lost (C-D). A residual resistance can be considered (c), until the deformation arrives to point E, that is the real collapse. The parameters a, b and c, that define the backbone curve of the plastic hinges, depend on the ratio of reinforcing steel area to gross concrete area, on the stirrup spacing, on the shear overstrength of the beam/column and, for columns also on the compression overstrength. Axial force in columns reduces their ductility. The parameters defining plastic hinges are evaluated through tables 10-7 (for beams) and 10-8 (for columns) of the standard (see Figure 3-21 and Figure 3-22). In the same tables also the acceptance criteria for three limit states are defined: Immediate Occupancy (IO), Life Safety (LS) and Collapse limit state (CP). No parameter in the tables indicates the ultimate

moment and the residual strength, but these two are always taken by default: the hardening is 10% and the residual strength is 20% of the yielding moment (parameter *c* in the tables). For the part C–D a constant difference of rotation between the two points is usually considered, equal to 0.0004.

Table 10-7. Modeling Parameters and Numerical Acceptance Criteria for Nonlinear Procedures—Reinforced Concrete Beams

			Modeling Parameters[a]			Acceptance Criteria[a]		
			Plastic Rotations Angle (radians)		Residual Strength Ratio	Plastic Rotations Angle (radians)		
						Performance Level		
Conditions			*a*	*b*	*c*	IO	LS	CP
Condition i. Beams controlled by flexure[b]								
$\dfrac{\rho - \rho'}{\rho_{bal}}$	Transverse reinforcement[c]	$\dfrac{V}{b_w d \sqrt{f_c'}}$ [d]						
≤0.0	C	≤3 (0.25)	0.025	0.05	0.2	0.010	0.025	0.05
≤0.0	C	≥6 (0.5)	0.02	0.04	0.2	0.005	0.02	0.04
≥0.5	C	≤3 (0.25)	0.02	0.03	0.2	0.005	0.02	0.03
≥0.5	C	≥6 (0.5)	0.015	0.02	0.2	0.005	0.015	0.02
≤0.0	NC	≤3 (0.25)	0.02	0.03	0.2	0.005	0.02	0.03
≤0.0	NC	≥6 (0.5)	0.01	0.015	0.2	0.0015	0.01	0.015
≥0.5	NC	≤3 (0.25)	0.01	0.015	0.2	0.005	0.01	0.015
≥0.5	NC	≥6 (0.5)	0.005	0.01	0.2	0.0015	0.005	0.01
Condition ii. Beams controlled by shear[b]								
Stirrup spacing ≤ *d*/2			0.0030	0.02	0.2	0.0015	0.01	0.02
Stirrup spacing > *d*/2			0.0030	0.01	0.2	0.0015	0.005	0.01
Condition iii. Beams controlled by inadequate development or splicing along the span[b]								
Stirrup spacing ≤ *d*/2			0.0030	0.02	0.0	0.0015	0.01	0.02
Stirrup spacing > *d*/2			0.0030	0.01	0.0	0.0015	0.005	0.01
Condition iv. Beams controlled by inadequate embedment into beam–column joint[b]								
			0.015	0.03	0.2	0.01	0.02	0.03

NOTE: f_c' in lb/in.[2] (MPa) units.
[a]Values between those listed in the table should be determined by linear interpolation.
[b]Where more than one of conditions i, ii, iii, and iv occur for a given component, use the minimum appropriate numerical value from the table.
[c]"C" and "NC" are abbreviations for conforming and nonconforming transverse reinforcement, respectively. Transverse reinforcement is conforming if, within the flexural plastic hinge region, hoops are spaced at ≤ *d*/3, and if, for components of moderate and high ductility demand, the strength provided by the hoops (V_s) is at least 3/4 of the design shear. Otherwise, the transverse reinforcement is considered nonconforming.
[d]*V* is the design shear force from NSP or NDP.

Figure 3-21: Table for the determination of modelling parameters and numerical acceptance criteria for nonlinear procedures – reinforced concrete beams (ASCE/SEI 41-13).

It should be noted that the plastic hinges are not necessarily symmetric, on the opposite, especially for existing buildings, that were designed for just gravitational loads, with different quantity of rebar at the bottom and the top of the beams, plastic hinges are usually not symmetric. This asymmetry is not visible in Figure 3-23, because the diagram is normalised to the positive and negative yield moments.

For the concrete walls of the stairwell the non-linearities are modelled with fiber hinges, that consider the constitutive laws of the materials defined in the 5 layers of the "Area section": 2 with rebar and 3 with unconfined concrete, as seen in Figure 3-18.

Also force-controlled brittle shear hinges can be defined automatically. They have been applied to the middle (relative distance 0.5) of the elements (beams -V2 and columns – V2 and V3) and the program automatically calculates the shear resistance of each element, without accounting for axial force. It has been defined that these hinges lose all load carrying capacity when maximum force is reached.

_____

Table 10-8. Modeling Parameters and Numerical Acceptance Criteria for Nonlinear Procedures—Reinforced Concrete Columns

			Modeling Parameters[a]			Acceptance Criteria[a]		
			Plastic Rotations Angle (radians)		Residual Strength Ratio	Plastic Rotations Angle (radians)		
						Performance Level		
Conditions			a	b	c	IO	LS	CP
Condition i.[b]								
$\dfrac{P}{A_g f_c'}$ [c]	$\rho = \dfrac{A_v}{b_w s}$							
≤0.1	≥0.006		0.035	0.060	0.2	0.005	0.045	0.060
≥0.6	≥0.006		0.010	0.010	0.0	0.003	0.009	0.010
≤0.1	=0.002		0.027	0.034	0.2	0.005	0.027	0.034
≥0.6	=0.002		0.005	0.005	0.0	0.002	0.004	0.005
Condition ii.[b]								
$\dfrac{P}{A_g f_c'}$ [c]	$\rho = \dfrac{A_v}{b_w s}$	$\dfrac{V}{b_w d \sqrt{f_c'}}$ [d]						
≤0.1	≥0.006	≤3 (0.25)	0.032	0.060	0.2	0.005	0.045	0.060
≤0.1	≥0.006	≥6 (0.5)	0.025	0.060	0.2	0.005	0.045	0.060
≥0.6	≥0.006	≤3 (0.25)	0.010	0.010	0.0	0.003	0.009	0.010
≥0.6	≥0.006	≥6 (0.5)	0.008	0.008	0.0	0.003	0.007	0.008
≤0.1	≤0.0005	≤3 (0.25)	0.012	0.012	0.2	0.005	0.010	0.012
≤0.1	≤0.0005	≥6 (0.5)	0.006	0.006	0.2	0.004	0.005	0.006
≥0.6	≤0.0005	≤3 (0.25)	0.004	0.004	0.0	0.002	0.003	0.004
≥0.6	≤0.0005	≥6 (0.5)	0.0	0.0	0.0	0.0	0.0	0.0
Condition iii.[b]								
$\dfrac{P}{A_g f_c'}$ [c]	$\rho = \dfrac{A_v}{b_w s}$							
≤0.1	≥0.006		0.0	0.060	0.0	0.0	0.045	0.060
≥0.6	≥0.006		0.0	0.008	0.0	0.0	0.007	0.008
≤0.1	≤0.0005		0.0	0.006	0.0	0.0	0.005	0.006
≥0.6	≤0.0005		0.0	0.0	0.0	0.0	0.0	0.0
Condition iv. Columns controlled by inadequate development or splicing along the clear height[b]								
$\dfrac{P}{A_g f_c'}$ [c]	$\rho = \dfrac{A_v}{b_w s}$							
≤0.1	≥0.006		0.0	0.060	0.4	0.0	0.045	0.060
≥0.6	≥0.006		0.0	0.008	0.4	0.0	0.007	0.008
≤0.1	≤0.0005		0.0	0.006	0.2	0.0	0.005	0.006
≥0.6	≤0.0005		0.0	0.0	0.0	0.0	0.0	0.0

NOTE: f_c' is in lb/in.² (MPa) units.
[a] Values between those listed in the table should be determined by linear interpolation.
[b] Refer to Section 10.4.2.2.2 for definition of conditions i, ii, and iii. Columns are considered to be controlled by inadequate development or splices where the calculated steel stress at the splice exceeds the steel stress specified by Eq. (10-2). Where more than one of conditions i, ii, iii, and iv occurs for a given component, use the minimum appropriate numerical value from the table.
[c] Where $P > 0.7 A_g f_c'$, the plastic rotation angles should be taken as zero for all performance levels unless the column has transverse reinforcement consisting of hoops with 135-degree hooks spaced at ≤ $d/3$ and the strength provided by the hoops (V_s) is at least 3/4 of the design shear. Axial load P should be based on the maximum expected axial loads caused by gravity and earthquake loads.
[d] V is the design shear force from NSP or NDP.

Figure 3-22: Table for the determination of modelling parameters and numerical acceptance criteria for nonlinear procedures – reinforced concrete columns (ASCE/SEI 41-13).

_____
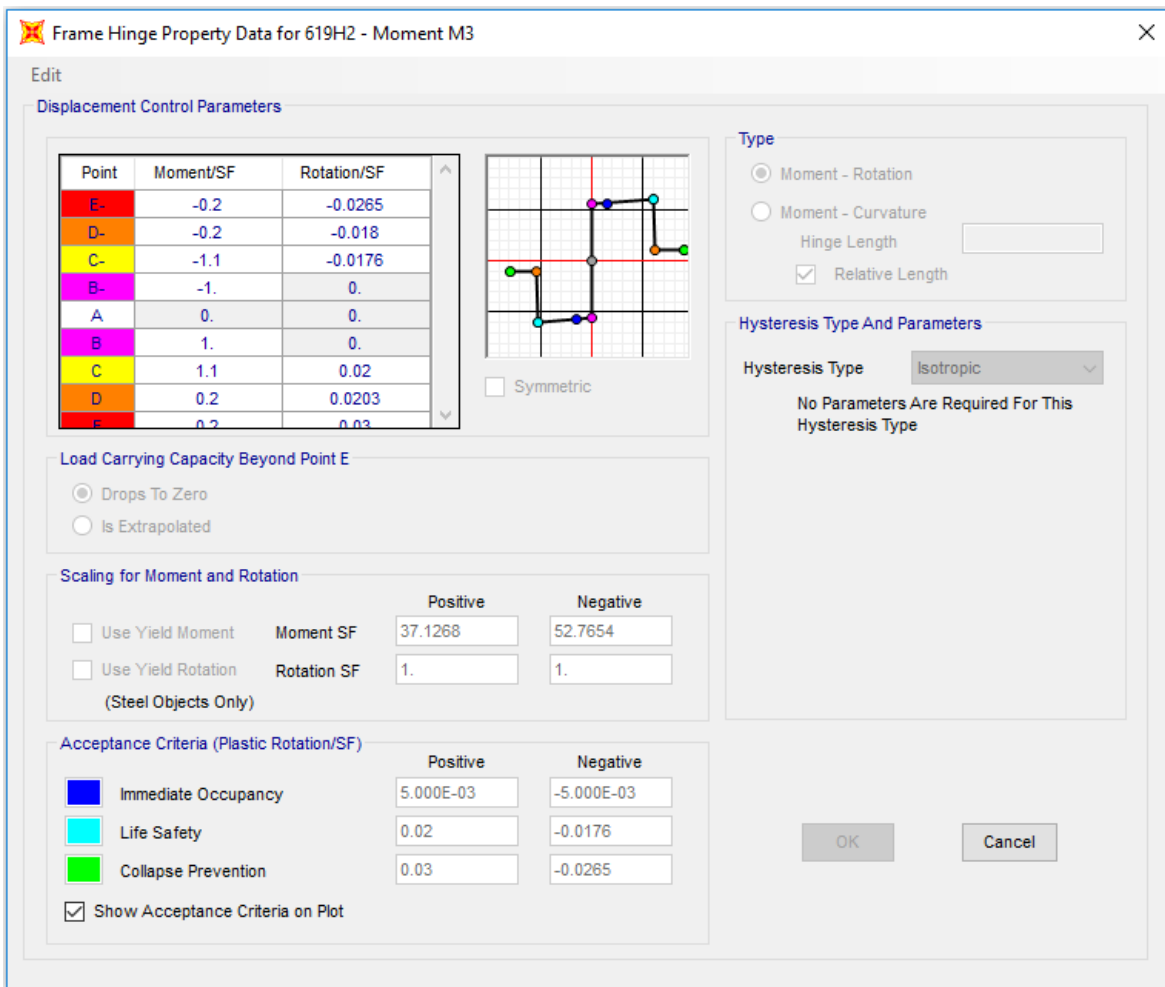
Figure 3-23: Properties of an automatically generated plastic hinge of a beam.

3.2. RC building 2

This second case study building has been built right after the first one, at the end of 60's - beginning of 70's and is part of a complex of buildings (building B in Figure 3-24). Building D in Figure 3-24 is another high-rise building, while building F-G is a connection building between D and B and has just two floors over the ground level. Under the yard in the middle of these buildings there is an underground garage with 80 parking places. Building B, the case study building (Figure 3-25), covers an area of 314 m² and has a basement, a ground floor and 10 other storeys. At the ground floor there are two shops, while at the upper storeys there are in total 38 flats: three or four at each storey from 1 to 9 and just 2 flats at the 10th floor, the attic.

Also for this second case study building the original project documentation has been found, kindly provided by a colleague of the structural engineer that designed it. Also in this case the handwritten calculation report, the final drawings and a testing certificate have been found.

As the construction period is the same of the RC building 1, the same standards has been used for the design (Regio Decreto 16/11/1939 n.2229 and updates – see §3.1).

3.2.1. *Geometry of the building and load-bearing elements*

The shape of the plan of the building is a T-shape. The "square shaped" part on one side of the building contains the staircase and the elevators, but also apartments. The stair-elevator-well is made of concrete walls, while the rest is made of concrete columns and beams, as also the whole "rectangle shaped" part of the building.
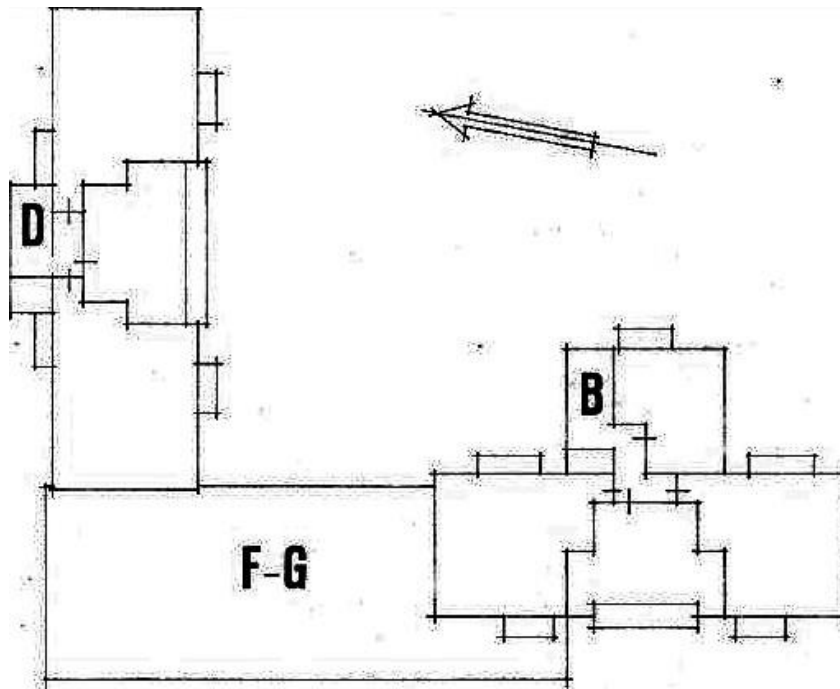
Figure 3-24: Scan of the original project documentation.

Figure 3-25: Side view of case study RC building 2.
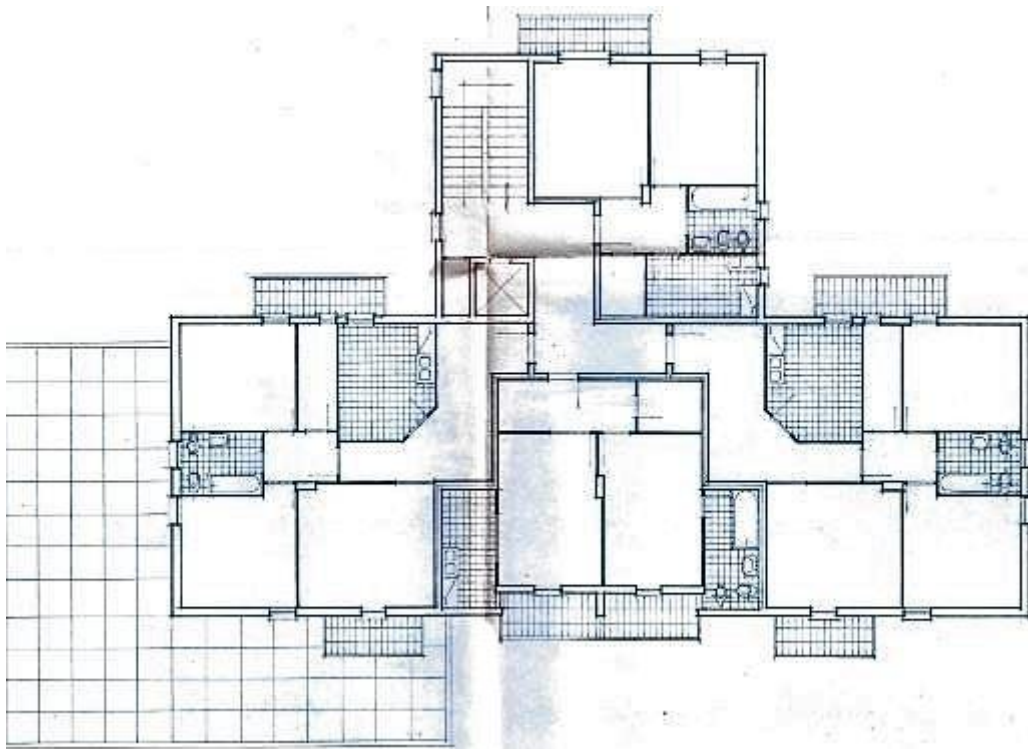
Figure 3-26: Plan of the typical storey.

The building F-G from Figure 3-24 is not spaced from building B, but each building has its own columns, so that the columns are doubled at the first two storeys on that side of the building and the interaction can be neglected. The total height of building B is about 40 m. The plan of a typical storey can be seen in Figure 3-26 and the main façade in Figure 3-27.

The structure of the building is a R.C. frame, the most common construction system of the time when it was built, for buildings higher than three storeys. The stair-elevator-well and the outer walls of the basement are made of concrete walls.

The foundation is very similar to the one of RC building 1 and is composed of concrete plinths and reverse T foundation beams (110 to 130 cm wide and 40 cm deep).

The load-bearing beams of the upper floors are all hidden in the thickness of the slabs.

The roof of the rectangular part of the building is a hip roof, supported by the perimetral beams and by two trusses. The roof of the square part (stair-elevator-well) is a lean-o roof, supported by perimetral beams and an intermediate beam.

Also for this case-study building, as for the first one, the design of concrete walls was not specified in the project documentation and the quantity of rebar is unknown. Moreover, it is not clear if the columns of the ground floor continue through the basement to the foundation or they just settle in the concrete walls of the basement.

The quantity of rebar has been investigated with a covermeter, at the ground floor. In a wall of the stairwell two directions of reinforcing bars have been found: vertically $\phi 10/40$ cm and horizontally $\phi 8/50$ cm. It has not been possible to access the basement of building B, so no tests have been made there, but there was the opportunity to access the basement of building D (Figure 3-24), so some tests have been made there. As the two buildings are part of the same complex, it can be supposed that the construction system is the same. Here in the concrete walls of the basement a similar quantity of rebar has been found as in the walls of the ground floor of building B. Unfortunately, as it was not possible to access the private cellars, it has not been possible to discover if the rebars of the columns of the ground floor were continuing to the foundation through the walls. The assumption of columns embedded in the top of concrete walls has then been made.
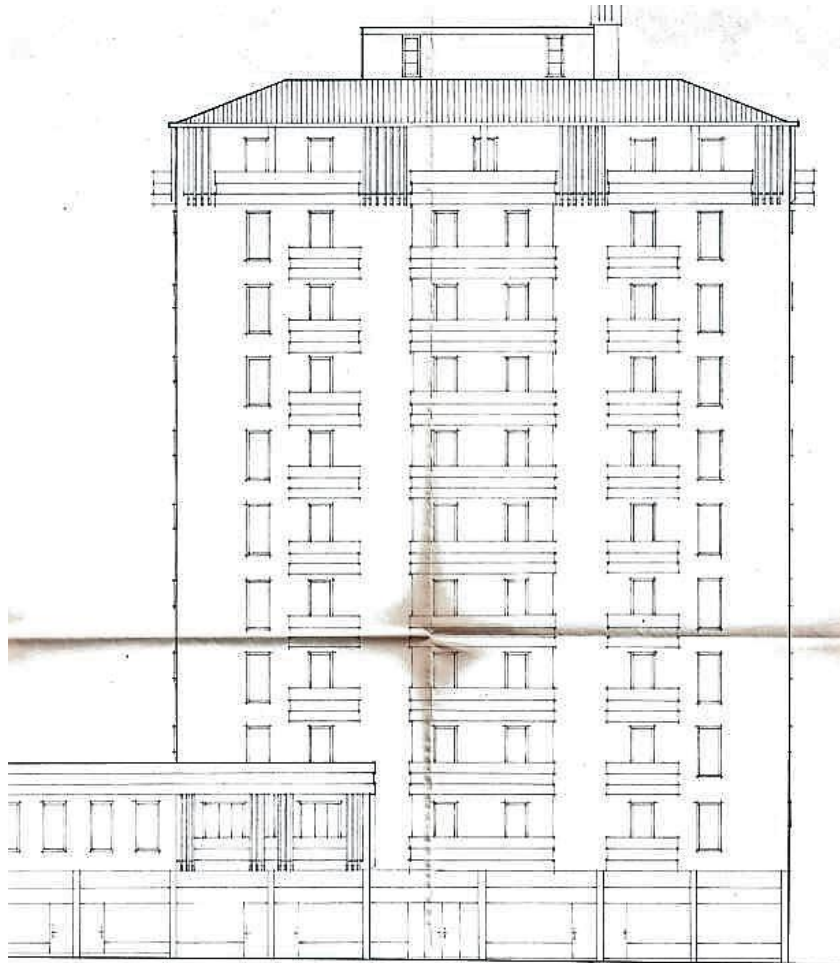
Figure 3-27: Scan of the drawing of the main façade.

Also two columns have been tested with the covermeter (nr. 11 and nr. 17 – see Figure 3-28), in order to check if the rebars were the same specified in the project documentation and it has been confirmed.

Concrete walls

The concrete walls of the basement are 30 cm thick and are supported by the reverse T foundation beams. They support two beams and the slab of the ground floor. As it has been detected with the covermeter, their reinforcement is made of $\phi 8/50$ cm horizontally and $\phi 10/40$ cm vertically.

The concrete walls of the stair-elevator-well are continuous over the whole height of the building and they are 30 cm thick in the basement and 20 cm thick at all the other storeys. The quantity of rebar seems to remain the same in all walls at all storeys.

Columns

There are 27 columns at the ground floor and first floor (Figure 3-28). In the upper floors the number reduces to 24, as a part of the building does not continue over the first floor. The dimension of the columns, that are rectangular, decreases along the height of the building.

Beams

The beams (and thus the frames) are oriented mainly in X direction (the long side of the building) and are hidden in the thickness of the slabs. In the other direction there are just some secondary beams, with curb function, although some of them also support some parts of the slab.
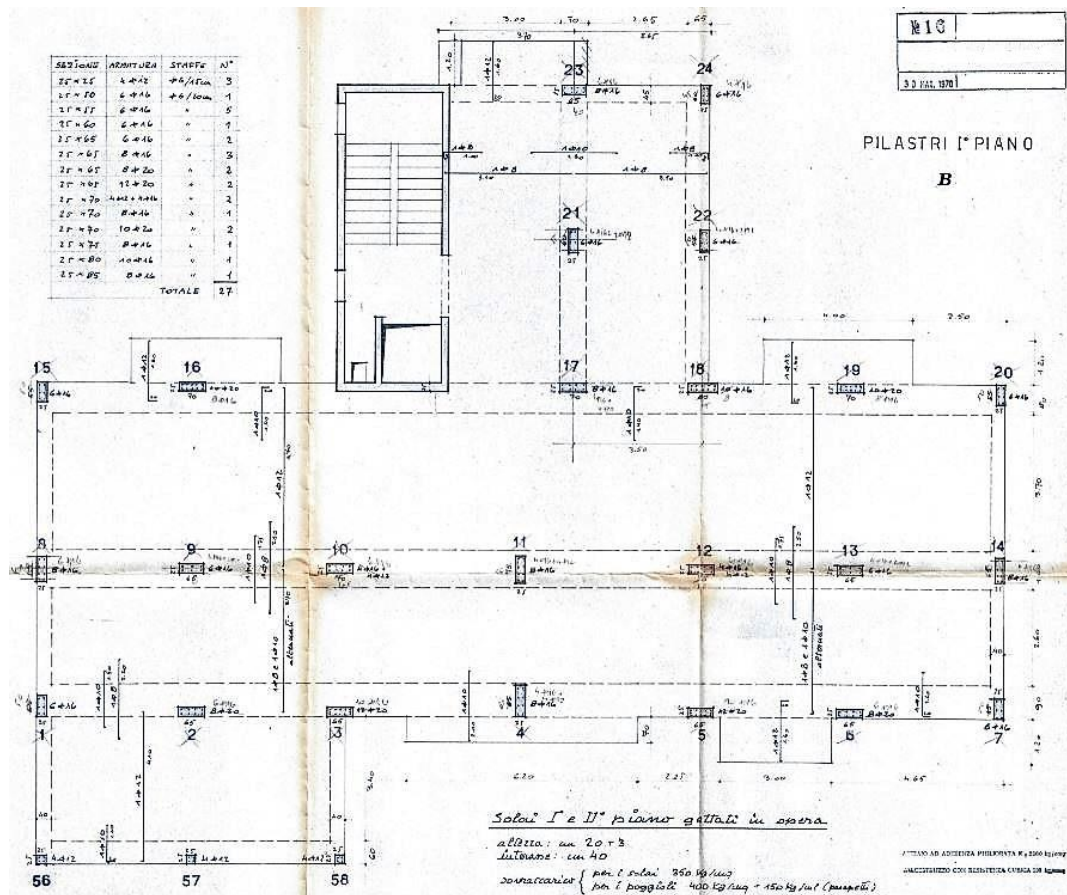
Figure 3-28: Plan of the first floor – numbering of columns.

The typical dimension of the beams is 100 x 23 cm, and they go over six spans of different length, but symmetrical with respect to the midpoint (Figure 3-29). The diameter and the number of reinforcing bars vary along the length of the beam. The stirrups are disposed with the same spacing along the whole beam: $\phi 6/30$ cm.
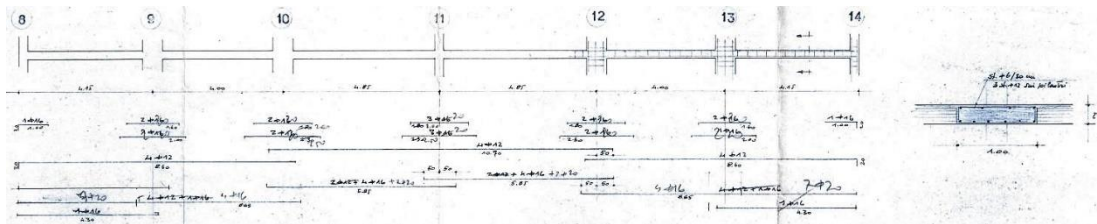
Figure 3-29: Original drawing of the main beam of the typical storey (1st to 9th).

The type of reinforcing is quite different from the one that was common at the construction time. Usually the bent bars were used to pass from the bottom to the top of the beam, with a slope of 45°, where the moment was passing from positive to negative. They were used also to resist shear forces at the supports, but in this structure there are almost no bent bars.

The perimetral beams of the last storey are meant to transmit vertical loads from the roof to the structure below and to connect the roof to the slab of the attic, that has the function of a tie-beam. This slab is hang to the ridge of the roof as no internal column has been constructed in the attic.

Trusses

The hip roof needs four hip rafters. These rafters are supported at one end by the perimetral beams and columns at the corners of the building, but they need another support at the other end.

This support is given by two r.c. trusses. The tie-rod (bottom chord) of the truss (Figure 3-30) is made of a beam that is slightly deeper than the thickness of the slab and it is hang to the apex of the truss through the king-post (15 cm x 15 cm).
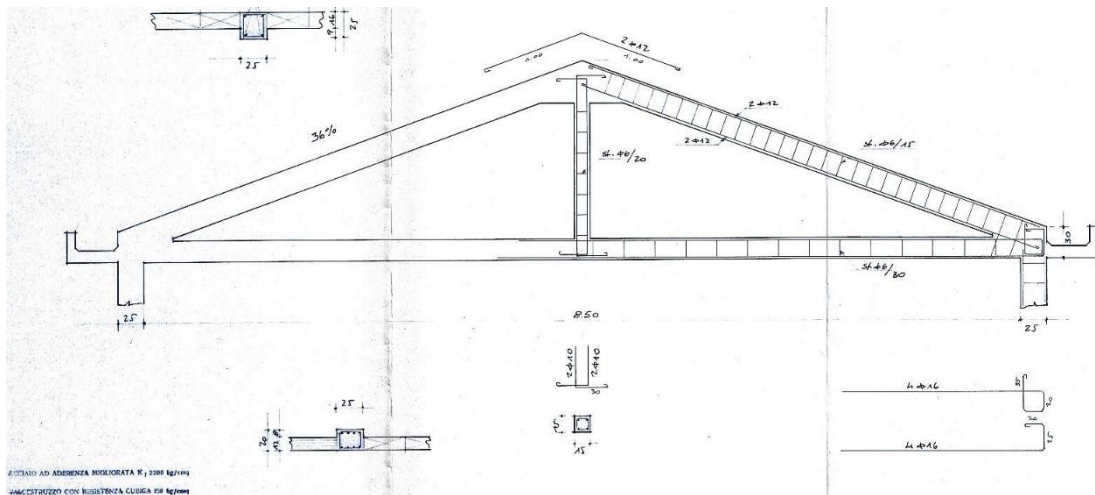
Figure 3-30: Original drawing of the trusses.

Slabs

There are more than one type of slab in the building. The slab of the ground floor is a kind of hollow pot slab made of prestresses joists and concrete blocks, with spacing 65 cm. The height of the slab is 23 cm (20 + 3).

The slabs of other storeys are cast in place hollow pot slabs with clay hollow bricks spaced 40 cm. The thickness of these slabs is also 23 cm (20 cm of bricks and 3 cm of concrete topping). Just the reinforcing bars are different from storey to storey. The slabs of the staircase are of the same kind, but they are thinner. Their total thickness is 20 cm (16 + 4).

The slab of the last floor of the square part of the building (walkable loft) is made with the same type of slab, 23 cm thick. The slab of the last floor of the rectangular part of the building (not walkable loft), that has the function of tie-rod for the roof, is a cast in place slab with clay blocks 12 cm high and spaced 50 cm. The total thickness is 12 cm, as the concrete topping is not present.

The roof is made of reinforced masonry, 16 cm thick and with 60 cm spacing. There is no concrete topping.

3.2.2. Knowledge level

For this case study building, as for the first one, project documentation has been found. It has been verified the correspondence with reality. The majority of construction details are represented in the original drawings. Materials are known from the prescriptions and tests in the project documentation. Some rebars have been verified with a covermeter. Although no in-situ tests have been performed, it has been assumed a knowledge level LC2, corresponding to a confidence factor CF= 1.2.

The current Italian building code defines the use of the confidence factors. When linear analyses with behaviour factor q or non-linear analyses are performed, for ductile elements the properties of existing materials should be divided by CF, for brittle elements the properties should be divided both by CF and by the partial factor for the material (Circolare 21 gennaio 2019, n. 7 CSLLPP, §C8.7.2.2).

3.2.3. Materials

The information about the materials used for the construction of the building are collected form the project documentation. From the technical report and from the drawings it can be learned that the two materials used are:

- Concrete with cubic strength 250 kg/cm²;
- Steel bars with rib pattern with $\sigma_f = 2200$ kg/cm².

The use of the prescribed materials in the real construction is confirmed by the test certificate that has been found together with the project documentation.

Concrete

The prescribed concrete has a cubic strength equal to 250 kg/cm², that corresponds to a current class C20/25, with a cubic strength of 25 N/mm². As there are no experimental values available (the code suggests using the average value of experimental tests), the properties are calculated starting from the characteristic values of the material (precautionary).

The properties of this concrete are divided by the confidence factor CF=1.2 for ductile elements:

Table 3-13: Design properties of concrete for ductile elements.

Design compression strength (f_{ck})	**20 N/mm² /1.2** = 16.67 N/mm²
Elastic modulus (E_{cm})	**29,962 N/mm²**

In case of brittle elements, the strength to use is:

Table 3-14: Design properties of concrete for brittle elements.

Design compression strength (f_{ck})	**20 N/mm² /1.2/ 1.5** = 11.11 N/mm²

Steel reinforcement

The prescribed reinforcing bars have rib pattern and are made of steel with a design strength of $\sigma_f = 2200$ kg/cm². The data reported in the testing certificate of the building show that the elastic modulus is equal to 2 000 000 kg/cm².

The same sources have been used to obtain more information about the steel, as for RC building 1 (see §3.1.3). This steel corresponds to a FeB44k (introduced later with D.M. 30/05/1972).

The properties that are used in the numerical model are the following:

Table 3-15: Design properties of reinforcing steel for ductile elements.

Design yielding stress (f_y)	**430 N/mm² /1.2** = 358.33 N/mm²
Design ultimate stress (f_u)	540 N/mm² /1.2 = **450.00 N/mm²**
Elastic modulus (E)	**206,000 N/mm²**

In case of brittle elements, the strength to use is:

Table 3-16: Design properties of reinforcing steel for brittle elements.

Design yielding stress (f_y)	**430 N/mm² /1.2/ 1.15** = 311.59 N/mm²
Design ultimate stress (f_u)	540 N/mm² /1.2/ 1.15 = **391.30 N/mm²**

3.2.4. *Loads*

Characteristics of the construction site

- Site: Gorizia
- Geographic coordinates: longitude 13.622 °E, latitude 45.937 °N
- Higth: 84 m a.s.l. (above sea level)
- Distance from the sea: about 18 km (as the crow flies)

- Ground type (for seismic load): B (deposits of very dense sand, gravel, or very stiff clay, at least several tens of metres in thickness, characterised by a gradual increase of mechanical properties with depth and by average shear wave velocity values $v_{s,30}$ between 360m/s and 800m/s)
- Topographic category: T1 (planar surface, isolated reliefs with average slope i≤15°)

Permanent and accidental loads

The dead loads of the beams and the columns are automatically considered by the program (SAP2000 is used), by taking into account a specific weight of reinforced concrete of 25 kN/m³. This represents the self-weight of structural members G_1, that for Italian building code is treated separately from the non-structural self-weight, G_2, that is specified in the following.

Structural (G_1), non-structural permanent loads (G_2) of slabs and walls and imposed loads (Q) are specified in Table 3-17 and Table 3-18.

The load due to the external infills (Table 3-17) is applied with its full value to the load-bearing beams without taking into account the presence of openings. The area loads from Table 3-18 are then transformed into linear loads applied to beams, based on their influence areas.

Table 3-17: Dimensions and load of the external infills.

Walls	height [m]	G_2 [kN/m²]	G_2 [kN/m]
External infills	2.70	2.70	7.30

Table 3-18: Loads from the slabs.

Slabs	G1 [kN/m²]	G2 [kN/m²]	Q [kN/m²]
Slab of ground floor	2.50	2.00	4.00
Slab of floors 1 to 10	2.40	1.60	2.00
Slab of balconies	2.40	2.60	4.00
Slab of not-walkable loft	1.10	0.50	0.00
Slab of walkable loft	2.40	1.60	2.00
Roof	1.60	1.20	0.50
Stairs	-	4.00	4.00

The permanent loads of the slabs have been extracted from the project documentation. The imposed loads have been precautionary chosen according to the current code. In the original project the imposed load of the slab of the ground floor and of balconies was slightly lower (300 kg/m²) and no permanent non-structural load was considered for the roof.

For the partition walls no load is considered, as in the original project and calculation report is also not considered or considered together with the imposed load, without explicitly mentioning it.

The loads due to the staircase and balconies are applied to the walls of the stairwell in the model.

Snow and wind load

As the seismic vulnerability is investigated and wind and snow load are not supposed to occur simultaneously with earthquake, these two loads are not considered.

3.2.5. *Structural regularity check*

The building satisfies almost all the requirements for regularity in plan. The plan is compact, although the stiffness distribution is not really symmetric with respect to the two main directions, as the "square shaped" part is eccentric and even more are eccentric the concrete walls of the stairwell. The slabs have concrete topping and can be considered rigid in their plan.

The regularity in elevation is not really satisfied. Some of the vertical load-bearing elements do not continue to the roof (because the attic misses the internal columns), the mass and the stiffness has some higher values of variation (over the code limit od 25% for masses and 30% for stiffness). The variations are reported in Table 3-19 and Table 3-20. The masses of the storeys have been extracted from the file "model.out", that is created from SAP2000 during the analyses. The stiffness of each storey in each direction has been computed as already described for RC building 1 (see §3.1.5) on the numerical model without infills.

Table 3-19: List of the storeys and variations in their mass.

Mass of storeys and variations			
Storey	Height [m]	Mass [ton]	Variation
GF	0,67	506,8	-
1	3,82	324,5	-36,0%
2	6,97	319,3	-1,6%
3	10,12	309,8	-3,0%
4	13,27	306,6	-1,0%
5	16,42	303,4	-1,0%
6	19,57	300,9	-0,8%
7	22,72	299,4	-0,5%
8	25,87	298,6	-0,3%
9	29,02	297,8	-0,3%
10	32,17	307,3	3,2%
Loft	35,26	180,8	-41,2%
Roof	37,56	31,7	-82,5%

The noticeable increment of stiffness at the roof is due to the minor height of the storey.

Table 3-20: List of the storeys and variations of their stiffness in the two main directions.

Stiffness of storeys and variations					
Storey	Height [m]	Kx [kN/m]	Ky [kN/m]	ΔKx	ΔKy
GF	0,67	39301997	21588946	-	-
1	3,82	2389486	2370792	-93,9%	-89,0%
2	6,97	2168727	2107038	-9,2%	-11,1%
3	10,12	2066116	2009646	-4,7%	-4,6%
4	13,27	1916810	1882885	-7,2%	-6,3%
5	16,42	1774623	1731302	-7,4%	-8,1%
6	19,57	1623904	1599488	-8,5%	-7,6%
7	22,72	1542496	1539883	-5,0%	-3,7%
8	25,87	1480385	1495663	-4,0%	-2,9%
9	29,02	1466491	1495886	-0,9%	0,0%
10	32,17	1397038	1429184	-4,7%	-4,5%

Loft	35,26	1388503	1456452	-0,6%	1,9%
Roof	37,56	5104645	2426595	267,6%	66,6%

The building cannot be considered regular in plan nor in elevation.

3.2.6. Numerical model of the structure

The building is modelled with the software SAP2000, by Computer and Structures inc., Berkeley, distributed in Italy by CSI-Italia s.r.l. [43].

Geometric model

First the materials have been defined, by modifying the strength value of the default materials from SAP2000 libraries, according to the ones specified in §3.2.3.

The second step is the definition of frame sections, with their rebar. For this case study building no shell elements have been used. Then the numerical model has been built. The eccentricities inside the structure (e.g. the beams connected to one end of the wall) are modelled with the introduction of rigid links that connect the ends of the elements. These rigid links have been created by defining a section of 0.2 m x 0.2 m and assigning them a material with a very high elasticity modulus and zero specific weight.

All the columns and walls (also modelled with frame elements) are fully restrained at the base and the foundations are not modelled. The stiffness of the slabs in their plan has been represented by the introduction of rigid diaphragms at each storey. The numerical model can be seen in Figure 3-31.

The loads have been assigned as specified in §3.2.4.

Modelling of non-linearities

Also for this case-study building the non-linearities have been considered through the concentrated plasticity method – all the non-linearities are concentrated in plastic hinges, while all the rest of the elements remain elastic.

When using this method, special attention should be paid to the definition of plastic hinges, that should represent the real non-linear behaviour of the whole element. In this model the length of the hinges is zero and they are positioned at the endings of each element (beam and column). No rigid zones have been applied in the nodes where more structural elements merge.

Basically, three types of hinges are applied to the model:

- Deformation controlled moment hinges (M3) to the endings of the beams (relative distance 0 and 1)
- Deformation controlled Interacting P-M2-M3 hinges to the endings of the columns and concrete walls (relative distance 0 and 1)
- Force controlled (brittle) shear hinges in the middle of beams and columns (just one direction for beams, two directions for columns).

For moment (M3) and interacting hinges (P-M2-M3), the automatic hinges have been used, calculated by SAP2000 based on ASCE 41-13 as described in §3.1.6. As already done for RC building 1, also for RC building 2 the shear forces in the beams due to the vertical loads are considered neglectable compared to the shear forces due to the seismic action, so that placing the shear hinges in the middle of the beams is considered acceptable.
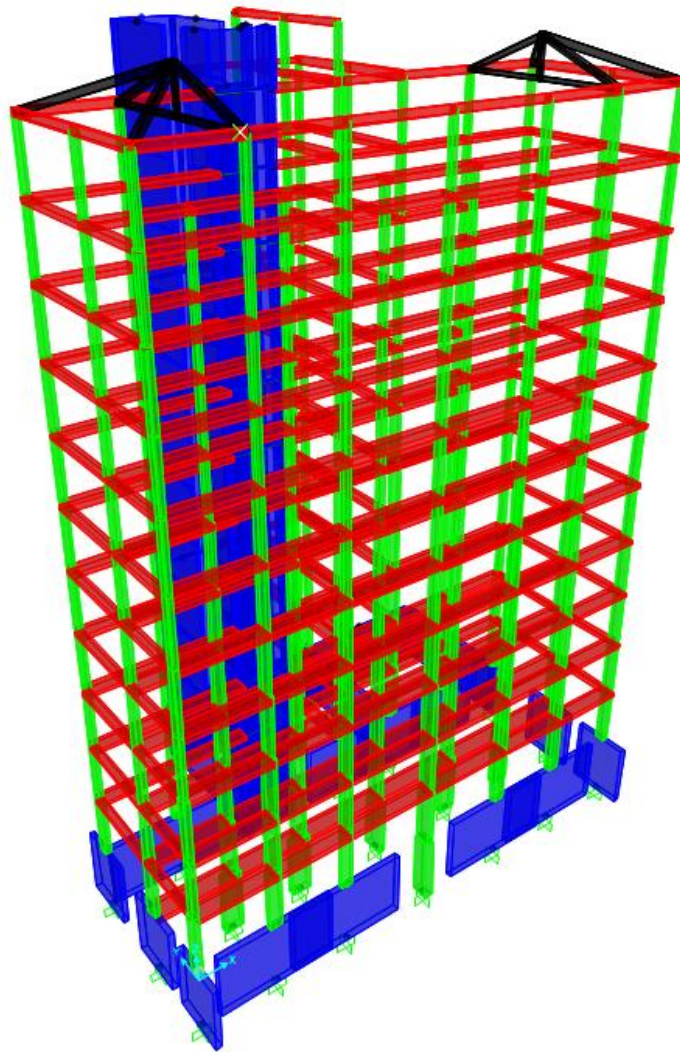
Figure 3-31: Numerical model of the building.
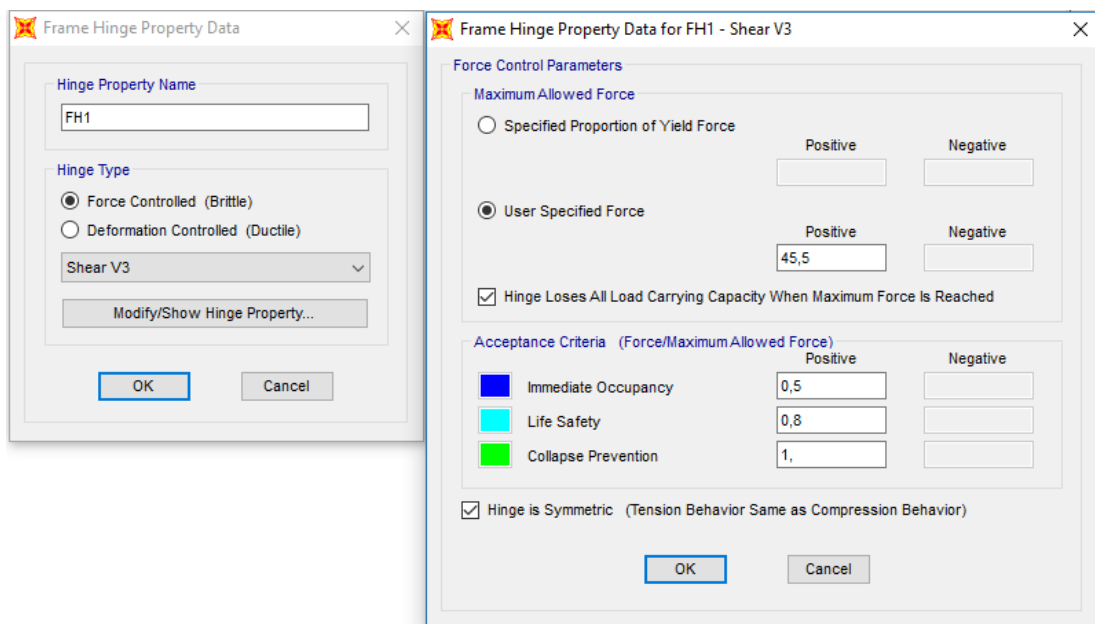
Figure 3-32: Screenshot of the window in SAP2000 for the definition of the brittle shear hinge.

For the force controlled brittle shear hinges, the shear resistance has been defined manually for each different section in the model. After the imposed ultimate shear strength the hinge loses all

load carrying capacity. The acceptance criteria have been chosen by the default of the program: 0.5 for Immediate Occupancy, 0.8 for Life Safety and 1 for Collapse Prevention (Figure 3-32).

For the calculation of the shear strength the Italian code NTC 2018 and the Circolare 21 gennaio 2019, n. 7 CSLLPP have been used. For beams and columns the shear strength has been calculated as prescribed at §4.1.2.3.5.2 of NTC 2018 for elements with shear reinforcement and §4.1.2.3.5.1 for elements without shear reinforcement. The maximum between the two results has been considered.

For the concrete walls also the specific prescription for walls (§7.4.4.5.1 of NTC 2018) has been considered, where three more checks need to be satisfied, that are not needed for beams and columns: shear-compression of the concrete web, shear-tension of the rebar in the web, sliding in dissipative zones. As the final values are very similar to the ones calculated according to §4.1.2.3.5.2, the latest have been used.

3.3. Masonry building A

This case study building is the oldest building of the group of buildings composing the City hall of Gorizia (Figure 3-33). A project has been run by the Department of Engineering and Architecture of the University of Trieste and the Municipality of Gorizia, in which seismic vulnerability of these buildings and retrofitting solutions have been evaluated. The project was comprising all the buildings of the city hall, but here just two are considered: building A and a part of building C. In order to achieve a knowledge level LC2, many in situ tests have been performed, as very few documentations have been found, especially for some buildings.

Building A is the oldest building of this complex and is called Palazzo Attems Santa Croce. It was built in 1740 as the first important project of the architect Nicolò Pacassi from Gorizia (that was afterwards the court architect of the queen Maria Teresa) and then completely modified after 1823 with a more neoclassical style. It became the headquarter of the City hall in 1908. After the First World War the front façade has been renewed with major modifications. After that also the entrance hall has been renewed with new claddings in aurisina and travertine stone and the creation of new accesses to the stairwell. At the entrance and at the exit (on the courtyard) there are, strangely, two different dates indicating the year of reconstruction: 1827 at the entrance and 1829 and the exit. The building is protected by the Ministry of Cultural Heritage, Activities and Tourism. In the back side of the buildings there is a huge garden/courtyard, probably designed at the same time of the building, also visible in Figure 3-34. Some information about the building has been extracted from "Il palazzo municipal di Gorizia – Palazzo Attems Santa Croce", by Stefano Cosma, Annibel Cunoldi Attems, Diego Kuzmin, Francesco Marani, Emanuela Uccello, Tanja Curto – Edizioni della Laguna.

The plan of Palazzo Attems Santa Croce is divided in three parts, symmetric with respect to the symmetry axis of the fasade: two side bands with four rooms each and a central part that continues from the front façade to the back façade. At the ground floor the central part connects the Piazza del Municipio (in the past Piazzetta Santa Croce) with the courtyard, used as a public passage until the 30's. The central part of the building was originally without partitions also at the first floor, but then Ritter, who bought the building in 1823, divided it with in two rooms, as it is today. The partition wall is fortunately thin, about 15 cm, so that it does not affect the structural behaviour of the building.

The modifications of the building that can be important from a structural point of view are the openings. From some drawings that have been found, it can be noticed that many openings changed their position over the years. The openings that have been closed, usually result in a clay brick part of walls, while the original structure of the building was stone masonry. Analysing the building in detail it can be noticed that it has been modified in many parts. One example is the ceiling of a part of the basement of the building, that is made of reinforced concrete beams, for sure built in the latest years. The slabs are probably original, while the roof has been for sure reconstructed, as it has clay hollow bricks in the last layer.
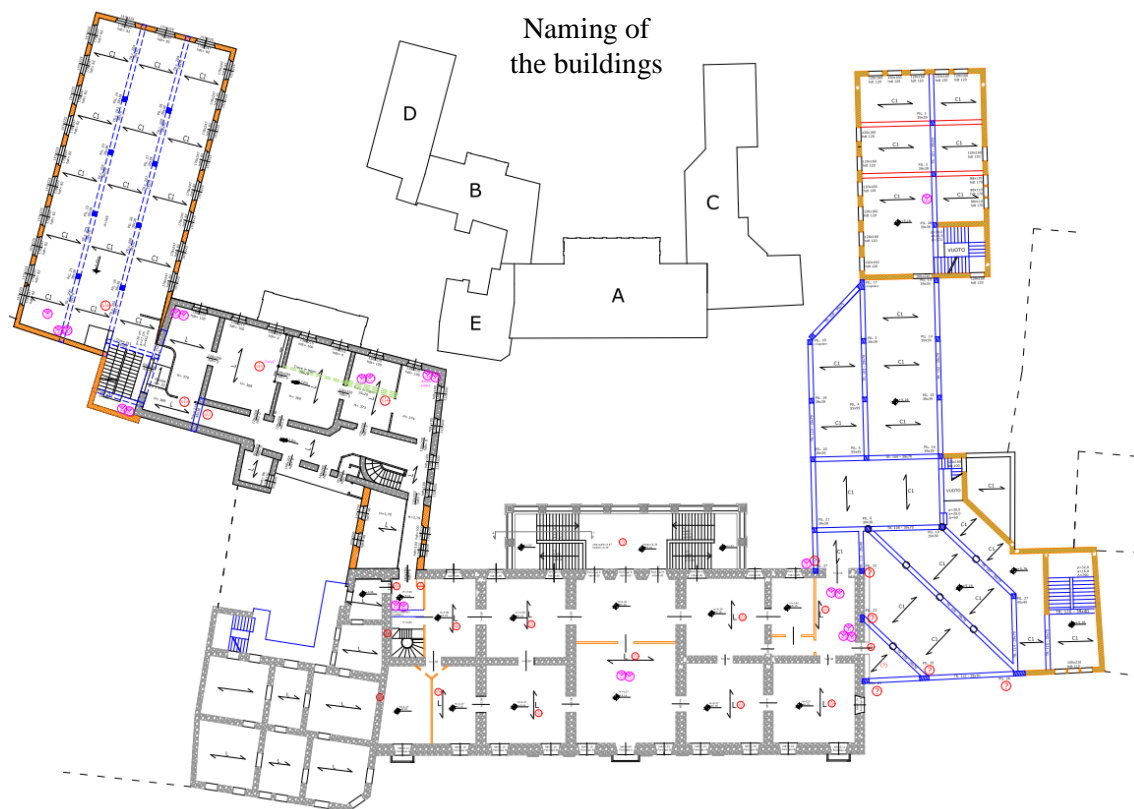
Figure 3-33: Plan of the 1st floor of the buildings of the City hall of Gorizia.

Figure 3-34: Image from the land registry of 1966.

A photo of the main façade of the building is visible in Figure 3-35.

Figure 3-35: Photo of the main façade of Palazzo Attems Santa Croce (Piazza del Municipio, 1).

3.3.1. Geometry of the building and load-bearing elements

In order to better identify the parts of the building, names have been given to the rooms. "A" indicates building A, the first number is the number of the storey (0 is the basement, 1 the ground floor, 2 the first floor and 3 the second floor), the last two numbers indicate the number of the room in the given storey. The plans of the storeys of the building are shown in Figure 3-36, Figure 3-37, Figure 3-38 and Figure 3-39. The geometry of the building has been accurately measured and reported in Autocad by the working team of the project with the City hall of Gorizia.
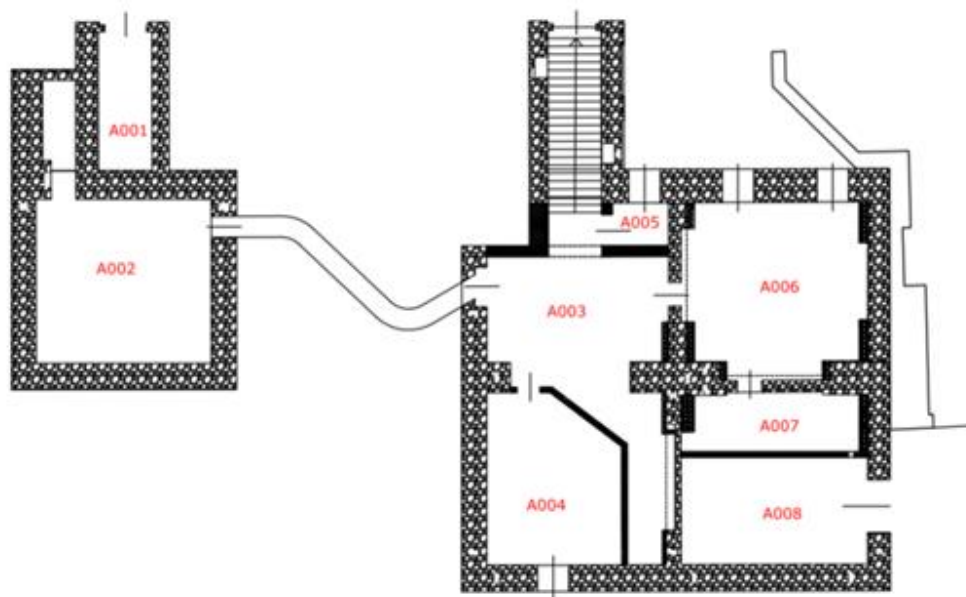
Figure 3-36: Rooms in the basement.
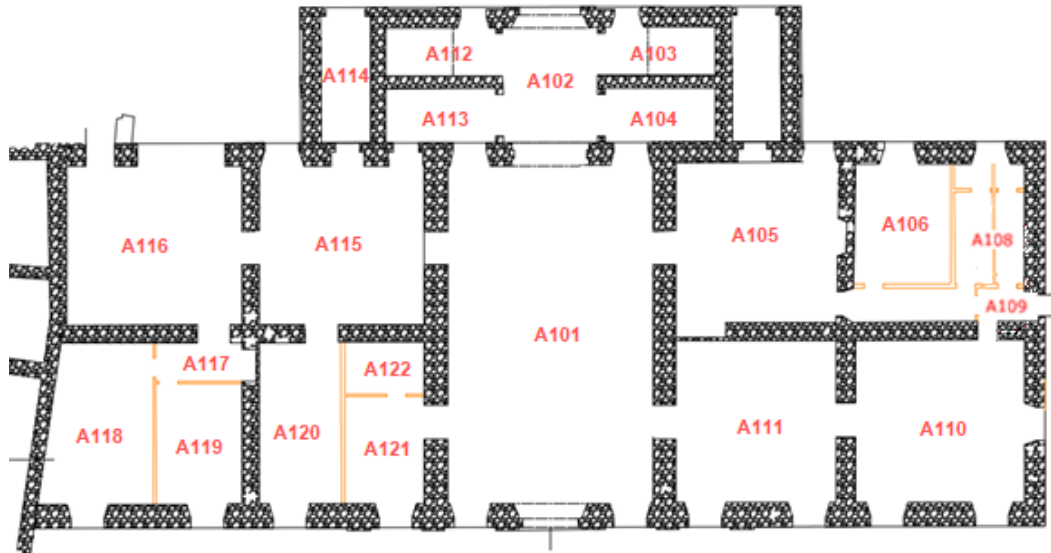
Figure 3-37: Rooms at the ground floor.

The building can be divided in two parts: the main rectangular part and the lodge with the stairwell, facing the courtyard. Both parts have three storeys above the ground level. The basement is 3.90 m deep under the ground level and it doesn't cover the whole plan of the building, so that the foundations are at different levels. The larger side of the basement (on the right side in the plans) is characterized by cross vaults. The other part of the basement is accessible from a narrow tunnel (80-93 cm).

The slab of the central part of the ground floor (entrance hall) has a slight slope (1.80%), so that the stairwell is 0.25 m higher than the entrance. The side bands have a constant level, higher than the entrance hall.
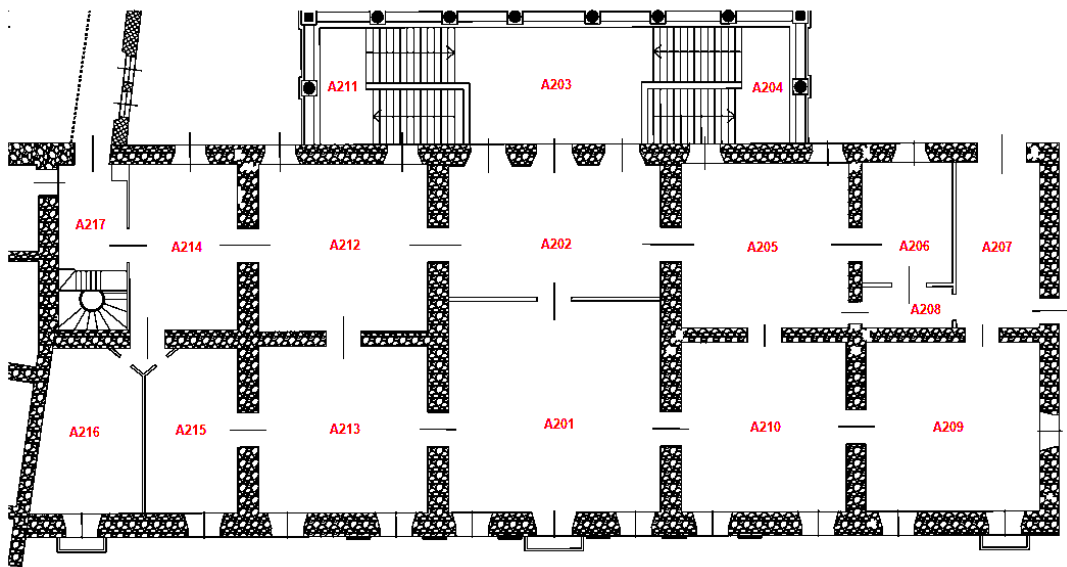
Figure 3-38: Rooms at the first floor.

The lintels are made of different materials. In the internal openings (that have rectangular shape) they seem to be wooden, while in the external openings there are brick arches. Some internal lintels are also made of concrete, where some reconstruction has been done (e.g. between rooms A115 and A116). Another type of lintel that has been found is a HEA 200 steel profile (at the border with building C).
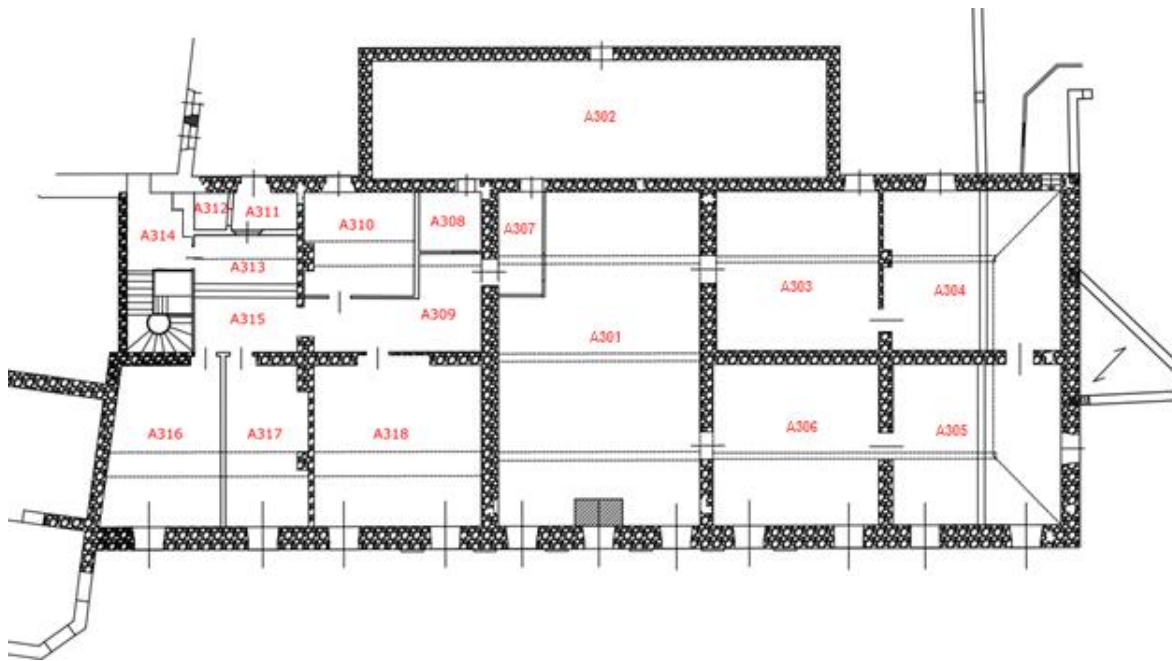
Figure 3-39: Rooms at the second floor (loft).

In the numerical model, all the internal lintels have been considered as wooden, all the external as brick arches, exception made for the openings on the borders with building B and C, where steel lintels have been considered.

The slabs are made of wood and in the side bands at all storeys they have the direction of the short side of the building (Y). Here the dimensions of the joists is 15 x 20 cm. Just in the rooms A206 (with A207 and A208) and A209 have been detected 2 larger beams (20 x 25.5 cm) in the other direction that seem to support the joists. In the central part of the building the joists have the direction of the long side of the building (X). In the ceiling of the room A213 a double direction structure has been observed: beams approximately 20 x 25 cm in Y direction and approximately 10 x 10 cm in X direction. In the lodge the central slab is a cross vault, while the rooms A103 and A112 have a barrel vault, as also A114 and the symmetrical one (access to the basement).

3.3.2. Knowledge level

The building has been accurately measured, investigated and subjected to many in situ tests in order to reach a knowledge level LC2.

The in situ tests that have been executed are: video-endoscopies, plaster removal, two flat jack tests (one in the side wall of the lodge – room A114, the other in an internal clay brick wall in the left wing of the building at the ground floor). Also sclerometric surveys have been performed on the mortar in many parts of the building. In the following figures the location of the tests can be seen. Video-endoscopies are denoted by the letter E, plaster removal by Sa and the flat jack tests by Mp.
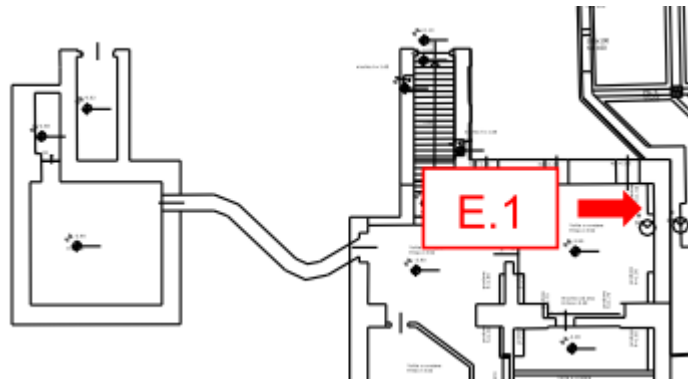
Figure 3-40: Location of video-endoscopies in the basement of building A.
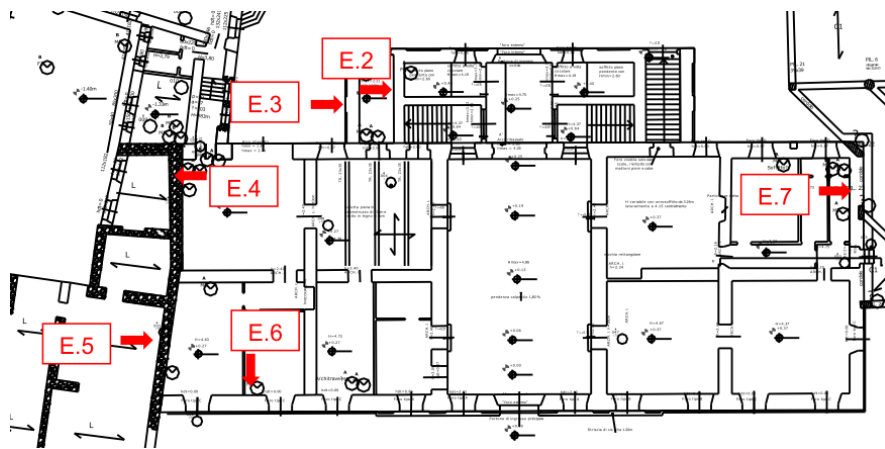
Figure 3-41: Location of video-endoscopies at the ground floor of building A.
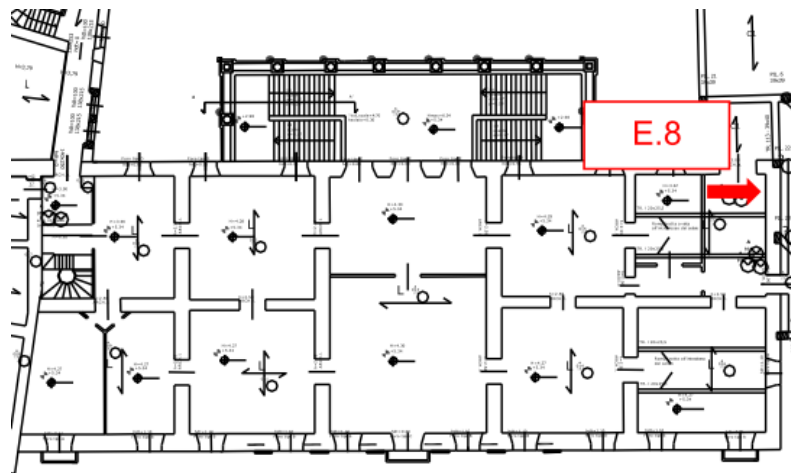
Figure 3-42: Location of video-endoscopies at the first floor of building A.
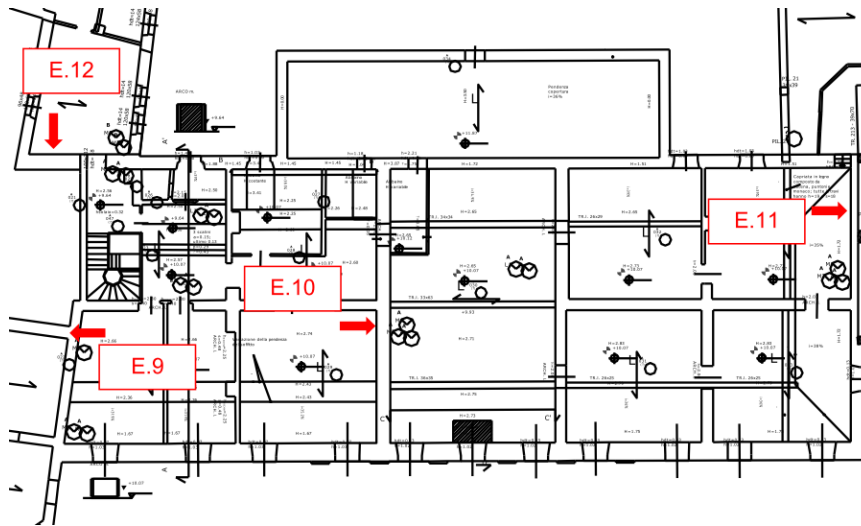
Figure 3-43: Location of video-endoscopies at the second floor of building A.
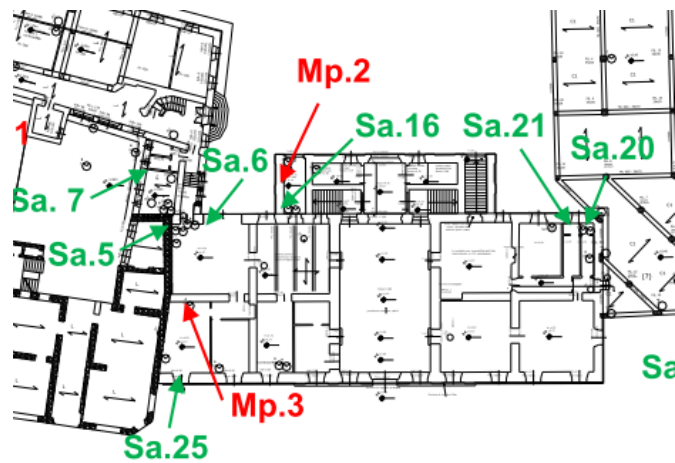
Figure 3-44: Location of plaster removal (Sa) and flat jack tests (Mp) at the ground floor of building A.
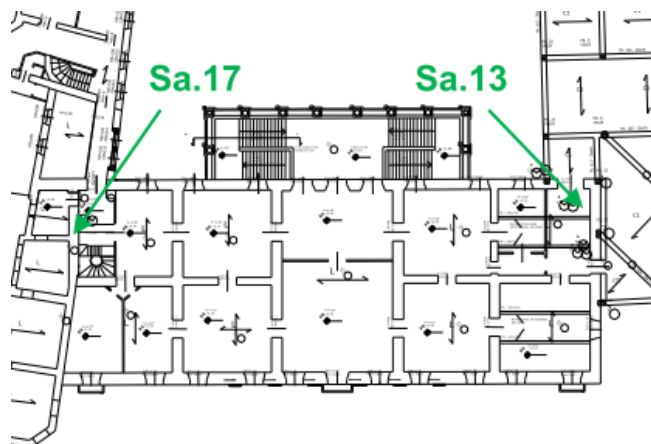
Figure 3-45: Location of plaster removal (Sa) at the first floor of building A.
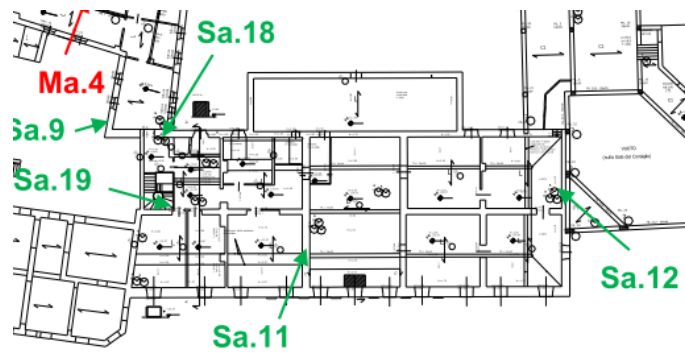
Figure 3-46: Location of plaster removal (Sa) at the second floor of building A.

3.3.3. *Materials*

The structure of the building is made of stone masonry and in some parts clay brick masonry.

The results of the flat jack test Mp2 are reported in Table 3-21. The test has been performed on masonry made of irregular stone with ashlars of different sizes.

Table 3-21: Results of the flat jack test made on stone masonry.

Test	Present stress		Ultimate stress		Elastic moduli			Poisson	
					E1	E2	G	ν	
	[bar]	[daN/cm^2]	[bar]	[daN/cm^2]	[N/mm^2]	[N/mm^2]	[N/mm^2]	from	to
MP2	4,0	2,99	11	8,23	742	741	296,4	0,23	0,32

The results of the flat jack test Mp3 are reported in Table 3-22.

Table 3-22: Results of the flat jack test made on clay brick masonry.

Test	Present stress		Ultimate stress		Elastic moduli			Poisson	
					E1	E2	G	ν	
	[bar]	[daN/cm^2]	[bar]	[daN/cm^2]	[N/mm^2]	[N/mm^2]	[N/mm^2]	from	to
MP3	3,0	2,24	20	14,98	1283	1320	513,2	0,12	0,33

The 12 plaster removals on building A show:

Sa.5: Stone masonry of various compact size, without noticeable voids and stone masonry of various sizes with common solid brick battens.

Sa.6: Common solid brick masonry (25 x 12 x 6h)

Sa.11: Stone masonry of various sizes packed in bulk

Sa.12: Stone masonry of various sizes packed in bulk with brick inserts

Sa.13: Stone masonry and pebbles of various sizes packed in bulk

Sa.16: Stone masonry of various sizes packed in bulk and with no bond at the corner

Sa.17: Solid brick masonry (25 x 3h)

Sa.18: Common solid brick masonry and hollow clay brick masonry, weak bond at the corner

Sa.19: Stone masonry of various sizes packed in bulk with brick inserts; stone masonry of various sizes packed in bulk – presence of reinforced plaster (net Ø4/10x10), weak bond at the corner

Sa.20: Common brick masonry; stone masonry of various sizes packed in bulk with brick inserts and no bonds

Sa.21: No perimetral curb; the beams enter the façade masonry for more than 30 cm.

Sa.25: Stone masonry of various sizes packed in bulk and brick arch lintel (common bricks 25 x 13 x 3 h).

The main material is clearly stone masonry of various sizes packed in bulk and the bond at the corners are usually missing or very weak. Some walls and part of walls are made of common solid clay bricks. These two types of materials will be considered in the numerical model.

Also the video-endoscopies show that the masonry varies from compact stone (mainly in the basement and at the ground floor, but also at the first floor), to a stone masonry with less or more noticeable voids between ashlars (from ground floor up). During the tests E.4, E.7 and E.11 clay brick masonry has been detected in some parts of the wall (in two whytes walls), but they will not be considered in the numerical model as in the test point E.4 the clay bricks are positioned on the side of building B (also because from plastr removal Sa.5 it can be seen that the wall of building A is made of stone masonry), the test point E.7 could be right where an old opening has been walled up, while at E.11 the load-bearing structure is made of stone masonry.

The results of sclerometric tests on the mortar are reported in Table 3-23 and they are compatible with the values that define the mechanical characteristics of masonries in Table C8.5.I of Circolare 21 gennaio 2019, n. 7 CSLLPP, where mortar with moderate characteristics is considered (average compression strength between 0.7 N/mm^2 and 1.5 N/mm^2). The strength found with the test Scl.3 is slightly lower than 0.7 N/mm^2 but however all the properties from the table are lowered based on the results of the flat jack tests.

Table 3-23: Results of the sclerometric tests on the mortar (class 0 corresponds to a very soft mortar with hardness <15).

Building	Material	Test	Zone	Average Rebound Index	Class	Cubic compression strength
			[-]	[IR]		[N/mm^2]
A – G.F.	Stone masonry	Scl.2	Mp.2	13.5	0	0.74
A – G.F.	Clay brick masonry	Scl.3	Mp.3	12.2	0	0.60

Stone masonry

The masonry is visible in some parts of the building, mainly in the basement and in the loft of the lodge. Masonry from the basement is shown in Figure 3-47. If we consider the type of masonries from Table C8.5.I of Circolare 21 gennaio 2019, n. 7 CSLLPP, there are some descriptions that could correspond to the visible masonry, but when comparing the strength values with the ones obtained with the flat jack test, just the worse masonry could be chosen, even by lowering its strength and elastic modulus. For the numerical model is thus considered a "Random rubble masonry (pebbles, erratic and irregular stones)", with knowledge level LC2, of which elastic moduli (E, G) and strength are lowered to meet the results from the flat jack test (the results found with the flat jack test are considered as average values). The characteristics are reported in Table 3-24. Shear behaviour is based on Turnsek-Cacovic.

Just for the stone columns of the lodge a better masonry has been considered ("Split stone masonry with good texture"), with the values from the code table and always a knowledge level LC2.

Figure 3-47: Stone masonry visible in the room A004 of the basement.

Table 3-24: Mechanical characteristics of stone masonry used in the numerical model.

E [N/mm²]	G [N/mm²]	w [kN/m³]	fm [N/cm²]	fhm [N/cm²]	fk [N/cm²]	τ [N/cm²]	CF
741	296	19	82.3	61.7	57.6	2.5	1.2

Clay brick masonry

In a similar way as for the stone masonry, the material "Solid brick masonry with lime mortar" has been considered from the code table and then the values of elastic moduli (E,G) and the strength have been lowered to meet the results obtained by the flat jack test. The values are reported in Table 3-25. In this case, shear behaviour is based on Mohr-Coulomb.

Table 3-25: Mechanical characteristics of brick masonry used in the numerical model.

E [N/mm²]	G [N/mm²]	w [kN/m³]	fm [N/cm²]	fk [N/cm²]	fb [N/mm²]	fv0 [N/cm²]	CF
1300	513	18	150	105	7.5	9	1.2

3.3.4. Loads

The self-weight of the walls is automatically computed by the program, based on the specified specific weight. The additional loads that have been used in the model are the area loads of the slabs. The loads are applied to the slabs and the direction of the slab is specified, so that the program can automatically apply the loads to the walls.

The slabs have an approximate thickness of 35 cm. Many of them have also a dropped ceiling. In the model the following composition is considered everywhere, but in rooms A108 and A110:

- Wooden beams 15 cm x 20 cm, spaced 50 cm
- Wooden planking 5 cm thick
- Parquet 2 cm
- Dropped ceiling

For rooms A108 and A110, as there are larger beams in the opposite direction of the other slabs, beams 20 cm x 25 cm are considered, with spacing 230 cm and the smaller beams are considered as an additional wooden planking.

In the loft, that is mainly used as an archive, there are heavy archive cabinets around the whole perimeter of the central area and a lot of random documents and objects in the middle of the room. For this reason in this area an imposed load of category B1 (offices not open to the public) is considered and linear load is added on the perimeter (approximately 60 kg/m).

The partition walls are very few and the slabs are not able to spread the load, so they are considered as a linear load on the slab in their actual position. The load from the partition walls depends also on their height: at the first floor 4.45 m, at the second floor 2.70 m.

The ceiling of the loft (a horizontal slab under the roof) is made of small 10 cm x 10 cm beams, with 50 cm spacing and wooden laths 3cm x 5 cm spaced 25 cm. The loads from this slab is manually computed and assigned to the walls that support it (linear or concentrated). In order to give a certain stiffness in the plan of this slab over the whole building, a slab with 10 cm x 10 cm beams is modelled, but with zero weight.

The roof is composed of wooden beams (the main are modelled), laths 3 cm x 6 cm with 25 cm spacing, hollow clay pots, waterproof sheath and tiles (considered as loads). The wooden structure varies in different zones of the roof. In the central zone there are 14 cm x 19 cm beams with 75 cm spacing (in the lodge there are additional truss beams 16 cm x 22 cm with 195 cm spacing) in the side bands there are 10 cm x 14 cm beams with 70 cm spacing and 19 cm x 26 cm beams with 175 cm spacing. The snow load is 80 daN/m^2.

Table 3-26: Permanent and imposed loads from slabs and walls.

Slabs	G1 [daN/m^2]	G2 [daN/m^2]	Q [daN/m^2]
Slab of the 1st and 2nd floor	44.0	46.0	200 (B1)
Slab of A108 and A110	52.7	46.0	200 (B1)
Slab of the lodge	24.0	34.0	50.0
Roof of the lodge	35.9	97.1	50.0 (H)
Roof – central part	14.2	97.1	50.0 (H)
Roof – side bands	19.3	97.1	50.0 (H)
Central balcony	330	575	400 (B)
Side balconies	330	630	400 (B)

Walls	1st floor G2 [daN/m]	2nd floor G2 [daN/m]
10 cm partition walls 1st and 2nd floor	400.3	242.9
15 cm partition walls 1st and 2nd floor	533.7	323.8
20 cm partition walls 1st and 2nd floor	800.6	485.8
Linear load of archive cabinets		294.3
Linear load of archive cabinets lower wall on lodge side		176.6

3.3.5. *Numerical model of the structure*

For the analysis of this masonry building the software TreMuri from StaData has been used. It uses macroelements and an equivalent frame method. With this software just modal analysis and non-

_____

linear static analysis can be performed. The non linearities are considered automatically, based on the input data of the materials.

In order to build the numerical model some simplification has been made. The openings have been transformed in equivalent rectangular openings and they have been slightly moved to align them vertically. The foundations are modelled as a prosecution of the walls of the ground floor, with a wall width and height of 50 cm. The basement has not been modelled and the ground is considered as rigid. The columns of the lodge are modelled with a square section, although they are cilindrical. The height of the columns in the model is limited by the definition of the levels of the storeys in the program. They are positioned at the first floor and then the wall above them is modelled, becoming higher than it is in reality. For this reason the specific weight of this wall has been lowered to obtain the real weight of the structure. In a similar way, the outer wall of the second floor (the loft) is modelled with the height of the central walls (about 120 cm more than in reality) and then the specific weight of this wall is adjusted to have the right total mass.

When modelling the whole structure, it has been noticed (with modal analysis) that the lodge was showing an independent behaviour from the main building. It is actually very poorly connected to the main building (just with the wooden slab of the loft, that is very deformable) and the columns don't have any seismic resistance. In case of an earthquake the lodge would probably collapse without almost no damage to the main structure. For this reason it has been decided to analyse the main building separately and connect it to the lodge at the end, with a retrofit proposal.

As the slabs are made of wooden beams, they are considered flexible and not able to distribute the horizontal actions among the vertical elements proportionally to their stiffness.

In the numerical model, all the internal lintels have been considered as wooden, all the external as brick arches, exception made for the openings on the borders with building B and C, where steel lintels have been considered.

The numerical model of the building is shown in Figure 3-48 and Figure 3-49.
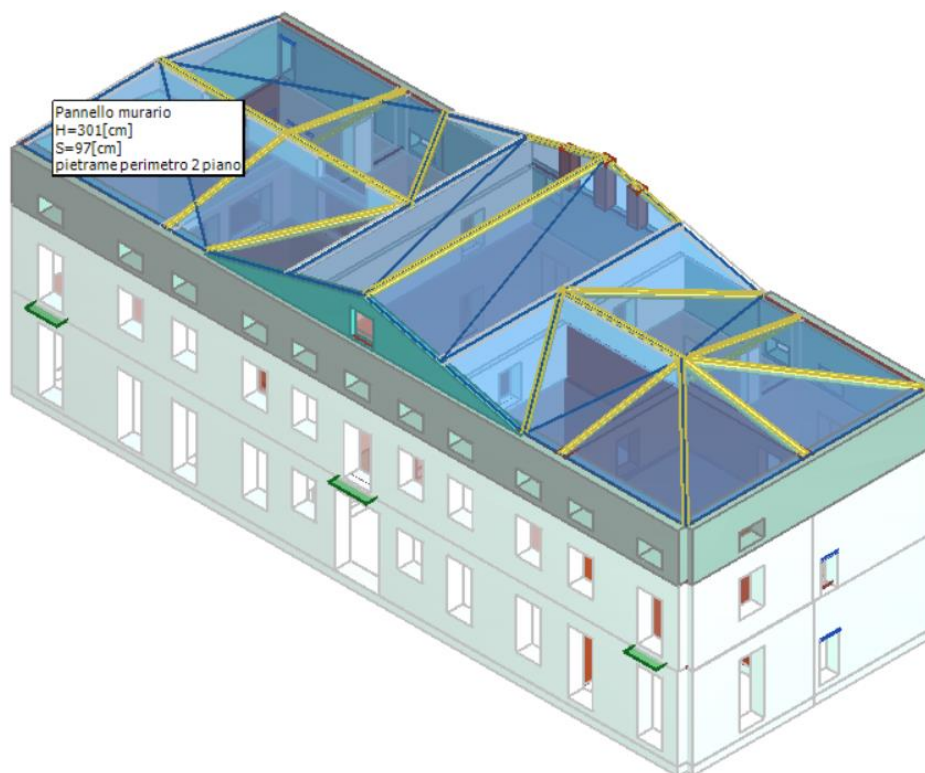
Figure 3-48: 3D view of the numerical model of the main building (without the lodge), front façade (facing Piazza del Municipio).

_____
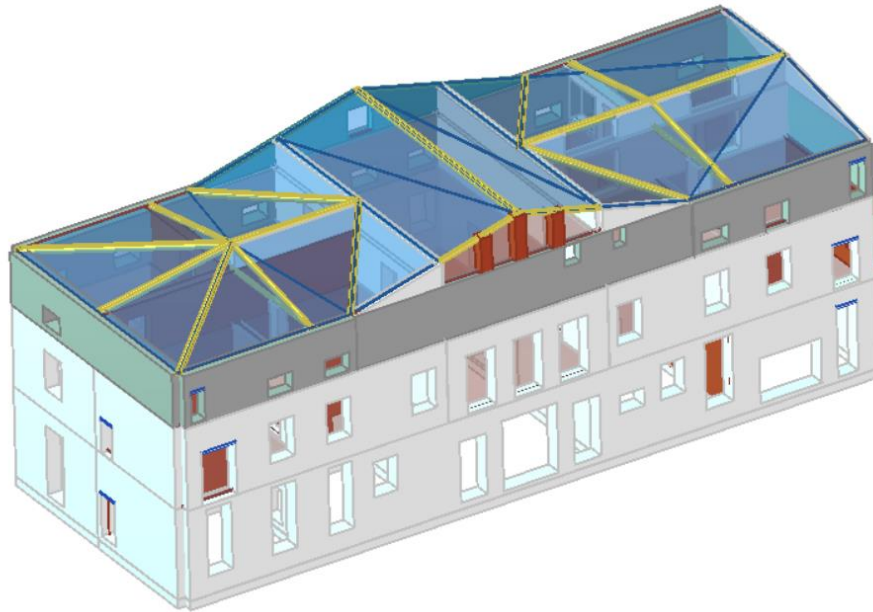
Figure 3-49: 3D view of the numerical model of the main building (without the lodge), back façade (facing the internal courtyard).

3.4. Masonry building B

This case study building is a residential building with a rectangular plane. It has 4 storeys over the ground level and a basement. All the apartments in the building, two in each storey, are accessible from the staircase, with the exception of the one at the ground floor, that is accessible from the back yard. The building is from 1903, as it can be seen at the entrance (Figure 3-50), and it was probably a refined, elegant building, with high ceilings (about 3.64 m) of the Austro-Hungarian Empire. The structure is composed of clay brick masonry, as it can be seen in many spots (in the basement and on one façade that is damaged). No in situ tests have been carried out on this building.

Figure 3-50: Front façade of the case study building and the construction year written at the entrance. Below, the damaged lateral façade where the clay bricks are visible.

The project documents have been found at the State Archive in Gorizia, they have the date 1902 and are composed of simple hand-drawings of the planes of the storeys of the building, of one section and of the drawing of the facades (Figure 3-51). There is also a section of a previous version of the project with one storey less. The ceilings of the basement are made of clay brick vaults.
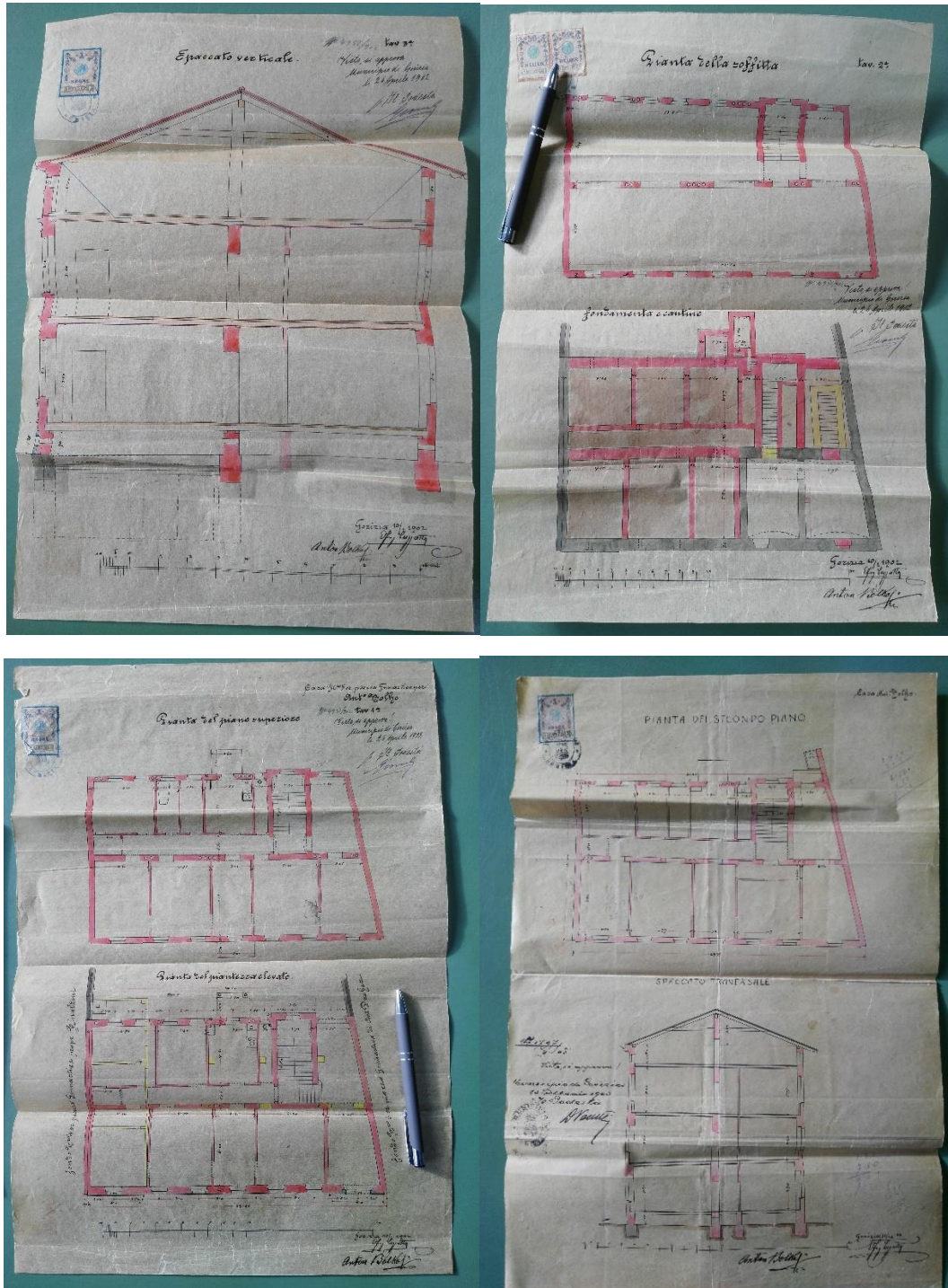
Figure 3-51: Project documents of the case study building, found at the State Archive.

3.4.1. *Geometry of the building and load-bearing elements*

The geometry of the building has been read from the project documents and verified with some measurements. The planes of each storey have been re-drawn in Autocad in order to have a clear base for the composition of the model. The drawings are reported in Figure 3-52 to Figure 3-55. The building is quite regular, it has a rectangular plane shape and four storeys over the ground level (three storeys + the loft). The load bearing walls are mainly the facades, one inner wall in the long

direction of the building and the walls of the stairwell. All the other inner walls are just 10 cm to 15 cm thick, so they cannot be considered as load-bearing, but just partition walls. They have not been modelled but they have been considered as loads. The building has a lot of openings (windows and doors), especially in the inner wall, where also flues pass to go to the roof. On the contrary, in the direction of the short side of the building there is almost no opening. The two short facades are totally full. The thickness of the walls is specified in Table 3-27. X direction is conventionally the long side of the building, while Y direction is the direction of the short side of the building. The interstorey height is 390 cm in the first two levels and 377 cm at the third level. The height of the loft goes from 1.50 m to 4.03 m (the slope of the roof is 20° on one side and 22° on the other side, as the ridge of the roof is not in the middle of the building). The basement is not modelled. The total height of the building is approximately 15.70 m.

The slabs are made of wood. The building has been modelled with the software 3Muri (STA DATA). It automatically considers the eccentricities of the walls, when they are aligned on the outer side.
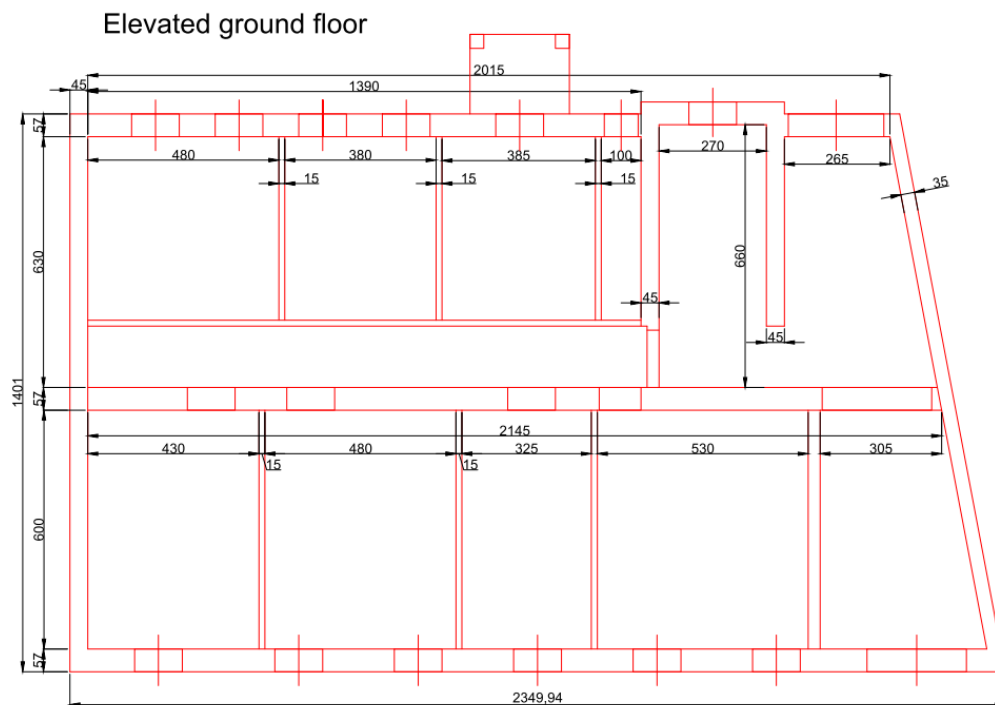
Figure 3-52: Plan of the ground floor.
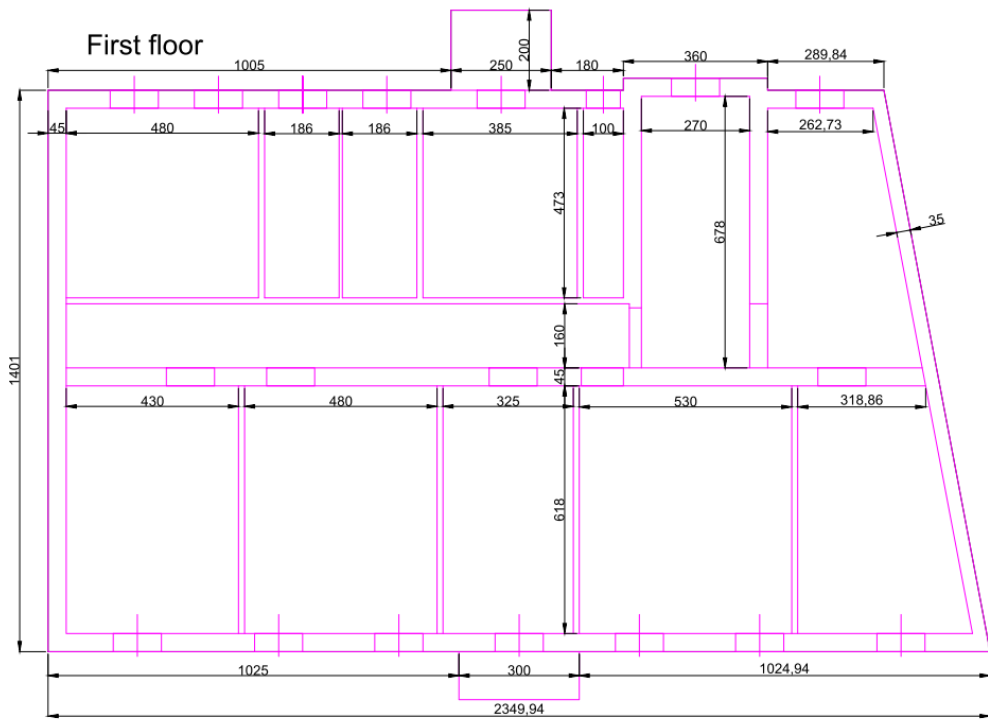
Figure 3-53: Plan of the first floor.
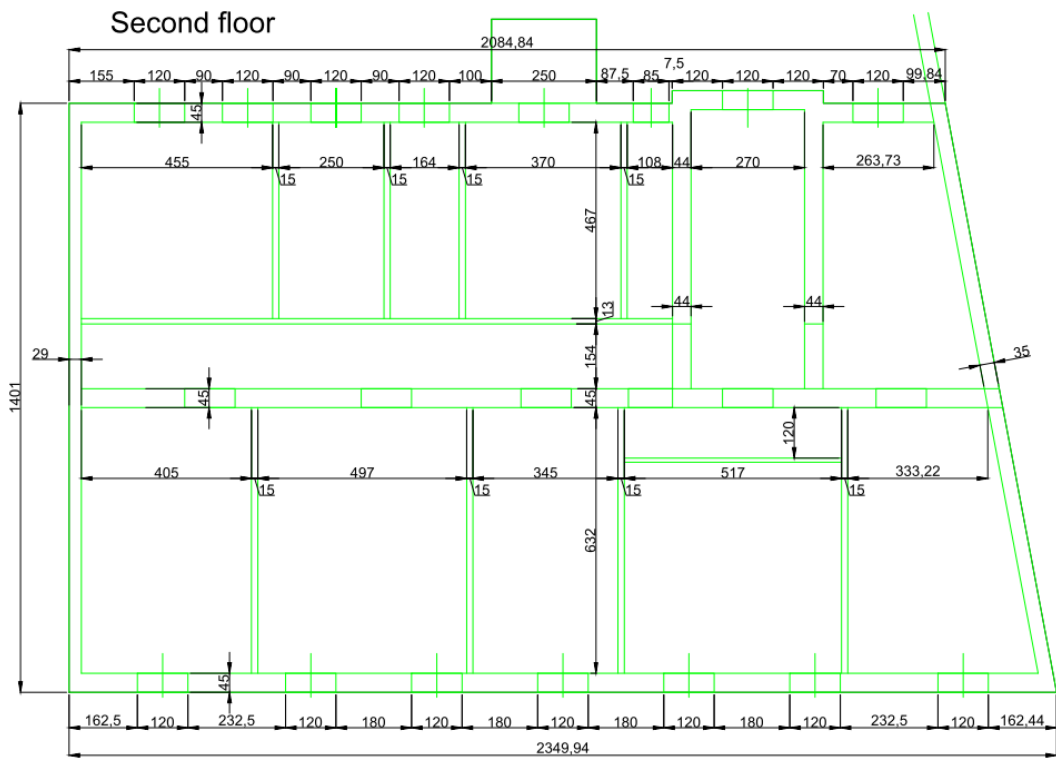
Figure 3-54: Plan of the second floor.
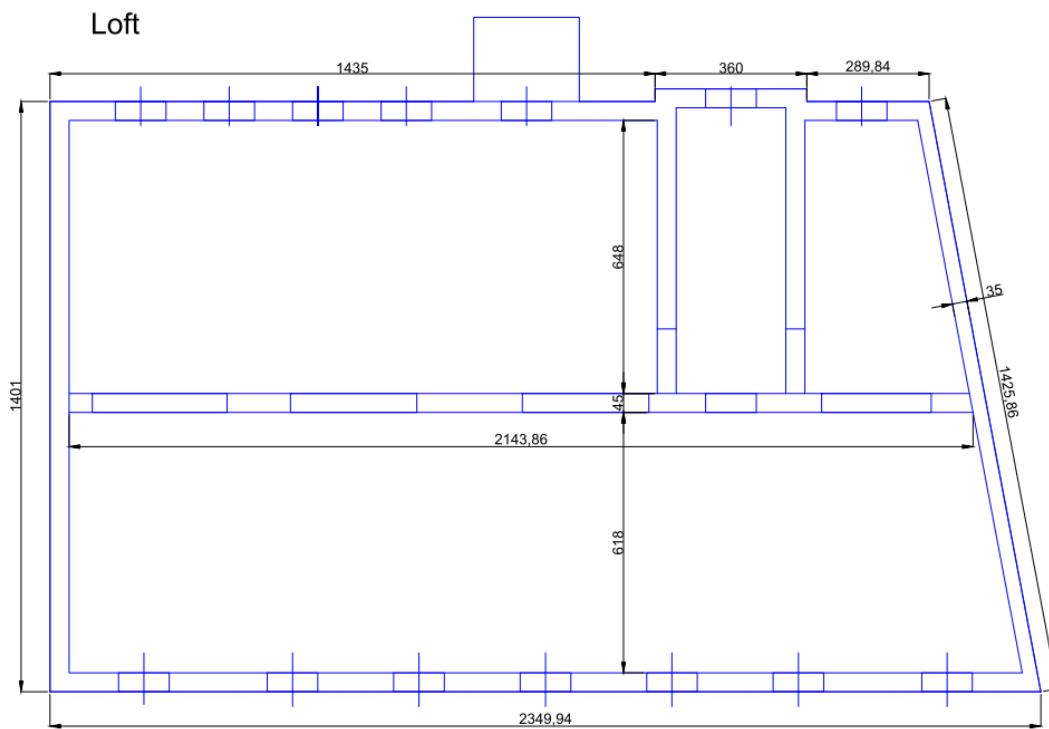
Figure 3-55: Plan of the loft.

Table 3-27: Thickness of the load-carrying walls.

Walls	Ground floor (level 1)	1st floor (level 2)	2nd floor (level 3)	Loft (level roof)
X direction (3 walls)	57 cm	45 cm	45 cm	45 cm
Left façade and stairwell in Y direction	45 cm	45 cm	29 cm façade, 44 cm stairwell	45 cm
Right façade in Y direction	35 cm	35 cm	35 cm	35 cm

3.4.2. Knowledge level

As no tests have been performed on the building, the knowledge level is low (LC1) and the confidence factor is 1.35.

3.4.3. Materials

The building is made of solid brick masonry. As no tests have been performed on the building, the characteristics from the code are considered (Circ. 2009 alle NTC2008, Tab. C8A.2.I), with a knowledge level LC1 (CF=1.35).

Table 3-28: Mechanical characteristics of masonry.

E [N/mm²]	G [N/mm²]	w [kN/m³]	fm [N/cm²]	fk [N/cm²]	τ [N/cm²]	CF
1500.00	500.00	18	240.00	124.44	6.00	1.35

3.4.4. Loads

The self load of the walls is automatically calculated by the program. As additional load are considered just the load of the slabs and the loads of the partition walls. As the stratigraphy of the slabs is not known, an approximate value of 70 daN/m² is considered. As the load of the partition

walls is considered just for the seismic mass and the load is applied as a linear load on the slab, it is calculated by considering half of the partition wall of the storey below the slab and half of the wall over the slab. It has been considered as linear in the actual position of the wall, because the partition walls have a load that is greater than 5 kN/m (10 kN/m^3 * 0.15 m * 3.9 m = 5.85 kN/m).

Table 3-29: Loads of the slabs.

Slabs	G1 [daN/m²]	G2 [daN/m²]	Q [daN/m²]
Over 1ˢᵗ, 2ⁿᵈ and 3ʳᵈ level	70.0	0.0	200.0
Roof	70.0	70.0	50.0

Table 3-30: Loads of the partition walls.

Walls	G1 [daN/m]	G2 [daN/m]	Q [daN/m]
15 cm thick walls	0.0	585.0	0.0
30 cm thick walls	0.0	1170.0	0.0
Load of the stairs	0.0	360.0	0.0
10 cm thick walls	0.0	390.0	0.0

3.4.5. Numerical model of the structure

The roof is considered just as mass and not for its stiffness, as it is wooden and not stiff in its plane. The slabs, including the roof, have been modelled as wood beam floors with double planking. The considered properties can be seen in Figure 3-56.
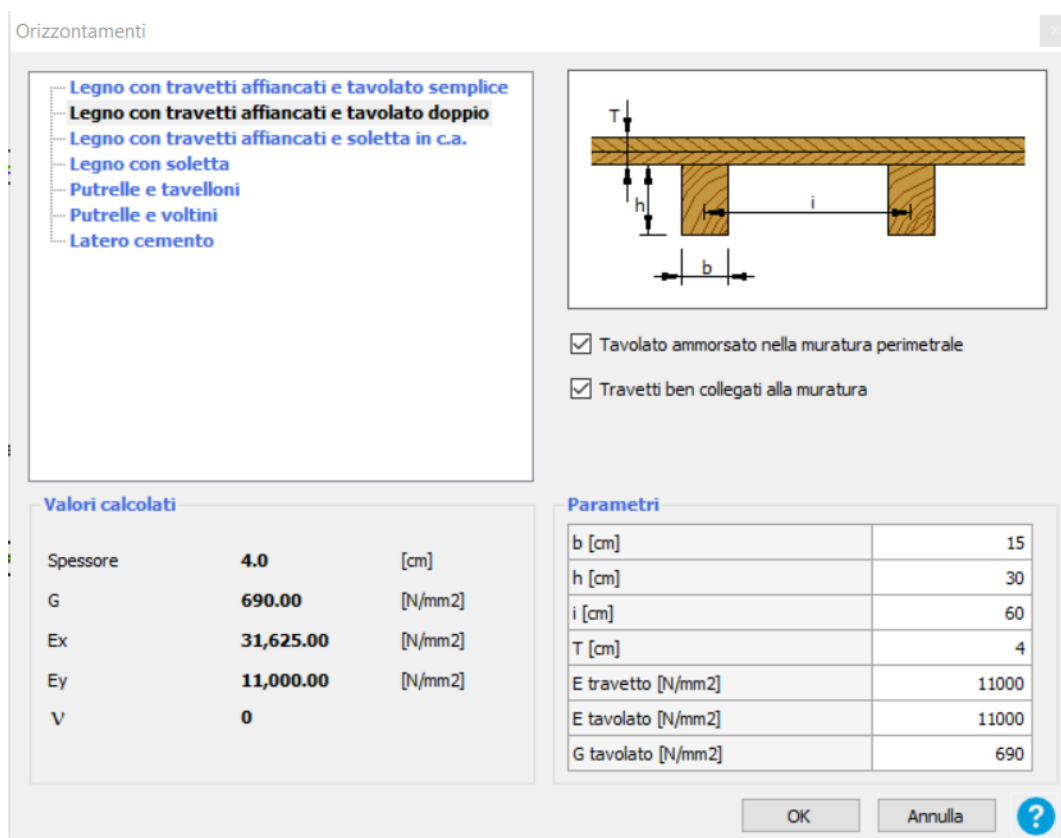
Figure 3-56: Definition of the wooden slabs in the software 3Muri (in Italian).

The holes for the flues in the central wall in X direction have not been considered. The part of the building on the backyard side, over the entrance on the right side, that is visible in the plan of

the second storey, has not been considered. It is for sure not designed to resist earthquakes, but it is negligible for the analysis of the behaviour of the main building. The added part should be verified separately. The stairwell is slightly moved forward with respect to the back façade, but in the model it has been aligned with the façade, as the shift can be neglected (it is equal to the thickness of the wall and it is connected to the perpendicular walls of the stairwell).
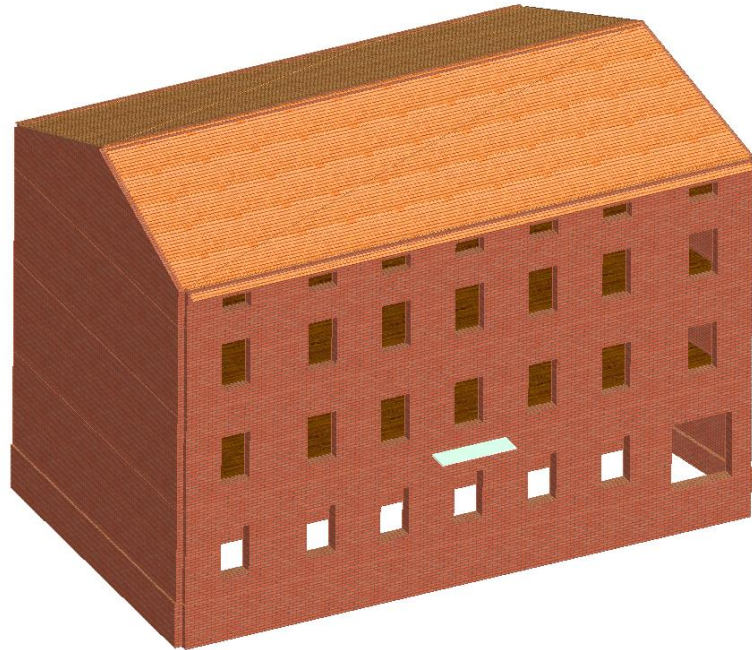
Figure 3-57: 3D view of the numerical model of the building – front façade.

Figure 3-58: 3D view of the numerical model of the building – back façade.

4. ANALYSES AND RETROFITTING SOLUTIONS

4.1. Seismic actions used in the analyses

4.1.1. PSHA method (code method) – response spectra

For the non-linear static analysis, the elastic response spectrum is needed in order to evaluate seismic vulnerability of the building. In the software TreMuri (used for the masonry case study buildings) it is possible to calculate the spectrum automatically, by giving some input parameters and it is automatically used in order to check the building. In SAP 2000 it is also possible to calculate the spectrum with the Italian code, but the program cannot use it for the checks of the pushover analyses. For this reason, the response spectra have been calculated separately, with an excel file provided by the Consiglio Superiore del Lavori Pubblici (Superior Council of Public Works). According to the Italian building code, the response spectra can be calculated for different limit states, based on the probability of exceedance P_{VR} during the reference life V_R of the building. The spectral shape is defined, for each probability of exceedance P_{VR} during the reference life V_R, based on the parameters of seismic hazard on rigid horizontal soil a_g (maximum horizontal acceleration at the site), F_0 (maximum value of the amplification factor of the response spectrum of horizontal accelerations) and T_C* (reference value for the determination of the starting period for the horizontal part of the spectrum of horizontal accelerations). The probabilities of exceedance that define the four limit states that are considered are defined in the Italian code NTC2018, Tab.3.2.I (Table 4-1).

Table 4-1: Table from NTC2018, defining the probabilities of exceedance for each limit state (SLO= Operational Limit State, SLD = Damage Limit State, SLV = Life safety Limit State and SLC = Collapse Limit State).

Tab. 3.2.I – *Probabilità di superamento P_{V_R} in funzione dello stato limite considerato*

Stati Limite		P_{V_R}: Probabilità di superamento nel periodo di riferimento V_R
Stati limite di esercizio	SLO	81%
	SLD	63%
Stati limite ultimi	SLV	10%
	SLC	5%

The elastic response spectra for RC building 1, RC building 2 and Masonry building B are the same (Figure 4-1):

- Reference life of 50 years is considered (ordinary buildings);
- Geographic coordinates: longitude 13.622 °E, latitude 45.937 °N ;
- Ground category B;
- Topographic category T1.
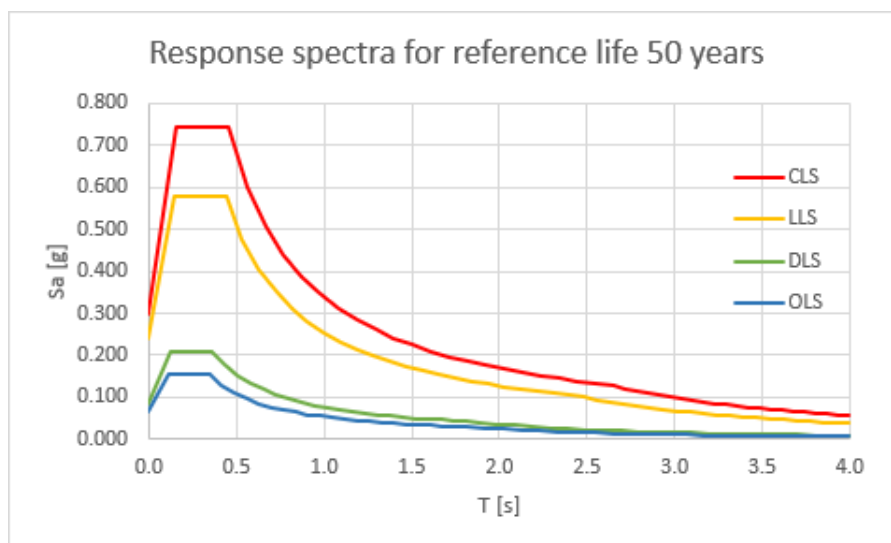
Figure 4-1: Code response spectra for buildings with reference life 50 years, for four limit states (CLS= Collapse Limit State; LLS= Life safety Limit State; DLS= Damage Limit State and OLS= Operational Limit State).

For Masonry building A, that is considered strategic, as it is the headquarter of the City hall, a reference life of 100 years is considered (Figure 4-2):

- Reference life 100 years (V_N= 50 years, C_U= 2);
- Geographic coordinates: longitude 13.6228, latitude 45.9416;
- Ground category B;
- Topographic category T1.
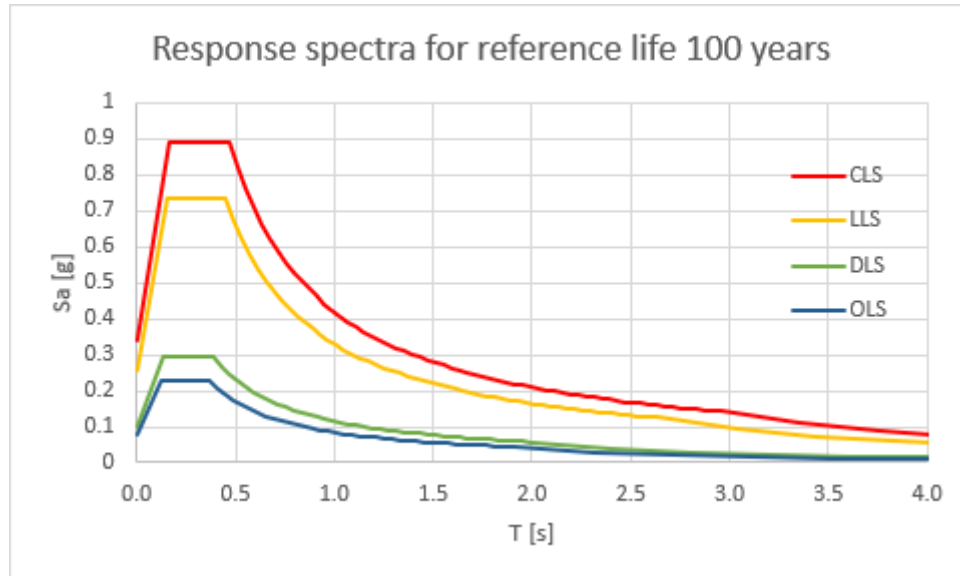
Figure 4-2: Response spectra for four limit states, calculated for reference life V_R= 100 years.

4.1.2. *Recorded accelerograms used for fragility curves*

A selection of recorded accelerograms has been made in order to develop fragility curves for the RC case study buildings. The accelerograms have been selected from the Engineering Strong Motion database (ESM database). From the website it is possible to download the ESM flat_file, where all the recorded signals are listed with some significant information (e.g. ground type, PGA, distance of the recording station from the epicentre and many others). Among other information, also spectral accelerations at some given periods are specified. The signals have been selected in such a way that they cover a wide range of Peak ground accelerations (PGA's) and spectral accelerations for the approximate fundamental periods of the two analysed buildings. The choice of using historical earthquakes for the analyses has been made in order to compare the obtained fragility curves with other results from literature.

Some general information about the seismic events to which the recordings belong, are reported in Table 4-2. For each building the component of each recording to use is later chosen based on the characteristics of the analysed building.

Table 4-2: Table with some characteristics of the chosen accelerograms

	Name	Mw	Focal mechanism	Ground type	Epicentral distance [km]	Duration [s]
1	A.496	7.3	SS		27.4	29.9
2	A.ATS	7.6	SS		109.3	150.205
3	A.BUR	7.6	SS		93.1	238.455
4	A.GZL	6.7	TF	D*	1.8	12.835
5	A.YPT	7.6	SS		16	175.015
6	BA.MIRE	6	TF	C*	4.1	61.97

7	BA.MIRH	6	TF	C*	4.5	64.99
8	EU.BAR	6.9	TF	B*	6.8	47.83
9	EU.PETO	6.9	TF	B*	19.7	48.24
10	EU.ULA	6.9	TF	A*	19.7	55.39
11	EU.ULO	6.9	TF	B*	22	46.18
12	HI.KAL1	5.9	NF	B	6.6	30.02
13	HL.AIGA	6.5	NF	B	23.6	39.79
14	HL.KALA	5.9	NF	B	5.5	35.875
15	HL.KORA	6.6	NF		32	50.695
16	HL.XLCA	6.6	NF		33.8	41.92
17	IT.ACC	6.5	NF	A*	18.6	35
18	IT.AMT	6	NF	B	8.5	27.895
19	IT.AQA	6.1	NF	E	5	40
20	IT.AQG	6.1	NF	B	5	100
21	IT.AQK09	6	NF	B	41.6	141.605
22	IT.AQK16	6.1	NF	B	1.8	100
23	IT.BGI	6.9	NF	B	21.9	129.95
24	IT.CLF	5.7	NF	D	2.8	44.45
25	IT.CLO	6.5	NF	A*	7.8	60
26	IT.CLT	6.9	NF	B	18.9	130
27	IT.CMI	5.9	NF	C*	7.1	30
28	IT.CNE	6.5	NF	C*	7.7	100
29	IT.GBP	6	NF	C	38.4	100.225
30	IT.MOG0	6	TF	C*	15.8	115
31	E.ATR	5.5	Normal faulting	B (inferred from geology)	17.4	60.435
32	E.FRC	5.6	Thrust faulting	B	18.6	18.56
33	IT.ASS	5.7	Normal faulting	A (inferred from geology)	24.2	25.6
34	IT.BGN	5.1	Normal faulting	B	24.2	92.145
35	IT.CR1			B (inferred from geology)	17.1	26.33
36	IT.MCV	6.5	Normal faulting	C (inferred from geology)	20	80
37	IT.MRC	5	Normal faulting	B (inferred from geology)	22.5	92.02
38	IT.MSC	5.8	Normal faulting	B	39.6	13.295
39	IT.NRC	4.5	Normal faulting	B	5.7	51.57
40	IT.PCH	5.6	Strike-slip faulting	B	63.2	30.99
41	IT.SGV	4.2	Thrust faulting	A	51	50
42	IT.SNO	4.3	Strike-slip faulting	B (inferred from geology)	20.8	50.545
43	IT.TDG			B	78.6	11.385
44	IT.TRL	6	Normal faulting	B	36.1	48.76
45	IT.UMB	6.5	Normal faulting	B (inferred from geology)	84	47.04
46	IT.VZZ	5.6	Strike-slip faulting	B (inferred from geology)	63.4	49.625
47	IV.NRCA	4.4	Normal faulting	B	7	71.81

48	MN.CEL	6.2	Strike-slip faulting	B (inferred from geology)	394	207.13
49	OX.SABO	5.9	Normal faulting	B (inferred from geology)	344.5	239.1
50	TK.2501	5.6	Strike-slip faulting	B	64.6	49.86

4.2. RC building 1

4.2.1. Modal analysis and comparison between different modelling choices

The first case study building has been analysed with different analyses and types of model in order to verify the reliability of the model, before using it to define its seismic vulnerability.

Building a reliable numerical model is the first, and probably the most sensitive step in order to define the seismic vulnerability of a structure. If it does not simulate the real behaviour of the analysed building, all the following calculations and evaluations could be totally wrong. The numerical model is, on the other hand, a tool that needs to find a balance between simplicity (in order to not burden the computational process to much) and detail. It is not possible yet to model every detail of a building, because buildings are very complex structures, composed of many materials and structural, but also non-structural elements, but all the most important details, that influence the behaviour of the building, need to be modelled [48]. Every construction system has its peculiarities. This case study building is a typical RC frame structure from the Italian 60's - 70's. They usually had masonry infills that were directly in contact with the load-bearing columns and beams, thus influencing the behaviour of the whole structure. The influence of the modelling choices for this kind of structures has been investigated with linear dynamic analysis, also considering or not considering the non-structural infill elements. The investigation does not take into account the normal uncertainties that are typical of existing structures, for which there is usually very few documentation available or nothing and many details remain unknown also if many in situ tests are performed [49].

At the time when the building was built, the dynamic behaviour of structures in Gorizia was not considered at all. The design was considering just gravitational loads, so that no importance was given to the infills, that were built directly in contact with the columns and beams and that increase a lot the stiffness and also lateral strength of the building. For sure such infills are very brittle and have low lateral strength compared to the RC frame, so that they collapse after the first stronger shake, but they could influence the seismic force that hits the building. A higher stiffness means a lower vibration period and this usually brings higher seismic forces acting on the building.

When a professional wants to evaluate the seismic vulnerability of an existing building, different type of analyses can be chosen. With a non-linear static (pushover) analysis, if all the elements are realistically modelled (also the infills can be modelled in different ways), it can be seen that the influence of the infills is just in the initial elastic phase, before the formation of plastic hinges in the RC elements. When a linear analysis is chosen, e.g. linear dynamic analysis, the increment of stiffness causes different vibration modes and periods and thus really different actions on the building, which brings to very different results in the seismic vulnerability evaluation.

In this research a linear dynamic analysis is used to evaluate the influence of modelling choices on the vulnerability of a structure.

The case study building, as described in § 3.1, has a stairwell made of concrete walls, while the rest of the building has an RC frame structure, that is very flexible (as the structure was not designed to withstand seismic forces). If just the load-bearing structure is considered, the centre of stiffness is shifted towards the concrete walls, that means far away from the centre of mass. The distance between the two centres depends on the stiffness distribution in plan, so it depends on modelling choices. Five different models have been considered and some result parameters are compared in order to evaluate the differences. The results of the models are also compared with the results of some vibrational measurements on the real building. For the analyses, as the linear (elastic)

behaviour is considered, a code response spectrum corresponding to DLS is used. The software used for modelling and analysis is SAP2000 (CSI Inc.).

The five models have the following differences:

- N1 – reference model – just structural elements are modelled – beams and columns are modelled with "frame" elements, while concrete walls are modelled with bi-dimensional "shell" elements.
- N2 – also this model considers just structural elements, but the concrete walls are modelled with "frame" elements, as the columns are.
- N3 – the same as the N1 model, but also masonry infills are modelled, with equivalent diagonals that do not consider openings (Figure 4-3).
- N4 – the same as N3 model, but the sections of the diagonals are reduced in order to consider the openings.
- N5 – the same as N2 model, but the "frame" elements of the concrete walls are connected among them with rigid links that allow for a spatial behaviour of the stairwell (Figure 4-4).

For modelling the infills many ways exist in the literature [50]. In this case it was chosen to model them as equivalent diagonals in models N3 and N4, according to an old Italian standard DM 16-1-96 and CM 10/04/1997 n. 65. The infills are modelled with equivalent compressed diagonals, pinned at the ends, with a thickness equal to the thickness of the infill wall, t, and width s, equal to the 10% of the length of the diagonal. As linear analysis is used, it was not possible to use non-linear elements (just compression) for the diagonals. For this reason, just one diagonal is modelled, that works in compression but also in tension, when the force direction is inverted. The elastic modulus of the masonry is 17600 N/mm^2. So as to consider the openings, the method proposed by Chen and Liu (2015) is used [51]. According to this method, the reducing factor for the stiffness and strength of the infill due to the opening, is a function of the dimension and position of the opening (eccentricity with respect to the centre of the infill and the direction of the action). As just one diagonal has been modelled, the reduction factor is taken as the average between the two values found for the two load directions.
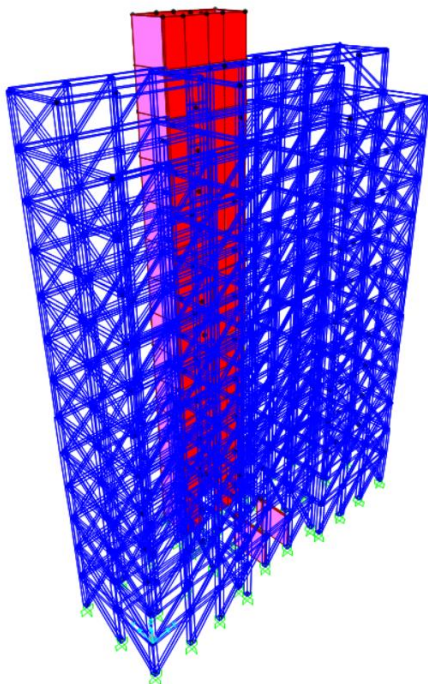
Figure 4-3: Model N3 or N4 where masonry infills are modelled with equivalent diagonals
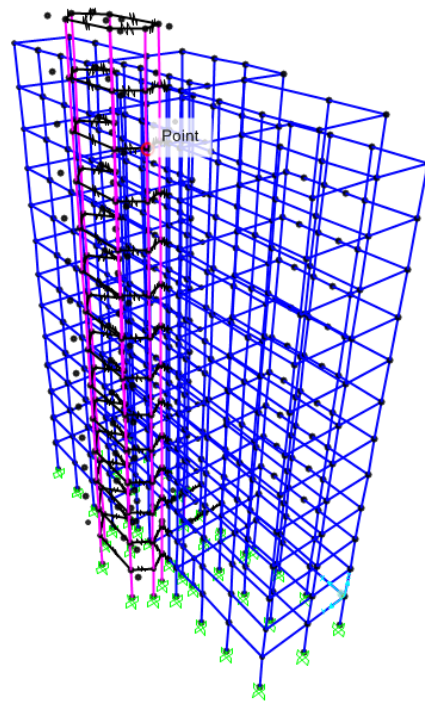
Figure 4-4: Model N5 where concrete walls are modelled with "frame" elements.

The Italian code, but also Eurocodes, do not specify exactly when the infills should be modelled and how, so that each of these five models (or even other different models with different elastic modulus of masonry) could be chosen by a professional, obtaining different results of seismic vulnerability. Usually the fastest to build and analyse is chosen, so that N2 could be the choice or N5, but almost nobody would choose N1, N3 or even less, N4. Shell elements need more computational capacity and time and they are more complex to "read", so that they are not a good choice for a professional. Modelling the infills is also an extra work that a professional could choose not to do, as the code does not require it. The Italian code NTC 2018 just pays few words on the negative influence of non-structural elements on new buildings, but nothing is said for existing buildings. In addition, also for new buildings, nothing is said about how to consider non-structural elements. The Eurocode 8 takes into account the irregularity in elevation that non-structural elements can cause by considering a coefficient that amplifies the seismic forces.

The comparison between the results of the five models is done in terms of natural periods, of the shape of vibration modes (through the participating mass ratios) and of base shear (obtained with linear dynamic analysis in both directions X and Y, combined according to the Italian code). The results of the analysis of the five different numerical models are summarized in Table 4-3 and a comparison is made in Table 4-4. The natural period can change of up to 67% (N2 compared to N1) and also the base shear changes of up to 67% (N3 compared to N1), as they depend on the combination of the modes. It can be seen that the model N5 is quite similar to the model N1.

The results of the numerical models have been also compared to some data obtained with vibrational measurements. The measurements have been performed with two velocimeters, positioned in two opposite corners of the roof of the building (positions P1 and P2 in Figure 4-5), for approximately 15 minutes. The acquired data have been processed with GHM method (Gaussian-filtered Horizontal Motion – Dal Moro et al., 2018 [52]) and six vibration modes have been clearly identified (signals M1 to M6 in Figure 4-6). Signal S (Figure 4-6) is a transient spurious signal and is not a vibrational mode of the building.

Table 4-3: Results of the five numerical models, in terms of natural periods (T), participating mass ratios (Ux and Uy) and base shear (Tb) for Damage Limit State (DLS).

Mode	N1			N2			N3			N4			N5		
	T [s]	UX [-]	UY [-]	T [s]	UX [-]	UY [-]	T [s]	UX [-]	UY [-]	T [s]	UX [-]	UY [-]	T [s]	UX [-]	UY [-]
1	1.96	**0.20**	**0.12**	3.18	0.00	**0.63**	1.01	0.00	**0.65**	1.10	0.00	**0.65**	1.93	**0.45**	0.00
2	1.75	0.06	**0.50**	2.60	**0.07**	0.00	0.64	**0.59**	0.00	0.76	**0.55**	0.00	1.74	0.00	**0.62**
3	1.02	**0.42**	0.00	1.72	**0.61**	0.00	0.52	**0.12**	0.00	0.59	**0.15**	0.00	0.76	**0.31**	0.00
Tb (X) [kN]	1840.69			1444.54			3068.20			2568.56			1404.16		
Tb (Y) [kN]	2024.21			1039.19			2542.95			2371.42			1934.49		

Table 4-4: Comparison of the results of N2, N3, N4 and N5 with results of N1, in terms of natural period (T) and base shear (Tb).

N2			N3			N4			N5		
ΔT	ΔTb (X)	ΔTb (Y)	ΔT	ΔTb (X)	ΔTb (Y)	ΔT	ΔTb (X)	ΔTb (Y)	ΔT	ΔTb (X)	ΔTb (Y)
62%			-49%			-44%			-2%		
48%	-22%	-49%	-64%	**67%**	26%	-57%	40%	17%	0%	-24%	-4%
67%			-49%			-42%			-26%		
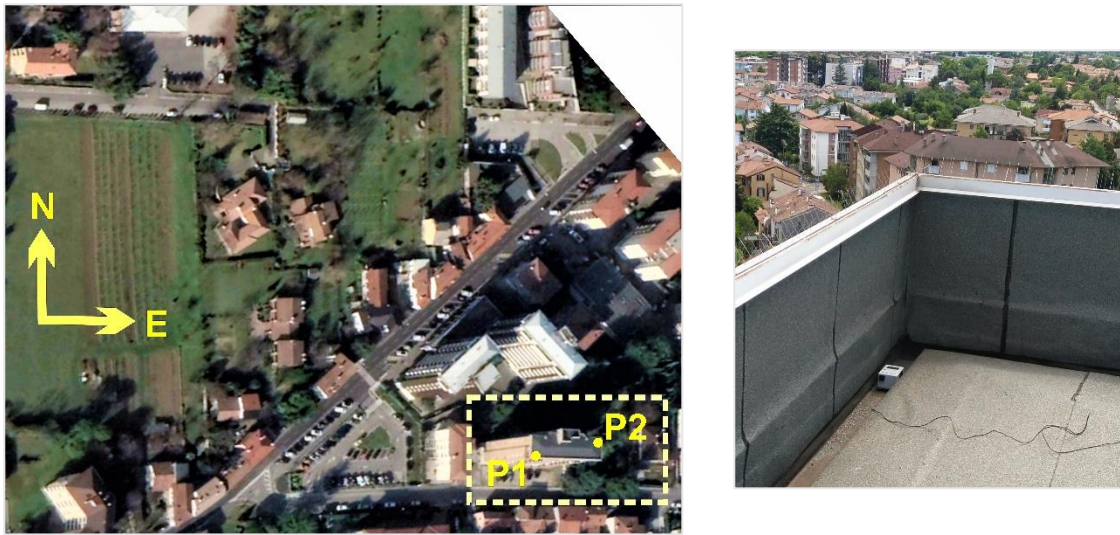
Figure 4-5: Position of the velocimeters on the roof of the building (left) and an image of the velocimeter (right)

In order to make a comparison between the periods resulting from the numerical models and the periods from the measurements, the first 6 periods are reported in Table 4-5. As the measurements reflect the elastic phase of the building, they can be compared with the numerical models that consider masonry infills. Between the two models (N3 and N4), N3 is chosen because it is the stiffest. The periods in this case are comparable, but the measured ones are still lower than the ones resulting from the numerical model.
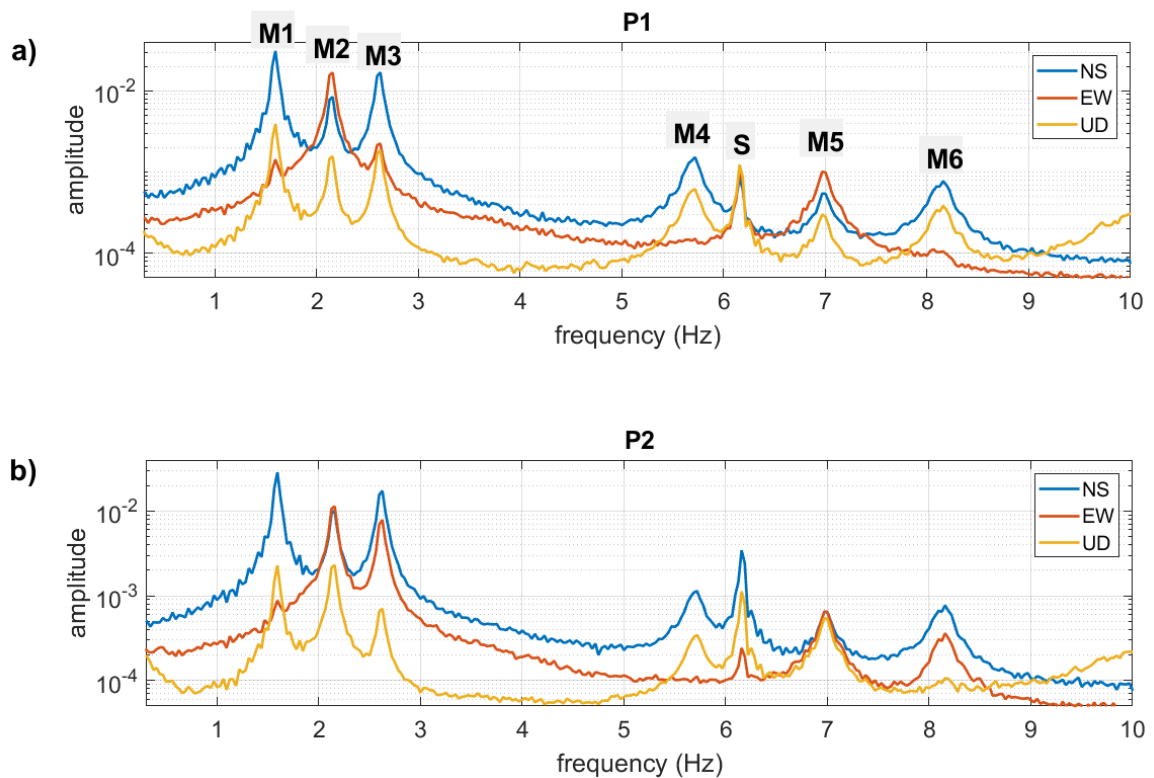
Figure 4-6: Amplitude spectra of the three components (NS, EW, vertical) for the measurement position P1 (a) and P2 (b) on the roof top. There are six clearly visible vibration modes of 1.6 Hz, 2.16 Hz, 2.63 Hz, 5.72 Hz, 7.00 Hz and 8.16 Hz. Signal S is a transient spurious signal, probably caused by motor that was working for some minutes during the measurements.

Table 4-5: Comparison between measured and computed periods of the case-study building. Among the numerical models, for the comparison the periods of model N3 are reported, that is the one with lower periods and for this reason closer to the measured ones.

Mode	Measured	From numerical model N3
M1	0.625 s	1.01 s
M2	0.463 s	0.64 s
M3	0.380 s	0.52 s
M4	0.175 s	0.27 s
M5	0.143 s	0.20 s
M6	0.123 s	0.17 s

In Figure 4-7, GHM graphs can be seen for the first three modes. They represent the recorded movements of the two measuring positions for a given frequency – in this case 1.60 Hz, 2.16 Hz and 2.63 Hz. The first mode, M1, is mainly translational in direction NS (short side of the building), mode M2 is almost purely rotational, while mode M3 seems to be a combination of translation and rotation (torsion). The following three modes (M4, M5 and M6) are very similar to the first three, but have higher frequencies and one order of magnitude lower amplitude.
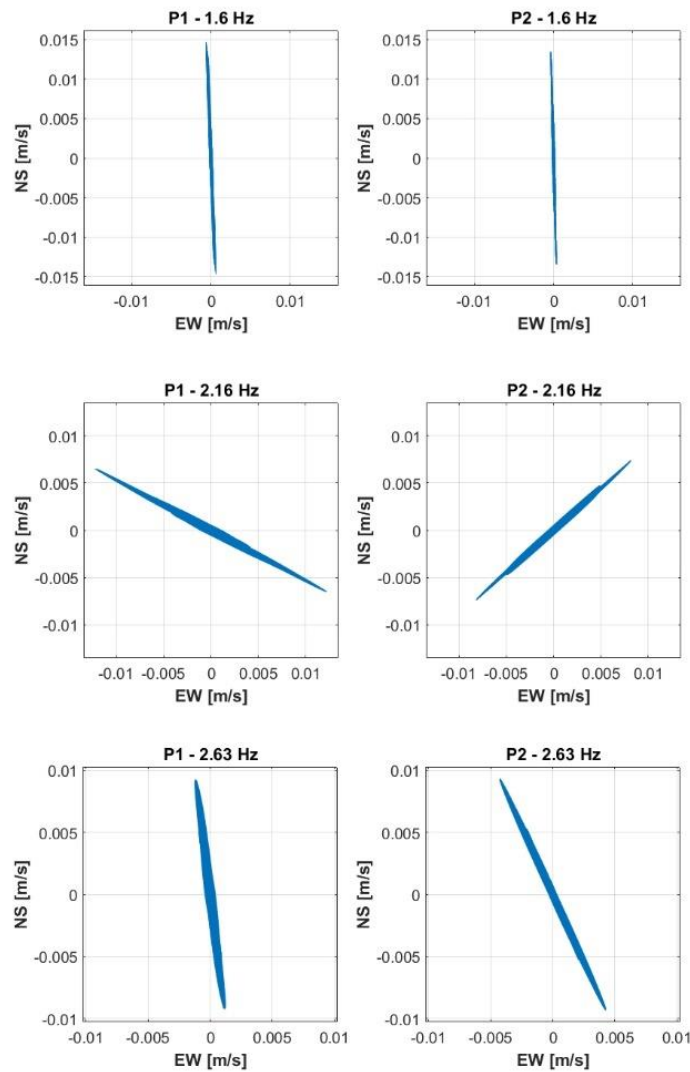
Figure 4-7: GHM graphs for the first three vibration modes. From the top down: mode M1 (flexural mode along NS axis, at 1.60 Hz – 0.625 s); mode M2 (torsional mode at 2.16 Hz - 0.463 s); mode M3 (mixed mode at 2.63 Hz – 0.380 s). The NS direction coincides with the short side of the building. P1 and P2 are the measuring positions on the roof of the building.

4.2.1.1.   Conclusions

As it has been shown, modelling choices have a great influence on the outcome of the vulnerability evaluation of an existing building. Although just the elastic phase has been investigated, the simplest to deal with, as less variables enter in the calculation, it is possible to verify that the results of numerical analyses are quite different from the results of the measurements of reality. The lowest natural period found with numerical analyses, T= 1.01 s (N3), remains significantly higher than the highest measured period (0.625 s). A credible cause is the effect of non-structural elements that are not considered in numerical models (as for example partition walls) and the additional mass of the imposed design loads in the models, that is probably higher than the loads that were actually present at the moment of measurements.

A fundamental difference in the models is the choice of modelling concrete walls with "shell" elements or "frame" elements. The difference in periods of model N1 and N2 is comparable with the difference between models N3 and N1 (considering masonry infills or not). This difference is around 60% and causes differences in base shear of around 35%. The most accurate modelling solution for concrete walls seems to be the one with "shell" elements, but an effective alternative is the use of "frame" elements in combination with rigid links (model N5) in order to create a connection between walls, simulating the behaviour of a C section.

In the elastic phase of the building's behaviour the contribute of masonry infills seems to be essential and this should be considered when evaluating the vulnerability of an existing building for damage limit state (DLS). As it can be noticed in Table 4-3, considering the infills does not change just the periods but also the mode shapes. They add stiffness to the part of the building that is otherwise more flexible, where there are no concrete walls, so that the stiffness centre moves closer to the mass centre and the behaviour of the building becomes less torsional and more regular. If the existing building is modelled with frame elements without rigid links and without considering infills, seismic forces for this case study building are underestimated of 59%. Similar results would be obtained also for other high-rise buildings as this is.

At last, also the stiffness of the compressed diagonal representing the infill is important for the final result. The contribute of the infills can vary with the type of bricks that have been used, so that a mechanical characterization of masonry and of the connection with the concrete structure is fundamental for a proper vulnerability analysis.

According to the code, if the knowledge level of the existing building is low (LC1) or if the building does not fulfil the requirements for using pushover analysis (regularity, period, participating mass of the first mode etc.), just linear analysis can be used (or non-linear dynamic, but it is not used by professionals as it requires high computational resources). In this case, a sensitivity analysis should be done on some different models in order to evaluate the best choices to approximate reality, before using the numerical model to evaluate seismic vulnerability or design retrofit solutions.

4.2.2. Non - linear static analysis (pushover)

The case study building, as already described at §3.1.5, is not regular and thus not really suitable for pushover analysis. For research purposes and for comparison with dynamic analysis, pushover analysis is performed in any case, knowing that the results could be not reliable.

For the following analysis a model like the model N5 in the previous paragraph has been chosen. Just the structural elements are modelled (RC beams, columns and walls – no infills) and concrete walls are modelled with "frame" elements that are connected to each other with rigid links. Some modal results are reported in Table 4-6 in order to better describe the building. The first mode has 62% of participating mass in Y direction (the short side of the building), while the next 3 modes are mainly translational in X direction, although all the modes that involve more participating mass in X direction are rotational, as the stairwell is asymmetrical with respect to X axis.

Table 4-6: Periods and participating mass ratios for the first 20 modes (total mass 89%).

Mode	Period	UX	UY	UZ	SumUX	SumUY	SumUZ	RZ
-	Sec	Unitless	Unitless	Unitless -	Unitless	Unitless	Unitless	Unitless
1	1.736	1.19E-05	0.622	1.99E-05	1.19E-05	0.622	1.99E-05	4.04E-06
2	1.260	0.341	1.03E-06	5.38E-07	0.341	0.622	2.04E-05	0.434
3	0.716	0.314	4.13E-07	8.29E-06	0.655	0.622	2.87E-05	0.352
4	0.410	0.079	4.57E-05	1.91E-07	0.734	0.622	2.89E-05	0.035
5	0.358	2.42E-05	0.198	3.25E-05	0.734	0.820	6.14E-05	8.44E-07
6	0.244	2.32E-03	1.56E-07	1.95E-06	0.736	0.820	6.33E-05	0.043
7	0.183	0.149	5.22E-06	6.28E-05	0.885	0.820	1.30E-04	0.042
8	0.171	2.50E-04	8.08E-05	4.32E-06	0.886	0.820	1.30E-04	0.028
9	0.155	6.11E-05	0.070	5.20E-04	0.886	0.890	6.50E-04	5.79E-07
10	0.133	4.35E-06	8.55E-06	0.331	0.886	0.890	0.331	3.35E-06
11	0.133	4.00E-04	8.45E-08	3.70E-04	0.886	0.890	0.332	2.10E-04
12	0.132	6.56E-03	9.21E-07	2.10E-04	0.893	0.890	0.332	7.87E-03
13	0.131	9.44E-05	4.79E-05	0.044	0.893	0.890	0.376	1.20E-04
14	0.123	2.34E-08	1.53E-07	0.087	0.893	0.890	0.463	3.84E-11
15	0.123	1.28E-05	1.16E-07	3.00E-05	0.893	0.890	0.463	5.26E-05
16	0.122	2.97E-06	2.83E-10	1.76E-06	0.893	0.890	0.463	1.53E-07
17	0.122	1.19E-09	2.45E-06	0.021	0.893	0.890	0.484	4.55E-08
18	0.118	3.54E-06	3.70E-09	1.76E-05	0.893	0.890	0.484	3.04E-07
19	0.117	4.19E-08	3.96E-06	0.067	0.893	0.890	0.552	1.16E-08
20	0.110	2.17E-10	1.29E-05	0.059	0.893	0.890	0.611	1.86E-07

Pushover analysis is usually performed with two different load patterns. According to the Italian code (NTC2018, §7.3.4.2), one should be from Group 1 and the second from Group 2. As the building has a participating mass for the first mode (in both directions X and Y) that is lower than 75% and the fundamental period is higher than 1.3 Tc (T1=1.736 > 1.3*0.439 s), the only possible load pattern from Group 1 is a load pattern that is proportional to the forces acting on each slab in a linear dynamic response spectrum analysis where a number of modes comprising at least 85% of the mass has been considered. This load pattern is called "spectral" load pattern in the following text. The second load pattern used for the pushover analysis is a "uniform" pattern, based on lateral forces that are proportional to mass regardless of elevation (uniform response acceleration). Lateral loads are applied at the location of the masses in the model and accidental eccentricity is taken into account. Forces shown in Table 4-7 are applied to the building for performing non-linear static analysis in X and Y direction separately. As the non-linear static analyses have found many difficulties to converge, it has been decided to perform a simulated static analysis also with a slow non-linear dynamic (direct-integration time-history) analysis. For this purpose, the same forces taken for the pushover analysis are applied to the structure by using a time-history function of 200 s that linearly increases, so that a pushover curve is also found with this method. In this case a damping of 90% is applied to the building in the period range from 0.005 s to 2.45 s in order to simulate a static behaviour and avoid the effects of the higher modes. It can be seen from the results that the curves obtained with static and with slow dynamic analyses are following almost exactly the same path, so that the analysis choices are validated.

Table 4-7: Lateral load distribution for pushover analysis (forces calculated based on the results of a response spectrum analysis with elastic LLS response spectrum, applied separately to X and Y direction).

H	Fx	Fy
0	172.4	137.0
3.1	285.4	323.5
6.2	384.0	513.7
9.3	387.8	573.1
12.4	345.8	519.0
15.5	302.5	392.5
18.6	286.9	240.2
21.7	302.7	87.7
24.8	363.1	13.0
27.9	482.1	121.2
31	671.1	439.8
34.1	1008.2	1005.2
37.2	726.0	814.3
40.3	188.8	208.4

The results of these analyses are shown in Figure 4-8 and Figure 4-9. The four curves have two different origins, as two curves are the results of the pushover analyses in X direction, while the other two are the results in Y direction. The origin is not zero, due to the initial deformation of the building because of vertical loads. Non-linear static analysis has more troubles to converge, so that the curves stop quite soon (especially in X direction), while the slow non-linear dynamic analysis converges more easily and finds further theoretical resistance and ductility. In any case, in all the analyses, the building arrives soon to the collapse of many plastic hinges and the dashed lines after the collapse of the building are not significant. In X direction the curves have been cut after the collapse. In the curves derived from the slow non-linear dynamic analyses, the theoretical further resistance is just a numerical result due to the high dumping that has been imposed in order to avoid the effects of higher modes. The first hinges that collapse are in all cases brittle shear hinges of the concrete walls in the first storeys of the building. In the static pushover analyses, at each step, many brittle shear hinges collapse or reach a worse damage level, so that the analyses cannot reach the numeric convergence and a proper drop of strength in the capacity curve. For this reason, the capacity of the building has been defined in the following way: the collapse limit state is reached when many plastic hinges collapse (become red on the screen) and the base shear reaches a local maximum (Figure 4-10). The Life Safety limit state is reached when some hinges first reach 0.8 of the ultimate shear (light blue colour on the screen) and it usually happens just one step before the collapse. CLS and LLS capacities are shown in the graphs with a red cross or circle. For the curves obtained with slow dynamic analysis, collapse is set at the step when the same number of hinge collapses is reached as for the collapse defined with the static analysis.
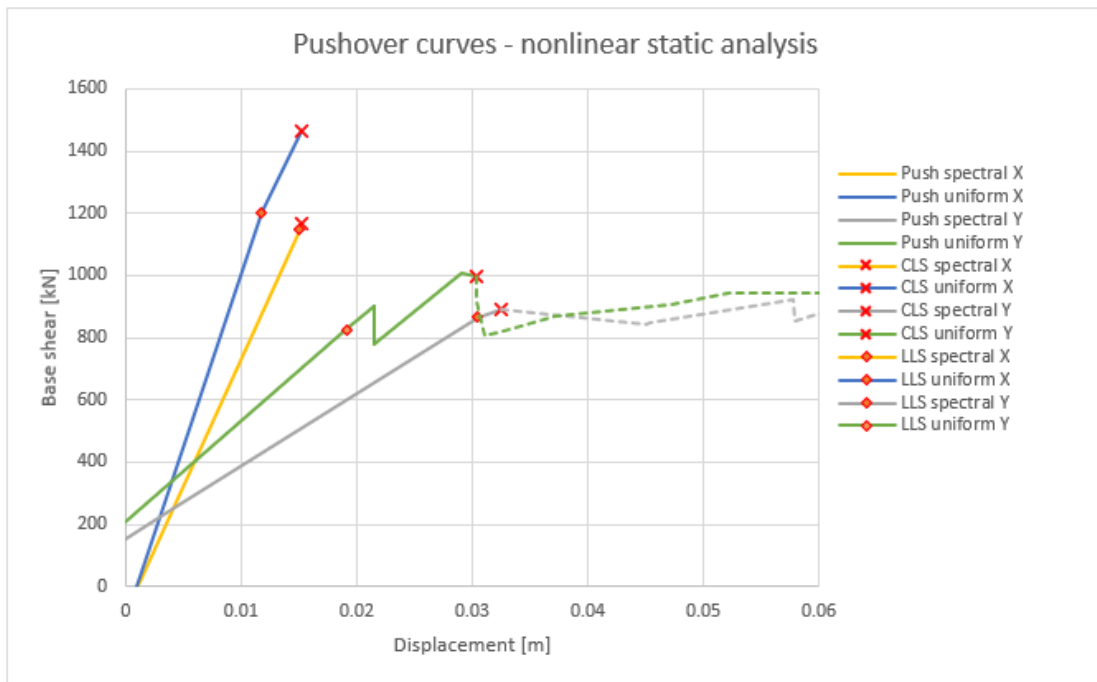
Figure 4-8: Pushover curves in X (higher curves) and Y (lower curves) direction. The curves are obtained with non-linear static analysis. The capacity of the building for CLS and LLS is shown on the curves with a symbol (see the legend). The dashed lines, after the collapse of the building, are not significant.
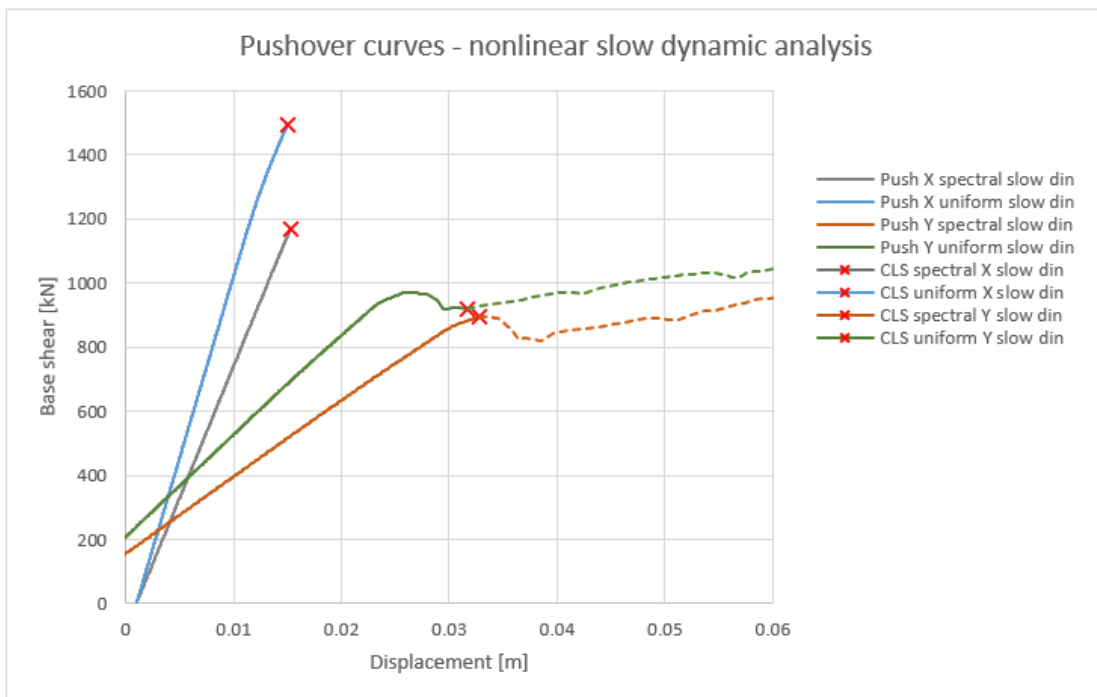
Figure 4-9: Pushover curves in X (higher curves) and Y (lower curves) direction. The curves are obtained with slow non-linear dynamic analysis. The capacity of the building for CLS is shown on the curves with an "x". The dashed lines, after the collapse of the building, are not significant.
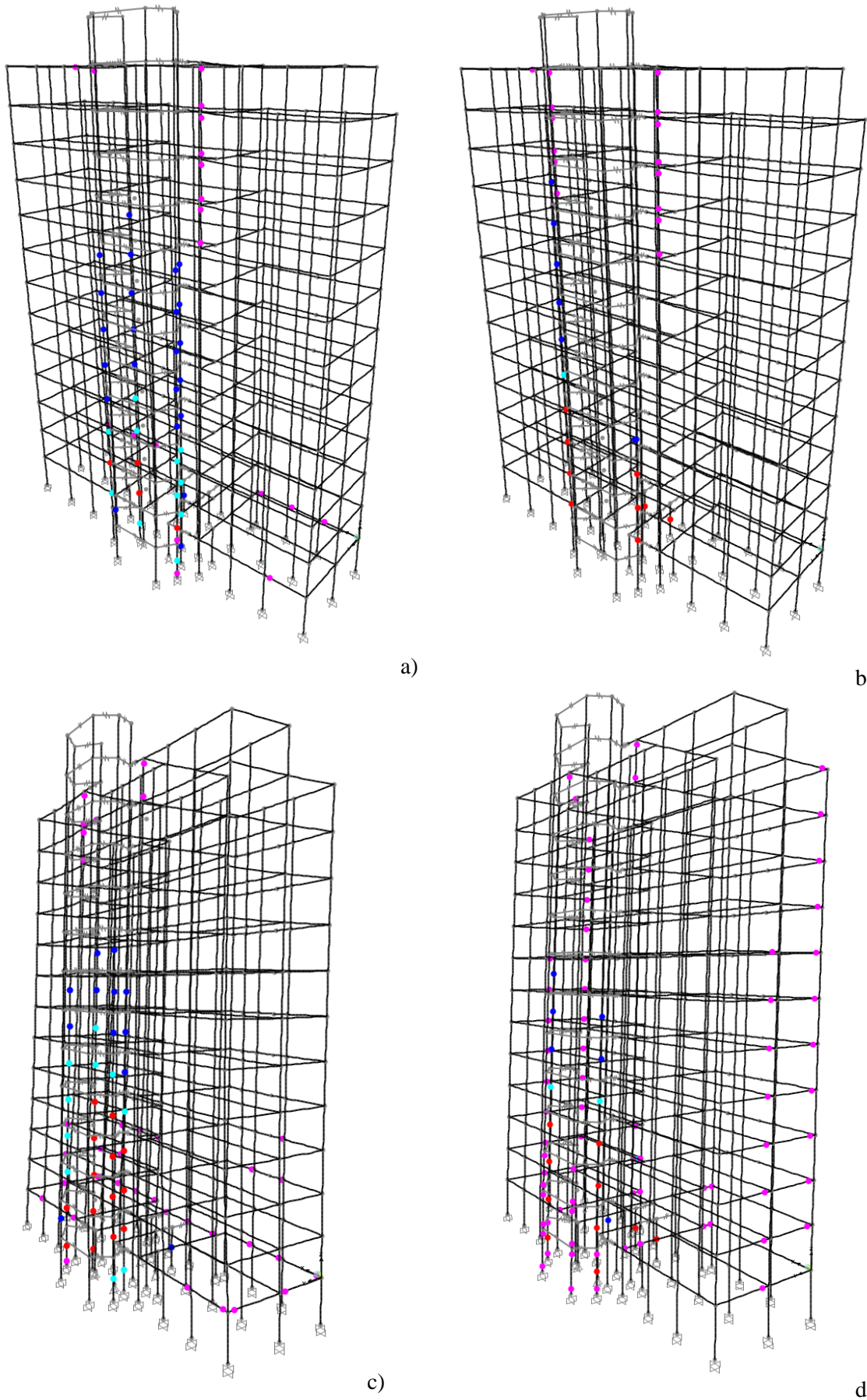
Figure 4-10: Deformed shape of the building at the step when CLS is reached: a) Spectral load distribution in X direction, b) spectral load distribution in Y direction, c) Uniform load distribution in X direction, d) Uniform load distribution in Y direction.

It can be noticed that the building is more ductile but less strong in Y direction. The curves stop for convergence reasons, however, if the number of collapsed plastic hinges is checked, it can be noticed that the building could be already considered collapsed at the end of the elastic phase, because many brittle shear hinges collapse right after it. The building is thus not ductile at all, as it presents brittle failure. It is interesting to notice that for this reason it is practically impossible to define the capacity at Serviceability Limit States (DLS or OLS), as the collapse is reached so soon that the slight damage cannot be seen from the analysis. The capacity of the building is checked and shown also in ADRS format in Figure 4-11, where it is clear that the structure is very vulnerable and brittle, compared to the seismic demand according to the code.
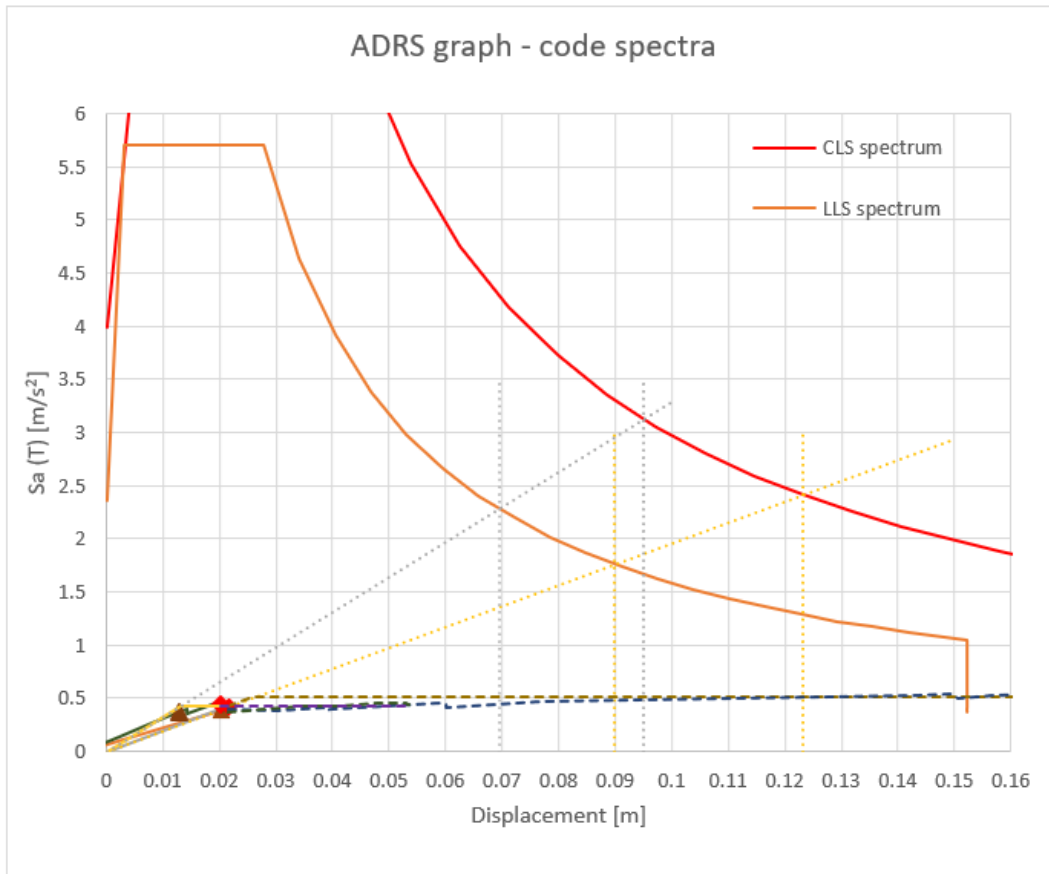
Figure 4-11: Capacity curves in Y direction with spectral and uniform load patterns in ADRS format, together with the code response spectrum for LLS and CLS. The displacement demand is shown with a yellow and grey vertical dotted line, for spectral and uniform load pattern respectively.

The vulnerability of the building is then checked also based on the scenario response spectra. Three percentiles are considered for each scenario: 50th, 84th and 95th. For each of these response spectra, the check, in terms of displacement, is made for CLS and LLS. The graphical check for Y direction of the building can be seen in Figure 4-12 and Figure 4-13, while the numeric data are shown in Table 4-8 in terms of Capacity displacement/Demand displacement. It can be noticed that the displacement demand of the 95th percentile of Medea scenario is very similar to the demand of the LLS code spectrum and is slightly higher. The only seismic input for which the building is verified, is the 50th percentile of Medea scenario. All the other cases show a very vulnerable building. It should be noticed that the collapse of the building happens at very low top displacements, around 0.032 m. As the building is 40.6 m heigh, the displacement corresponds to an average interstorey drift of **0.8‰.**
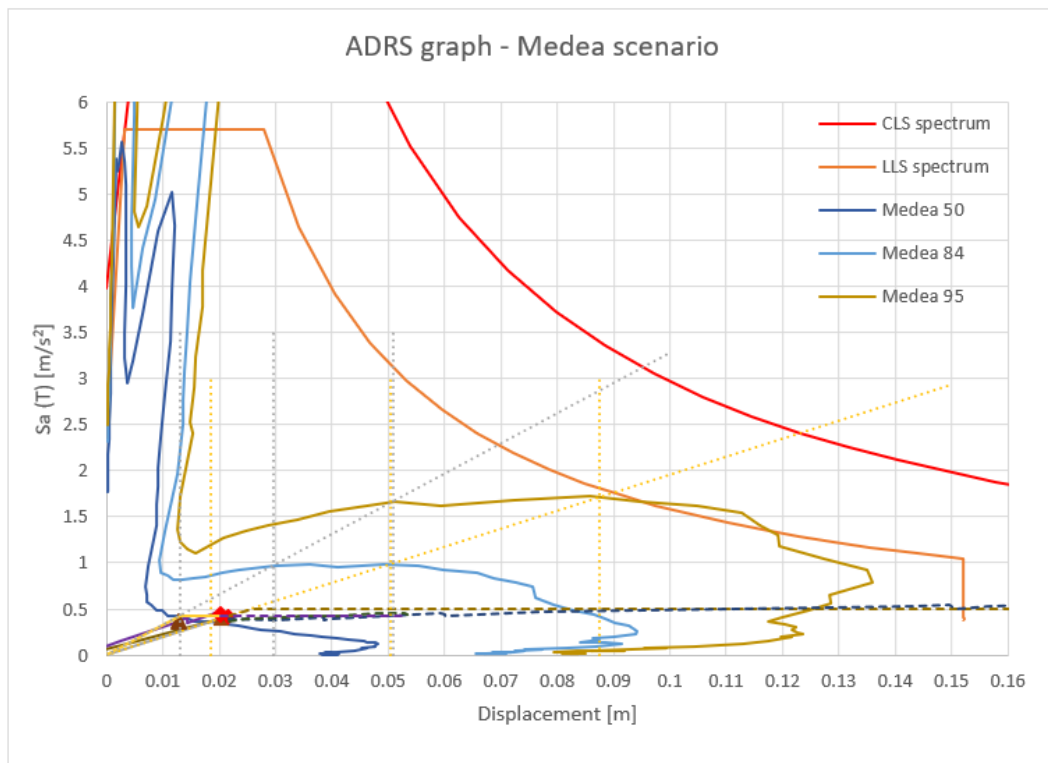
Figure 4-12: Capacity curves in Y direction with spectral and uniform load patterns in ADRS format, together with the Medea scenario response spectra (50th, 84th and 95th percentiles). For both load patterns, the LLS and CLS capacity of the building is marked with triangles and diamonds respectively. The displacement demand is shown with yellow and grey vertical dotted lines, for spectral and uniform load pattern respectively.

Figure 4-13: Capacity curves in Y direction with spectral and uniform load patterns in ADRS format, together with the Idrija scenario response spectra (50th, 84th and 95th percentiles). For both load patterns, the LLS and CLS capacity of the building is marked with triangles and diamonds respectively. The displacement demand is shown with yellow and grey vertical dotted lines, for spectral and uniform load pattern respectively.
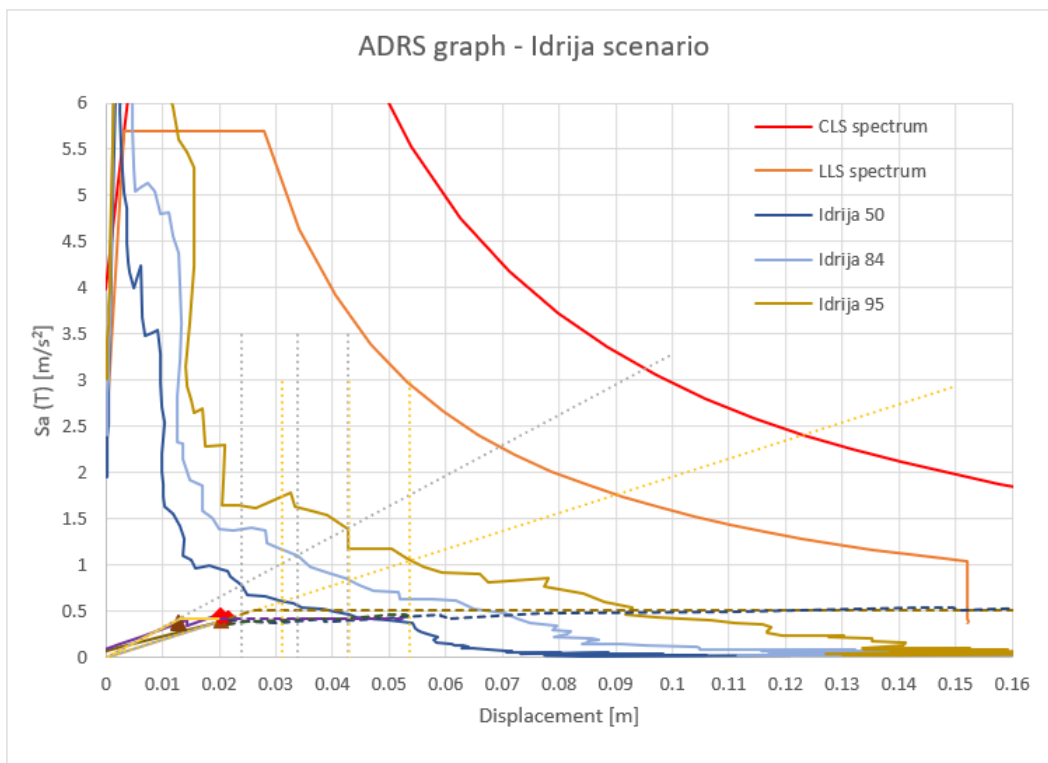
Table 4-8 shows, in the first line, the results of the check based on the code response spectra. In this case, one check is made with the demand from the CLS response spectrum, compared to the CLS capacity of the structure, and another check is made with the demand based on the LLS code spectrum, compared to the LLS capacity of the building. For this reason, the vulnerability index is lower for CLS than for LLS. On the contrary, in all the other lines, the vulnerability index is lower for LLS than for CLS, because the demand is calculated based on scenario response spectra (the same for both limit states CLS and LLS), while the capacity of the structure is lower for LLS than for CLS. It could be reasonable for example to compare the demand found for the 95th percentile of scenarios, just with the CLS capacity and the demand found for the 50th percentile, just with the LLS capacity. For completeness, all the indexes are calculated nevertheless.

Table 4-8: C/D ratios in terms of displacement for the capacity curves in Y direction, for CLS and LLS.

Seismic input	Load pattern	CLS	LLS
code spectra		0.176	0.225
Medea 50		1.170	1.094
Medea 84		0.431	0.403
Medea 95	Spectral	0.248	0.231
Idrija 50		0.698	0.653
Idrija 84		0.506	0.473
Idrija 95		0.404	0.377
code spectra		0.212	0.183
Medea 50		1.563	0.987
Medea 84		0.679	0.429
Medea 95	Uniform	0.397	0.251
Idrija 50		0.843	0.533
Idrija 84		0.596	0.377
Idrija 95		0.473	0.299

4.2.3. Non - linear dynamic analysis

The aim of this research is to evaluate seismic vulnerability of typical structures in the town of Gorizia. To do so, the evaluation of the vulnerability of the single building is not very significant and it is not extendable to other buildings, but fragility curves can show more data, that can be also usable in order to extend the results to similar buildings, as they are defined in probability terms.

Fragility curves are defined as the probability of exceeding a given damage level (or performance) as a function of a chosen parameter of intensity measure (IM) representing the ground motion. There are many methods to calculate fragility curves. In this case it has been chosen to use a cloud analysis. The procedure is the following:

1) **Build a numerical model**: just one have been used, uncertainties about the model have not been considered in the curves. The model used for the dynamic analyses is the same described in §4.2.2. The hysteretic behaviour of plastic hinges is automatically determined by the programme, based on the plastic hinges previously defined.

2) **Choose accelerograms** (30 to 50 accelerograms): the records already described in §4.1.2 have been considered. In order to better understand the behaviour of the building and also to better control the reliability of results, it has been chosen to perform analyses in just one main direction of the building with just one component of the accelerograms. The component of each record to be used for the analysis has

been chosen based on the highest value (for the first 30 accelerograms) or the lowest value (for the last 20 accelerograms) of the spectral acceleration for the fundamental period 1.7 s. The list of the chosen components of the records, with their PGA, Sa (T1) and Sa,eq,y (later specified) is reported in Table 4-9.

3) **Perform non-linear dynamic analyses** with all the accelerograms. Dumping is defined for each load case. A damping of 5% in the range of periods from 0.05 s to 2.45 s has been chosen. In a couple cases, an analysis stopped for convergence reasons, then the damping has been increased to 7% in the same range of periods.

4) **Choose an Engineering demand parameter (EDP)**, a parameter that can measure the damage/performance of the building (e.g. maximum interstorey drift or displacement at the top of the building).

5) **Choose an Intensity Measure of the ground motion**: the most common IM used in literature are the Peak Groud Acceleration (PGA) and the Spectral Acceleration for the fundamental period (Sa(T1)) [53][54], although also other parameters can be used (e.g. Housner index, Arias intensity I_A, spectral pseudo-velocity – PSV, spectral displacement S_d, equivalent input energy $E_{i,eq}$, elastic energy of spectral deformation $E_{e,mod}$ or others).

6) **Draw a graph with the cloud of dots given by (IM, EDP)** of each accelerogram.

7) **Calculate the linear regression** that fits the points (slope and intercept of the line and standard deviation are needed).

8) **Choose EDP$_0$** (the limit of the EDP for the considered damage level, for example one limit for each considered limit state).

9) **Calculate fragility curves**

The formulation for the calculation of fragility curves is the following:

$$P[EDP \geq EDP_0|IM] = 1 - \Phi\left(\frac{\ln(EDP_0) - \ln(aIM^b)}{\sigma}\right) \tag{4.1}$$

Where aIM^b is the equation of the regression line, σ is the standard deviation of the correlation and EDP_0 is the limit value of the EDP, for the considered limit state. The probability of exceedance of this limit is calculated with a log-normal distribution function.

Equation (4.1) can be rewritten as follows:

$$
\begin{aligned}
P[EDP \geq EDP_0|IM] &= 1 - \Phi\left(\frac{\ln(EDP_0) - \ln(aIM^b)}{\sigma}\right) = \\
&= \Phi\left(\frac{-\ln(EDP_0) + \ln(aIM^b)}{\sigma}\right) = \\
&= \Phi\left(\frac{b\ln(IM) - \ln(EDP_0) - \ln(a)}{\sigma}\right) = \\
&= \Phi\left(\frac{\ln(IM) - \dfrac{\ln(EDP_0) - \ln(a)}{b}}{\dfrac{\sigma}{b}}\right) = \\
&= \Phi\left(\frac{\ln(IM) - \lambda}{\zeta}\right)
\end{aligned}
\tag{4.2}
$$

Where $\lambda = \frac{\ln(EDP_0) - \ln(a)}{b}$ and $\zeta = \frac{\sigma}{b}$.

Table 4-9: Table with the used components of the records and their Intensity Measures used for the correlations.

	Load case	Component	PGA [g]	Sa(T1) [g]	Sa,eq,y [g]	Housner index [cm]
1	A.496	E	0.7578	0.179	0.288	96.818
2	A.ATS	E	0.1852	0.272	0.239	150.532
3	A.BUR	E	0.0999	0.183	0.141	81.804
4	A.GZL	E	0.7217	0.472	0.459	198.941
5	A.YPT	N	0.3222	0.331	0.270	175.441
6	BA.MIRE	N	0.2706	0.401	0.315	186.655
7	BA.MIRH	N	0.2701	0.338	0.265	176.514
8	EU.BAR	E	0.3600	0.495	0.382	251.279
9	EU.PETO	N	0.4537	0.123	0.289	148.907
10	EU.ULA	E	0.2139	0.271	0.221	124.280
11	EU.ULO	E	0.2368	0.412	0.324	182.864
12	HI.KAL1	E	0.2322	0.155	0.197	99.480
13	HL.AIGA	E	0.4982	0.146	0.281	118.074
14	HL.KALA	E	0.2162	0.191	0.183	118.773
15	HL.KORA	E	0.2404	0.193	0.180	98.067
16	HL.XLCA	E	0.2899	0.142	0.237	111.523
17	IT.ACC	E	0.4341	0.223	0.249	139.782
18	IT.AMT	N	0.3755	0.149	0.185	112.955
19	IT.AQA	E	0.4024	0.128	0.144	88.830
20	IT.AQG	E	0.4459	0.167	0.238	115.178
21	IT.AQK09	E	0.3300	0.314	0.258	59.906
22	IT.AQK16	N	0.0581	0.158	0.113	137.453
23	IT.BGI	E	0.1871	0.261	0.196	120.028
24	IT.CLF	E	0.2566	0.149	0.253	85.593
25	IT.CLO	E	0.4267	0.480	0.401	234.313
26	IT.CLT	E	0.1748	0.239	0.203	116.846
27	IT.CMI	E	0.6507	0.184	0.514	141.767
28	IT.CNE	N	0.2939	0.172	0.180	91.369
29	IT.GBP	E	0.0978	0.231	0.168	93.407
30	IT.MOG0	N	0.1703	0.214	0.178	95.065
31	E.ATR	E	0.0416	0.007	0.017	6.436
32	E.FRC	E	0.2338	0.017	0.247	28.288
33	IT.ASS	N	0.1547	0.008	0.062	10.139
34	IT.BGN	N	0.0432	0.002	0.014	2.440
35	IT.CR1	N	0.1066	0.008	0.039	8.845
36	IT.MCV	N	0.3591	0.021	0.113	19.822
37	IT.MRC	N	0.0137	0.018	0.015	10.173
38	IT.MSC	E	0.0387	0.020	0.028	9.506
39	IT.NRC	N	0.1469	0.004	0.041	5.238
40	IT.PCH	N	0.0458	0.002	0.011	2.542
41	IT.SGV	E	0.0026	0.000	0.001	0.211

42	IT.SNO	N	0.0101	0.000	0.006	0.756
43	IT.TDG	E	0.0167	0.005	0.010	5.669
44	IT.TRL	N	0.0392	0.014	0.021	12.015
45	IT.UMB	N	0.0129	0.003	0.009	3.733
46	IT.VZZ	N	0.0726	0.016	0.042	16.014
47	IV.NRCA	E	0.1262	0.002	0.027	2.558
48	MN.CEL	N	0.0002	0.000	0.000	0.089
49	OX.SABO	N	0.0034	0.006	0.004	2.798
50	TK.2501	N	0.0070	0.002	0.004	2.150

Fragility curves have been calculated for three limit states: Collapse limit state (CLS), Life Safety limit state (LLS) and Damage limit state (DLS).

In this first phase the analyses have been performed just in Y direction, the most flexible direction of the building. It has been chosen to analyse separately the two main directions of the building for better understanding its behaviour and control the numeric results. The first 30 signals have been first used, then it has been noticed that the building was reaching collapse with all the accelerograms, so lower intensity signals have been added.

Some combinations of EDP and IM have been tried in order to check the variability of the resulting fragility curves. As first, the simplest two parameters have been used: the **maximum interstorey drift as EDP and PGA as IM**. The choice of these parameters, that are the most common in literature [55][56], permits to compare the obtained results with literature results for similar structures.

The maximum interstorey drift has been calculated by considering the displacements of the nodes in a barycentric position. The drift has been calculated based on the total displacement of the nodes in X and Y direction. The results of the correlations found with all 50 signals are shown in Figure 4-14. The values of the maximum interstorey drifts are reported in Attachment, in Table 0-2. Fragility curves are reported for three limit states: CLS, LLS and DLS.

The limits for the interstorey drifts for the three limit states have been determined based on the results of pushover analysis. It has been seen that the failure is always brittle and that the first hinges collapse at around 0.032 m of displacement at the top of the building. As the building is 40.6 m high, the average insterstorey drift at collapse is around 0.8‰, that is much lower than the code limit for damage limit state in ordinary masonry buildings (2‰). For LLS and DLS the limit has been set to 80% and 50% of the limit for CLS respectively (Table 4-10). The correlation and the fragility curves are presented in Figure 4-14 and Figure 4-15.

Table 4-10: Chosen EDP_0 for fragility curves.

Limit State	Top displacement (from pushover)	Interstorey drift limit
CLS	0.032 m	0.8‰
LLS	0.025 m (80% of CLS)	0.6‰
DLS	0.016 m (50% of CLS)	0.4‰
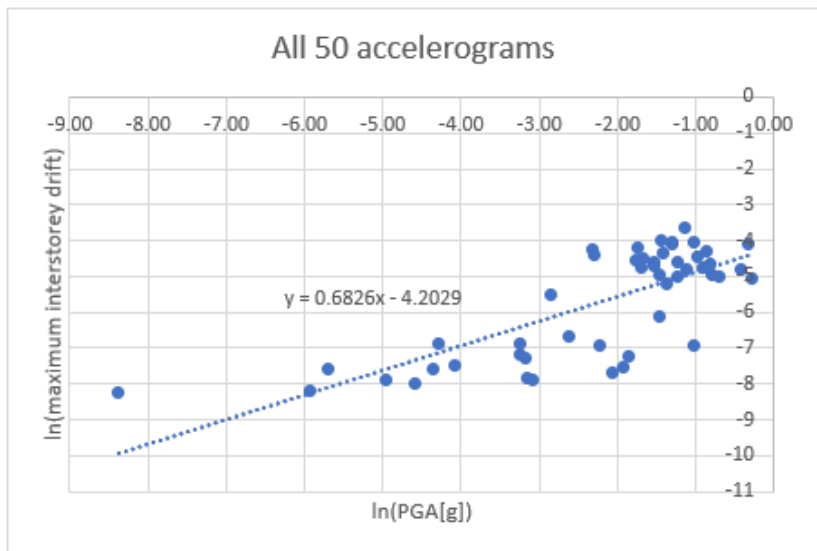
Figure 4-14: Bi-logarithmic correlation between the maximum interstorey drift and the PGA (σ =0.975).
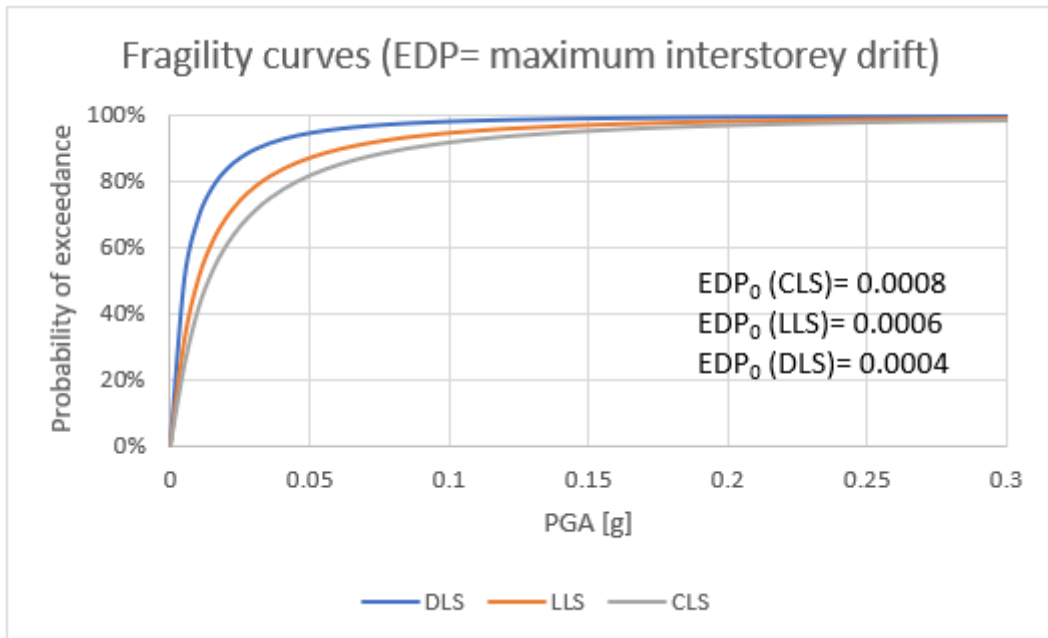
Figure 4-15: Fragility curves obtained considering the maximum interstorey drift in the building and PGA.

As the dots in the cloud of the correlation have a high dispersion and the standard deviation is high (σ=0.975), another IM has been adopted to make the correlation: spectral acceleration at T1=1.73 s (Sa(T1)). The correlation and the resulting fragility curves, calculated with respect to the same EDP_0, are presented in Figure 4-16 and Figure 4-17.

It can be seen that the dispersion of the dots of the cloud is much lower (σ=0.435) than in the case of correlation with PGA. It shows that the Sa(T1) is much more correlated to the effects of ground shaking on the building. This affects the fragility curves, that show in this case a very vulnerable building.
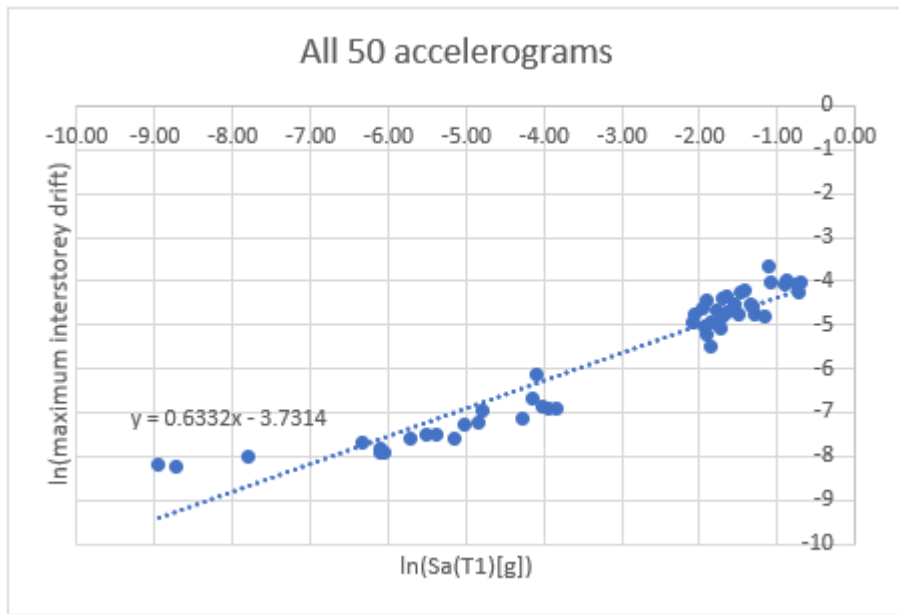
Figure 4-16: Bi-logarithmic correlation between the maximum interstorey drift and the spectral acceleration of the fundamental period Sa(T1) (σ =0.435).
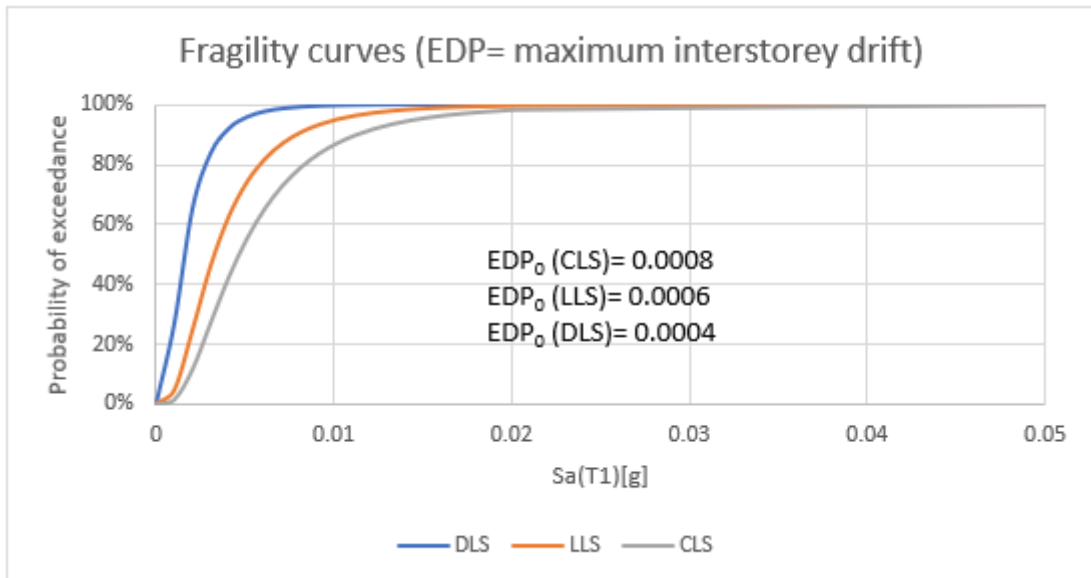
Figure 4-17: Fragility curves obtained considering the maximum interstorey drift in the building and spectral acceleration of the fundamental period Sa(T1).

As the building has a low participating mass ratio for the first period (<75%), it appeared to be rational to include in some way also spectral accelerations of the other modes. For this reason an experiment has been done by using a new IM, the equivalent spectral acceleration, in Y direction, Sa,eq,y, calculated on the first 10 modes. The equivalent spectral acceleration has been calculated based on the base shear of each mode and an SRSS combination of the modes. The result has been divided by the total participating mass (ratio) in order to find an acceleration:

$$S_{a,eq,y} = \frac{\sqrt{\sum_{i=1}^{10}(S_{a,y}(T_i) \cdot U_{y,i})^2}}{\sum_{i=1}^{10} U_{y,i}} \tag{4.3}$$

Where $U_{y,i}$ is the participating mass ratio, in this case in y direction, of the ith mode.

The correlation of the maximum interstorey drift with this IM and the consequent fragility curves are presented in Figure 4-18 and Figure 4-19.

The curves are slightly moved to the right, but as the standard deviation σ is higher than in the case of the correlation with Sa(T1), this IM does not seem to be more suitable than the spectral acceleration of the fundamental period.
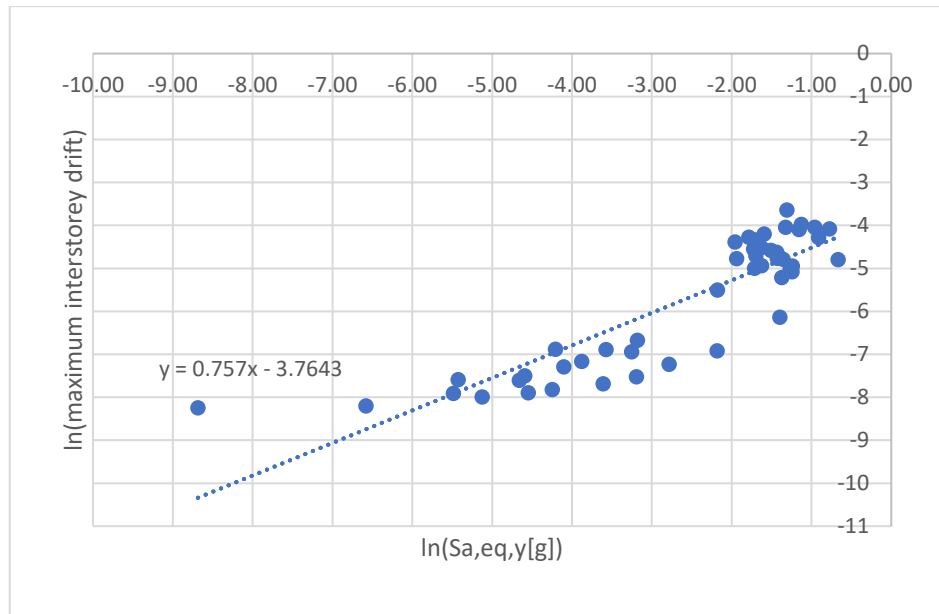
Figure 4-18: Bi-logarithmic correlation between the maximum interstorey drift and the equivalent spectral acceleration Sa,eq,y (σ =0.708).
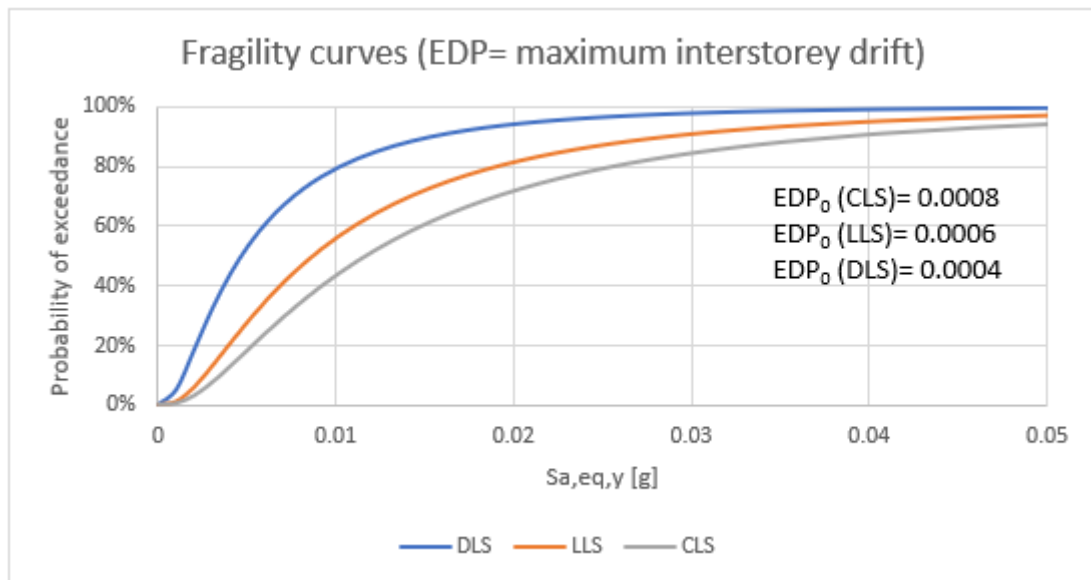
Figure 4-19: Fragility curves obtained considering the maximum interstorey drift in the building and Equivalent spectral acceleration Sa,eq,y.

As a last combination, also Housner index is used to check the correlation and calculate fragility curves (Figure 4-20 and Figure 4-21). Housner idex is defined as:

$$I_H = \int_{0.1}^{2.5} S_v(T, \xi = 0.05)dT$$

_____

where S_v is the pseudo-velocity spectrum, T is the fundamental period and ξ is the dumping ratio.
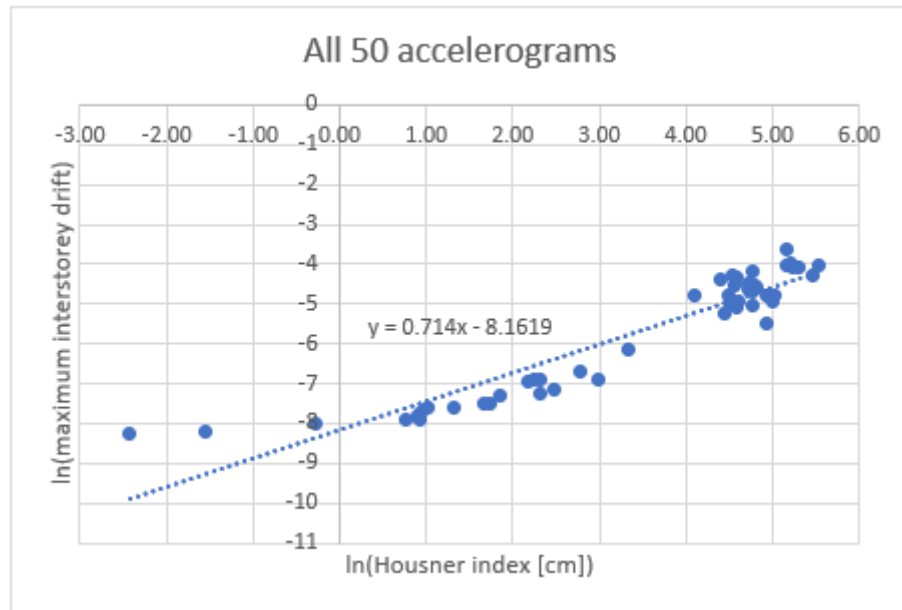
Figure 4-20: Bi-logarithmic correlation between the maximum interstorey drift and the Housner index (σ =0.510).
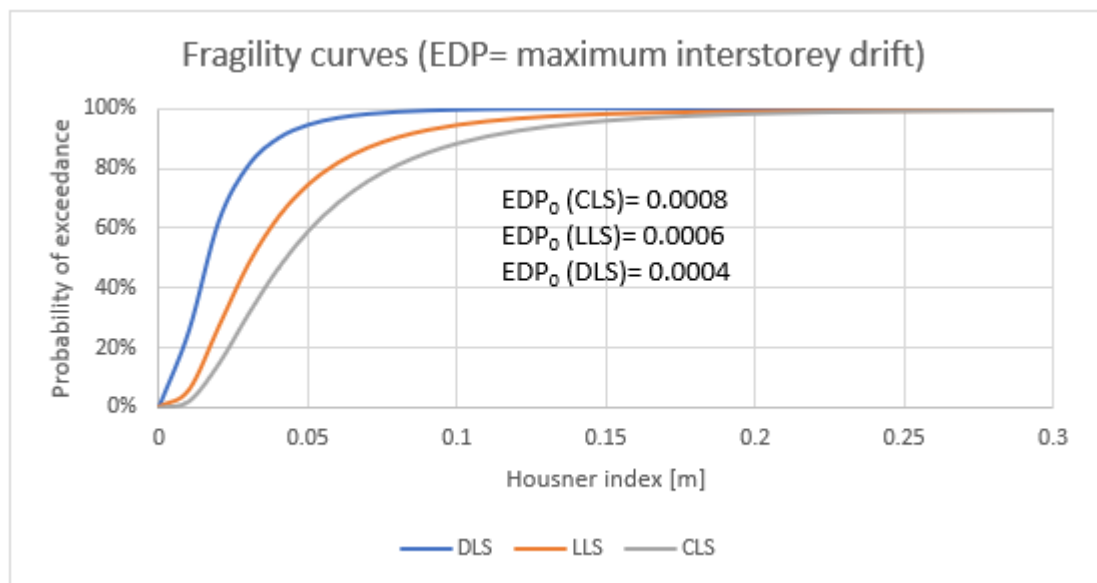
Figure 4-21: Fragility curves obtained considering the maximum interstorey drift in the building and Housner index as IM.

The behaviour of the building has been further investigated by considering another EDP. By manually checking the status of plastic hinges in the model during the dynamic analyses, it has been noticed that for all the analyses where some hinges reach the collapse, the first to collapse is a brittle shear hinge in the concrete walls of the stairwell (as already observed in pushover analyses). With the aim to find the best parameter that governs the brittle shear collapse, the maximum displacement at the top of the building has been considered (barycentrical joint 302). In order to find a suitable limit for this EDP, the displacement at the top of the building at the collapse of the first hinge has been considered. The value of the displacement has been checked for each of the first 30 analyses that caused at least one hinge collapse. Then an average value has been taken as a reference. The total displacement (resultant of X and Y direction) has been considered. All the considered values are shown in Figure 4-22, where also the median value and the standard deviation are displayed. The average value of 0.0107 m, compared to the height of the building of 40.6 m, means a drift of

_____

_____

0.000264= 0.3‰, that is really low (less than half of the value found with pushover analysis). When this limit is used for the calculation of the fragility curves based on the interstorey drift, very different results are obtained. The capacity reference values for the three limit states are listed in Table 4-11.

Table 4-11: Capacity of the building in terms of top displacement.

	Absolute top displacement	**Drift (H=40.6 m)**
CLS	0.0107 m	0.3‰
LLS	0.0086 m (80% of CLS)	0.2‰
DLS	0.0054 m (50% of CLS)	0.1‰

The chosen EDP is the ratio between the demand and the capacity (D/C) in terms of top displacement. The EDP_0 for CLS is thus 1, while for the LLS and DLS have been chosen 80% and 50% of the collapse. The correlation and fragility curves obtained from this last EPD and PGA as intensity measure, are displayed in Figure 4-23 and Figure 4-24. The data used for the correlation are reported in Attachment, in Table 0-3.
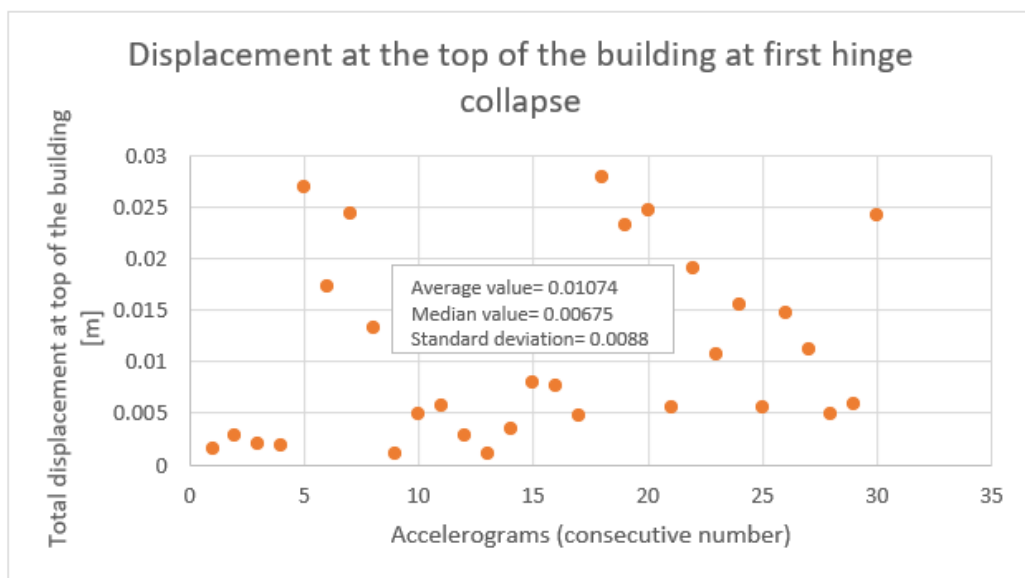
Figure 4-22: Displacement at the top of the building at the first hinge collapse for the first 30 analyses.

It can be noticed that the standard deviation in the correlation with PGA is just slightly lower than the one for the same correlation made with maximum interstorey drifts. Spectral acceleration of the first period appears to be a better choice for the IM. The standard deviation of this last correlation is the minimum among all the presented correlations (see Figure 4-25 and Figure 4-26).

_____

Figure 4-23: Bi-logarithmic correlation between the D/C ratio in terms of top displacement and the PGA (σ =0.973).

Figure 4-24: Fragility curves obtained considering the D/C ratio and PGA.

Figure 4-25: Bi-logarithmic correlation between the D/C ratio in terms of top displacement and the spectral acceleration Sa(T1) (σ =0.413).
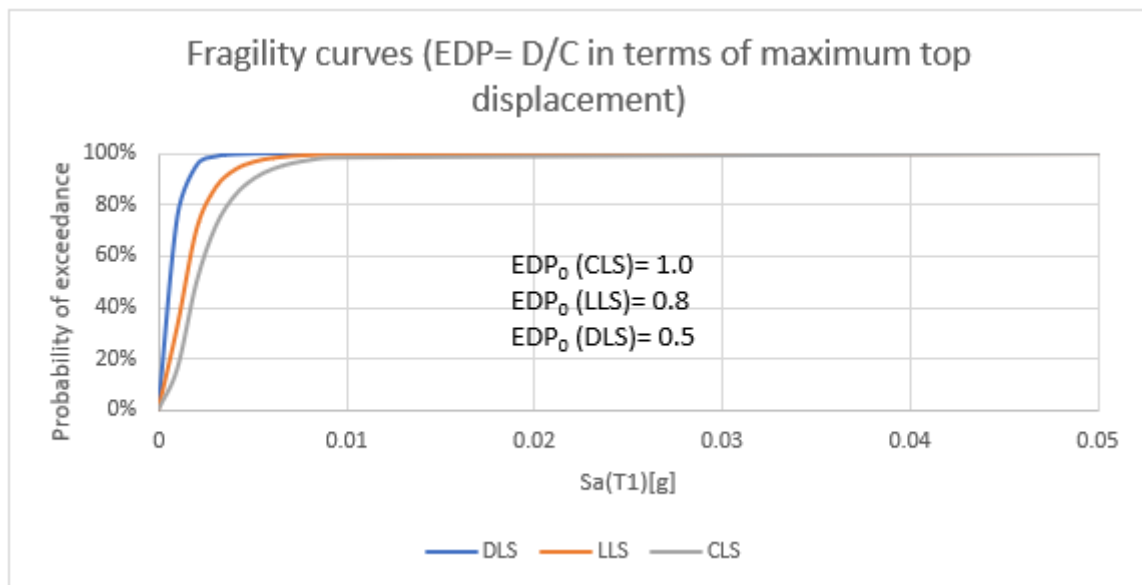
Figure 4-26: Fragility curves obtained considering the D/C ratio and Sa(T1).

As a last combination, also Housner index is used to check the correlation and calculate fragility curves (Figure 4-27 and Figure 4-28).
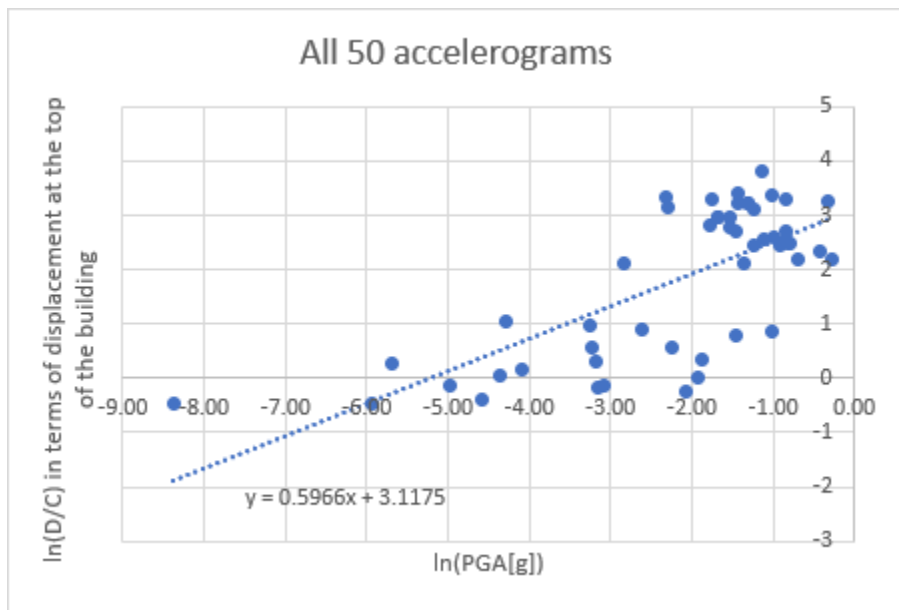
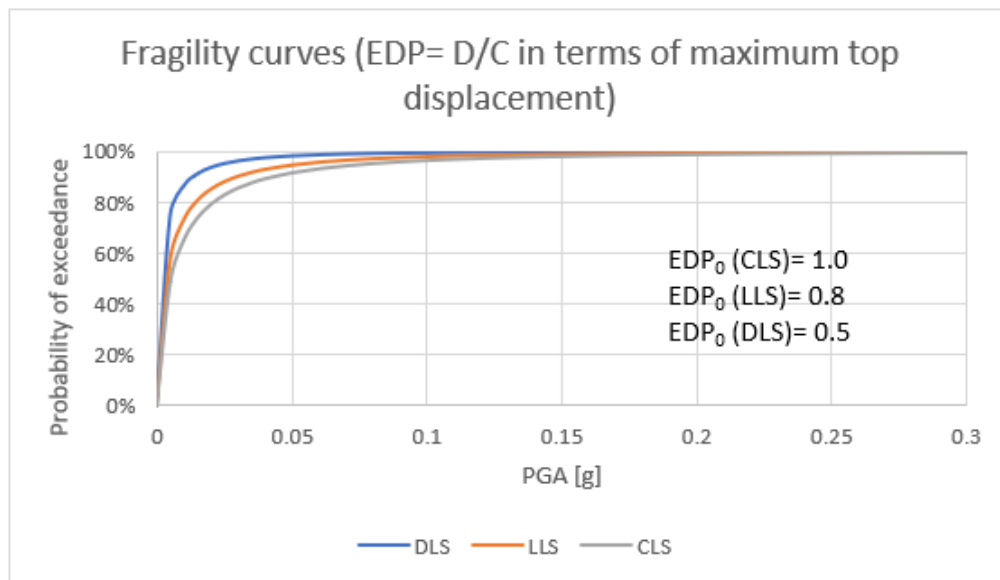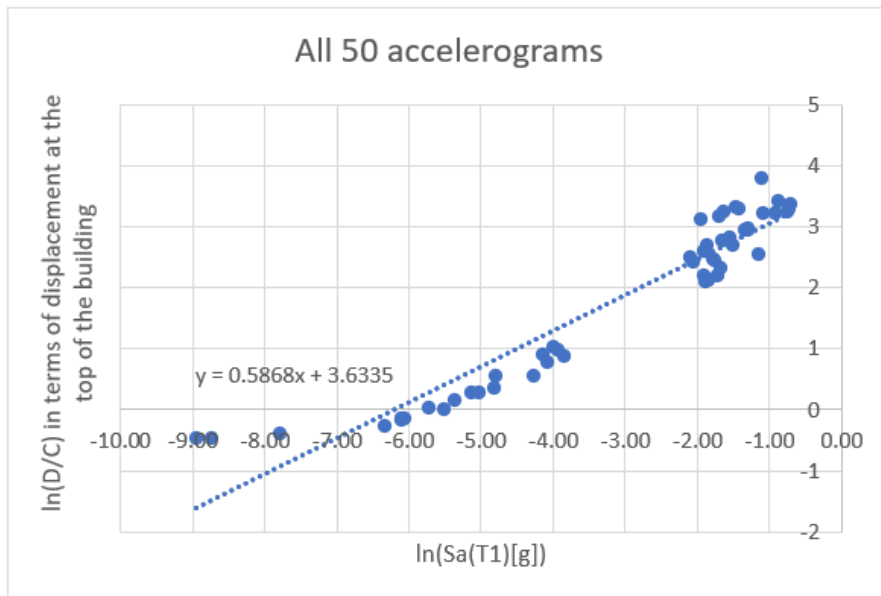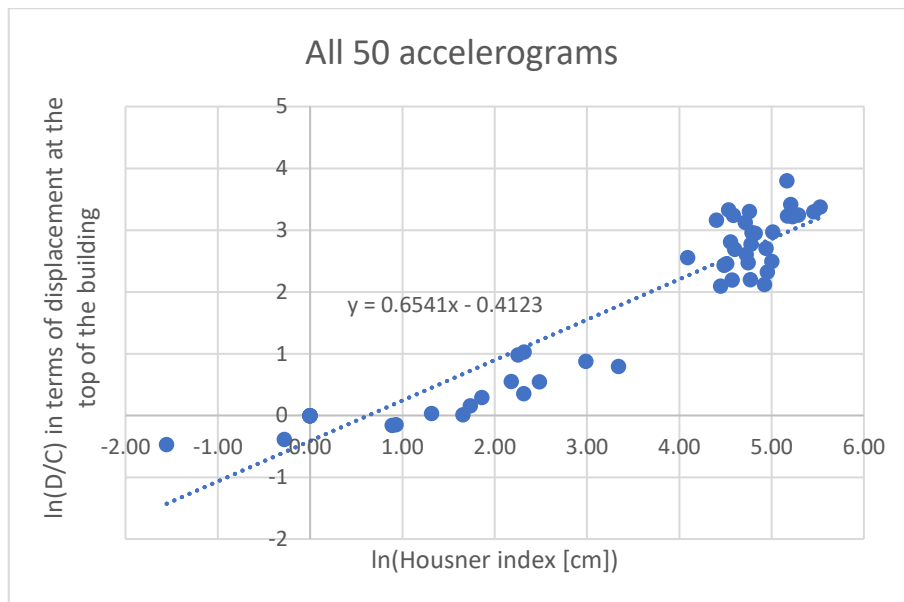**Figure 4-27: Bi-logarithmic correlation between the D/C ratio in terms of top displacement and the Housner index (σ =0.515).**
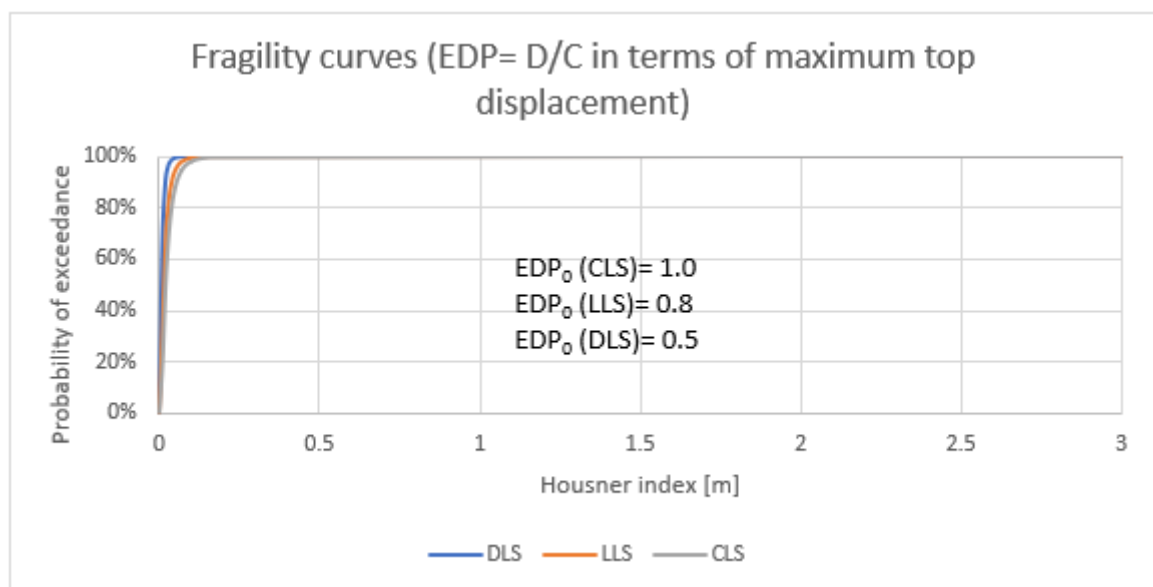
Figure 4-28: Fragility curves obtained considering the D/C ratio and the Housner index.

Among all the presented sets of fragility curves, one should be chosen as the representative of the building. For the calculation of the curves, two criteria have been used to set the damage state thresholds: the first is based on the top displacement at the collapse in non-linear static analysis, the second is based on the top displacement in the non-linear dynamic analyses at the moment of the first hinge collapse. It has been noticed that the second criterium leads to fragility curves that have too high probabilities to exceed CLS for very low intensity measures, corresponding to frequent and low intensity seismic events. This is due to the definition of CLS capacity of the building, that has been set at the collapse of the first plastic hinge, while the building has usually a not negligible capacity of plastic redistribution. For this reason, the first criterium is considered more reliable.

The fragility curves of the building are then compared to fragility curves of similar buildings from literature [57] [56]. Although this type of structures in Italy is very diffuse, there are just few research studies about RC buildings with RC walls (core) [58][59] and usually just framed structures are investigated. It can be noticed that the case study building results to be much more vulnerable

than the average building with similar, but framed only, structure (Figure 4-29, Figure 4-30, Figure 4-31 and Figure 4-32).

For the comparison of the fragility curves, it is fundamental to know the data with which they have been built. In [57] the building has been defined with simulated design. It is not a real existing building. It has been designed based on the Italian code Regio Decreto del 1939 n. 2229, that was used before 1971, for non-seismic areas (design for gravitational loads only). The chosen EDP is the maximum interstorey drift. The interstorey height is 3 m. The strength of the concrete is assumed equal to 16 MPa, while the steel is a Aq42 (yielding stress 250 MPa). The difference with the RC building 1 is that the building from [57] has no concrete walls, but just concrete frames. Also the number of storeys is different, as RC building 1 has 5 storeys more than the building in [57]. The most important parameter, that influences the fragility curves, is the interstorey drift limit for each damage level. Four damage levels have been considered in [57], defined in Table 4-12.

Table 4-12: Definition of the limits of the interstorey drift for four damage levels in [57].

Damage level	Drift/h (%)
Null	<0.1
Slight	0.1 – 0.25
Moderate	0.25 – 0.5
Severe	0.5 – 1.0
Collapse (partial or total)	>0.1

It can be noticed that the allowed interstorey drift for the collapse is 1.25 times higher than the one considered for RC building 1 (collapse at 0.8‰). Moreover, as the considered building has no concrete walls, the collapse probably occurs in a ductile way (moment plastic hinges) and not for brittle shear collapse.

The fragility curves in [56] are built for a reinforced concrete (RC) frame structure representative of 1980s construction in the Central United States. "A five-story flat-slab RC case study building with a moment frame system was used in this study. It was designed based on the code requirements used in the Central US region during the early 1980s. Performance levels were described in terms of drift limits based on the global-level and member-level limits found in the Prestandard and commentary for the seismic rehabilitation of buildings (FEMA 356), along with additional quantitative drift limits based on the specific response characteristics of the structure." The non-linear dynamic analyses were conducted with synthetic ground motion data. Also in this case, the building does not have any concrete wall. The drift demand value is the maximum interstorey drift. The limits, based on FEMA 356, are shown in Table 4-13.

Table 4-13: Interstorey drift limits used for the definition of fragility curves in [56].

Interstory drift limits based on FEMA 356 global-level criteria (percent)

Structure	Drift limits (%)		
	IO	LS	CP
Concrete frame	1	2	4 (2.9[a])
Concrete wall	0.5	1 (0.85[b])	2 (1.2[b])

[a] Punching shear, CP limited to 2.9% versus 4% based on punching shear prediction.
[b] Shear wall failure, LS and CP limited to 0.85% and 1.2% versus 1% and 2% based on shear wall failure in shear.

_____

Table 4-14: Interstorey drift limits based on FEMA 356 member-level and additional quantitative limits (percent) [56].

Interstory drift limits based on FEMA 356 member-level and additional quantitative limits (percent)

Structure	FEMA 356 global			FEMA 356 member (Regular push-over)			FEMA 356 member (Critical response push-over)		
	IO	LS	CP	IO	LS	CP	IO	LS	CP
Unretrofitted	1	2	2.9[a]	0.88	0.88	1.07	0.62	0.62	0.69
Retrofit 1	0.5	0.85[b]	1.2[b]	0.4[c]	0.6[c]	0.75[c]	0.4[c]	0.6[c]	0.75[c]
Retrofit 2	1	2	2.9[a]	0.96	1.29	1.29	0.88	1.37	1.37
Retrofit 3	1	2	2.9[a]	1.07	1.74	1.89	0.83	1.46	1.81

[a] Drift limits for CP limited to 2.9% versus 4% based on punching shear prediction.

[b] Drift limits for LS and CP limited to 0.85% and 1.2% versus 1% and 2% based on shear wall failure in shear.

[c] Drift limits governed by the FEMA 356 member-level criteria for shear wall members in Table 2.8 [11].

[d] PMI limited to 1.2% based on shear wall failure in shear.
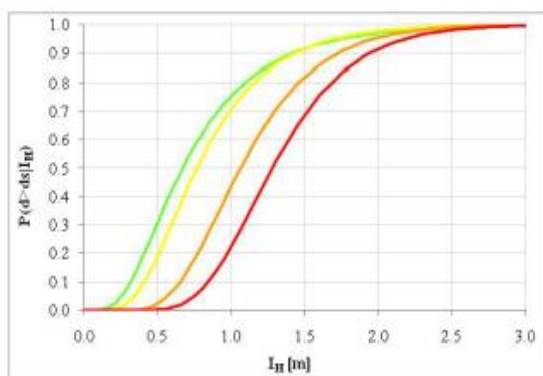
Figure 4-29: Fragility curves for 8-storey bare frame built before 1971, for four damage levels (slight, moderate, severe and partial or total collapse) [57].
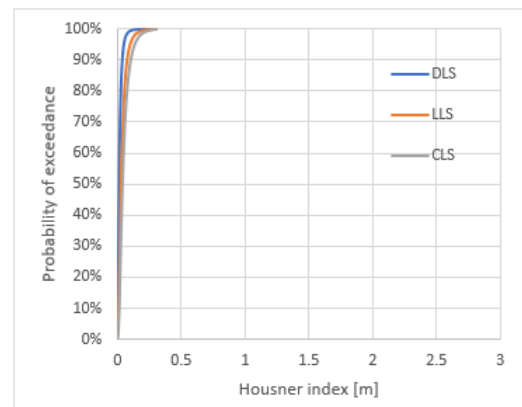
Figure 4-30: Fragility curves for RC building 1, in Y direction – 13 storeys, frame + concrete walls, built in 1968. Three limit states (collapse, life safety and damage limit states). IM= Housner index.
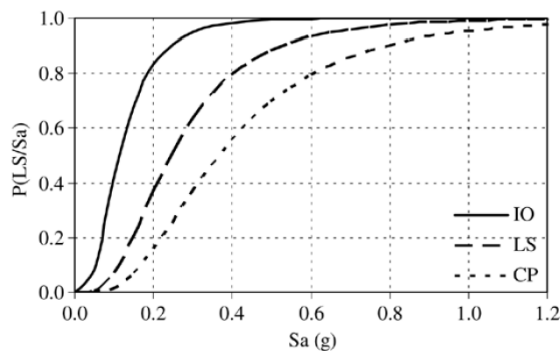
Figure 4-31: Global-level fragility curves for unretrofitted RC frame structure representative of 1980's construction in the Central United States – 5 storeys [56].
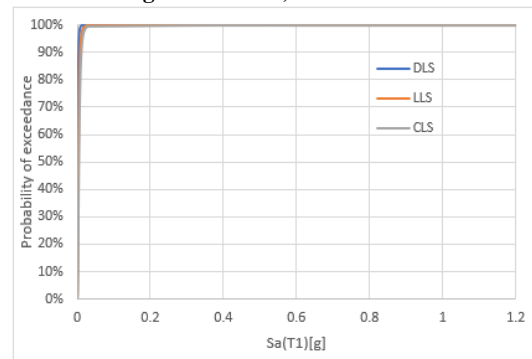
Figure 4-32: Fragility curves for RC building 1, in Y direction – 13 storeys, frame + concrete walls, built in 1968. Three limit states (collapse, life safety and damage limit states). IM=spectral acceleration.

Figure 4-33 shows another set of fragility curves obtained by [56] for the same unretrofitted building, together with some fragility curves obtained for the retrofitted building (not of interest in this case). These ones were obtained for drift limits of the FEMA 356 member-level limits, based on the storey-by-storey push-over analysis (critical response push-over) – see Table 4-14. It can be noticed that the

_____

curves for the unretrofitted building are translated to the left, in a similar way as the ones found for RC building 1.
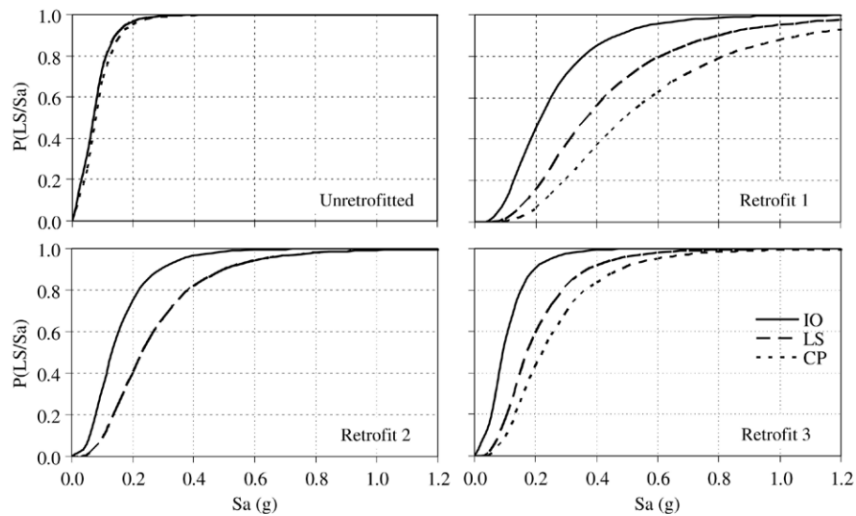
Figure 4-33: Fragility curves based on FEMA 356 member-level limits [56].

4.2.4. *Vulnerability evaluation*

As already mentioned, for the calculation of fragility curves, two criteria have been used to set the damage state thresholds and the first has been considered more reliable. Among the different IM used, fragility curves obtained from the correlation with the lowest standard deviation are chosen as the most indicative, that is spectral acceleration at the fundamental period. They show that the building has collapsed for sure for a spectral acceleration of 0.028 g = 0.27 m/s^2, that is a very low value.
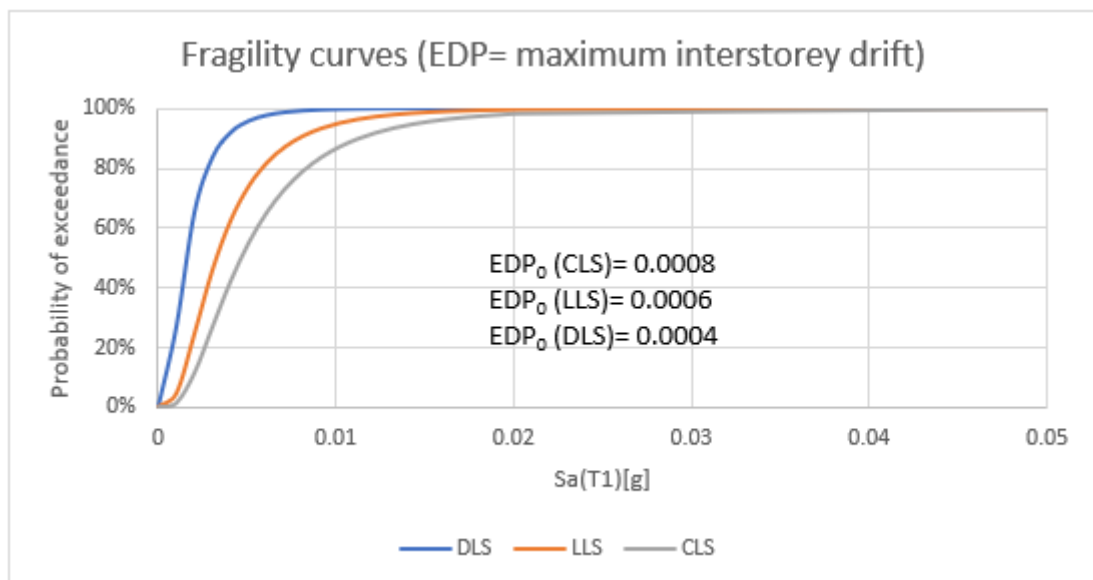
Figure 4-34: Final fragility curve for RC building 1.

If the scenario response spectra are considered, the spectral acceleration for the fundamental period of 1.7 s, for Idrija fault is 0.031 g for the 5th percentile, 0.039 g for the 16th percentile, 0.053 g for the 50th percentile, while for Medea fault is 0.011 g for the 5th percentile, 0.014 g for the 16th percentile and 0.033 g for the 50th percentile. These values are almost all over the 0.028 g (just Medea 5th and 16th percentiles are lower), so that the probability of exceedance of all three limit states is high.

If we consider the code spectra, there is a value for each limit state (Table 4-15):

Table 4-15: Spectral accelerations for the fundamental period of the case study building (code spectra).

Limit state	Spectral acceleration
CLS	0.198g
LLS	0.147g
DLS	0.044g

It is evident that the code spectral accelerations are higher than scenario accelerations for the given fundamental period and that the scenario values are almost all under the DLS value. In every case the building exceeds the limit states with 100% probability.

In order to better see the vulnerability results, the probability of the structure of being in a given limit state, for a given Sa value, is plotted in the histogram in Figure 4-35 for three values of Sa: the value from the code response spectrum for the DLS, the value of the 5th percentile for Idrija scenario and for Medea scenario. Just with Medea 5th percentile, there is 4% probability to be in DLS and 7% probability to be in LLS for the structure, otherwise there is certainty of collapse.

Figure 4-35: Histogram with the probability of the structure to be in a given Limit State, for three different values of Sa: value from the code response spectrum for DLS and values of the 5th percentile of the two analysed scenarios, Idrija and Medea.
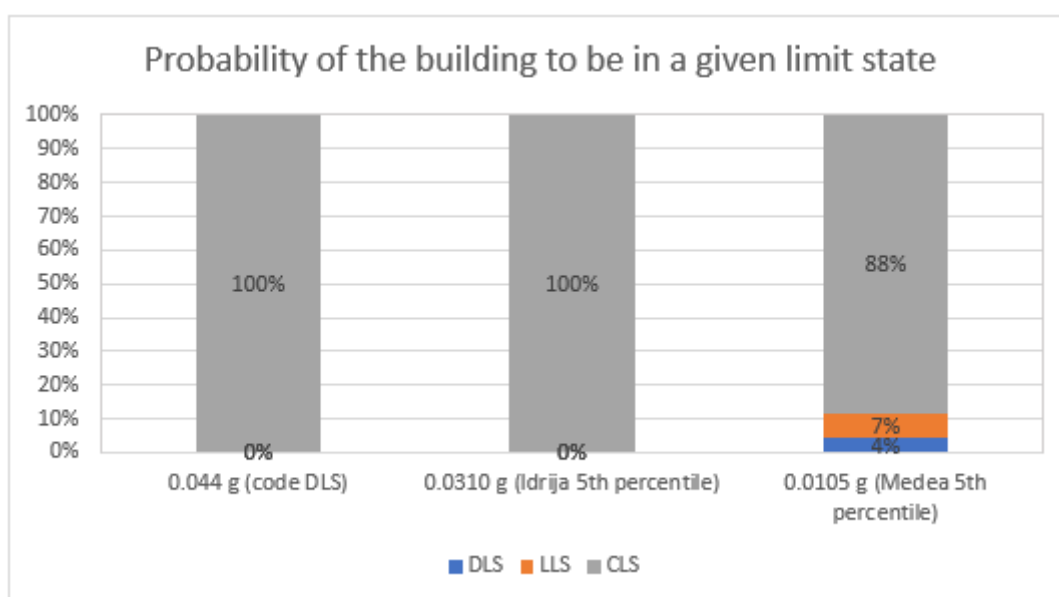
4.3. RC building 2

4.3.1. Modal analysis and comparison between different modelling choices

Also this second case study building has been analysed with different analyses and types of model in order to verify the reliability of the model, before using it to define its seismic vulnerability.

A similar comparison, as done for RC building 1, has been done, in order to see the difference in the results, when masonry infills are considered in the model or not. According to the code, for performing linear dynamic analysis (response spectrum analysis) a minimum number of modes for considering at least 85% of participating mass in both directions is needed. For RC building 2, 44 modes have been considered in order to satisfy this requirement. This shows the irregularity of the structure, that has already been exposed in §3.2.5. The first 12 modes are presented in Table 4-16.

Table 4-16: Participating mass ratios for the first 12 modes of the structure including the basement.

_____

Participating mass ratios

Mode	Period [s]	UX	UY	SumUX	SumUY	RX	RY	RZ	SumRX	SumRY	SumRZ
1	2.469	0.012	0.244	0.012	0.244	0.151	0.003	0.344	0.151	0.003	0.344
2	2.009	0.032	0.334	0.044	0.578	0.234	0.014	0.236	0.386	0.017	0.579
3	1.832	0.568	0.005	0.611	0.583	0.003	0.307	0.028	0.389	0.324	0.608
4	0.749	0.021	0.019	0.632	0.603	0.015	0.028	0.073	0.404	0.352	0.681
5	0.495	0.111	0.019	0.743	0.622	0.012	0.077	0.014	0.416	0.429	0.695
6	0.389	0.003	0.027	0.746	0.650	0.015	0.002	0.068	0.431	0.431	0.763
7	0.385	0.014	0.114	0.760	0.764	0.069	0.008	0.003	0.500	0.440	0.766
8	0.241	0.006	0.003	0.766	0.767	0.003	0.007	0.019	0.503	0.447	0.786
9	0.209	0.044	0.006	0.810	0.773	0.006	0.032	0.008	0.509	0.479	0.793
10	0.167	0.004	0.003	0.814	0.776	0.003	0.004	0.010	0.512	0.483	0.803
11	0.151	0.001	0.054	0.815	0.830	0.048	0.000	0.015	0.560	0.483	0.818
12	0.146	0.000	0.000	0.815	0.830	0.000	0.000	0.000	0.560	0.483	0.818

The first mode (T1=2.47 s) is rotational and translational, with a greater mass participation in Y direction. The second mode (T2=2.01 s) is very similar, while the third mode is mainly translational in X direction (T3=1.83 s). All the other modes have very low participating mass ratios.

After this modal analysis, another model of the building has been built, considering also the masonry infills. As done for RC building 1, also for this case study building, the infills have been modelled as equivalent pinned compressed diagonals (single-strut model), according to Decreto Ministeriale del 16 gennaio 1996 and to the Circolare Ministeriale n.65 del 10 aprile 1997.

The available information about the infills is just the statement in the technical report that describes the infills as made of an outer wythe of 13 cm thick bricks and an 8 cm inner wythe. As the two wythes are separated, it has been chosen to consider just the thicker wythe in the model. The equivalent diagonals have thus a section that is 13 cm deep and the height of the section is calculated as 1/10 of the length of the diagonal itself. The diagonals have been positioned in all the outer walls, considering the reduced stiffness given by the openings. They have been drawn in such a direction so that they are compressed when performing pushover analysis in positive direction (Figure 4-36).

The facades are full of windows and balcony doors, that have a great influence on the strength of the infills. For this case-study building the influence of the openings is taken into account according to [60][51], with a reduction factor that depends on the area of the infill (A_P) and the area of the opening (A_0):

$$R_F = 1 + 0{,}6 \cdot \left(\frac{A_0}{A_P}\right)^2 - 1{,}6 \cdot \left(\frac{A_0}{A_P}\right) \tag{4.4}$$

It does not consider the influence of the position of the opening in the infill, as [51] does, but in this case the openings are all approximately in the centre of the infills, so that this methodology has been chosen. The reduction factor is suitable for both stiffness and strength and there is no limitation on the A_0/A_P ratio.

The openings have not been considered influencing the stiffness of the infills, but just their strength. The factor has been thus applied to the strength of the plastic hinges of the infills (see below), while the section of the diagonals remains the same, when there is an opening in the infill.

As no information is available about the material of the infills, parameters from the Italian code (Circolare n.617 del 2 febbraio 2009- Tabella C8B.1) have been considered (see Table 4-17),

but they have been lowered in order to obtain stiffness and strength that are not excessively higher than the ones of the bare frame.

Table 4-17: Mechanical properties of masonry made of clay bricks with <45% of voids (code parameters).

Mechanical characteristics of masonry from Circolare n.617	
Compression strength f_k	4.0 N/mm²
Shear strength f_{vk0}	0.3 N/mm²
Elastic modulus E_m	3600 N/mm²

The parameters considered in the model are listed in Table 4-18.

Table 4-18: Mechanical properties of the masonry considered for the infills.

Mechanical characteristics of masonry infills	
Compression strength f_k	1.20 N/mm²
Shear strength f_{vk0}	0.05 N/mm²
Elastic modulus E_m	1200 N/mm²

As also pushover analysis is performed on the model, it is needed to calculate the strength of the infills, in order to assign them a plastic hinge. According to Allegato A della Circolare Ministeriale n.65 del 10 aprile 1997, there are three different collapse mechanisms: shear slip, diagonal tension and corner crushing. The strength in the three different cases can be calculated as follows:

Shear-slip:

$$H_0 \leq \frac{\tau_u}{\phi} \cdot l \cdot t \tag{4.5}$$

$$\tau_u = f_{vk0} \sqrt{1 + \frac{(\frac{0,8h}{l} - 0,2)}{1,5 \cdot f_{vk0}} \cdot \frac{H_0}{l/t}} \tag{4.6}$$

Diagonal tension:

$$H_0 \leq \frac{f_{vk0}}{0,6 \cdot \phi} \cdot l \cdot t \tag{4.7}$$

Corner crushing:

$$H_0 \leq 0,8 \cdot \frac{f_k}{\phi} \cdot \cos^2 \theta \cdot \sqrt[4]{\frac{E_c}{E_m} \cdot I \cdot h \cdot t^3} \tag{4.8}$$

Where h, l and t are the dimensions of the masonry infill;

H_0 is the horizontal seismic force acting on the masonry element (horizontal component of the force in the equivalent diagonal), considering behaviour factor β;

f_{vk0} is the characteristic shear strength without vertical loads;

f_k is the characteristic compression strength of masonry;

θ = arctg (h/l) is the angle between the diagonal and the horizontal direction;

φ is a reduction factor for the stresses: it is equal to 2 for verification with admissible stresses, it is equal to 1 for verification with limit states;

E_c is concrete elastic modulus;

_____

E_m is masonry elastic modulus;

I is the moment of inertia of the section of the column, calculated with respect to the axis perpendicular to the plane of the infill.

4.3.1.1. *Plastic hinges for the infills*

With the purpose to perform non-linear static analysis on the model with the infills, axial force brittle plastic hinges are applied to the middle of the equivalent diagonals representing the infills. The strength of the infills has been calculated as the minimum value among the three collapse mechanisms, the reduction factor due to the openings has been applied and then it has been transformed into the diagonal component (see equation (4.9)) in order to apply it to the equivalent diagonals:

$$P_{Rd} = \frac{H_{Rd}}{\cos\theta} \tag{4.9}$$

The defined strength is the force after which there is the collapse of the plastic hinge, while the acceptance criteria for Immediate Occupancy, Life Safety and Collapse Prevention are automatically set at 0.5, 0.8 and 1 respectively.

4.3.1.2. *Modal analysis of the building with infills*

The first differences between considering and not considering the masonry infills in the model can be seen by performing a modal analysis. Table 4-19 shows some results, in terms of natural periods and participating mass ratios for the first 12 modes. It can be noticed that the structure has a much more regular behaviour, compared to the model where the infills were not considered. The first mode (T1=1.76 s) has 58.4% of participating mass in Y direction, the second mode (T2=1.43 s) is rotational and the third mode (T3=1.36 s) has 60% of participating mass in X direction. All the other modes have much lower participating masses.

As it has been noted for RC building 1, also for RC building 2 the infills have a fundamental role in the elastic phase of the building's behaviour. They increase the stiffness of the part of the load-bearing structure that is otherwise very flexible (the RC frames), so that the huge stiffness of the decentred stairwell is not anymore the prevalent stiffness and the centre of stiffness moves closer to the centre of mass, regularizing the whole behaviour. Moreover, the natural periods noticeably decrease, meaning higher seismic forces in case of linear dynamic response spectrum analysis.

Table 4-19: Periods and participating mass ratios for the numerical model of the building where also masonry infills are considered.

|					Participating mass ratios						
Mode	Period [s]	UX	UY	SumUX	SumUY	RX	RY	RZ	SumRX	SumRY	SumRZ
1	1.761	0.003	0.584	0.003	0.244	0.364	0.001	0.016	0.364	0.001	0.016
2	1.433	0.041	0.015	0.044	0.578	0.016	0.012	0.599	0.380	0.013	0.615
3	1.360	0.599	0.000	0.611	0.583	0.000	0.292	0.032	0.380	0.306	0.648
4	0.496	0.020	0.034	0.632	0.603	0.032	0.036	0.047	0.413	0.342	0.695
5	0.406	0.088	0.035	0.743	0.622	0.027	0.104	0.003	0.440	0.445	0.698
6	0.356	0.008	0.092	0.746	0.650	0.063	0.007	0.061	0.503	0.452	0.760
7	0.275	0.012	0.009	0.760	0.764	0.007	0.006	0.019	0.509	0.459	0.778
8	0.189	0.029	0.009	0.766	0.767	0.009	0.016	0.012	0.518	0.474	0.790
9	0.185	0.014	0.000	0.810	0.773	0.001	0.018	0.010	0.519	0.492	0.800
10	0.147	0.002	0.052	0.814	0.776	0.043	0.001	0.011	0.562	0.493	0.811
11	0.146	0.000	0.000	0.815	0.830	0.000	0.000	0.000	0.562	0.493	0.811
12	0.146	0.000	0.001	0.815	0.830	0.001	0.000	0.003	0.562	0.493	0.814

_____
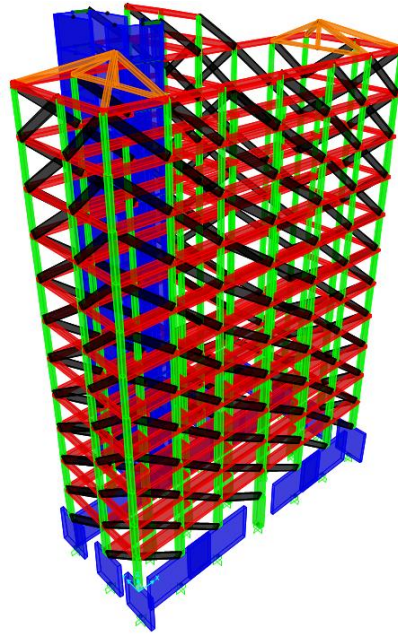
Figure 4-36: 3D view of the numerical model of RC building 2, where also masonry infills in the outer walls have been modelled.

4.3.1.3.   Non-linear static analysis

For this case study building a further investigation is made, in order to evaluate the influence of masonry infills after the linear elastic phase. As the behaviour of the model with infills is different from the model without infills, the load patterns used for the non-linear static analysis should be different, but as the infills collapse, the structure tends to return to the behaviour of the model without infills. For this reason the load pattern is calculated on the model without masonry infills and it is applied to both models.

The lateral loads are calculated in the same manner as it has been explained for RC building 1. The first load pattern ("spectral") is proportional to the storey forces, obtained from a response spectrum analysis (LLS response spectrum) separately in X and Y direction. The second load pattern is a "uniform" load pattern, proportional to the storey masses. Figure 4-37 shows the collapse of the model during the analysis in X direction with spectral load pattern. It can be seen that many hinges of the infills are collapsed (red dots).
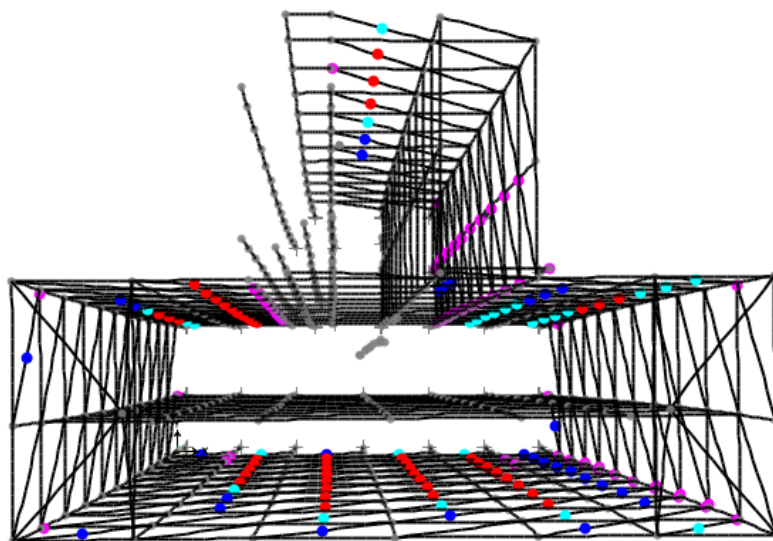

Figure 4-37: Activated plastic hinges at the collapse limit state (CLS) for the analysis in X direction with spectral lateral load.

The following images (Figure 4-38, Figure 4-39, Figure 4-40 and Figure 4-41) show the pushover curves for the two models (with and without considering masonry infills). Both curves have been cut when the CLS is reached.

The structure is not actually considered collapsed, when just the infills are collapsed, but the software cannot find the convergence for continuing the analysis after many hinges collapse. On the other hand it is clear that if the infills are not effective anymore and they are taken away, the behaviour of the model becomes equal to the behaviour of the model without infills, where just the load-bearing structure withstands lateral forces. In a static situation (as in this analysis) it is probable that there is a strength drop with respect to the strength obtained with effective infills (vertical red arrow in the graphs), but in a dynamic situation, where the seismic force cannot just disappear in the moment when the infills collapse, it is more credible that the RC frame absorbs the whole load insisting on the structure at the moment of the collapse of the infills, becoming more deformable and so having a sudden greater deformation for the same load. For this reason also a horizontal red arrow has been added to the graph, to show a possible evolution of the behaviour of the structure. The real behaviour is thus in the range between the horizontal and vertical red arrows, shown with the orange dashed line.

From the curves it can be noticed that the masonry infills increase not just the stiffness of the building but also the strength, on the other hand they collapse very soon with brittle mechanisms. The collapse intervenes in correspondence of small displacements.

This shows that the choice of modelling or not the masonry infills for sure influences the results of the vulnerability evaluation, but when modelling the infills, the choices of how to model them is also fundamental and affects the results. It also shows that the level of influence of the infills on the building's behaviour depends on the material of the infills and thus it should be investigated with the same attention as the materials and details of the main load-bearing structure.

In a limit condition when the masonry infills have ductility and strength comparable with the ones of the concrete walls of the staircase, that for buildings like the presented case studies are very brittle, it could happen that they collapse more or less simultaneously. In this case it is fundamental to model also the masonry infills, when analysing the structure, as its stiffness and strength is fully dependant on the behaviour of the infills, until the collapse of both of them.
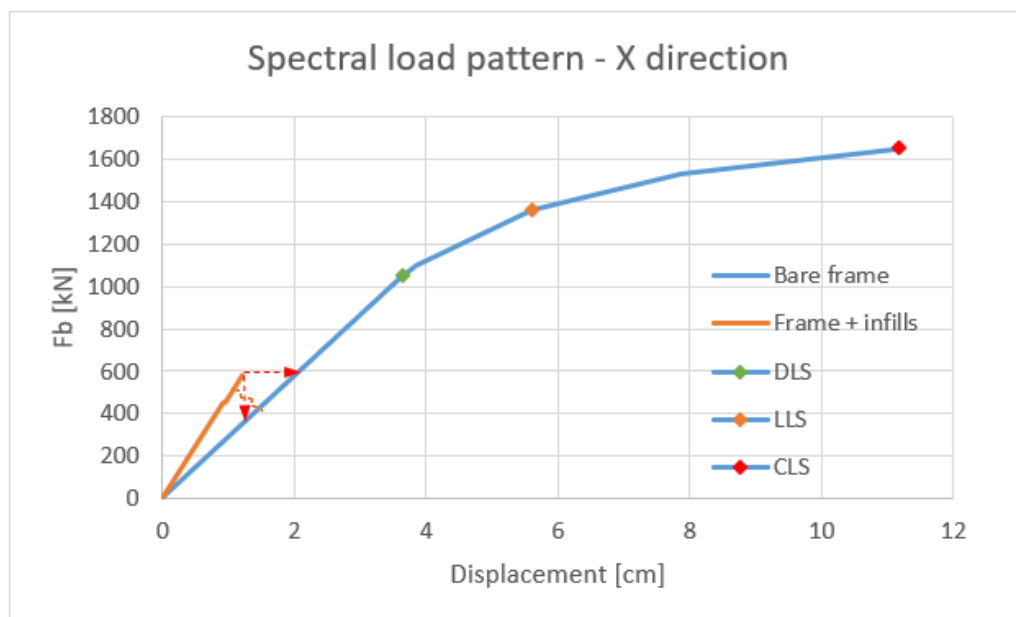
Figure 4-38: Non - linear static analysis in X direction with spectral load pattern, for the model with and without masonry infills. The diamonds indicate the capacity of the bare frame building at CLS, LLS and DLS. The red arrows and the orange dashed line show a possible path of transition between the structure with infills and the structure without infills, that have collapsed.
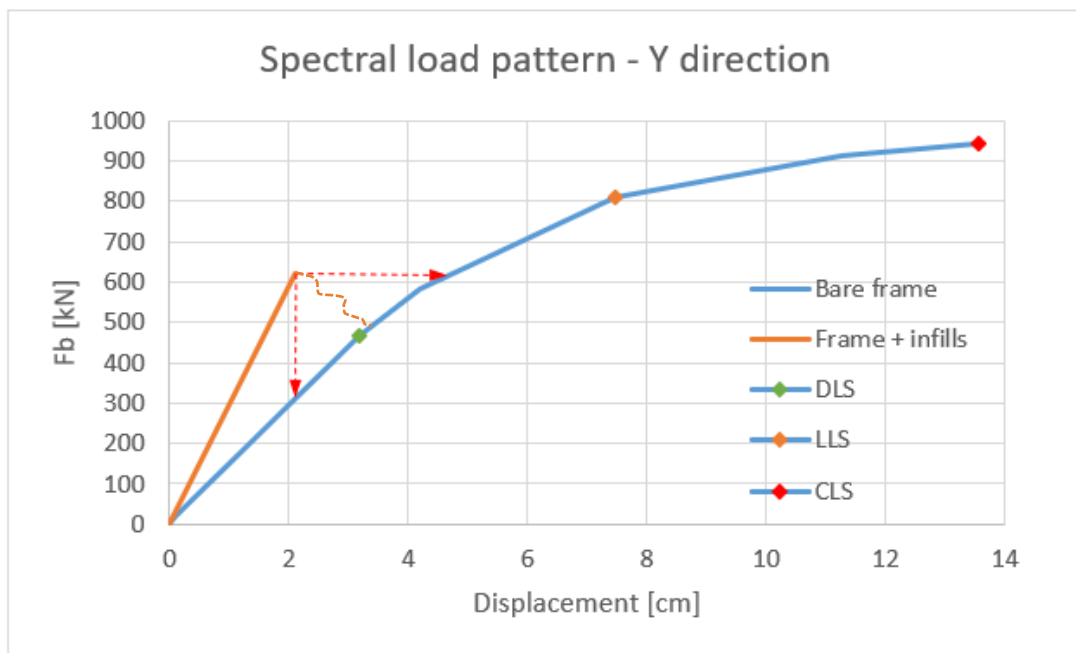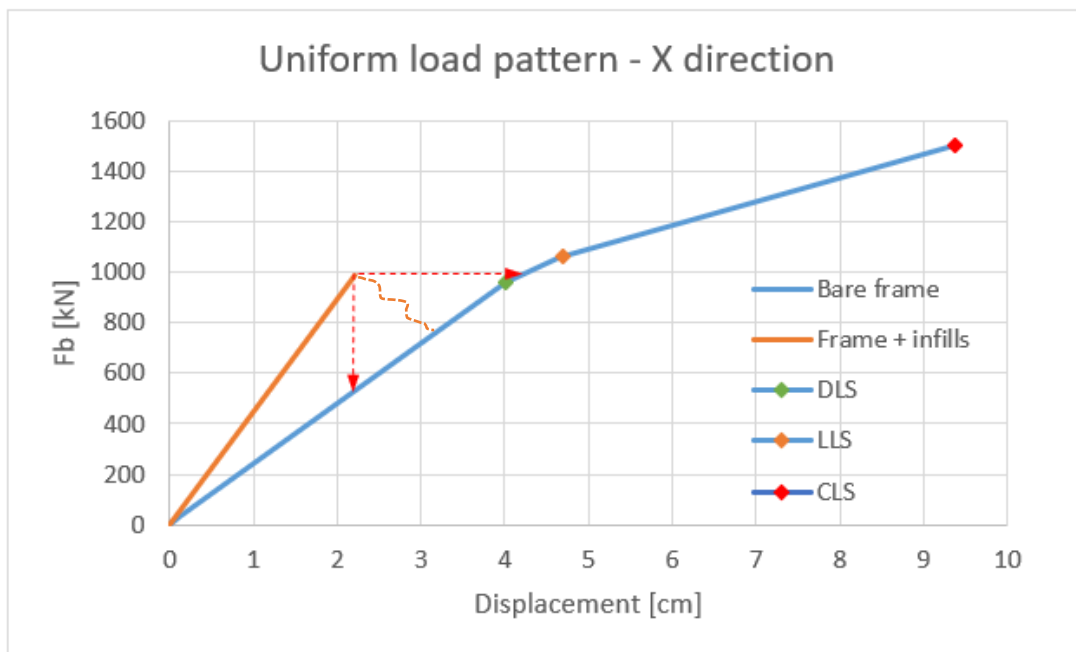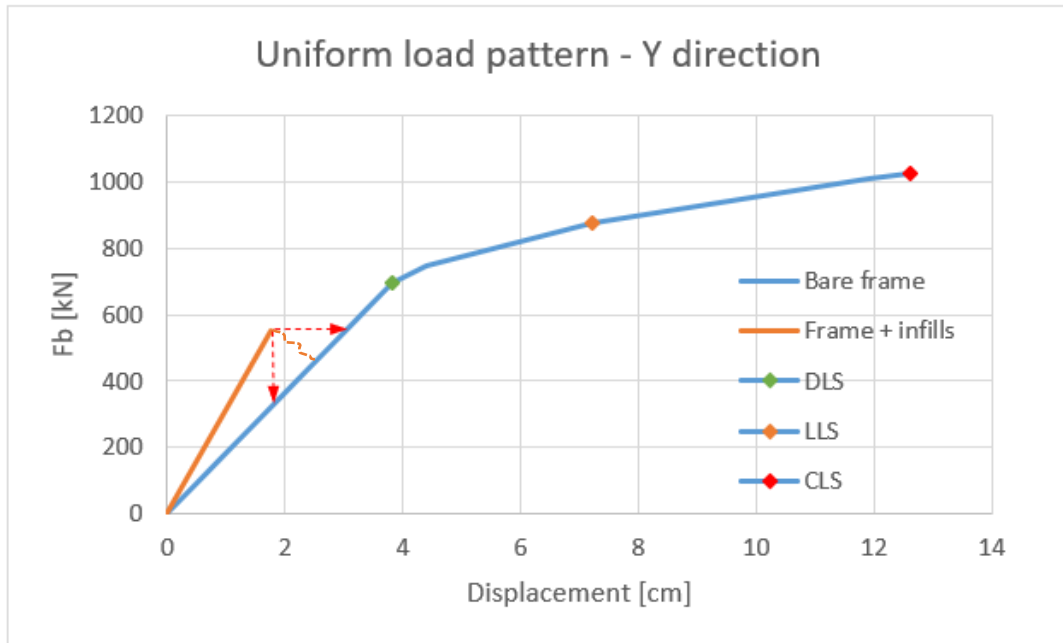
Figure 4-39: Non - linear static analysis in Y direction with spectral load pattern, for the model with and without masonry infills. The diamonds indicate the capacity of the bare frame building at CLS, LLS and DLS. The red arrows and the orange dashed line show a possible path of transition between the structure with infills and the structure without infills, that have collapsed.

Figure 4-40: Non - linear static analysis in X direction with uniform load pattern, for the model with and without masonry infills. The diamonds indicate the capacity of the bare frame building at CLS, LLS and DLS. The red arrows and the orange dashed line show a possible path of transition between the structure with infills and the structure without infills, that have collapsed.

Figure 4-41: Non - linear static analysis in Y direction with uniform load pattern, for the model with and without masonry infills. The diamonds indicate the capacity of the bare frame building at CLS, LLS and DLS. The red arrows and the orange dashed line show a possible path of transition between the structure with infills and the structure without infills, that have collapsed.

4.3.2. Non – linear static analysis (pushover)

In the following investigations the model of the building has been modified: the basement, made of concrete walls, has been taken away and the new model starts from the ground floor with an RC frame structure (concrete walls just for the stairwell).

For the sake of completeness, a table with the new modal results is reported (Table 4-20). The vibration modes are very similar to the ones already seen for the model with the basement, but the periods are slightly lower. The first mode is rotational with some translation in Y direction, the second mode is mainly translational in Y direction, with some torsion, while the third mode is mainly translational in X direction.

Table 4-20: Modal participating mass ratios and periods for the first 12 modes for the model without the basement.

StepNum	Period	UX	UY	UZ	SumUX	SumUY	SumUZ
Unitless	Sec	Unitless	Unitless	Unitless	Unitless	Unitless	Unitless
1	2.41	0.0220	0.2287	0.0000	0.0220	0.2287	0.0000
2	1.90	0.0981	0.3883	0.0000	0.1202	0.6169	0.0000
3	1.77	0.5690	0.0299	0.0000	0.6891	0.6469	0.0000
4	0.74	0.0248	0.0218	0.0000	0.7139	0.6687	0.0000
5	0.48	0.1263	0.0206	0.0000	0.8403	0.6893	0.0000
6	0.38	0.0132	0.0012	0.0000	0.8535	0.6905	0.0000
7	0.36	0.0051	0.1568	0.0000	0.8586	0.8473	0.0000
8	0.24	0.0071	0.0029	0.0000	0.8657	0.8502	0.0000
9	0.20	0.0493	0.0071	0.0000	0.9150	0.8573	0.0000
10	0.17	0.0049	0.0028	0.0000	0.9199	0.8601	0.0000
11	0.15	0.0000	0.0000	0.0001	0.9199	0.8601	0.0001
12	0.15	0.0009	0.0002	0.0000	0.9208	0.8603	0.0001

StepNum	Period	RX	RY	RZ	SumRX	SumRY	SumRZ
Unitless	Sec	Unitless	Unitless	Unitless	Unitless	Unitless	Unitless
1	2.41	0.1063	0.0042	0.4502	0.1063	0.0042	0.4502
2	1.90	0.2241	0.0332	0.1695	0.3304	0.0374	0.6197
3	1.77	0.0163	0.2329	0.0753	0.3467	0.2703	0.6950
4	0.74	0.0266	0.0496	0.0850	0.3733	0.3199	0.7800
5	0.48	0.0189	0.1297	0.0204	0.3922	0.4496	0.8004
6	0.38	0.0019	0.0138	0.0433	0.3941	0.4634	0.8437
7	0.36	0.1368	0.0045	0.0337	0.5309	0.4679	0.8774
8	0.24	0.0053	0.0131	0.0221	0.5362	0.4810	0.8995
9	0.20	0.0092	0.0535	0.0105	0.5454	0.5345	0.9100
10	0.17	0.0041	0.0072	0.0120	0.5496	0.5416	0.9219
11	0.15	0.0000	0.0000	0.0000	0.5496	0.5416	0.9219
12	0.15	0.0002	0.0007	0.0001	0.5497	0.5423	0.9220

For performing pushover analysis two load patterns have been used, as already described previously, one proportional to the forces obtained from a response spectrum analysis and one proportional to the storey masses. The analyses have been performed with non-linear static analysis and also with slow non-linear dynamic analysis, as already described for RC building 1 in §4.2.2. The monitored joint is a joint at the top of the stairwell. The forces used as the load pattern for the analyses are shown in Table 4-21 and Table 4-22:

Table 4-21: Load pattern for the "uniform" lateral load, in X and Y direction, applied to the centre of mass

	X unif	Y unif
H	FX	FY
37.56	31.66	31.66
35.26	180.78	180.78
32.17	307.27	307.27
29.02	297.76	297.76
25.87	298.61	298.61
22.72	299.36	299.36
19.57	300.92	300.92
16.42	303.43	303.43
13.27	306.64	306.64
19.12	309.75	309.75
6.97	319.31	319.31
3.82	324.48	324.48
0.67	506.82	506.82
Total	3786.79	3786.79

Table 4-22: Load pattern for the "spectral" lateral load, in X and Y direction, with specified application point.

	X mod			Y mod		
H	FX	FY	MZ	FX	FY	MZ
37.56	46	14	174	24	45	296

35.26	184	56	697	95	183	1185
32.17	688	270	3649	252	715	6639
29.02	645	185	2576	187	608	5930
25.87	377	27	469	53	207	2078
22.72	234	-4	103	-11	34	579
19.57	188	-29	856	-69	-24	1210
16.42	224	-47	1389	-58	56	2859
13.27	267	68	1216	55	294	3602
19.12	314	176	916	183	477	2572
6.97	331	214	1098	228	531	3072
3.82	318	180	1248	190	495	2867
0.67	183	93	890	90	310	1731
Application point (X,Y):		14.225		8.75		

The following figures (Figure 4-42, Figure 4-43, Figure 4-44 and Figure 4-45) show the plastic hinges at the final step of the analyses with static procedure. The colours of the hinges correspond to the stages of the hinges, as already explained in §3.1.6. It should be noticed that many plastic hinges are activated (pink colour – just over yielding point) already with just gravitational loads.

If the structure is considered collapsed at the first collapsed plastic hinge, it can be seen that the collapse is brittle (the first collapsed hinges are shear hinges, with the exception of the analysis in Y direction with uniform lateral load) and that it happens for low displacements at the top of the building. Table 4-23 summarizes the collapse data, in terms of displacement at the top of the building and base shear. The analysis in Y direction with uniform lateral load is very different from the others, as the displacement at collapse is nearly 1 m (10 times all the other analyses). In this case the first hinges to collapse are flexural (interacting PMM) hinges at the base of concrete walls or columns. This can be seen from the results of the slow dynamic analysis, as the static analysis stops before reaching the collapse of any plastic hinge. This difference (all the other analyses show a brittle collapse of shear hinges) for just one direction and one load pattern could be due to the irregularity of the structure and to the fact that also superior modes relevantly contribute to the seismic behaviour of the building. Later on, the results are going to be compared with the results of dynamic analyses.

The pushover curves are shown in Figure 4-46 and Figure 4-47. The four curves have two different origins, as two curves are the results of the pushover analyses in X direction, while the other two are the results in Y direction. The origin is not zero, due to the initial deformation of the building because of vertical loads. The results show that the slow dynamic analyses follow the same curves as the static analyses, but are able to continue further, with the exception of the analysis in X direction with uniform lateral load, that stops earlier with the slow dynamic analysis than with the static one, for convergence reasons. Static analyses find troubles in converging when a lot of plastic hinges are activated or collapsed, so that no significant strength degradation is reached in the capacity curves and the collapse is defined based on the status of the plastic hinges in the model. All the curves have been cut after the collapse capacity.

Table 4-23: Forces and displacements at the collapse of the building for the four different analyses.

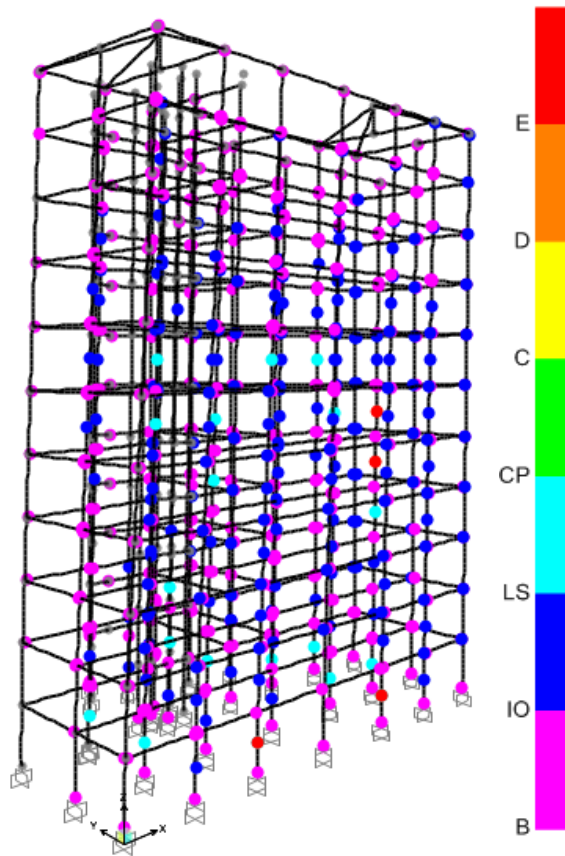| Analysis	Displacement at collapse	Base shear at collapse
X spectral	0.12 m	1576 kN
Y spectral	0.14 m	881 kN
X uniform	0.06 m	1220 kN
Y uniform	0.91 m	854 kN

Figure 4-42: Final step of non-linear static analysis in X direction with "spectral" lateral load.
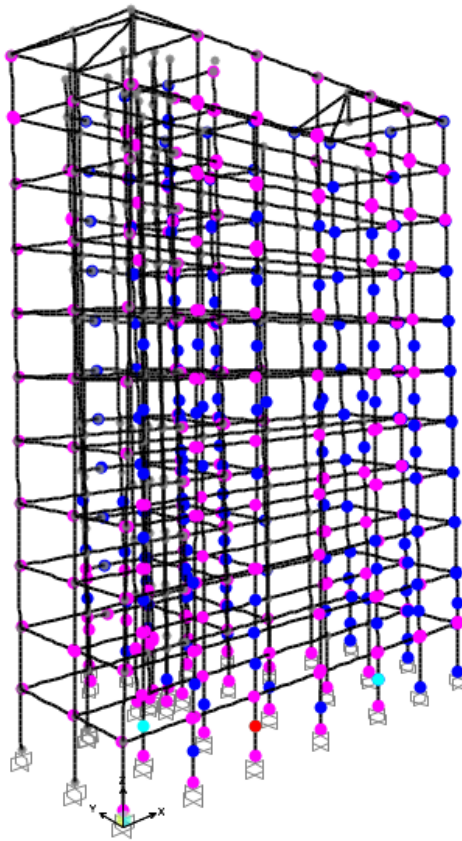

Figure 4-43: Final step of non-linear static analysis in Y direction with "spectral" lateral load.
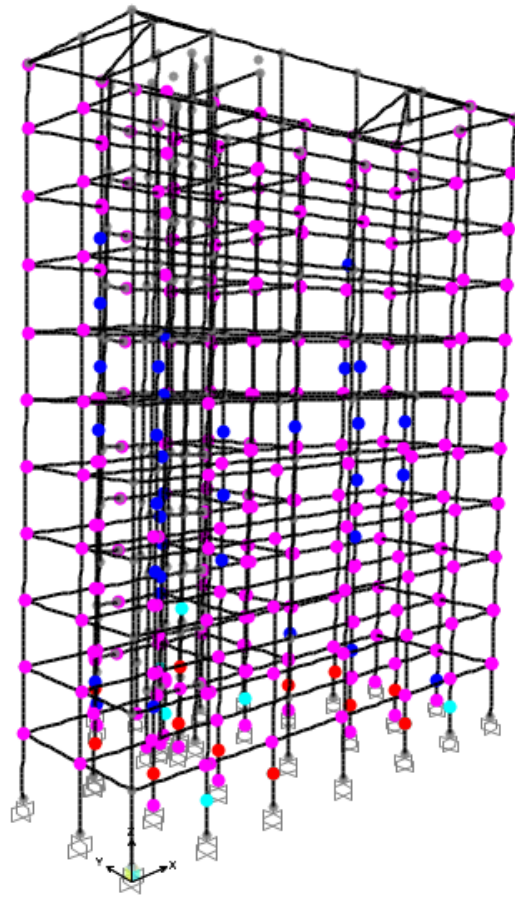
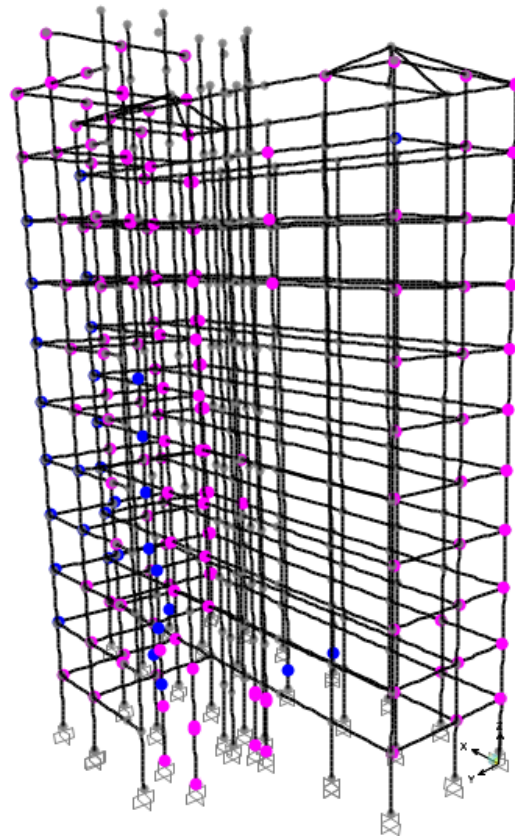**Figure 4-44: Final step of non-linear static analysis in X direction with "uniform" lateral load.**

Figure 4-45: Final step of non-linear static analysis in Y direction with "uniform" lateral load.

The definition of the capacity of the building is made based on the stage of the plastic hinges: the Collapse limit state is reached when at least one plastic hinge collapses (becomes red on the screen),the Life Safety limit state is reached when one or more hinges first reach 0.8 of the ultimate shear or displacement (light blue colour on the screen), depending on the rupture mode (shear or flexural), Damage limit state is reached when one or more hinges first reach 0.5 of the ultimate shear or displacement. In Figure 4-46 and Figure 4-47all the defined capacities are shown with a symbol. In some cases it is not possible to define a capacity, for example because the LLS coincides with CLS or the curve stops before reaching the capacity. It can be seen that the curves obtained with the two methods (static and slow dynamic) are very similar, also in terms of capacities.
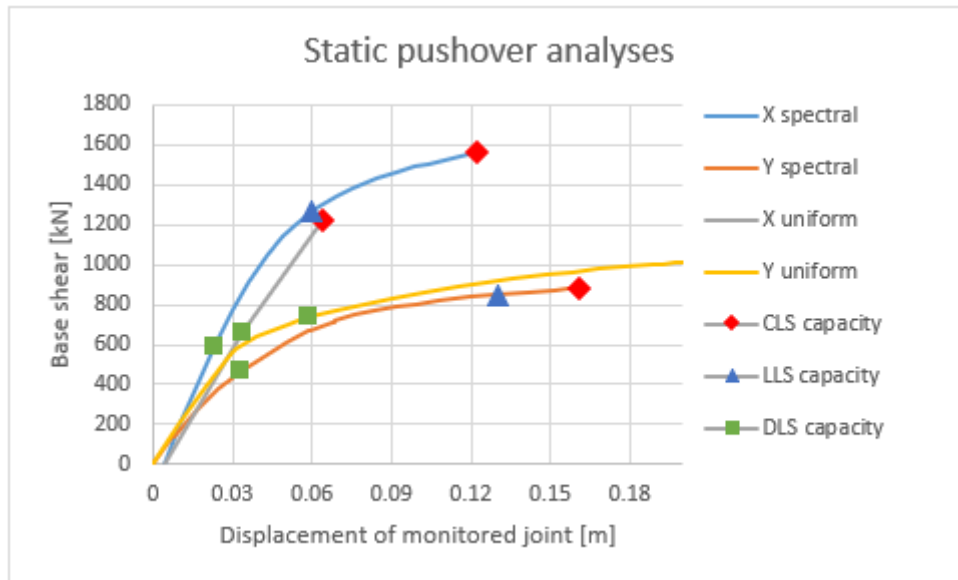
Figure 4-46: Pushover curves of the building in X and Y positive directions with two different load patterns, obtained with non-linear static analysis. The capacity of the building for three limit states (CLS, LLS and DLS) is shown on each curve with symbols.
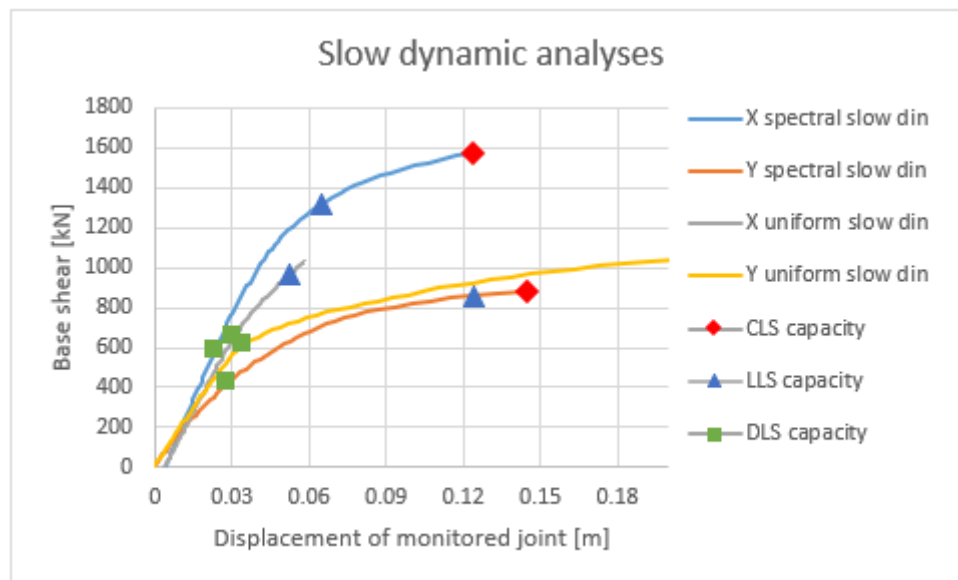

Figure 4-47: Pushover curves of the building in X and Y positive directions with two different load patterns, obtained with slow non-linear dynamic analysis. The capacity of the building for three limit states (CLS, LLS and DLS) is shown on each curve with symbols.

It can be noticed that the building is more ductile but less strong in Y direction. The capacity of the building is checked and shown also in ADRS format in Figure 4-48 and Figure 4-49, for X

and Y direction respectively, where it is clear that the structure is very vulnerable and brittle, compared to the code seismic demand.
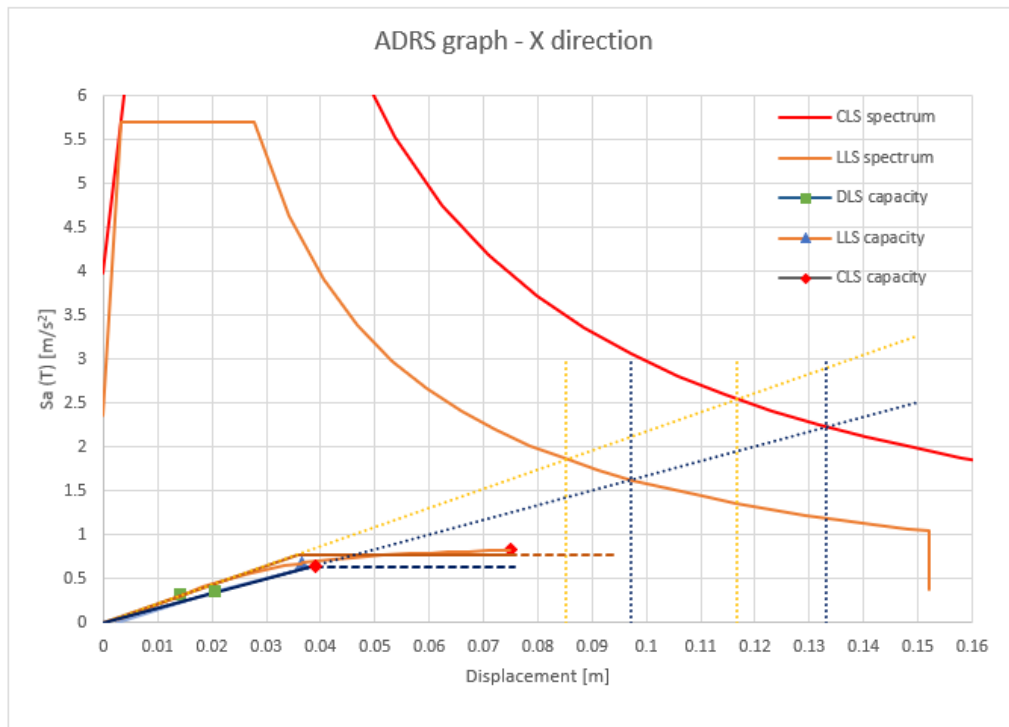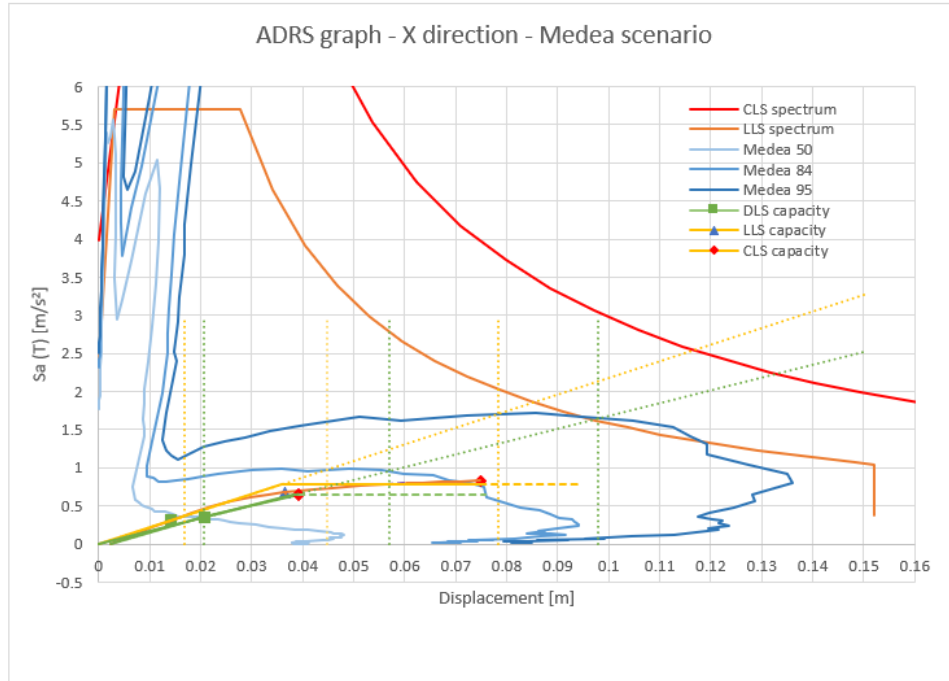

Figure 4-48: Capacity curves in X direction with spectral and uniform load patterns in ADRS format, together with the CLS and LLS code response spectra. For both load patterns, the DLS, LLS and CLS capacity of the building is marked with squares, triangles and diamonds respectively. The displacement demand is shown with yellow and blue vertical dotted lines, for spectral and uniform load pattern respectively.
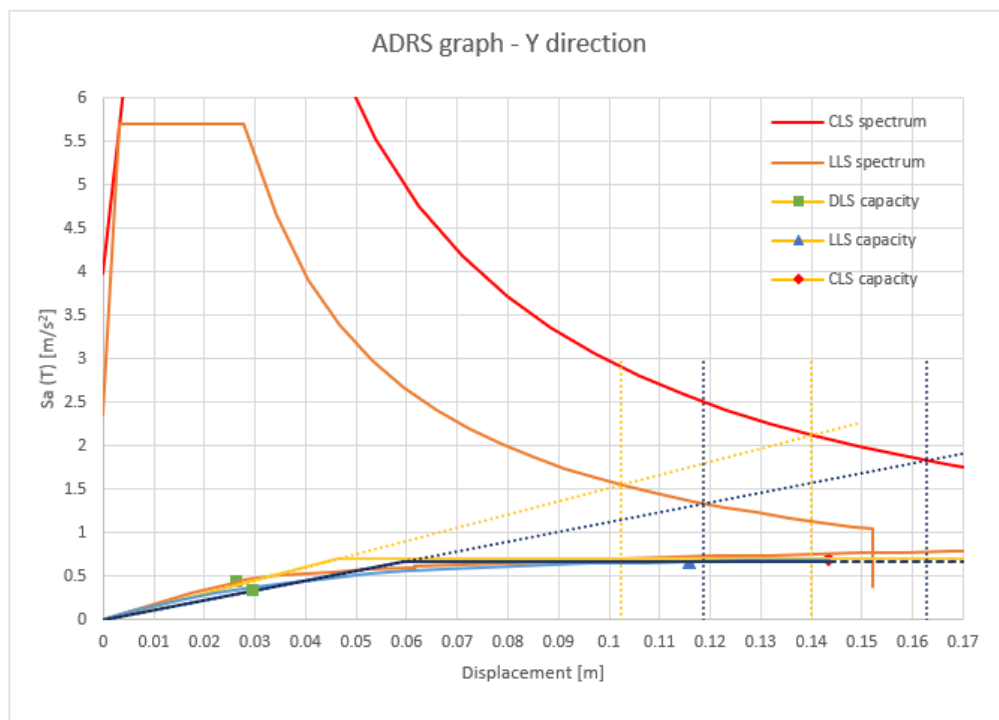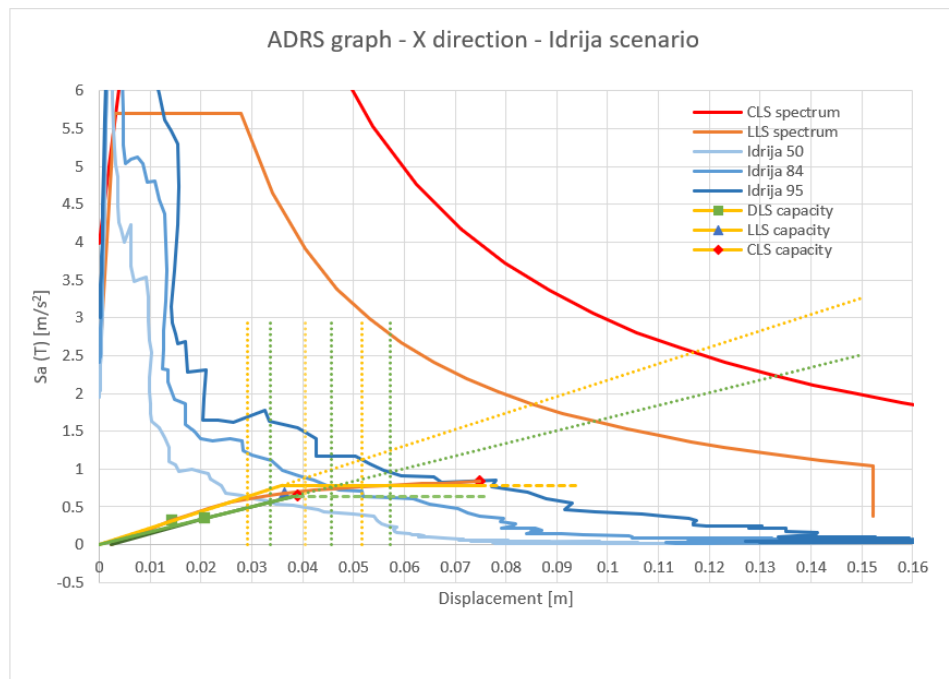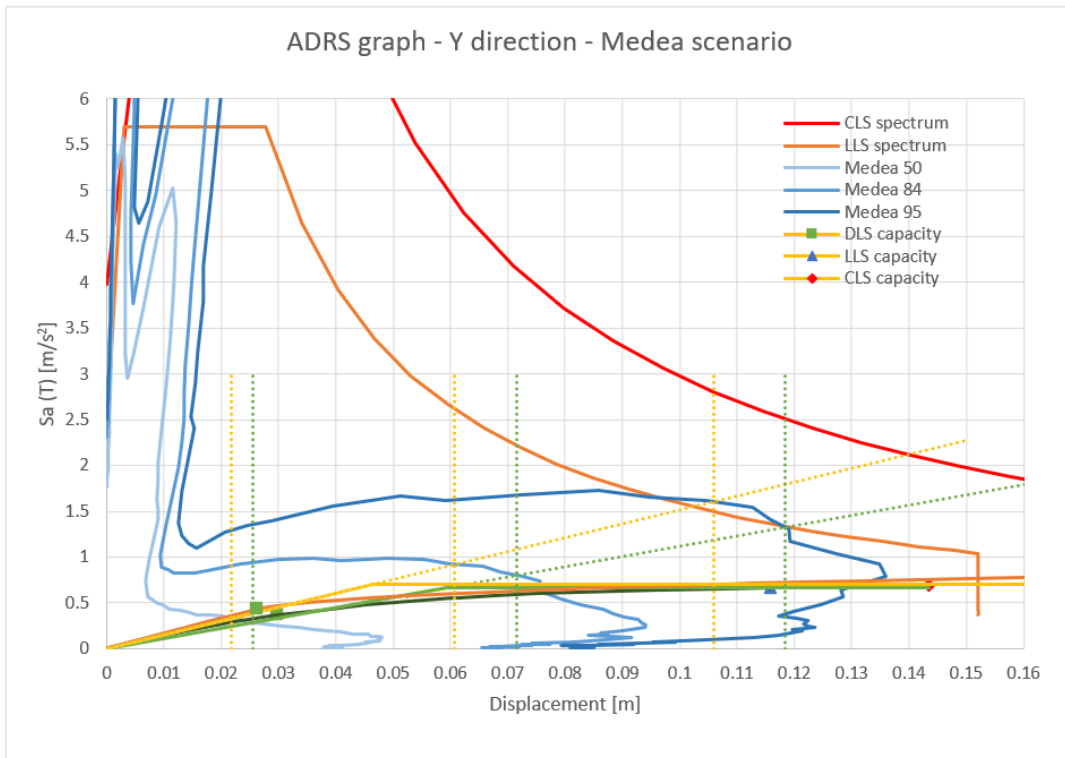

Figure 4-49: Capacity curves in Y direction with spectral and uniform load patterns in ADRS format, together with the CLS and LLS code response spectra. For both load patterns, the DLS, LLS and CLS capacity of the building is marked with squares, triangles and diamonds respectively. The displacement demand is shown with yellow and blue vertical dotted lines, for uniform and spectral load pattern respectively.

The vulnerability of the building is then checked also based on the scenario response spectra. Three percentiles are considered for each scenario: 50th, 84th and 95th. For each of these response spectra, the check, in terms of displacement, is made for CLS and LLS. The capacity of the building for DLS is also shown, but it is not explicitly checked. The graphical check for X direction can be seen in Figure 4-50 and Figure 4-51 for Medea and Idrija scenario respectively and for Y direction in Figure 4-52 and Figure 4-53.

Figure 4-50: Capacity curves in X direction with spectral and uniform load patterns in ADRS format, together with the Medea scenario response spectra (50th, 84th and 95th percentiles). For both load patterns, the DLS, LLS and CLS capacity of the building is marked with squares, triangles and diamonds respectively. The displacement demand is shown with yellow and green vertical dotted lines, for spectral and uniform load pattern respectively.

Figure 4-51: Capacity curves in X direction with spectral and uniform load patterns in ADRS format, together with the Idrija scenario response spectra (50th, 84th and 95th percentiles). For both load patterns, the DLS, LLS and CLS capacity of the building is marked with squares, triangles and diamonds respectively. The displacement demand is shown with yellow and green vertical dotted lines, for spectral and uniform load pattern respectively.

Figure 4-52: Capacity curves in Y direction with spectral and uniform load patterns in ADRS format, together with the Medea scenario response spectra (50th, 84th and 95th percentiles). For both load patterns, the DLS, LLS and CLS capacity of the building is marked with squares, triangles and diamonds respectively. The displacement demand is shown with yellow and green vertical dotted lines, for uniform and spectral load pattern respectively.
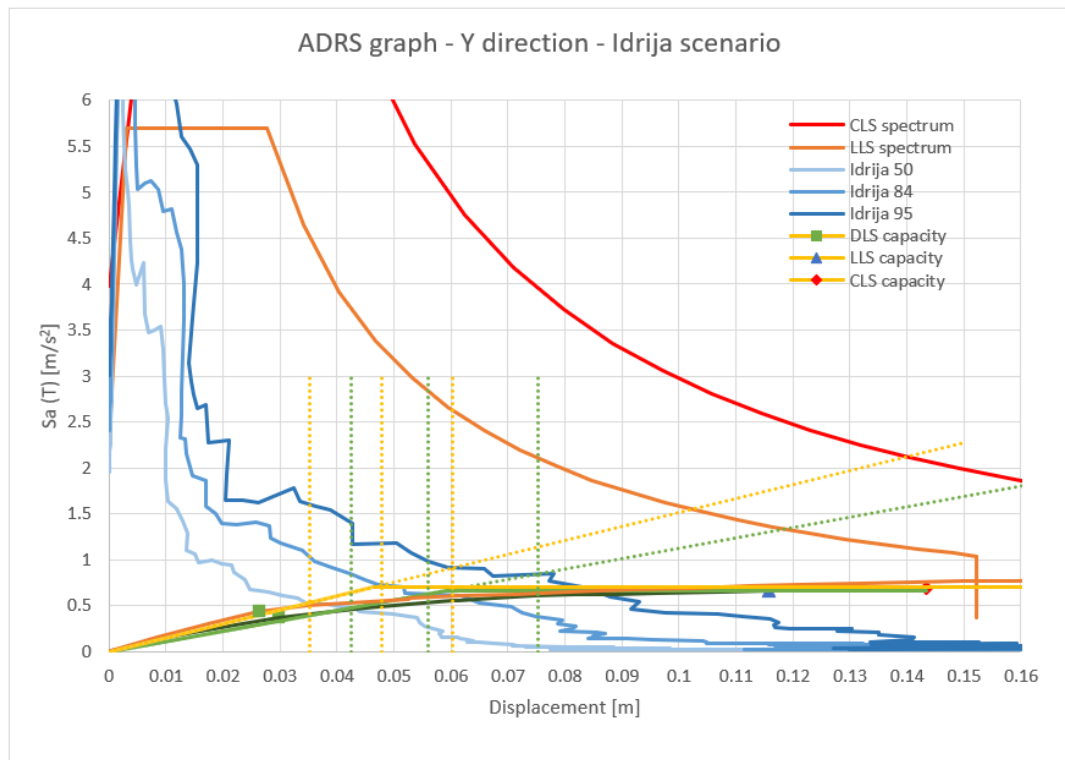
Figure 4-53: Capacity curves in Y direction with spectral and uniform load patterns in ADRS format, together with the Idrija scenario response spectra (50th, 84th and 95th percentiles). For both load patterns, the DLS, LLS and CLS capacity of the building is marked with squares, triangles and diamonds respectively. The displacement demand is shown with yellow and green vertical dotted lines, for uniform and spectral load pattern respectively.

The numeric data are shown in Table 4-24 in terms of Capacity displacement/Demand displacement. In the first line, the results of the check based on the code response spectra is shown. In this case, one check is made with the demand from the CLS response spectrum, compared to the CLS capacity of the structure, and another check is made with the demand based on the LLS code spectrum, compared to the LLS capacity of the building. For this reason, the vulnerability index is generally lower for CLS than for LLS. On the contrary, in all the other lines, the vulnerability index is lower for LLS than for CLS, because the demand is calculated based on scenario response spectra (the same for both limit states CLS and LLS), while the capacity of the structure is lower for LLS than for CLS.

It can be noticed that the building is never verified for the code seismic demand, but it is verified in many cases for scenario seismic inputs. Medea 95 scenario is comparable with LLS code demand for both X and Y direction of the building. All the other percentiles of the scenarios have lower demands. It is clear that Y direction of the building is less vulnerable, as the C/D ratios are in some cases (uniform load pattern) very high. This means that the main problem of the building is the fragility of the concrete walls, that are not designed to withstand lateral forces and have a very few steel reinforcements. An effective retrofit intervention certainly needs to address those walls and make them more ductile.

Table 4-24: C/D ratios in terms of displacement for the capacity curves of RC building 2, for CLS and LLS.

Seismic input	Load pattern	CLS	LLS
code spectra		0.642	0.428
Medea 50		4.467	2.176
Medea 84		1.674	0.816
Medea 95	Spectral X	0.955	0.465
Idrija 50		2.567	1.250
Idrija 84		1.844	0.898
Idrija 95		1.451	0.707
code spectra		0.294	0.402
Medea 50		1.899	1.899
Medea 84		0.687	0.687
Medea 95	Uniform X	0.399	-
Idrija 50		1.162	1.162
Idrija 84		0.856	0.856
Idrija 95		0.684	0.684
code spectra		0.882	0.975
Medea 50		5.625	4.542
Medea 84		2.003	1.617
Medea 95	Spectral Y	1.212	0.979
Idrija 50		3.384	2.733
Idrija 84		2.557	2.065
Idrija 95		1.904	1.538
code spectra		5.758	5.366
Medea 50		37.092	25.246
Medea 84		13.275	9.035
Medea 95	Uniform Y	7.615	5.183
Idrija 50		22.940	15.614
Idrija 84		16.839	11.461
Idrija 95		13.362	9.095

4.3.3. Non - linear dynamic analysis and fragility curves

As already done for RC building 1, also for this case study building, non-linear dynamic analyses are carried out in order to calculate fragility curves for three limit states: CLS, LLS and DLS. The technique used to calculate the fragility curves is the cloud analysis. The procedure is the same described at §4.2.3.

The numerical model used for this purpose is the model without infills (bare frame) and without the basement storey described in §4.3.2.

The same 50 time histories have been used, already presented in §4.1.2. In order to better understand the behaviour of the building and also to better control the reliability of results, it has been chosen to perform analyses separately for the two main directions of the building with just one component of the accelerograms. The component of the accelerogram has been chosen in two different ways. For the higher intensity signals (the first 30), the component with the highest PGA has been chosen. For the lower intensity signals (the next 20), the component with the lowest PGA has been chosen. The analyses have been performed with the same signals in X and Y directions. The selected components of the records and their intensity measures, used for the correlations and fragility curves, are shown in Table 4-25.

Dumping is defined for each load case. A damping of 5% in the range of periods from 0.05 s to 2.45 s have been chosen. In a couple cases, an analysis stopped for convergence reasons, then the damping has been increased to 7% in the same range of periods.

The chosen EDP's are the same already introduced for RC building 1: maximum interstorey drift and D/C ratio in terms of displacement at the top of the building.

The chosen intensity measures of the ground motion are the same used for RC building 1: PGA, spectral acceleration Sa(T1), equivalent spectral acceleration Sa,eq calculated on the first 10 modes and Housner index.

Table 4-25: Table with the used components of the records and their Intensity Measures used for the correlations.

	Load case	Component	PGA [g]	Sa(T1) [g]	Sa,eq,y [g]	Housner index [cm]
1	A.496	N	-1.029	0.049	0.390	98.04974
2	A.ATS	N	-0.253	0.078	0.136	104.2932
3	A.BUR	N	-0.101	0.068	0.069	58.32067
4	A.GZL	E	-0.722	0.221	0.314	198.9406
5	A.YPT	N	-0.322	0.194	0.172	175.4408
6	BA.MIRE	N	0.271	0.260	0.215	186.6554
7	BA.MIRH	N	0.270	0.296	0.204	176.5144
8	EU.BAR	N	0.372	0.155	0.162	202.9978
9	EU.PETO	N	-0.454	0.077	0.235	148.9071
10	EU.ULA	E	0.214	0.135	0.138	124.2796
11	EU.ULO	N	0.282	0.142	0.165	156.8833
12	HI.KAL1	N	-0.270	0.059	0.174	90.82298
13	HL.AIGA	N	0.521	0.087	0.188	110.1562
14	HL.KALA	N	-0.296	0.063	0.161	114.6064
15	HL.KORA	N	0.296	0.126	0.119	95.16337
16	HL.XLCA	E	-0.290	0.121	0.185	111.5231
17	IT.ACC	E	0.434	0.125	0.172	139.7818
18	IT.AMT	E	-0.867	0.035	0.317	74.91207
19	IT.AQA	N	-0.442	0.042	0.151	76.52077

20	IT.AQG	N	-0.489	0.040	0.121	91.68268
21	IT.AQK09	N	-0.354	0.145	0.160	59.90569
22	IT.AQK16	N	-0.058	0.039	0.055	141.7027
23	IT.BGI	E	0.187	0.143	0.122	120.0285
24	IT.CLF	N	-0.277	0.041	0.103	81.23187
25	IT.CLO	N	0.582	0.139	0.374	204.3615
26	IT.CLT	E	-0.175	0.112	0.137	116.846
27	IT.CMI	E	-0.651	0.068	0.407	141.7672
28	IT.CNE	E	0.476	0.058	0.161	128.1226
29	IT.GBP	E	0.098	0.130	0.134	93.40728
30	IT.MOG0	E	0.240	0.034	0.098	70.74732
31	E.ATR	E	0.042	0.006	0.013	6.436053
32	E.FRC	N	-0.129	0.010	0.048	21.02296
33	IT.ASS	E	0.113	0.004	0.034	11.54466
34	IT.BGN	E	0.035	0.003	0.004	2.529356
35	IT.CR1	E	0.099	0.003	0.012	7.15888
36	IT.MCV	E	0.292	0.017	0.045	24.3522
37	IT.MRC	N	0.014	0.010	0.010	10.17329
38	IT.MSC	N	0.035	0.011	0.010	10.48822
39	IT.NRC	E	0.119	0.005	0.028	11.37202
40	IT.PCH	N	0.046	0.001	0.005	2.541577
41	IT.SGV	N	-0.002	0.000	0.001	0.229445
42	IT.SNO	N	-0.010	0.000	0.004	0.756294
43	IT.TDG	E	0.017	0.004	0.008	5.668645
44	IT.TRL	E	0.036	0.010	0.015	12.3092
45	IT.UMB	E	-0.011	0.005	0.007	4.096958
46	IT.VZZ	E	-0.065	0.008	0.017	15.02651
47	IV.NRCA	E	0.126	0.001	0.009	2.557977
48	MN.CEL	N	0.000	0.000	0.000	0.088819
49	OX.SABO	E	-0.003	0.006	0.005	3.965804
50	TK.2501	E	-0.011	0.005	0.004	3.618672

4.3.3.1.   Analyses and fragility curves in Y direction

The analyses have been first performed in Y direction, the most flexible direction of the building. The first 30 signals have been first used, then it has been noticed that the building was reaching collapse with all the accelerograms, so lower intensity signals have been added.

Some combinations of EDP and IM have been tried in order to check the variability of the resulting fragility curves. As first, the simplest two parameters have been used: the maximum interstorey drift as EDP and PGA as IM.

The maximum interstorey drift has been calculated by considering the displacements of the nodes in a barycentric position. The nodes of the structure on the line between the RC frame main building and the concrete walls stairwell has been chosen. The drift has been calculated based on the total displacement of the nodes in X and Y direction. The results of the correlations found with just the first 30 accelerograms and then with all 50 signals are shown in Figure 4-54 and Figure 4-55. The values of the maximum interstorey drifts are reported in Attachment, in Table 0-4. Fragility

curves are reported just for the case with all 50 accelerograms for three limit states: Collapse limit state (CLS), Life Safety limit state (LLS) and Damage limit state (DLS).
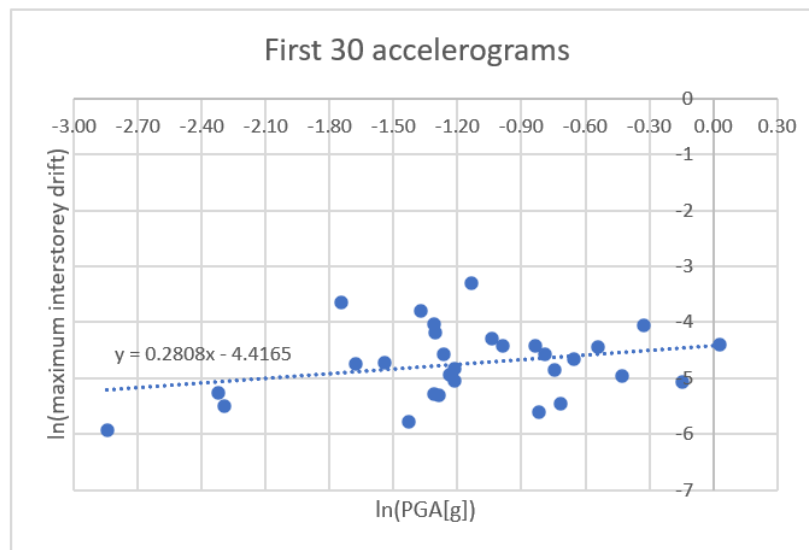

Figure 4-54: Correlation between the maximum interstorey drift and the PGA for the first 30 accelerograms used
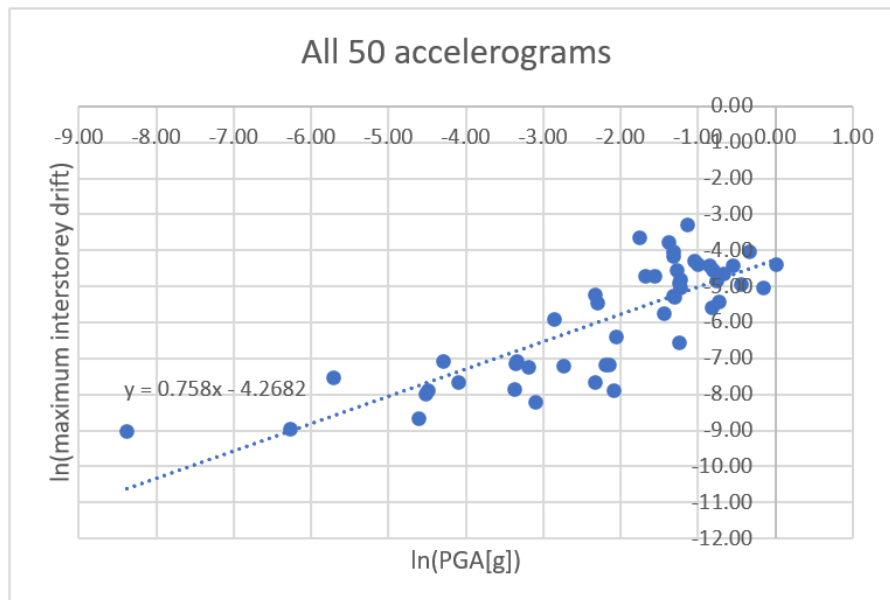

Figure 4-55: Correlation between the maximum interstorey drift and the PGA for all the 50 accelerograms used (σ=0.924).

The limits for the interstorey drifts for the three limit states have been determined based on the results of pushover analysis. It has been seen that the failure is almost always brittle and that the first hinge collapses at around 0.1 m of displacement at the top of the building. As the building is 34.59 m high, the average insterstorey drift at collapse would be of 3‰, that is slightly higher than the code limit for damage limit state in ordinary masonry buildings (2‰). For LLS and DLS the limit has been set to 80% and 50% of the limit for CLS respectively (Table 4-26).

Table 4-26: Chosen EDP$_0$ for fragility curves.

Limit State	Top displacement (from pushover)	Interstorey drift limit
CLS	0.10 m	3.0‰
LLS	0.08 m (80% of CLS)	2.4‰
DLS	0.05 m (50% of CLS)	1.5‰
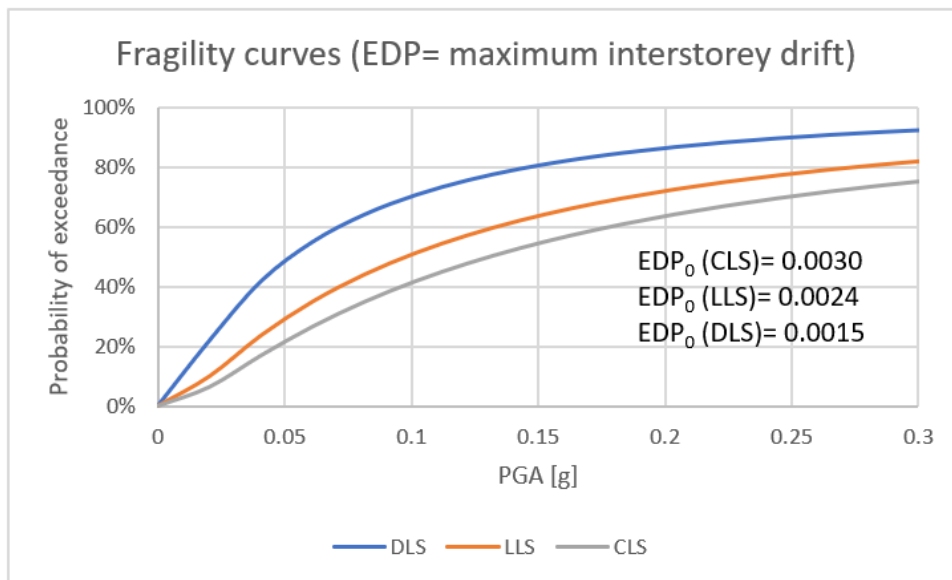
Figure 4-56: Fragility curves calculated based on maximum interstorey drift and PGA.

As the dots in the cloud of the correlation have a high dispersion and the standard deviation is high (0.924 in the correlation with all 50 accelerograms), another IM has been adopted to make the correlation: spectral acceleration at T1=2.41 s (Sa(T1)). The correlation and the resulting fragility curves, calculated with respect to the same EDP_0, are presented in Figure 4-57 and Figure 4-58.
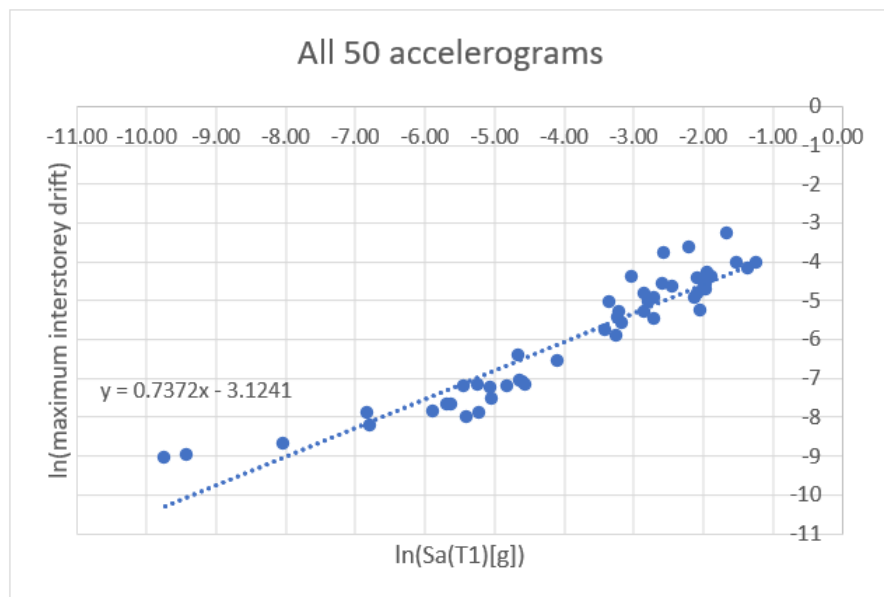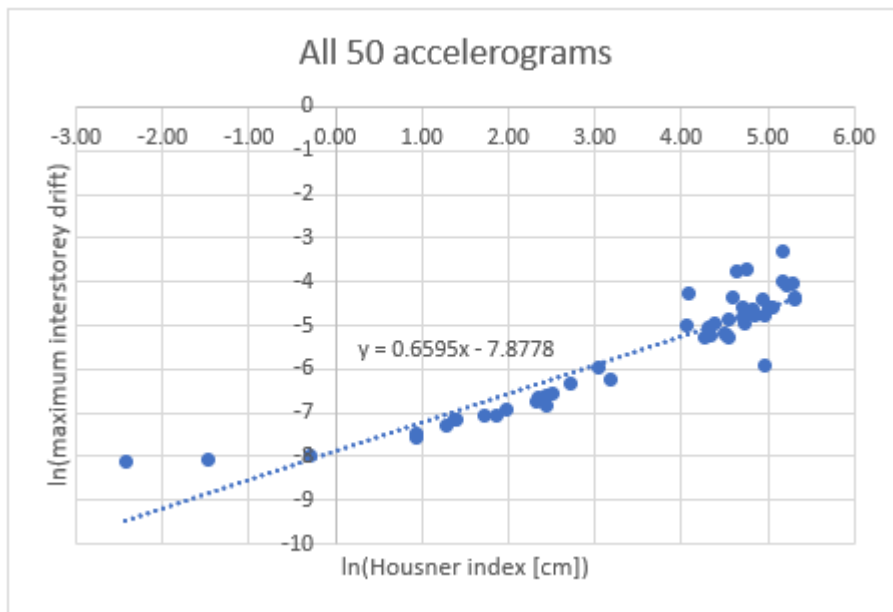

Figure 4-57: Correlation between the maximum interstorey drift and the Sa(T1) for all the 50 accelerograms used (σ=0.540).

It can be seen that the dispersion of the dots of the cloud is much lower (σ=0.540 is much lower than in the case of correlation with PGA). It shows that the Sa(T1) is much more correlated to the effects of ground shaking on the building. This affects the fragility curves, that show in this case a very vulnerable building.
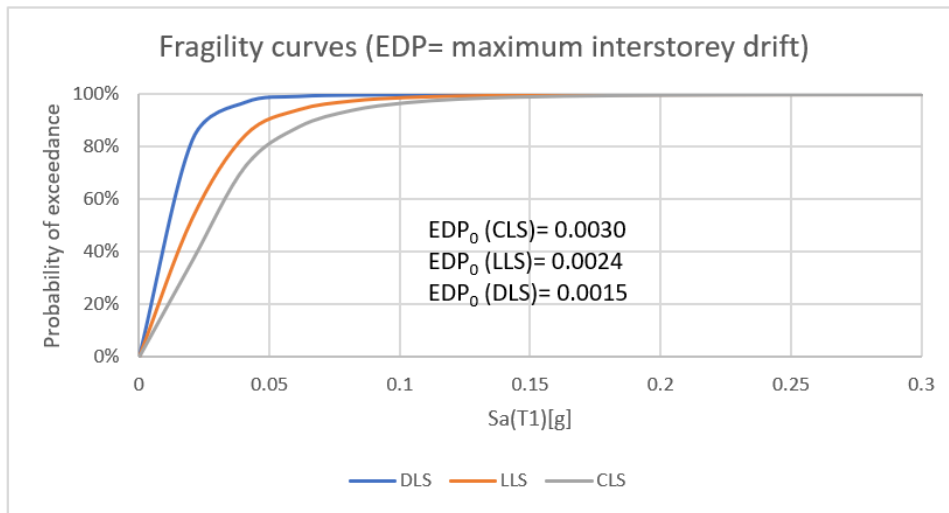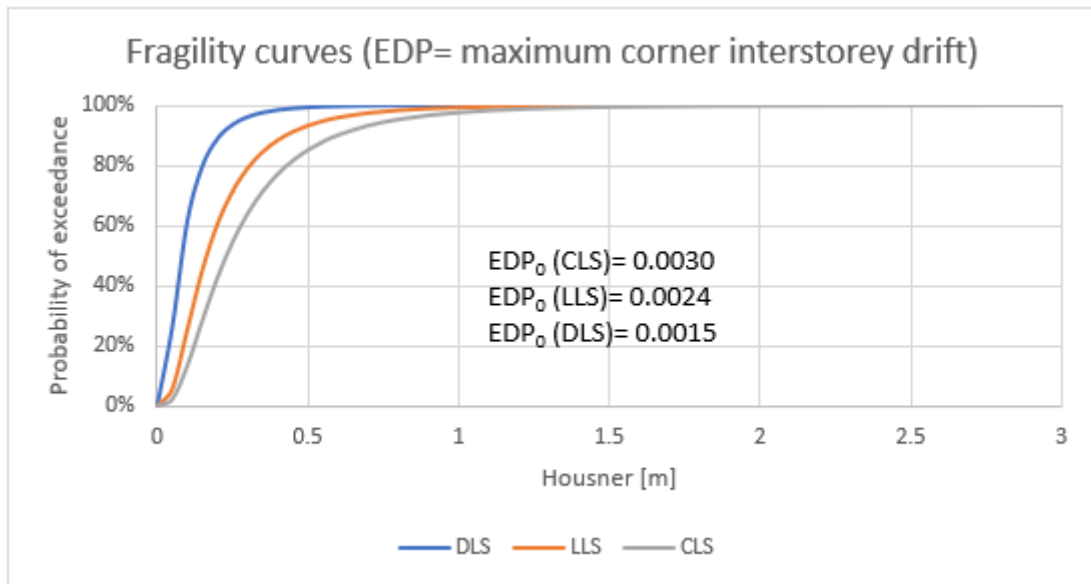
Figure 4-58: Fragility curves calculated based on maximum interstorey drift and spectral acceleration (Sa(T1)).

As the building has a low participating mass ratio for the first period, it appeared to be rational to include in some way also spectral accelerations of the other modes. For this reason an experiment has been done by using a new IM, the equivalent spectral acceleration Sa,eq,y, calculated on the first 10 modes. The equivalent spectral acceleration for the y direction has been calculated based on the base shear of each mode and an SRSS combination of the modes. The result has been divided by the total participating mass (ratio) in order to find an acceleration:

$$S_{a,eq,y} = \frac{\sqrt{\sum_{i=1}^{10}(S_{a,y}(T_i) \cdot U_{y,i})^2}}{\sum_{i=1}^{10} U_{y,i}} \tag{4.10}$$

Where $U_{y,i}$ is the participating mass ratio, in this case in y direction, of the ith mode.
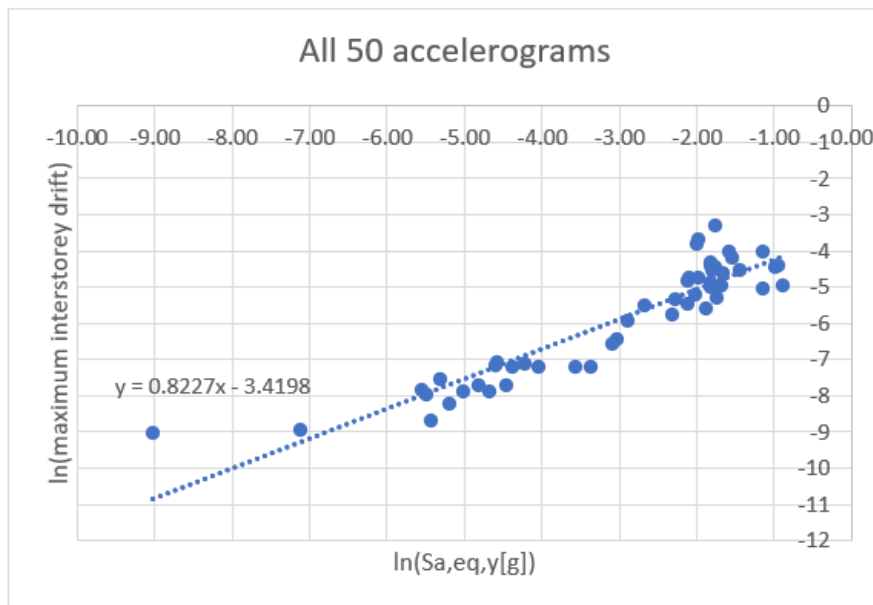
Figure 4-59: Correlation between the maximum interstorey drift and the Sa,eq,y for all the 50 accelerograms used (σ=0.619).
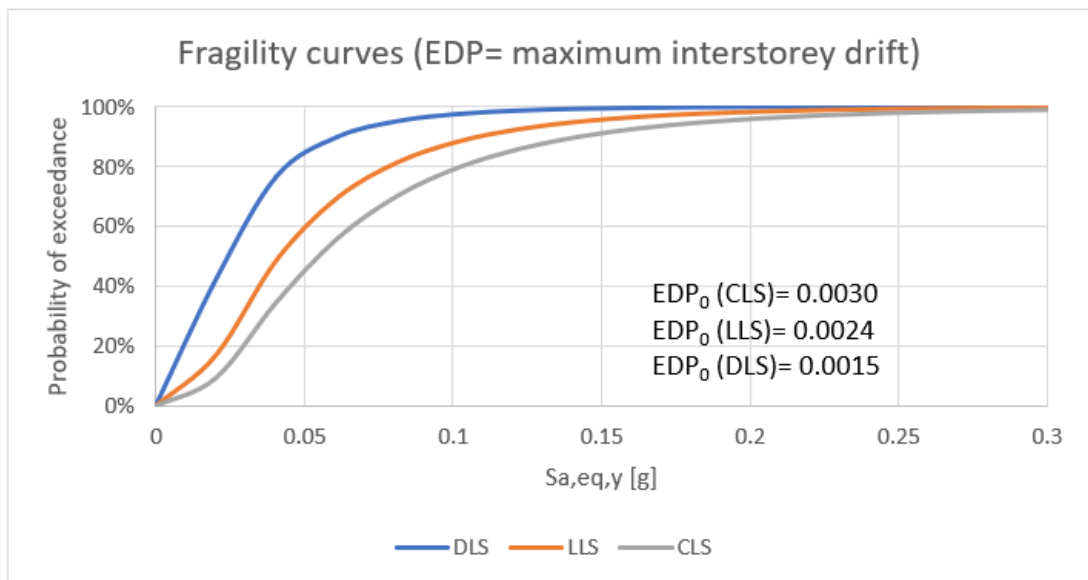
Figure 4-60: Fragility curve calculated based on maximum interstorey drift and equivalent spectral acceleration (Sa,eq,y).

The correlation of the maximum interstorey drift with this IM and the consequent fragility curves are presented in Figure 4-59 and Figure 4-60.

The curves are slightly moved to the right, but as the standard deviation σ is higher than in the case of the correlation with Sa(T1), this IM does not seem to be more suitable than the spectral acceleration of the fundamental period.

As the building has mainly rotational modes and it appears strange that the maximum drifts occur in the high storeys, similar correlations have been calculated by taking the interstorey drifts of an outer corner of the building (on the side of the main façade). The resulting standard deviation of the linear regression (σ=0.489) is lower than the one calculated on the barycentric interstorey drift (σ=0.540), so the maximum interstorey drift of the corner of the building appears to be a better EDP. As the variability of the response is lower (lower standard deviation), the fragility curves are moved to the left and indicate a more vulnerable building, that at Sa(T1) = 0.13 g is already 100% collapsed.
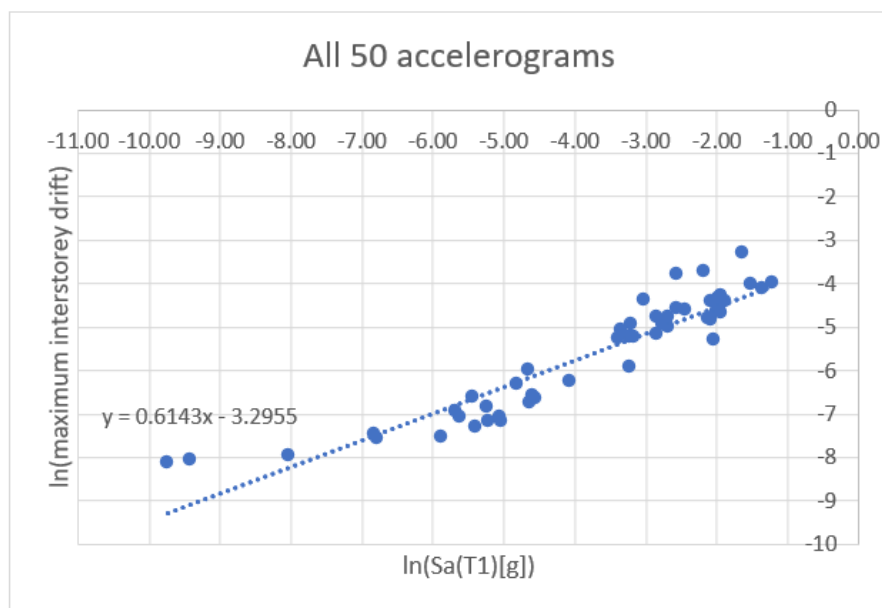
Figure 4-61: Correlation between the maximum interstorey drift in a corner of the building and the Sa(T1) for all the 50 accelerograms used (σ=0.489).
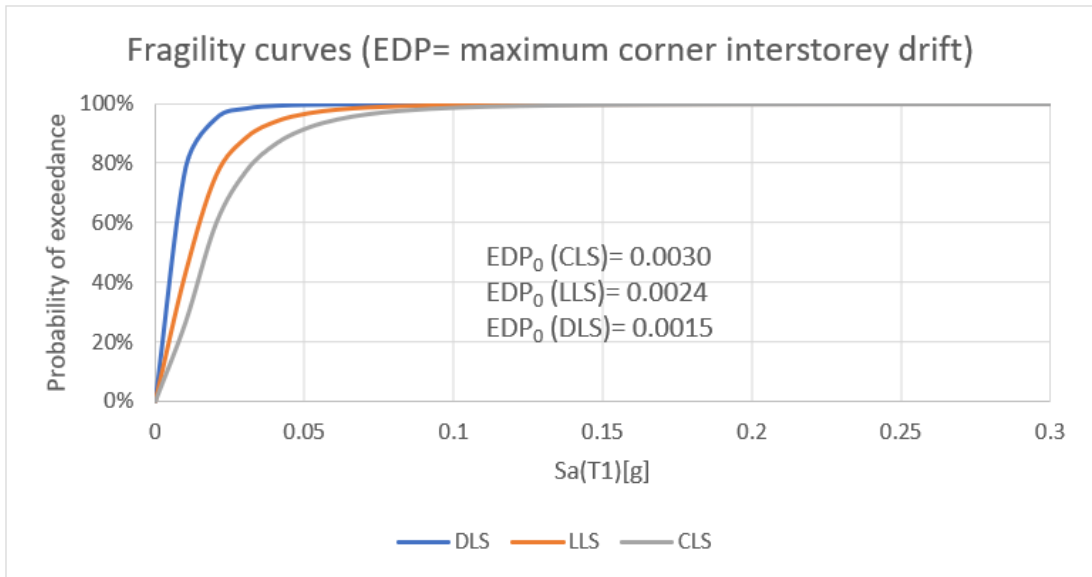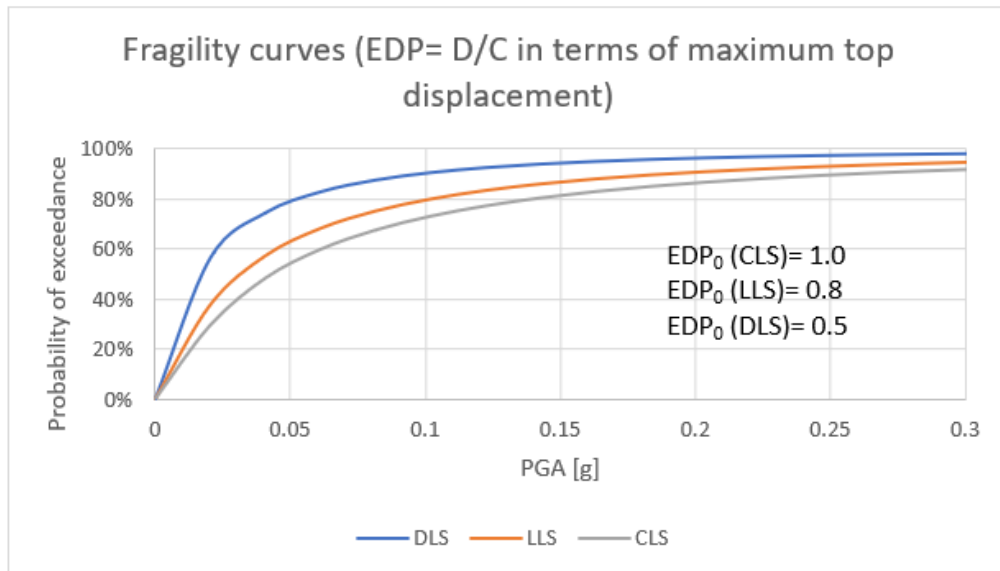
Figure 4-62: Fragility curves calculated based on maximum interstorey drift in a corner of the building and spectral acceleration (Sa(T1)).

As a last combination, also Housner index is used to check the correlation and calculate fragility curves (Figure 4-63 and Figure 4-64).

Figure 4-63: Bi-logarithmic correlation between the maximum interstorey drift in a corner of the building and the Housner index for all the 50 accelerograms used (σ=0.493).

Figure 4-64: Fragility curves calculated based on maximum interstorey drift in a corner of the building and Housner index.

The behaviour of the building has been further investigated by considering another EDP. As already done for RC building 1, by manually checking the status of plastic hinges in the model during the dynamic analyses, it has been noticed that for all the analyses where some hinges reach the collapse, the first to collapse is a brittle shear hinge in the concrete walls of the stairwell. With the aim to find the best parameter that governs the brittle shear collapse, the maximum displacement at the top of the building has been considered (joint 209, on the limit between the rectangular main building and the square shaped part with the stairwell). In order to find a suitable limit for this EDP, the displacement at the top of the building at the collapse of the first hinge has been considered. The value of the displacement has been checked for each of the first 30 analyses that caused at least one hinge collapse. Then an average value has been taken as a reference. The total displacement in X and Y direction (resultant) has been considered. All the considered values are shown in Figure 4-65, where also the median value and the standard deviation are displayed. The average value of 0.0253 m, compared to the height of the building of 34.59 m, means a drift of $0.000731 = 0.7‰$, that is extremely small. When this limit is used for the calculation of the fragility curves based on the interstorey drift, very different results would be obtained.

The capacity reference values for the three limit states are listed in Table 4-27.

Table 4-27: Capacity of the building in terms of top displacement.

	Top displacement	Drift (H=34.6 m)
CLS	0.0253 m	0.7‰
LLS	0.0202 m (80% of CLS)	0.6‰
DLS	0.0127 m (50% of CLS)	0.4‰
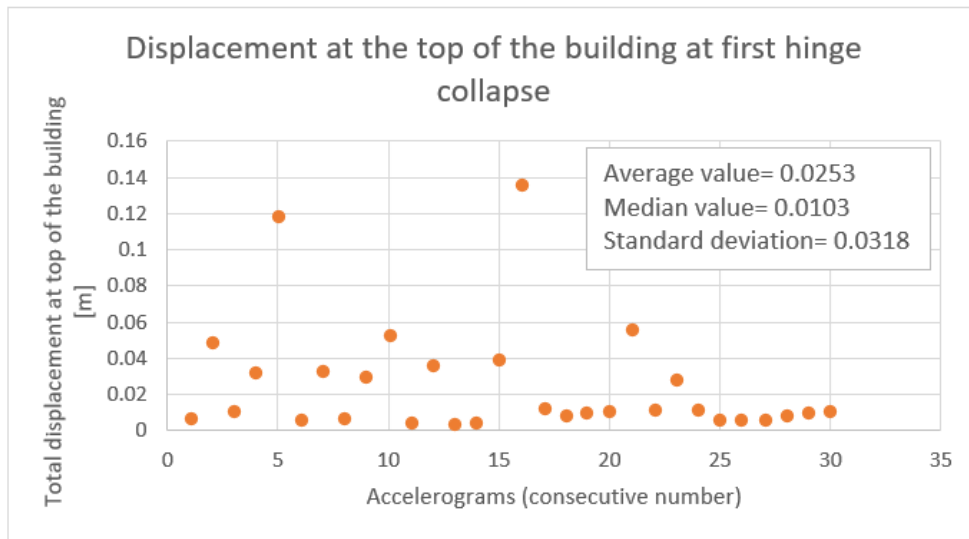
Figure 4-65: Values of the displacement at the top of the building at the moment of the collapse of the first hinge.

The result of fragility curves, based on interstorey drift of corner joints (correlation in Figure 4-61), with spectral acceleration of the first mode as IM, but with the new limit (EDP$_{0,\,CLS}$=0.7‰), are shown in Figure 4-66.
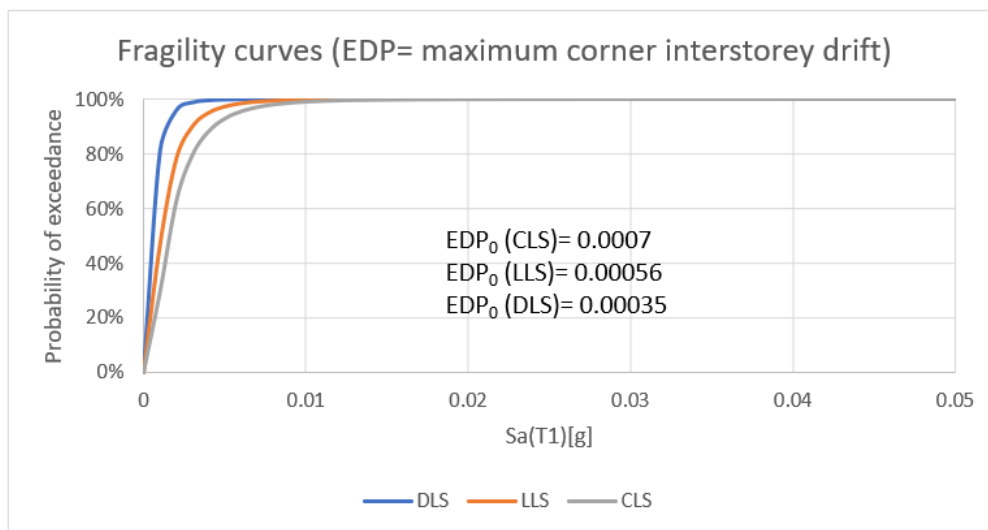
Figure 4-66: Fragility curves calculated based on maximum interstorey drift in a corner of the building and spectral acceleration (Sa(T1)).

Then the maximum displacement at the top of the building has been considered and the ratio between demand and capacity (D/C) has been calculated, by taking as capacity the average value of the displacements at the top of the building at the moment of the collapse of the first hinge, as described above. The correlation of D/C has been made with PGA and Sa(T1) as intensity measures. The correlation and the fragility curves derived with PGA as intensity measure, are shown in Figure 4-67 and Figure 4-68. The same graphs found with Sa(T1) as intensity measure are shown in Figure 4-69 and Figure 4-70. All the data used are reported in Attachment, in Table 0-5.
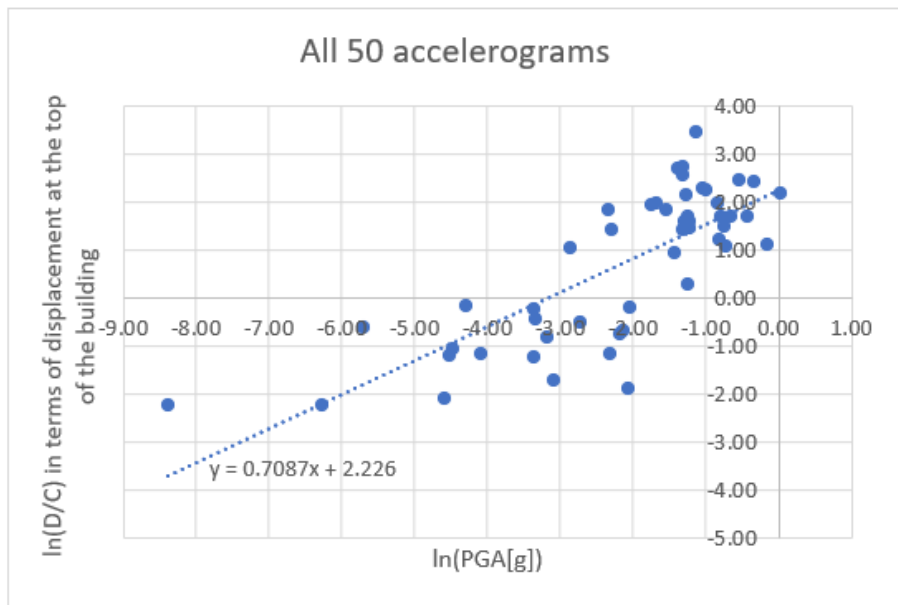
Figure 4-67: Correlation between the ratio D/C in terms of maximum displacement at the top of the building and the PGA for all the 50 accelerograms used (σ=0.989).

Figure 4-68: Fragility curves calculated based on the ratio D/C in terms of maximum displacement at the top of the building and PGA.

It can be noticed that the standard deviation in the correlation with PGA is even higher than the one for the same correlation made with maximum interstorey drifts. Spectral acceleration of the first period appears to be a better choice for the IM. The standard deviation of this last correlation is the minimum among all the presented correlations.
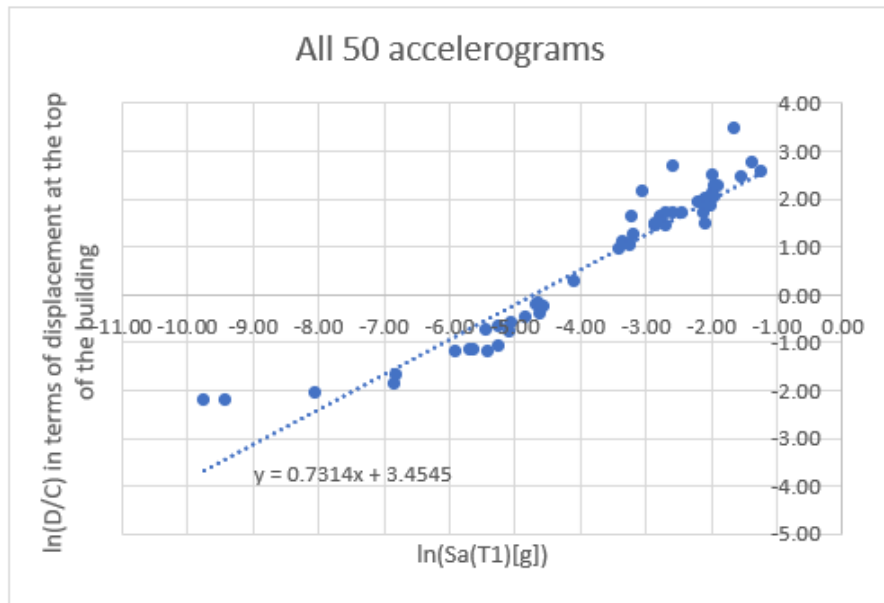
Figure 4-69: Correlation between the ratio D/C in terms of maximum displacement at the top of the building and the Sa(T1) for all the 50 accelerograms used (σ=0.487).
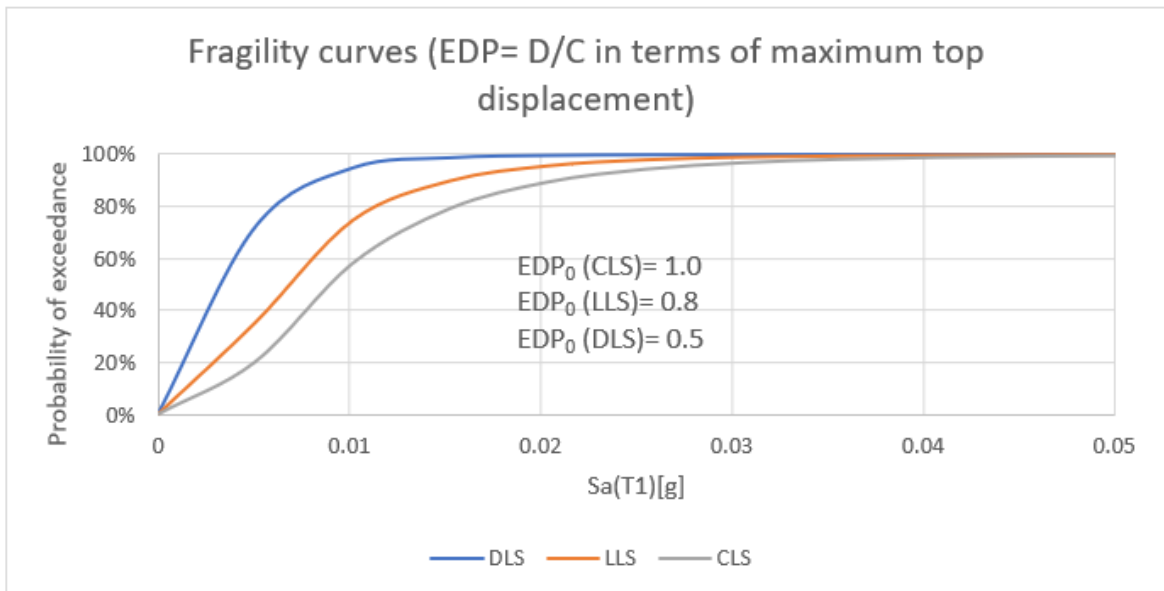
Figure 4-70: Fragility curves calculated based on the ratio D/C in terms of maximum displacement at the top of the building and spectral acceleration (Sa(T1)).

As a last combination, also Housner index is used to check the correlation and calculate fragility curves (Figure 4-71 and Figure 4-72).
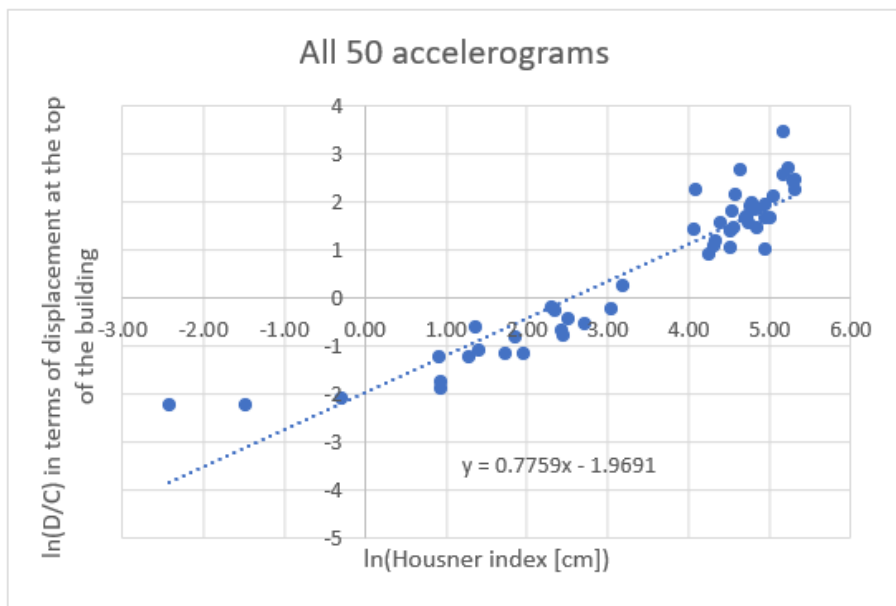
Figure 4-71: Correlation of the logarithm of the D/C ratio in terms of displacement at the top of the building vs. the logarithm of the Housner index (σ=0.544).
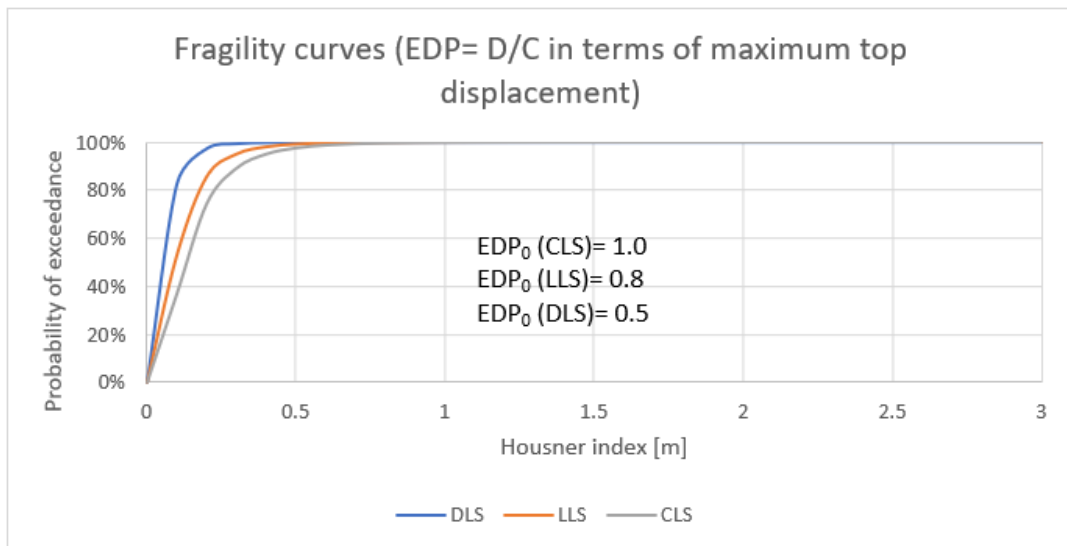
Figure 4-72: Fragility curves calculated based on the ratio D/C in terms of maximum displacement at the top of the building and Housner index [m].

As already done for RC building 1 (**§4.2.3**), also for RC building 2, the first criterium used to set the damage state thresholds is considered more reliable. The fragility curves of the building, obtained with the first criterium, are thus compared to fragility curves of similar buildings from literature [57] [56], already described in §4.2.3. It can be noticed that the case study building results to be much more vulnerable than the average building with similar structure (Figure 4-73, Figure 4-74, Figure 4-75 and Figure 4-76).
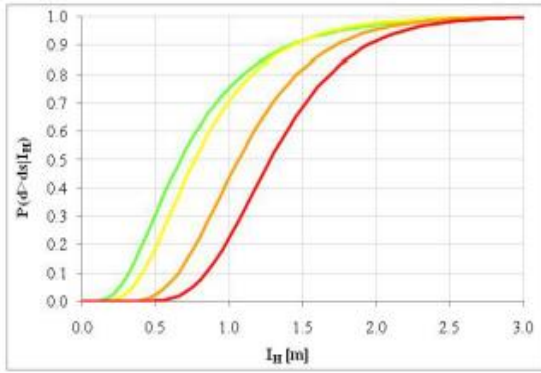
Figure 4-73: Fragility curves for 8-storey bare frame built before 1971, for four damage levels (slight, moderate, severe and partial or total collapse) [57].
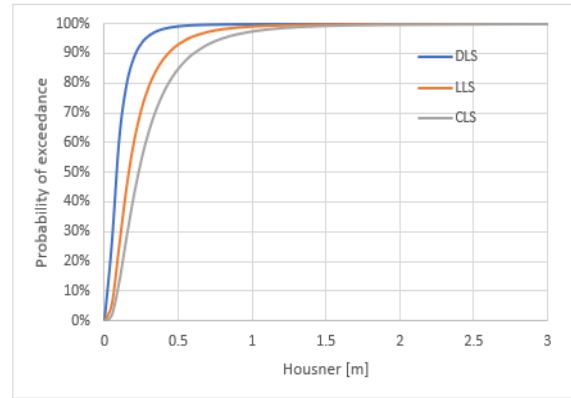
Figure 4-74: Fragility curves for RC building 2, in Y direction – 11 storeys, frame + concrete walls, built in 1970. Three limit states (collapse, life safety and damage limit states). IM= Housner index.
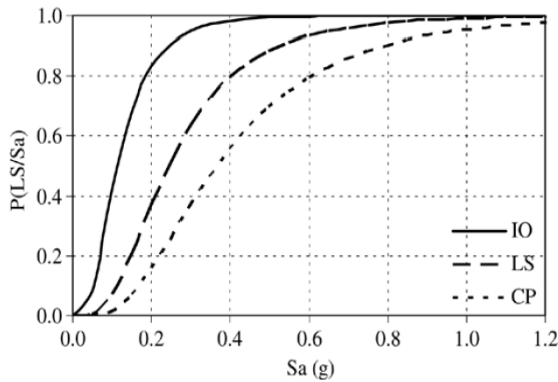
Figure 4-75: Global-level fragility curves for unretrofitted RC frame structure representative of 1980's construction in the Central United States [56].
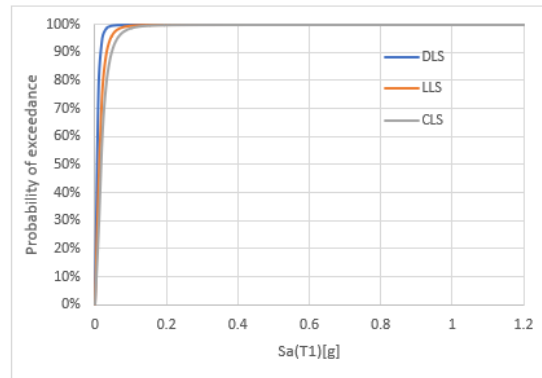
Figure 4-76: Fragility curves for RC building 2, in Y direction – 11 storeys, frame + concrete walls, built in 1970. Three limit states (collapse, life safety and damage limit states). IM=spectral acceleration.

Figure 4-77 shows another set of fragility curves obtained by [56], already shown in §4.2.3, but reported here for a faster comparison. It can be noticed that the curves for the unretrofitted building are translated to the left, in a similar way as the ones found for RC building 2.
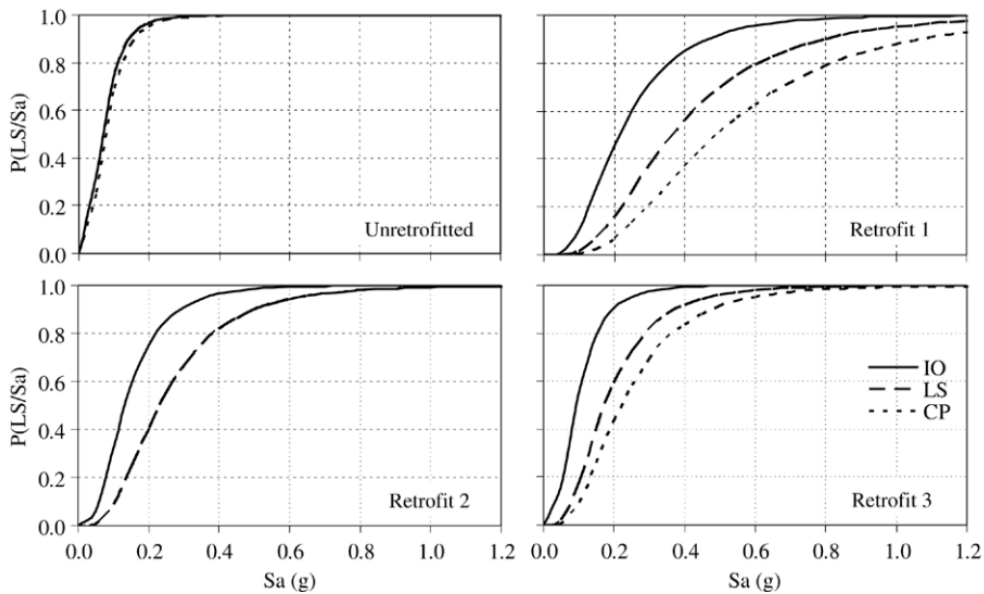
Figure 4-77: Fragility curves based on FEMA 356 member-level limits [56].

4.3.3.2. Analyses and fragility curves in X direction

The same analyses carried out in Y direction of the building, have been then performed also in X direction of the building, the stiffer and more irregular direction (long side of the building). The same accelerograms have been used to carry out the analyses. In this case just the best correlations are shown:

- maximum interstorey drift as EDP, calculated with barycentric joints and with corner joints, with spectral acceleration of the fundamental period (Sa(T1)) and with Housner index as IM;
- D/C ratio as EDP, calculated for the displacement at the top of the building, considering three different IMs – PGA, Sa(T1) and Housner index.

The same limits considered for Y direction have been chosen. The maximum interstorey drift for CLS is 0.3% and the limits for LLS and DLS are 0.8 and 0.5 of the CLS limit respectively.

All the data of the interstorey displacements, drifts, top dispacements and intensity measures used for the correlations are reported in Attachment, in Table 0-6 and Table 0-7.

The correlations and the fragility curves found with maximum interstorey drifts for barycentric joints and for corner joints, can be seen in Figure 4-78, Figure 4-79, Figure 4-80 and Figure 4-81.
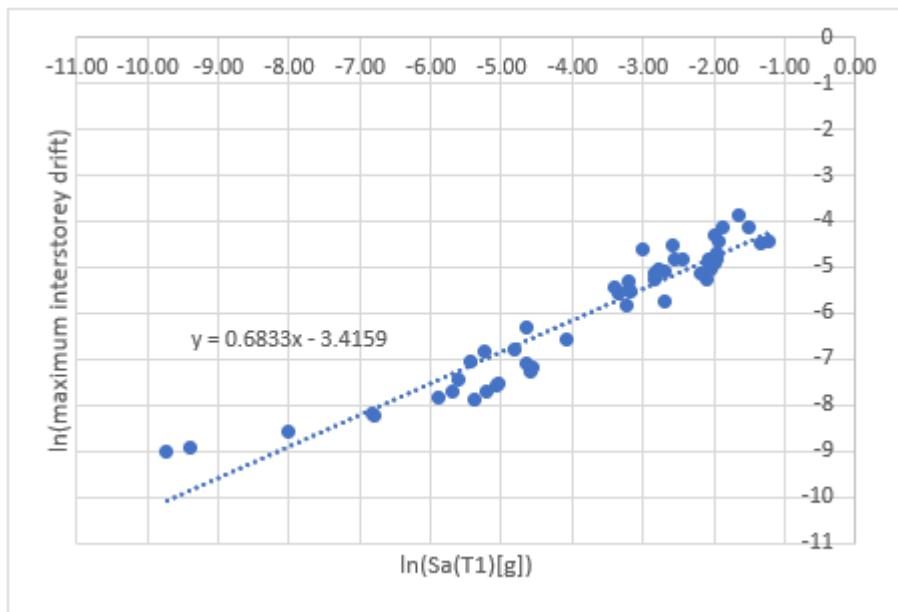
Figure 4-78: Correlation between the maximum interstorey drift and the Sa(T1) for all the 50 accelerograms used (σ=0.450).
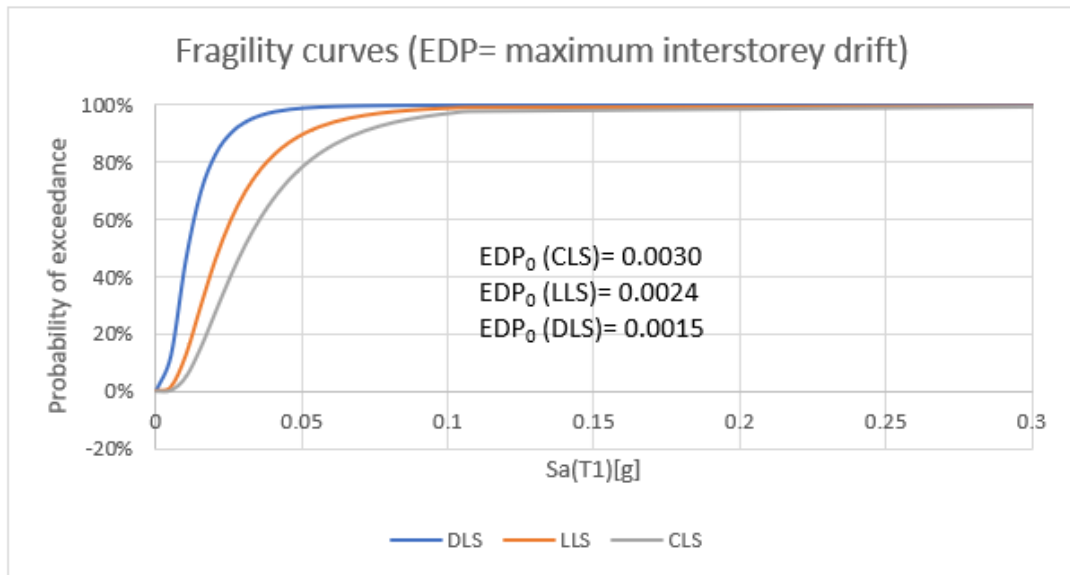
Figure 4-79: Fragility curves calculated based on maximum interstorey drift and spectral acceleration (Sa(T1)).
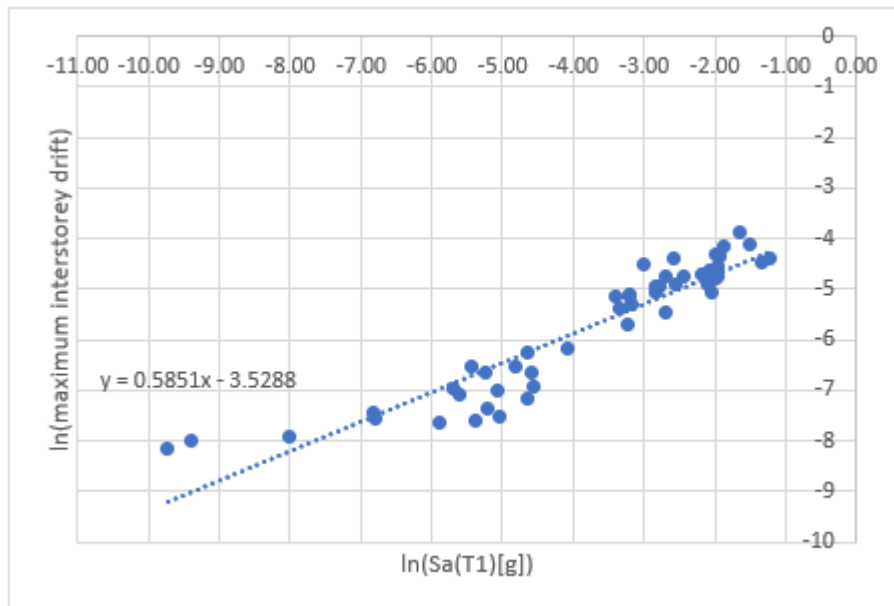
Figure 4-80: Correlation between the maximum interstorey drift in a corner of the building and the Sa(T1) for all the 50 accelerograms used (σ=0.466).
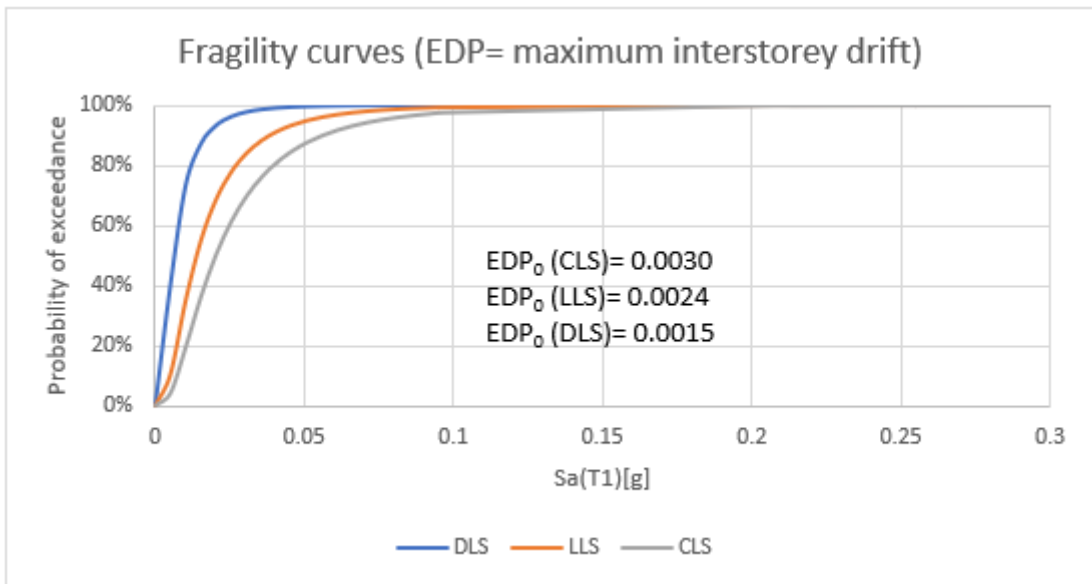
Figure 4-81: Fragility curves calculated based on maximum interstorey drift in a corner of the building and spectral acceleration (Sa(T1)).

As a last combination, also Housner index is used to check the correlation and calculate fragility curves (Figure 4-82 and Figure 4-83), just for the corner joints.
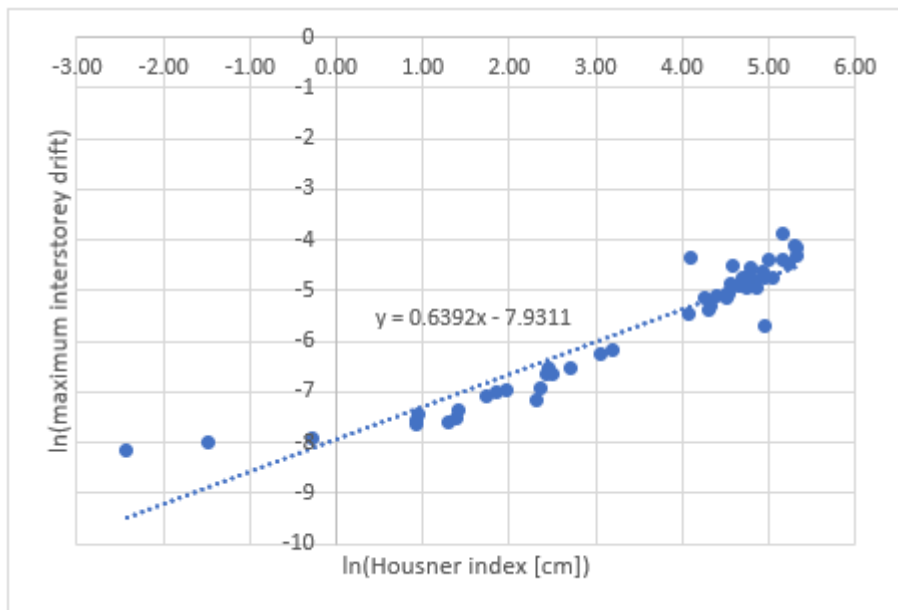
Figure 4-82: Bi-logarithmic correlation between the maximum interstorey drift in a corner of the building and the Housner index for all the 50 accelerograms used (σ=0.413).
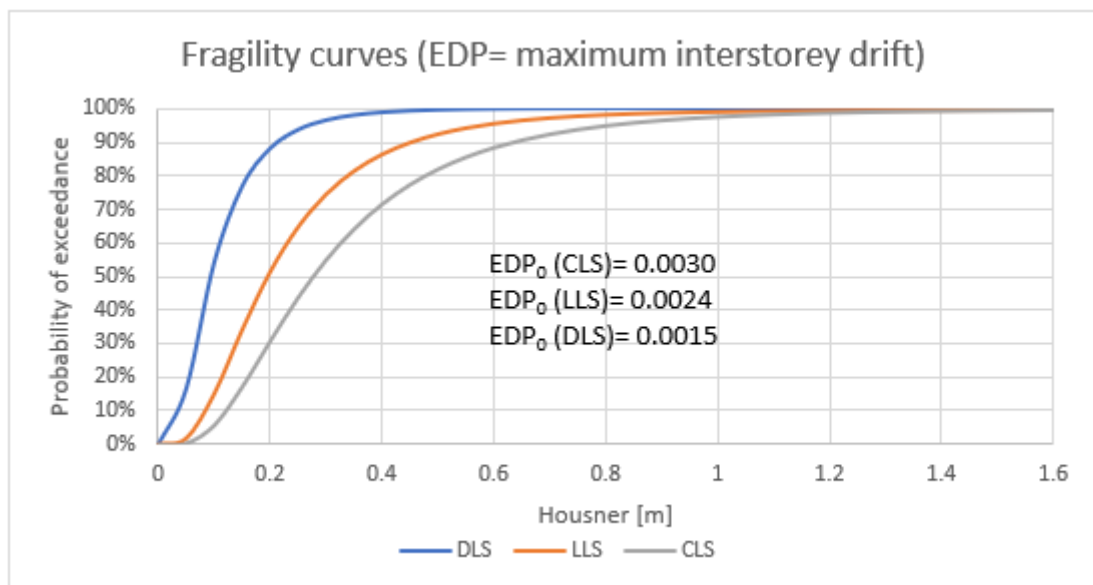
Figure 4-83: Fragility curves calculated based on maximum interstorey drift in a corner of the building and Housner index.

In order to use the ratio D/C as EDP, the capacity of the building has been checked for the first 30 signals. As already done for Y direction, also for X direction the displacement at the top of the building has been considered. The capacity in terms of top displacement has been calculated as the average value of the capacity in each of the first 30 analyses. The building has been considered collapsed when the first plastic hinge (or the first group of plastic hinges, if they collapse simultaneously) collapses and the displacement of the top of the building has been checked at that moment. The values of this capacity for each of the 30 analyses are reported in Figure 4-84, where also the median value and the standard deviation are displayed. The resultant displacement in X and Y direction has been considered.

The average value of 0.0148 m, compared to the height of the building of 34.59 m, means a drift of 0.000429= 0.4‰, that is even smaller than the value found for Y direction, as expected. When this limit is used for the calculation of the fragility curves based on the interstorey drift, very different results would be obtained.
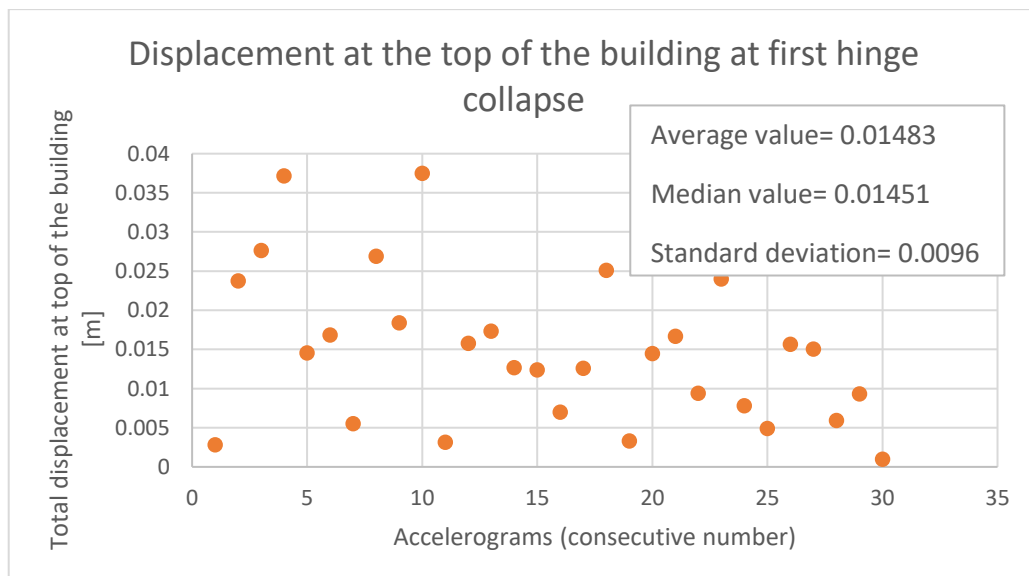
Figure 4-84: Values of the displacement at the top of the building at the moment of the collapse of the first hinge.

The correlation of D/C has been made with PGA and Sa(T1) as intensity measures.
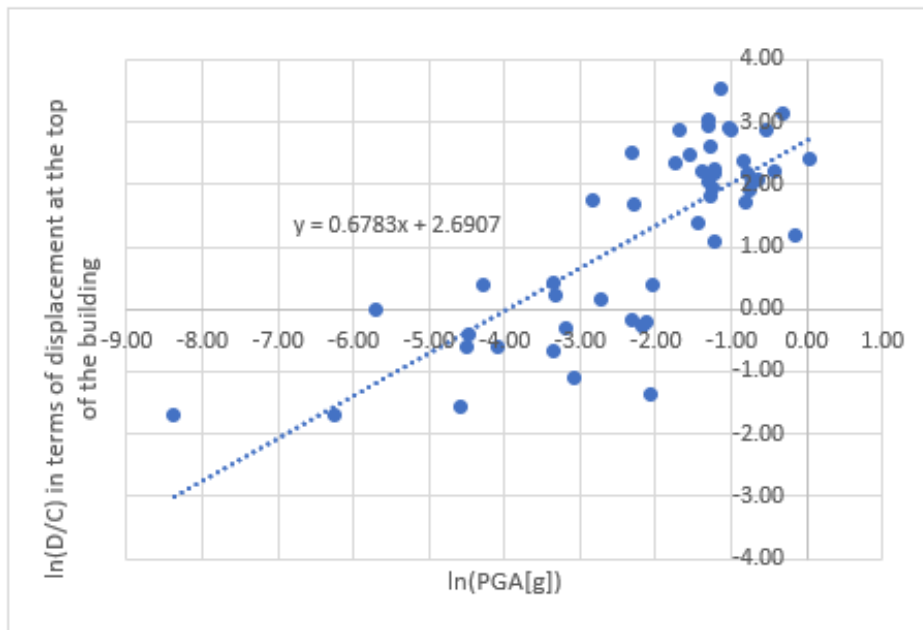
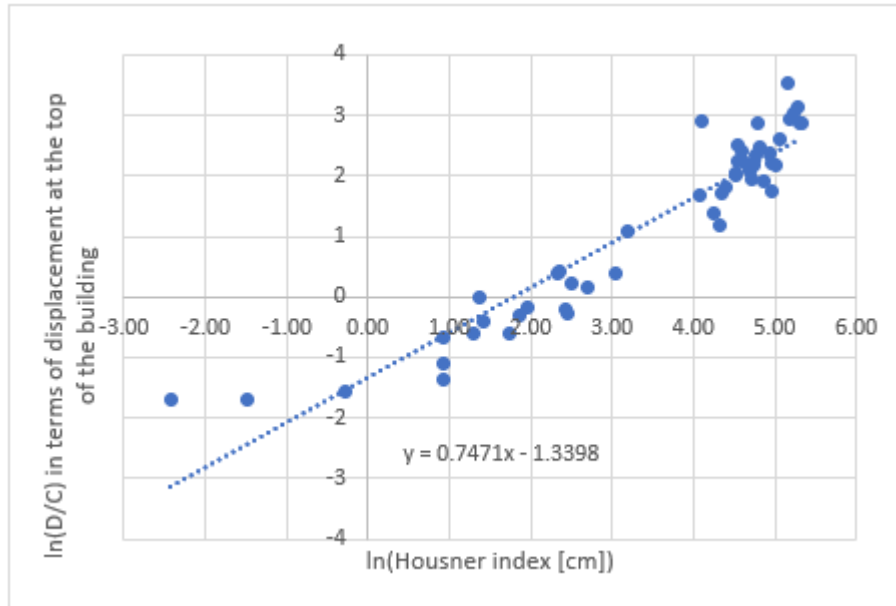**Figure 4-85: Correlation of the logarithm of the D/C ratio in terms of displacement at the top of the building vs. the logarithm of the PGA (σ=0.940).**
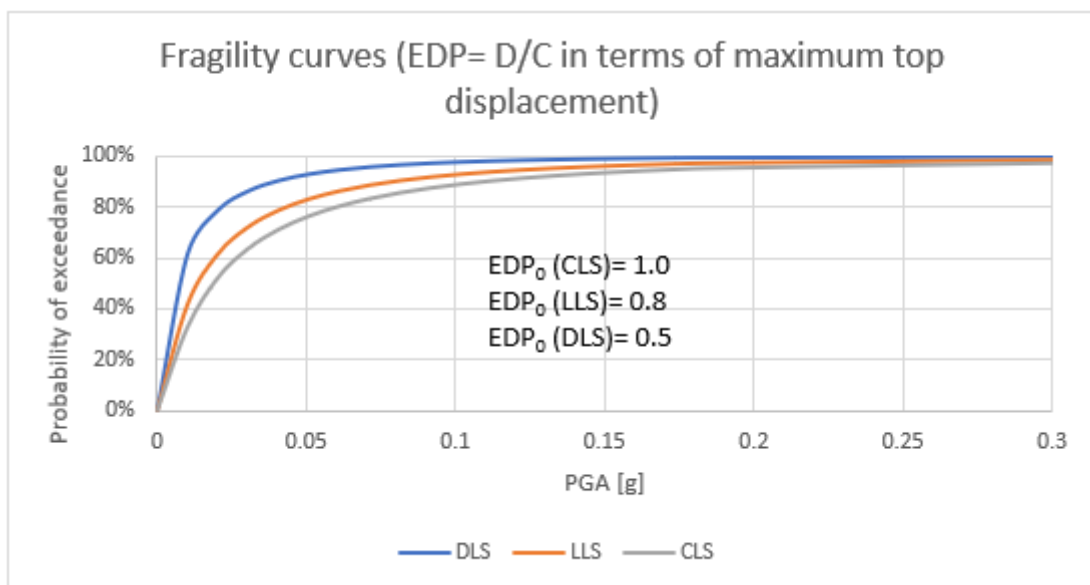
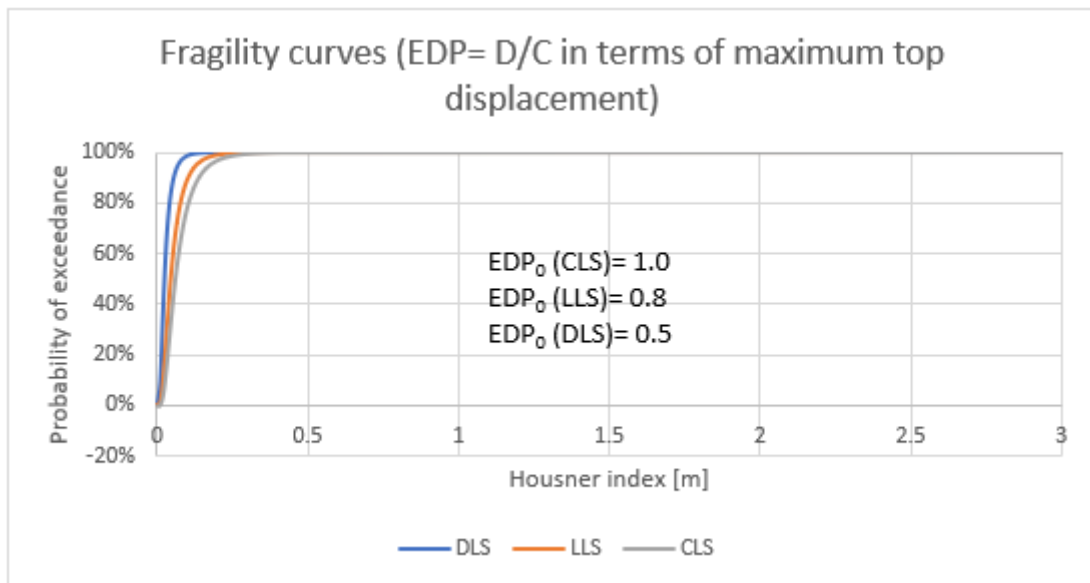**Figure 4-86: Fragility curves calculated based on the ratio D/C in terms of maximum displacement at the top of the building and PGA.**
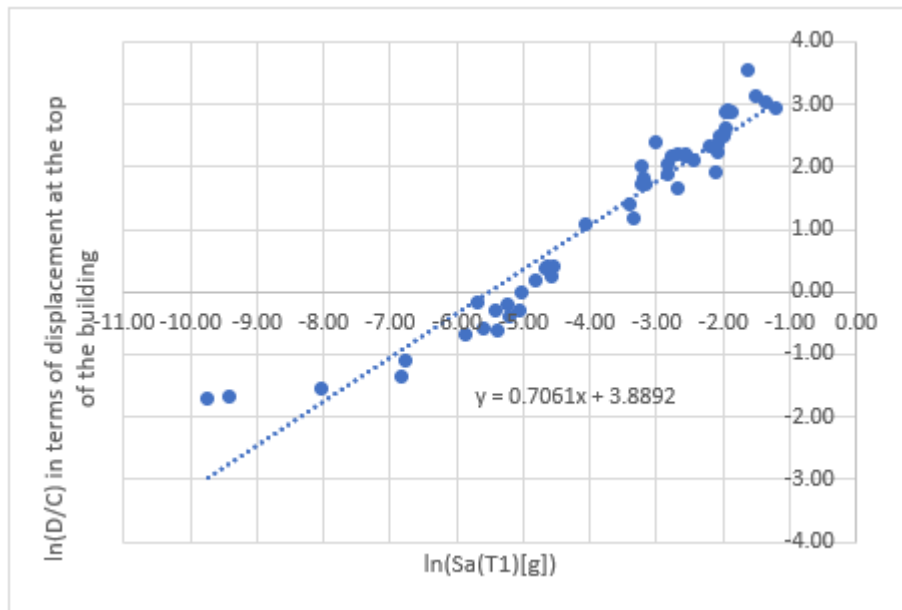
Figure 4-87: Correlation of the logarithm of the D/C ratio in terms of displacement at the top of the building vs. the logarithm of the spectral acceleration Sa(T1) (σ=0.413).
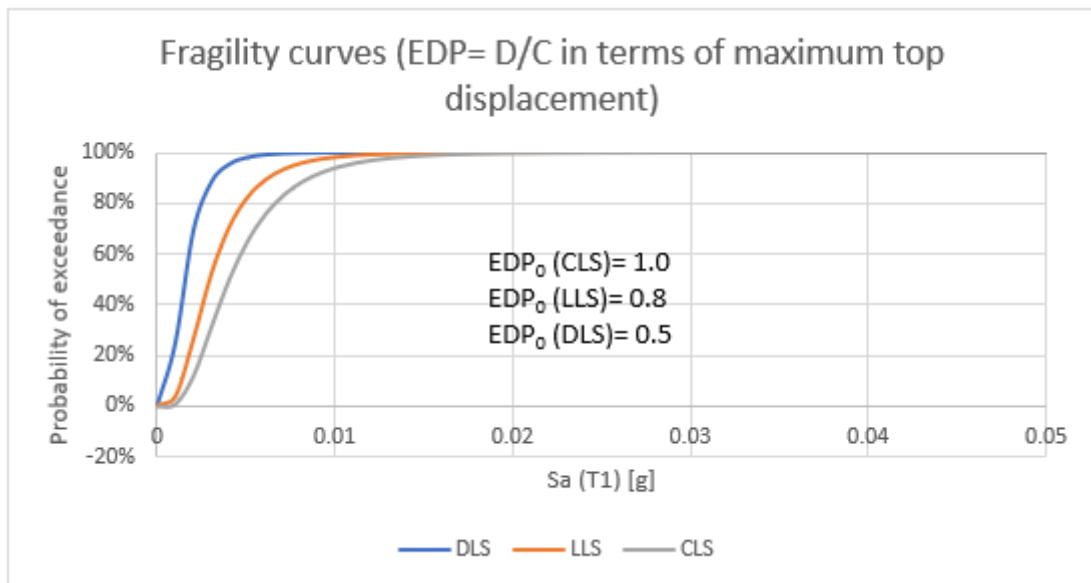
Figure 4-88: Fragility curves calculated based on the ratio D/C in terms of maximum displacement at the top of the building and spectral acceleration Sa(T1).

At the end also Housner index has been used as an IM (Figure 4-89 and Figure 4-90).

Figure 4-89: Correlation of the logarithm of the D/C ratio in terms of displacement at the top of the building vs. the logarithm of the Housner index (σ=0.486).

Figure 4-90: Fragility curves calculated based on the ratio D/C in terms of maximum displacement at the top of the building and Housner index.

4.3.4. Vulnerability evaluation

In the previous paragraph some combinations of Engineering demand parameters (EDPs) and Intensity measures (IM) have been made in order to calculate the fragility curves of the case study building in X and Y direction. For a vulnerability evaluation, the curves calculated with the damage states thresholds set based on the results of the pushover analyses have been considered (as already mentioned in §4.2.3 for RC building 1).

Among the different IMs used, fragility curves obtained from the correlation with the lowest standard deviation are chosen as the most indicative, that is spectral acceleration at the fundamental period, for both X and Y directions of the building. The curves are shown in Figure 4-91 and Figure

_____

4-92. As the considered damage state thresholds are the same in the two directions, the curves are very similar, although the ones in Y direction are slightly higher. Both directions are very vulnerable compared to fragility curves from literature, as shown in §4.3.3.1. They show that the building has collapsed for sure for a spectral acceleration of 0.158 g = 1.55 m/s^2 for X direction and of 0.130 g = 1.28 m/s^2 for Y direction, that are very low values.
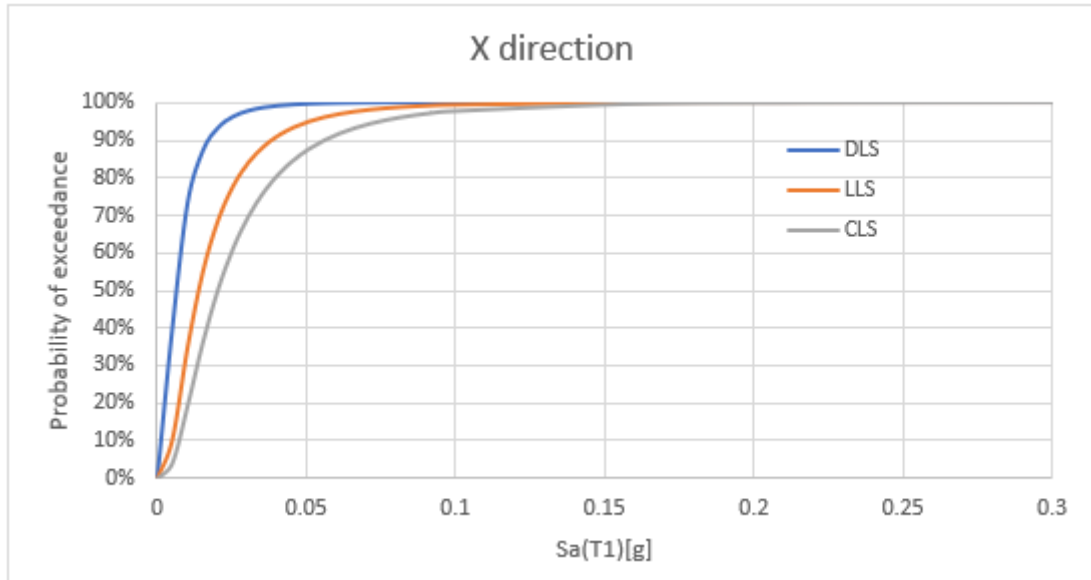
Figure 4-91: Fragility curves for three limit states for X direction of the RC building 2.
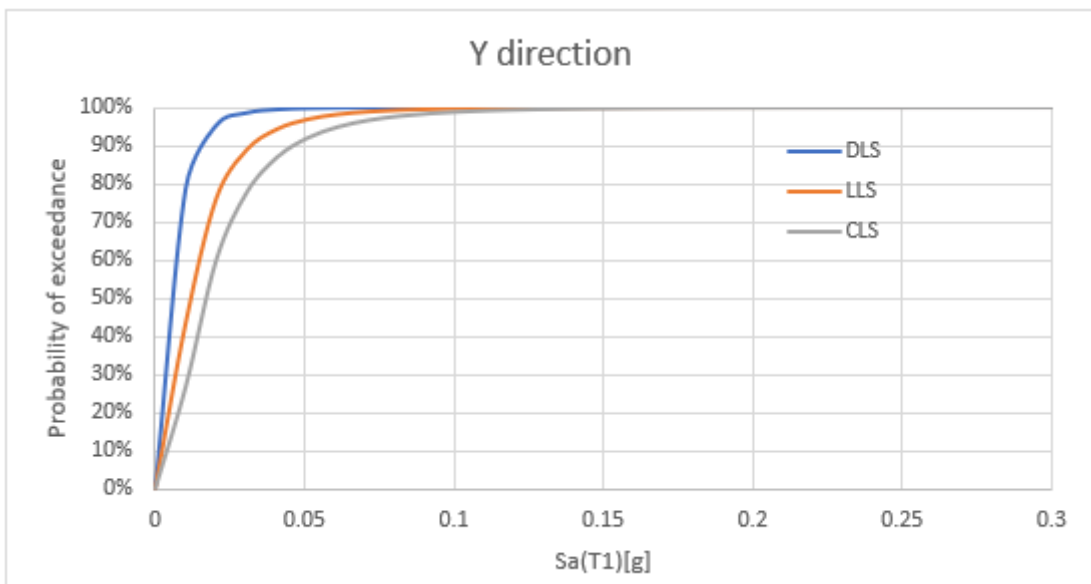
Figure 4-92: Fragility curves for three limit states for Y direction of the RC building 2.

If the scenario response spectra are considered, the spectral acceleration for the approximate fundamental period of 2.4 s, for Idrija fault is 0.038 g for the 50th percentile, 0.049 g for the 84th percentile and 0.061 g for the 95th percentile, while for Medea fault is 0.023 g for the 50th percentile, 0.055 g for the 84th percentile and 0.094 g for the 95th percentile. These values are all below the 0.130 g, but the probability of exceedance of collapse limit state with the scenario seismic input is nevertheless higher than 70%. Some values are investigated more in detail in Figure 4-93.

_____

_____

If we consider the code spectra, there is a value for each limit state (Table 4-28):

Table 4-28: Spectral accelerations for the fundamental period of the case study building (code spectra).

Limit state	Spectral acceleration (T=2.4 s)
CLS	0.138g
LLS	0.106g
DLS	0.024g

It is evident that the code spectral accelerations are higher than scenario accelerations for the given fundamental period (with the exception of the DLS) and that the scenario values are between the ones of DLS and LLS.

In order to better see the vulnerability results, the probability of the structure of being in a limit state, for a given Sa value, is plotted in the histogram in Figure 4-93 for Y direction of the building and for six values of Sa: the values from the code response spectra for the DLS, LLS and CLS and the values of the 95th percentile for Idrija scenario and for Medea scenario and the 50th percentile of Medea scenario. Each column of the histogram refers to one of the six spectral acceleration values, for which the probabilities of being in a given limit state is calculated. In each column the red part is the probability of exceeding the collapse limit state and can be directly read from the fragility curve of the CLS. The blue part is the probability of the building to exceed LLS, but not exceed CLS, that means to be in LLS. It is calculated as the difference between the probability of exceeding LLS and the probability of exceeding CLS. In the same way, the probability of exceeding DLS, but not LLS (green part) is calculated as the difference of the two probabilities of exceeding each of the two limit states. The grey part is eventually the probability that not even DLS is exceeded, so that the building remains operational and undamaged. The graph shows that just with Medea 50th percentile and the code DLS spectrum, there is some probability for the structure not to be damaged (3%) or to be in a DLS, not exceeding LLS (15-16%). For the other cases the probability to exceed the CLS is very hight and over 90%, but they are related to stronger seismic events.
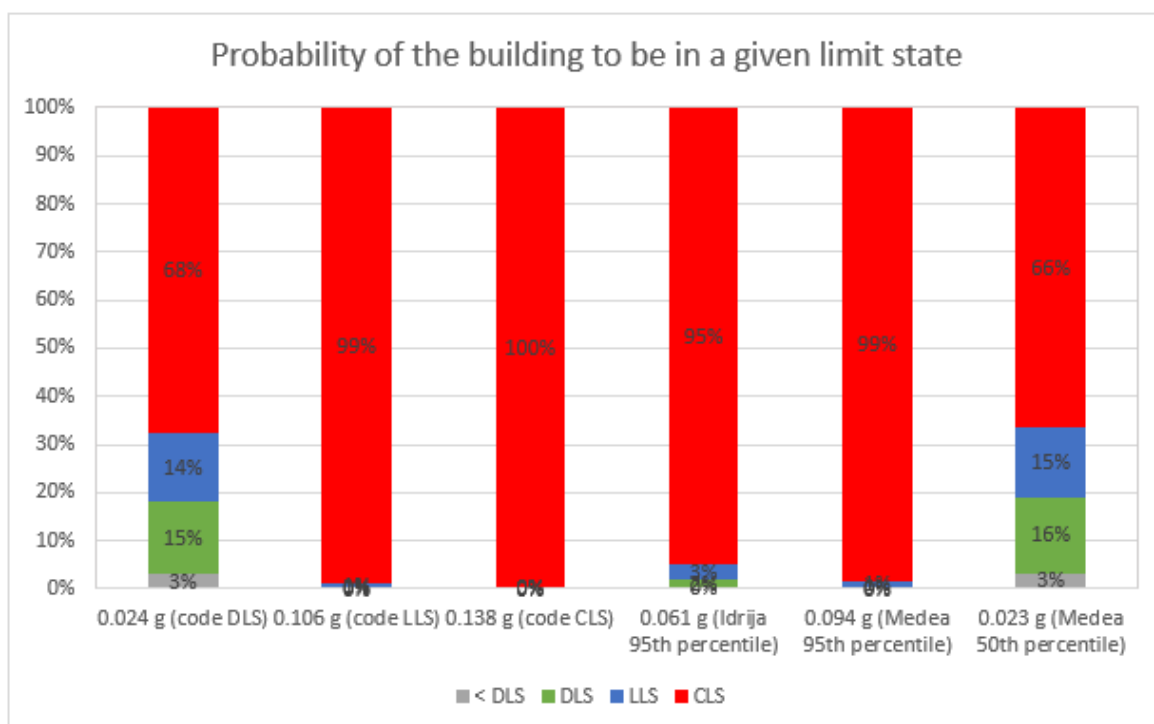
Figure 4-93: Histogram with the probability of the structure to be in a given Limit State, for three different values of Sa: value from the code response spectrum for DLS and values of the 5th percentile of the two analysed scenarios, Idrija and Medea. The grey part indicates the probability of the building to be under the damage limit state (Operational limit state or without any damage).

_____

For a comparison of the vulnerability of the two case study buildings, also the fragility curve for RC building 1 is reported in Figure 4-94 with the same scale than the curves for RC building 2. It can be seen that the Y direction of building 1 is much more fragile of both directions of building 2. This is probably due to the additional 2 storeys of building 1 compared to building 2 and to a stiffer staircase, although it is more centred along the long side of the building, compared to building 2.
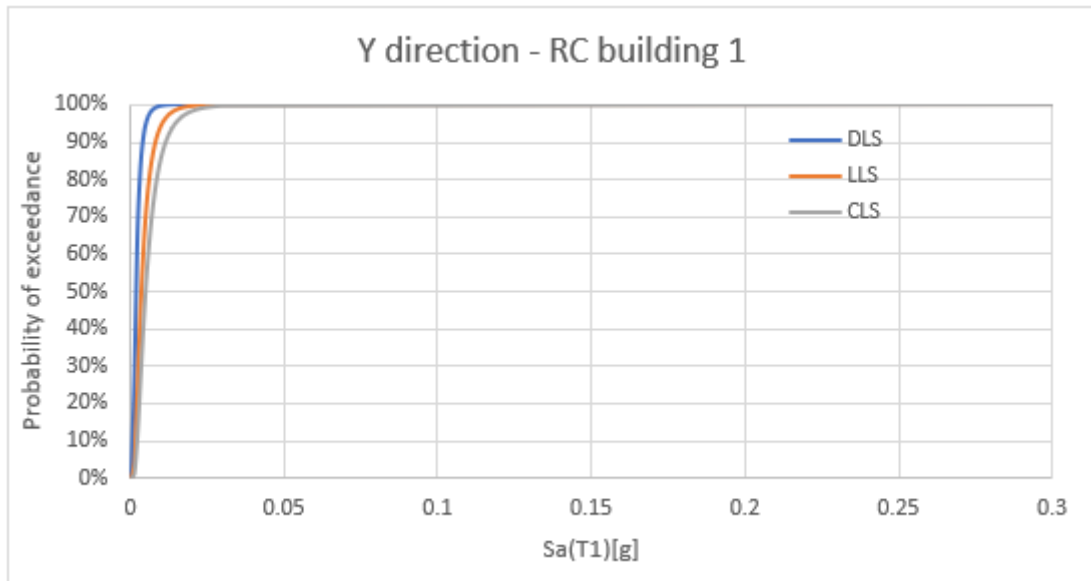

Figure 4-94: Fragility curves for three limit states for Y direction of the RC building 1, for comparison with RC building 2.

4.4. Masonry building A

As already discussed in §3.3.5, just the main part of the building (without the lodge) is analysed.

4.4.1. Modal analysis

The stone masonry building has a fundamental period in X direction of 0.39 s (61.6% of participating mass) and in Y direction of 0.40 s (26.9% of participating mass). For achieving a participating mass ratio of at least 85%, 9 or 10 modes are needed, for X and Y direction respectively (Table 4-29). The first modal shapes in X and Y direction of the building are shown in Figure 4-95 for the last storey of the building.

Table 4-29: Modal participating masses and mass ratios for the main part of Masonry building A.

Mode	T [s]	mx [kg]	Mx [%]	my [kg]	My [%]	mz [kg]	Mz [%]	Mx sum [%]	My sum [%]	Mz sum [%]
1	0.40671	32,861	1.08	143,146	4.71	40	0	1.08	4.71	0
2	0.39541	213,264	7.02	816,577	26.88	118	0	8.1	31.59	0
3	0.3891	1,872,124	61.63	345,251	11.36	98	0	69.73	42.95	0
4	0.3795	103,084	3.39	285,054	9.38	3	0	73.12	52.33	0
5	0.36388	5,121	0.17	574,010	18.9	3	0	73.29	71.23	0
6	0.35419	1,930	0.06	11,591	0.38	14	0	73.35	71.61	0
7	0.31679	231,015	7.6	167,971	5.53	122	0	80.95	77.14	0
8	0.30897	0	0	159,829	5.26	110	0	80.95	82.4	0
9	0.28591	251,060	8.26	59,931	1.97	36	0	89.21	84.37	0
10	0.26265	3,459	0.11	151,074	4.97	18	0	89.32	89.34	0
11	0.17237	10,921	0.36	28	0	3,513	0.12	89.68	89.34	0.12
12	0.1608	1,402	0.05	2,066	0.07	24	0	89.73	89.41	0.12

13	0.15323	10,888	0.36	16,954	0.56	2,140	0.07	90.09	89.97	0.19
14	0.15193	1,380	0.05	25,460	0.84	1,538	0.05	90.14	90.81	0.24
15	0.1448	46,609	1.53	55,409	1.82	29	0	91.67	92.63	0.24
16	0.13876	149	0	101,544	3.34	14	0	91.67	95.97	0.24
17	0.13587	47,028	1.55	22,220	0.73	1,751	0.06	93.22	96.7	0.3
18	0.13267	14,272	0.47	39,792	1.31	1,604	0.05	93.69	98.01	0.35
19	0.13	100,912	3.32	8,834	0.29	671	0.02	97.01	98.3	0.37
20	0.12709	23,351	0.77	4,104	0.14	2	0	97.78	98.44	0.37
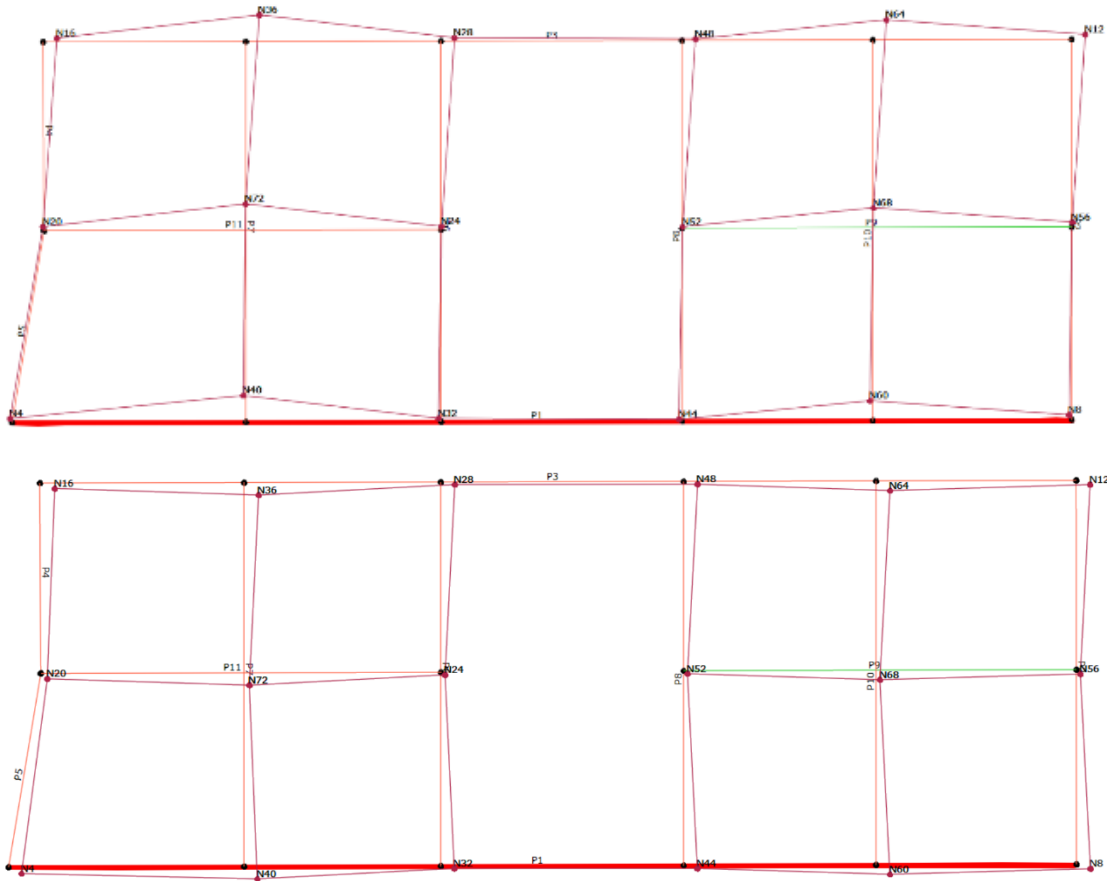
Figure 4-95: (a) 2ⁿᵈ (fundamental in Y direction) and (b) 3ʳᵈ (fundamental in X direction) mode deformed shape of the third (and last) storey of the building.

The great flexibility of the slabs in their plane (as they are wooden) causes a quite independent motion of each wall of the building. For this reason, the pushover analyses are carried out on the single wall and not on the whole building.

In order to validate the model and check if the fundamental modes correspond to reality, some vibrational measures have been carried out, in a similar way as described for RC building 1 (§4.2.1). The measures are based on the natural vibration of the building without external forces, so that the measured vibrations have very low amplitudes and they reflect the very linear elastic behaviour of the building. They are not expected to be the same as in the numerical model, but they can give some hints about the quality of modelling and on the nature of the building.

The measures have been carried out in the loft of the building, where the motion has usually the maximum amplitude. The location of the measuring points is shown in Figure 4-96 and Figure 4-97. The measuring time is 16 minutes, a good compromise in order to be able to distinguish natural

vibration of the building from spurious signals (as people walking by or vibrations from machines or traffic), without losing too much time for each measurement.
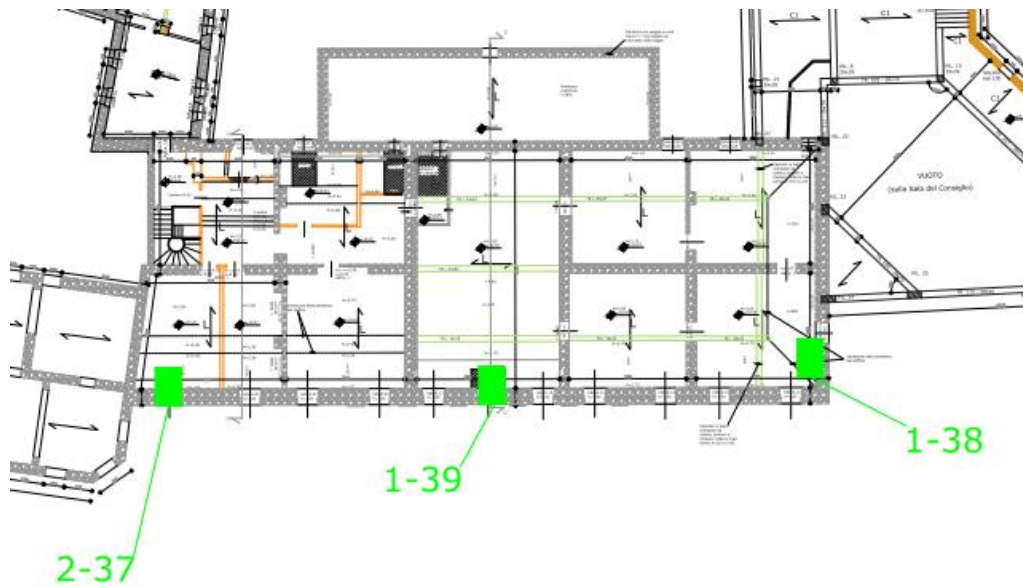
Figure 4-96: Location of velocimeters and name of the records – loft
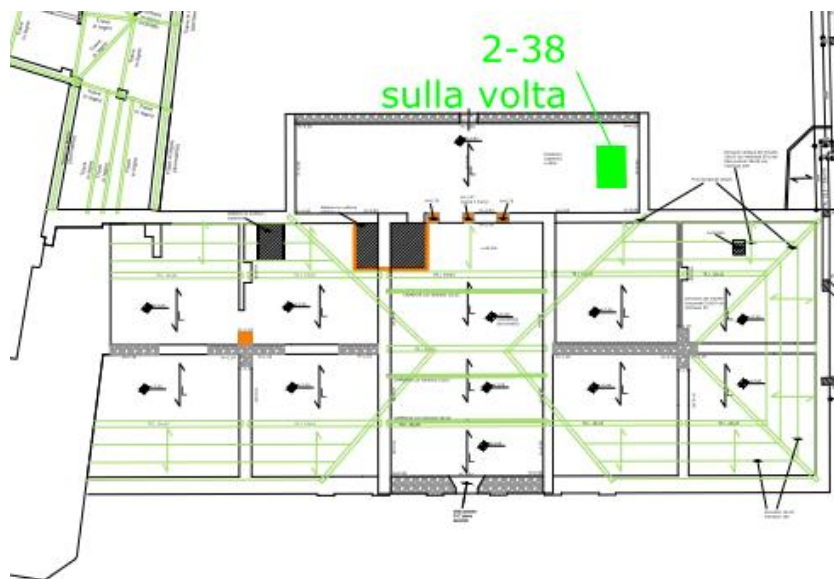
Figure 4-97: Location of velocimeters and name of the records – roof

The results of the measures carried out on the case study building are summarized in Table 4-30. The N-S direction is in the direction of the short side of the building (Y direction), while the E-W is in the direction of the long side of the building (X direction). The frequencies automatically found by the software of the velocimeters (Tromini – software Grilla) have a slight variation from measure to measure. However, Peak 1 (2.0 Hz or 0.5 s) is quite similar to the period found with the numerical analysis (0.41s). The ratio between the spectra of horizontal and vertical components (H/V) and the spectra of the single recorded components are shown in Figure 4-98 to Figure 4-101.

Table 4-30: Results of the measures – in the first two columns are reported the peaks automatically found by the software Grilla that is sold together with the velocimeters (inferred form H/V spectra); the following three columns report the peaks that are read on the spectra of the single components. In the cells both frequency and periods are reported.

Record	Frequency N-S	Frequency E-W	Peak 1	Peak 2	Peak 3	Peak 4
2-37	4.78 Hz → 0.209s	4.78 Hz → 0.209s	2.00 Hz → 0.5s	3.50 Hz → 0.29s	5.00 Hz → 0.2s	5.50 Hz → 0.18s
1-38	5.88 Hz → 0.170s	5.72 Hz → 0.175s	2.00 Hz → 0.5s	3.50 Hz → 0.29s	4.50 Hz → 0.22s	6.00 Hz → 0.17s
2-38 lodge	3.59 Hz → 0.279s	4.38 Hz → 0.228s	2.00 Hz → 0.5s	3.50 Hz → 0.29s	4.50 Hz → 0.22s	6.00 Hz → 0.17s
1-39	3.56 Hz → 0.281s	4.75 Hz → 0.211s	2.00 Hz → 0.5s	3.50 Hz → 0.29s	4.80 Hz → 0.21s	6.50 Hz → 0.15s

Max.(N-S)/V: 4.78 ± 0.82 Hz. Max.(E-W)/V: 4.78 ± 0.67 Hz. (In the range 0.0 - 10.0 Hz).
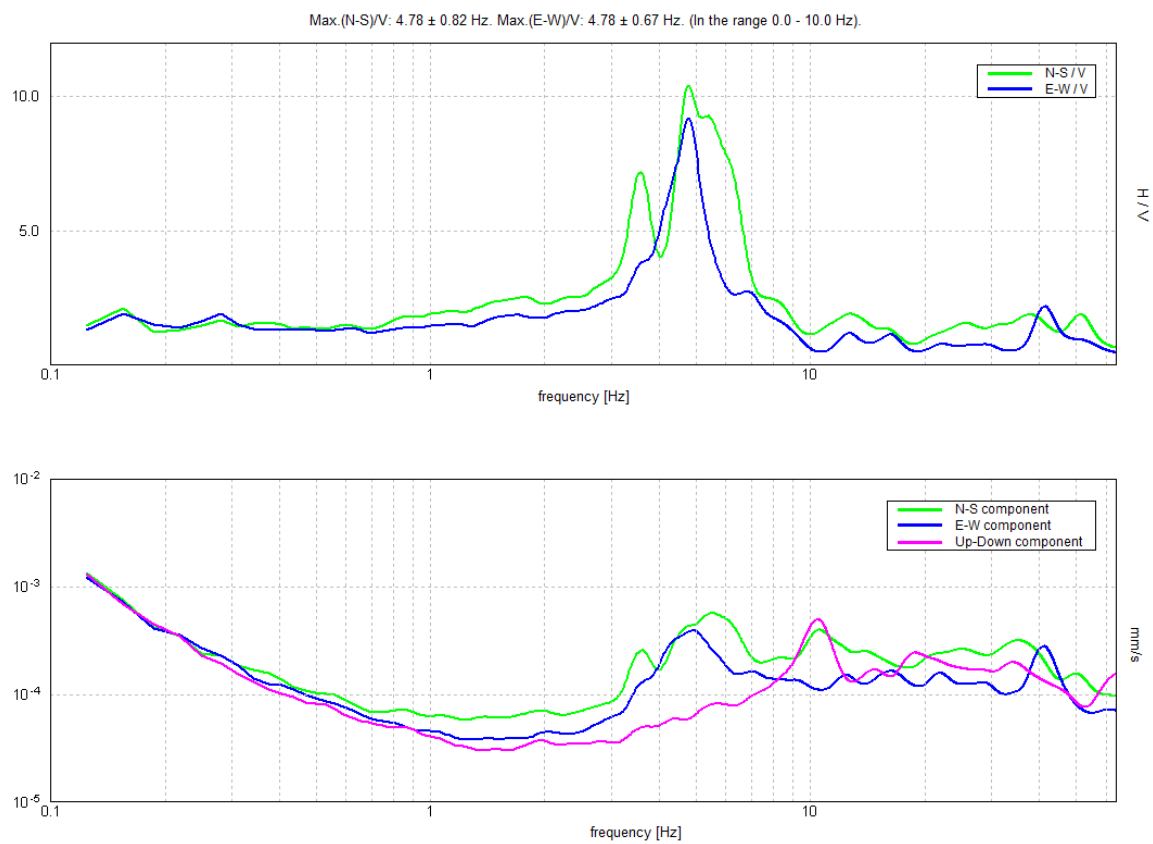
Figure 4-98: Spectra of the record 2-37 – H/V and spectra of the single components

Max.(N-S)/V: 5.88 ± 1.51 Hz. Max.(E-W)/V: 5.72 ± 1.85 Hz. (In the range 0.0 - 10.0 Hz).
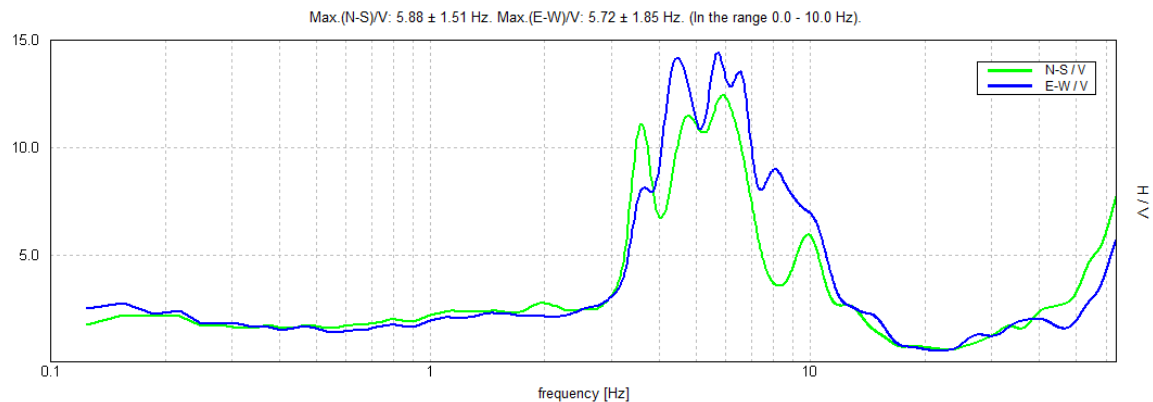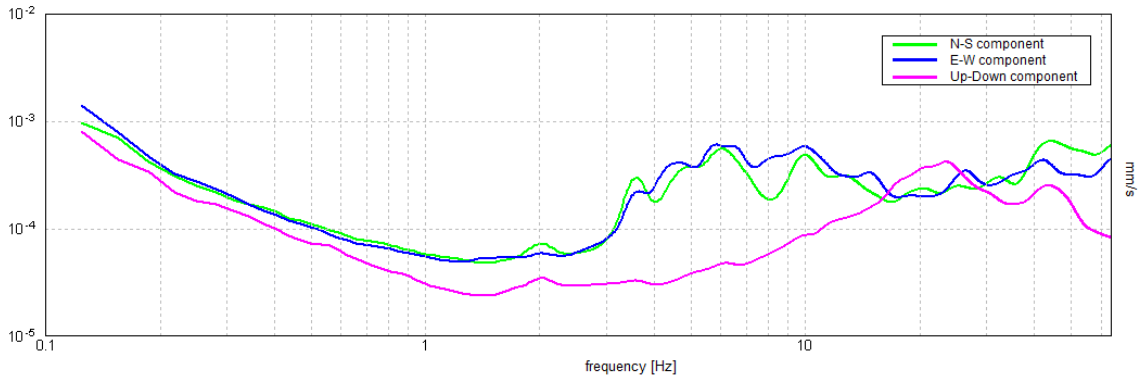
Figure 4-99: Spectra of the record 1-38 – H/V and spectra of the single components

Max.(N-S)/V: 3.59 ± 0.22 Hz. Max.(E-W)/V: 4.38 ± 0.17 Hz. (In the range 0.0 - 10.0 Hz).
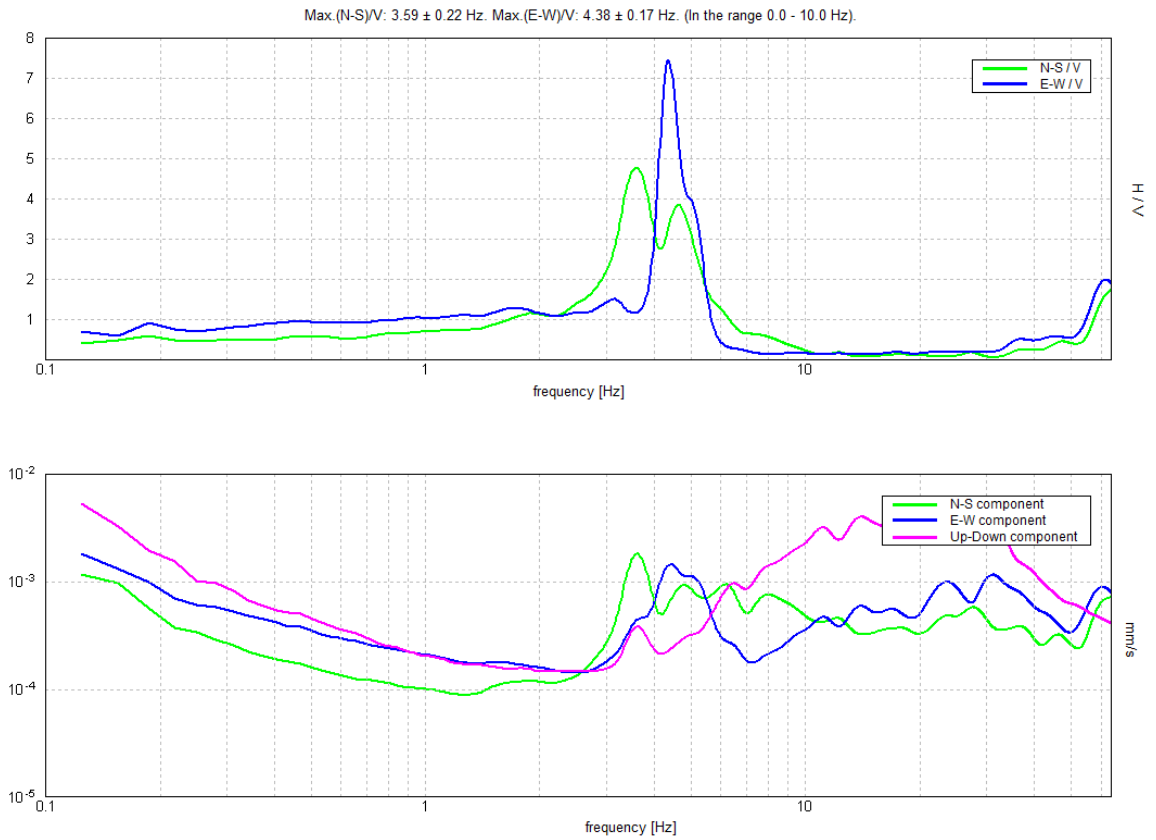
Figure 4-100: Spectra of the record 2-38 – H/V and spectra of the single components

Max.(N-S)/V: 3.56 ± 1.07 Hz. Max.(E-W)/V: 4.75 ± 1.28 Hz. (In the range 0.0 - 10.0 Hz).
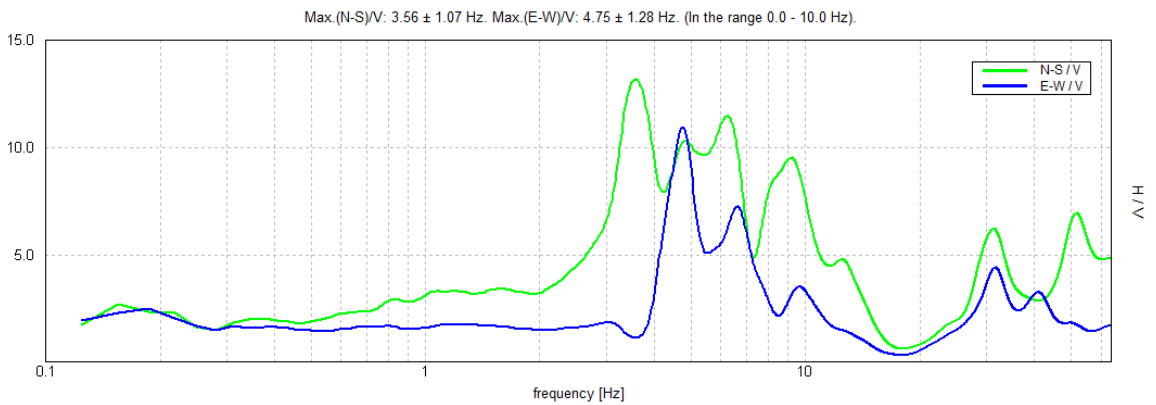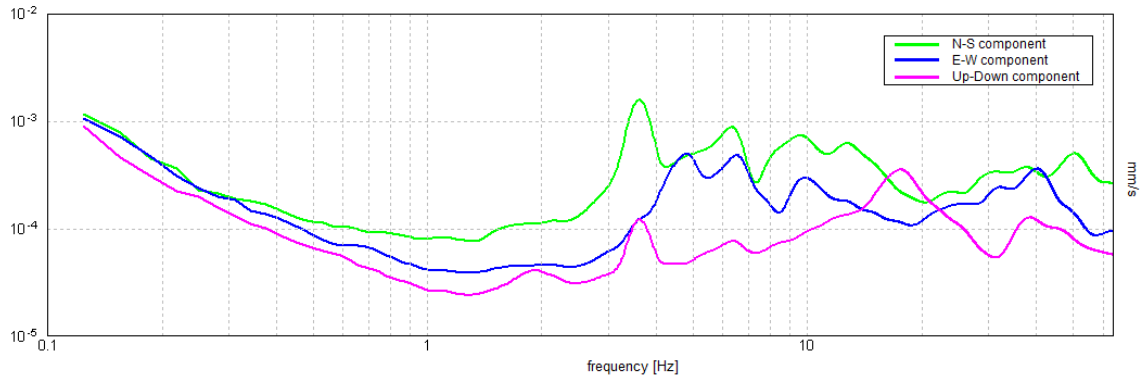
Figure 4-101: Spectra of the record 1-39 – H/V and spectra of the single components

4.4.2. *Non - linear static analysis (pushover)*

The analyses have been carried out with 3Muri computer software from STA DATA. It is a software that is specialized in the analysis of masonry buildings and it considers an equivalent frame model with nonlinear macroelements. It is possible to carry out modal analysis and static non-linear analyses with this software. The load patterns used for this study are the "uniform" pattern, proportional to the storey masses, and a load pattern with a distribution proportional to the equivalent static forces (triangular lateral load). For each wall, four analyses are performed: for each of the two distributions of lateral load, the analyses are carried out in positive and negative direction along the plane of the wall. The names of the walls are visible in Figure 4-102.
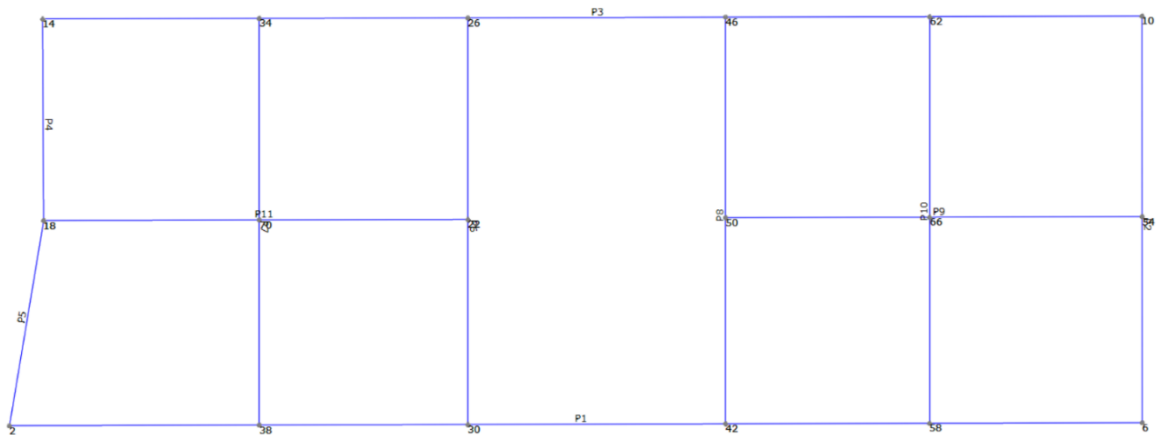
Figure 4-102: Names of the walls of the building in the model in 3Muri (plan of the ground floor).

The results of the analyses are expressed in terms of seismic vulnerability indices α, calculated for each limit state (α_{CLS}, α_{LLS}, α_{DLS}, α_{OLS}) as the ratio between the capacity PGA and the demand PGA:

$$\alpha_{SL,i} = \frac{(PGA_i)_C}{(PGA_i)_D} \tag{4.11}$$

4.4.2.1. *Vulnerability evaluation based on code response spectra*

The results of the analyses are summarized in Table 4-31. For the analyses that did not reach a decay of 20% of the maximum base shear, the last step has been chosen as the collapse and the vulnerability has been calculated based on that step. The new results are reported at the bottom of the table.

Table 4-31: Results of the pushover analyses on all the walls of the building. The analyses highlighted in violet did not reach a decay of 20%, the ones in red are "not verified" and the ones in green are "verified". The yellow analysis is the most severe. The software is in Italian language, so that a small legend is needed: Parete = Wall, Nodo = control joint, Dir.sisma= Direction of the load, Carico sismico= Load pattern, SLC = CLS, SLV = LLS, SLD = DLS and SLO = OLS.

Parete	N.	Inserisci in relazione	Nodo	Dir. sisma	Carico sismico	Dmax SLC [cm]	Du SLC [cm]	q* SLC	Dmax SLV [cm]	Du SLV [cm]	q* SLV	Dmax SLD [cm]	Du SLD [cm]	Dmax SLO	Du SLO [cm]	α SLC	α SLV	α SLD	α SLO
1	1	✓	4	+	Uniforme	12.80	11.58	5.00	10.05	8.69	3.93	3.47	2.56	2.53	1.71	0.800	0.764	0.737	0.674
1	2	✓	4	+	Forze statiche	14.00	11.91	5.30	10.99	8.93	4.16	3.80	2.64	2.77	1.76	0.755	0.722	0.696	0.637
1	3	✓	8	-	Uniforme	12.65	11.96	4.98	9.93	8.97	3.91	3.43	2.54	2.50	1.70	0.804	0.768	0.741	0.678
1	4	✓	8	-	Forze statiche	0.00	12.02	0.00	0.00	12.02	0.00	0.00	0.00	0.00	0.00	0.000	0.000	0.000	0.000
2	1	✓	12	+	Uniforme	4.40	3.10	3.11	3.43	2.33	2.56	1.16	1.11	0.89	0.74	0.732	0.710	0.963	0.829
2	2	✓	12	+	Forze statiche	4.93	3.28	3.36	3.86	2.46	2.77	1.37	1.21	1.04	0.81	0.689	0.662	0.891	0.775
2	3	✓	8	-	Uniforme	4.32	3.75	2.66	3.36	2.81	2.19	1.15	1.29	0.89	0.86	0.881	0.855	1.127	0.969
2	4	✓	8	-	Forze statiche	4.90	4.47	2.88	3.84	3.35	2.37	1.38	1.43	1.05	0.96	0.920	0.884	1.042	0.911
3	1	✓	16	+	Uniforme	7.24	5.49	6.34	5.68	4.12	4.98	1.96	1.14	1.43	0.76	0.631	0.603	0.581	0.532
3	2	✓	16	+	Forze statiche	8.15	6.09	6.37	6.39	4.57	5.00	2.21	1.28	1.61	0.85	0.628	0.600	0.579	0.530
3	3	✓	12	-	Uniforme	5.73	2.94	6.10	4.52	2.20	5.02	1.58	0.87	1.15	0.58	0.520	0.491	0.553	0.506
3	4	✓	12	-	Forze statiche	6.35	3.30	6.55	4.98	2.47	5.14	1.72	0.97	1.25	0.65	0.520	0.497	0.563	0.515
4	1	✓	16	+	Uniforme	4.58	10.00	2.85	3.55	7.50	2.35	1.18	1.24	0.91	0.82	1.403	1.279	1.051	0.904
4	2	✓	16	+	Forze statiche	5.18	10.12	3.24	4.05	7.59	2.67	1.41	1.30	1.09	0.86	1.234	1.125	0.924	0.795
4	3	✓	20	-	Uniforme	4.43	10.28	2.28	3.43	7.71	1.88	1.18	1.55	0.91	1.03	1.755	1.600	1.315	1.131
4	4	✓	20	-	Forze statiche	5.07	10.40	2.59	3.96	7.80	2.13	1.40	1.62	1.09	1.08	1.545	1.408	1.157	0.996
5	1	✓	4	+	Uniforme	5.37	10.05	3.11	4.22	7.54	2.56	1.53	1.48	1.13	0.99	1.287	1.173	0.964	0.869
5	2	✓	4	+	Forze statiche	6.03	10.17	3.52	4.77	7.63	2.90	1.70	1.55	1.24	1.04	1.136	1.036	0.916	0.838
5	3	✓	20	-	Uniforme	5.31	10.22	2.69	4.18	7.67	2.22	1.53	1.71	1.13	1.14	1.486	1.354	1.113	1.004
5	4	✓	20	-	Forze statiche	6.00	10.35	3.04	4.75	7.76	2.50	1.70	1.80	1.24	1.20	1.314	1.198	1.060	0.970
6	1	✓	28	+	Uniforme	5.92	5.92	6.66	4.66	4.44	5.48	1.63	0.80	1.19	0.53	0.600	0.547	0.489	0.448
6	2	✓	28	+	Forze statiche	6.74	6.15	7.62	5.29	4.61	6.04	1.83	0.88	1.33	0.58	0.525	0.497	0.480	0.439
6	3	✓	32	-	Uniforme	5.37	5.22	3.61	4.23	3.92	2.97	1.53	1.29	1.11	0.86	0.975	0.930	0.845	0.773
6	4	✓	32	-	Forze statiche	5.93	5.53	4.12	4.69	4.15	3.39	1.65	1.32	1.20	0.88	0.935	0.885	0.800	0.732
7	1	✓	36	+	Uniforme	6.03	3.46	3.43	4.68	2.60	2.82	1.53	1.30	1.15	0.87	0.615	0.602	0.873	0.751
7	2	✓	36	+	Forze statiche	7.70	3.28	5.54	6.05	2.46	4.56	2.15	1.15	1.58	0.77	0.447	0.428	0.540	0.487
7	3	✓	40	-	Uniforme	6.18	3.50	3.29	4.81	2.63	2.70	1.59	1.43	1.21	0.95	0.608	0.594	0.912	0.784
7	4	✓	40	-	Forze statiche	7.88	3.20	5.35	6.19	2.40	4.40	2.21	1.25	1.61	0.83	0.427	0.408	0.564	0.516
8	1	✓	44	+	Uniforme	7.44	7.50	4.77	5.84	5.63	3.74	2.02	1.56	1.47	1.04	0.839	0.802	0.773	0.708
8	2	✓	44	+	Forze statiche	8.19	11.80	5.03	6.43	8.85	3.95	2.22	1.63	1.62	1.09	0.795	0.760	0.733	0.671
8	3	✓	48	-	Uniforme	7.59	11.56	5.24	5.96	8.67	4.11	2.06	1.45	1.50	0.97	0.763	0.729	0.704	0.644
8	4	✓	48	-	Forze statiche	8.35	11.85	5.44	6.56	8.89	4.27	2.27	1.53	1.65	1.02	0.735	0.702	0.677	0.620
9	1	✓	52	+	Uniforme	1.86	2.44	1.41	1.29	1.83	1.16	0.45	0.95	0.35	0.64	1.190	1.222	2.118	1.822
9	2	✓	52	+	Forze statiche	2.33	2.38	1.65	1.70	1.79	1.36	0.55	0.99	0.43	0.66	1.014	1.033	1.814	1.561
9	3	✓	56	-	Uniforme	2.32	3.60	2.15	1.72	2.70	1.77	0.47	0.65	0.36	0.43	1.407	1.399	1.392	1.197
9	4	✓	56	-	Forze statiche	2.74	3.78	2.47	2.06	2.83	2.03	0.57	0.69	0.44	0.46	1.300	1.284	1.215	1.045
10	1	✓	60	+	Uniforme	0.00	11.91	0.00	0.00	11.91	0.00	0.00	0.00	0.00	0.00	0.000	0.000	0.000	0.000
10	2	✓	60	+	Forze statiche	0.00	11.91	0.00	0.00	11.91	0.00	0.00	0.00	0.00	0.00	0.000	0.000	0.000	0.000
10	3	✓	64	-	Uniforme	0.00	11.99	0.00	0.00	11.99	0.00	0.00	0.00	0.00	0.00	0.000	0.000	0.000	0.000
10	4	✓	64	-	Forze statiche	0.00	11.99	0.00	0.00	11.99	0.00	0.00	0.00	0.00	0.00	0.000	0.000	0.000	0.000
11	1	✓	20	+	Uniforme	5.62	4.37	4.01	4.42	3.28	3.30	1.59	1.19	1.17	0.79	0.787	0.753	0.747	0.679
11	2	✓	20	+	Forze statiche	6.45	6.21	4.54	5.10	4.66	3.73	1.79	1.31	1.30	0.87	0.882	0.803	0.733	0.670
11	3	✓	24	-	Uniforme	5.76	4.93	2.38	4.55	3.70	1.96	1.67	2.18	1.22	1.45	0.866	0.824	1.304	1.193
11	4	✓	24	-	Forze statiche	6.78	4.99	3.23	5.40	3.74	2.66	1.87	2.02	1.36	1.34	0.741	0.695	1.077	0.985
1	4	✓	8	-	Forze statiche	14.09	11.60	5.17	11.06	8.70	4.06	3.82	2.73	2.79	1.82	0.774	0.740	0.714	0.653
10	1	✓	60	+	Uniforme	9.85	11.91	4.31	7.73	8.94	3.38	2.67	2.29	1.95	1.52	0.928	0.887	0.856	0.783
10	2	✓	60	+	Forze statiche	11.01	11.91	4.43	8.65	8.94	3.48	2.99	2.48	2.18	1.66	0.902	0.862	0.832	0.761
10	3	✓	64	-	Uniforme	9.59	11.99	4.10	7.53	9.00	3.22	2.60	2.34	1.90	1.56	0.975	0.931	0.899	0.822
10	4	✓	64	-	Forze statiche	10.75	11.93	4.21	8.44	8.95	3.31	2.92	2.55	2.13	1.70	0.950	0.907	0.875	0.801

The minimum seismic vulnerability indices for each wall and for each limit state are summarized in Table 4-32, with the information of which analysis led to the result. Overall seismic vulnerability of the building is determined by the walls with the minimum indices in X and Y direction (Table 4-33). It can be noticed that the building is more vulnerable in Y direction (the short side of the building) than in X direction. The building is capable of resisting just 43% of the seismic demand for the CLS, 41% for LLS, 48% for DLS and 44% for OLS, considering the code response spectra of strategic buildings (reference life 100 years). In the analyses the out of plane kinematics are not considered, but they could be possible, as the bonds between perpendicular walls are very weak or absent. A proper retrofit intervention needs to consider the improvement of such bonds.

Table 4-32: Minimum seismic vulnerability indices. For each wall the most burdensome analysis is specified.

Minimum vulnerability indices - wall analysis				
Wall	α CLS	α LLS	α DLS	α OLS
1	0.755	0.722	0.696	0.637
Analysis	2	2	2	2
2	0.689	0.662	0.891	0.775
Analysis	2	2	2	2
3	0.520	0.491	0.553	0.506
Analysis	3	3	3	3
4	1.234	1.125	0.924	0.795
Analysis	2	2	2	2
5	1.136	1.036	0.916	0.838
Analysis	2	2	2	2
6	0.525	0.497	0.480	0.439
Analysis	2	2	2	2
7	0.427	0.408	0.540	0.487
Analysis	4	4	2	2
8	0.735	0.702	0.677	0.620
Analysis	4	4	4	4
9	1.014	1.033	1.215	1.045
Analysis	2	2	4	4
10	0.902	0.862	0.832	0.761
Analysis	2	2	2	2
11	0.741	0.695	0.733	0.670
Analysis	4	4	2	2

Table 4-33: Determination of the seismic vulnerability of the case study building. In X direction, wall 3 is the most vulnerable for all limit states, in Y direction wall 7 is the most vulnerable for ULS, while wall 6 is the most vulnerable for SLS.

Wall	Load pattern	α CLS	αLLS	α DLS	α OLS
[-]	[-]	[-]	[-]	[-]	[-]
3 (-X)	Uniform	0,520	0,491	0,553	0,506
7 (-Y)	Static forces	0,427	0,408	0,564	0,516
6 (+Y)	Static forces	0,525	0,497	0,480	0,439

The results of the most burdensome analyses are reported in the following. The legend to understand the type of damage of the piers and spandrels in the walls is shown in Figure 4-103.
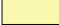
Figure 4-103: Colour legend with the specification of the type of damage (from the software 3Muri, in Italian): Non-damaged, Starting plasticity, Shear plasticity, Incipient shear collapse, Shear collapse, Flexural plasticity, Incipient flexural collapse, Flexural collapse, Severe crisis, Compression collapse, Tension collapse, Collapse in elastic phase, Non-effective element

Wall nr. 3 (analysis 3)

Figure 4-104: Deformed shape of wall 3 at the last step of the analysis

Figure 4-105: Pushover curve of analysis 3 of wall 3

The capacity checks that are carried out on the walls are: check if Dmax<Du for each limit state, q*>4 for CLS and q*>3 for LLS, seismic vulnerability index α.

None of the capacity checks of wall 3 are verified. At Ultimate limit states (ULS) the displacement demand is higher than the capacity and also the behaviour fact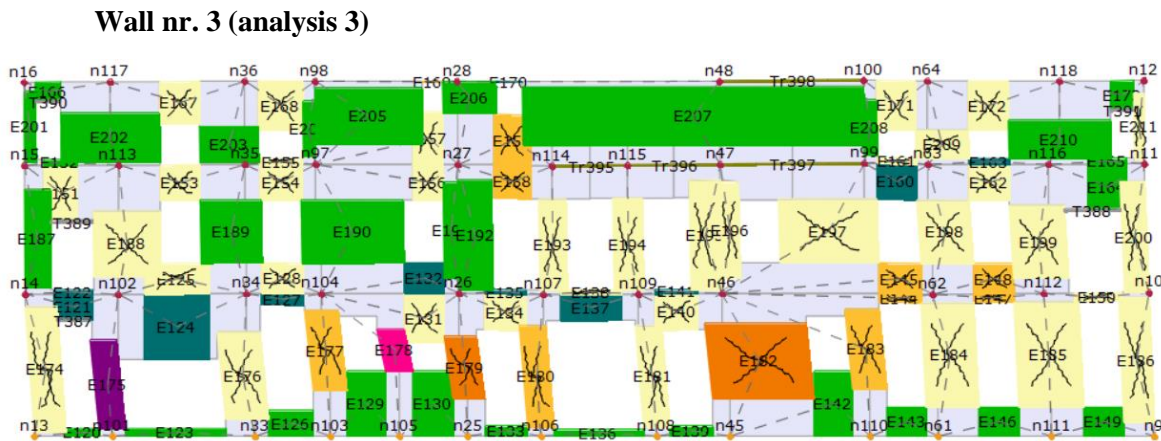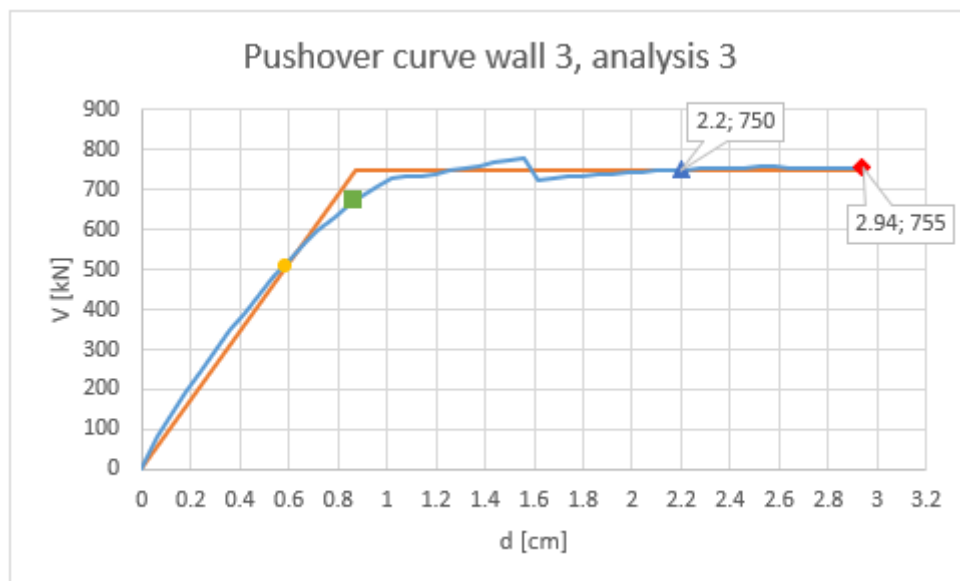ors overcome the limits. At the final step of the analysis two piers at the ground floor reach shear collapse. The displacements of some nodes of the wall are reported in Table 4-34 and the interstorey drifts are computed. It can be noticed that the collapse occurs for a maximum interstorey drift of 5‰ at the ground storey of the building, that is the limit that has been set in the software for shear collapse of piers (the drift limit for flexural collapse is 10‰, while the drift limit for shear and flexural collapse of spandrels is 15‰).

Table 4-34: Displacements of the nodes of the left end of the wall at the last step of analysis 3 of wall 3.

Node	Ux [cm]	Uy [cm]	Uz [cm]	Rot X [rad]	Rot Y [rad]	Interstorey displ [cm]	Interstorey height [cm]	Interstorey drift
13	0	0	0	0	0			
14	-2.59	0	-0.4	0	0.0001	-2.59	518	0.50%
15	-2.77	0	-0.67	0	0.0003	-0.18	468	0.04%
16	-2.93	0	-0.74	0	0.0002	-0.16	301	0.05%

Figure 4-106: Details of capacity checks.

Wall nr. 6 (analysis 2)

Figure 4-107: Deformed shape of wall 6 at the last step of the analysis.
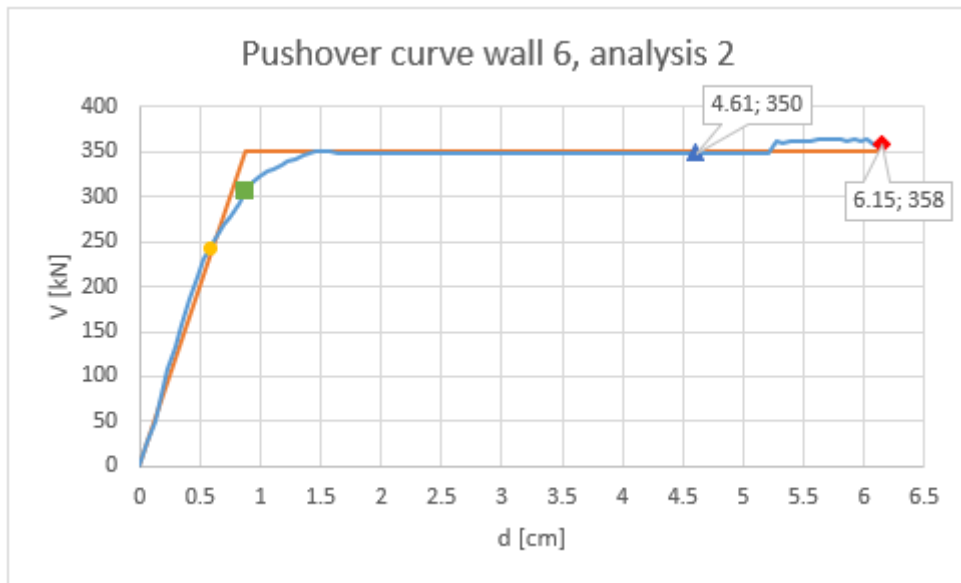
Figure 4-108: Pushover curve of analysis 2 of wall 6.
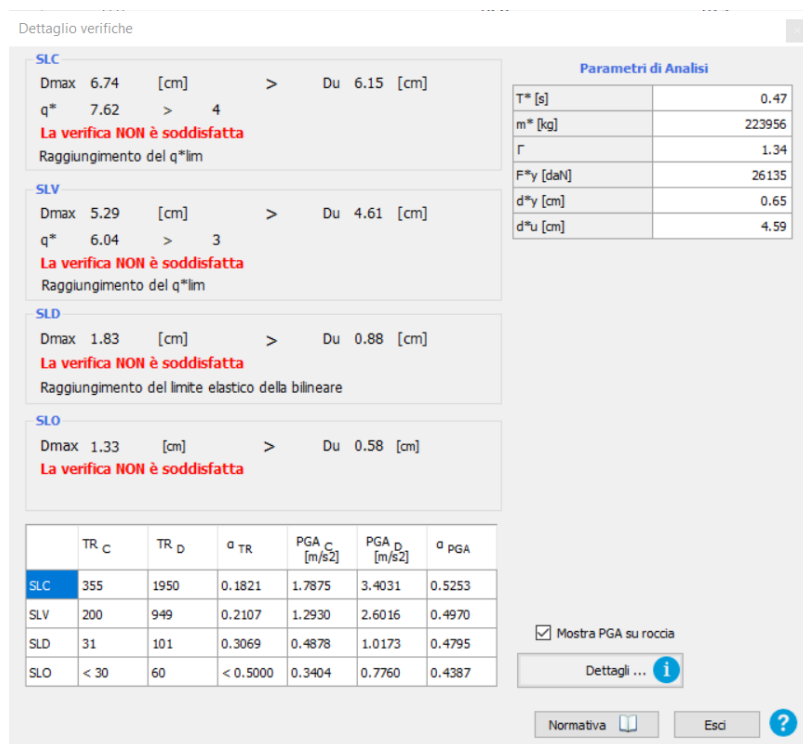
Figure 4-109: Details of capacity checks.

Table 4-35: Displacements of the nodes of the left end of the wall at the last step of analysis 2 of wall 6.

Node	Ux [cm]	Uy [cm]	Uz [cm]	Rot X [rad]	Rot Y [rad]	Interstorey displ [cm]	Interstorey height [cm]	Interstorey drift
25	0	0	0	0	0			
26	3.14	0	0.47	0	-0.0052	3.14	518	0.61%
27	5.2	0	0.16	0	-0.0042	2.06	468	0.44%
28	6.44	0	0.11	0	-0.0041	1.24	301	0.41%

None of the capacity checks of wall 6 are verified. At ULS the displacement demand is higher than the capacity and also the behaviour factors overcome the limits. At the final step of the analysis two piers at the ground floor have incipient shear collapse and other two piers at the ground floor have compression collapse. The displacements of some nodes of the wall are reported in Table 4-35 and the interstorey drifts are computed. It can be noticed that the collapse occurs for a maximum interstorey drift of 6‰ at the ground storey of the building.
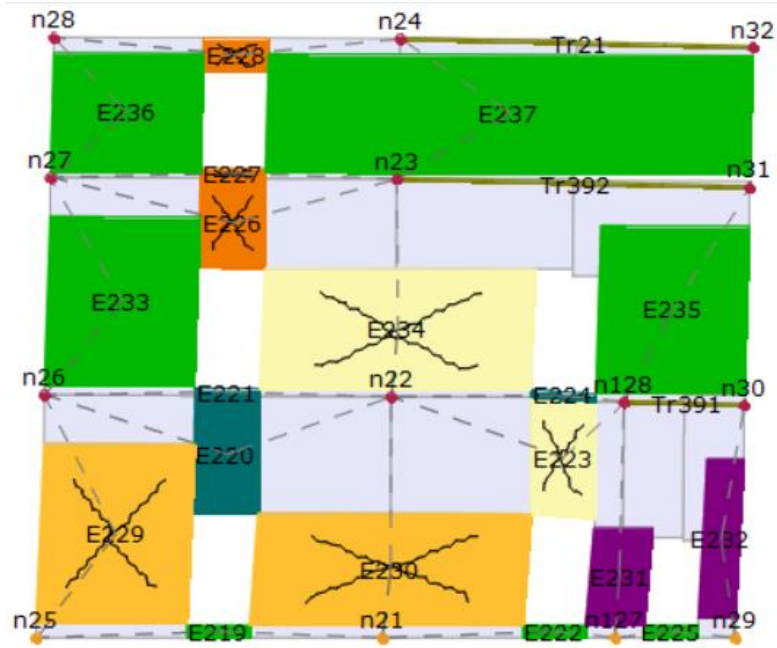
Wall nr. 7 (analysis 4)
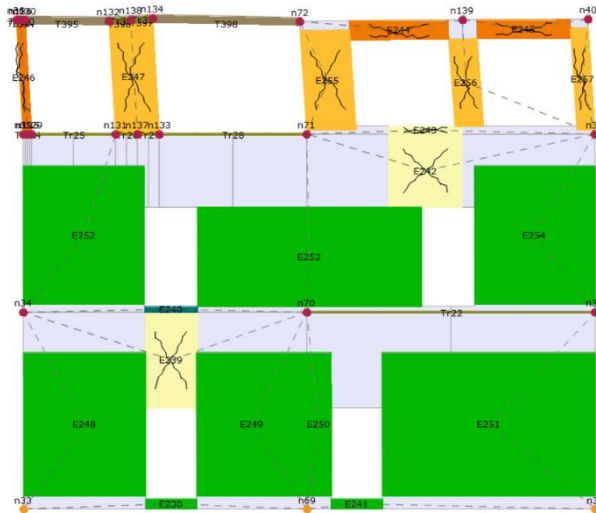
Figure 4-110: Deformed shape of wall 7 at the last step of the analysis.
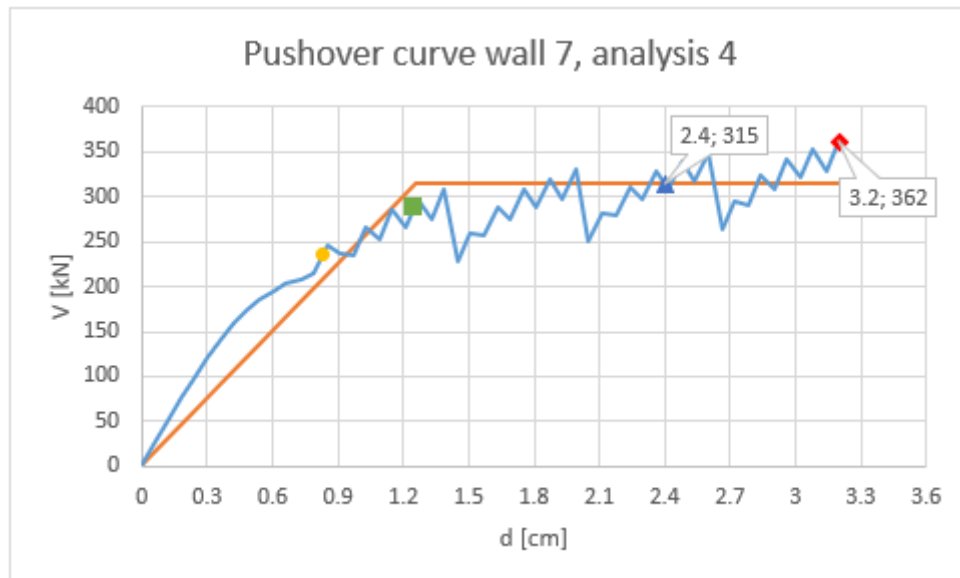
**Figure 4-111: Pushover curve of analysis 4 of wall 7.**
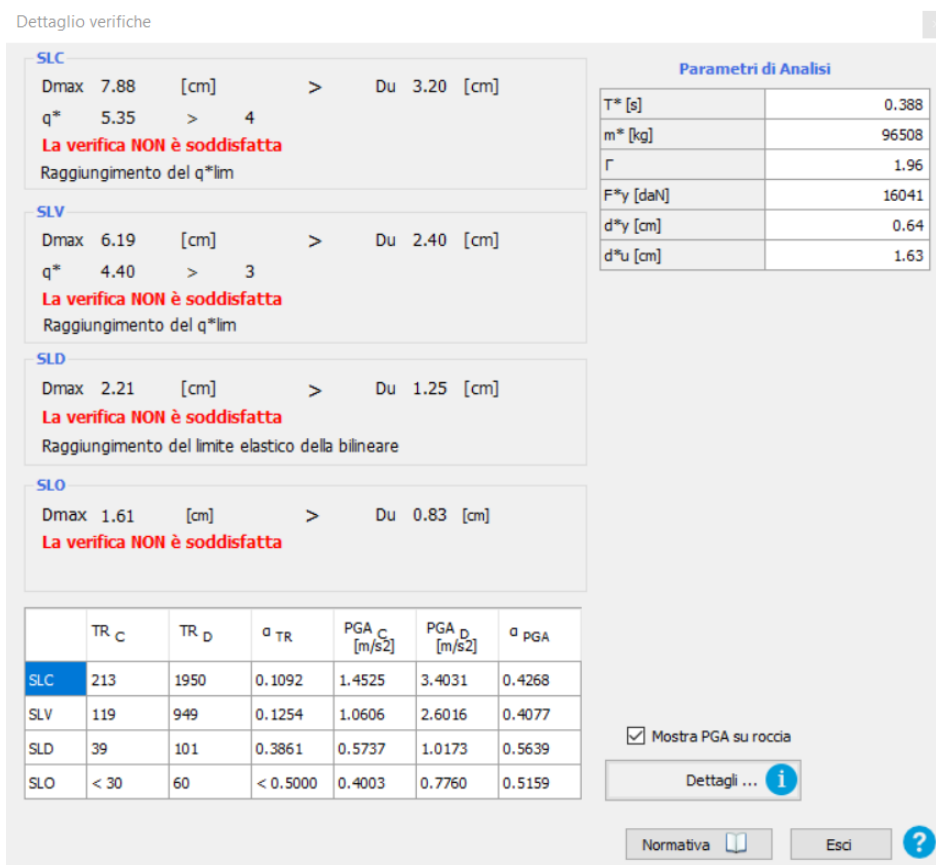
Figure 4-112: Details of capacity cheks.

None of the capacity checks of wall 7 are verified. At ULS the displacement demand is higher than the capacity and also the behaviour factors overcome the limits. At the final step of the analysis there is shear collapse of piers and spandrels at the last floor. The displacements of some nodes of the wall are reported in Table 4-36 and the interstorey drifts are computed. It can be noticed that the collapse occurs for a maximum interstorey drift of 1% at the last storey of the building.

Table 4-36: Displacements of the nodes of the right end of the wall at the last step of analysis 4 of wall 7.

Node	Ux [cm]	Uy [cm]	Uz [cm]	Rot X [rad]	Rot Y [rad]	Interstorey displ [cm]	Interstorey height [cm]	Interstorey drift
37	0	0	0	0	0			
38	-0.1	0	-0.21	0	0	-0.1	518	0.02%
39	-0.22	0	-0.28	0	0.0003	-0.12	468	0.03%
40	-3.18	0	-0.08	0	0.0133	-2.96	301	0.98%

4.4.2.2. *Vulnerability evaluation based on simulated scenario response spectra*

As discussed in §2.2, the PSHA method, used by the codes, is not the only one that can be used to evaluate the seismic action in the site of interest. SPBSHA allows to calculate realistic scenarios of earthquakes in the site of interest with their seismograms, accelerograms and consequently response spectra. For this case study, two scenarios have been considered, calculated based on the characteristics of earthquakes that could derive from the two faults that are the closest to the town of Gorizia: Medea and Idria. The considered response spectra (percentiles of all the 100 realizations for each scenario) are shown in Figure 2-16 and Figure 2-17.

The pushover curves of the building remain the same as already shown in the previous paragrah, but the demand is calculated based on the scenario response spectra. The minimum seismic vulnerability indices are reported in Table 4-37. The maximum demand displacements for the two scenarios are reported in Table 4-38 together with the ratio between the two scenarios, in order to find the most burdensome. In most of the cases Medea, the closest fault to Gorizia, has higher demand displacements.

Table 4-37: Minimum seismic vulnerability indices calculated for three percentiles for each scenario (Medea and Idrija), for each of the 11 walls of the building.

Min vulnerability indices - MEDEA 50					Min vulnerability indices - IDRIJA 50			
Wall	α CLS	α LLS	α DLS	α OLS	Wall	α CLS	α LLS	α DLS	α OLS
1	7.088	5.316	1.772	1.182	1	3.681	2.761	0.920	0.614
2	1.609	1.281	0.702	0.468	2	1.973	1.571	0.861	0.575
3	2.469	1.915	0.773	0.516	3	2.248	1.743	0.704	0.469
4	2.788	2.091	0.697	0.465	4	3.595	2.696	0.899	0.599
5	4.042	3.032	1.011	0.674	5	4.232	3.174	1.058	0.706
6	2.636	1.977	0.659	0.44	6	2.410	1.807	0.602	0.402
7	1.169	0.938	0.551	0.367	7	1.447	1.134	0.593	0.395
8	5.027	3.77	1.257	0.838	8	3.633	2.725	0.908	0.606
9	2.947	2.465	1.157	0.772	9	2.200	1.840	0.867	0.578
10	8.94	6.705	2.235	1.491	10	4.627	3.470	1.157	0.771
11	2.55	2.001	0.802	0.535	11	2.632	2.065	0.827	0.552

Min vulnerability indices - MEDEA 84					Min vulnerability indices - IDRIJA 84			
Wall	α CLS	α LLS	α DLS	α OLS	Wall	α CLS	α LLS	α DLS	α OLS
1	3.177	2.382	0.794	0.53	1	2.644	1.983	0.661	0.441
2	1.061	0.845	0.463	0.309	2	1.485	1.182	0.648	0.432
3	1.631	1.265	0.511	0.341	3	1.756	1.362	0.550	0.367
4	1.88	1.41	0.47	0.313	4	2.678	2.008	0.669	0.447
5	2.832	2.124	0.708	0.472	5	3.168	2.376	0.792	0.528
6	1.728	1.296	0.432	0.288	6	1.880	1.410	0.470	0.313
7	0.794	0.637	0.374	0.249	7	1.105	0.866	0.443	0.296
8	3.588	2.691	0.897	0.598	8	2.865	2.149	0.716	0.478
9	2.215	1.852	0.857	0.572	9	1.770	1.480	0.704	0.470
10	6.322	4.741	1.58	1.054	10	3.619	2.714	0.905	0.603
11	1.778	1.395	0.559	0.373	11	1.984	1.556	0.624	0.416

Min vulnerability indices - MEDEA 95					Min vulnerability indices - IDRIJA 95			
Wall	α CLS	α LLS	α DLS	α OLS	Wall	α CLS	α LLS	α DLS	α OLS
1	1.874	1.405	0.468	0.312	1	2.07	1.552	0.517	0.345
2	0.812	0.646	0.354	0.236	2	1.229	0.979	0.537	0.358
3	1.372	1.064	0.43	0.287	3	1.554	1.205	0.486	0.324
4	1.5	1.125	0.375	0.25	4	2.249	1.687	0.562	0.375
5	2.311	1.733	0.578	0.385	5	2.711	2.033	0.678	0.452
6	1.407	1.055	0.352	0.235	6	1.694	1.271	0.424	0.283
7	0.649	0.521	0.306	0.204	7	0.946	0.743	0.379	0.253
8	2.903	2.177	0.726	0.484	8	2.367	1.775	0.592	0.395
9	1.901	1.59	0.75	0.5	9	1.366	1.143	0.545	0.364
10	4.732	3.549	1.183	0.789	10	2.935	2.202	0.734	0.489
11	1.457	1.143	0.458	0.306	11	1.706	1.338	0.536	0.358

A comparison to the results obtained with the code response spectra is made in the following for the two worst-case walls: wall 7 and wall 3. The following results are highlighted:

- Capacity curves (blue) of each analysis are reported, with dots that indicate the capacity limit states (red, blue, green and yellow, respectively for CLS, LLS, DLS and OLS). On the same graphs also the demand displacements are reported as vertical lines (brown dashed lines for code spectra, full black lines for Medea and green full lines for Idrija (Figure 4-113 for wall 7 and Figure 4-116 for wall 3).
- Displacements capacity check is reported in tables (Table 4-39 and Table 4-40 for wall 7 and Table 4-42 and Table 4-43 for wall 3).

- Comparison between Medea and Idrija is also made (Table 4-41 for wall 7 and Table 4-44 for wall 3).
- The results are also shown in ADRS format, where pushover curves have been transformed to an equivalent SDOF system with the transformation factor Γ (Figure 4-114 and Figure 4-115 for wall 7 and Figure 4-117 and Figure 4-118 for wall 3).

Table 4-38: Maximum displacement demands Dmax for the two scenarios for all the 11 walls. On the right ratio between such demand from Medea and Idrija. A coefficient > 1 means that Medea has a higher demand, in the opposite Idrija.

Dmax (cm) MEDEA				Dmax (cm) IDRIJA				COMPARISON Dmax MEDEA/IDRIJA			
Wall	50° PERC	84° PERC	95° PERC	Wall	50° PERC	84° PERC	95° PERC	Wall	50° PERC	84° PERC	95° PERC
1	1.51	3.38	5.74	1	2.89	4.03	5.14	1	0.522	0.839	1.117
2	1.76	2.90	3.92	2	1.36	1.95	2.44	2	1.294	1.487	1.607
3	1.15	1.77	2.12	3	1.64	2.12	2.63	3	0.701	0.835	0.806
4	2.01	3.25	4.21	4	1.48	2.14	2.63	4	1.358	1.519	1.601
5	1.46	2.23	2.81	5	1.41	1.96	2.35	5	1.035	1.138	1.196
6	1.34	2.07	2.54	6	1.39	1.85	2.16	6	0.964	1.119	1.176
7	2.87	4.52	5.69	7	2.13	2.94	3.49	7	1.347	1.537	1.630
8	1.19	1.67	2.04	8	1.69	2.14	2.59	8	0.704	0.780	0.788
9	0.59	0.92	1.15	9	0.90	1.27	1.84	9	0.656	0.724	0.625
10	1.05	1.57	2.10	10	2.04	2.75	3.12	10	0.515	0.571	0.673
11	1.55	2.34	2.91	11	1.49	2.07	2.45	11	1.040	1.130	1.188

Wall 7 (Y direction)
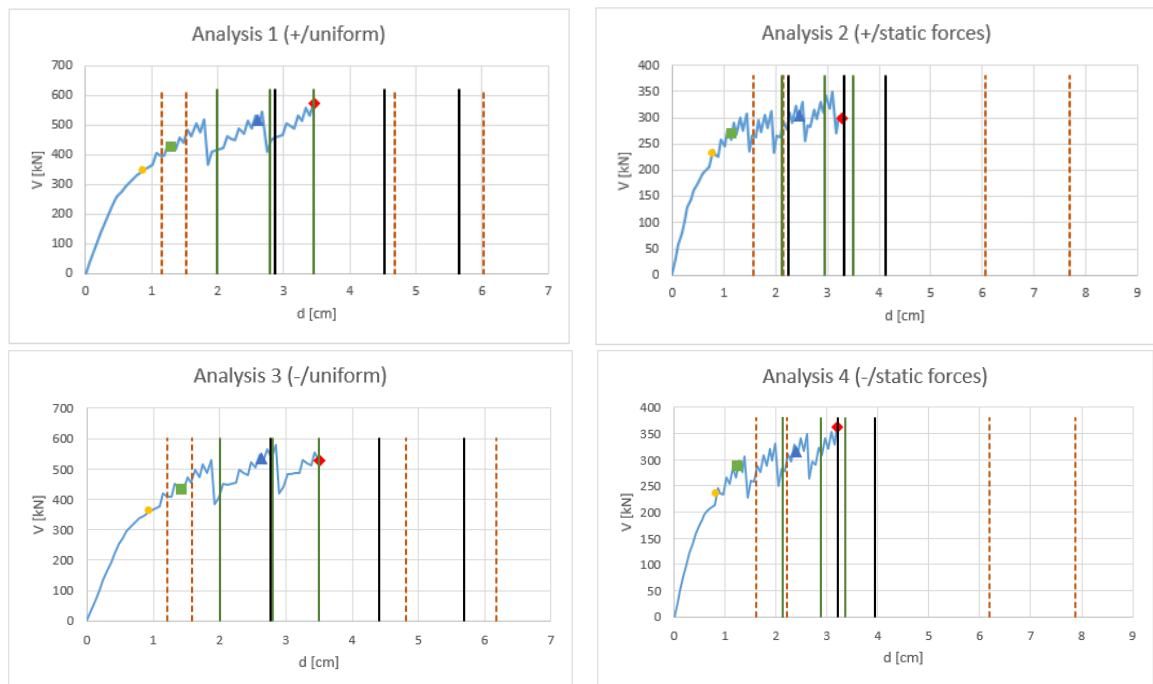
Figure 4-113: Pushover curves (blue) of each of the four analyses performed on wall 7 are reported, with dots that indicate the capacity limit states (yellow, green, blue and red, respectively for OLS, DLS, LLS and CLS). On the same graphs also the demand displacements are reported as vertical lines (brown dashed lines for code spectra, full black lines for Medea and green full lines for Idrija - 50th, 84th and 95th percentile).

All the checks with code response spectra are not satisfied. The seismic vulnerability index is the minimum for LLS.

Table 4-39: Results of pushover analyses for the wall 7 (code response spectra, reference life 100 years).

	Dmax CLS [cm]	Du CLS [cm]	V CLS [kN]	C/D
Analysis 1	6.03	3.46	575	0.574
Analysis 2	7.7	3.28	299	0.426
Analysis 3	6.18	3.5	529	0.566
Analysis 4	7.88	3.2	362	0.406
	Dmax LLS [cm]	**Du LLS [cm]**	**V LLS [kN]**	**C/D**
Analysis 1	4.68	2.6	518	0.556
Analysis 2	6.05	2.46	304	0.407
Analysis 3	4.81	2.63	535	0.547
Analysis 4	6.19	2.4	315	0.388
	Dmax DLS [cm]	**Du DLS [cm]**	**V DLS [kN]**	**C/D**
Analysis 1	1.53	1.3	426	0.850
Analysis 2	2.15	1.15	268	0.535
Analysis 3	1.59	1.43	431	0.899
Analysis 4	2.21	1.25	288	0.566
	Dmax OLS [cm]	**Du OLS [cm]**	**V OLS [kN]**	**C/D**
Analysis 1	1.15	0.87	348	0.757
Analysis 2	1.58	0.77	232	0.487
Analysis 3	1.21	0.95	360	0.785
Analysis 4	1.61	0.83	235	0.516

Table 4-40: Results of pushover analyses for the wall 7 (scenario response spectra for Medea and Idrija faults). The check is made in terms of Capacity/Demand.

	Medea scenario					Idrija scenario				
	50th percentile					**50th percentile**				
	Dmax [cm]	C/D (CLS)	C/D (LLS)	C/D (DLS)	C/D (OLS)	Dmax [cm]	C/D (CLS)	C/D (LLS)	C/D (DLS)	C/D (OLS)
Analysis 1	**2.870**	1.206	0.906	0.453	0.303	**2.000**	1.730	1.300	0.650	0.435
Analysis 2	**2.250**	1.458	1.093	0.511	0.342	**2.130**	1.540	1.155	0.540	0.362
Analysis 3	**2.770**	1.264	0.949	0.516	0.343	**2.010**	1.741	1.308	0.711	0.473
Analysis 4	**2.140**	1.495	1.121	0.584	0.388	**2.130**	1.502	1.127	0.587	0.390
	84th percentile					**84th percentile**				
Analysis 1	**4.520**	0.765	0.575	0.288	0.192	**2.790**	1.240	0.932	0.466	0.312
Analysis 2	**3.320**	0.988	0.741	0.346	0.232	**2.940**	1.116	0.837	0.391	0.262
Analysis 3	**4.410**	0.794	0.596	0.324	0.215	**2.800**	1.250	0.939	0.511	0.339
Analysis 4	**3.220**	0.994	0.745	0.388	0.258	**2.870**	1.115	0.836	0.436	0.289
	95th percentile					**95th percentile**				
Analysis 1	**5.660**	0.611	0.459	0.230	0.154	**3.450**	1.003	2.592	0.377	0.252
Analysis 2	**4.140**	0.792	0.594	0.278	0.186	**3.490**	0.940	2.618	0.330	0.221
Analysis 3	**5.690**	0.615	0.462	0.251	0.167	**3.490**	1.003	2.622	0.410	0.272
Analysis 4	**3.950**	0.810	0.608	0.316	0.210	**3.350**	0.955	2.513	0.373	0.248

On the other hand, in the checks with scenario response spectra, the demands of the 84th and 95th percentile of Medea are always higher than the capacity for CLS and the 50th percentile already exceeds the LLS almost in all cases. The scenario demand is never under the DLS capacity.

Medea has always higher demand than Idrija (Table 4-41).

Table 4-41: Comparison between Medea and Idrija demands.

COMPARISON Dmax MEDEA/IDRIJA			
Analysis	50th percentile	84th percentile	95th percentile
1	1.435	1.620	1.641
2	1.056	1.129	1.186
3	1.378	1.575	1.630
4	1.005	1.122	1.179
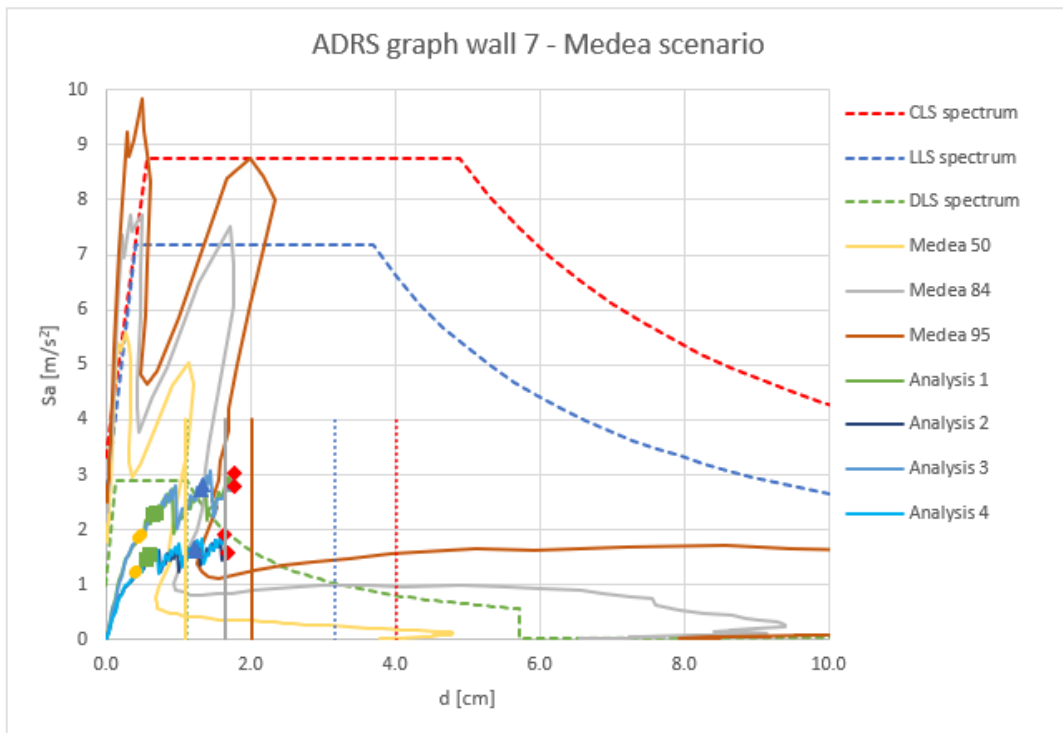
Figure 4-114: Pushover curves and response spectra in ADRS format for Medea scenario – wall 7. The coloured dots on the pushover curves indicate the capacities of the building for four limit states (CLS, LLS, DLS and OLS), while the vertical lines show the displacement demand of the response spectra for analysis 4. The vertical line has the same colour of the spectrum to which it belongs.
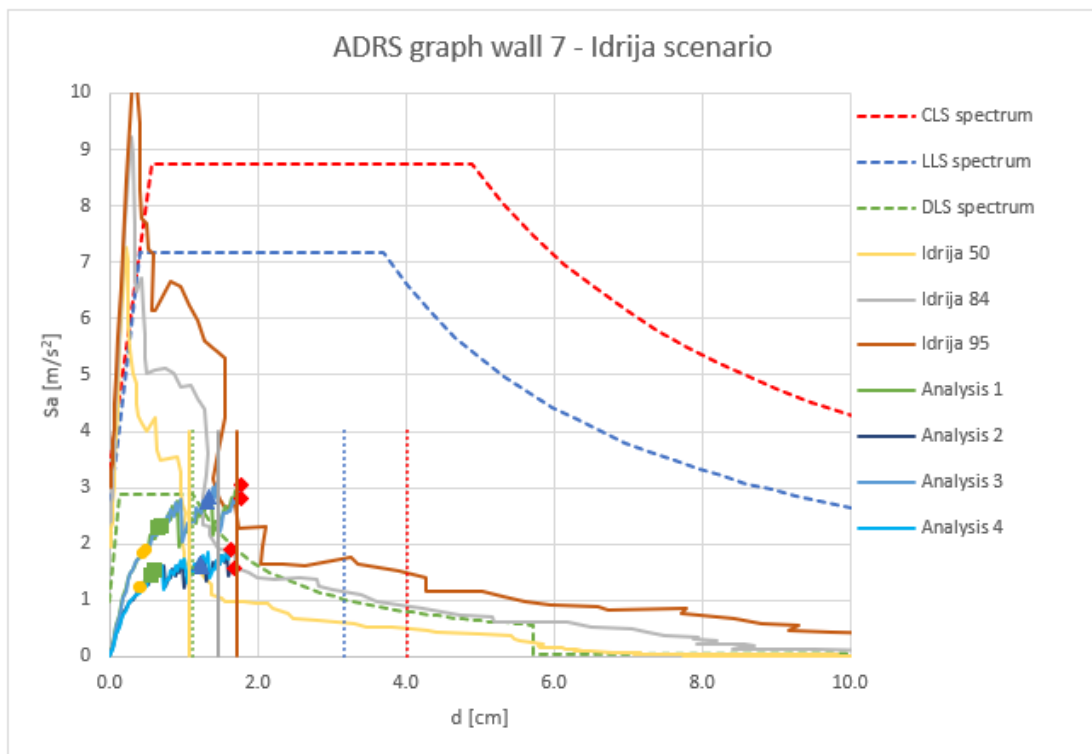
Figure 4-115: Pushover curves and response spectra in ADRS format for Idrija scenario – wall 7. The coloured dots on the pushover curves indicate the capacities of the building for four limit states (CLS, LLS, DLS and OLS), while the vertical lines show the displacement demand of the response spectra for analysis 4. The vertical line has the same colour of the spectrum to which it belongs.

Wall 3 (X direction)
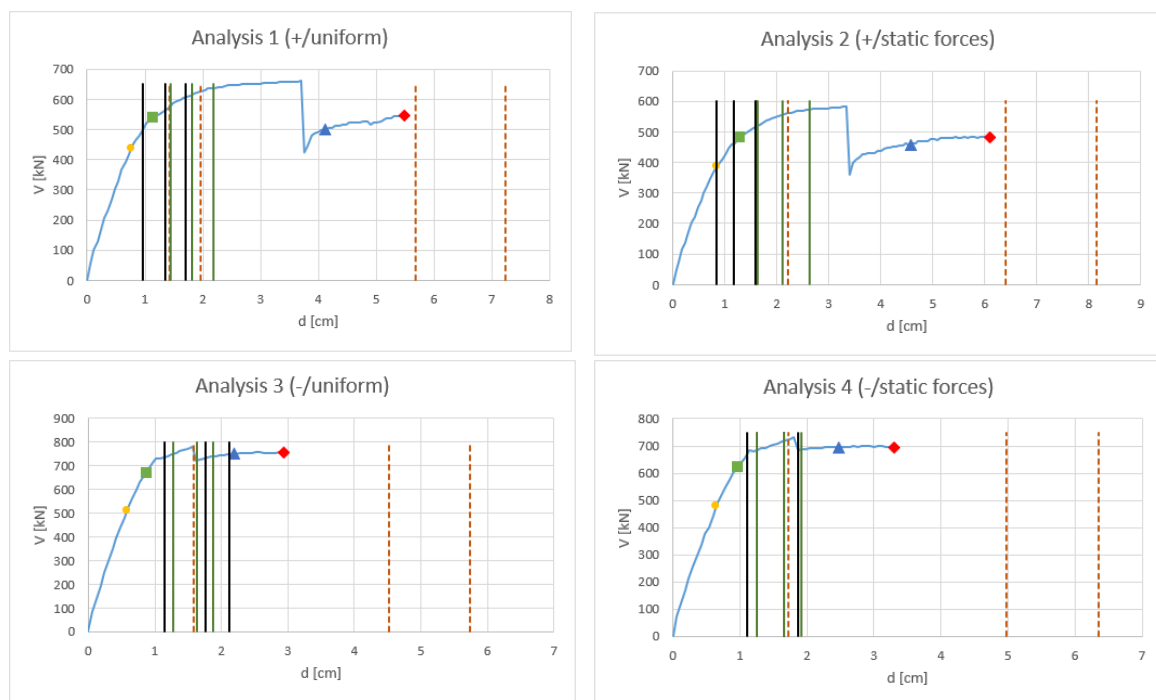
Figure 4-116: Pushover curves (blue) of each of the four analyses performed on wall 3 are reported, with dots that indicate the capacity limit states (red, blue, green and yellow, respectively for CLS, LLS, DLS and OLS). On the same graphs also the demand displacements are reported as vertical lines (brown dashed lines for code spectra, full black lines for Medea and green full lines for Idrija - 50th, 84th and 95th percentile).

All the checks with code response spectra are not satisfied.

Table 4-42: Results of pushover analyses for the wall 3 (code response spectra, reference life 100 years).

	Dmax $_{CLS}$ [cm]	Du $_{CLS}$ [cm]	V $_{CLS}$ [kN]	C/D
Analysis 1	7.24	5.49	548	0.758
Analysis 2	8.15	6.09	483	0.747
Analysis 3	5.73	2.94	755	0.513
Analysis 4	6.35	3.3	694	0.520
	Dmax $_{LLS}$ [cm]	Du $_{LLS}$ [cm]	V $_{LLS}$ [kN]	C/D
Analysis 1	5.68	4.12	499	0.725
Analysis 2	6.39	4.57	458	0.715
Analysis 3	4.52	2.2	750	0.487
Analysis 4	4.98	2.47	695	0.496
	Dmax $_{DLS}$ [cm]	Du $_{DLS}$ [cm]	V $_{DLS}$ [kN]	C/D
Analysis 1	1.96	1.14	538	0.582
Analysis 2	2.21	1.28	481	0.579
Analysis 3	1.58	0.87	671	0.551
Analysis 4	1.72	0.97	624	0.564
	Dmax $_{OLS}$ [cm]	Du $_{OLS}$ [cm]	V $_{OLS}$ [kN]	C/D
Analysis 1	1.43	0.76	435	0.531
Analysis 2	1.61	0.85	386	0.528
Analysis 3	1.15	0.58	509	0.504
Analysis 4	1.25	0.65	477	0.520

The demands by the scenarios are mainly concentrated around the DLS and LLS capacity of the wall. Almost all the demands exceed the DLS and OLS capacity.

Table 4-43: Results of pushover analyses for the wall 3 (scenario response spectra, Medea and Idrija).

	Medea scenario					Idrija scenario			
	50th percentile					50th percentile			
	Dmax [cm]	C/D (CLS)	C/D (LLS)	C/D (DLS)	C/D (OLS)	Dmax [cm]	C/D (CLS)	C/D (LLS)	C/D (DLS)	C/D (OLS)
Analysis 1	0.960	5.719	4.292	1.188	0.792	1.450	3.786	2.841	0.786	0.524
Analysis 2	0.850	7.165	5.376	1.506	1.000	1.640	3.713	2.787	0.780	0.518
Analysis 3	1.150	2.557	1.913	0.757	0.504	1.270	2.315	1.732	0.685	0.457
Analysis 4	1.110	2.973	2.225	0.874	0.586	1.260	2.619	1.960	0.770	0.516
	84th percentile					84th percentile			
Analysis 1	1.350	4.067	3.052	0.844	0.563	1.820	3.016	2.264	0.626	0.418
Analysis 2	1.180	5.161	3.873	1.085	0.720	2.120	2.873	2.156	0.604	0.401
Analysis 3	1.770	1.661	1.243	0.492	0.328	1.640	1.793	1.341	0.530	0.354
Analysis 4	1.650	2.000	1.497	0.588	0.394	1.650	2.000	1.497	0.588	0.394
	95th percentile					95th percentile			
Analysis 1	1.700	3.229	2.424	0.671	0.447	2.180	2.518	1.636	0.523	0.349
Analysis 2	1.580	3.854	2.892	0.810	0.538	2.630	2.316	1.974	0.487	0.323
Analysis 3	2.120	1.387	1.038	0.410	0.274	1.870	1.572	1.399	0.465	0.310
Analysis 4	1.870	1.765	1.321	0.519	0.348	1.920	1.719	1.437	0.505	0.339

Table 4-44: Comparison between Medea and Idrija demands.

COMPARISON Dmax MEDEA/IDRIJA		
Analysis	50th percentile	84th percentile	95th percentile
1	0.662	0.742	0.780
2	0.518	0.557	0.601
3	0.906	1.079	1.134
4	0.881	1.000	0.974

The comparison between the two scenarios for this wall shows that Idrija is more burdensome.
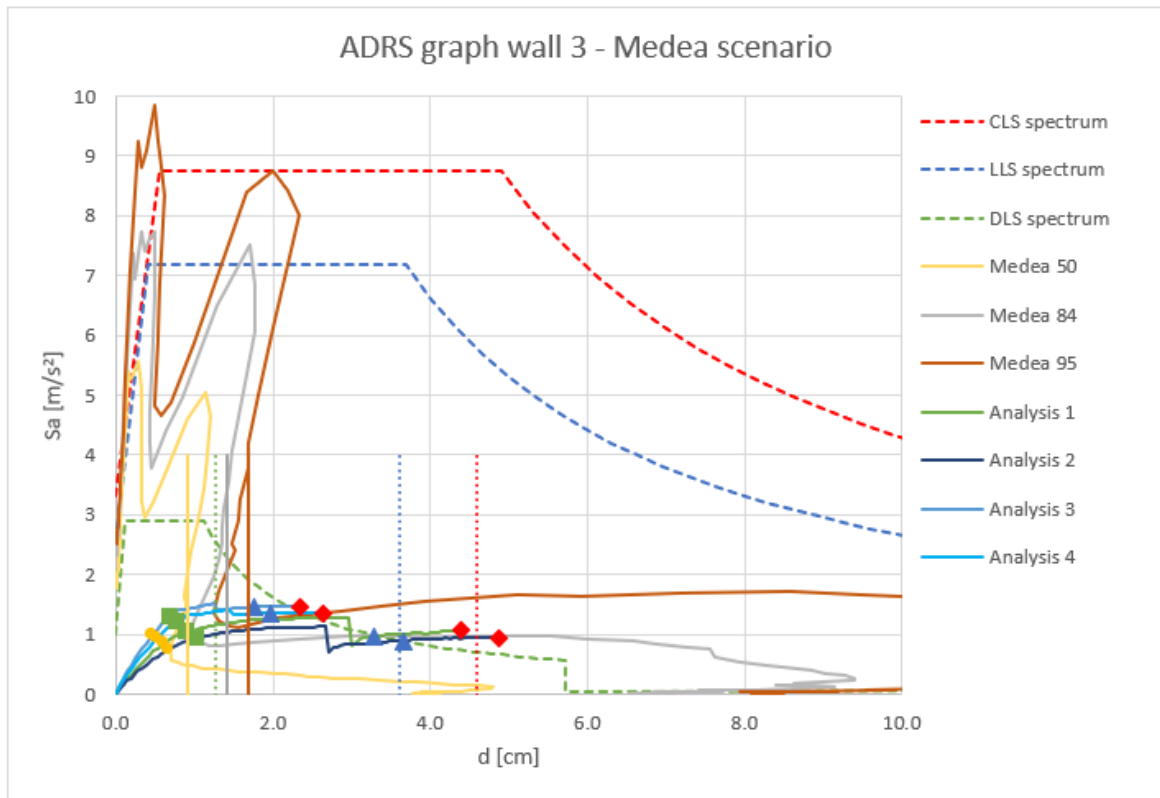
Figure 4-117: Pushover curves and response spectra in ADRS format for Medea scenario - wall 3. The coloured dots on the pushover curves indicate the capacities of the building for four limit states (CLS, LLS, DLS and OLS), while the vertical lines show the displacement demand of the response spectra for analysis 3. The vertical line has the same colour of the spectrum to which it belongs.
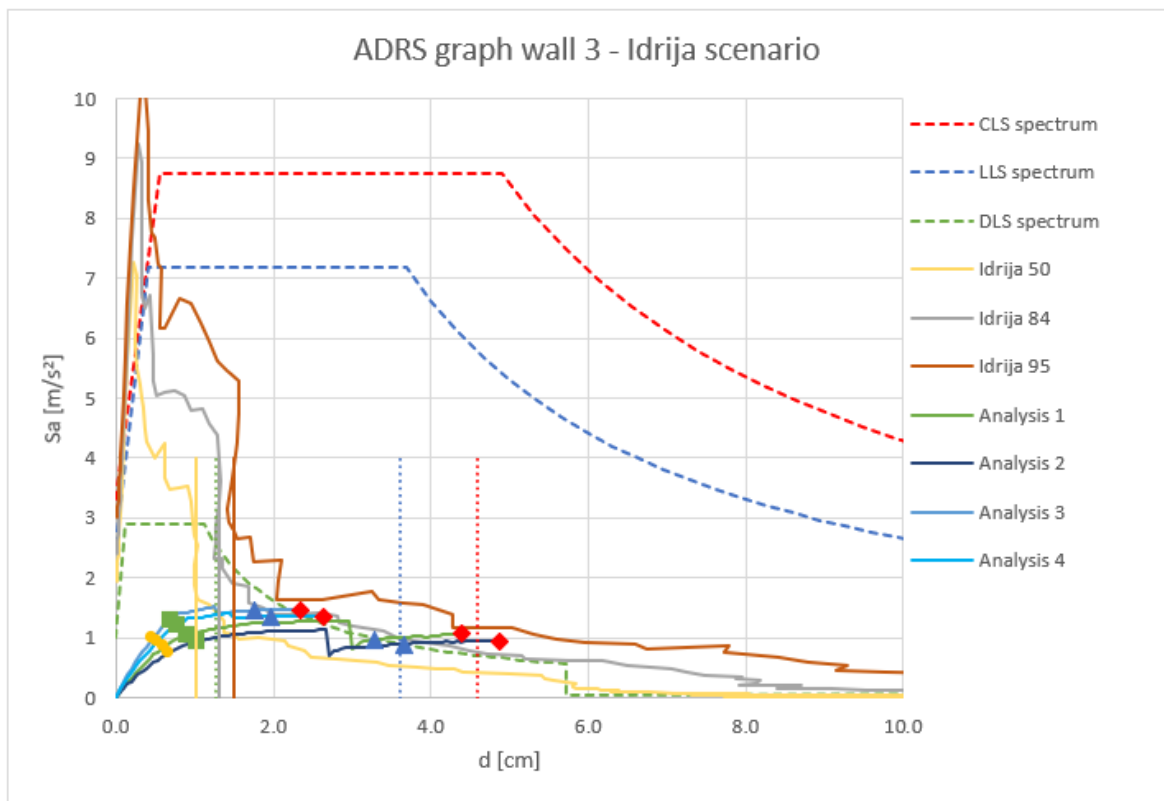
Figure 4-118: Pushover curves and response spectra in ADRS format for Idrija scenario -wall 3. The coloured dots on the pushover curves indicate the capacities of the building for four limit states (CLS, LLS, DLS and OLS), while the vertical lines show the displacement demand of the response spectra for analysis 3. The vertical line has the same colour of the spectrum to which it belongs.

4.4.2.3. Conclusions about the comparison between PSHA and SPBSHA seismic demands

It can be noticed that the demands of all the considered percentiles (50th, 84th and 95th) of the scenario response spectra are lower than the ones of the SLU code spectra (CLS and LLS). For this case (it depends on the site, but also on the fundamental period of the analysed building), if seismic vulnerability is evaluated based on scenario response spectra, Ultimate limit states (ULS) checks give higher vulnerability indices than the ones found with code response spectra, while Serviceability limit states (SLS) give lower indices. Also with the scenario demands, wall 7 is the one in the worst state in Y direction. For X direction, the worst wall is wall 3. The results confirm the findings from the checks with the code spectra. Although Medea has a lower maximum magnitude compared to Idrija (Mw, max for Medea is 6.5, while for Idrija is 6.8), it is closer to Gorizia (the minimum distance from Idrija fault is about 35 km, while Medea is just 15 km away from the town) and thus constitutes an equal or higher hazard for the town as it has been shown in Table 4-38.

4.4.3. Non – linear dynamic analyses

With the aim to deeper analyse the dynamic non-linear behaviour of the case study building, also some non-linear dynamic analyses have been carried out on some walls of the building. The academic version of the software Tremuri (STA DATA) has been used to perform the dynamic analyses. This software needs an input file in .txt format where the numerical model is specified. It is not possible to model the structure through a graphic interface. The software accepts just 3D models, for this reason the wall has been modelled with an equivalent structure, where the wall of interest is doubled and positioned parallel to the original one, at a distance of 1.5 m. The interstorey slabs have been modelled as stiff in their plane and without loads. The loads to apply on each of the two walls (as linear loads) have been calculated, by considering the slab directions and influence areas in the real building. Wall 8 has been analysed in Y direction and wall 11 in X direction. The

position of the two walls in the building and their aspect are shown in Figure 4-119 and Figure 4-120. The two numerical models are shown in Figure 4-121.
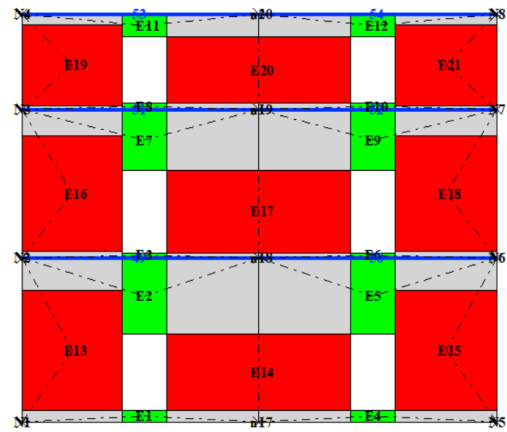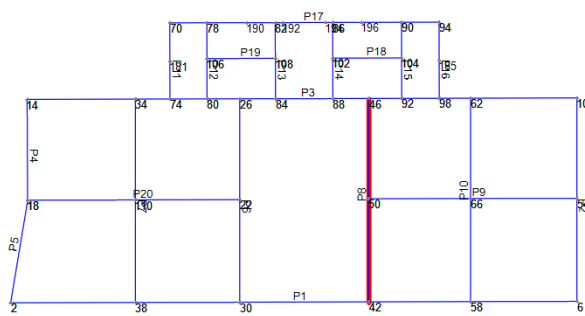
Figure 4-119: Wall 8 (Y direction)
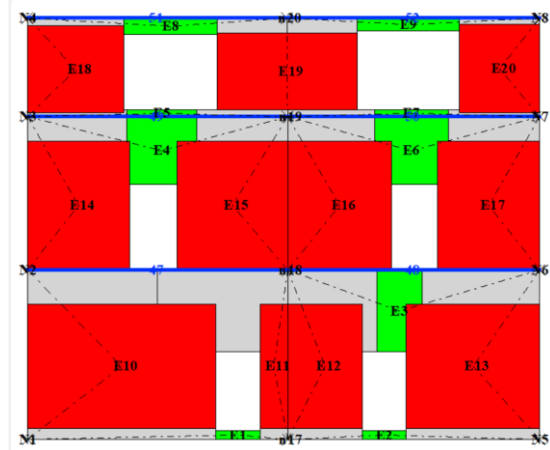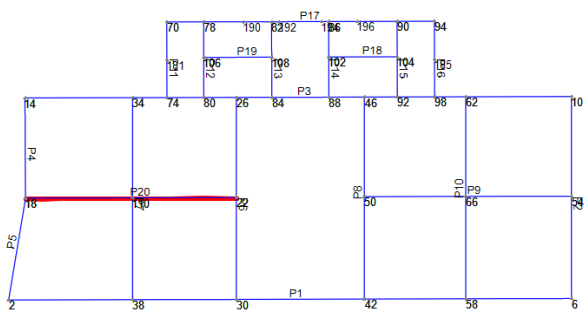
Figure 4-120: Wall 11 (X direction)
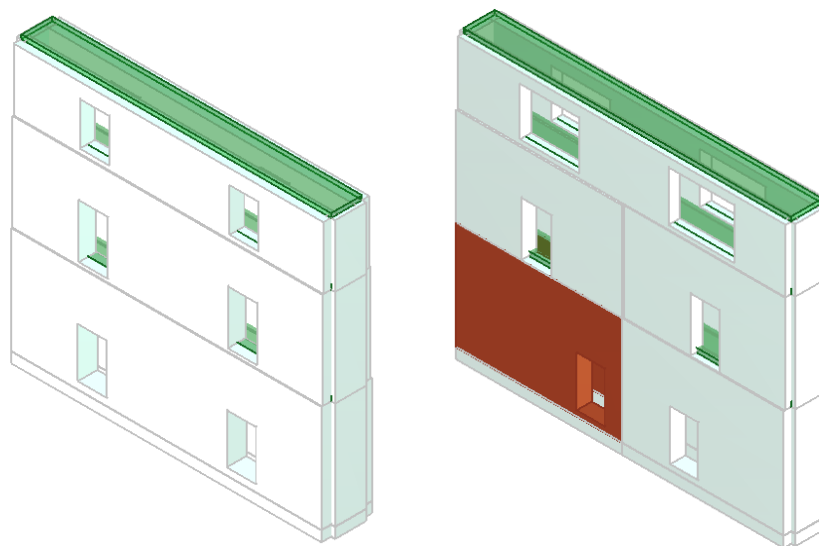
Figure 4-121: Numerical model of the equivalent structure used to analyse wall 8 (left) and wall 11 (right).

The accelerograms used for the non-linear dynamic analyses have been chosen among all the simulated signals for the two scenarios, Idrija and Medea, already used in terms of percentile

response spectra and described in §2.5.1. Three accelerograms have been selected, so that their response spectrum is the closest to the 50th and 95th percentile spectrum for the fundamental period T=0.3 s, approximately the fundamental period of the analysed structures. The choice of the component to use is made based on the response spectrum of the single component. The component with the highest spectral acceleration for the fundamental period of the wall is selected. The accelerogram of the selected component has been further amplified in order to consider the uncertainty about the direction of the earthquake with respect to the wall. The amplification factor used for the signal is the ratio between the spectral acceleration in the resultant response spectrum of the realization and the spectral acceleration of the selected component. The chosen realizations, for each wall, are reported in Table 4-45 and Table 4-46. Their response spectra, compared to the percentile response spectrum and the vertical line showing the fundamental period of the analysed walls, are displayed in Figure 4-122.

Table 4-45: Selected simulated scenario signals for the non-linear dynamic analyses of wall 8 of Masonry building A.

Wall 8				
Percentile	Realization	Component	$S_{a,max}$ [m/s^2]	$a_{max\ amplified}$ [m/s^2]
Medea 50	11	EAST	4.283	1.704
Medea 50	17	EAST	4.438	1.966
Medea 50	81	EAST	7.293	2.216
Medea 95	13	EAST	6.125	2.196
Medea 95	37	EAST	5.979	2.065
Medea 95	99	EAST	6.143	1.590
Idrija 50	12	EAST	4.819	1.451
Idrija 50	21	EAST	3.46	1.62
Idrija 50	60	NORTH	3.038	1.248
Idrija 95	41	NORTH	4.248	2.247
Idrija 95	42	EAST	6.195	2.082
Idrija 95	70	NORTH	4.509	2.22

Table 4-46: Selected simulated scenario signals for the non-linear dynamic analyses of wall 11 of Masonry building A.

Wall 11				
Percentile	Realization	Component	$S_{a,max}$ [m/s^2]	$a_{max\ amplified}$ [m/s^2]
Medea 50	11	EAST	5.881	1.695
Medea 50	17	EAST	5.612	1.92
Medea 50	81	EAST	9.529	2.236
Medea 95	15	EAST	8.719	1.792
Medea 95	77	EAST	9.285	1.852
Medea 95	99	EAST	9.63	1.586
Idrija 50	12	EAST	4.232	1.507
Idrija 50	45	EAST	3.165	1.254
Idrija 50	96	EAST	3.335	1.714
Idrija 95	41	NORTH	4.245	2.083
Idrija 95	42	EAST	5.148	2.121
Idrija 95	70	NORTH	5.394	2.318
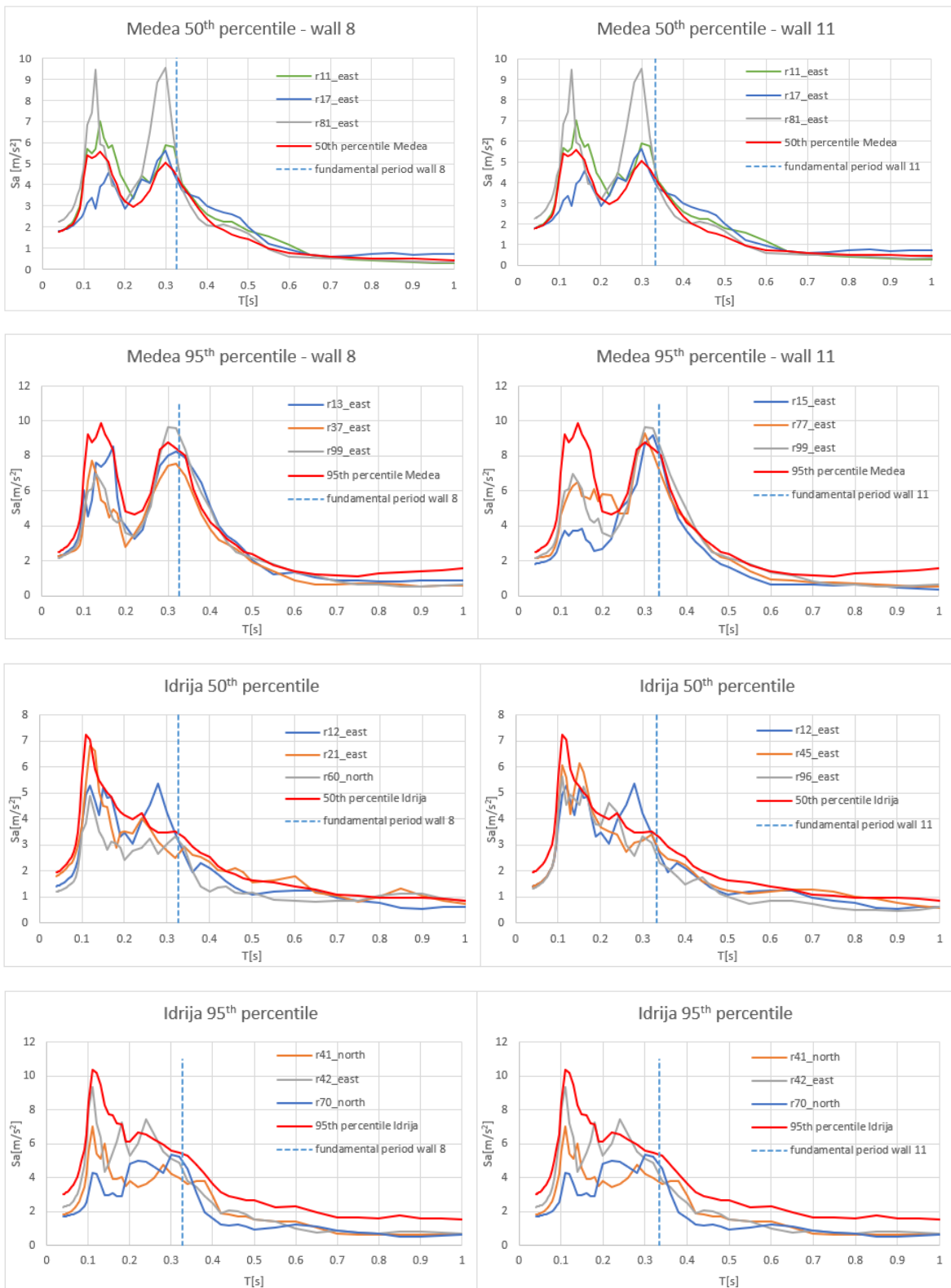
Figure 4-122: Response spectra of the scenario accelerograms selected for performing non-linear dynamic analyses on two walls of Masonry building A.

Wall 8

In the following figures, the results are reported in terms of base shear – top displacement. The base shear is calculated as the sum of the shear at the base of the ground floor piers. The reference displacement is the displacement of a joint at one end of the top of the wall, consistently with the

control joint of the pushover curves, that are also reported in the graphs. The capacity of the wall for fours limit states (CLS, LLS, DLS and OLS) is shown in the figures with coloured symbols. Four graphs are presented, two for Medea scenario (Figure 4-123 and Figure 4-124) and two for Idrija scenario (Figure 4-125 and Figure 4-126).

The displacement capacities (Du), compared to the highest displacements achieved with the dynamic analyses (Dmax), have been then used to calculate a C/D ratio, a kind of vulnerability index for the dynamic analyses (Table 4-47, Table 4-48, Table 4-49 and Table 4-50).

Figure 4-123: Base shear (V) – displacement (uy) graph with the results of pushover analysis and of dynamic analysis with 3 accelerograms close to the 50th percentile of Medea scenario (realizations 11, 17, and 81). On pushover curves also wall's capacities are shown with symbols, for four limit states. For the dynamic analysis, the displacement of a node at the top of the wall is taken as a reference (node 8).

Table 4-47: Check of the maximum top displacements requested by the non – linear dynamic analyses for wall 8, compared to the capacity of the wall, defined based on the pushover analysis (Medea 50th percentile).

Results of dynamic analysis - Medea 50th percentile				
	Dmax	Du,CLS	Du,LLS	Du,DLS	Du,OLS
uy_8 + [mm]	13.03	75	56.3	15.6	10.4
CHECK		5.756	4.321	1.197	0.798
uy_8 – [mm]	-10.38	-115.6	-86.7	-14.5	-9.7
CHECK		11.137	8.353	1.397	0.934
Minimum coefficients		**CLS**	**LLS**	**DLS**	**OLS**
		5.756	**4.321**	**1.197**	**0.798**

Figure 4-124: Base shear (V) – displacement (uy) graph with the results of pushover analysis and of dynamic analysis with 3 accelerograms close to the 95th percentile of Medea scenario (realizations 13, 37, and 99). On pushover curves also wall's capacities are shown with symbols, for four limit states. For the dynamic analysis, the displacement of a node at the top of the wall is taken as a reference (node 8).

Table 4-48: Check of the maximum top displacements requested by the non – linear dynamic analyses for wall 8, compared to the capacity of the wall, defined based on the pushover analysis (Medea 95th percentile).

Results of dynamic analysis - Medea 95th percentile					
	Dmax	Du,CLS	Du,LLS	Du,DLS	Du,OLS
uy_8 + [mm]	13.97	75	56.3	15.6	10.4
CHECK		5.369	4.030	1.117	0.744
uy_8 – [mm]	-13.26	-115.6	-86.7	-14.5	-9.7
CHECK		8.718	6.538	1.094	0.732
Minimum coefficients		**CLS**	**LLS**	**DLS**	**OLS**
		5.369	**4.030**	**1.094**	**0.732**

Figure 4-125: Base shear (V) – displacement (uy) graph with the results of pushover analysis and of dynamic analysis with 3 accelerograms close to the 50th percentile of Idrija scenario (realizations 12, 21, and 60). On pushover curves also wall's capacities are shown with symbols, for four limit states. For the dynamic analysis, the displacement of a node at the top of the wall is taken as a reference (node 8).

Table 4-49: Check of the maximum top displacements requested by the non – linear dynamic analyses for wall 8, compared to the capacity of the wall, defined based on the pushover analysis (Idrija 50th percentile).

Results of dynamic analysis - Idrija 50th percentile					
	Dmax	Du,CLS	Du,LLS	Du,DLS	Du,OLS
uy_8 + [mm]	10.86	75	56.3	15.6	10.4
CHECK		6.906	5.184	1.436	0.958
uy_8 – [mm]	-11.46	-115.6	-86.7	-14.5	-9.7
CHECK		10.087	7.565	1.265	0.846
Minimum coefficients		**CLS**	**LLS**	**DLS**	**OLS**
		6.906	**5.184**	**1.265**	**0.846**

Figure 4-126: Base shear (V) – displacement (uy) graph with the results of pushover analysis and of dynamic analysis with 3 accelerograms close to the 95th percentile of Idrija scenario (realizations 41, 42, and 70). On pushover curves also wall's capacities are shown with symbols, for four limit states. For the dynamic analysis, the displacement of a node at the top of the wall is taken as a reference (node 8).

Table 4-50: Check of the maximum top displacements requested by the non – linear dynamic analyses for wall 8, compared to the capacity of the wall, defined based on the pushover analysis (Idrija 95th percentile).

Results of dynamic analysis - Idria 95th percentile					
	Dmax	Du,CLS	Du,LLS	Du,DLS	Du,OLS
uy_8 + [mm]	11.58	75	56.3	15.6	10.4
CHECK		6.477	4.862	1.347	0.898
uy_8 – [mm]	-14.08	-115.6	-86.7	-14.5	-9.7
CHECK		8.210	6.158	1.030	0.689
Minimum coefficients		**CLS**	**LLS**	**DLS**	**OLS**
		6.477	**4.862**	**1.030**	**0.689**

The displacements of the wall during the dynamic analyses with the scenario accelerograms are clearly low and exceed just the OLS capacity of the wall. This is credibly due to the shape of the response spectrum of the scenario signals, that present low spectral accelerations for the fundamental period of the analysed structure. This hypothesis can be confirmed by performing an analysis with a signal that has a different shape of the response spectrum, with higher accelerations for the periods of interest. The chosen signal is a recorded signal (El Centro, 1940, north - south component, 1559 points with 0.02 s intervals), modified so that it becomes compatible with the code response spectrum

for CLS (the closest to the 95th percentile spectrum for Medea scenario). The signal has been prepared in SAP2000 software with which it is possible to modify accelerograms so that their response spectrum gets close to a given code response spectrum. In this case the compatibility has been calculated with CLS spectrum (elastic spectrum, reference life 100 years, ground category B). The result of the non-linear dynamic analysis performed with this accelerogram is shown in Figure 4-127. It can be seen that the displacement demand for such a seismic event are clearly higher, although they remain under the LLS capacity.
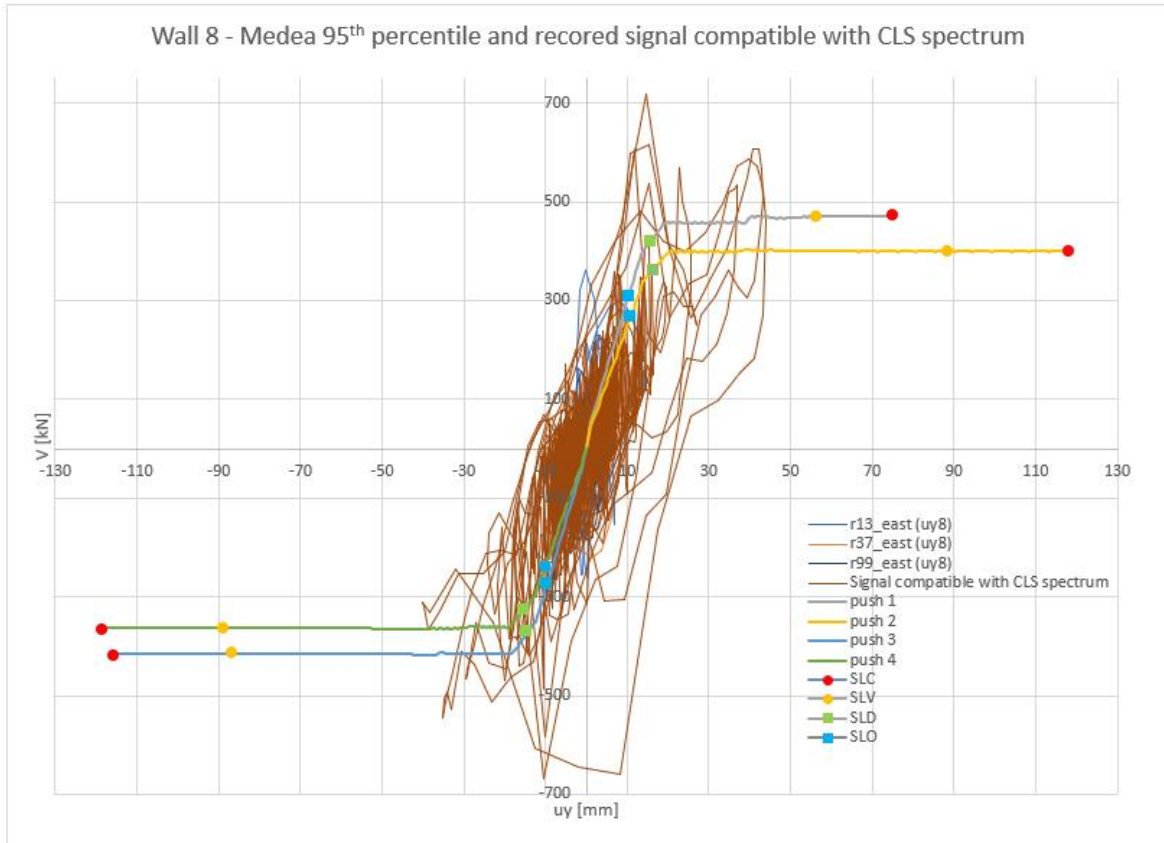
Figure 4-127: Base shear (V) – displacement (uy) graph with the results of pushover analysis and of dynamic analysis with 3 accelerograms close to the 95th percentile of Medea scenario (realizations 13, 37, and 99) and with an accelerogram compatible with the code CLS response spectrum. On pushover curves also wall's capacities are shown with symbols, for four limit states. For the dynamic analysis, the displacement of a node at the top of the wall is taken as a reference (node 8).

Wall 11

The same analyses and graphs are displayed for wall 11, as already done for wall 8. Four graphs are presented, two for Medea scenario (Figure 4-128 and Figure 4-129) and two for Idrija scenario (Figure 4-130 and Figure 4-131).

The displacement capacities (Du), compared to the highest displacements achieved with the dynamic analyses (Dmax), have been then used to calculate a C/D ratio, a kind of vulnerability index for the dynamic analyses (Table 4-51, Table 4-52, Table 4-53 and Table 4-54).
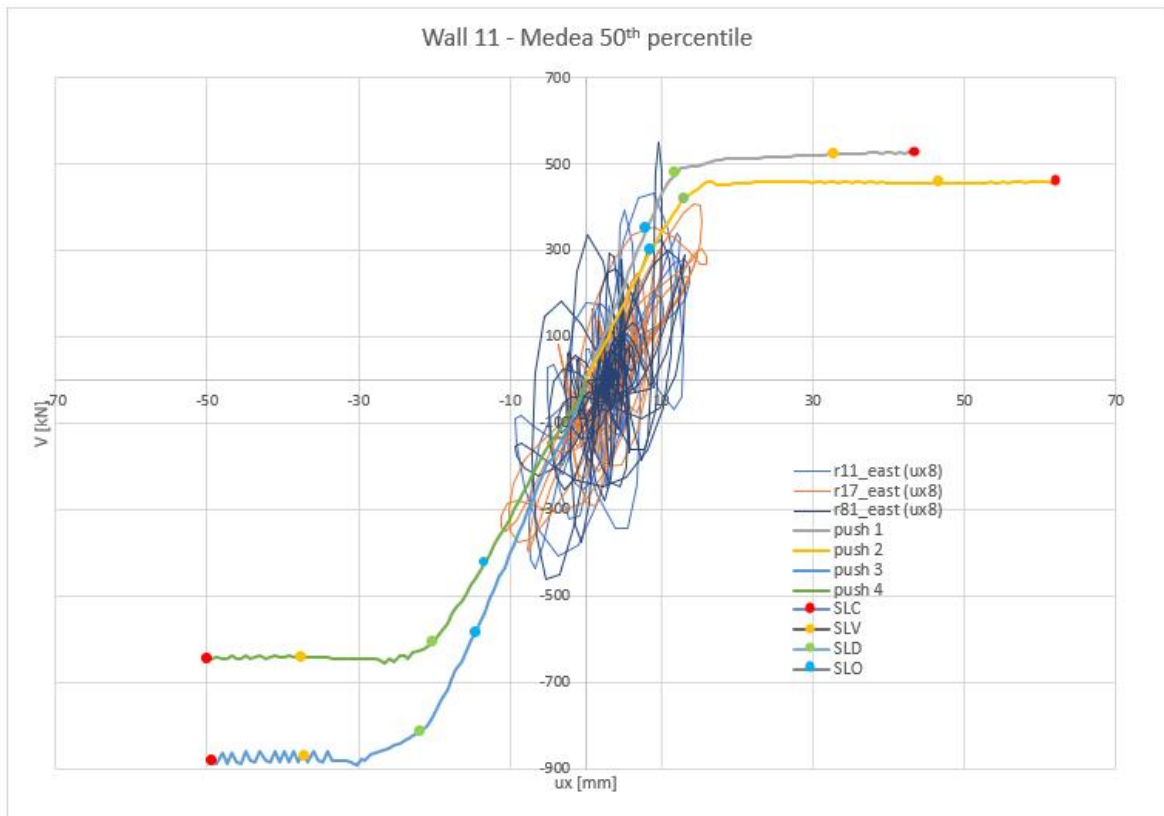
Figure 4-128: Base shear (V) – displacement (ux) graph with the results of pushover analysis and of dynamic analysis with 3 accelerograms close to the 50th percentile of Medea scenario (realizations 11, 17, and 81). On pushover curves also wall's capacities are shown with symbols, for four limit states. For the dynamic analysis, the displacement of a node at the top of the wall is taken as a reference (node 8).

Table 4-51: Check of the maximum top displacements requested by the non – linear dynamic analyses for wall 11, compared to the capacity of the wall, defined based on the pushover analysis (Medea 50th percentile).

Results of dynamic analysis - Medea 50th percentile					
	Dmax	Du,CLS	Du,LLS	Du,DLS	Du,OLS
uy_8 + [mm]	16.03	43.7	32.8	11.9	7.9
CHECK		2.726	2.046	0.742	0.493
uy_8 – [mm]	-11.2	-49.3	-37	-20.2	-13.4
CHECK		4.402	3.304	1.804	1.196
Minimum coefficients		**CLS**	**LLS**	**DLS**	**OLS**
		2.726	**2.046**	**0.742**	**0.493**
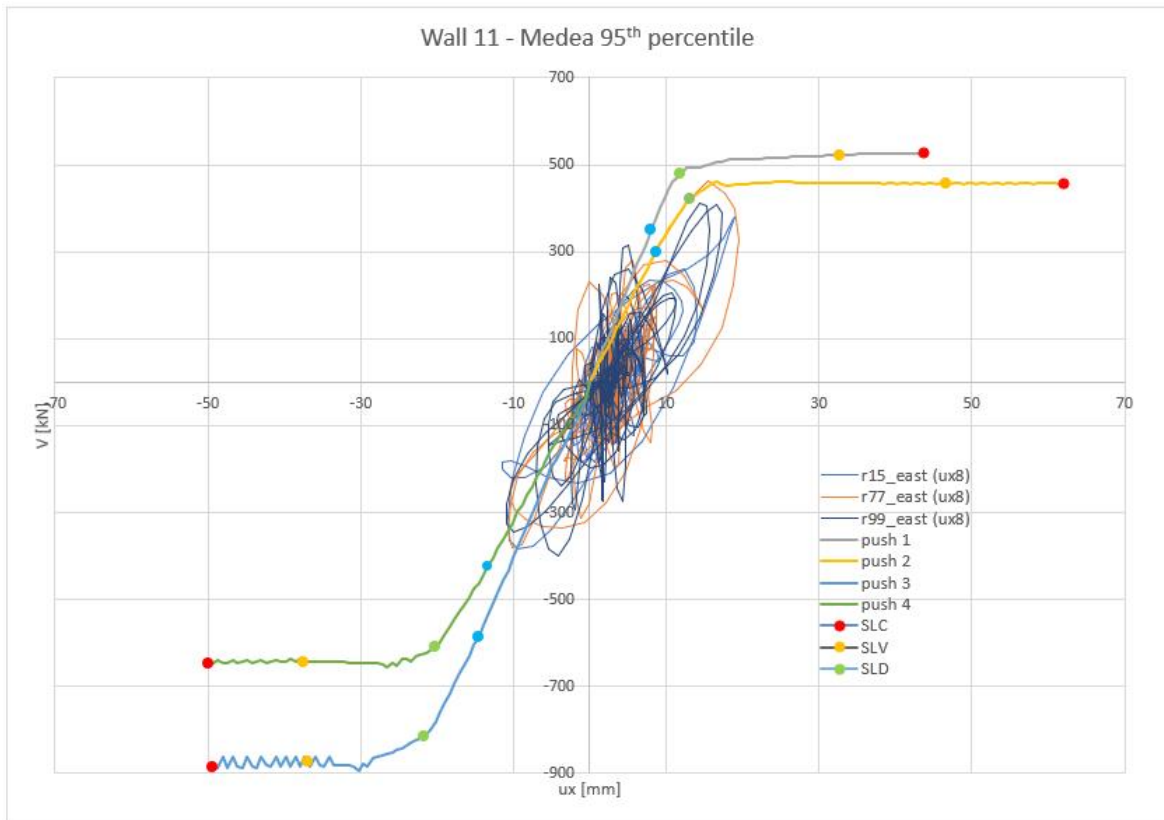
Figure 4-129: Base shear (V) – displacement (ux) graph with the results of pushover analysis and of dynamic analysis with 3 accelerograms close to the 95th percentile of Medea scenario (realizations 15, 77, and 99). On pushover curves also wall's capacities are shown with symbols, for four limit states. For the dynamic analysis, the displacement of a node at the top of the wall is taken as a reference (node 8).

Table 4-52: Check of the maximum top displacements requested by the non – linear dynamic analyses for wall 11, compared to the capacity of the wall, defined based on the pushover analysis (Medea 95th percentile).

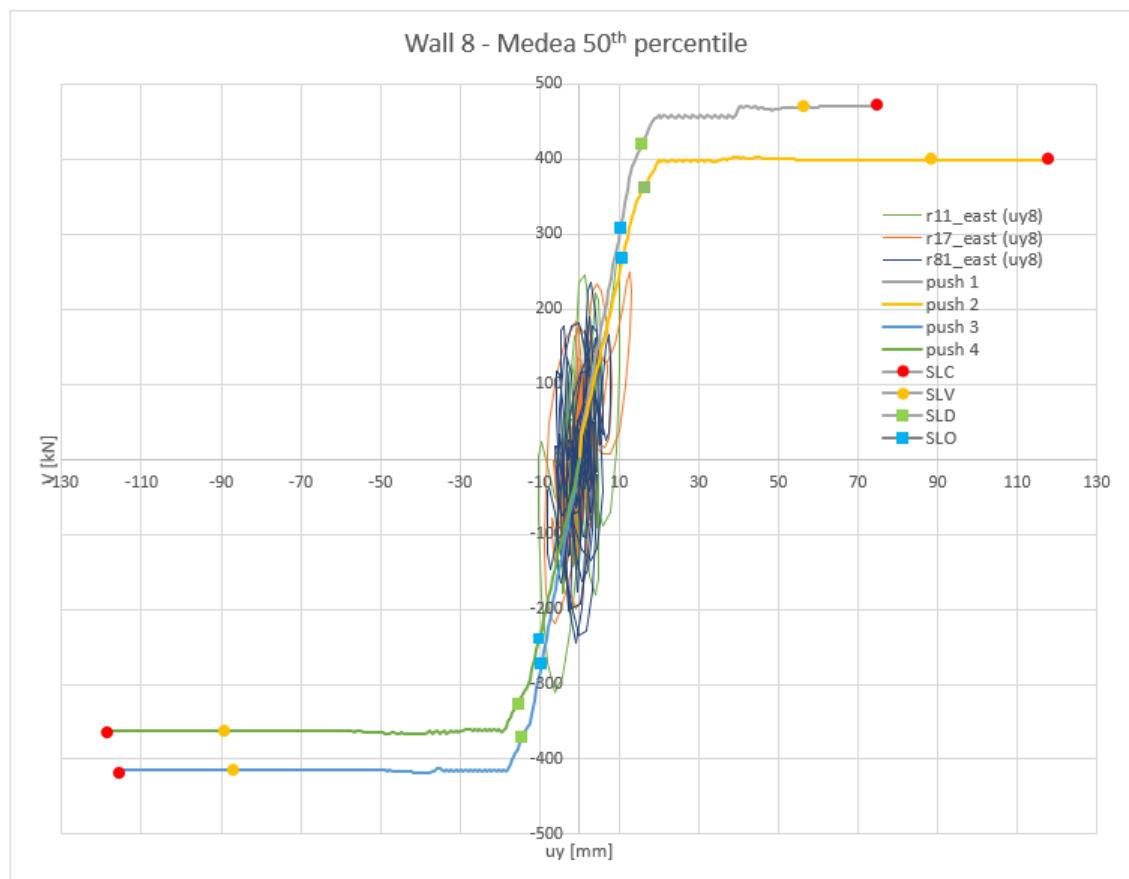| Results of dynamic analysis - Medea 95th percentile					
	Dmax	Du,CLS	Du,LLS	Du,DLS	Du,OLS
uy_8 + [mm]	19.46	43.7	32.8	11.9	7.9
CHECK		2.246	1.686	0.612	0.406
uy_8 – [mm]	-11.38	-49.3	-37	-20.2	-13.4
CHECK		4.332	3.251	1.775	1.178
Minimum coefficients		**CLS**	**LLS**	**DLS**	**OLS**
		2.246	**1.686**	**0.612**	**0.406**
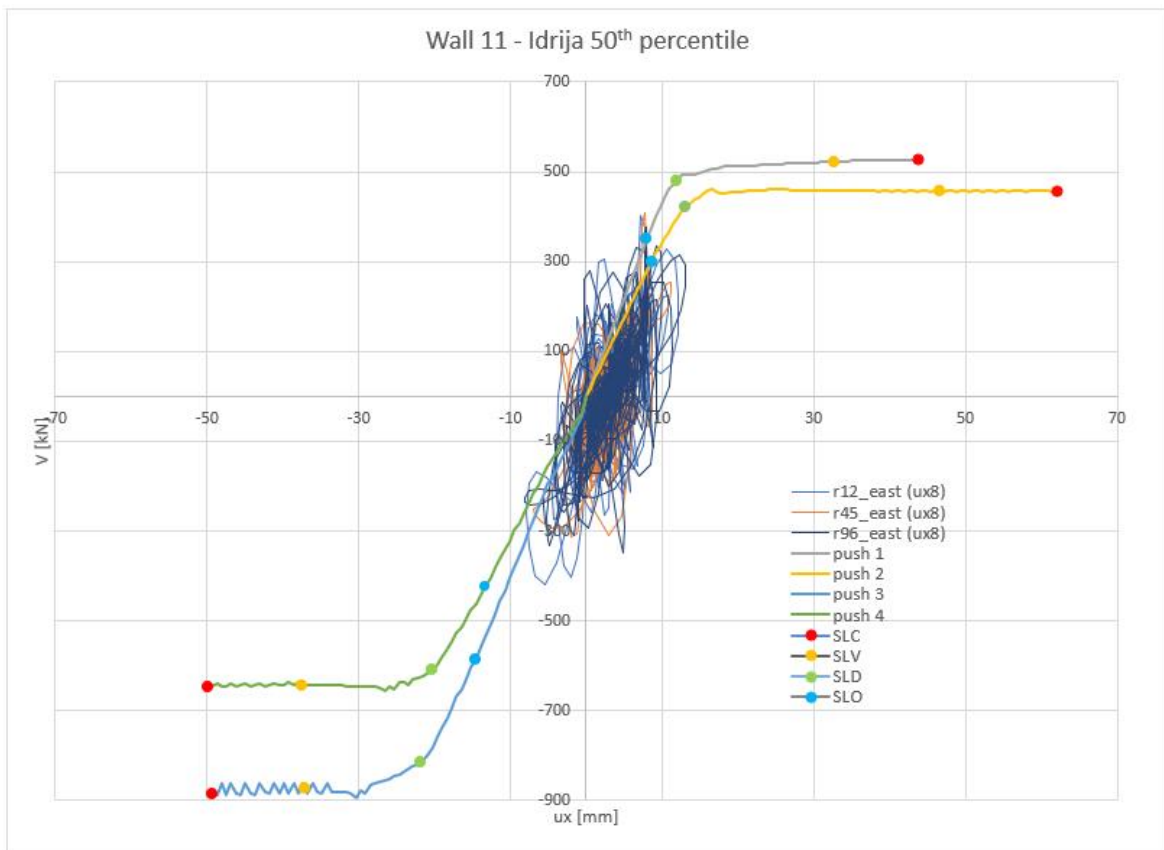
Figure 4-130: Base shear (V) – displacement (ux) graph with the results of pushover analysis and of dynamic analysis with 3 accelerograms close to the 50th percentile of Idrija scenario (realizations 12, 45, and 96). On pushover curves also wall's capacities are shown with symbols, for four limit states. For the dynamic analysis, the displacement of a node at the top of the wall is taken as a reference (node 8).

Table 4-53: Check of the maximum top displacements requested by the non – linear dynamic analyses for wall 11, compared to the capacity of the wall, defined based on the pushover analysis (Idrija 50th percentile).

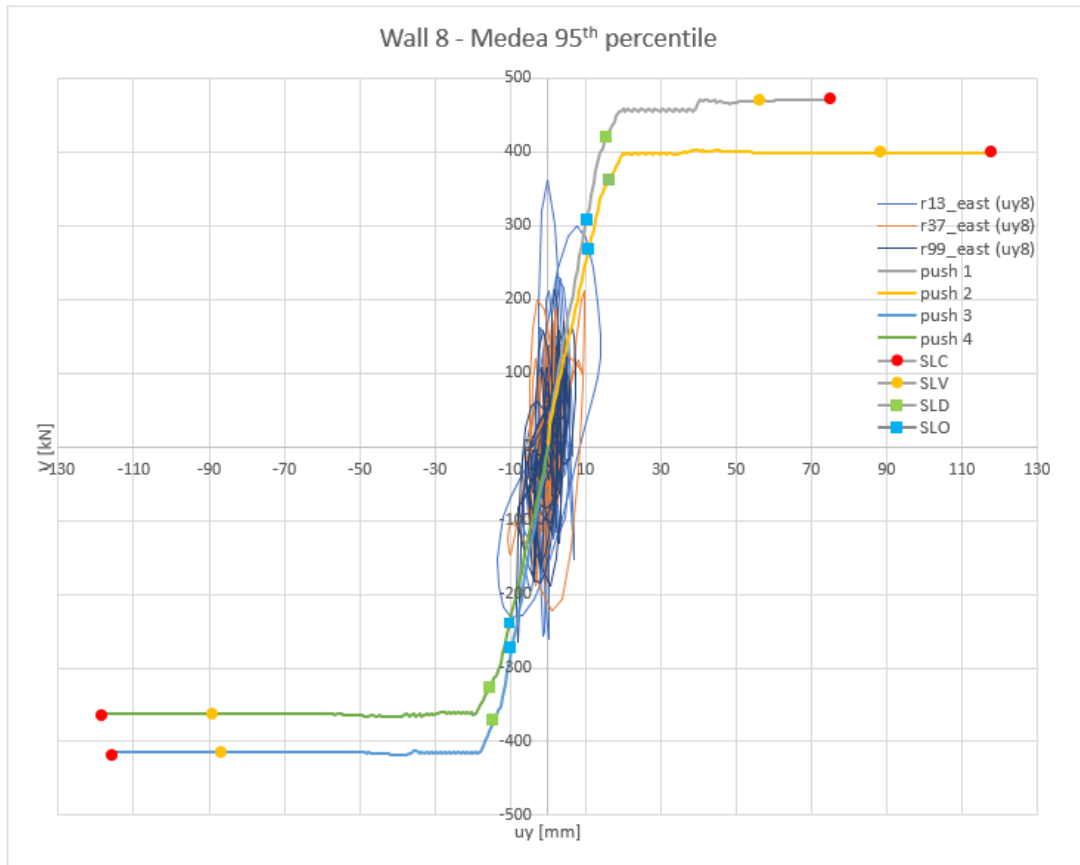| Results of dynamic analysis - Idrija 50th percentile					
	Dmax	Du,CLS	Du,LLS	Du,DLS	Du,OLS
uy_8 + [mm]	13.12	43.7	32.8	11.9	7.9
CHECK		3.331	2.500	0.907	0.602
uy_8 – [mm]	-8.16	-49.3	-37	-20.2	-13.4
CHECK		6.042	4.534	2.475	1.642
Minimum coefficients		**CLS**	**LLS**	**DLS**	**OLS**
		3.331	**2.500**	**0.907**	**0.602**
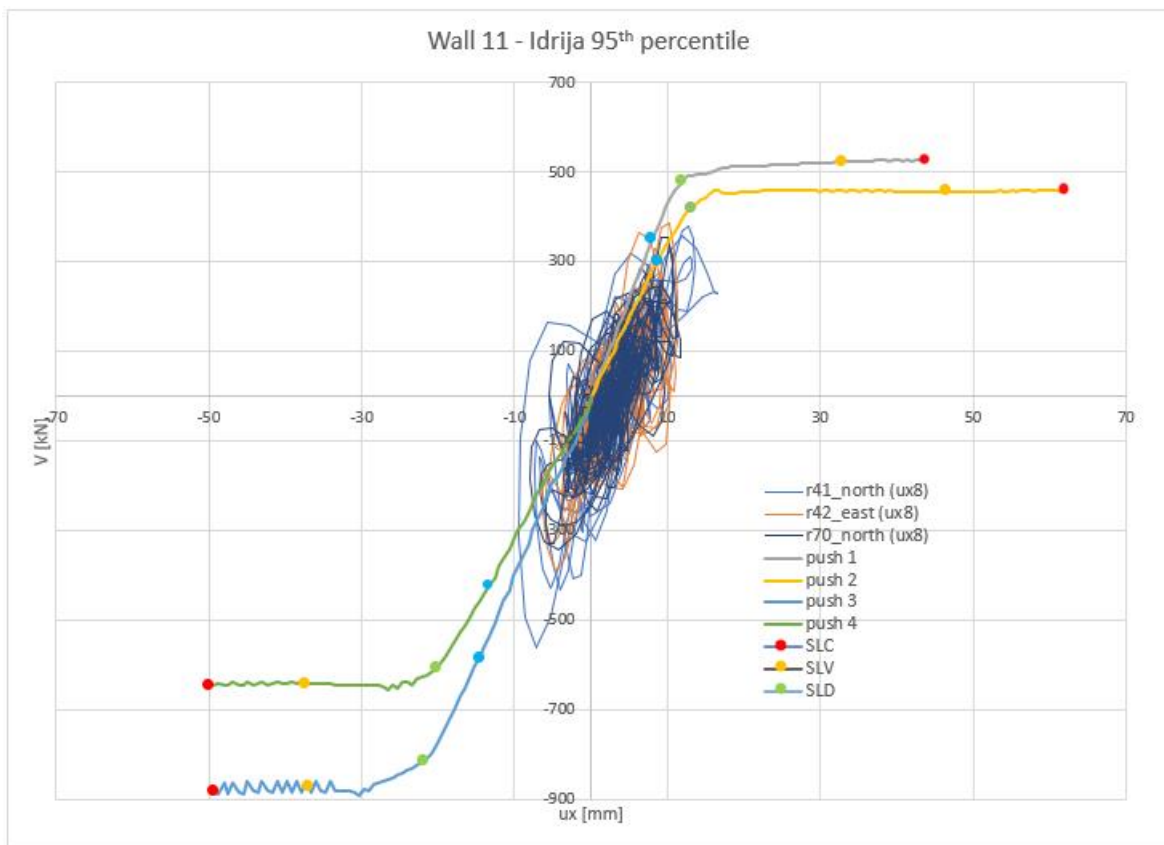
Figure 4-131: Base shear (V) – displacement (ux) graph with the results of pushover analysis and of dynamic analysis with 3 accelerograms close to the 95th percentile of Idrija scenario (realizations 41, 42, and 70). On pushover curves also wall's capacities are shown with symbols, for four limit states. For the dynamic analysis, the displacement of a node at the top of the wall is taken as a reference (node 8).

Table 4-54: Check of the maximum top displacements requested by the non – linear dynamic analyses for wall 11, compared to the capacity of the wall, defined based on the pushover analysis (Idrija 95th percentile).

Results of dynamic analysis - Idrija 95th percentile					
	Dmax	Du,CLS	Du,LLS	Du,DLS	Du,OLS
uy_8 + [mm]	16.53	43.7	32.8	11.9	7.9
CHECK		2.644	1.984	0.720	0.478
uy_8 – [mm]	-9.37	-49.3	-37	-20.2	-13.4
CHECK		5.261	3.949	2.156	1.430
Minimum coefficients		**CLS**	**LLS**	**DLS**	**OLS**
		2.644	**1.984**	**0.720**	**0.478**

As already noticed for wall 8, also for wall 11, the displacements required by the scenario accelerograms are quite low and exceed just OLS and DLS capacity of the wall. This is credibly due to the shape of the response spectrum of the scenario signals, that present low spectral accelerations for the fundamental period of the analysed structure. This hypothesis can be confirmed by performing an analysis with a signal that has a different shape of the response spectrum, with higher accelerations for the periods of interest. The same signal used for wall 8 is used also for wall 11. The result is shown in Figure 4-132. It can be seen that the displacement demand for such a seismic event is clearly higher, although it remains under the LLS capacity almost in all cases.
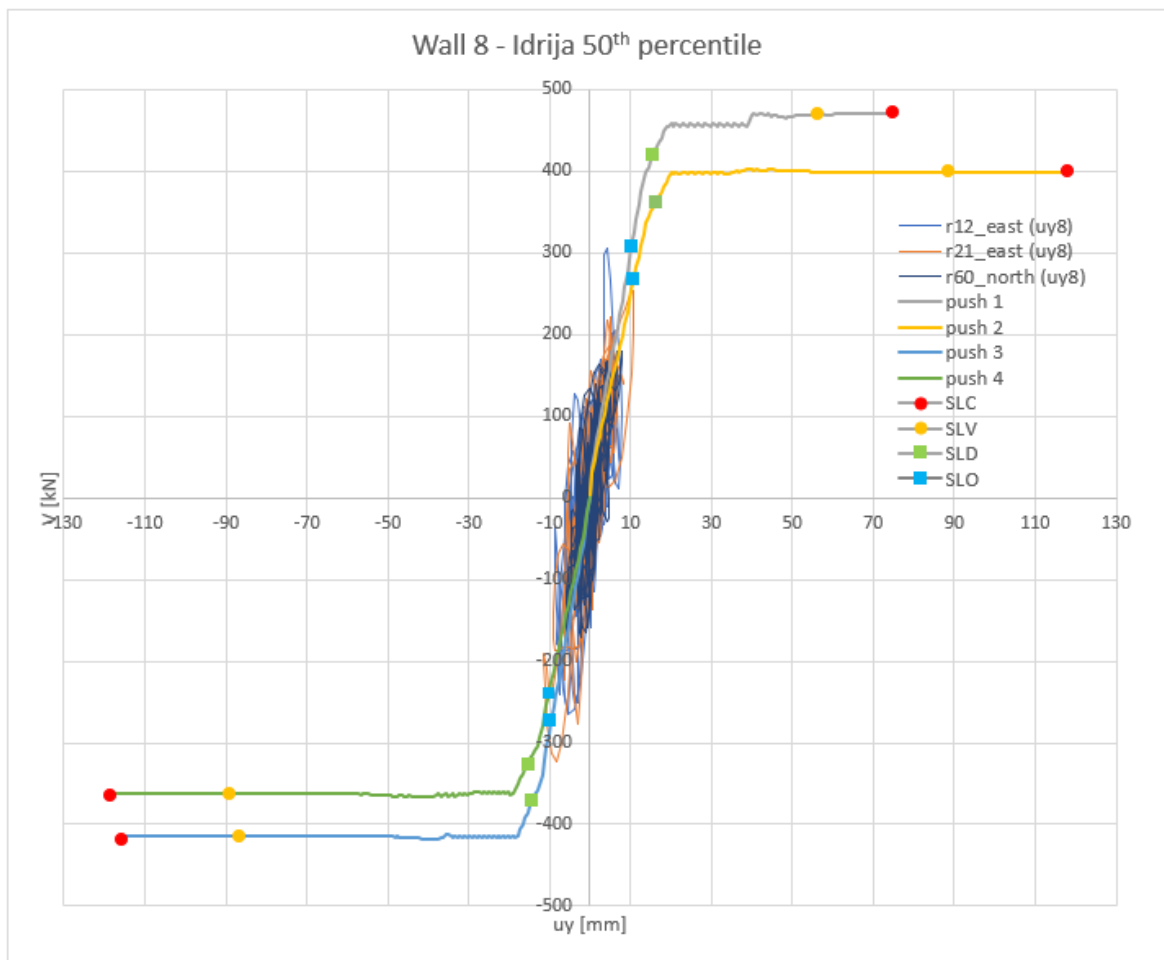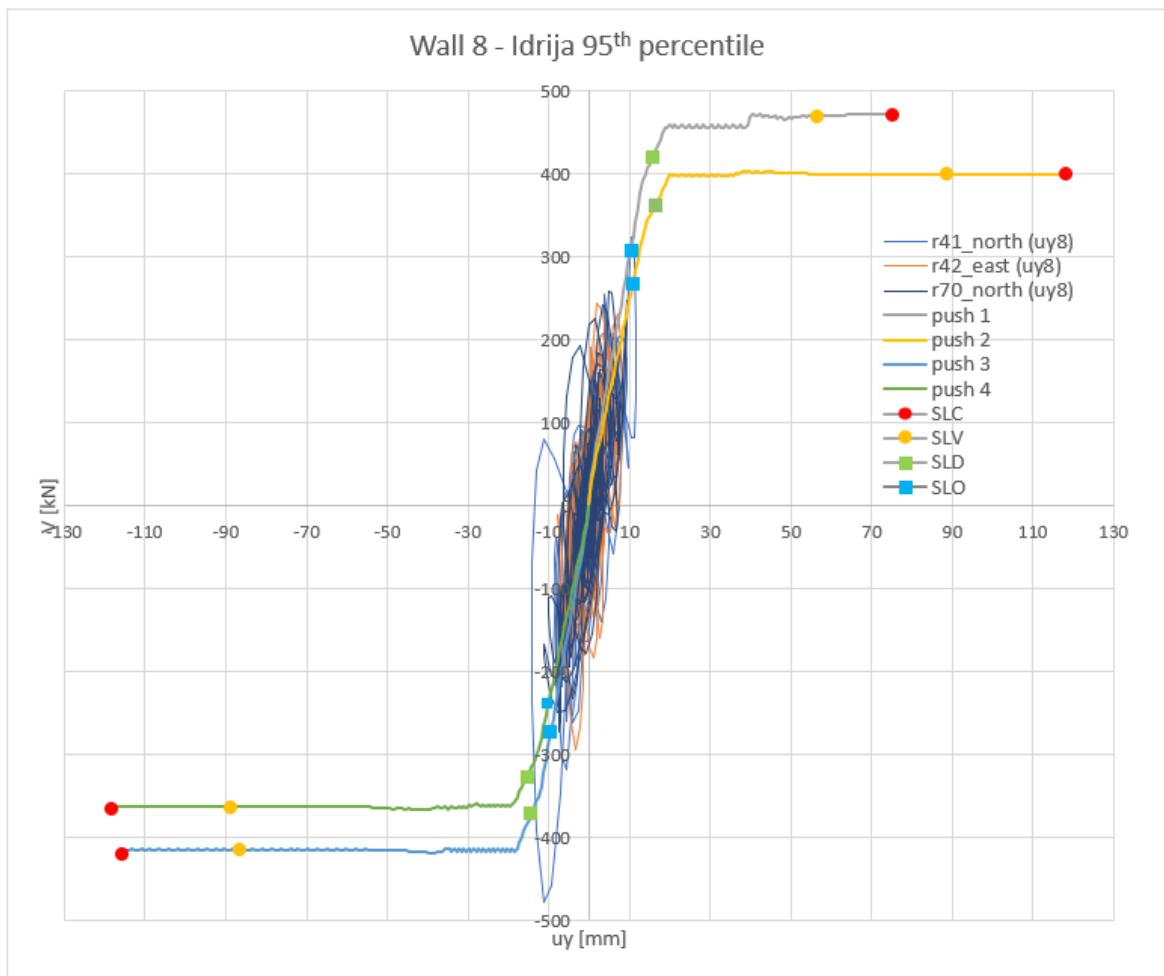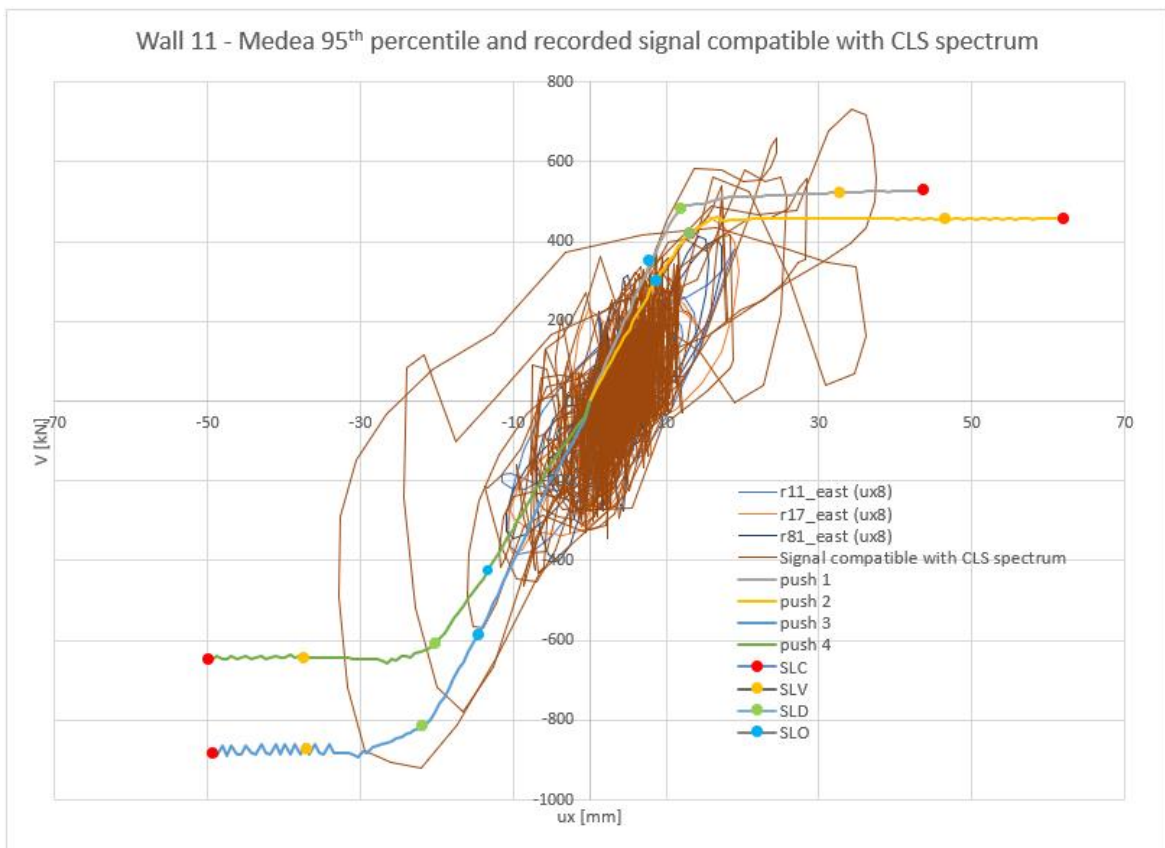
Figure 4-132: Base shear (V) – displacement (ux) graph with the results of pushover analysis and of dynamic analysis with 3 accelerograms close to the 95th percentile of Medea scenario (realizations 11, 17, and 81) and with an accelerogram compatible with the code CLS response spectrum. On pushover curves also wall's capacities are shown with symbols, for four limit states. For the dynamic analysis, the displacement of a node at the top of the wall is taken as a reference (node 8).

The results found with non - linear dynamic analyses confirm the results found with the pushover analyses with scenario seismic input (percentile scenario response spectra - Table 4-37). The displacement demand of the scenarios is low and exceeds just DLS and OLS capacity of the building.

4.4.4. *Vulnerability evaluation and retrofitting solutions*

The first important weakness of the building is the lack of bond between perpendicular walls. This allows the possibility of out-of-plane collapse of single walls and does not allow a proper collaboration between walls. This, combined with flexible wooden slabs, that are not properly bonded to the walls, leads to a building that does not have a box behaviour at all, while the box behaviour is the best way for a masonry building to resist seismic forces.

Also the masonry itself is not of good quality, as it has been noticed from the in situ tests. The mortar is weak and deteriorated. Masonry is randomly positioned and has small to evident voids between blocks.

Moreover, all the analyses have been carried out just on the main rectangular building, without the lodge. The lodge is a very vulnerable part, without almost any seismic resistance (especially at the level of the stone columns), but it contains the stairwell, so that it is fundamental to improve its behaviour under horizontal action. One option is to connect it efficiently to the main building, another option is to create a seismic joint at the border with the main building and retrofit the lodge so that it can withstand seismic actions by itself.

The last, but not less important, also for usability and not just for seismic actions, is the state of the roof, that, at the moment is very bad. It leaks water in many points, so that the rooms under

the roof are deteriorated by the water. The remaking of the sheats is urgent, before the wooden structural elements are damaged too.

In order to retrofit this building, including the lodge, it is necessary to solve all the mentioned weaknesses [61]. When designing the interventions, it should be considered that the building has artistic importance, so that the exterior and the valuable internal finishes should be left as they are, as much as possible. For this reason the law prescribes that in this kind of buildings the seismic behaviour can be just improved, without adapting it to current requirements (ξ, the ratio between capacity and demand can be lower than 1, but it should be at least 0.6 and it needs to be incremented of at least 0.1).

The bonds between the walls can be improved with different solutions:

- *Scuci e cuci* technique – it can be used to repair cracks in the masonry, but also to guarantee the connection between perpendicular walls (Figure 4-133);
- *Reinforced stitching* – steel rods are inserted at the corners of the building in order to connect perpendicular walls (Figure 4-134);
- *Horizontal tie rods* (Figure 4-135).
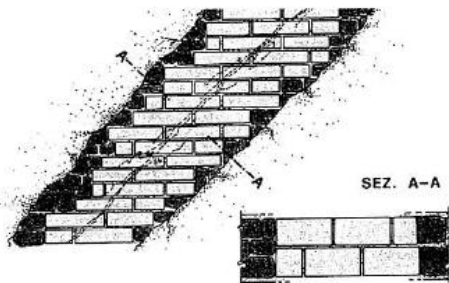
Figure 4-133: Scuci e cuci technique.
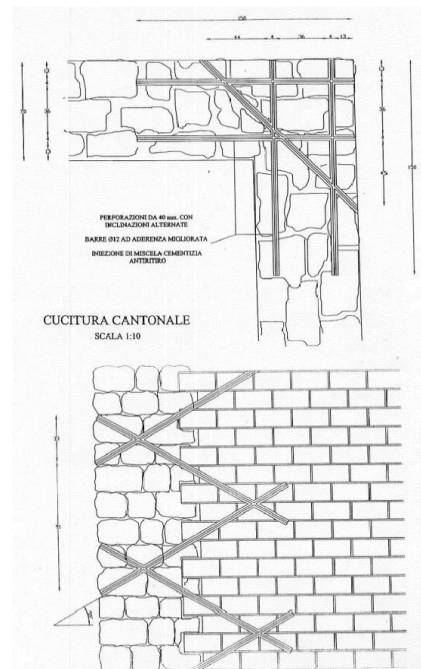
Figure 4-134: Example of reinforced stitching.

For making the wooden slabs more effective in distributing horizontal forces to the walls, their connection to the walls needs to be improved and also their in-plane stiffness. A good solution, that does not add mass to the structure, is to build a bracing system with metal straps, as the ones shown in Figure 4-136. These elements can be applied to the extrados or the intrados of the slab, depending on which side has the more valuable layer. For a better connection of the slabs to the walls, a steel L profile can be positioned around the whole perimeter and fixed to the walls with injected rods (diameter 30-35 mm).
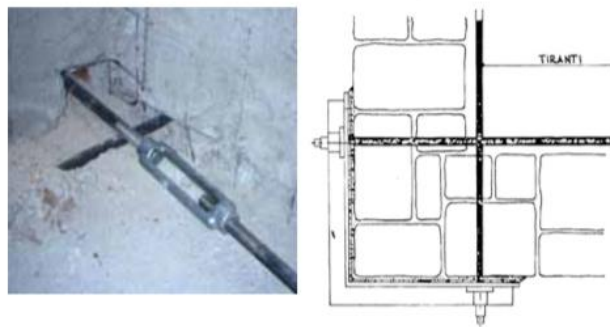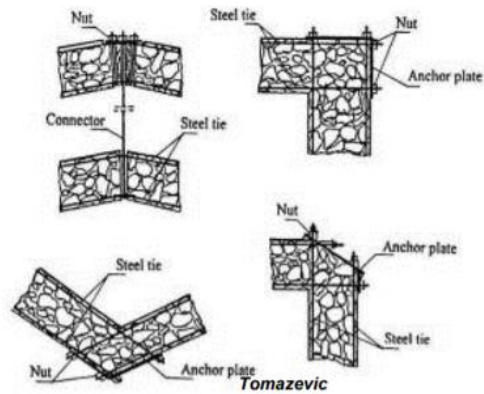
Figure 4-135: Examples of installation of tie rods for the connection of perpendicular walls.

Figure 4-136: Example of bracing system of the slabs made of metal straps (www.rothoblaas.it)

For strengthening the masonry, there are many types of intervention possible.

- **Injection of binder mixtures**: it is effective in masonries with many voids between the blocks, as the one of the case study building. The voids are filled with cementitious material (or hydraulic lime or lime with pozzolan) that can significantly increase the strength of the masonry.
- **Reinforced plaster**: steel reinforcing nets are placed on the two sides of the masonry wall, connected through passing bars, then a concrete sheet 3-4 cm thick, is applied. The intervention is effective, if it is applied to both sides of the wall. It is very invasive as it covers all the surface of the old masonry.

The existing building needs all these interventions in order to improve all the weaknesses that have been found during the analysis of the actual state. An important part is the connection of the lodge to the main building. The very flexible wooden slab of the last floor needs to be connected

and stiffened, as described before. The same solution can be applied also to the roof, then the lodge can be considered in the analyses together with the main building.

The interventions used for the strengthening of the masonry are visible in Figure 4-137 to Figure 4-141. The colours of the walls are associated to a specific intervention, as described in the legend in Table 4-55. The wall of the front façade has been left untouched for its artistic importance.
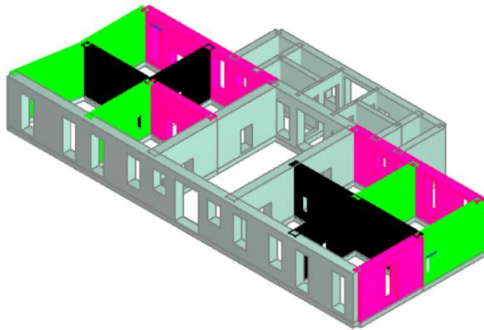
Figure 4-137: Level 1
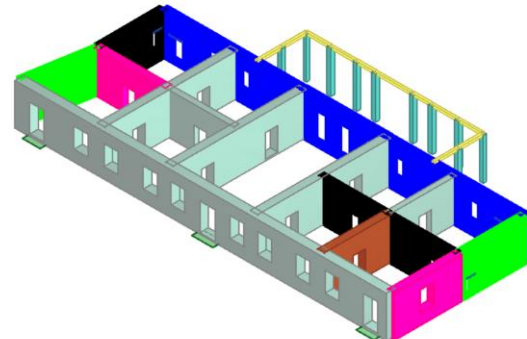
Figure 4-138: Level 2
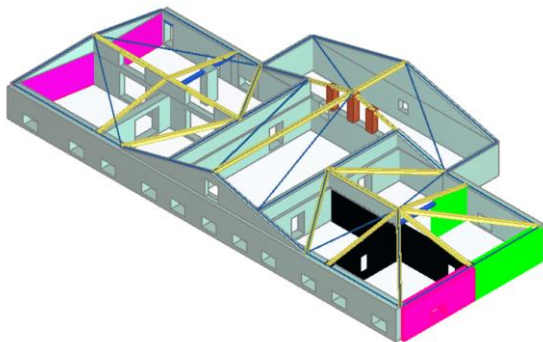
Figure 4-139: Level 3
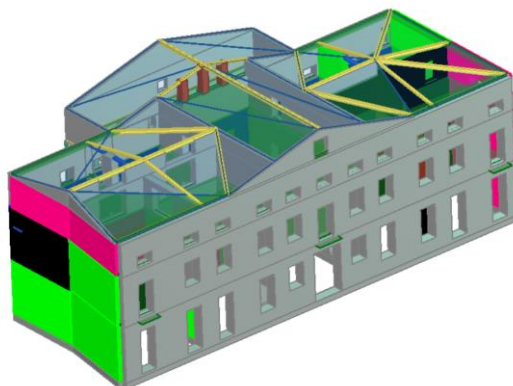
Figure 4-140: Front view of the whole building
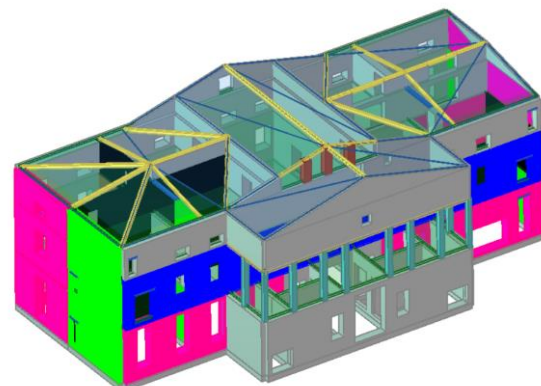
Figure 4-141: Back view of the whole building

Table 4-55: Legend of the interventions proposed for the seismic retrofit of the case study building.

LEGEND	
'White'	Stone masonry (without intervention)
Brown	Brick masonry (without intervention)
Blue	Stone masonry + injections
Fuchsia	Stone masonry + injections + artificial diatons
Green	Stone masonry + injections + reinforced plaster
Black	Brick masonry + reinforced plaster
Blue beam	Steel beam
Yellow beam	Wooden beam

The displayed retrofitting interventions are taken into account in the numerical model, as specified by the Italian code "Circolare 21 gennaio 2019, n. 7 C.S.LL.PP.", table C8.5.II, by considering amplification factors for the strength and stiffness of the material, based on the type of intervention.

The modes of vibration of such retrofitted building are shown in Table 4-56.

Table 4-56: Results of modal analysis carried out on the model of the whole retrofitted building.

Mode	T [s]	mx [kg]	Mx [%]	my [kg]	My [%]	mz [kg]	Mz [%]	Mx sum [%]	My sum [%]	Mz sum [%]
1	0.303	3,059,330	86.11	31,623	0.89	120	0	86.11	0.89	0
2	0.288	18,542	0.52	2,747,768	77.34	210	0.01	86.63	78.23	0.01
3	0.245	76,902	2.16	151,763	4.27	6	0	88.79	82.5	0.01
4	0.201	12,291	0.35	802	0.02	256	0.01	89.14	82.52	0.02
5	0.171	29	0	35,450	1	101,732	2.86	89.14	83.52	2.88
6	0.119	25,151	0.71	473,293	13.32	92,636	2.61	89.85	96.84	5.49
7	0.116	322,443	9.08	27,656	0.78	34,733	0.98	98.93	97.62	6.47
8	0.109	2,737	0.08	32,041	0.9	708,785	19.95	99.01	98.52	26.42
9	0.102	1,536	0.04	2,418	0.07	21,469	0.6	99.05	98.59	27.02
10	0.099	2,343	0.07	2,567	0.07	220,618	6.21	99.12	98.66	33.23
11	0.094	705	0.02	1,048	0.03	224,527	6.32	99.14	98.69	39.55
12	0.090	3	0	115	0	600,503	16.9	99.14	98.69	56.45
13	0.089	37	0	2,176	0.06	293	0.01	99.14	98.75	56.46
14	0.082	49	0	1,323	0.04	2,849	0.08	99.14	98.79	56.54
15	0.081	33	0	431	0.01	72,799	2.05	99.14	98.8	58.59
16	0.080	2	0	4,126	0.12	46,115	1.3	99.14	98.92	59.89
17	0.079	41	0	600	0.02	22,838	0.64	99.14	98.94	60.53
18	0.077	398	0.01	481	0.01	73,344	2.06	99.15	98.95	62.59
19	0.076	270	0.01	238	0.01	407,347	11.47	99.16	98.96	74.06
20	0.075	212	0.01	509	0.01	229,336	6.46	99.17	98.97	80.52

These interventions are not enough for adapting the building to the requirements of current codes, but they allow to achieve a box behaviour, including the lodge, and improve the seismic response of the building. The minimum seismic vulnerability indices of the retrofitted building are reported in Table 4-57. They are almost all over 0.6. Moreover, comparing them to the seismic vulnerability indices of the existing non-retrofitted building, the increment is almost in all cases (but for SLS in X direction) higher than 0.1 (Table 4-58).

Table 4-57: Minimum seismic vulnerability indices found with pushover analysis after the retrofitting solutions have been applied to the model.

αPGA – RETROFITTED BUILDING				
	α CLS	α LLS	α DLS	α OLS
X	0,711	0,663	0,604	0,545
Y	0,609	0,595	0,662	0,579

Table 4-58: Increment of seismic vulnerability indices, compared to the non-retrofitted building

Variations of indices				
	αCLS	α LLS	α DLS	α OLS
X	+0,191	+0,172	+0,051	+0,039
Y	+0,182	+0,187	+0,182	+0,140

4.5.Masonry building B

4.5.1. Modal analysis

The clay brick masonry building has a fundamental period in Y direction of 0.39 s (80.5% of participating mass). The second and the third modes are in X direction with 25.7% and 55.4% of participating mass ratios respectively. With the first 5 modes the participating mass ratios in both directions exceed 85% (see Table 4-59), that means that the building is quite regular, as expected.

Table 4-59: First 10 modes resulting from the modal analysis of the building.

Mode	T [s]	mx [kg]	Mx [%]	Sum Mx [%]	my [kg]	My [%]	Sum My [%]	mz [kg]	Mz [%]
1	0.39405	48,313	4	4	973,018	80.54	80.54	309	0.03
2	0.34668	310,925	25.74	29.74	26,617	2.2	82.74	103	0.01
3	0.32468	668,828	55.36	85.1	24,742	2.05	84.79	13	0
4	0.16832	8,598	0.71	85.81	25	0	84.79	151	0.01
5	0.13636	2,255	0.19	86	131,792	10.91	95.7	2,529	0.21
6	0.13501	5,070	0.42	86.42	6,459	0.53	96.23	6	0
7	0.1207	71,717	5.94	92.36	1,274	0.11	96.34	3,384	0.28
8	0.11784	35,499	2.94	95.3	19,936	1.65	97.99	4,758	0.39
9	0.10085	8	0	95.3	270	0.02	98.01	597,846	49.49
10	0.10011	7,833	0.65	95.95	460	0.04	98.05	62,683	5.19
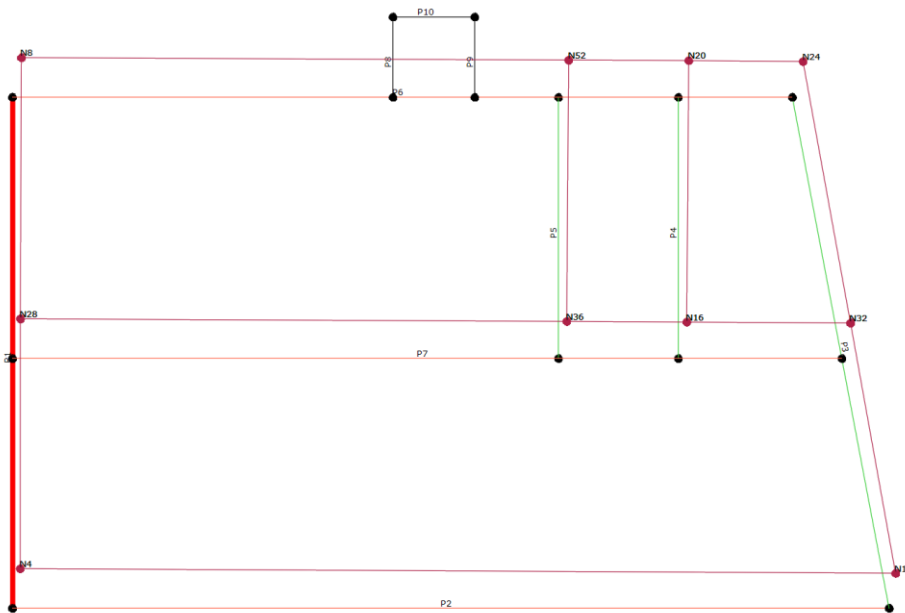
Figure 4-142: Deformed shape of the 1st mode at level 3.
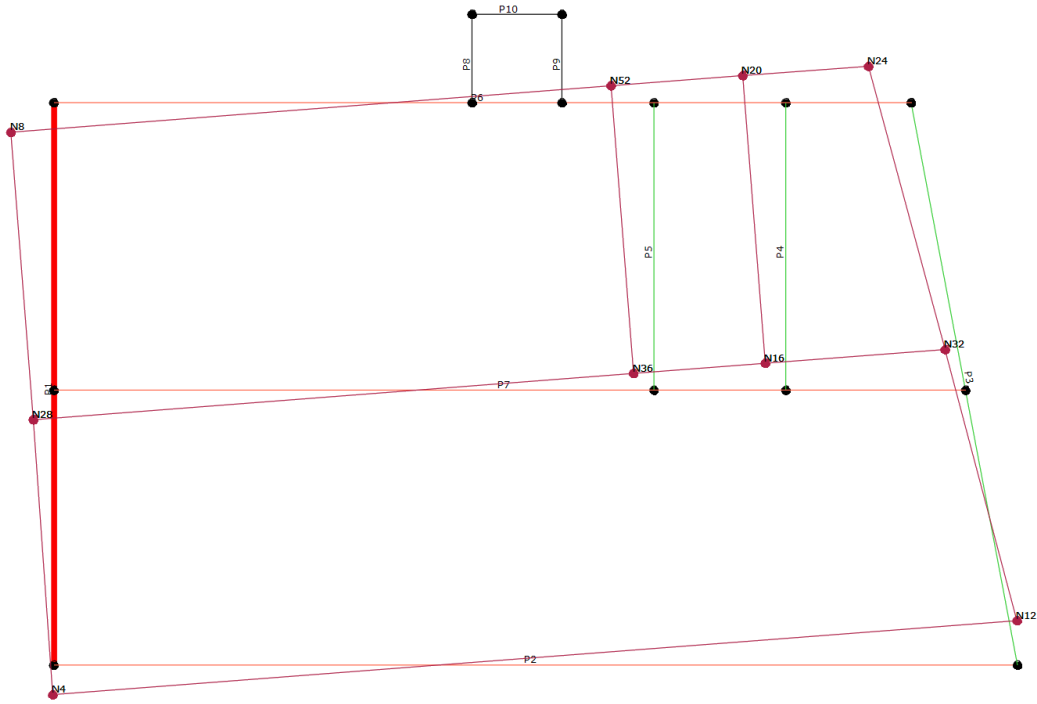
Figure 4-143:Deformed shape of the 2nd mode at level 3.

Although the slabs are wooden and presumably not stiff enough in their plane, the building has a box behaviour. For this reason, both results of global analysis and of analyses of the single walls are presented in the following.

4.5.2. Non - linear static analysis (pushover)

The analyses have been carried out with 3Muri computer software from STA DATA, as done for Masonry building A. The load patterns used for this study are the "uniform" pattern, proportional to the storey masses, and a load pattern with a distribution proportional to the equivalent static forces (triangular lateral load). The analyses are first performed on the whole building (24 analyses), then also separately for each wall. For each wall, four analyses are performed: for each of the two distributions of lateral load, the analyses are carried out in positive and negative direction along the plane of the wall. The names of the walls are visible in Figure 4-144.
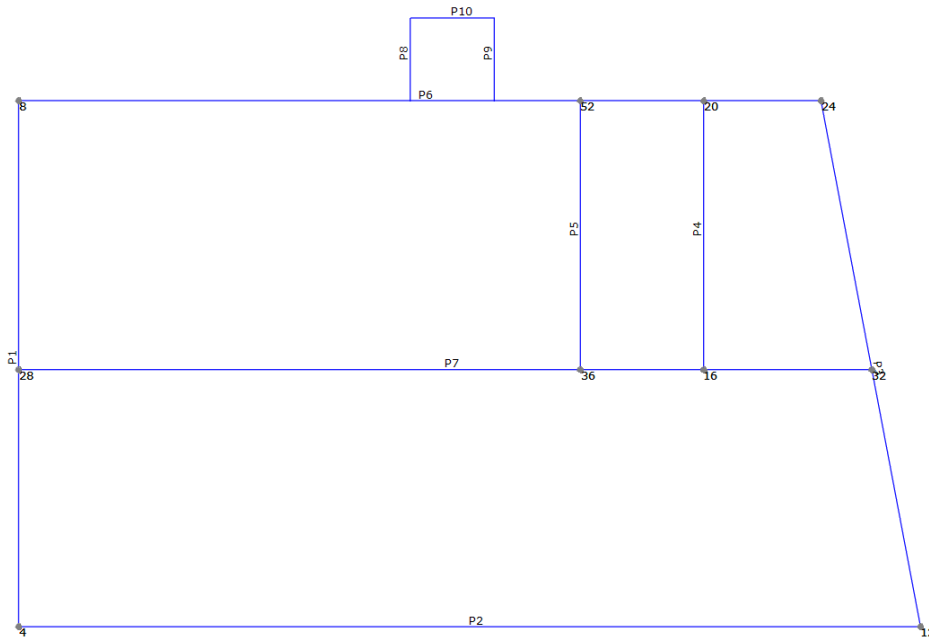
Figure 4-144: Names of the walls of the building in the model in 3Muri (plan of the second floor).

The results of the analyses are expressed in terms of seismic vulnerability indices α, calculated for each limit state (α_{CLS}, α_{LLS}, α_{DLS}, α_{OLS}) as the ratio between the capacity PGA and the demand PGA:

$$\alpha_{SL,i} = \frac{(PGA_i)_C}{(PGA_i)_D} \tag{4.12}$$

4.5.2.1. Vulnerability evaluation based on code response spectra

Global analysis

The results of the global analyses are summarized in Table 4-60. None of the 24 analyses are verified for the Life Safety limit state, while all of them, but two, are verified for Serviceability limit states (DLS and OLS). For this building CLS is not considered, as it is an ordinary building.

At the end of the worse analysis in X direction, the 16th (highlighted in yellow in the table), the most damaged wall is wall 7, with 21% of the wall elements collapsed (4.5% of the whole building – see Table 4-61). As it can be seen in Table 4-62, the maximum interstorey displacement in the same analysis is the one at the last level of the model in wall 2 – 0.93 cm= 0.0093 m. As the third level has an interstorey height of 3.77 m, the interstorey drift is 0.25 %. The displacements of the joints of all the storeys of wall 2 (left end) and the calculation of the interstorey drifts are reported in Table 4-63. The interstorey drift limits set in the software for shear collapse and for flexural collapse are 0.4% and 0.6%, respectively. The interstorey drift of 0.25% is very low, considering that wall 2 at the end of analysis has just some spandrels collapsed for compression or compression-bending interaction, but as the analysis is global, the low value of interstorey drifts is due to the shape of the building, to the early collapse of some parts of the building and to the slight torsion that happens during the pushover analysis. The deformed shape of the last floor at the last step of analysis 16 is shown in Figure 4-145.

Table 4-60: Results of the global pushover analyses. Dmax is the demand displacement, Du is the ultimate capacity displacement. The analyses highlighted in red are "not verified" and the ones in green are "verified". The yellow analyses are the most severe in each main direction. The software is in Italian language, so that a small legend is needed: Dir.sisma= Direction of the load, Carico sismico= Load pattern, SLV = LLS, SLD = DLS and SLO = OLS.

N.	Inserisci in relazione	Dir. sisma	Carico sismico	Eccentricità [cm]	Dmax SLV [cm]	Du SLV [cm]	q* SLV	Dmax SLD [cm]	Du SLD [cm]	Dmax SLO	Do SLO [cm]	a SLV	a SLD	a SLO
1	☑	+X	Uniforme	0.00	4.02	5.59	4.50	1.19	2.43	0.85	1.72	0.666	2.043	2.028
2	☑	+X	Forze statiche	0.00	4.37	7.33	4.68	1.29	1.22	0.92	1.22	0.642	0.941	1.317
3	☑	-X	Uniforme	0.00	4.41	2.06	3.30	1.31	1.78	0.93	1.78	0.467	1.366	1.912
4	☑	-X	Forze statiche	0.00	4.90	2.03	3.55	1.45	1.78	1.04	1.78	0.413	1.230	1.721
5	☑	+Y	Uniforme	0.00	2.80	2.22	2.98	0.87	1.27	0.62	1.27	0.802	1.460	2.044
6	☑	+Y	Forze statiche	0.00	3.14	2.46	3.12	0.95	1.38	0.68	1.38	0.786	1.452	2.032
7	☑	-Y	Uniforme	0.00	2.84	2.12	2.63	0.88	1.39	0.63	1.39	0.762	1.574	2.204
8	☑	-Y	Forze statiche	0.00	3.19	3.19	2.89	0.96	1.85	0.69	1.40	0.999	1.925	2.036
9	☑	+X	Uniforme	77.75	4.02	5.14	4.65	1.19	2.44	0.85	1.73	0.645	2.051	2.033
10	☑	+X	Uniforme	-77.75	4.07	4.54	3.36	1.20	1.33	0.86	1.33	0.892	1.101	1.541
11	☑	+X	Forze statiche	77.75	4.34	5.79	4.66	1.29	1.29	0.92	1.29	0.644	1.003	1.403
12	☑	+X	Forze statiche	-77.75	4.47	5.65	3.71	1.32	1.21	0.95	1.21	1.265	0.911	1.275
13	☑	-X	Uniforme	77.75	4.37	2.64	3.22	1.29	1.86	0.92	1.86	0.604	1.435	2.009
14	☑	-X	Uniforme	-77.75	4.39	2.17	3.48	1.30	1.77	0.93	1.77	0.494	1.361	1.905
15	☑	-X	Forze statiche	77.75	4.87	2.17	3.51	1.44	1.80	1.03	1.80	0.444	1.250	1.750
16	☑	-X	Forze statiche	-77.75	4.90	1.95	3.65	1.45	1.95	1.04	1.83	0.397	1.343	1.764
17	☑	+Y	Uniforme	115.21	2.85	2.16	3.04	0.88	1.27	0.63	1.27	0.768	1.440	2.016
18	☑	+Y	Uniforme	-115.21	2.77	1.40	3.14	0.86	1.33	0.62	1.06	0.529	1.543	1.716
19	☑	+Y	Forze statiche	115.21	3.20	2.23	3.17	0.96	1.77	0.69	1.44	0.703	1.839	2.085
20	☑	+Y	Forze statiche	-115.21	3.10	1.86	3.26	0.94	1.59	0.67	1.38	0.610	1.691	2.059
21	☑	-Y	Uniforme	115.21	2.87	2.77	2.63	0.89	1.27	0.64	1.27	0.966	1.426	1.996
22	☑	-Y	Uniforme	-115.21	2.81	1.59	2.87	0.88	1.39	0.63	1.18	0.587	1.585	1.889
23	☑	-Y	Forze statiche	115.21	3.23	3.09	2.94	0.97	1.89	0.69	1.55	0.955	1.939	2.224
24	☑	-Y	Forze statiche	-115.21	3.16	2.44	3.15	0.95	1.75	0.68	1.25	0.778	1.835	1.836

Table 4-61: Percentage of the walls and of the building that is damaged at the end of the analysis 16 (X direction). The walls are in order from the most damaged to the less damaged.

Wall	% of wall damaged	% of building damaged
7	21.4	4.5
2	15.3	3.8
4	13.7	0.7
5	6.1	0.4
6	3.4	0.8
1	0	0
3	0	0
8	0	0
9	0	0
10	0	0

Table 4-62: Interstorey displacement at the final step of analysis 16 (X direction). The highest interstorey drift is in the wall 2 (front façade) at the third level.

Parete principale	Nodo sotto	Nodo sopra	Spostamento relativo [cm] ▽	Livello	Pareti interessate
2	3	4	0.93	3	1-2
7	27	28	0.87	3	1-7
6	7	8	0.83	3	1-6
2	2	3	0.74	2	1-2
10	41	42	0.73	2	8-10
6	6	7	0.72	2	1-6
7	26	27	0.68	2	1-7
7	25	26	0.40	1	1-7
2	1	2	0.38	1	1-2
6	5	6	0.36	1	1-6
10	40	41	0.33	1	8-10

Table 4-63: Displacements of the nodes of the left end of the wall 2 at the last step of analysis 16 (X direction).

Node	Ux [cm]	Uy [cm]	Uz [cm]	Rot X [rad]	Rot Y [rad]	Interstorey displ [cm]	Interstorey height [cm]	Interstorey drift
1	0	0	0	0	0			
2	-0.38	0	-0.16	0	-0.0014	-0.38	390	0.10%
3	-1.12	-0.01	-0.27	0	-0.0021	-0.74	390	0.19%
4	-2.05	-0.01	-0.37	0	-0.0027	-0.93	377	0.25%
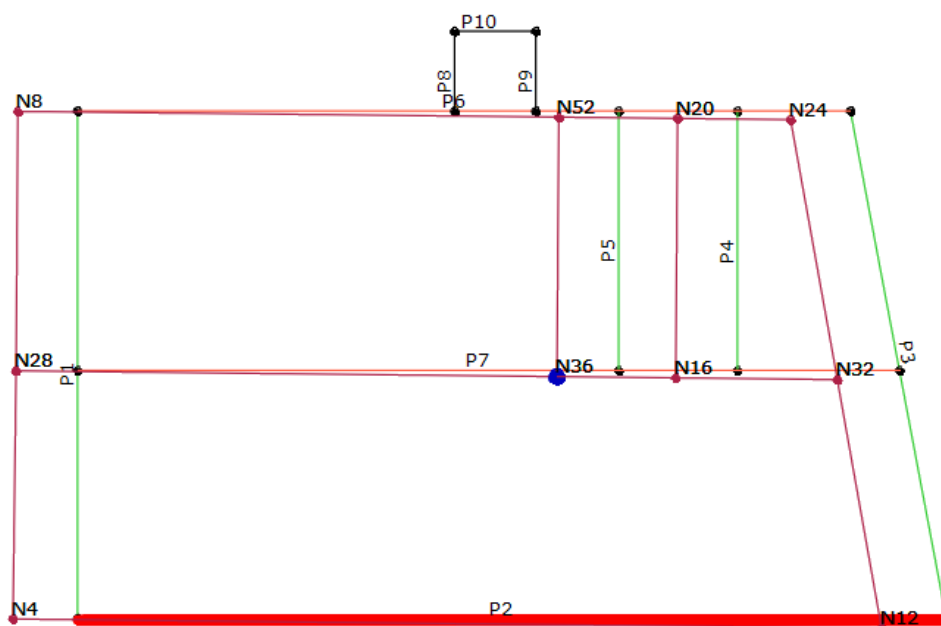
Figure 4-145: Deformed shape at the last step of analysis 16, at the third level (deformation scale 10).

The deformed shape of the most damaged wall, wall 7, is shown in Figure 4-146, where it can be seen that the majority of the piers are plastic for compression-bending interaction or for shear, some are collapsed and some spandrels are collapsed too. In the figure it is clear that the critical point of the building is the large opening on the right, at the ground floor.
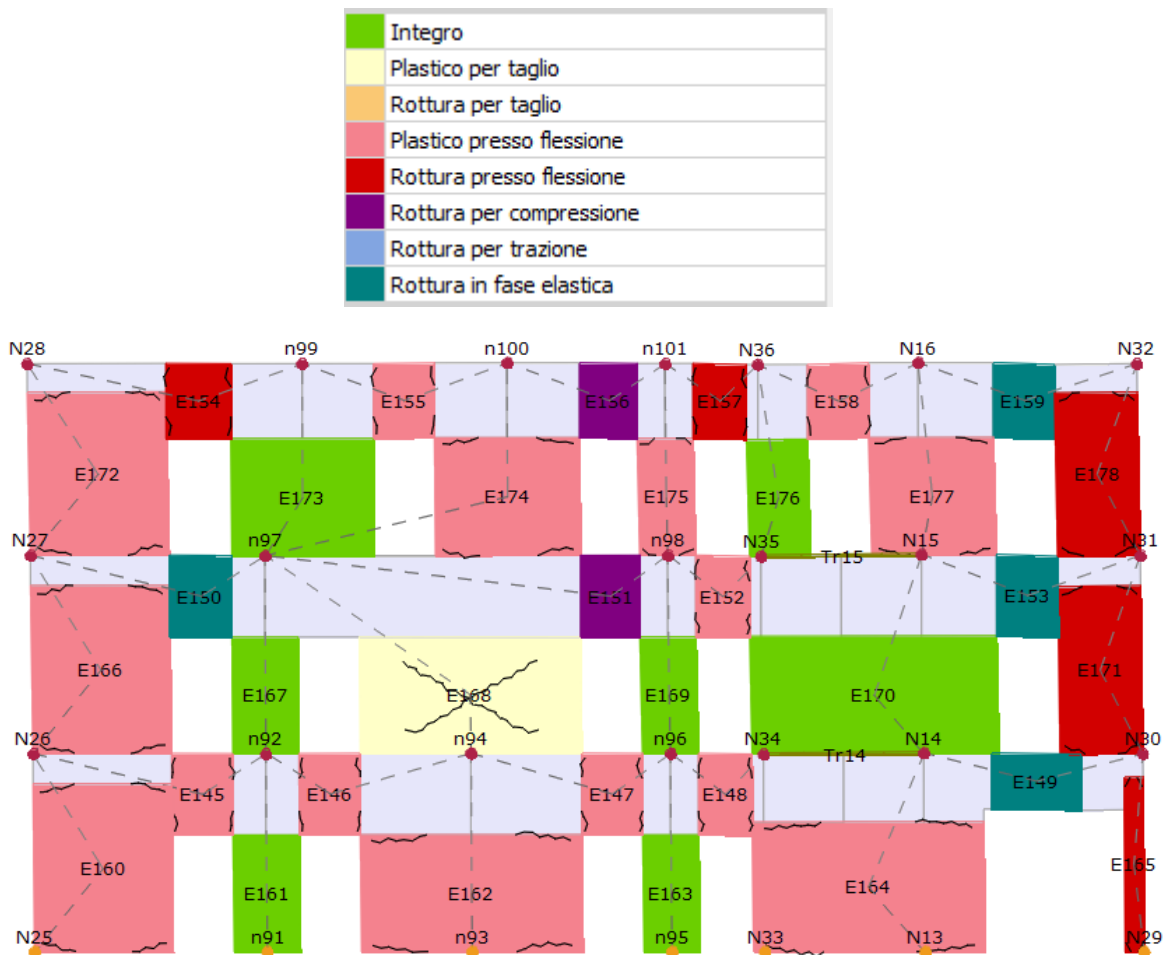
Figure 4-146: Wall 7 at the last step of analysis 16 (X direction). Above, colour legend with the specification of the type of damage (from the software 3Muri, in Italian): Non-damaged, Shear plasticity, Shear collapse, Flexural plasticity, Flexural collapse, Compression collapse, Tension collapse, Collapse in elastic phase.

Pushover curve of the analysis 16 is reported in Figure 4-147, with the capacity of the building and the bilinearization.
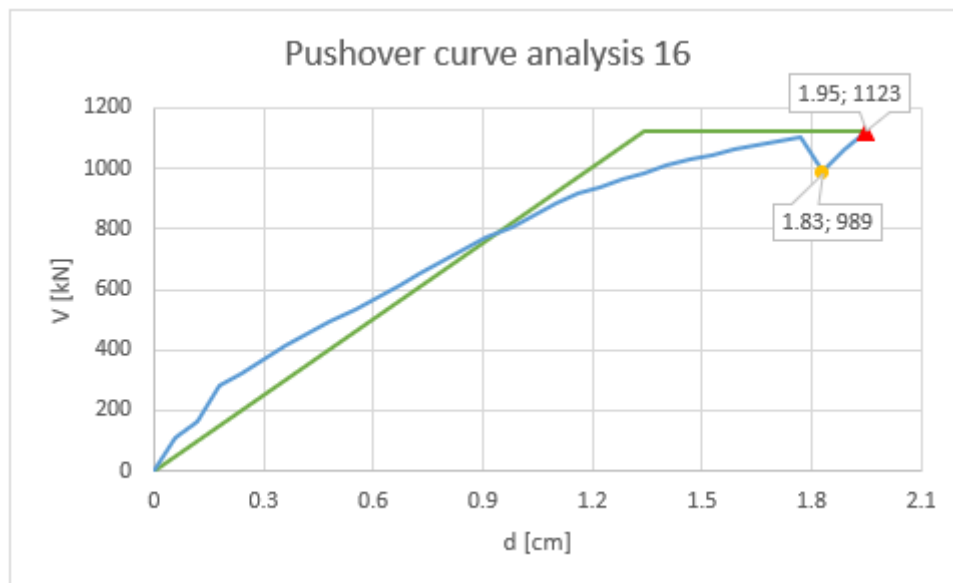
Figure 4-147: Pushover analysis nr. 16 (X direction). The red triangle indicates the SLV capacity, that in this case coincides with the DLS capacity. The yellow dot is the OLS capacity of the building. Also the bilinearization of the curve is shown.

In Y direction the worse analysis is the nr. 18. In this case the most damaged wall is wall 1, with 37.8% of the wall damaged (3.8% of the building - Table 4-64). The maximum interstorey displacement in the same analysis is the one at the ground floor of the model in the wall 1 – 2.85 cm = 0.0285 m. As the first level has an interstorey height of 3.90 m, the interstorey drift is 0.73 % (see Table 4-65 and Table 4-66), that is a high value for a shear plastification, but as it can be noticed from the deformed shape of the plan of the building in Figure 4-148, a noticeable torsion occurs during the pushover analysis, so that the drift of the control joint (1.4 cm/(390+390+377)cm =0,00121=0.12%) is much lower than the drift of the left corner of the building (3.09 cm/1157 cm = 0.00267 = 0.27%).

Table 4-64: Percentage of the walls and of the building that is damaged at the end of the analysis 18 (Y direction).

Wall	% of wall damaged	% of building damaged
1	37.8	3.8
5	24.2	1.4
4	21.0	1.1
7	11.1	2.3
2	0	0
3	0	0
6	0	0
8	0	0
9	0	0
10	0	0

Table 4-65: Interstorey displacement at the final step of analysis 18 (Y direction). The highest interstorey drift is in the wall 1 (left side façade) at the first level.

Parete principale	Nodo sotto	Nodo sopra	Spostamento relativo [cm]	Livello	Pareti interessate
1	1	2	2.85	1	1-2
8	37	38	1.62	1	6-8
9	43	44	1.36	1	6-9
5	33	34	1.09	1	5-7
4	13	14	0.69	1	4-7
3	22	23	0.24	2	3-6
3	21	22	0.23	1	3-6
4	14	15	0.16	2	4-7
3	23	24	0.16	3	3-6
5	34	35	0.15	2	5-7
9	44	45	0.14	2	6-9
8	38	39	0.14	2	6-8
4	15	16	0.13	3	4-7
5	35	36	0.13	3	5-7
1	3	4	0.13	3	1-2
1	2	3	0.11	2	1-2

Table 4-66: Displacements of the nodes of the left end of the wall 1 at the last step of analysis 18 (Y direction).

Node	Ux [cm]	Uy [cm]	Uz [cm]	Rot X [rad]	Rot Y [rad]	Interstorey displ [cm]	Interstorey height [cm]	Interstorey drift
1	0	0	0	0	0			
2	-0.58	2.85	-0.06	-0.0001	0.0003	2.85	390	0.73%
3	-0.61	2.96	-0.11	-0.0001	0.0007	0.11	390	0.03%
4	-0.59	3.09	-0.18	-0.0001	0.0003	0.13	377	0.03%
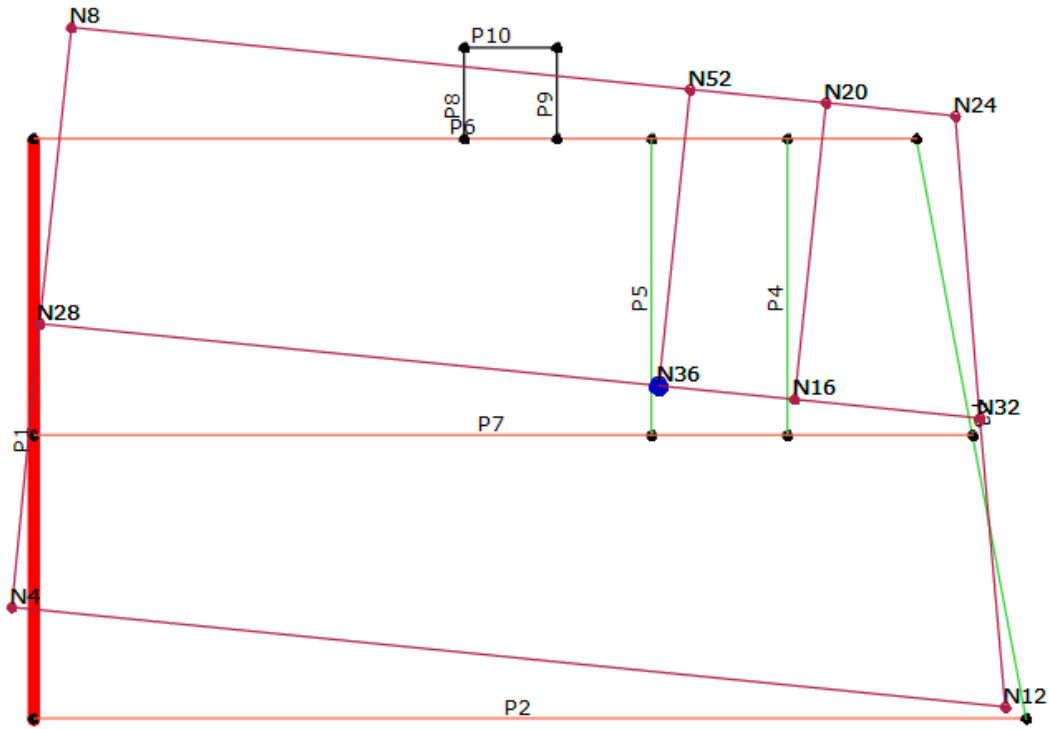
Figure 4-148: Deformed shape at the last step of analysis 18, at the third level (deformation scale 10).

The deformed shape of the most damaged wall, wall 1, is shown in Figure 4-149, where just the ground floor is damaged and the pier is plastic for shear, while the upper levels are undamaged. The great percentage of damage is due to the fact that the wall has no openings and thus the area of the pier is huge.
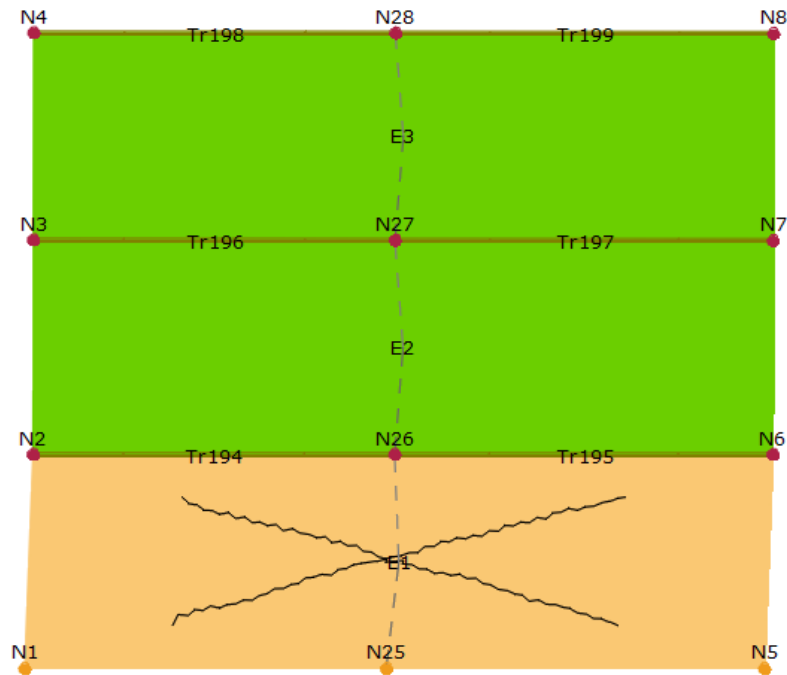
Figure 4-149: Wall 1 at the last step of analysis 18 (Y direction). Ground floor plastic for shear.

Pushover curve of the analysis 18 is reported in Figure 4-150, with the capacity of the building (LLS, DLS and OLS) and the bilinearization.
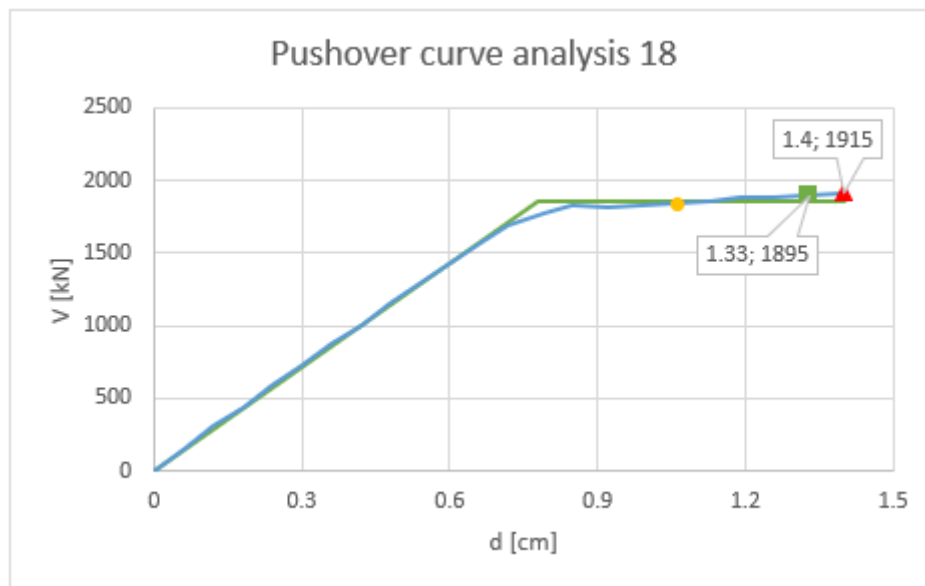
Figure 4-150: Pushover analysis nr. 18 (Y direction)

The lowest vulnerability indices for the global analyses of the building are the ones in Table 4-67. The global analysis has shown that the building is good at resisting Serviceability limit states (DLS and OLS), as the lowest vulnerability index is 0.911, but has some problems at LLS, especially in X direction (index 0.397). This is due to the great amount of openings in the walls in X direction.

Table 4-67: Vulnerability indices for the global analyses of the building (minimum in each direction).

direction	α LLS	α DLS	α OLS
X	0.397 (nr. 16)	0.911 (nr. 12)	1.275 (nr.12)
Y	0.529 (nr. 18)	1.426 (nr. 21)	1.716 (nr. 18)

Single wall analysis

Pushover analyses have been carried out also on the single wall, as the slabs are wooden and not rigid enough to distribute the horizontal forces to the walls proportionally to their stiffness. The results are shown in Table 4-68.

Table 4-68: Results of the pushover analyses performed on each wall. Dmax is the demand displacement, Du is the ultimate capacity displacement. The analyses highlighted in red are "not verified" and the ones in green are "verified". The yellow analysis is the most severe. The software is in Italian language, so that a small legend is needed: Parete = Wall, Nodo = control joint, Dir.sisma= Direction of the load, Carico sismico= Load pattern, SLV = LLS, SLD = DLS and SLO = OLS.

Parete	N.	Inserisci in relazione	Nodo	Dir. sisma	Carico sismico	Dmax SLV [cm]	Du SLV [cm]	q* SLV	Dmax SLD [cm]	Du SLD [cm]	Dmax SLO	Do SLO [cm]	α SLV	α SLD	α SLO
1	1	☑	4	+	Uniforme	0.71	3.00	0.76	0.26	2.40	0.19	1.74	2.623	6.781	7.357
1	2	☑	4	+	Forze statiche	0.87	2.40	0.77	0.31	1.32	0.23	1.32	2.025	3.972	5.397
1	3	☑	8	-	Uniforme	0.71	3.00	0.76	0.26	2.40	0.19	1.74	2.623	6.781	7.357
1	4	☑	8	-	Forze statiche	0.87	2.40	0.77	0.31	1.32	0.23	1.32	2.025	3.972	5.397
2	1	☑	4	+	Uniforme	5.41	7.01	3.33	1.60	2.70	1.14	1.86	0.901	1.683	1.623
2	2	☑	4	+	Forze statiche	6.06	7.25	3.53	1.79	2.58	1.28	1.80	0.850	1.436	1.402
2	3	☑	12	-	Uniforme	5.14	6.94	3.31	1.52	2.71	1.09	1.81	0.906	1.783	1.664
2	4	☑	12	-	Forze statiche	5.80	7.12	3.49	1.72	2.59	1.23	1.75	0.860	1.510	1.426
3	1	☑	24	+	Uniforme	0.82	2.94	0.86	0.29	2.34	0.22	1.68	2.346	6.018	6.422
3	2	☑	24	+	Forze statiche	0.97	3.24	0.86	0.35	2.58	0.26	1.92	2.309	5.883	6.391
3	3	☑	12	-	Uniforme	0.82	3.00	0.86	0.29	2.10	0.22	1.74	2.379	5.529	6.583
3	4	☑	12	-	Forze statiche	0.97	3.24	0.86	0.35	2.64	0.26	1.92	2.306	5.985	6.383
4	1	☑	16	+	Uniforme	3.34	5.91	2.53	0.99	2.28	0.71	2.15	1.187	2.294	3.037
4	2	☑	16	+	Forze statiche	3.68	5.97	2.81	1.09	3.57	0.78	2.09	1.068	3.275	2.687
4	3	☑	20	-	Uniforme	3.12	5.16	2.10	0.95	2.99	0.68	1.64	1.429	3.150	2.421
4	4	☑	20	-	Forze statiche	3.52	5.27	2.33	1.04	3.11	0.75	1.46	1.290	2.978	1.966
5	1	☑	36	+	Uniforme	2.87	5.55	1.48	0.91	1.97	0.65	1.97	1.876	2.176	3.045
5	2	☑	36	+	Forze statiche	3.32	5.68	1.69	0.99	2.10	0.71	2.10	1.705	2.119	2.966
5	3	☑	52	-	Uniforme	2.90	4.90	2.17	0.90	2.86	0.64	1.75	1.381	3.180	2.725
5	4	☑	52	-	Forze statiche	3.28	5.02	2.48	0.98	2.98	0.70	1.58	1.211	3.037	2.250
6	1	☑	8	+	Uniforme	3.09	0.06	46.90	0.92	0.06	0.65	0.06	0.021	0.065	0.091
6	2	☑	8	+	Forze statiche	3.42	0.06	57.29	1.01	0.06	0.72	0.06	0.017	0.059	0.083
6	3	☑	24	-	Uniforme	8.13	7.26	2.84	2.41	2.66	1.72	1.70	0.893	1.106	0.985
6	4	☑	24	-	Forze statiche	9.06	7.69	3.01	2.68	2.54	1.92	1.70	0.848	0.948	0.884
7	1	☑	28	+	Uniforme	2.81	5.04	2.69	0.87	1.74	0.62	1.14	1.114	1.997	1.831
7	2	☑	28	+	Forze statiche	3.23	5.88	3.13	0.96	1.62	0.69	1.08	0.957	1.680	1.568
7	3	☑	32	-	Uniforme	3.53	4.85	2.29	1.04	2.85	0.75	1.82	1.312	2.730	2.439
7	4	☑	32	-	Forze statiche	3.87	5.52	2.38	1.14	2.42	0.82	1.64	1.263	2.119	2.002

The worst wall appears to be wall 6. Most of the walls, analysed by themselves, are entirely verified for all three limit states. Just wall 2, wall 6 and wall 7 are not verified (wall 2 and wall 7 just for LLS, while wall 6 for all three limit states). The lowest vulnerability indices are reported in Table 4-69.

Table 4-69: Vulnerability indices for the wall analyses of the building (minimum in each direction).

direction	α LLS	α DLS	α OLS
X	0.017 (wall 6)	0.059 (wall 6)	0.083 (wall 6)
Y	1.068 (wall 4)	2.119 (wall 5)	1.966 (wall 4)

It can be noticed that wall 6 alone is very vulnerable, while if the whole building is considered (in the global analysis previously discussed), wall 7 is more damaged. The main problem of wall 6 are the spandrels, that collapse for compression. A critical point is also the large opening at the ground floor for the entrance to the building. The deformed shape of the wall at the last step of the analysis and the pushover curve of the same analysis are shown in Figure 4-151 and Figure 4-152 for wall 6 and in Figure 4-153 and Figure 4-154 for wall 4. Pushover curves of all the walls can be seen in Figure 4-155, where it is clear which walls are stiffer and stronger and which have more openings.

It can be noticed that the building is more vulnerable in X direction, the long side of the building, as all the openings are in this direction. The walls in Y direction are verified and have no problems. The building in X direction, if just the single wall is checked, is capable of resisting just 1.7% of the seismic demand for the LLS, 5.9% for DLS and 8.3% for OLS, considering the code

response spectra of ordinary buildings (reference life 50 years). In the analyses the out of plane kinematics are not considered. The capacity in this case is very low, but it should be noted that all the other walls, also in X direction, are not in such a bad condition. Just wall 2 and wall 7 (just for one analysis) are not verified for LLS. All the rest of the building is able to resist the code seismic actions. A retrofitting solution should thus focus on those 3 walls and their openings. Especially the huge entrance, that is like a tunnel in the building, should be retrofitted in order to not become a critical point in case of a seismic event.
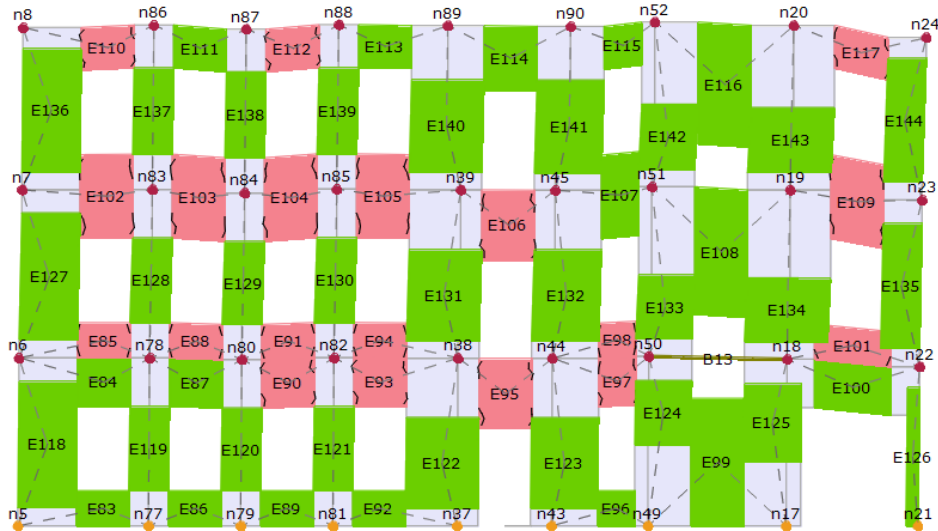
Figure 4-151: Wall 6 at the last step of the analysis 2.
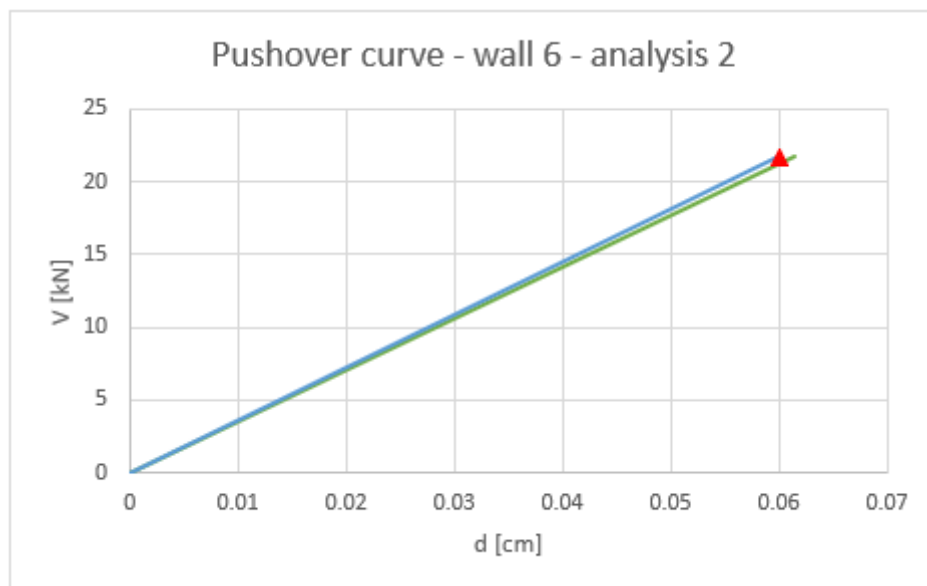
Figure 4-152: Pushover curve of the wall 6, analysis 2 (positive direction, static forces)
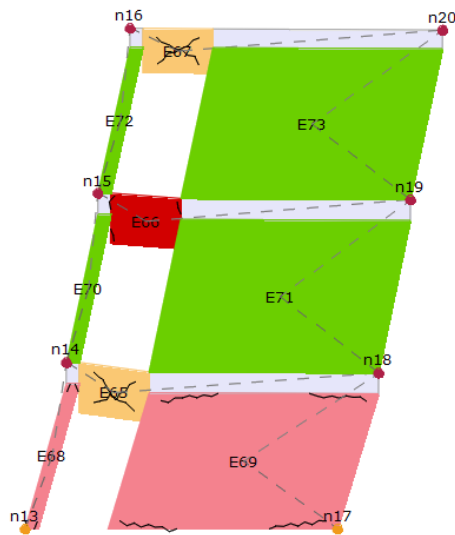
Figure 4-153: Wall 4 at the last step of the analysis 2.
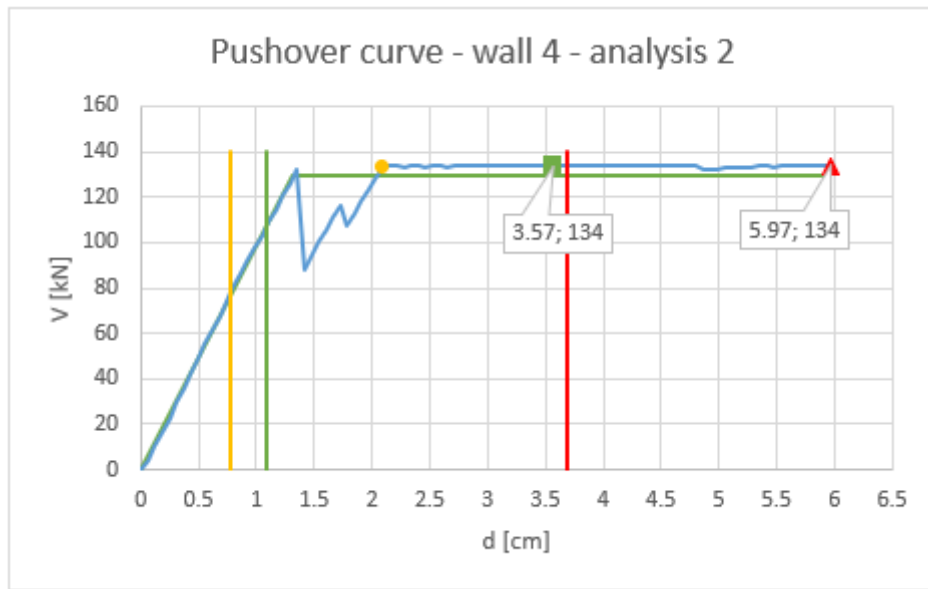
Figure 4-154: Pushover curve of the wall 4, analysis 2 (positive direction, static forces).
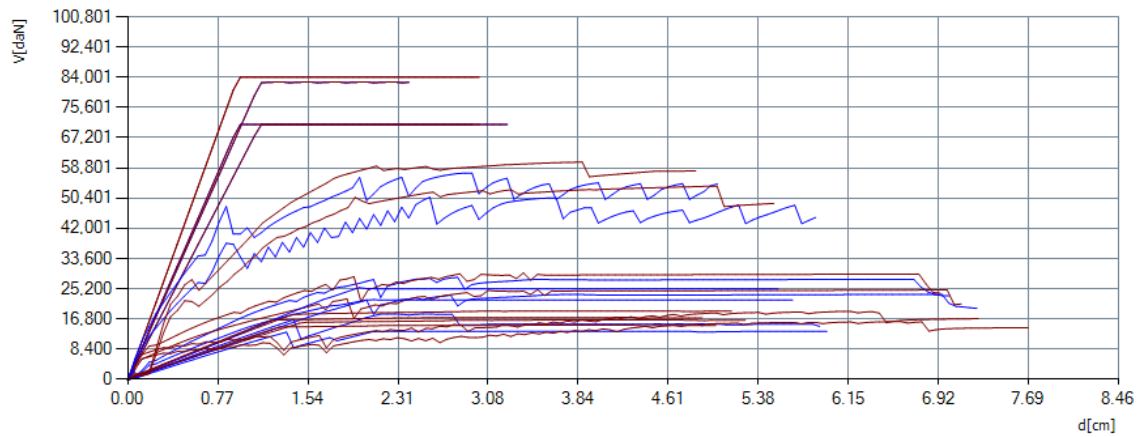
Figure 4-155: Pushover curves of all the walls (4 analyses/wall). The highest group of curves are related to the full facades in Y direction (wall 1 and 3), the group of curves in the middle are related to wall 7 (X direction) and the lowest group of curves is related to all the other walls in X and Y direction.

4.5.2.2. *Vulnerability evaluation based on simulated scenario response spectra*

As discussed in §2.2, the PSHA method, used by the codes, is not the only one that can be used to evaluate the seismic action in the site of interest. SPBSHA allows to calculate realistic scenarios of earthquakes in the site of interest. For this case study, the same scenarios considered for Masonry building A, are chosen to check the seismic vulnerability of the building: Medea and Idrija.

The pushover curves of the building remain the same, but the demand is calculated based on the scenario response spectra. The minimum seismic vulnerability indices for the analyses of the single walls are reported in Table 4-70. With the exception of the 50th percentile, for which Idria seems to be slightly more demanding, for the other percentiles the demand of the two scenarios are comparable, but Medea is slightly more burdensome.

Table 4-70: Minimum vulnerability indices for each wall with the scenario seismic input.

Minimum vulnerability indices - MEDEA 50				Minimum vulnerability indices - MEDEA 84				Minimum vulnerability indices - MEDEA 95			
Wall	α LLS	α DLS	α OLS	Wall	α LLS	α DLS	α OLS	Wall	α LLS	α DLS	α OLS
1	3.848	2.715	2.727	1	3.006	2.121	2.13	1	2.452	1.73	1.737
2	5.13	2.566	1.79	2	3.341	1.671	1.166	2	2.375	1.188	0.829
3	4.159	3.7	3.066	3	3.072	2.816	2.265	3	2.701	2.387	1.991
4	3.581	2.073	1.373	4	2.369	1.371	0.893	4	2.004	1.16	0.77
5	3.156	1.682	1.434	5	2.147	1.135	0.946	5	1.798	0.957	0.791
6	0.051	0.051	0.051	6	0.034	0.034	0.034	6	0.029	0.029	0.029
7	2.362	1.427	0.935	7	1.633	0.981	0.646	7	1.348	0.814	0.534

Minimum vulnerability indices - IDRIA 50				Minimum vulnerability indices - IDRIA 84				Minimum vulnerability indices - IDRIA 95			
Wall	α LLS	α DLS	α OLS	Wall	α LLS	α DLS	α OLS	Wall	α LLS	α DLS	α OLS
1	2.848	2.01	2.018	1	2.239	1.58	1.586	1	1.718	1.212	1.217
2	2.683	1.342	0.936	2	1.98	0.99	0.691	2	1.679	0.84	0.586
3	3.119	2.769	2.3	3	2.539	2.205	1.872	3	1.968	1.718	1.451
4	3.183	1.885	1.199	4	2.395	1.473	0.96	4	2.082	1.3	0.804
5	3.021	1.576	1.307	5	2.36	1.243	1.021	5	2.08	1.103	0.906
6	0.047	0.047	0.047	6	0.037	0.037	0.037	6	0.033	0.033	0.033
7	2.373	1.358	0.905	7	1.812	1.06	0.707	7	1.572	0.944	0.622

The check of demand and capacity for code and scenario spectra is presented in ADRS format in Figure 4-156 and Figure 4-157 for wall 4, the worst wall in Y direction.
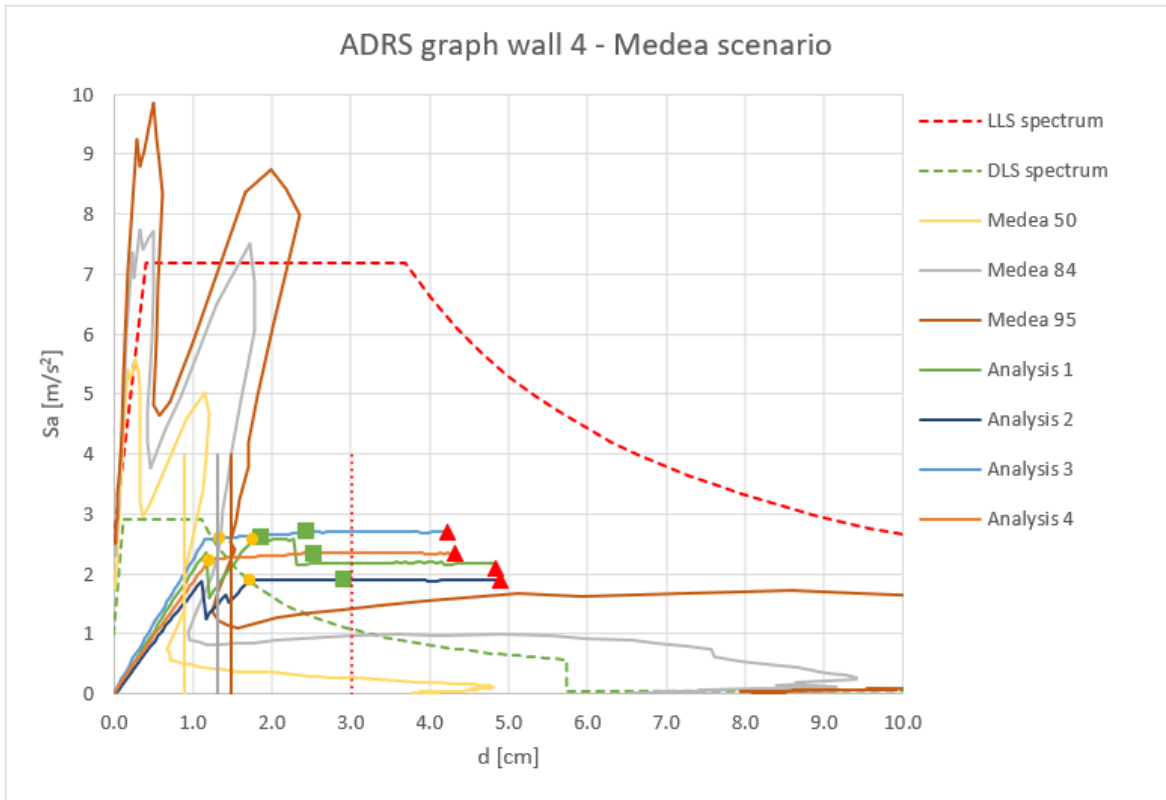
Figure 4-156: Pushover curves and response spectra in ADRS format for Medea scenario -wall 4. The coloured dots on the pushover curves indicate the capacities of the building for three limit states (LLS, DLS and OLS), while the vertical lines show the displacement demand of the response spectra for analysis 2. The vertical line has the same colour of the spectrum to which it belongs.
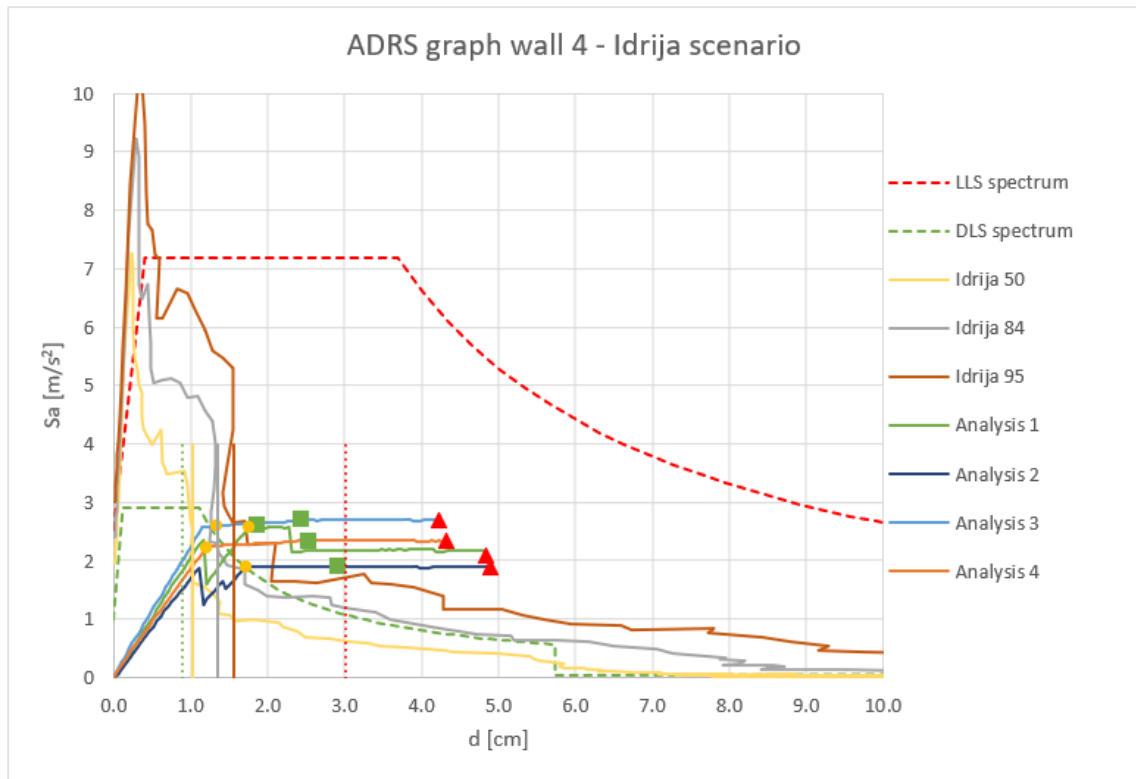
Figure 4-157: Pushover curves and response spectra in ADRS format for Idrija scenario -wall 4. The coloured dots on the pushover curves indicate the capacities of the building for three limit states (LLS, DLS and OLS), while the vertical lines show the displacement demand of the response spectra for analysis 2. The vertical line has the same colour of the spectrum to which it belongs.

As done for the code response spectra, also the scenario demands are checked for the global analysis of the building too. The results are summarised in Table 4-71, for each scenario and main direction of the building. The most burdensome analyses for LLS are also checked graphically in ADRS format in Figure 4-158 and Figure 4-159 for Medea scenario and in Figure 4-160 and Figure 4-161 for Idrija scenario. It should be mentioned that the results in the figures are the ones obtained for analysis 16 and 18 only, while the vulnerability indices in Table 4-71 summarize all the lowest indices for each main direction, where for example one analysis could have the lowest index for LLS, but another analysis could have the lowest index for another limit state.

Table 4-71: Minimum vulnerability indices for each main direction of global analysis with the scenario seismic input. The indices for all the limit states of the same direction are not necessarily the result of the same analysis.

Min vulnerability indices - MEDEA 50			
Direction	α LLS	α DLS	α OLS
X	2.266	1.272	1.272
Y	0.989	0.981	0.800

Min vulnerability indices - MEDEA 84			
Direction	α LLS	α DLS	α OLS
X	1.636	0.908	0.908
Y	0.692	0.688	0.56

Min vulnerability indices - MEDEA 95			
Direction	α LLS	α DLS	α OLS
X	1.217	0.733	0.733
Y	0.561	0.56	0.454

Min vulnerability indices - IDRIJA 50			
Direction	α LLS	α DLS	α OLS
X	1.169	0.785	0.785
Y	1.071	1.023	0.866

Min vulnerability indices - IDRIJA 84			
Direction	α LLS	α DLS	α OLS
X	0.923	0.619	0.619
Y	0.798	0.776	0.645

Min vulnerability indices - IDRIJA 95			
Direction	α LLS	α DLS	α OLS
X	0.750	0.511	0.511
Y	0.679	0.663	0.549

Figure 4-158: Pushover curves and response spectra in ADRS format for Medea scenario - global analysis 16. The coloured dots on the pushover curve indicate the capacities of the building for three limit states (LLS, DLS and OLS). In this case DLS coincides with LLS, so that just LLS is reported. The vertical lines show the displacement demand of the response spectra and they have the same colour of the spectrum to which they belong.
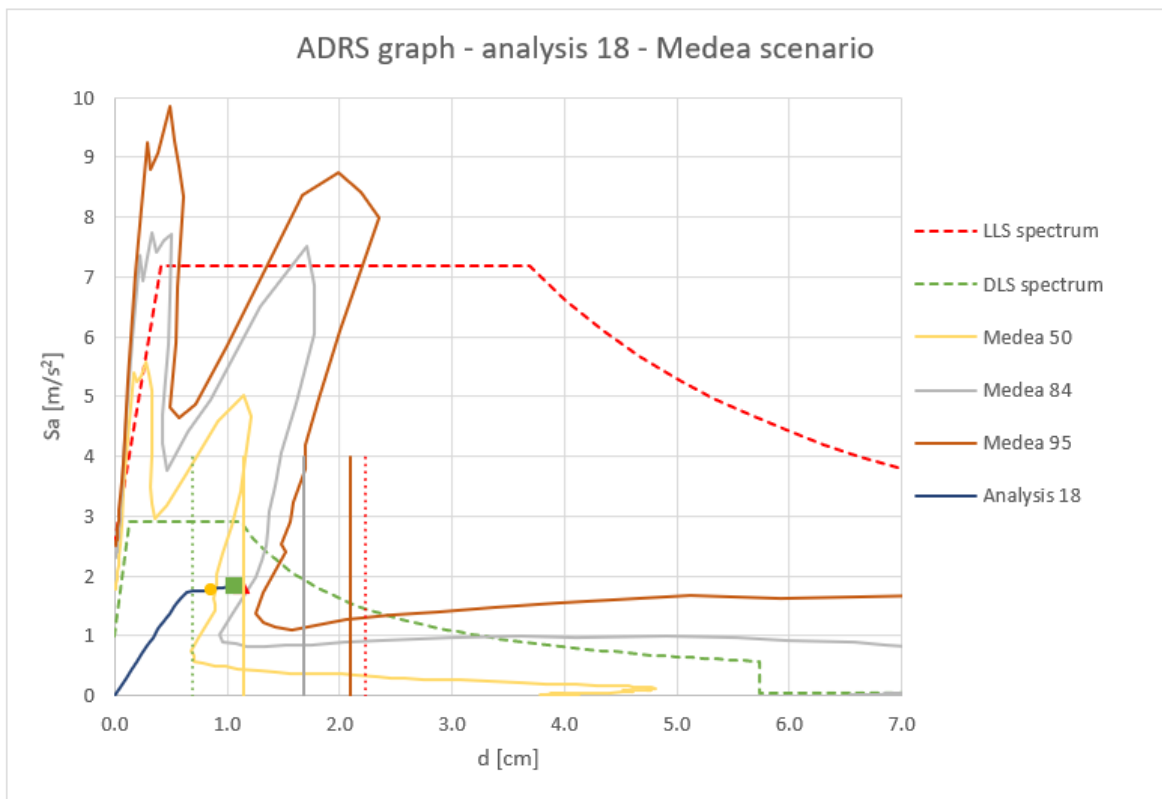
Figure 4-159: Pushover curves and response spectra in ADRS format for Medea scenario – global analysis 18. The coloured dots on the pushover curve indicate the capacities of the building for three limit states (LLS, DLS and OLS). The vertical lines show the displacement demand of the response spectra and they have the same colour of the spectrum to which they belong.
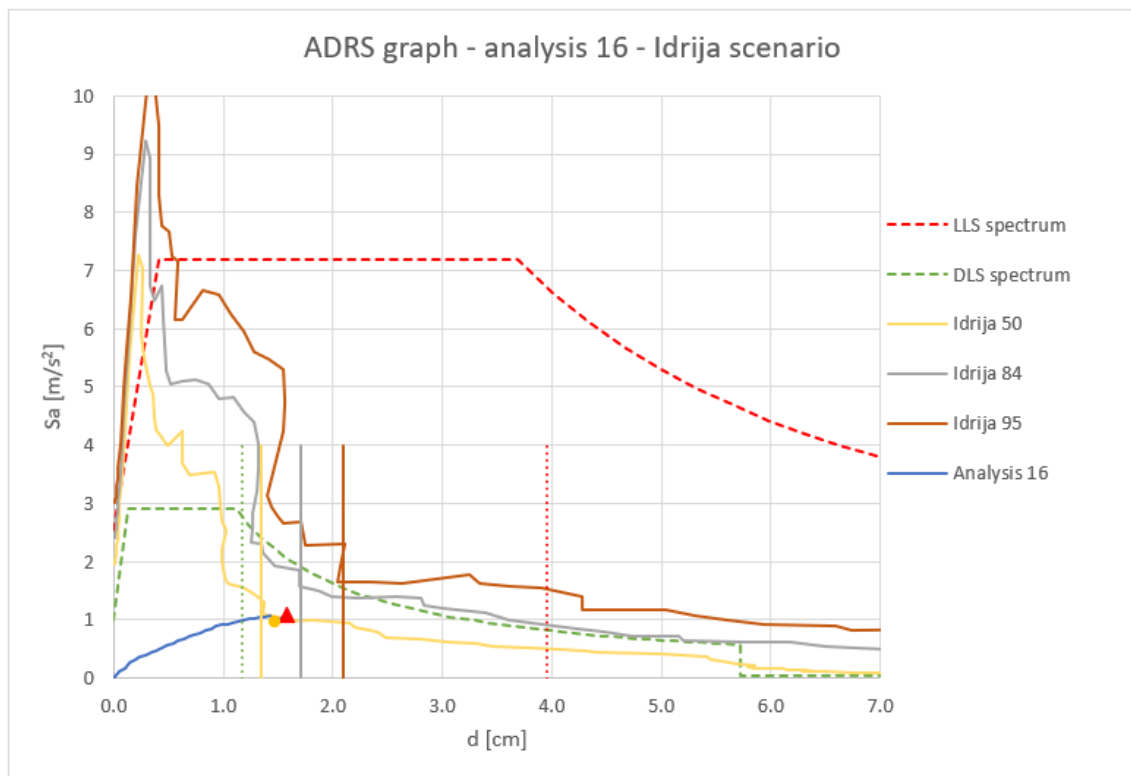
Figure 4-160: Pushover curves and response spectra in ADRS format for Idrija scenario - global analysis 16. The coloured dots on the pushover curve indicate the capacities of the building for three limit states (LLS, DLS and OLS). In this case DLS coincides with LLS, so that just LLS is reported. The vertical lines show the displacement demand of the response spectra and they have the same colour of the spectrum to which they belong.

211
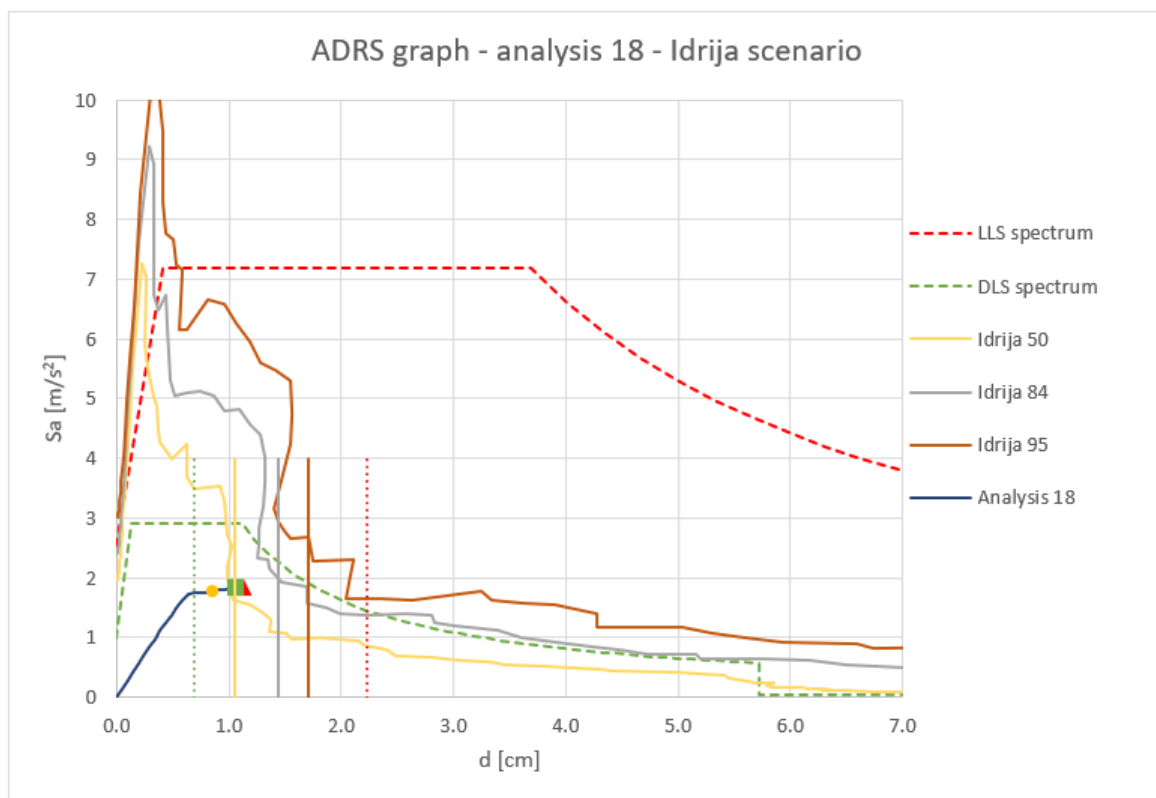
Figure 4-161: Pushover curves and response spectra in ADRS format for Idrija scenario – global analysis 18. The coloured dots on the pushover curve indicate the capacities of the building for three limit states (LLS, DLS and OLS). The vertical lines show the displacement demand of the response spectra and they have the same colour of the spectrum to which they belong.

4.5.2.3. Conclusions about the comparison between PSHA and SPBSHA seismic demands

If the lowest vulnerability indices with the scenario input in both directions (X and Y) are compared to the indices found with code spectra, it can be noticed that the demands are very similar. The weakest wall is wall 6 (in X direction). In Y direction the walls are totally verified with code spectra, but they have more demand from scenarios. In both Medea and Idrija scenarios, the walls of the stairwell (wall 4 and 5) are not verified for OLS and in some cases DLS, but they are always ok for LLS, so that it can be deduced that, on the contrary of the case of Masonry building A, the scenarios are more demanding than the code. The reason could be the great dependence that the scenario response spectra have on the period. As the scenario spectra are not smoothed, they can have some minimum right at the fundamental period of the investigated building and thus result in a low demand, but, as in reality, they can have a high demand for a building that has a slightly different fundamental period. For this reason, the best choice, in case of pushover analysis, should be to check both seismic inputs and, especially when designing new structures or retrofitting solutions, select the worse scenario.

As already noticed for Masonry building A, although Medea has a lower maximum magnitude compared to Idrija (Mw, max for Medea is 6.5, while for Idrija is 6.8), it is closer to Gorizia (the minimum distance from Idrija fault is about 35 km, while Medea is just 15 km away from the town) and thus represents an equal or higher hazard for the town.

4.5.3. Vulnerability evaluation and retrofitting solutions

As it has been noticed from the results of the analyses, the main weakness of this building is the number of openings in X direction. The retrofitting solution should be focused on the walls in X direction, wall 6 in particular, but also wall 7 and wall 2, and it could consist in steel ring-frames around the openings that increase the stiffness and resistance of the wall.

5. INNOVATIVE SEISMIC RETROFITTING STUDY

The analysed buildings, especially the reinforced concrete ones, have shown a very brittle behaviour. For this reason, an initial theoretical study has been carried out in order to find a suitable retrofitting solution for them. Traditional retrofitting solutions (reinforcement of RC nodes, columns and beams) are not suitable in this case, as the adaptation of the existing building to the current seismic demand is not achievable and they are very invasive. Exoskeletons have been thus considered and studied, but this solution has some weaknesses too, so that an innovative improvement has been proposed, making use of a sliding system at the base of the existing building, combined with a dissipative exoskeleton. The retrofitting solution has been investigated initially with a Single Degree of Freedom (SDOF) system, then with a 2D frame (Multi degree of freedom - MDOF system). It has not been yet applied to the case-study buildings, but this is the aim of future research and it is expected that the proposed solution could be extended to 3D structures, once the exoskeleton systems are optimally designed along the two principal directions of the hybrid structure to retrofit, achieving an effective retrofit of the existing building, with no damage expected.

Figure 5-1: Retrofit of an existing RC building with an exoskeleton (figure reproduced from [72] under the terms and conditions of the Creative Commons Attribution (CC BY) license.

Many research studies have been dedicated to several techniques that may be suitable for different existing structures ([62]-[66]), and especially for RC buildings ([67]-[69]). The solutions with masonry infill walls [67] and with BRBs applied directly to the RC frame [68] are for sure very invasive. The building needs to be totally emptied in order to retrofit it, with the consequent need to relocate the occupants. A simplified design method has been proposed in [70] for the use of diagrid exoskeletons in RC frames. The use of diagrid exoskeletons allows to retrofit the buildings by working from outside, without relocate occupants, but the exoskeleton is meant to remain elastic and it creates a very stiff structure that can cause high seismic actions on the retrofitted building. An example of a retrofit intervention with an exoskeleton is visible in Figure 5-1. It should be coupled with a dissipative system at the connections to the RC frame. In [71], the effects of the retrofit are investigated with a simplified model based on two coupled linear viscoelastic oscillators. Based on the "traditional" design concept of these exoskeletons, the optimal seismic retrofit of a given existing RC building derives from the mechanical interaction between weak and brittle RC members (through suitable links at the level of each floor) and a steel bracing system. The bracing system is typically characterized by high resistance, ductility and high dissipative capacity, which leads to the realization of a seismic efficient, hybrid steel-RC structure ([72][73]). Due to the specific features of the RC building itself (element dimensions, rebars, geometry and masses) and to the characteristics of the steel system (stiffness, stiffness ratio between storeys, type of diagonals, resistance), the behaviour of the hybrid system can vary markedly.

5.1. Parametric investigation on a SDOF system

The aim of this research is to investigate how the response of the hybrid RC-steel system changes based on the variation of the characteristics of the exoskeleton. For this purpose, a Single Degree of Freedom (SDOF) model is first analysed. Based on a parametric study, some limit

conditions are explored. In particular, the in-plane seismic response of such a relatively simple mechanical model is examined and the analysis is separately conducted on:

- the RC building;
- the steel exoskeleton and
- the hybrid steel-RC assembly.

The steel exoskeleton and the RC building are modelled as rigid bars, connected between them with a rigid link and connected to the base through nonlinear rotational springs, as shown in Figure 5-2. The stiffness of the exoskeleton is K_1, plastic rotational resistance is M_1 and ductility μ_1. The RC building is actually modelled through three rigid bars that are connected by rotational nonlinear springs with initial rotational stiffness $K_2/2$ and yielding bending resistance $M_2/2$.

Until the springs are linear elastic, their constitutive law is given by:

$$M_i = K_i \varphi_i \tag{5.1}$$

where K_i and φ_i are the rotational stiffness and the rotation of each spring in Figure 5-2. The shear force sustained by each building component can be expressed as a function of the displacement δ:

$$R_i = \frac{K_i}{H^2} \delta \tag{5.2}$$

At the foundation level, the RC frame is equipped with a rigid restraint against possible rotations and vertical displacements. In order to analyse and improve the behaviour of the retrofitted structure, two additional translational springs, characterized by a linear elastic behaviour ("spring #3" in Figure 5-2), are introduced at the base of the building to represent the level of connection of the building to the ground. The stiffness of these springs can vary from $K_3 \to \infty$ (to represent a traditional fix based building) to $K_3 \to 0$, to represent the introduction of a sliding system at the base of the existing building, an innovative way to improve the performance of the retrofitting solution. The proposed sliding system is composed of planar steel-PTFE (polytetrafluoroethylene or commonly known as Teflon) bearings. This sliding system is simple, economic and insensitive to variations in frequency content of seismic excitations ([74]-[76]). The PTFE devices are placed at the base (or in the middle of the base columns) of the existing RC building to uncouple its motion from the ground motion and transfer all the seismic load to the steel exoskeleton, maximizing its efficiency and making the original building weakly stressed.
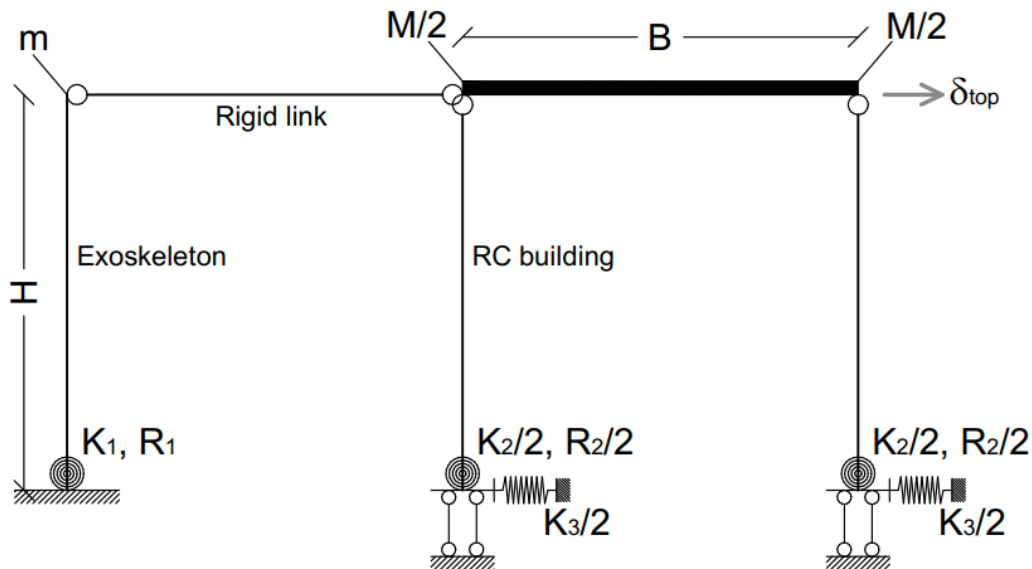
Figure 5-2: Reference model for the parametric analysis of the SDOF system, showing the RC building, the steel exoskeleton and the base sliding device. The circles at the top of the bars represent pinned connections.

The total mass is set in m and M for the exoskeleton structure and the RC frame, respectively. The mass of the RC frame is placed half at each end of the beam, as shown in Figure 5-2 ($M/2$). The constitutive laws of the used springs are shown in Figure 5-3. According to Figure 5-3 b), the nonlinear behaviour of the existing structure is characterized by limited ductility μ_2 of springs, as it is typical of existing RC structures, and by a brittle collapse mechanism.

For an optimal seismic retrofit of the building, and thus a maximization of the efficiency of the exoskeleton, it is usually expected that the ductility μ_1 of the steel structure is fully exploited by the hybrid structure. The latter one should result in a structure with enhanced ductility and dissipative capacity, compared to the initial existing RC frame, and thus have an improved capacity to withstand the imposed seismic loads.

From a seismic design point of view, the key dynamic parameters to account for the definition of input seismic loads are represented by the mass and stiffness of the structural components. These parameters also define the fundamental vibration period of structures: T_2 for the RC frame, T_1 for the independent steel exoskeleton and T_{TOT} for the hybrid system in which the steel bracing members fully interact with the RC building.

In the design of the retrofit intervention, T_{TOT} is thus responsible of possible variations in the seismic demand. The acceleration affecting the hybrid structure could be strongly sensitive to stiffness modifications and thus the variation of T_{TOT} could even increase the seismic demand.

(a)

(b)

(c)
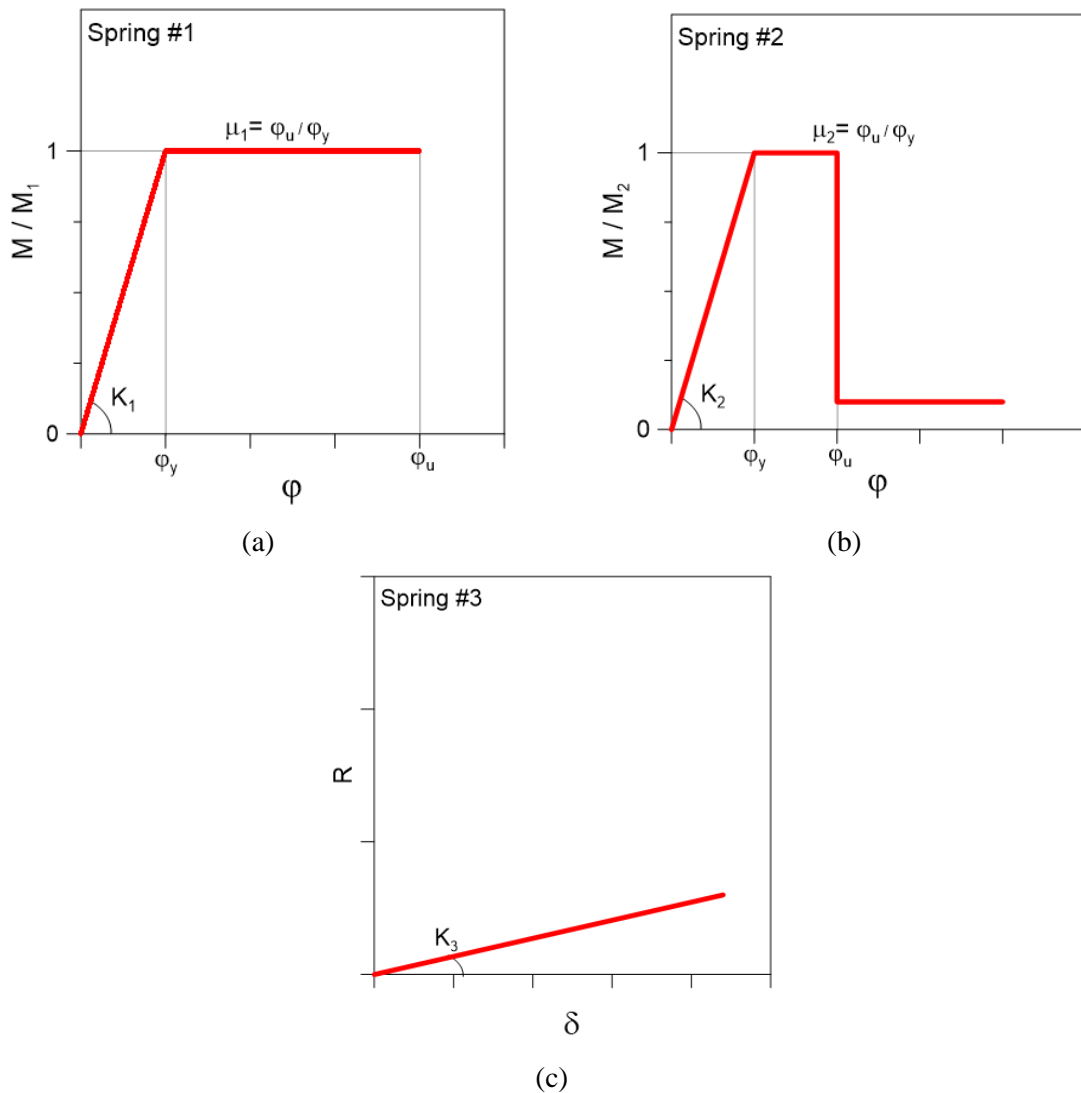
Figure 5-3: Constitutive laws of the used springs with the input mechanical properties: (a) steel exoskeleton, (b) RC building and (c) sliding system.

_____

      Among the possible combinations for the mechanical parameters in Figure 5-3, the attention of this paper is focused on some limit configurations for the examined system, and namely represented by:

- BLD: un-retrofitted building, with K_2 the stiffness, R_2 the resistance and $\mu_2=2$ its ductility ($K_3 \to \infty$);

- EXO-1: existing building ($K_3 \to \infty$), with an exoskeleton less rigid ($K_1= 0.5\ K_2$) but much more resistant ($R_1= 1.5\ R_2$) and ductile ($\mu_1= 7\ \mu_2$) than the building;

- EXO-2: existing building ($K_3 \to \infty$), with an exoskeleton much more rigid ($K_1= 10\ K_2$), but less resistant ($R_1= 0.75\ R_2$) than the RC building ($\mu_1= 7\ \mu_2$);

- EXO-3: hybrid RC-steel system with an additional coupled sliding system ($K_3 = 0$), where the steel exoskeleton has a given stiffness K_1, high resistance ($R_1= 1.2\ R_2$), and ductility μ_1 (to define based on the input seismic design loads, independently from the RC building mechanical characteristics). The additional advantage is represented by the introduction of a series of sliding devices at the base (or at the level of the 1st floor, in case of multi-storey buildings) of the RC columns, in order to achieve a coupled sliding-hybrid solution that can maximize the potential and the benefits due to the steel exoskeleton.

The above described configurations have been assessed with the support of nonlinear static analyses (push-over analyses), that were carried out in SAP2000.

The analysis of the parametric results is focused on the typical base-shear R / top displacement δ response of the systems, in order to assess their global in-plane lateral response. For sake of clarity, all the parametric estimates are proposed in non-dimensional form, as a function of the measured base shear R (compared to the RC frame shear resistance, R_2) at any instant of the analysis, and the corresponding top displacement δ of each building component. The latter is presented as a function of the lateral displacement leading the RC columns to the first yielding configuration, $\delta_{y,2}$. The attention is thus focused on the response of the RC frame, the steel exoskeleton and the hybrid system. The results are shown in Figure 5-4.

In Figure 5-4 a), the typical brittle response of the **BLD system** is proposed. Until the yielding configuration is achieved (P_1), the plot evidences a linear elastic response in the initial stage of the seismic event. The plastic response, and thus the overall ductility of the BLD structure, is relatively small, and the brittle collapse mechanism initiates at point P_2 and has null residual capacity (P_3).

The **EXO-1** solution represents the typical application of a steel bracing system that is expected to optimally react to the input seismic loads, given its limited (and thus positive) stiffness K_1 and relatively high resistance ($R_1/R_2= 1.5$), with large ductility ($\mu_1/\mu_2= 7$). As shown in Figure 5-4 b), however, a limit towards the potential benefits of such an exoskeleton is represented by the limited stiffness itself, compared to the original building. The stiffness of the exoskeleton alone can be clearly perceived from the 0-P_3 segment. As such, a direct effect is that the original stiffness of the BLD system is only minimally increased by the collaborating steel exoskeleton. This effect can be perceived from the segment 0-P_1, where:

$$K_{TOT} = K_1 + K_2 \tag{5.3}$$

and

$$R_{TOT} = R_2 + K_1 \delta_{y,2} \tag{5.4}$$

is the maximum resistance that can be achieved.

_____

The steel structure, due to the relatively low stiffness but high resistance, can sustain part of the input seismic loads, as shown by the segment P_1-P_2. Key mechanical parameters are in this case the stiffness that can be expected from the hybrid system:

$$K_{TOT} = K_1 \tag{5.5}$$

and the maximum resistance:

$$R_{TOT} = R_2 + K_1 \delta_{y,2} \mu_2 \tag{5.6}$$

Due to the limited stiffness, however, the potential plastic deformations and dissipative phenomena of the steel bracing system are activated only once the BLD structure is already collapsed. Even in presence of a residual stiffness and high ultimate resistance for the steel structure (P_3), the latter is not able to preserve the RC frame from a brittle collapse mechanism. Accordingly, the third stage of the overall seismic response starts at a lateral displacement:

$$\delta_{TOT} = \delta_{y,2} \mu_2 \tag{5.7}$$

and is characterized by a total stiffness that still equals the exoskeleton alone.

From a seismic design point of view, the EXO-1 retrofit intervention is thus not successful, and the hybrid assembly is still strongly sensitive to the initial BLD features. On the other hand, the increased initial stiffness of the hybrid assembly is associated to a reduction of the period of vibration of the system, T_{TOT}, thus in increased input seismic loads.

In **EXO-2** system a markedly high stiffness and a moderate resistance are assigned to the steel exoskeleton. The achieved response is shown in Figure 5-4 c). Compared to the original BLD system, it is possible to perceive that the hybrid solution can take strong benefit of the exoskeleton features, thus achieving a relatively higher stiffness (segment 0-P_1) and maximum resistance (R/R_2 ≈1.75), where:

$$R_{TOT} = R_1 + R_2 \tag{5.8}$$

It is however possible to see that the final result does not always preserve the RC building from a potential brittle collapse, thus vanishing the benefits due to the elasto-plastic steel members. The hybrid structure can work efficiently for limited deformations only (segment P_1-P_2). In order to ensure an optimal efficiency of the retrofit intervention, the exoskeleton itself must be over-designed, both for stiffness (K_1) and resistance (R_1) parameters. The resistance itself, accordingly, should be generally defined by taking into account a conservative input seismic load for design, and thus minimizing the potential risk of collapse. From P_0, the steel structure starts to dissipate part of the incoming energy, through plastic deformations, in support of the RC frame that has already achieved the yielding configuration.

In conclusion, the BLD system itself could be safe as far as the exoskeleton behaves linear-elastically only (segment 0-P_1), with obvious effects on the design of details and related costs. In terms of input seismic forces, such a stiffness increase corresponds to a marked reduction in the period of vibration T_{TOT} of the hybrid assembly, and thus in a corresponding increase of expected seismic demand for the composite structural system. The exoskeleton structure, accordingly, should be optimally designed to withstand this relevant increase of input seismic loads. Also in this case, as in the previous one, the possible plastic capacities of the exoskeleton cannot be exploited, due to the premature collapse of the RC frame.

Finally, the in-plane seismic response of the hybrid **EXO-3** system inclusive of coupled sliding devices for the RC columns is proposed in Figure 5-4 d). Compared to the previous retrofit solutions, the intrinsic advantage is that the BLD frame behaves as a fully isolated rigid body under seismic loads. Accordingly, the stiffness (segment 0-P_1) and resistance (P_1) parameters of the total hybrid assembly fully reflect the behaviour of the steel exoskeleton alone. In other words, the hybrid solution assumes the structural features (and thus benefits) of the steel exoskeleton.
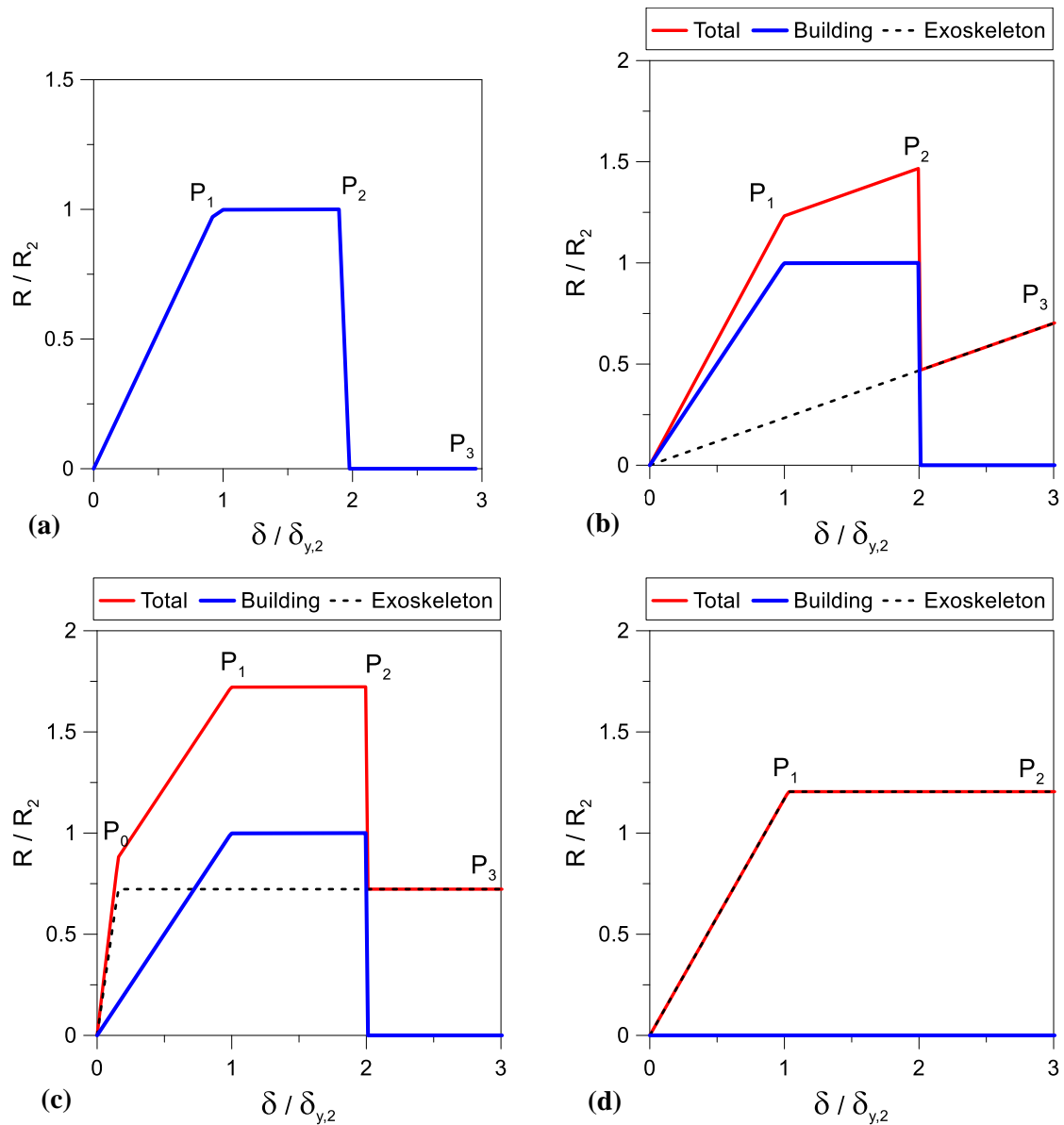
Figure 5-4: Shear-displacement response of BLD system (a), EXO-1 system (b), EXO-2 system (c) and EXO-3 system (d). P1 and P2 denote yielding and collapse of the RC frame, respectively, while P3 is the post-failure stage. P0 represents the yielding point of the steel exoskeleton. In (d) P1 denotes the yielding configuration for the exoskeleton / hybrid system, while P2 is the post-yielding stage.

In this context, it is clear that the steel structure should be optimally designed, based on the expected input seismic loads. At the same time, the sliding devices for the RC columns must be also optimized in the design of details. In general, the advantage of such an approach derives from the decoupled response of the base stiffness for the RC structure to retrofit. For this reason, the stiffness of the steel exoskeleton should be high enough to limit the lateral displacements due to the sliding system.

In these conditions, however, the overall design process can efficiently take advantage of the high ductility and plastic dissipation of the exoskeleton itself (segment P_1-P_2, in the example).

5.2. Analysis of a plane multi storey building

As a further attempt of validation and assessment of the proposed design concept, a plane multi-storey building is also investigated. In order to define the optimal configuration for the design of the key parameters for a steel exoskeleton applied to an MDOF system of an existing RC building, a multi-storey plane frame is analysed with SAP2000 computer software [38]. The RC frame is a

_____

two-bay, four-storey frame, with 5m wide spans and 3m high floors (R_{ck} 300 the resistance class for concrete and FeB44k for the steel reinforcement).

The frame members are loaded with a seismic combination of permanent and accidental vertical loads, that were taken into account during the seismic analysis of the structure, and in particular:

- G_1: dead loads of all the RC elements (automatically computed by the software);
- G_2= 26.12kN/m and Q_k= 8kN/m: additional distributed permanent and accidental vertical loads assigned to the RC beams (based on a slab with a 4m influence length).

The design detailing (beam and column sections and reinforcement details) are summarized in Table 5-1.

Table 5-1: Reference input features for the full-size multi-storey RC frame (SAP2000). Key for plastic hinges: h= hardening, φu= ultimate rotation (ASCE/SEI 41-13)

Floor	Columns			Beams		
	Section [cm^2]	Rebars	Plastic hinges	Section [cm^2]	Rebars at support	Plastic hinges
1st	65×45	4Φ14 + Φ6/15 stirrups	M3 + P-M2-M3 (h=1%, φ_u=4.86×10^{-3})	30×45	4Φ16 top + 0 bottom	M3 (h=1%, φ_u =20×10^{-3})
2nd	65×45	4Φ14 + Φ6/15 stirrups	P-M2-M3 (h=1%, φ_u =4.86×10^{-3})	30×45	4Φ16top + 0 bottom	M3 (h=1%, φ_u =20×10^{-3})
3rd	50×45	4Φ14 + Φ6/20 stirrups	P-M2-M3 (h=1%, φ_u =4.83×10^{-3})	30×45	4Φ16 top + 0 bottom	M3 (h=1%, φ_u =20×10^{-3})
4th	50×45	4Φ14 + Φ6/20 stirrups	P-M2-M3 (h=1%, φ_u =4.83×10^{-3})	30×45	4Φ16 top + 0 bottom	M3 (h=1%, φ_u =20×10^{-3})

For this planar MDOF model, five configurations have been investigated, namely consisting in three main different models and two additional models that are derived from MOD_02, where:

- MOD_00: is the existing fixed base RC frame;
- MOD_01: represents the RC frame connected to a traditional exoskeleton system (with steel members for the bracing system that yield simultaneously at different storey levels);
- MOD_02: the RC frame, with a cut at the base of the columns (for the installation of the sliding devices) and connected to a steel braced exoskeleton (in practice the sliding devices can be placed more easily in the middle of the base columns). Differing from MOD_01, the bracing members of the 1st floor are only expected to yield and a BRB (Buckling Restrained Brace) is proposed, while all the other steel members of the exoskeleton are expected to remain elastic and stiff under the

_____

imposed seismic loads. It is worth mentioning, for this design solution, that the plasticization of upper-floor diagonals does not allow to maximize the structural performance of the coupled system. The hyperstaticity of the hybrid structure and the congruence of floor displacements would in fact manifest in internal moments (and thus progressive damage) of the RC beams.

Two additional models (MOD_03 and MOD_04) are finally added to investigate how a possible high friction of the sliding devices could affect the retrofit solution:

- MOD_03: is the RC frame with sliding devices at the base, accounted for with a rigid-plastic link, with a yielding force calculated as the friction force for a high friction coefficient of 5%. Such RC frame is connected to the same steel exoskeleton of MOD_02 (just the bracing member of the 1st floor is expected to yield);
- MOD_04: represents the RC frame with sliding devices at the base, accounted for with a rigid-plastic link, with a yielding force calculated as the friction force for a friction coefficient of 10%, to simulate, on the safe side, the real behaviour of the sliding device (usually the friction coefficient is around 5%). Such RC frame is connected to the same steel exoskeleton of MOD_02 (just the bracing member of the 1st floor is expected to yield).

In the analysis, for the MOD_01, MOD_02, MOD_03 and MOD_04 solutions, the exoskeleton is connected to the RC frame by rigid links at the level of each storey. In the case of the MOD_02 solution, the sliding devices at the base of the RC building are introduced without any friction, in MOD_03 and MOD_04 the sliding devices are deeper investigated by considering that they can present different levels of static friction. For this reason, the constitutive law of the link representing the sliding device is characterized by a yielding force equal to the static friction force and a hardening of 1% representing a small kinetic friction. The exoskeleton is designed as a rigid pinned structure composed of HE450B columns and HE360B beams (S355 the resistance class). Additional bracing diagonals were separately calibrated for each one of the examined design solutions. In particular, in the case of MOD_01 (rigid base for the RC frame), a concentric X bracing steel system with dissipative zones in tension diagonals only is coupled with the RC frame. All diagonals are assumed to yield almost simultaneously, under the effects of a triangular-shaped in-plane lateral load. For this reason, the diagonals are designed to resist the shear forces at each storey, calculated for a linear static analysis of the frame. In this case-study example, among other possible solutions, the bracing diagonals are thus assumed with sections HEA180 at the 1st floor, HEA160 at the 2nd, HEA140 at the 3rd and HEA100 at the 4th floor respectively, considering only the tensile braces active.

In the case of MOD_02, MOD_03 and MOD_04, where the RC frame is cut at the base and sliding devices are introduced, the bracing system is composed of stiff X diagonal bracings at the 2nd, 3rd and 4th floor (2×HEA300), that do not buckle and remain elastic. At the level of the 1st storey, a single BRB diagonal (HEA120) is calibrated on the base of the input design seismic load. In this case, the bracing of the 1st storey gives the whole plastic behaviour of the hybrid structure, while the RC frame and the upper part of the steel brace remain elastic. An important intrinsic advantage of this hybrid system is that the ductility of the exoskeleton can be chosen independently from the characteristics of the existing RC building, that remains in every case undamaged until the collapse of the exoskeleton. In Table 5-2 the first three modes of each configuration are presented, with their periods of vibration and modal masses. The vibrational modes of MOD_03 and MOD_04 are not reported as they are very similar to MOD_02.

Figure 5-5 shows the deformed shape of MOD_01 and MOD_02. In MOD_01 the RC frame is deformed; its inter-storey drifts are due to the deformation of the exoskeleton and for this reason it can be damaged during an earthquake if the exoskeleton is less stiff. In MOD_02 the RC frame moves almost like a rigid body, as the exoskeleton is rigid in the upper storeys and concentrates all the deformation in the 1st (or ground) floor, where the RC frame is decoupled from the soil.

Nonlinear static (pushover) analyses have been carried out on the five models, with a triangular load pattern. The results are shown in Figure 5-6. The introduced red cross points highlight the collapse for the plastic hinges at the base of the 1st storey RC columns. In this regard, it is interesting to see that the base section of the RC columns (1st storey) collapses at the same amplitude of lateral displacement δ for the MOD_00 and MOD_01 solutions, although the resistance of the braced MOD_01 system is much higher. On the contrary, in MOD_02, no significant damage in the hinges of RC beams and columns is observed.

Table 5-2: First three modes of each FE model - periods of vibration and participating modal masses (SAP2000)

	Mode n°	Period [s]	Modal mass	Sum of modal masses
MOD_00	1	**0.469388**	0.774	0.774
	2	0.139137	0.135	0.908
	3	0.069277	0.055	**0.963**
MOD_01	1	**0.305313**	0.79234	0.79234
	2	0.099741	0.134	0.92635
	3	0.05326	0.05167	**0.97802**
MOD_02	1	**0.346573**	0.98557	0.98557
	2	0.09735	0.01428	0.99985
	3	0.052022	0.00003	**0.99989**

(a)   (b)
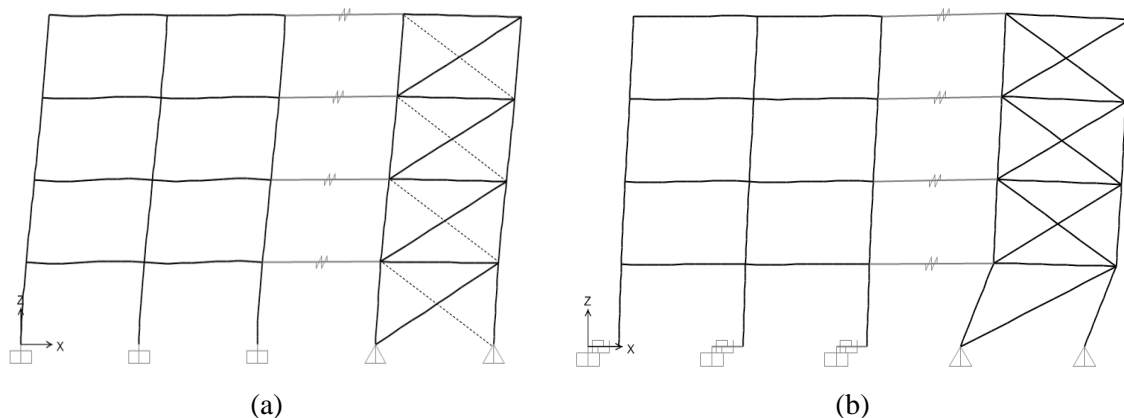
Figure 5-5: Deformed shape of the first mode in the (a) MOD_01 and (b) MOD_02 models (SAP2000)

In order to avoid the collapse of the hinges of the RC building, the solution of MOD_02 is then the most suitable and efficient. The overall resistance of the hybrid solution is significantly enhanced, compared to the un-retrofitted RC frame. At the same time also the ductility is increased and it can be estimated and compared to the RC frame alone in Figure 5-6 (a). In the same way, also the MOD_03 and MOD_04 solutions in Figure 5-6 (b) give similar results, although the sliding devices are accounted for with their real friction forces.

In all three cases with sliding devices, the RC frame is in fact subjected to almost null deformations and all the resistance and ductility of the retrofitted hybrid system are given by the braces of the 1st floor, that can be easily calibrated at the design stage and even replaced during the lifetime of the structure, in case of damage.

The seismic demand is efficiently transferred from the brittle RC members towards the steel assembly. The overall design benefit can be noticed at different levels. First, the RC building can in fact behave in the same way of a fully base-isolated system under a general input seismic event. At the same time, the steel exoskeleton itself can be optimally designed for the given design seismic loads, thus exploiting at best its resistance, ductility and dissipation capacities.

Figure 5-7 shows how the base shear is subdivided between the RC frame and the steel exoskeleton, for all the five numerical models, compared to the total seismic response of the system. Red cross symbols in Figure 5-7 (a) and (b) give evidence of collapse mechanisms at the base columns for the RC frame while the same symbols Figure 5-7 (c), (d) and (e) show the collapse in the ground floor steel brace of the exoskeleton (hybrid solution).

(a)

(b)
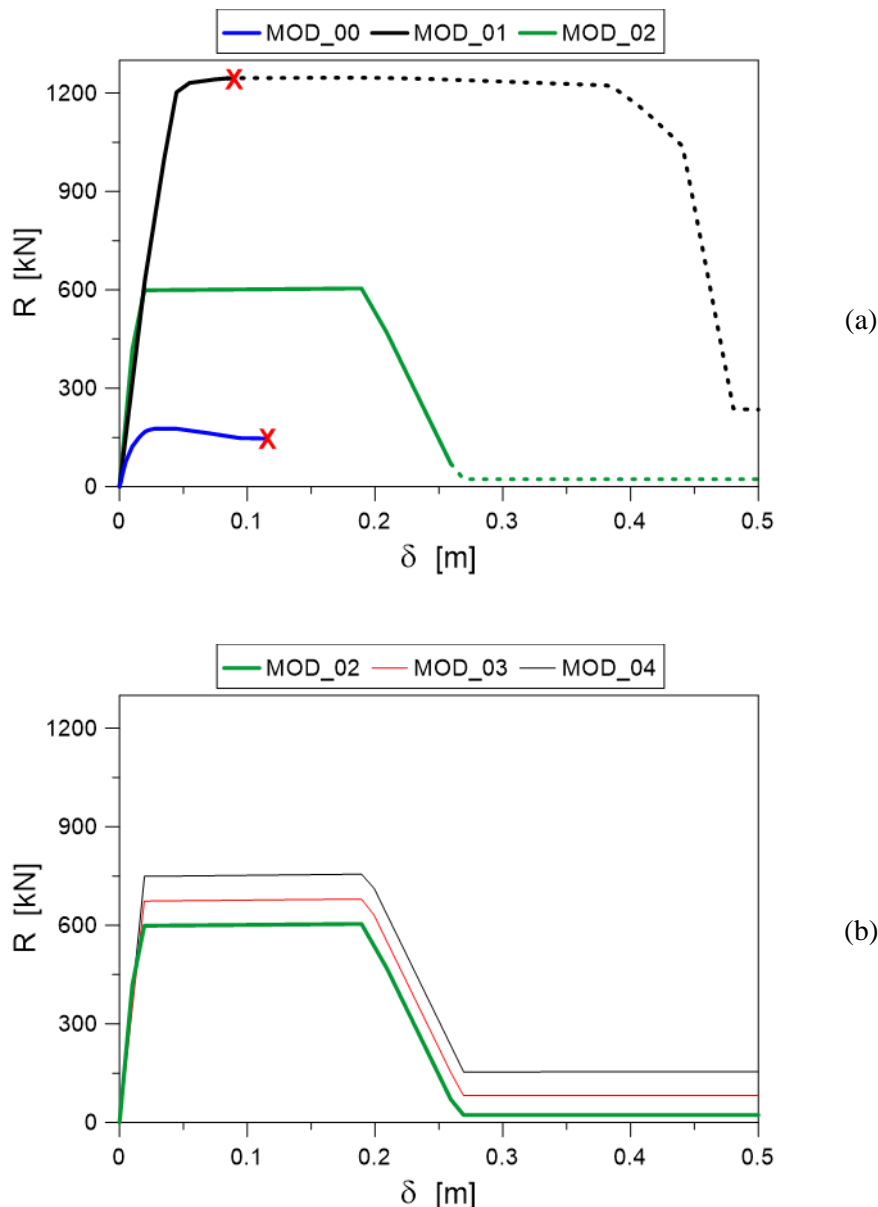
Figure 5-6: Push-over curves from the nonlinear static analyses (triangular load pattern): (a) analysis of MOD_00, MOD_01 and MOD_02, or (b) friction effects for the MOD_02, MOD_03 and MOD_04 models (SAP2000)

The collapse mechanisms of the analysed models can be seen in the following figures that show the deformed shape of the models at the last step of the nonlinear push-over analyses performed with SAP200. The coloured dots indicate the formation of plastic hinges, as described in the legend (the letters correspond to the points of the definition of plastic hinges).

_____

Figure 5-8 shows the behaviour at collapse for the RC frame alone. Besides the very low resistance (around 200kN) and limited displacement capacity of the structure, the overall collapse of the frame is governed by the plastic hinges at the base (level "E" in Figure 5-8 (b), thus beyond the "Collapse Prevention" performance limit). It is worth of interest that relevant damage can be noticed also for some RC beams (level "C", that still exceeds the "CP" limit). Figure 5-9 and Figure 5-10 show the behaviour at collapse of the other four models of the retrofitted structure.
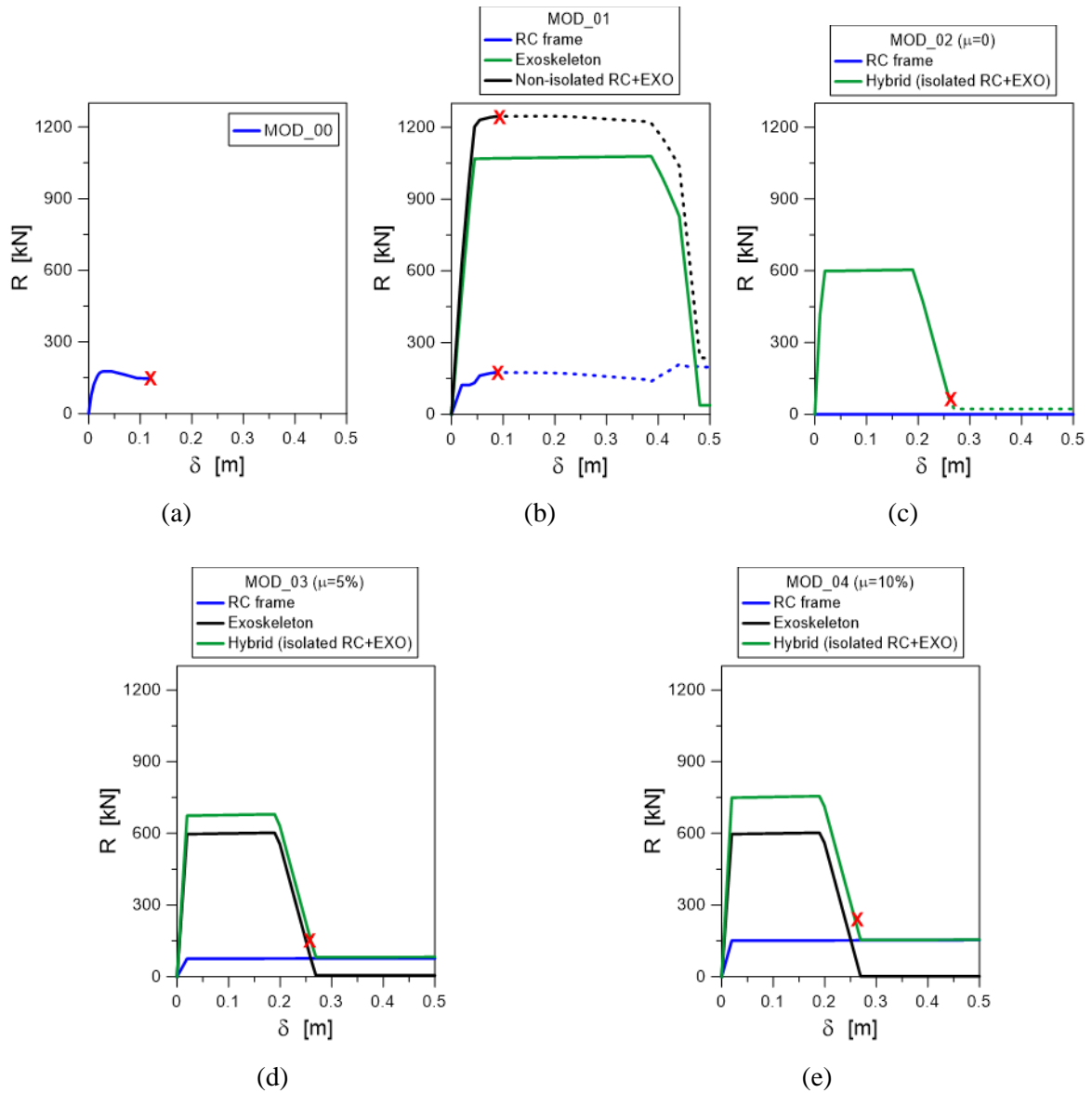
Figure 5-7: Push-over curves for (a) MOD_00; (b) MOD_01; (c) MOD_02; (d) MOD_03 and (e) MOD_04, with evidence of the global and component performance (SAP2000).

When the steel exoskeleton is first introduced for the fixed base RC frame, the MOD_01 collapse configuration can be seen in Figure 5-9 (a). Due to the high ductility of the bracing system, the in-plane deformation of the hybrid system causes the collapse of some of the plastic hinges in the beams of the RC frame ("C" level) and at the base section of the RC columns (level "E" for all the plastic hinges).

This is a strong limitation for the design of the steel structure. The total resistance of the hybrid system is high (more than 1200kN, as it can be seen in Figure 5-6, that is ≈6 times the RC

_____

_____

frame alone for the selected members), and suggests the potential capacity of the retrofitted structure to resist the input design seismic load. On the other hand, when the brace enters the plastic phase, the RC structure is already severely damaged.

On the contrary, in MOD_02, MOD_03 and MOD_04, when the base brace of the exoskeleton collapses, the RC frame has almost no damage, as it can be seen in Figure 5-9 (b) and Figure 5-10.

In case of MOD_02, it is possible to notice that the RC frame remains mostly elastic (just one hinge reaches level "B" corresponding to a slight activation of the plastic hinge, under the "Immediate Occupancy" limit). At the same time, the exoskeleton withstands all the input seismic loads, thus resulting in a total resistance that is in the order of ≈3÷4 times the un-retrofitted RC frame and a ductility that can be around 2÷3 times higher. Such an effect is mostly governed by the diagonal member at the base of the steel structure, whose axial force-horizontal displacement coincides with the push-over curve earlier presented in Figure 5-6. As the RC structure remains elastic, the base diagonal of the exoskeleton can be designed for even stronger seismic events and be easily changed in case the regulations during the lifespan of the structure change the input design horizontal forces. The rigid connections between the existing RC frame and the exoskeleton can be engineered with stiff steel elements.

(a)   (b)
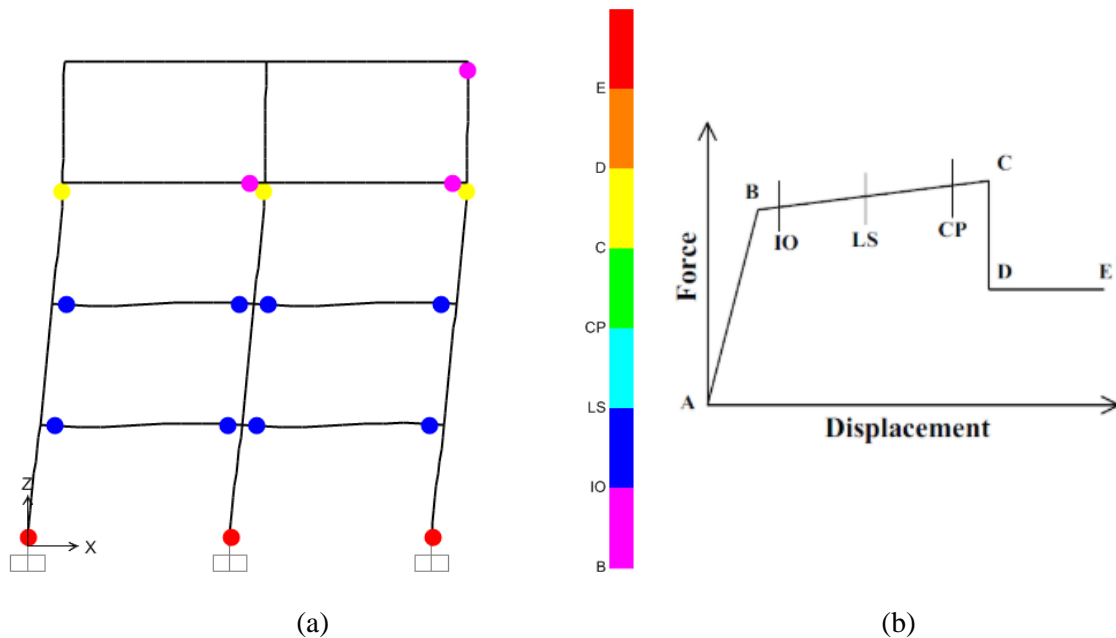
Figure 5-8: MOD_00: (a) deformed shape at the last step of the push-over analysis of the RC frame, with (b) general definition of plastic hinges (SAP2000), compared to "Immediate Occupancy" (IO), "Life Safeguard" (LS) and "Collapse Prevention" (CP) performance limits.

_____
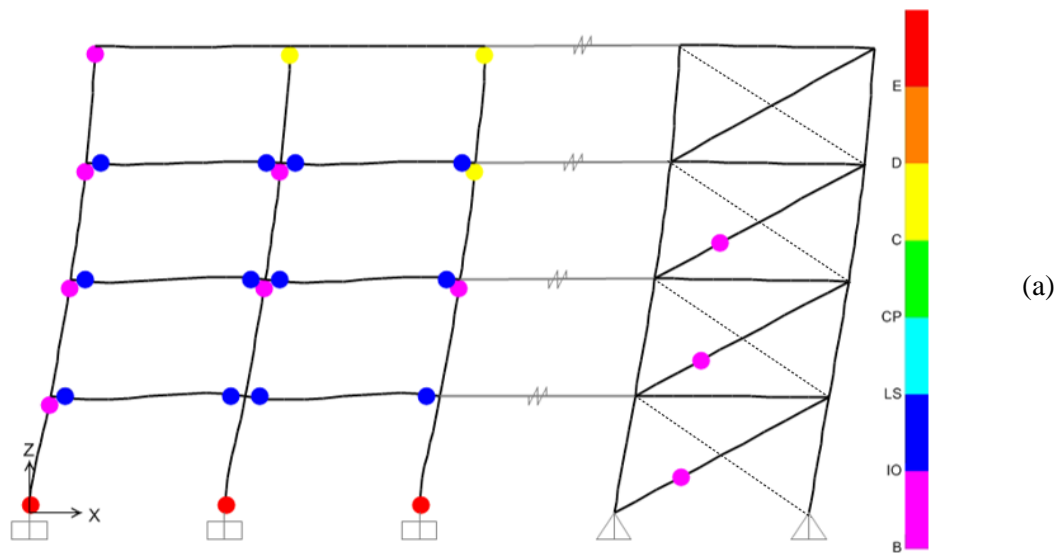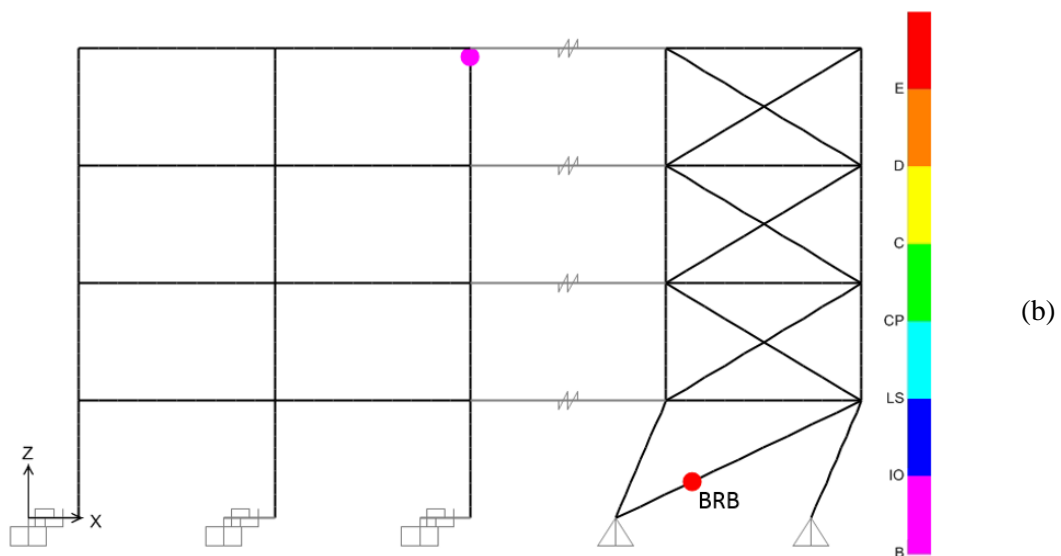
Figure 5-9: Deformed shape at the last step of push-over analysis for models (a) MOD_01 and (b) MOD_02 (SAP2000).
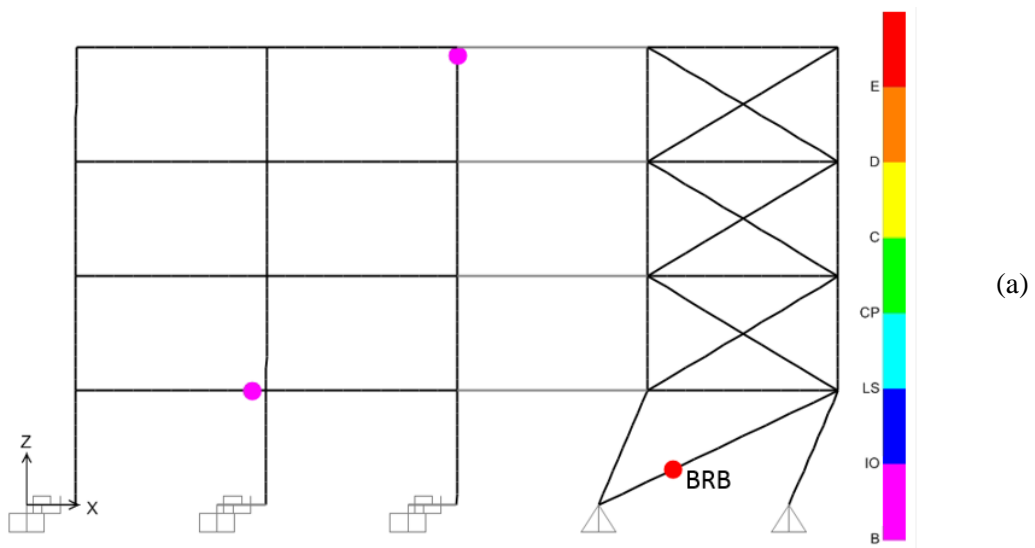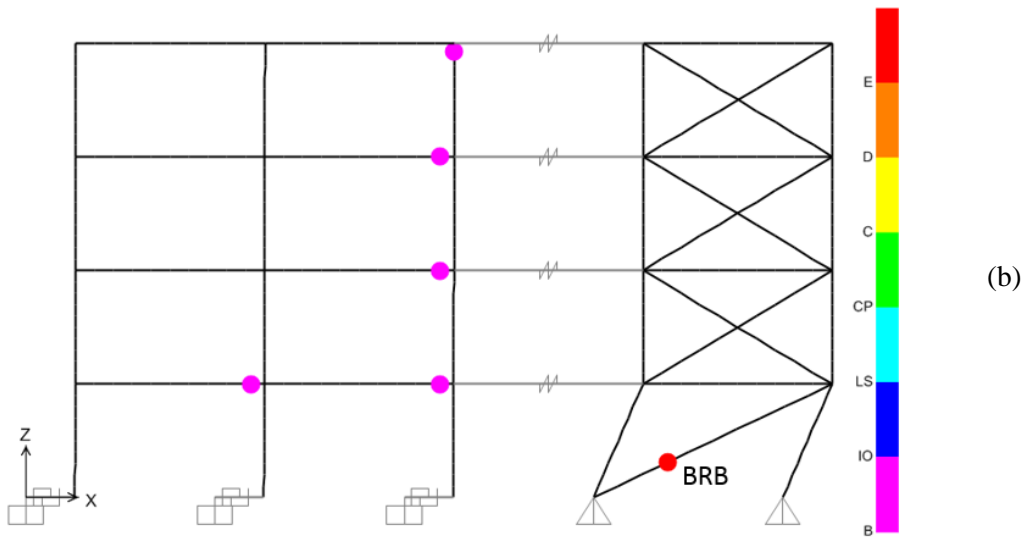
Figure 5-10: Deformed shape at the last step of push-over analysis for models (a) MOD_03 and (b) MOD_04 (SAP2000).

5.3. Design procedure

In order to draft a practical guideline for the design of the proposed hybrid solution (isolated RC frame + exoskeleton) some basic steps to follow are herein summarized. The overall design method is based on non-linear static analysis, in order to account for the non-linear behaviour of both the existing RC frame and the newly introduced steel exoskeleton. As a simple alternative, a design procedure that is based on linear analyses with the use of the exoskeleton' behaviour factor q is still possible, but not advisable, as it is always recommended to run a pushover analysis to check that all the elements behave as desired.
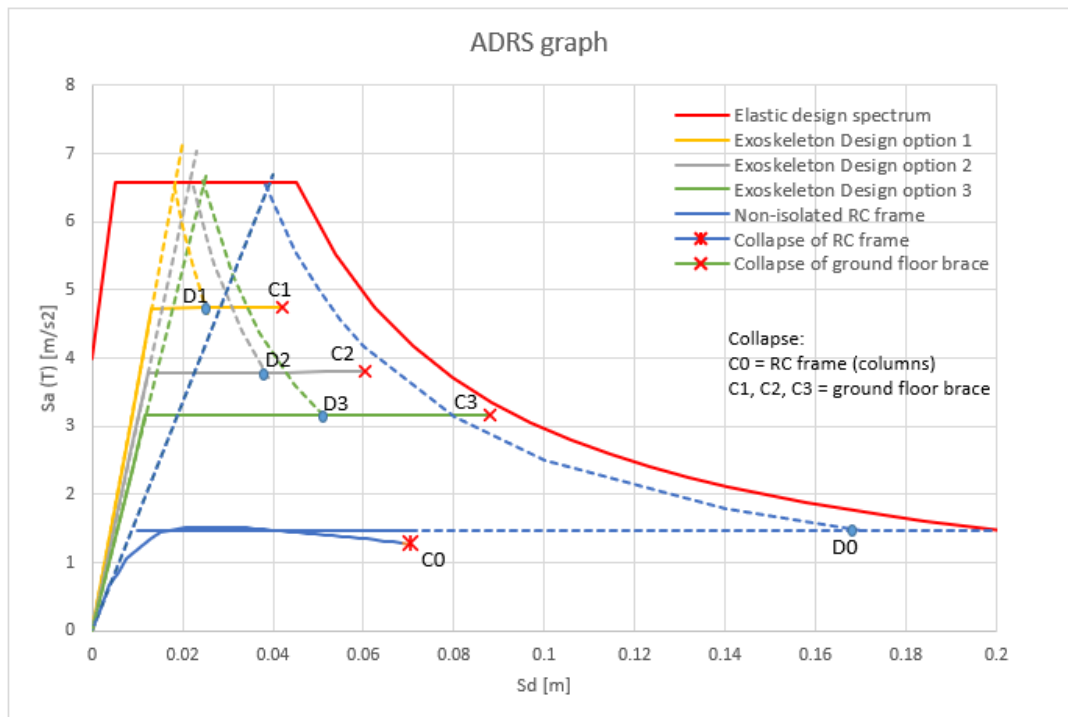
Figure 5-11: ADRS graph with the Design response spectrum, three of the possible different options for the design of the exoskeleton and the capacity curve of the existing RC frame (Di=displacement demand, Ci= capacity of the building)

In this context, the fundamental steps can be summarized as in the following:

1) **Analysis of the existing building**. The capacity curve needs to be plotted in the ADRS format as in Figure 5-11, where the capacity of the building can be checked, based on the given response spectrum at Ultimate Limit State (ULS). The Modified Capacity Spectrum Method (MCSM) proposed by Fajfar [77] and reported in Eurocode 8 [13] provisions can be used for this purpose.

2) **Elastic stiffness and resistance of the exoskeleton**. Fix the desired stiffness (and thus the fundamental period) of the exoskeleton and its resistance. The stiffness and the resistance are regulated by the BRB element at the ground floor. The stiffness of the steel exoskeleton should be high enough to limit the lateral displacements of the sliding system. The stiffness of the upper storeys must guarantee very limited inter-storey drifts (max 0.5%) and a totally elastic behaviour of the braces.

3) **Ultimate displacement of the exoskeleton**. The ultimate displacement capacity of the exoskeleton (based on the current code in the designer's country) must be calculated. To optimize the intervention, this parameter should be approximately in the order of 5-10 times the elastic displacement.

4) **Analysis**. The non-linear static (pushover) analysis is carried out on the hybrid structure (RC frame + sliding devices + exoskeleton). The capacity of the system is positive as far as the structural elements of the upper storeys and the exoskeleton remain both elastic, while the RC building is nearly undamaged.

5) **Final check**. If all the requirements are satisfied, the design approach can be considered appropriate. On the contrary, the iterative procedure restarts from step #2.

As it can be seen in Figure 5-11, the design of the exoskeleton is a designer's choice and is quite independent from the existing RC building. The base diagonal can be for example chosen to be (design option 1) stiffer and more resistant of options 2, 3, which are less stiff, less resistant but more ductile. The major limitations are given by the input design response spectrum. For the three different design options that are presented in Figure 5-11, expected capacity and demand parameters can be compared to the existing RC frame. C1, C2 and C3 points are representative of the displacement capacities of the exoskeleton with three different base diagonals, while C0 is the displacement capacity of the existing RC frame. Further, D0, D1, D2 and D3 denote the displacement demands given by the design response spectrum. From the figure it is thus possible to see that the original RC frame is not verified for the assigned seismic input. Conversely, all three the proposed hybrid retrofit solutions are positively verified for the seismic demand and prove the efficiency of the proposed approach.

5.4. Conclusions

Based on the results of this theoretical study, the proposed retrofitting solution seems to be optimal for the retrofit of very brittle structures, as the case study buildings analysed in the previous chapters. In this case, on the contrary of the traditional exoskeleton or in the retrofitting solutions with the introduction of dissipative bracings, as the existing building is not connected to the ground (it has vertical support but it can slide), it cannot be damaged by the bracing system and can continue to bear just the vertical loads. The reason for choosing sliding devices instead of seismic isolators is their cost. Sliding devices are cheaper and the recentring of the structure is guaranteed by the bracing system. A major limitation for the application of this method, is for sure the space around the buildings that is needed for placing the exoskeleton and reinforcing the foundations. Especially in the towns, the buildings are usually one next to the other and have no private land around them, but just public sidewalks. However, the advantage of using a sliding system at the base of the existing building is that the exoskeleton could also be realized inside the existing structure, as an endo-skeleton, by the installation of rigid diagonals, columns and beams at the upper storeys, in the masonry infills and the ductile bracing system at the ground floor, supported by the new steel columns rigidly connected to the foundation. In this way, the advantage of the realization of the exoskeleton just from the outside, without disturbing the inhabitants, il loosen, but the retrofitting solution can be installed also where there is no additional space. The main achievement of the

proposed retrofitting solution with an endo – or exo skeleton and a combined sliding system at the base of the existing building is that the hybrid configuration can be designed to withstand every expected seismic event without damage. The application of the method to existing buildings and the details for creating an endo-skeleton must be investigated in the future research. Also a cost comparison is going to be carried out in the future with a full seismic isolation solution (without bracing and exoskeleton).

_____

6. CONCLUSIONS

The aim of this research study is to investigate the vulnerability of the building heritage in Gorizia, a town in north-eastern Italy, on the border with Slovenia. As shown in **§ 1**, the majority of buildings in the town are old masonry buildings and reinforced concrete buildings from the 60's-70's. All the buildings built before the year 2003 were not designed under earthquake hazard and just after 2010, the seismic hazard has been considered at the level that we now consider credible, due to the evolution of the seismic classification of Italian territory.

Based on the statistical data about the building heritage in Gorizia, four existing buildings have been chosen and analysed with different methods in order to evaluate their seismic vulnerability and critical points. The case study buildings are representative of the main types of buildings that can be found in the town; two reinforced concrete buildings from the 60's-70's, named RC building 1 and RC building 2, and two masonry buildings from 1740 and 1903 (one made of stone masonry, the other of clay brick masonry), named Masonry building A and B.

For the evaluation of the seismic vulnerability of the analysed buildings, two types of seismic inputs have been considered: the Italian code response spectra, calculated based on the Probabilistic Seismic Hazard Assessment (PSHA) method, and compatible recorded time histories and the simulated response spectra of two specific possible scenarios for the town of Gorizia and correlated time histories, calculated with SPBSHA method. The physics-based simulations for the scenarios are calculated based on the latest evolutions of the Neo Deterministic Seismic Hazard Assessment (NDSHA) method. The differences, strengths and weaknesses of the two methods are analysed in **§ 2**.

The geometry of the structures, materials, loads and some preliminary regularity checks for each of the four case study buildings are described in **§ 3**, where also the numeric model's features are specified. The two RC buildings and one masonry building are residential buildings, while the older stone masonry building is the city hall of the town of Gorizia. For this reason, it has been possible to develop a project between the University of Trieste, Department of Engineering and Architecture and the Municipality of Gorizia and this allowed to perform some in situ tests on the building, in order to have a higher knowledge level of the analysed structure.

The results of the analyses performed on each of the case study buildings are reported in **§ 4**. The seismic actions used in the analyses are reported in **§ 4.1**. The simulated response spectra described in **§2.5.1** are the 50th, 84th and 95th percentile resultant response spectra of two scenarios, connected to the two faults that are the closest to Gorizia: Idrija fault and Medea fault. These data are the results of a research study developed at the University of Trieste, Department of Engineering and Architecture. For each scenario 100 realizations have been performed, response spectra have been calculated and statistically analysed in order to find the percentile response spectra. The two RC buildings have been modelled with the software SAP2000 from CSI [38], while for masonry buildings the software TreMuri from STA DATA has been used.

For **_RC building 1_** (**§ 4.2**) a sensitivity study is carried out about the differences in seismic behaviour found with different models of the same building. Based on a linear dynamic response spectrum analysis (the only suitable when the knowledge level about the building is low), it is shown how masonry infills influence the stiffness, resistance, but also the vibration mode shapes of the model (and of the real structure), at least in the elastic phase and until the collapse of the infills. The results obtained with the numerical models have been compared to the vibration periods found with some measurements of the natural vibrations of the building. The lowest natural period found with numerical analyses, T= 1.01 s (model with masonry infills), remains significantly higher than the highest measured period (0.625 s). A credible cause is the effect of non-structural elements that are not considered in numerical models (as for example partition walls) and the additional mass of the imposed design loads in the models, that is probably higher than the loads that were actually present at the moment of measurements. Another cause could be that the model includes also the basement

_____

storey, because it is almost not in touch with the ground (there is a gap between the walls of the basement and the ground, but the ground floor is connected to the ground with a sidewalk), but for such low-amplitude vibrations this storey could be considered fixed. The results of this study also show that the most accurate modelling solution for concrete walls seems to be the one with "shell" elements, but an effective alternative is the use of "frame" elements in combination with rigid links in order to create a connection between walls. On the selected model (without infills) are then carried out non-linear analyses. First some non-linear static (pushover) analyses are carried out in both main directions of the building. The capacity results are compared to the displacement demands of the code CLS and LLS spectra (Collapse and Life Safety limit states) and to the demands of scenario response spectra (three percentiles for each of the two scenarios). The vulnerability indices (C/D ratios, in terms of displacement) are reported in Table 6-5, where the displacement demand of the 84th and 95th percentiles of the scenarios (Medea and Idrija) are compared to the Life Safety and Collapse limit state capacity of the building, respectively. Based on the results of the pushover analysis, interstorey drifts at the collapse of the building have been computed and used to calculate fragility curves of the building. The curves have been obtained by performing 50 non-linear dynamic analyses on the numerical model, extracting the maximum interstorey drifts and top displacements and by using the results for carrying out a cloud analysis. The resulting fragility curves, derived for three limit states (Collapse limit state - CLS, Life safety limit state - LLS and Damage limit state - DLS) have been compared with literature fragility curves. The case-study building has a much higher probability of exceeding all three limit states, compared to the literature ones. In particular, the difference and main critical point of the studied building is that it has a brittle stairwell made of concrete walls, that were not designed to resist any lateral load. They have very few steel reinforcement bars and are very brittle, so that for all the analysed time histories, the first hinges that collapse are shear hinges in the concrete walls. The results of the fragility curves show that such a building has 100% probability of reaching collapse already for very low spectral accelerations (0.03 g), a lower value than the code spectral acceleration for the fundamental period of the building for Damage limit state response spectrum. Also for the 5th percentile of the Idrija scenario response spectrum, there is 100% probability to exceed the collapse limit state. In Table 6-1 the spectral acceleration for which the fragility curve shows that there is 100% probability for the building to reach the Collapse ($Sa_{res, CLS,100}$) is compared to the capacity of the building, in terms of spectral acceleration, found with pushover analysis, for the equivalent SDOF system ($Sa_{res, CLS,SDOF}$). It can be noticed that they are similar, although the value found with the fragility curve is slightly lower. Non - linear dynamic analyses are, in fact more variable. They involve many more parameters (of the numerical model and of the seismic input), vibration modes and dynamic forces compared to the static analysis. On the other hand, during an earthquake this is what happens. The real behaviour could be slightly different from the one forecast with a static analysis. Moreover, fragility curves are a statistical analysis of the behaviour of the building, so even more parameters influence the result.

Table 6-1: Comparison between capacities of the building, in terms of spectral acceleration, found with non-linear static analysis and with fragility curve.

Analysis	$Sa_{res,CLS, SDOF}$ [g]	$Sa_{res,CLS, 100}$ [g]
Y uniform	0.0455	0.0275
Y spectral	0.0406	

RC building 2 (§ **4.3**) has been analysed with and without masonry infills too. In this case, the difference between the two models has been investigated with pushover analysis. It has been shown that the masonry infills increase not just the stiffness of the building but also the strength, although they collapse very soon with brittle mechanisms. The collapse intervenes in correspondence of small displacements. On the other hand, it should be noticed that the strength and stiffness of the infills in the model depends on the chosen parameters (material) and modelling choices for the masonry infills. For this reason, they should be investigated with the same attention as the materials and details of the main load-bearing structure, when there is the opportunity to carry out in situ tests.

In a limit condition when the masonry infills have ductility and strength comparable with the ones of the concrete walls of the staircase, that for buildings like the presented case studies are very brittle, it could happen that they collapse more or less simultaneously. In this case it is fundamental to model also the masonry infills, when analysing the structure, as its stiffness and strength fully depend on the behaviour of the infills, until the collapse of both of them. After this preliminary study, the model without masonry infills and without the basement storey has been used to carry out more non-linear analyses. First some non-linear static (pushover) analyses are carried out in both main directions of the building. The capacity results are compared to the displacement demands based on the code CLS and LLS spectra (Collapse and Life Safety) and the demands of scenario response spectra (three percentiles for each of the two scenarios). The vulnerability indices (C/D ratios, in terms of displacement) are reported in Table 6-5 also for this building. On the contrary of the case of RC building 1, in this case, one analysis (pushover in Y direction with uniform load pattern) shows a very ductile behaviour (first collapsed hinges are flexural), so that in that case the building is all verified, with both code and scenario seismic inputs, but just the lowest values (among the two main directions and the two load patterns) of the vulnerability indices are reported in Table 6-5. Based on the results of the pushover analysis, interstorey drifts at the collapse of the building have been computed and used to calculate fragility curves of the building. The curves have been obtained by performing 50 non-linear dynamic analyses on the numerical model, extracting the maximum interstorey drifts and top displacements and by using the results for carrying out a cloud analysis. The resulting fragility curves, derived for three limit states (CLS, LLS and DLS) have been compared to fragility curves from literature. Also this case-study building has a much higher probability of exceeding all three limit states, compared to the literature ones. The difference and main critical point of the studied building is the same observed for RC building 1: the stairwell made of brittle concrete walls. They were not designed to resist any lateral load and they have very few steel reinforcement bars, so that for all the analysed time histories, the first hinges that collapse are shear hinges in the concrete walls. The results of the fragility curves show that such a building has 100% probability of reaching collapse for low spectral accelerations, that is 0.13 g in Y direction and 0.16 g in X direction. In Table 6-2 the spectral acceleration for which the fragility curve shows that there is 100% probability for the building to reach the Collapse ($Sa_{res,\ CLS,100}$) is compared to the capacity of the building, in terms of spectral acceleration, found with pushover analysis, for the equivalent SDOF system ($Sa_{res,\ CLS,SDOF}$). It can be noticed that the value found with the fragility curve is higher and this could be due to the fact that it refers to 100% probability of collapse, but the collapse could occur, with lower probability, also for lower spectral accelerations.

Table 6-2: Comparison between capacities of the building, in terms of spectral acceleration, found with non-linear static analysis and with fragility curve.

Analysis	$Sa_{res,CLS,\ SDOF}$ [g]	$Sa_{res,\ cls,\ 100}$ [g]
X uniform	0.066314	0.1580
X spectral	0.084875	
Y uniform	0.068092	0.1325
Y spectral	0.070197	

Masonry building A (**§ 4.4**) is the central building of the city hall of Gorizia. It was built in 1740 and then modified during the years. The main structure is made of stone masonry and it has a quite regular shape. The critical point of this building is the lodge, that is positioned along the long side of the building, but it is not well connected and it has no strength at all towards horizontal actions, especially in the upper part, where it has high stone columns. For this reason, the building has been first analysed without the lodge and then a retrofitting solution has been designed to include the lodge and achieve an enhancement of the behaviour of the whole building. First a modal analysis has been carried out and the vibration periods have been compared to measured periods (as already done for RC building 1). Then non-linear static (pushover) analyses have been carried out on the single wall of the building. This choice is due to the fact that the in situ investigations have shown

very low or absent connections between perpendicular walls. Moreover, the structure of the interstorey slabs is made of wood, so that it is not stiff enough to guarantee a box behaviour of the building. The results of the pushover analyses in this case are computed in terms of capacity and demand PGA. Overall seismic vulnerability of the building is determined by the walls with the minimum indices in X and Y direction. The vulnerability is checked with respect to the code response spectra and also with scenario response spectra. In addition, some non-linear dynamic analyses are carried out on two walls of the building, by using the scenario simulated accelerograms. The building is more vulnerable in Y direction (the short side of the building) than in X direction. The capacity of the building in terms of spectral acceleration found for the equivalent SDOF system with pushover analysis is reported in Table 6-3 for all the considered limit states. In the analyses the out of plane kinematics are not considered, but they could be possible, as the bonds between perpendicular walls are very weak or absent. A proper retrofit intervention needs to consider the improvement of such bonds. The vulnerability indices found for the un-retrofitted building are reported in Table 6-5. With the designed retrofit intervention, including the lodge, an increment of the vulnerability indices is achieved, higher than 0.1 for all limit states, but for Serviceability limit states in X direction.

Table 6-3: Capacity of Masonry building A in terms of spectral acceleration found from pushover analysis, for the equivalent SDOF system, for all limit states.

Analysis	$Sa_{,\ res,\ SDOF}$			
	CLS	LLS	DLS	OLS
X direction (wall 3, analysis 3)	1.466 m/s² = 0.149 g	1.457 m/s² = 0.148 g	1.303 m/s² = 0.133 g	0.989 m/s² = 0.101 g
Y direction (wall 7, an. 4 for ULS and wall 6, an.2 for SLS)	1.912 m/s² = 0.195 g	1.666 m/s² = 0.170 g	1.017 m/s² = 0.104 g	0.812 m/s² = 0.083 g

The last case study building, ***Masonry building B*** (**§ 4.5**) is a residential building built in 1903. No in situ tests have been performed, but from some details is visible a clay brick masonry. The building is very regular and although the slabs are wooden and presumably not stiff enough in their plane, the building has a box behaviour. For this reason, both results of global analysis and of analyses of the single walls are carried out. Also in this case the results of the analyses are expressed in terms of seismic vulnerability indices calculated as the ratio between the capacity PGA and the demand PGA, for each limit state. For this building the collapse limit state has not been considered, as for residential buildings is usually not required to check it. The vulnerability index (minimum index found for all the global pushover analyses carried out on the whole building) for LLS (for code demand and scenarios demand) is reported in Table 6-5. The index found with global analysis is, in this case, considered a better parameter for the evaluation of the vulnerability of the building, since the results obtained from the pushover analysis of the single walls are very different one from the other. Almost all the walls are totally verified, while just 2 walls are not strong and ductile enough for the code demands, achieving very low indices, that are not representative of the whole building. The capacity of the building in terms of spectral acceleration found for the equivalent SDOF system with global pushover analysis is reported in Table 6-4 for all the considered limit states.

Table 6-4: Capacity of Masonry building B in terms of spectral acceleration found from global pushover analysis, for the equivalent SDOF system, for all limit states.

Analysis	$Sa_{,\ res,\ SDOF}$		
	LLS	DLS	OLS
X direction (analysis 16 for LLS and analysis 12 SLS)	1.083 m/s² = 0.110 g	1.019 m/s² = 0.104 g	1.019 m/s² = 0.104 g
Y direction (analysis 18 for LLS and OLS, analysis 21 for DLS)	1.840 m/s² = 0.188 g	2.191 m/s² = 0.223 g	1.771 m/s² = 0.181 g

The vulnerability indices for all the analysed buildings, for code and scenario seismic inputs, are reported in Table 6-5 for comparison.

Table 6-5: Table of the vulnerability indices of the four case study buildings obtained with pushover analysis. The 84th percentile spectrum demand of the scenarios is compared to LLS capacity of the building, while the 95th percentile is compared to CLS capacity of the building.

Building	CLS	LLS	Medea 84 - LLS	Medea 95 - CLS	Idrija 84 - LLS	Idrija 95 - CLS
RC building 1	0.176	0.183	0.403	0.248	0.377	0.404
RC building 2	0.294	0.402	0.687	0.399	0.856	0.684
Masonry building A	0.427	0.408	0.637	0.649	0.866	0.946
Masonry building B	-	0.397	0.692	-	0.798	-

As it can be noticed from the presented results, masonry buildings, especially with respect to code seismic demand, are in a better condition than the RC ones, although the vulnerability indices are low for all the analysed buildings. Masonry building A, that is the one in the best condition according to the results, resists just to 43% of the total seismic demand for the collapse limit state. On the other hand, it should be remarked that the check for this building is made with th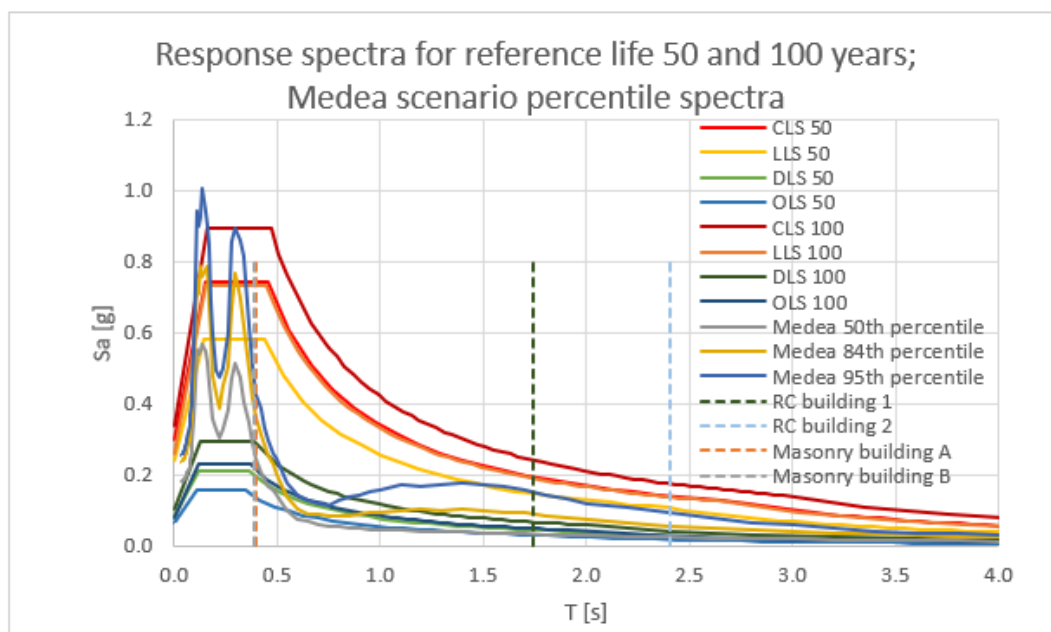e code response spectra for a reference life of 100 years and not 50 years as for the other three buildings. The RC buildings are in general more vulnerable, with a capacity that is less than 30% of the one needed for the collapse limit state demand. When considering the scenario seismic inputs, the situation is better. The seismic demand of the 95th percentile of Medea scenario is more similar to the LLS code demand than to the CLS demand, but still lower, while all the other percentiles of the scenarios have lower demands. This is due to the position and soil of Gorizia, because the shape of the scenario response spectra has low values of spectral accelerations for the periods of the analysed structures. This does not mean that the scenario demand is lower for every kind of building. It can be seen in Figure 6-1 that the scenario spectral accelerations for very low periods are even higher than the code accelerations, but for the fundamental periods of the analysed buildings, the scenario response spectra are very low.
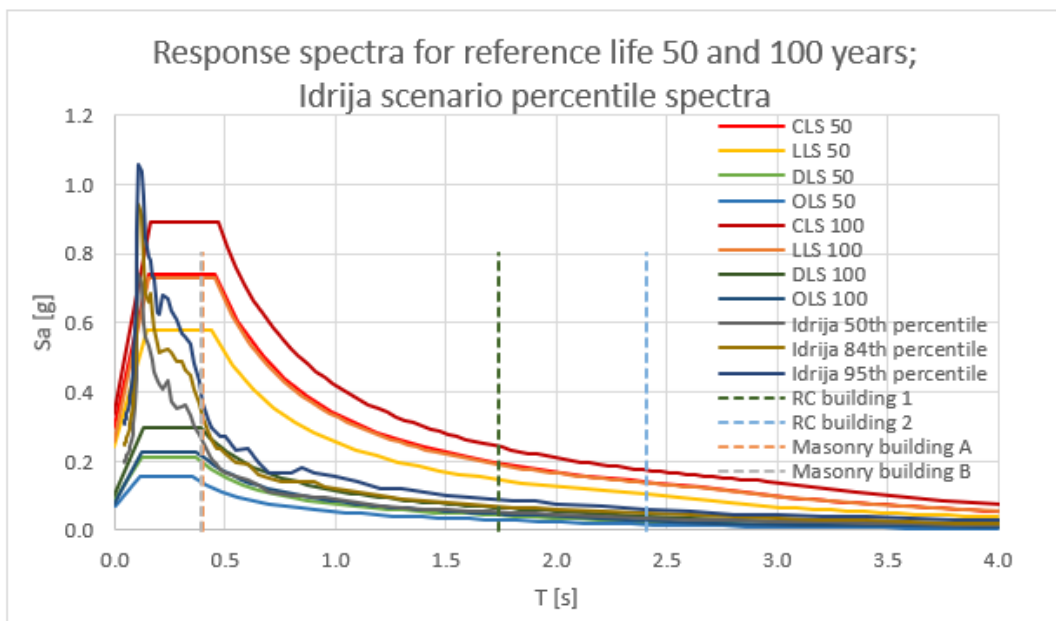
Figure 6-1: Code response spectra for all limit states, for reference life 50 years and 100 years, compared to the scenario percentile spectra for Idrija (above) and Medea (below). On the same graphs also vertical lines are drawn at the periods of the four analysed buildings.

The studied buildings could be considered an indicator of the average state of the building heritage in Gorizia. They are representative of the two types of buildings that are the most frequent in the town. For RC buildings built in the same period of the case study buildings (60's -70's), it can be said that the probability of having the same type of structure and the same critical points is very high, not just in Gorizia, but also in many other Italian cities. In that period the standard design was made for gravitational loads only, the frames were present just in one direction, while in the other direction just the slabs and some curbs were connecting the structure. Generally the staircase was made of concrete walls, that had very low reinforcement, as they were supposed to withstand just vertical loads. Buildings like these are very vulnerable, due to the very brittle concrete walls, as it has been shown in this research and they should be retrofitted as soon as possible, with priority towards masonry buildings. Their ductility should be checked and improved and masonry infills should be also carefully analysed and considered in the evaluation of the seismic response of the buildings. The vulnerability and the importance of retrofitting interventions rises with the height of the buildings. High-rise buildings are more vulnerable than lower buildings. Old masonry buildings also need retrofitting interventions and, as it has been noticed in this research study, the critical points are the openings and the bonds between perpendicular walls, in some cases also the quality of the masonry should be improved.

A theoretical study has been carried out within the present research study in order to find an innovative and effective solution for the retrofit of the RC high-rise buildings. It is described in **§ 5** and consists in the application of an exoskeleton, that could also be transformed into an endo-skeleton in a future development, with the additional introduction of a sliding system at the base of the RC building, in order to decouple the ground motion from the existing building. In this way, the exo- or endo-skeleton can be designed independently from the features of the existing building and no damage is expected in the existing building. Just the bracing system of the exoskeleton, at the first storey over the level of the sliding devices in the RC building, is designed to yield and so it is also the only element that could need a substitution after a stronger seismic event. The proposed solution has been analysed in a simple SDOF system and also in a plane MDOF system. A design procedure is proposed, based on non-linear static analysis.

When possible (technically and economically), a retrofit solution that guarantees no damage after a strong seismic event, should be applied, as for example base isolation or damping systems or the solution proposed in this research study (**§ 5**). The aim is to avoid the activation of plastic hinges

in the existing structure and thus its damage. In this case, a design based on both seismic hazard assessment methods (PSHA and SPBSHA) should be used. The economic difference between the design with the two seismic inputs is very low and allows to have a more complete view about the possible seismic actions on the building. Moreover, as they are calculated based on the physical numerical modelling of the propagation of seismic waves, the scenario response spectra are more reliable for longer fundamental periods, as the ones of a high-rise building or a base isolated one.

The results of this research study show some important critical points for the seismic vulnerability of the building heritage in the town of Gorizia. While the results obtained for the two masonry case study buildings are more site-specific (the types of masonry on Italian territory are very different from one region to the other and from one construction period to the other), the results obtained for the RC buildings are of great importance also for other Italian cities. The RC buildings built in the 60's and 70's, especially in places that were not considered yet seismic, were very frequently designed in the same way as the two case-study buildings, with brittle concrete staircase. It should be remarked that in those years, the seismic classification of Italy was still based on the R.D. 640 of 25/03/1935. It had 2 categories, based on experienced earthquakes, so that a great part of Italy was not considered seismic. Despite this, the majority of the research studies on existing RC buildings, are based on simulated structures, that don't consider brittle concrete walls, but just RC frames. This type of buildings should be further analysed and as shown in the present study, also the interaction with the masonry infills should be accurately considered, when the collapse of the building is so brittle. The stiffness and strength of the concrete walls and of the masonry infills could be comparable and thus crucial in the collapse mechanism. The knowledge about this interaction is fundamental when using numerical models for the evaluation of the seismic vulnerability of existing buildings and the design of retrofitting interventions. The results obtained in this research are just some preliminary results, therefore some more work should still be done. The fragility curves could be calculated for any direction (not just for each main direction separately), they could be calculated also with site-specific accelerograms (for better assessing the specific vulnerability in Gorizia), in-situ tests should be performed on the materials in order to have more realistic values, other parameters could be chosen for measuring the damage level. On the other hand, also the retrofit intervention needs a great research effort. The proposed solution with sliding devices and bracing system should be applied to real existing buildings, in the form of endo – or exo-skeleton, for finding the additional parameters that enter in the design of a 3D intervention (as just a 2D has been investigated). It would be interesting to investigate the differences in the cost, but also in the behaviour of a full isolation solution. The proposed solution could be particularly suitable for very brittle RC buildings.

Beside the research studies about the best retrofitting solution, the main real problem is usually the awareness of people. In the public opinion, seismic vulnerability is not considered so important as the issue of energy efficiency of buildings, where people see immediate advantage in thermically isolating their homes in order to spend less in everyday life. Earthquakes are relatively rare events and we always hope they will never destroy our homes. So that a retrofit intervention is usually seen as something not very necessary. Based on the results obtained with this research study, that shows the great vulnerability of the building heritage, awareness campaigns should be organised by the public authority (City hall, Region or State), that should encourage, also financially and with less bureaucracy, the retrofitting of this kind of vulnerable buildings.

REFERENCES

[1]   Presidenza del Consiglio dei Ministri (2017), Struttura di Missione Casa Italia. Rapporto sulla Promozione della sicurezza dai Rischi naturali del Patrimonio abitativo

[2]   Presidenza del Consiglio dei Ministri, Dipartimento della Protezione Civile (2017): rapporto predisposto al fine di accedere ai finanziamenti del Fondo di Solidarietà dell'Unione Europea (FSUE) per gli eventi sismici del Centro Italia.

[3]   ISTAT, Rapporto Bes 2017, Istituto nazionale di statistica, Via Cesare Balbo, 16 - Roma. Il benessere equo e sostenibile in Italia. ISBN 978-88-458-1935-3

[4]   ISTAT data (censimento 2011)

[5]   Ordinanza del Presidente del Consiglio dei Ministri – OPCM n. 3274 del 2003

[6]   Ministero delle Infrastrutture e dei Trasporti, Decreto 17 gennaio 2018: Aggiornamento delle "Norme tecniche per le costruzioni" (NTC2018)

[7]   Sabetta, F. and Pugliese, A. (1996), Estimation of response spectra and simulation of nonstationary earthquake ground motions. Bulletin of the Seismological Society of America (April 1996) Vol. 86 (No.2): 337-352.

[8]   DISS Working Group (2018), Database of Individual Seismogenic Sources (DISS), Version 3.2.1: A compilation of potential sources for earthquakes larger than M 5.5 in Italy and surrounding areas. http://diss.rm.ingv.it/diss/, Istituto Nazionale di Geofisica e Vulcanologia, doi: 10.6092/INGV.IT-DISS3.2.1.

[9]   INGV, Parametric Catalogue of Italian Earthquakes, https://emidius.mi.ingv.it/CPTI15-DBMI15/

[10]   Consiglio Superiore dei Lavori Pubblici - C.S.L.P. (2018), Italian Building Code (NTC18).

[11]   Consiglio Superiore dei Lavori Pubblici - C.S.L.P. (2008), Italian Building Code (NTC08).

[12]   CEN (2005), Eurocode 8: Design of structures for earthquake resistance - Part 3: Assessment and retrofitting of buildings (EC8-3). European Committee for Standardization

[13]   CEN (2004), Eurocode 8: Design of structures for earthquake resistance - Part 1: General rules, seismic actions and rules for building (EC8-1). European Committee for Standardization.

[14]   Baker, Jack W. (2015), Introduction to Probabilistic Seismic Hazard Analysis. White Paper Version 2.1, 77 pp.

[15]   Baker, Jack W., (2011), Conditional mean spectrum: Tool for ground motion selection. Journal of Structural Engineering 137, 322–331. doi:10.1061/(ASCE)ST.1943-541X.0000215

[16]   Rovida, A., Locati, M., Camassi, R., Lolli, B., Gasperini, P. (eds) (2016), CPTI15, the 2015 version of the Parametric Catalogue of Italian Earthquakes. Istituto Nazionale di Geofisica e Vulcanologia. doi:http://doi.org/10.6092/INGV.IT-CPTI15

[17]   Gruppo di Lavoro (2004), Redazione della mappa di pericolosità sismica prevista dall'Ordinanza PCM del 20 marzo 2003, n. 3274, All.1. Rapporto Conclusivo per il Dipartimento della Protezione Civile, INGV, Milano-Roma, aprile 2004, 65 pp. + 5 appendici

[18]   Ministero delle infrastrutture e dei trasporti, Circolare 2 febbraio 2009, n. 617: Istruzioni per l'applicazione delle "Nuove norme tecniche per le costruzioni" di cui al decreto ministeriale 14 gennaio 2008

[19]   Cornell, C.A. (1968), Engineering seismic risk analysis. Bull. Seismol. Soc. Am., Vol. 58 (No.5) (1968), pp. 1583-1606.

[20]   Fasan, M. (2017), Advanced Seismological and Engineering Analysis for Structural Seismic Design. PhD thesis, Università degli Studi di Trieste, Dipartimento di Ingegneria e Architettura

[21]   Panza, G.F. (1985), Synthetic seismograms: the Rayleigh modal summation technique. Journal of Geophysics 58, 125–145.

_____

[22] Panza, G.F., Romanelli, F., Vaccari, F. (2001), Seismic wave propagation in laterally heterogeneous anelastic media: Theory and applications to seismic zonation. Advances in Geophysics. pp. 1–95. doi:10.1016/S0065-2687(01)80002-9

[23] Panza, G.F., Kossobokov, V.G., Peresan, A., Nekrasova, A. (2014), Why are the Standard Probabilistic Methods of Estimating Seismic Hazard and Risks Too Often Wrong, Earthquake Hazard, Risk and Disasters. Elsevier Inc., pp. 309-357. doi:http://dx.doi.org/10.1016/B978-0-12-394848-9.00012-2.

[24] Magrin, A. (2013), Multi-Scale Seismic Hazard Scenarios. PhD thesis, University of Trieste, Italy.

[25] Gorshkov, A., Panza, G.F., Soloviev, A.A., Aoudia, A. (2002), Morphostructural Zonation and Preliminary Recognition of Seismogenic Nodes Around the Adria Margin in Peninsular Italy and Sicily. Journal of Seismology and Earthquake Engineering 4, 1–24.

[26] Gorshkov, A.I., Panza, G.F., Soloviev, A., Aoudia, A. (2004), Restricted access Identification of seismogenic nodes in the Alps and Dinarides. Italian Journal of Geoscience 123, 3–18.

[27] Gorshkov, A.I., Panza, G.F., Soloviev, A.A., Aoudia, A., Peresan, A. (2009), Delineation of the geometry of nodes in the Alps-Dinarides hinge zone and recognition of seismogenic nodes (M ≥ 6). Terra Nova 21, 257–264. doi:10.1111/j.1365-3121.2009.00879.x

[28] CPTI Working Group (2004), Catalogo Parametrico dei Terremoti Italiani, versione 2004 (CPTI04). Bologna, Italy. doi:10.6092/INGV.IT-CPTI04

[29] Živčić, M., Suhadolc, P., Vaccari, F. (2000), Seismic Zoning of Slovenia Based on Deterministic Hazard Computations. Seismic Hazard of the Circum-Pannonian Region. Birkhäuser Basel, Basel, pp. 171–184. doi: 10.1007/978-3-0348-8415-0_10

[30] Markušić, S., Suhadolc, P., Herak, M., Vaccari, F. (2000), A Contribution to Seismic Hazard Assessment in Croatia from Deterministic Modeling. Seismic Hazard of the Circum-Pannonian Region. Birkhäuser Basel, Basel, pp. 185–204. doi:10.1007/978-3-0348-8415-0_11

[31] Meletti, C., Galadini, F., Valensise, G., Stucchi, M., Basili, R., Barba, S., Vannucci, G., Boschi, E. (2008), A seismic source zone model for the seismic hazard assessment of the Italian territory. Tectonophysics 450, 85–108. doi:10.1016/j.tecto.2008.01.003

[32] Vaccari, F. (2014), Computational aspects of the Neodeterministic Seismic Hazard Assessment – presentation at the International School on "Advanced Modeling of Seismic Hazard in Africa"

[33] Fasan, M., Amadio, C., Noè, S., Panza, G.F., Magrin, A., Romanelli, F., Vaccari, F. (2015), A new design strategy based on a deterministic definition of the seismic input to overcome the limits of design procedures based on probabilistic approaches. XVI Convegno ANIDIS. L'Aquila, pp. 1–11

[34] Peresan, A., Magrin, A., Nekrasova, A., Kossobokov, V.G., Panza, G.F. (2013), Earthquake Recurrence and Seismic Hazard Assessment: A Comparative Analysis Over The Italian Territory. WIT Transactions on The Built Environment 132, 23–34. doi:10.2495/ERES130031

[35] Panza, G., Peresan, A. (2016), Difendersi dal terremoto si può: l'approccio neo-deterministico. EPC editore

[36] Panza, G.F., La Mura, C., Peresan, A., Romanelli, F., Vaccari, F. (2012), Seismic Hazard Scenarios as Preventive Tools for a Disaster Resilient Society. Advances in Geophysics. pp. 93–165. doi:10.1016/B978-0-12-380938-4.00003-3

[37] Hassan, H.M., Fasan, M., Sayed, M.A., Romanelli, F., ElGabry, M.N., Vaccari, F., Hamed A. (2020), Site-specific ground motion modeling for a historical Cairo site as a step towards computation of seismic input at cultural heritage sites. Engineering Geology, Vol. 268, 105524, ISSN 0013-7952. https://doi.org/10.1016/j.enggeo.2020.105524.

[38] Barnaba, M., Fasan, M., Amadio, C., Noè, S., Romanelli, F., Vaccari, F. (2019), Scenari di pericolosità sismica e di danno per la città di Gorizia. Associazione Nazionale Italiana Di Ingegneria Sismica ANIDIS

_____

[39] Panza, G.F., La Mura, C., Peresan, A., Romanelli, F., Vaccari, F. (2012), Seismic Hazard Scenarios as Preventive Tools for a Disaster Resilient Society. Advances in Geophysics, Vol. 53, 2012, pp. 93-165. https://doi.org/10.1016/B978-0-12-380938-4.00003-3

[40] Panza, G.F., Romanelli, F., Vaccari, F. (2001), Seismic wave propagation in laterally heterogeneous anelastic media: Theory and applications to seismic zonation. Advances in Geophysics, Vol. 43, pp. 1-95. ISBN 9780120188437, https://doi.org/10.1016/S0065-2687(01)80002-9

[41] Bisiani, F. (1989), Indagine geologico-tecnica del territorio comunale di Gorizia.

[42] Grego, B., Iadarola, F. (1998), Relazione geologica per la variante generale al piano regolatore generale comunale.

[43] CSI, "SAP2000 Integrated Software for Structural Analysis and Design," Computers and Structures Inc., Berkeley, California

[44] Verderame, G.M., Ricci, P., Esposito, M., Sansiviero, F. C. (2011), Le caratteristiche meccaniche degli acciai impiegati nelle strutture in c.a. realizzate dal 1950 al 1980. Atti del XXVI Convegno Nazionale AICAP "Le prospettive di sviluppo delle opere in calcestruzzo strutturale nel terzo millennio", Padova, 19-21 maggio 2011 (memorie 63)

[45] Decreto Ministeriale 30 maggio 1972 – Norme tecniche alle quali devono uniformarsi le costruzioni in conglomerato cementizio, normale e precompresso ed a struttura metallica.

[46] Sivocci, D. (2012), Verifica e proposte di adeguamento sismico del palazzetto dello sport di Castelfranco Veneto, Padova

[47] Decreto Ministeriale 9 gennaio 1996 – Norme tecniche per il calcolo, l'esecuzione ed il collaudo delle strutture in cemento armato, normale e precompresso e per le strutture metalliche.

[48] Gerardi, V., Ditommaso, R., Auletta, G., Ponzo, F.C. (2017), Strutture intelaiate in conglomerato cementizio armato: validazione numerica di due modelli di calcolo finalizzati a portare in conto il contributo irrigidente dei pannelli di tamponatura in condizioni di esercizio. Proceedings GNGTS 2017, 478-482.

[49] Jalayer, F., Iervolino, I., Manfredi, G. (2007), Influenza dei parametri di modellazione e dell'incertezza associata nella valutazione sismica di edifici esistenti in cemento armato. Proceedings XII Convegno ANIDIS, Giugno 2007.

[50] Liberatore, L., Mollaioli, F. (2015), Influence of Masonry Infill Modelling on the Seismic Response of Reinforced Concrete Frames, Proceedings of the Fifteenth International Conference on Civil, Structural and Environmental Engineering Computing, J. Kruis, Y. Tsompanakis and B.H.V. Topping (Editors), Civil-Comp Press, Stirlingshire, Scotland

[51] Chen, X., Liu, Y. (2015), The Effect of Openings on the In-Plane Behavior and Strength of Masonry Infills. Proceedings of the 15th International Conference on Civil, Structural and Environmental Engineering Computing, Civil-Comp Press, Stirlingshire, Scotland, Paper 69

[52] Dal Moro, G., Weber, T. M., Keller, L. (2018), Gaussian-filtered Horizontal Motion (GHM) plots of non-synchronous ambient microtremors for the identification of flexural and torsional modes of a building. Soil Dynamics and Earthquake Engineering, 112, 243-255.

[53] Zentner, I., Gundel, M., Bonfils, N. (2017). Fragility analysis methods: Review of existing approaches and application. Nuclear Engineering and design, Vol. 323, pp. 245-258, ISSN 0029-5493. https://doi.org/10.1016/j.nucengdes.2016.12.021.

[54] Rosti, A., Del Gaudio, C., Rota, M., Ricci, P., Di Ludovico, M., Penna, A., Verderame, G.M. (2021). Empirical fragility curves for Italian residential RC buildings. Bulletin of Earthquake Engineering 19, pp. 3165-3183. https://doi.org/10.1007/s10518-020-00971-4

[55] Di Sarno, L., Pugliese, F. (2020). Seismic fragility of existing RC buildings with corroded bars under earthquake sequences. Soil Dynamics and Earthquake Engineering, Vol. 134, 106169, ISSN 0267-7261. https://doi.org/10.1016/j.soildyn.2020.106169.

[56] Hueste, M. B. D., Bai, Jong-Wha (2007), Seismic retrofit of a reinforced concrete flat-slab structure: Part II – seismic fragility analysis. Engineering structures, Vol. 29, Issue 6, pp. 1178-1188. https://doi.org/10.1016/j.engstruct.2006.07.022

_____

[57]   Masi, A., Vona, M., Digrisolo, A. (2009), Costruzione di curve di fragilità di alcune tipologie strutturali rappresentative di edifici esistenti in c.a. mediante analisi dinamiche non lineari. ANIDIS 2009

[58]   Belletti, B., Martinelli, E., Michelini, E., Tavano, M., Vecchi, F. (2020), Seismic risk assessment of existing RC buildings with shear walls. 9th European Workshop on the seismic behaviour of irregular and complex structures (December 2020)

[59]   Belletti, B., Martinelli, E., Michelini, E., Vecchi, F. (2021), Evaluation of the seismic vulnerability of existing pre-code RC core structural systems through non-linear pushover analyses. COMPDYN 2021

[60]   Al-Chaar, G.; Lamb, G.E. (2003), Effect of openings on structural performance of unreinforced masonry infilled frames. ACI Spec. Publ.2003,211–212, 247–261

[61]   C.S.L.L.P.P. (2010), Linee guida per la valutazione e la riduzione del rischio sismico del patrimonio culturale con riferimento alle Norme tecniche per le costruzioni di cui al decreto del Ministero delle Infrastrutture e dei trasporti del 14 gennaio 2008", 26/11/2010

[62]   Wenk, T. (2008), Seismic retrofitting of structures: strategies and collection of examples in Switzerland. Federal Office for the Environment FOEN, Bern

[63]   Liu, W., Givens, J.D., Kanitkar, R., Blaney, C. (2009), Seismic Evaluation and Rehabilitation of a Three Story Pre-Northridge Steel Frame Essential Service Facility. ATC and SEI Conference on Improving the Seismic Performance of Existing Buildings and Other Structures, December 9-11, 2009, San Francisco, California, United States, doi: 10.1061/41084(364)6

[64]   Faiella, D., Calderoni, B., Mele, E. (2020), Seismic Retrofit of Existing Masonry Buildings through Inter-story Isolation System: A Case Study and General Design Criteria. Journal of Earthquake Engineering, doi: 10.1080/13632469.2020.1752854

[65]   Rizzo, S., Stempniewski, L. (2018), EQ-grid: A Multiaxial Seismic Retrofitting System for Masonry Buildings. Valentina Svalova, IntechOpen, doi: 10.5772/intechopen.78596. Available from: https://www.intechopen.com/books/earthquakes-forecast-prognosis-and-earthquake-resistant-construction/eq-grid-a-multiaxial-seismic-retrofitting-system-for-masonry-buildings

[66]   Bedon, C., Amadio, C. (2018), Numerical assessment of vibration control systems for multi-hazard design and mitigation of glass curtain walls. Journal of Building Engineering, 15, doi: 10.1016/j.jobe.2017.11.004

[67]   Griffith, M. (2008), Seismic Retrofit of RC Frame Buildings with Masonry Infill Walls: Literature Review and Preliminary Case Study. EUR 23289 EN – Joint Research Centre – Institute for the Protection and Security of the Citizen. Luxembourg: Office for Official Publications of the European Communities 2008, 72 pp., Scientific and Technical Research series – ISSN 1018-5593

[68]   Di Sarno, L., Manfredi, G. (2012), Experimental tests on full-scale RC unretrofitted frame and retrofitted with buckling-restrained braces. Earthquake Engineering & Structural Dynamics, 41(2): 315-333

[69]   Di Sarno, L., Manfredi, G. (2010), Seismic retrofitting with buckling restrained braces: Application to an existing non-ductile RC framed building. Soil Dynamics and Earthquake Engineering, 30(11): 1279-1297

[70]   Labò, S., Passoni, C., Marini, A., Belleri, A. (2020), Design of diagrid exoskeletons for the retrofit of existing RC buildings. Engineering Structures, 220: 110899, doi: 10.1016/j.engstruct.2020.110899

[71]   Reggio, A., Restuccia, L., Ferro, G.A. (2018), Feasibility and effectiveness of exoskeleton structures for seismic protection. Procedia Structural Integrity, 9: 303-310

[72]   D'Urso, S., Cicero, B. (2019), From the Efficiency of Nature to Parametric Design. A Holistic Approach for Sustainable Building Renovation in Seismic Regions. Sustainability, 11(5): 1227, doi: 10.3390/su11051227

[73]   Badini, L., De Stefano, C.A., Custodi, A. (2019), Seismic Strengthening of Existing RC Structure Through External 3D Exoskeleton. Proceedings of the 20th IABSE Congress, New

_____

York City, 2019 - The Evolving Metropolis, pp. 1018-1024, doi: 10.1080/10168664.2019.1599209

[74] Dolce, M., Cardone, D., Croatto, F. (2005), Frictional Behavior of Steel-PTFE Interfaces for Seismic Isolation. Bull. Earthquake Eng., 3: 75-99, doi: 10.1007/s10518-005-0187-9

[75] Higashino, M., Hamaguchi, H., Minewaki, S., Aizawa, S. (2003), Basic Characteristics and Durability of Low-Friction Sliding Bearings for Base Isolation. Earthquake Engineering and Engineering Seismology, 4(1): 95-105

[76] Jampole, E.A., Swensen, S.D., Fell, B., Miranda, E., Deierlein, G.G. (2014), Dynamic testing of a low-cost sliding isolation system for light-frame residential structures. Proceedings of the 10th U.S. National Conference on Earthquake Engineering Frontiers of Earthquake Engineering, July 21-25, 2014, Anchorage, Alaska, https://datacenterhub.org/resources/11637

[77] Fajfar, P. (1999), Capacity spectrum method based on inelastic demand spectra. Earthquake Engineering and Structural Dynamics, 28(9): 979–993

ATTACHMENT

1. Columns of RC building 1

Table 0-1: Dimensions of all the columns of the RC building 1, rebars, as specified in the design documents that have been found. The lines of the same color are columns with the same section and rebars.

N. Pilastro	cantina				piano terra				piano I			
	a	b	armatura	staffe	a	b	armatura	staffe	a	b	armatura	staffe
1	40	40	6Φ16	Φ6/20	40	40	6Φ16	Φ6/20	30	35	4Φ16	Φ6/15
2	40	50	6Φ16	Φ6/20	40	50	6Φ18	Φ6/20	30	45	6Φ16	Φ6/15
3	40	50	6Φ16	Φ6/20	40	50	6Φ18	Φ6/20	30	45	6Φ16	Φ6/15
4	40	40	4Φ16	Φ6/20	40	40	4Φ16	Φ6/20	30	30	4Φ16	Φ6/15
5	40	40	6Φ16	Φ6/20	40	40	6Φ16	Φ6/20	30	40	4Φ18	Φ6/15
6	40	50	4Φ16+4Φ18	Φ6/20	40	50	8Φ18	Φ6/20	30	50	8Φ18	Φ6/20
7	40	50	4Φ16+4Φ18	Φ6/20	40	50	8Φ18	Φ6/20	30	50	8Φ18	Φ6/20
8	40	40	6Φ16	Φ6/20	40	40	6Φ16	Φ6/20	30	40	4Φ18	Φ6/15
9	40	40	4Φ16	Φ6/20	40	40	4Φ16	Φ6/20	30	30	4Φ16	Φ6/15
10	40	50	6Φ16	Φ6/20	40	50	6Φ18	Φ6/20	30	45	6Φ16	Φ6/15
11	40	50	6Φ16	Φ6/20	40	50	6Φ18	Φ6/20	30	45	6Φ16	Φ6/15
12	40	40	6Φ16	Φ6/20	40	40	6Φ16	Φ6/20	30	35	4Φ16	Φ6/15
13	40	50	6Φ18	Φ6/20	40	50	6Φ18	Φ6/20	30	50	4Φ16+2Φ18	Φ6/15
14	50	50	8Φ18	Φ6/20	40	50	8Φ18	Φ6/20	30	50	4Φ16+2Φ18	Φ6/20
15	50	50	8Φ18	Φ6/20	40	50	8Φ18	Φ6/20	30	50	4Φ16+2Φ18	Φ6/20
16	40	50	6Φ16	Φ6/20	40	40	6Φ16	Φ6/20	30	40	4Φ16+2Φ12	Φ6/15
17	40	50	6Φ16	Φ6/20	40	40	6Φ16	Φ6/20	30	30	4Φ16	Φ6/15
17 bis	40	50	6Φ16	Φ6/20	-				-			
18	50	50	6Φ18	Φ6/20	40	40	6Φ16	Φ6/20	30	40	4Φ16+2Φ12	Φ6/15
19	50	50	6Φ18	Φ6/20	40	40	6Φ16	Φ6/20	30	40	4Φ16+2Φ12	Φ6/15
20	40	50	6Φ16	Φ6/20	40	40	6Φ16	Φ6/20	30	30	4Φ16	Φ6/15
20 bis	40	50	6Φ16	Φ6/20	-				-			
21	40	50	6Φ16	Φ6/20	40	40	6Φ16	Φ6/20	30	40	4Φ16+2Φ12	Φ6/15
22	50	50	8Φ18	Φ6/20	40	50	8Φ18	Φ6/20	30	50	4Φ16+2Φ18	Φ6/20
23	50	50	8Φ18	Φ6/20	40	50	8Φ18	Φ6/20	30	50	4Φ16+2Φ18	Φ6/20
24	40	50	6Φ18	Φ6/20	40	50	6Φ18	Φ6/20	30	50	4Φ16+2Φ18	Φ6/15
25	40	40	6Φ16	Φ6/20	40	40	6Φ16	Φ6/20	30	40	4Φ16+2Φ12	Φ6/15
26	40	50	6Φ18	Φ6/20	40	50	6Φ18	Φ6/20	30	45	4Φ16+2Φ12	Φ6/15
27	40	50	6Φ18	Φ6/20	40	50	8Φ18	Φ6/20	30	50	4Φ16+2Φ18	Φ6/15
28	40	40	6Φ16	Φ6/20	40	50	8Φ18	Φ6/20	30	50	6Φ18	Φ6/20
29	40	40	6Φ16	Φ6/20	40	50	8Φ18	Φ6/20	30	50	6Φ18	Φ6/20
30	40	50	6Φ18	Φ6/20	40	50	8Φ18	Φ6/20	30	50	4Φ16+2Φ18	Φ6/15
31	40	50	6Φ18	Φ6/20	40	50	6Φ18	Φ6/20	30	45	4Φ16+2Φ12	Φ6/15
32	40	40	6Φ16	Φ6/20	40	40	6Φ16	Φ6/20	30	40	4Φ16+2Φ12	Φ6/15

N. Pilastro	piano II				piano III				piano IV			
	a	b	armatura	staffe	a	b	armatura	staffe	a	b	armatura	staffe
1	30	35	4Φ16	Φ6/15	30	35	4Φ16	Φ6/15	30	35	4Φ16	Φ6/15
2	30	45	4Φ16+2Φ12	Φ6/15	30	40	4Φ16+2Φ12	Φ6/15	30	35	4Φ12+2Φ16	Φ6/15
3	30	45	6Φ16	Φ6/15	30	40	6Φ16	Φ6/15	30	40	4Φ16+2Φ12	Φ6/15
4	30	30	4Φ16	Φ6/15	30	30	4Φ16	Φ6/15	30	30	4Φ16	Φ6/15
5	30	35	4Φ16+2Φ12	Φ6/15	30	35	4Φ16+2Φ12	Φ6/15	30	30	4Φ16	Φ6/15
6	30	50	6Φ18	Φ6/15	30	50	6Φ18	Φ6/15	30	45	4Φ18+2Φ12	Φ6/15
7	30	50	6Φ18	Φ6/15	30	50	6Φ18	Φ6/15	30	45	4Φ18+2Φ12	Φ6/15
8	30	35	4Φ16+2Φ12	Φ6/15	30	35	4Φ16+2Φ12	Φ6/15	30	30	4Φ16	Φ6/15
9	30	30	4Φ16	Φ6/15	30	30	4Φ16	Φ6/15	30	30	4Φ16	Φ6/15
10	30	45	6Φ16	Φ6/15	30	40	6Φ16	Φ6/15	30	40	4Φ16+2Φ12	Φ6/15
11	30	45	4Φ16+2Φ12	Φ6/15	30	40	4Φ16+2Φ12	Φ6/15	30	35	4Φ12+2Φ16	Φ6/15
12	30	35	4Φ16	Φ6/15	30	35	4Φ16	Φ6/15	30	35	4Φ16	Φ6/15
13	30	45	6Φ16	Φ6/15	30	45	6Φ16	Φ6/15	30	40	6Φ16	Φ6/15
14	30	45	6Φ16	Φ6/15	30	45	6Φ16	Φ6/15	30	40	6Φ16	Φ6/15
15	30	45	6Φ16	Φ6/15	30	45	6Φ16	Φ6/15	30	40	6Φ16	Φ6/15
16	30	35	4Φ16+2Φ12	Φ6/15	30	35	4Φ16+2Φ12	Φ6/15	30	35	4Φ12+2Φ16	Φ6/15
17	30	30	4Φ16	Φ6/15	30	30	4Φ16	Φ6/15	30	30	4Φ16	Φ6/15
17 bis	-				-				-			
18	30	35	4Φ16+2Φ12	Φ6/15	30	35	4Φ16+2Φ12	Φ6/15	30	30	4Φ16	Φ6/15
19	30	35	4Φ16+2Φ12	Φ6/15	30	35	4Φ16+2Φ12	Φ6/15	30	30	4Φ16	Φ6/15
20	30	30	4Φ16	Φ6/15	30	30	4Φ16	Φ6/15	30	30	4Φ16	Φ6/15
20 bis	-				-				-			
21	30	35	4Φ16+2Φ12	Φ6/15	30	35	4Φ16+2Φ12	Φ6/15	30	35	4Φ12+2Φ16	Φ6/15
22	30	45	6Φ16	Φ6/15	30	45	6Φ16	Φ6/15	30	40	6Φ16	Φ6/15
23	30	45	6Φ16	Φ6/15	30	45	6Φ16	Φ6/15	30	40	6Φ16	Φ6/15
24	30	45	6Φ16	Φ6/15	30	45	6Φ16	Φ6/15	30	40	6Φ16	Φ6/15
25	30	40	4Φ16+2Φ12	Φ6/15	30	40	4Φ16+2Φ12	Φ6/15	30	40	4Φ16+2Φ12	Φ6/15
26	30	40	4Φ16+2Φ12	Φ6/15	30	40	4Φ16+2Φ12	Φ6/15	30	35	4Φ12+2Φ16	Φ6/15
27	30	45	6Φ16	Φ6/15	30	45	6Φ16	Φ6/15	30	45	4Φ16+2Φ12	Φ6/15
28	30	45	4Φ16+2Φ18	Φ6/15	30	45	4Φ16+2Φ18	Φ6/15	30	45	4Φ18+2Φ12	Φ6/15
29	30	45	4Φ16+2Φ18	Φ6/15	30	45	4Φ16+2Φ18	Φ6/15	30	45	4Φ18+2Φ12	Φ6/15
30	30	45	6Φ16	Φ6/15	30	45	6Φ16	Φ6/15	30	45	4Φ16+2Φ12	Φ6/15
31	30	40	4Φ16+2Φ12	Φ6/15	30	40	4Φ16+2Φ12	Φ6/15	30	35	4Φ12+2Φ16	Φ6/15
32	30	40	4Φ16+2Φ12	Φ6/15	30	40	4Φ16+2Φ12	Φ6/15	30	40	4Φ16+2Φ12	Φ6/15

N. Pilastro	piano V				piano VI				piano VII			
	a	b	armatura	staffe	a	b	armatura	staffe	a	b	armatura	staffe
1	30	30	4Φ16	Φ6/15	30	30	4Φ16	Φ6/15	30	30	4Φ12	Φ6/15
2	30	30	4Φ16	Φ6/15	30	30	4Φ16	Φ6/15	30	30	4Φ16	Φ6/15
3	30	30	4Φ16	Φ6/15	30	30	4Φ16	Φ6/15	30	30	4Φ16	Φ6/15
4	30	30	4Φ16	Φ6/15	30	30	4Φ16	Φ6/15	30	30	4Φ12	Φ6/15
5	30	30	4Φ16	Φ6/15	30	30	4Φ16	Φ6/15	30	30	4Φ12	Φ6/15
6	30	35	4Φ16+2Φ12	Φ6/15	30	35	4Φ16	Φ6/15	30	30	4Φ16	Φ6/15
7	30	35	4Φ16+2Φ12	Φ6/15	30	35	4Φ16	Φ6/15	30	30	4Φ16	Φ6/15
8	30	30	4Φ16	Φ6/15	30	30	4Φ16	Φ6/15	30	30	4Φ12	Φ6/15
9	30	30	4Φ16	Φ6/15	30	30	4Φ16	Φ6/15	30	30	4Φ12	Φ6/15
10	30	30	4Φ16	Φ6/15	30	30	4Φ16	Φ6/15	30	30	4Φ16	Φ6/15
11	30	30	4Φ16	Φ6/15	30	30	4Φ16	Φ6/15	30	30	4Φ16	Φ6/15
12	30	30	4Φ16	Φ6/15	30	30	4Φ16	Φ6/15	30	30	4Φ12	Φ6/15
13	30	35	4Φ16+2Φ12	Φ6/15	30	35	4Φ16	Φ6/15	30	30	4Φ16	Φ6/15
14	30	35	4Φ16+2Φ12	Φ6/15	30	35	4Φ16	Φ6/15	30	30	4Φ16	Φ6/15
15	30	35	4Φ16+2Φ12	Φ6/15	30	35	4Φ16	Φ6/15	30	30	4Φ16	Φ6/15
16	30	30	4Φ16	Φ6/15	30	30	4Φ16	Φ6/15	30	30	4Φ12	Φ6/15
17	30	30	4Φ16	Φ6/15	30	30	4Φ16	Φ6/15	30	30	4Φ12	Φ6/15
17 bis	-				-				-			
18	30	30	4Φ16	Φ6/15	30	30	4Φ16	Φ6/15	30	30	4Φ12	Φ6/15
19	30	30	4Φ16	Φ6/15	30	30	4Φ16	Φ6/15	30	30	4Φ12	Φ6/15
20	30	30	4Φ16	Φ6/15	30	30	4Φ16	Φ6/15	30	30	4Φ12	Φ6/15
20 bis	-				-				-			
21	30	30	4Φ16	Φ6/15	30	30	4Φ16	Φ6/15	30	30	4Φ12	Φ6/15
22	30	35	4Φ16+2Φ12	Φ6/15	30	35	4Φ16	Φ6/15	30	30	4Φ16	Φ6/15
23	30	35	4Φ16+2Φ12	Φ6/15	30	35	4Φ16	Φ6/15	30	30	4Φ16	Φ6/15
24	30	35	4Φ16+2Φ12	Φ6/15	30	35	4Φ16	Φ6/15	30	30	4Φ16	Φ6/15
25	30	30	4Φ16	Φ6/15	30	30	4Φ16	Φ6/15	30	30	4Φ12	Φ6/15
26	30	30	4Φ16	Φ6/15	30	30	4Φ16	Φ6/15	30	30	4Φ16	Φ6/15
27	30	30	4Φ16	Φ6/15	30	30	4Φ16	Φ6/15	30	30	4Φ16	Φ6/15
28	30	35	4Φ16	Φ6/15	30	35	4Φ16	Φ6/15	30	30	4Φ16	Φ6/15
29	30	35	4Φ16	Φ6/15	30	35	4Φ16	Φ6/15	30	30	4Φ16	Φ6/15
30	30	30	4Φ16	Φ6/15	30	30	4Φ16	Φ6/15	30	30	4Φ16	Φ6/15
31	30	30	4Φ16	Φ6/15	30	30	4Φ16	Φ6/15	30	30	4Φ16	Φ6/15
32	30	30	4Φ16	Φ6/15	30	30	4Φ16	Φ6/15	30	30	4Φ12	Φ6/15

N. Pil.	piano VIII				piano IX				piano X				attico			
	a	b	armatura	staffe	a	b	armatura	staffe	a	b	armatura	staffe	a	b	armatura	staffe
1	30	30	4Φ12	Φ6/15	30	30	4Φ12	Φ6/15	30	30	4Φ16	Φ6/15	-			
2	30	30	4Φ12	Φ6/15	30	30	4Φ12	Φ6/15	30	30	4Φ12	Φ6/15	-			
3	30	30	4Φ12	Φ6/15	30	30	4Φ12	Φ6/15	30	30	4Φ12	Φ6/15	-			
4	30	30	4Φ12	Φ6/15	30	30	4Φ12	Φ6/15	30	30	4Φ12	Φ6/15	-			
5	30	30	4Φ12	Φ6/15	30	30	4Φ12	Φ6/15	30	30	4Φ12	Φ6/15	30	30	4Φ12	Φ6/15
6	30	30	4Φ16	Φ6/15	30	30	4Φ12	Φ6/15	30	30	4Φ12	Φ6/15	30	30	4Φ12	Φ6/15
7	30	30	4Φ16	Φ6/15	30	30	4Φ12	Φ6/15	30	30	4Φ12	Φ6/15	30	30	4Φ12	Φ6/15
8	30	30	4Φ12	Φ6/15	30	30	4Φ12	Φ6/15	30	30	4Φ12	Φ6/15	30	30	4Φ12	Φ6/15
9	30	30	4Φ12	Φ6/15	30	30	4Φ12	Φ6/15	30	30	4Φ12	Φ6/15	-			
10	30	30	4Φ12	Φ6/15	30	30	4Φ12	Φ6/15	30	30	4Φ12	Φ6/15	-			
11	30	30	4Φ12	Φ6/15	30	30	4Φ12	Φ6/15	30	30	4Φ12	Φ6/15	-			
12	30	30	4Φ12	Φ6/15	30	30	4Φ12	Φ6/15	30	30	4Φ16	Φ6/15	-			
13	30	30	4Φ12	Φ6/15	30	30	4Φ12	Φ6/15	30	30	4Φ12	Φ6/15	30	30	4Φ12	Φ6/15
14	30	30	4Φ16	Φ6/15	30	30	4Φ12	Φ6/15	30	30	4Φ12	Φ6/15	30	30	4Φ12	Φ6/15
15	30	30	4Φ16	Φ6/15	30	30	4Φ12	Φ6/15	30	30	4Φ12	Φ6/15	-			
16	30	30	4Φ12	Φ6/15	30	30	4Φ12	Φ6/15	30	30	4Φ12	Φ6/15	30	30	6Φ16	Φ6/15
17	30	30	4Φ12	Φ6/15	30	30	4Φ12	Φ6/15	30	30	4Φ12	Φ6/15	30	30	4Φ12	Φ6/15
17 bis	-				-				-				-			
18	30	30	4Φ12	Φ6/15	30	30	4Φ12	Φ6/15	30	30	4Φ12	Φ6/15	30	30	4Φ12	Φ6/15
19	30	30	4Φ12	Φ6/15	30	30	4Φ12	Φ6/15	30	30	4Φ12	Φ6/15	30	30	4Φ12	Φ6/15
20	30	30	4Φ12	Φ6/15	30	30	4Φ12	Φ6/15	30	30	4Φ12	Φ6/15	30	30	4Φ12	Φ6/15
20 bis	-				-				-				-			
21	30	30	4Φ12	Φ6/15	30	30	4Φ12	Φ6/15	30	30	4Φ12	Φ6/15	30	30	6Φ16	Φ6/15
22	30	30	4Φ16	Φ6/15	30	30	4Φ12	Φ6/15	30	30	4Φ12	Φ6/15	-			
23	30	30	4Φ16	Φ6/15	30	30	4Φ12	Φ6/15	30	30	4Φ12	Φ6/15	30	30	4Φ12	Φ6/15
24	30	30	4Φ12	Φ6/15	30	30	4Φ12	Φ6/15	30	30	4Φ12	Φ6/15	30	30	4Φ12	Φ6/15
25	30	30	4Φ12	Φ6/15	30	30	4Φ12	Φ6/15	30	30	4Φ12	Φ6/15	30	30	4Φ12	Φ6/15
26	30	30	4Φ12	Φ6/15	30	30	4Φ12	Φ6/15	30	30	4Φ12	Φ6/15	30	30	4Φ12	Φ6/15
27	30	30	4Φ12	Φ6/15	30	30	4Φ12	Φ6/15	30	30	4Φ12	Φ6/15	30	30	4Φ12	Φ6/15
28	30	30	4Φ12	Φ6/15	30	30	4Φ12	Φ6/15	30	30	4Φ12	Φ6/15	30	30	4Φ12	Φ6/15
29	30	30	4Φ12	Φ6/15	30	30	4Φ12	Φ6/15	30	30	4Φ12	Φ6/15	30	30	4Φ12	Φ6/15
30	30	30	4Φ12	Φ6/15	30	30	4Φ12	Φ6/15	30	30	4Φ12	Φ6/15	30	30	4Φ12	Φ6/15
31	30	30	4Φ12	Φ6/15	30	30	4Φ12	Φ6/15	30	30	4Φ12	Φ6/15	30	30	4Φ12	Φ6/15
32	30	30	4Φ12	Φ6/15	30	30	4Φ12	Φ6/15	30	30	4Φ12	Φ6/15	30	30	4Φ12	Φ6/15

2. Results for non-linear dynamic analyses in Y direction of RC building 1

Table 0-2: Maximum interstorey displacements and drifts resulting from non-linear dynamic analyses in Y direction of RC building 1

	Load case	Maximum interstorey displacement [m]	Storey	Storey height [m]	Maximum interstorey drift [-]	ln (drift)
1	A.496	0.0193	2	3.1	0.0062	-5.08
2	A.ATS	0.0264	6	3.1	0.0085	-4.77
3	A.BUR	0.0387	5	3.1	0.0125	-4.38
4	A.GZL	0.0525	3	3.1	0.0169	-4.08
5	A.YPT	0.0813	3	3.1	0.0262	-3.64
6	BA.MIRE	0.0516	3	3.1	0.0166	-4.10
7	BA.MIRH	0.0544	3	3.1	0.0175	-4.04
8	EU.BAR	0.0546	4	3.1	0.0176	-4.04
9	EU.PETO	0.0222	1	3.1	0.0071	-4.94
10	EU.ULA	0.0318	3	3.1	0.0103	-4.58
11	EU.ULO	0.0581	3	3.1	0.0187	-3.98
12	HI.KAL1	0.0222	5	3.1	0.0072	-4.94
13	HL.AIGA	0.0206	2	3.1	0.0066	-5.02
14	HL.KALA	0.0281	5	3.1	0.0091	-4.70
15	HL.KORA	0.0408	4	3.1	0.0132	-4.33
16	HL.XLCA	0.0304	6	3.1	0.0098	-4.62
17	IT.ACC	0.0263	2	3.1	0.0085	-4.77
18	IT.AMT	0.0359	2	3.1	0.0116	-4.46
19	IT.AQA	0.0263	3	3.1	0.0085	-4.77
20	IT.AQG	0.0295	3	3.1	0.0095	-4.66
21	IT.AQK09	0.0258	4	3.1	0.0083	-4.79
22	IT.AQK16	0.0126	3	3.1	0.0041	-5.50
23	IT.BGI	0.0341	4	3.1	0.0110	-4.51
24	IT.CLF	0.0169	5	3.1	0.0054	-5.21
25	IT.CLO	0.0430	4	3.1	0.0139	-4.28
26	IT.CLT	0.0464	6	3.1	0.0150	-4.20
27	IT.CMI	0.0256	2	3.1	0.0083	-4.80
28	IT.CNE	0.0210	6	3.1	0.0068	-4.99
29	IT.GBP	0.0433	5	3.1	0.0140	-4.27
30	IT.MOG0	0.0329	4	3.1	0.0106	-4.55
31	E.ATR	0.0021	10	3.1	0.0007	-7.29
32	E.FRC	0.0067	1	3.1	0.0022	-6.13
33	IT.ASS	0.0023	10	3.1	0.0007	-7.23
34	IT.BGN	0.0012	11	3.1	0.0004	-7.82
35	IT.CR1	0.0030	11	3.1	0.0010	-6.94
36	IT.MCV	0.0031	10	3.1	0.0010	-6.92
37	IT.MRC	0.0032	11	3.1	0.0010	-6.88
38	IT.MSC	0.0032	11	3.1	0.0010	-6.89
39	IT.NRC	0.0017	11	3.1	0.0005	-7.52

40	IT.PCH	0.0012	11	3.1	0.0004	-7.90
41	IT.SGV	0.0009	11	3.1	0.0003	-8.20
42	IT.SNO	0.0010	11	3.1	0.0003	-7.99
43	IT.TDG	0.0017	11	3.1	0.0006	-7.50
44	IT.TRL	0.0024	11	3.1	0.0008	-7.16
45	IT.UMB	0.0015	11	3.1	0.0005	-7.60
46	IT.VZZ	0.0039	1	3.1	0.0013	-6.67
47	IV.NRCA	0.0014	11	3.1	0.0005	-7.68
48	MN.CEL	0.0008	11	3.1	0.0003	-8.24
49	OX.SABO	0.0016	11	3.1	0.0005	-7.59
50	TK.2501	0.0011	11	3.1	0.0004	-7.91

Table 0-3: Maximum top displacements and Demand/Capacity ratios resulting from non-linear dynamic analyses in Y direction of RC building 1. Also the logarithms of the IM's are reported.

	Load case	Maximum top displacement [m]	D/C ratio in terms of top displacement	ln (D/C)	ln (PGA)	ln (Sa(T1))	ln (Sa,eq,Y)	ln (Housner)
1	A.496	0.0966	8.9923	2.196371	-0.277	-1.72	-1.24	4.57
2	A.ATS	0.2100	19.5462	2.972783	-1.686	-1.30	-1.43	5.01
3	A.BUR	0.2545	23.6926	3.165164	-2.304	-1.70	-1.96	4.40
4	A.GZL	0.2766	25.7496	3.248418	-0.326	-0.75	-0.78	5.29
5	A.YPT	0.4805	44.7321	3.800692	-1.132	-1.11	-1.31	5.17
6	BA.MIRE	0.2695	25.0863	3.222323	-1.307	-0.91	-1.16	5.23
7	BA.MIRH	0.2719	25.3121	3.231282	-1.309	-1.08	-1.33	5.17
8	EU.BAR	0.3134	29.1772	3.373388	-1.022	-0.70	-0.96	5.53
9	EU.PETO	0.1301	12.1158	2.494511	-0.790	-2.10	-1.24	5.00
10	EU.ULA	0.2052	19.1053	2.949964	-1.542	-1.31	-1.51	4.82
11	EU.ULO	0.3278	30.5134	3.418164	-1.441	-0.89	-1.13	5.21
12	HI.KAL1	0.1584	14.7433	2.690789	-1.460	-1.86	-1.63	4.60
13	HL.AIGA	0.0971	9.0372	2.201352	-0.697	-1.92	-1.27	4.77
14	HL.KALA	0.1725	16.0597	2.776315	-1.531	-1.65	-1.70	4.78
15	HL.KORA	0.2739	25.4996	3.238663	-1.425	-1.65	-1.72	4.59
16	HL.XLCA	0.2451	22.8213	3.127693	-1.238	-1.95	-1.44	4.71
17	IT.ACC	0.1610	14.9908	2.707438	-0.834	-1.50	-1.39	4.94
18	IT.AMT	0.1458	13.5749	2.608219	-0.979	-1.91	-1.69	4.73
19	IT.AQA	0.1223	11.3830	2.432117	-0.910	-2.06	-1.94	4.49
20	IT.AQG	0.1277	11.8866	2.47541	-0.808	-1.79	-1.43	4.75
21	IT.AQK09	0.1386	12.9067	2.557749	-1.109	-1.16	-1.36	4.09
22	IT.AQK16	0.0898	8.3593	2.123373	-2.845	-1.85	-2.18	4.92
23	IT.BGI	0.2075	19.3224	2.961265	-1.676	-1.34	-1.63	4.79
24	IT.CLF	0.0875	8.1446	2.097351	-1.360	-1.90	-1.37	4.45
25	IT.CLO	0.2908	27.0742	3.29858	-0.852	-0.73	-0.91	5.46
26	IT.CLT	0.2928	27.2624	3.30551	-1.744	-1.43	-1.60	4.76
27	IT.CMI	0.1100	10.2386	2.326169	-0.430	-1.69	-0.67	4.95
28	IT.CNE	0.1256	11.6938	2.459055	-1.225	-1.76	-1.71	4.51

29	IT.GBP	0.3005	27.9759	3.331342	-2.325	-1.46	-1.79	4.54
30	IT.MOG0	0.1789	16.6587	2.812932	-1.770	-1.54	-1.73	4.55
31	E.ATR	0.0144	1.3435	0.295263	-3.180	-5.03	-4.10	1.86
32	E.FRC	0.0237	2.2109	0.793387	-1.453	-4.08	-1.40	3.34
33	IT.ASS	0.0154	1.4291	0.357034	-1.866	-4.83	-2.78	2.32
34	IT.BGN	0.0092	0.8547	-0.15698	-3.142	-6.11	-4.25	0.89
35	IT.CR1	0.0187	1.7367	0.55199	-2.239	-4.79	-3.26	2.18
36	IT.MCV	0.0258	2.4019	0.876259	-1.024	-3.85	-2.18	2.99
37	IT.MRC	0.0300	2.7955	1.028007	-4.289	-4.01	-4.21	2.32
38	IT.MSC	0.0287	2.6747	0.983833	-3.251	-3.94	-3.57	2.25
39	IT.NRC	0.0109	1.0133	0.013247	-1.918	-5.51	-3.19	1.66
40	IT.PCH	0.0093	0.8617	-0.14885	-3.083	-6.11	-4.55	0.93
41	IT.SGV	0.0067	0.6274	-0.46612	-5.935	-8.95	-6.58	-1.55
42	IT.SNO	0.0073	0.6816	-0.38336	-4.592	-7.79	-5.13	-0.28
43	IT.TDG	0.0126	1.1700	0.156981	-4.090	-5.37	-4.59	1.73
44	IT.TRL	0.0186	1.7307	0.548553	-3.240	-4.28	-3.88	2.49
45	IT.UMB	0.0111	1.0343	0.033703	-4.352	-5.73	-4.66	1.32
46	IT.VZZ	0.0264	2.4589	0.899706	-2.623	-4.15	-3.18	2.77
47	IV.NRCA	0.0083	0.7700	-0.26136	-2.070	-6.34	-3.61	0.94
48	MN.CEL	0.0068	0.6286	-0.46423	-8.377	-8.74	-8.69	-2.42
49	OX.SABO	0.0143	1.3267	0.282723	-5.690	-5.15	-5.43	1.03
50	TK.2501	0.0094	0.8705	-0.13864	-4.965	-6.05	-5.49	0.77

3. Results for non-linear dynamic analyses in Y direction of RC building 2

Table 0-4: Maximum interstorey drifts for non-linear dynamic analyses in Y direction of RC building 2

	Load case	Maximum interstorey displacement baricenter [m]	Storey	Storey height [m]	Maximum interstorey drift [-]	Maximum interstorey displacement corner [m]	Storey	Storey height [m]	Maximum interstorey drift [-]
1	A.496	0.039	3	3.15	0.0123	0.040	4	3.15	0.0125
2	A.ATS	0.071	4	3.15	0.0225	0.072	4	3.15	0.0229
3	A.BUR	0.013	9	3.15	0.0041	0.021	9	3.15	0.0068
4	A.GZL	0.055	9	3.15	0.0173	0.057	9	3.15	0.0180
5	A.YPT	0.116	4	3.15	0.0367	0.117	4	3.15	0.0370
6	BA.MIRE	0.048	8	3.15	0.0153	0.052	7	3.15	0.0165
7	BA.MIRH	0.055	3	3.15	0.0176	0.059	3	3.15	0.0187
8	EU.BAR	0.038	5	3.15	0.0121	0.038	5	3.15	0.0121
9	EU.PETO	0.032	3	3.15	0.0103	0.033	3	3.15	0.0103
10	EU.ULA	0.028	4	3.15	0.0088	0.030	3	3.15	0.0096
11	EU.ULO	0.032	5	3.15	0.0102	0.032	5	3.15	0.0102
12	HI.KAL1	0.016	3	3.15	0.0050	0.018	3	3.15	0.0057
13	HL.AIGA	0.030	2	3.15	0.0094	0.032	2	3.15	0.0101

14	HL.KALA	0.020	2	3.15	0.0064	0.022	2	3.15	0.0071
15	HL.KORA	0.025	3	3.15	0.0079	0.025	3	3.15	0.0079
16	HL.XLCA	0.023	4	3.15	0.0072	0.026	4	3.15	0.0083
17	IT.ACC	0.038	3	3.15	0.0119	0.038	2	3.15	0.0120
18	IT.AMT	0.020	2	3.15	0.0063	0.020	2	3.15	0.0063
19	IT.AQA	0.011	2	3.15	0.0036	0.017	9	3.15	0.0053
20	IT.AQG	0.013	1	3.15	0.0043	0.017	9	3.15	0.0053
21	IT.AQK09	0.043	3	3.15	0.0136	0.044	3	3.15	0.0139
22	IT.AQK16	0.008	8	3.15	0.0026	0.009	9	3.15	0.0027
23	IT.BGI	0.028	3	3.15	0.0088	0.030	3	3.15	0.0095
24	IT.CLF	0.015	9	3.15	0.0049	0.022	8	3.15	0.0071
25	IT.CLO	0.037	4	3.15	0.0118	0.040	3	3.15	0.0127
26	IT.CLT	0.081	9	3.15	0.0258	0.077	9	3.15	0.0244
27	IT.CMI	0.022	4	3.15	0.0070	0.027	9	3.15	0.0084
28	IT.CNE	0.025	2	3.15	0.0078	0.026	2	3.15	0.0083
29	IT.GBP	0.016	6	3.15	0.0052	0.016	4	3.15	0.0051
30	IT.MOG0	0.010	1	3.15	0.0031	0.016	9	3.15	0.0051
31	E.ATR	0.002	9	3.15	0.0007	0.003	9	3.15	0.0008
32	E.FRC	0.005	10	3.09	0.0016	0.008	10	3.09	0.0025
33	IT.ASS	0.002	10	3.09	0.0007	0.004	9	3.15	0.0013
34	IT.BGN	0.001	10	3.09	0.0004	0.002	7	3.15	0.0005
35	IT.CR1	0.001	10	3.09	0.0005	0.003	8	3.15	0.0010
36	IT.MCV	0.004	9	3.15	0.0014	0.006	9	3.15	0.0019
37	IT.MRC	0.003	8	3.15	0.0008	0.004	7	3.15	0.0012
38	IT.MSC	0.002	9	3.15	0.0008	0.004	7	3.15	0.0013
39	IT.NRC	0.002	9	3.15	0.0008	0.003	10	3.09	0.0011
40	IT.PCH	0.001	9	3.15	0.0003	0.002	10	3.09	0.0005
41	IT.SGV	0.000	9	3.15	0.0001	0.001	9	3.15	0.0003
42	IT.SNO	0.001	9	3.15	0.0002	0.001	9	3.15	0.0003
43	IT.TDG	0.001	9	3.15	0.0005	0.003	9	3.15	0.0009
44	IT.TRL	0.003	9	3.15	0.0008	0.004	7	3.15	0.0014
45	IT.UMB	0.001	9	3.15	0.0004	0.002	7	3.15	0.0008
46	IT.VZZ	0.002	8	3.15	0.0007	0.006	9	3.15	0.0018
47	IV.NRCA	0.001	10	3.09	0.0004	0.002	10	3.09	0.0006
48	MN.CEL	0.000	9	3.15	0.0001	0.001	9	3.15	0.0003
49	OX.SABO	0.002	9	3.15	0.0005	0.002	7	3.15	0.0008
50	TK.2501	0.001	9	3.15	0.0003	0.002	7	3.15	0.0007

Table 0-5: Maximum displacements at the top of the building and IM used in the correlations. Ln (drift) is the logarithm of the interstorey drift reported in Table 0-4.

	Load case	Maximum top displacement [m]	D/C ratio in terms of top displacement	ln (D/C)	ln (drift)	ln (PGA)	ln (Sa(T1))	ln (Sa,eq,Y)	ln (Housner)
1	A.496	0.2179	8.6160	2.1536	-4.40	0.029	-3.019	-0.942	4.585
2	A.ATS	0.3669	14.5088	2.6748	-3.80	-1.375	-2.552	-1.998	4.647

3	A.BUR	0.1035	4.0907	1.4087	-5.49	-2.292	-2.687	-2.670	4.066
4	A.GZL	0.2827	11.1784	2.4140	-4.06	-0.326	-1.508	-1.157	5.293
5	A.YPT	0.7920	31.3155	3.4441	-3.31	-1.132	-1.641	-1.758	5.167
6	BA.MIRE	0.3833	15.1560	2.7184	-4.18	-1.307	-1.347	-1.537	5.229
7	BA.MIRH	0.3262	12.8989	2.5571	-4.04	-1.309	-1.219	-1.588	5.173
8	EU.BAR	0.2383	9.4209	2.2429	-4.42	-0.990	-1.866	-1.822	5.313
9	EU.PETO	0.1345	5.3186	1.6712	-4.58	-0.790	-2.567	-1.448	5.003
10	EU.ULA	0.1574	6.2223	1.8281	-4.73	-1.542	-1.999	-1.981	4.823
11	EU.ULO	0.2099	8.2987	2.1161	-4.58	-1.264	-1.950	-1.799	5.056
12	HI.KAL1	0.1033	4.0843	1.4071	-5.30	-1.311	-2.834	-1.751	4.509
13	HL.AIGA	0.1345	5.3190	1.6713	-4.67	-0.653	-2.438	-1.669	4.702
14	HL.KALA	0.1208	4.7766	1.5637	-5.05	-1.216	-2.769	-1.828	4.742
15	HL.KORA	0.1075	4.2510	1.4471	-4.84	-1.216	-2.070	-2.129	4.556
16	HL.XLCA	0.1370	5.4177	1.6897	-4.93	-1.238	-2.111	-1.689	4.714
17	IT.ACC	0.1795	7.0969	1.9597	-4.43	-0.834	-2.077	-1.758	4.940
18	IT.AMT	0.0750	2.9663	1.0873	-5.07	-0.142	-3.340	-1.150	4.316
19	IT.AQA	0.0830	3.2819	1.1884	-5.62	-0.816	-3.167	-1.891	4.338
20	IT.AQG	0.0726	2.8713	1.0548	-5.46	-0.716	-3.213	-2.116	4.518
21	IT.AQK09	0.2437	9.6344	2.2653	-4.30	-1.040	-1.932	-1.830	4.093
22	IT.AQK16	0.0698	2.7597	1.0151	-5.94	-2.845	-3.232	-2.896	4.954
23	IT.BGI	0.1807	7.1438	1.9662	-4.74	-1.676	-1.945	-2.106	4.788
24	IT.CLF	0.1213	4.7944	1.5675	-5.31	-1.285	-3.200	-2.278	4.397
25	IT.CLO	0.2924	11.5600	2.4476	-4.44	-0.540	-1.973	-0.984	5.320
26	IT.CLT	0.1714	6.7763	1.9134	-3.66	-1.744	-2.187	-1.990	4.761
27	IT.CMI	0.1353	5.3489	1.6769	-4.96	-0.430	-2.689	-0.898	4.954
28	IT.CNE	0.1093	4.3212	1.4635	-4.86	-0.743	-2.840	-1.826	4.853
29	IT.GBP	0.1558	6.1616	1.8183	-5.26	-2.325	-2.040	-2.012	4.537
30	IT.MOG0	0.0633	2.5032	0.9176	-5.79	-1.426	-3.392	-2.322	4.259
31	E.ATR	0.0110	0.4353	-0.8317	-7.26	-3.180	-5.057	-4.380	1.862
32	E.FRC	0.0201	0.7954	-0.2289	-6.42	-2.047	-4.656	-3.043	3.046
33	IT.ASS	0.0116	0.4593	-0.7781	-7.21	-2.179	-5.432	-3.381	2.446
34	IT.BGN	0.0073	0.2900	-1.2378	-7.89	-3.361	-5.878	-5.550	0.928
35	IT.CR1	0.0079	0.3114	-1.1667	-7.69	-2.317	-5.679	-4.465	1.968
36	IT.MCV	0.0329	1.3018	0.2637	-6.58	-1.232	-4.077	-3.101	3.193
37	IT.MRC	0.0207	0.8192	-0.1994	-7.09	-4.289	-4.634	-4.582	2.320
38	IT.MSC	0.0195	0.7698	-0.2616	-7.18	-3.351	-4.548	-4.598	2.350
39	IT.NRC	0.0127	0.5018	-0.6896	-7.19	-2.131	-5.236	-3.578	2.431
40	IT.PCH	0.0044	0.1752	-1.7416	-8.24	-3.083	-6.784	-5.205	0.933
41	IT.SGV	0.0027	0.1067	-2.2381	-8.99	-6.262	-9.413	-7.117	-1.472
42	IT.SNO	0.0031	0.1224	-2.1006	-8.70	-4.592	-8.025	-5.432	-0.279
43	IT.TDG	0.0078	0.3082	-1.1769	-7.69	-4.090	-5.609	-4.812	1.735
44	IT.TRL	0.0161	0.6374	-0.4504	-7.11	-3.337	-4.590	-4.216	2.510
45	IT.UMB	0.0085	0.3363	-1.0899	-7.92	-4.473	-5.217	-5.016	1.410
46	IT.VZZ	0.0147	0.5804	-0.5440	-7.24	-2.727	-4.806	-4.054	2.710
47	IV.NRCA	0.0038	0.1512	-1.8890	-7.91	-2.070	-6.819	-4.686	0.939
48	MN.CEL	0.0027	0.1060	-2.2443	-9.05	-8.377	-9.734	-9.026	-2.421

49	OX.SABO	0.0136	0.5390	-0.6181	-7.56	-5.695	-5.038	-5.308	1.378
50	TK.2501	0.0075	0.2965	-1.2157	-8.02	-4.503	-5.390	-5.500	1.286

4. Results for non-linear dynamic analyses in X direction of RC building 2

Table 0-6: Maximum interstorey drifts for non-linear dynamic analyses in X direction of RC building 2 (barycentric point)

	Load case	Maximum interstorey displacement barycentre [m]	Storey	Storey height [m]	Maximum interstorey drift [-]	ln (drift)
1	A.496	0.0304	10.0000	3.0900	0.0098	-4.6223
2	A.ATS	0.0247	3.0000	3.1500	0.0078	-4.8476
3	A.BUR	0.0099	8.0000	3.1500	0.0031	-5.7627
4	A.GZL	0.0508	3.0000	3.1500	0.0161	-4.1265
5	A.YPT	0.0670	4.0000	3.1500	0.0213	-3.8503
6	BA.MIRE	0.0350	6.0000	3.1500	0.0111	-4.5005
7	BA.MIRH	0.0376	4.0000	3.1500	0.0119	-4.4280
8	EU.BAR	0.0502	10.0000	3.0900	0.0163	-4.1194
9	EU.PETO	0.0331	10.0000	3.0900	0.0107	-4.5370
10	EU.ULA	0.0227	3.0000	3.1500	0.0072	-4.9314
11	EU.ULO	0.0255	5.0000	3.1500	0.0081	-4.8163
12	HI.KAL1	0.0164	9.0000	3.1500	0.0052	-5.2550
13	HL.AIGA	0.0253	2.0000	3.1500	0.0080	-4.8250
14	HL.KALA	0.0199	9.0000	3.1500	0.0063	-5.0626
15	HL.KORA	0.0230	4.0000	3.1500	0.0073	-4.9208
16	HL.XLCA	0.0160	2.0000	3.1500	0.0051	-5.2799
17	IT.ACC	0.0253	4.0000	3.1500	0.0080	-4.8229
18	IT.AMT	0.0117	2.0000	3.1500	0.0037	-5.5920
19	IT.AQA	0.0124	9.0000	3.1500	0.0039	-5.5395
20	IT.AQG	0.0159	7.0000	3.1500	0.0050	-5.2897
21	IT.AQK09	0.0380	4.0000	3.1500	0.0121	-4.4166
22	IT.AQK16	0.0091	5.0000	3.1500	0.0029	-5.8492
23	IT.BGI	0.0287	4.0000	3.1500	0.0091	-4.6972
24	IT.CLF	0.0133	9.0000	3.1500	0.0042	-5.4641
25	IT.CLO	0.0425	1.0000	3.1500	0.0135	-4.3053
26	IT.CLT	0.0187	5.0000	3.1500	0.0059	-5.1246
27	IT.CMI	0.0193	3.0000	3.1500	0.0061	-5.0970
28	IT.CNE	0.0185	3.0000	3.1500	0.0059	-5.1376
29	IT.GBP	0.0205	8.0000	3.1500	0.0065	-5.0336
30	IT.MOG0	0.0138	9.0000	3.1500	0.0044	-5.4272
31	E.ATR	0.0016	9.0000	3.1500	0.0005	-7.5900
32	E.FRC	0.0057	9.0000	3.1500	0.0018	-6.3111
33	IT.ASS	0.0027	9.0000	3.1500	0.0008	-7.0716
34	IT.BGN	0.0012	9.0000	3.1500	0.0004	-7.8341

35	IT.CR1	0.0014	10.0000	3.0900	0.0005	-7.6947
36	IT.MCV	0.0044	9.0000	3.1500	0.0014	-6.5793
37	IT.MRC	0.0026	7.0000	3.1500	0.0008	-7.0999
38	IT.MSC	0.0024	9.0000	3.1500	0.0008	-7.1759
39	IT.NRC	0.0033	10.0000	3.0900	0.0011	-6.8502
40	IT.PCH	0.0008	9.0000	3.1500	0.0003	-8.2307
41	IT.SGV	0.0004	10.0000	3.0900	0.0001	-8.9091
42	IT.SNO	0.0006	10.0000	3.0900	0.0002	-8.5859
43	IT.TDG	0.0018	10.0000	3.0900	0.0006	-7.4537
44	IT.TRL	0.0022	9.0000	3.1500	0.0007	-7.2719
45	IT.UMB	0.0014	9.0000	3.1500	0.0004	-7.7274
46	IT.VZZ	0.0034	10.0000	3.0900	0.0011	-6.8121
47	IV.NRCA	0.0008	10.0000	3.0900	0.0003	-8.2011
48	MN.CEL	0.0004	9.0000	3.1500	0.0001	-9.0208
49	OX.SABO	0.0017	6.0000	3.1500	0.0005	-7.5520
50	TK.2501	0.0012	9.0000	3.1500	0.0004	-7.8901

Table 0-7: Maximum interstorey drifts calculated in a corner point and maximum top displacements for the non-linear dynamic analyses in X direction of RC building 2.

	Load case	Maximum interstorey displacement corner [m]	Storey	Storey height [m]	Maximum interstorey drift [-]	ln (drift)	Maximum top displacement [m]	D/C ratio in terms of top displacement	ln (D/C)
1	A.496	0.0335	10	3.09	0.0109	-4.5234	0.1650	11.1263	2.4093
2	A.ATS	0.0229	4	3.15	0.0073	-4.9235	0.1355	9.1355	2.2122
3	A.BUR	0.0131	2	3.15	0.0042	-5.4798	0.0787	5.3038	1.6684
4	A.GZL	0.0505	3	3.15	0.0160	-4.1324	0.3420	23.0622	3.1382
5	A.YPT	0.0641	4	3.15	0.0203	-3.8949	0.5144	34.6893	3.5464
6	BA.MIRE	0.0358	4	3.15	0.0114	-4.4764	0.3104	20.9303	3.0412
7	BA.MIRH	0.0384	5	3.15	0.0122	-4.4064	0.2796	18.8528	2.9367
8	EU.BAR	0.0483	10	3.09	0.0156	-4.1590	0.2599	17.5250	2.8636
9	EU.PETO	0.0378	10	3.09	0.0122	-4.4043	0.1308	8.8179	2.1768
10	EU.ULA	0.0258	4	3.15	0.0082	-4.8066	0.1769	11.9256	2.4787
11	EU.ULO	0.0276	7	3.15	0.0088	-4.7364	0.2042	13.7666	2.6222
12	HI.KAL1	0.0198	9	3.15	0.0063	-5.0694	0.1129	7.6127	2.0298
13	HL.AIGA	0.0270	3	3.15	0.0086	-4.7595	0.1203	8.1142	2.0936
14	HL.KALA	0.0228	9	3.15	0.0072	-4.9285	0.1292	8.7140	2.1649
15	HL.KORA	0.0245	5	3.15	0.0078	-4.8553	0.1383	9.3247	2.2327
16	HL.XLCA	0.0232	9	3.15	0.0074	-4.9117	0.1022	6.8897	1.9300
17	IT.ACC	0.0311	5	3.15	0.0099	-4.6185	0.1575	10.6237	2.3631
18	IT.AMT	0.0145	10	3.09	0.0047	-5.3632	0.0489	3.2961	1.1927
19	IT.AQA	0.0151	10	3.09	0.0049	-5.3185	0.0828	5.5823	1.7196
20	IT.AQG	0.0181	7	3.15	0.0057	-5.1600	0.1115	7.5195	2.0175
21	IT.AQK09	0.0404	4	3.15	0.0128	-4.3569	0.2717	18.3179	2.9079

22	IT.AQK16	0.0105	6	3.15	0.0033	-5.7082	0.0843	5.6850	1.7378
23	IT.BGI	0.0328	4	3.15	0.0104	-4.5648	0.2603	17.5539	2.8653
24	IT.CLF	0.0195	9	3.15	0.0062	-5.0867	0.0919	6.2001	1.8246
25	IT.CLO	0.0425	1	3.15	0.0135	-4.3058	0.2621	17.6743	2.8721
26	IT.CLT	0.0281	6	3.15	0.0089	-4.7198	0.1524	10.2772	2.3299
27	IT.CMI	0.0275	6	3.15	0.0087	-4.7420	0.1332	8.9800	2.1950
28	IT.CNE	0.0228	8	3.15	0.0072	-4.9293	0.0990	6.6758	1.8985
29	IT.GBP	0.0197	4	3.15	0.0063	-5.0737	0.1795	12.1011	2.4933
30	IT.MOG0	0.0184	10	3.09	0.0059	-5.1255	0.0599	4.0395	1.3961
31	E.ATR	0.0029	9	3.15	0.0009	-6.9961	0.0111	0.7460	-0.2930
32	E.FRC	0.0060	9	3.15	0.0019	-6.2677	0.0216	1.4582	0.3772
33	IT.ASS	0.0046	10	3.09	0.0015	-6.5144	0.0112	0.7533	-0.2834
34	IT.BGN	0.0015	9	3.15	0.0005	-7.6564	0.0076	0.5134	-0.6667
35	IT.CR1	0.0030	9	3.15	0.0009	-6.9690	0.0124	0.8377	-0.1771
36	IT.MCV	0.0063	10	3.09	0.0021	-6.1883	0.0440	2.9641	1.0866
37	IT.MRC	0.0025	9	3.15	0.0008	-7.1477	0.0222	1.5000	0.4055
38	IT.MSC	0.0031	9	3.15	0.0010	-6.9292	0.0226	1.5239	0.4213
39	IT.NRC	0.0041	9	3.15	0.0013	-6.6466	0.0121	0.8149	-0.2047
40	IT.PCH	0.0016	10	3.09	0.0005	-7.5597	0.0049	0.3322	-1.1021
41	IT.SGV	0.0010	9	3.15	0.0003	-8.0145	0.0028	0.1863	-1.6806
42	IT.SNO	0.0011	9	3.15	0.0004	-7.9156	0.0031	0.2109	-1.5563
43	IT.TDG	0.0027	9	3.15	0.0008	-7.0731	0.0081	0.5493	-0.5991
44	IT.TRL	0.0041	9	3.15	0.0013	-6.6464	0.0188	1.2648	0.2349
45	IT.UMB	0.0020	9	3.15	0.0006	-7.3793	0.0099	0.6692	-0.4016
46	IT.VZZ	0.0046	8	3.15	0.0015	-6.5269	0.0176	1.1861	0.1707
47	IV.NRCA	0.0018	10	3.09	0.0006	-7.4401	0.0038	0.2560	-1.3626
48	MN.CEL	0.0009	9	3.15	0.0003	-8.1386	0.0027	0.1841	-1.6923
49	OX.SABO	0.0017	9	3.15	0.0005	-7.5134	0.0146	0.9845	-0.0156
50	TK.2501	0.0016	9	3.15	0.0005	-7.6169	0.0081	0.5483	-0.6010